COPOLYMERIZATION OF CARBON DIOXIDE WITH TAILORED EPOXIDES: FROM TERPENE-BASED MONOMERS TO AMPHIPHILIC POLYMERS AND THERMOPLASTIC ELASTOMERS

DISSERTATION ZUR ERLANGUNG DES GRADES
„DOKTOR DER NATURWISSENSCHAFTEN“
IM PROMOTIONSFACH CHEMIE

AM FACHBEREICH CHEMIE, PHARMAZIE, GEOGRAPHIE UND GEOWISSENSCHAFTEN
DER JOHANNES GUTENBERG-UNIVERSITÄT MAINZ

Christina Gardiner

geboren in Lahnstein

Mainz, Oktober 2021

JOHANNES GUTENBERG UNIVERSITÄT MAINZ

JG|U

Die als Dissertation vorgelegte Arbeit wurde in der Zeit von Oktober 2018 bis November 2021 am Department Chemie der Johannes Gutenberg-Universität Mainz angefertigt.

1.Berichtersatter:

2.Berichterstatter:

Tag der mündlichen Prüfung: 16.12.2021

Hiermit versichere ich gemäß § 10 Abs. 3d der Promotionsordnung vom 24.07.2007:
Ich habe die jetzt als Dissertation vorgelegte Arbeit selbst angefertigt und alle benutzten Hilfsmittel (Literatur, Apparaturen, Material) in der Arbeit angegeben.
Ich habe oder hatte die jetzt als Dissertation vorgelegte Arbeit nicht als Prüfungsarbeit für eine andere staatliche oder andere wissenschaftliche Prüfung eingereicht.
Ich hatte weder die jetzt als Dissertation vorgelegt Arbeit noch Teile davon bei einer anderen Fakultät bzw. einem anderen Fachbereich als Dissertation eingereicht.

Christina Gardiner

Für meine Familie

„It´s okay to fail; it´s not okay to quit"

Chris Gardner, 'The pursuit of happyness'

DANKSAGUNG

COLLABORATIONS

TABLE OF CONTENT

MOTIVATION AND OBJECTIVES

The climate crisis can only be prevented through innovative processes by reducing greenhouse gases in the industry. Carbon dioxide causes the majority of the additional greenhouse effect created by humans.[1–4] One of these innovative processes is the synthesis of polycarbonates from CO_2.[1,5–13] Establishing the synthesis of polycarbonates based on carbon dioxide and epoxides in the industry could aid to face **three major challenges**.[14]

The first major challenge is the **CO_2 emission**.[14] The synthesis of polycarbonates based on CO_2 does not currently result in significant improvements in the carbon footprint, but with further developments and scale-up of production, the CO_2 emissions could be reduced (using directly high-purity CO_2 from combustion power plants).[1] First steps to introduce this method in the industry are already realized such as the application of polyols based on carbon dioxide for different polyurethanes, which are used as mattresses or in the automotive industry.[15]

The second major challenge of the fossil fuel-based plastic industry is the persistence of the produced materials: 8 million metric tons (Mt) of microplastic and 1.5 Mt of primary micro**plastic enter the ocean** annually, most of which based on persistent materials.[16] This could be reduced as polycarbonates are biodegradable.[9,17–19]

The last demanding task of the plastic industry is that mostly all polymers are **based on fossil fuels**.[14,20–22] Since CO_2 is readily available, non-toxic, and sustainable, it is a useful C1 building block and could be used as sustainable monomer in aliphatic polycarbonates.[23]

That mostly all polymers are based on fossil fuels, can additionally be addressed by using terpenes as an alternative of fossil fuel-based monomers.[24–26] Terpenes are non-food and biobased and are available not just through waste products like orange peel or pines, they can also be produced *via* biotechnological processes using simple C1-materials by applying yeast and bacteria.[26,27] In the field of polycarbonates terpene-based limonene oxide (LO) and menth-2-ene oxide (Men2O) are established as epoxide monomers.[28–35] The resulting polycarbonates of these monomers exhibit high T_gs around 120 °C. Current state-of-the art polycarbonates aiming at low T_gs are the often-used poly(propylene carbonate) (T_g: 28°C) and poly(octene carbonate) (POC) (T_g: -24 °C).[36] Additionally, Jia et al. introduced a new polycarbonate from 2-ethylhexyl glycidyl ether with a T_g of -46 °C.[36] Zhang et al. presented a fully biobased aliphatic polycarbonate based on fatty acid with a low T_g of -40 °C.[37] Apart from these polymers no fully aliphatic particularly terpene based polycarbonate structures with a low glass transition below -40 °C have been reported to date. Such structures would be crucial to realize elastomer properties in the typical desired service

temperature range. Citronellol is abundant in lemongrass and roses and is also a monoterpenoid with a long alkyl chain. Reacting citronellol with epichlorohydrin in a phase transfer reaction, citronellol glycidyl ether (CitroGE) can be synthesized.[38] CitroGE can then be used to produce flexible polycarbonates with promise low T_g,,since in the case of polyethers based on CitroGE the long side chain of the polymer may be considered as an additional solvent leading to low T_gs.[38]

In this thesis, we investigate the question of whether it is possible to prepare aliphatic polycarbonates with low T_g (under - 40 °C) using citronellol glycidyl ether and which influence the long alkyl side chain has on the properties of the resulting polycarbonates. *Is it possible to lower the glass transition temperature of the known aliphatic polycarbonates PPC and PCHC? Can PCitroGEC serve as a soft midblock for a thermoplastic ABA elastomer?*

ABA triblock copolymers are not only applicable as thermoplastic elastomers. Using a hydrophilic inner block and hydrophobic outer blocks can lead to hydrogels.[39] Moreover aliphatic polycarbonates are not merely of high interest due to their improved sustainability in various areas, they are also biodegradable and biocompatible. These attributes offer the possibility to use them in several biomedical fields. As a drug delivery system, they were already tested.[40] Moreover, hydrogels based on the ring-opening polymerization of cyclic carbonates like TMC are known.[41,42] The key question was:

Is it feasible to produce a thermoplastic hydrogel based on CO_2?

Thermoplastic hydrogels exhibit the advantage of forming various shapes and therefore constitute valuable materials for customized tissue engineering.[43,44]

The combination of PEG with aliphatic polycarbonates in a block-like manner can not just result in hydrogels. AB diblock copolymers based on PEG and aliphatic polycarbonates can form micelles and other structures in aqueous solution. In the last decade, the properties of mPEG-polycarbonates block copolymers with poly(propylene carbonate) (PPC) or poly(butylene carbonate) (PBC) as the second block was studied.[45–47] Since aliphatic polycarbonates and siloxanes both are known for their high CO_2 affinity, another aspect of this work was the synthesis of mPEG-*b*-PAGEC and subsequent hydrosilylation of the ene moiety. As the hydrophobic polycarbonate is then combined with the hydrophobic siloxane, this material could be an alternative for the persistent fluorinated oligomers, which are currently utilized as surfactants in a CO_2-in water emulsion.[48]

Moreover, anti-bacterial materials gained big attention in the biomedical field. In the case of polycarbonates based on CO_2, the quaternary amino group was introduced in the polycarbonate by thiol-ene clicks or protected amino-based epoxides.[10,49–51]

We wondered whether direct copolymerization of epoxides bearing a quaternary ammonium group with CO_2 is possible to obtain a water-soluble and probably anti-bacterial material.

CO_2-based polycarbonates are the first step to achieving biobased, biodegradable, and more CO_2 neutral polymers, and driving their innovation can support our society towards sustainability.

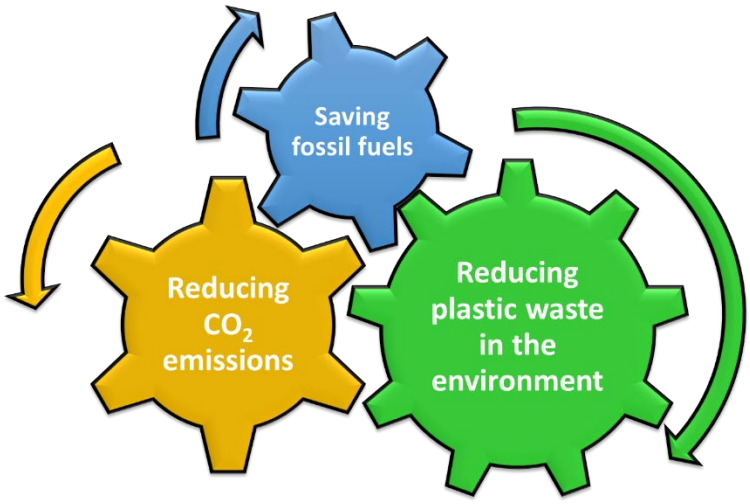

Facing three major challenges in plastic industry: Copolymerizing CO_2 with epoxides

REFERENCES

(1) Hepburn, C.; Adlen, E.; Beddington, J.; Carter, E. A.; Fuss, S.; Mac Dowell, N.; Minx, J. C.; Smith, P.; Williams, C. K. The technological and economic prospects for CO_2 utilization and removal. *Nature* **2019**, *575*, 87–97.

(2) Pinkse, J.; Kolk, A. Challenges and trade-offs in corporate innovation for climate change. *Bus. Strat. Env.* **2010**, n/a-n/a.

(3) Smithers, J.; Blay-Palmer, A. Technology innovation as a strategy for climate adaptation in agriculture. *Appl. Geogr.* **2001**, *21*, 175–197.

(4) Mwanza, B. G.; Mbohwa, C. Major Obstacles to Sustainability in the Plastic Industry. *Procedia Manuf.* **2017**, *8*, 121–128.

(5) Kember, M. R.; Buchard, A.; Williams, C. K. Catalysts for CO_2/epoxide copolymerisation. *Chem. Commun. (Camb)* **2011**, *47*, 141–163.

(6) Darensbourg, D. J.; Yeung, A. D. A concise review of computational studies of the carbon dioxide–epoxide copolymerization reactions. *Polym. Chem.* **2014**, *5*, 3949–3962.

(7) Lu, X.-B.; Darensbourg, D. J. Cobalt catalysts for the coupling of CO_2 and epoxides to provide polycarbonates and cyclic carbonates. *Chem. Soc. Rev.* **2012**, *41*, 1462–1484.

(8) Poland, S. J.; Darensbourg, D. J. A quest for polycarbonates provided via sustainable epoxide/CO_2 copolymerization processes. *Green Chem.* **2017**, *19*, 4990–5011.

(9) Scharfenberg, M.; Hilf, J.; Frey, H. Functional Polycarbonates from Carbon Dioxide and Tailored Epoxide Monomers: Degradable Materials and Their Application Potential. *Adv. Funct. Mater.* **2018**, *28*, 1704302.

(10) Hauenstein, O.; Agarwal, S.; Greiner, A. Bio-based polycarbonate as synthetic toolbox. *Nat. Commun.* **2016**, *7*, 11862.

(11) Zhang, Z.; Pan, S.-Y.; Li, H.; Cai, J.; Olabi, A. G.; Anthony, E. J.; Manovic, V. Recent advances in carbon dioxide utilization. *Renew. Sustain. Energy Rev.* **2020**, *125*, 109799.

(12) Omae, I. Recent developments in carbon dioxide utilization for the production of organic chemicals. *Coord. Chem. Rev.* **2012**, *256*, 1384–1405.

(13) Omae, I. Aspects of carbon dioxide utilization. *Catal. Today* **2006**, *115*, 33–52.

(14) Zheng, J.; Suh, S. Strategies to reduce the global carbon footprint of plastics. *Nat. Clim. Chang.* **2019**, *9*, 374–378.

(15) Turning waste into added value: CO_2 technology. https://solutions.covestro.com/en/highlights/articles/theme/product-technology/turning-waste-into-added-value-co2-technology (accessed October 9, 2021).

(16) Lau, W. W. Y.; Shiran, Y.; Bailey, R. M.; Cook, E.; Stuchtey, M. R.; Koskella, J.; Velis, C. A.; Godfrey, L.; Boucher, J.; Murphy, M. B.*; et al.* Evaluating scenarios toward zero plastic pollution. *Science (New York, N.Y.)* **2020**, *369*, 1455–1461.

(17) Darensbourg, D. J. Comments on the depolymerization of polycarbonates derived from epoxides and carbon dioxide: A mini review. *Polym. Degrad. Stab.* **2018**, *149*, 45–51.

(18) Huang, J.; Worch, J. C.; Dove, A. P.; Coulembier, O. Update and Challenges in Carbon Dioxide-Based Polycarbonate Synthesis. *ChemSusChem* **2020**, *13*, 469–487.

(19) Taherimehr, M.; Al-Amsyar, S. M.; Whiteoak, C. J.; Kleij, A. W.; Pescarmona, P. P. High activity and switchable selectivity in the synthesis of cyclic and polymeric cyclohexene carbonates with iron amino triphenolate catalysts. *Green Chem.* **2013**, *15*, 3083.

(20) Bentley, R. W. Global oil & gas depletion: an overview. *Energy Policy* **2002**, *30*, 189–205.

(21) CO2 and Climate Change. *Science*.

(22) Crowley, T. J.; Berner, R. A. Paleoclimate. CO_2 and climate change. *Science (New York, N.Y.)* **2001**, *292*, 870–872.

(23) Liu, Q.; Wu, L.; Jackstell, R.; Beller, M. Using carbon dioxide as a building block in organic synthesis. *Nat. Commun.* **2015**, *6*, 5933.

(24) Mosquera, M. E. G.; Jiménez, G.; Tabernero, V.; Vinueza-Vaca, J.; García-Estrada, C.; Kosalková, K.; Sola-Landa, A.; Monje, B.; Acosta, C.; Alonso, R.*; et al.* Terpenes and Terpenoids: Building Blocks to Produce Biopolymers. *Sustain. Chem.* **2021**, *2*, 467–492.

(25) Della Monica, F.; Kleij, A. W. From terpenes to sustainable and functional polymers. *Polym. Chem.* **2020**, *11*, 5109–5127.

(26) Rubulotta, G.; Quadrelli, E. A. Terpenes: A Valuable Family of Compounds for the Production of Fine Chemicals. *Horizons in Sustainable Industrial Chemistry and Catalysis*; Studies in Surface Science and Catalysis; Elsevier, 2019; pp 215–229.

(27) Moser, S.; Pichler, H. Identifying and engineering the ideal microbial terpenoid production host. *Appl. Microbiol. Biotechnol.* **2019**, *103*, 5501–5516.

(28) Wambach, A.; Agarwal, S.; Greiner, A. Synthesis of Biobased Polycarbonate by Copolymerization of Menth-2-ene Oxide and CO_2 with Exceptional Thermal Stability. *ACS Sustain. Chem. Eng.* **2020**, *8*, 14690–14693.

(29) Stößer, T.; Li, C.; Unruangsri, J.; Saini, P. K.; Sablong, R. J.; Meier, M. A. R.; Williams, C. K.; Koning, C. Bio-derived polymers for coating applications: comparing poly(limonene carbonate) and poly(cyclohexadiene carbonate). *Polym. Chem.* **2017**, *8*, 6099–6105.

(30) Parrino, F.; Fidalgo, A.; Palmisano, L.; Ilharco, L. M.; Pagliaro, M.; Ciriminna, R. Polymers of Limonene Oxide and Carbon Dioxide: Polycarbonates of the Solar Economy. *ACS Omega* **2018**, *3*, 4884–4890.

(31) Neumann, S.; Leitner, L.-C.; Schmalz, H.; Agarwal, S.; Greiner, A. Unlocking the Processability and Recyclability of Biobased Poly(limonene carbonate). *ACS Sustain. Chem. Eng.* **2020**, *8*, 6442–6448.

(32) Martín, C.; Kleij, A. W. Terpolymers Derived from Limonene Oxide and Carbon Dioxide: Access to Cross-Linked Polycarbonates with Improved Thermal Properties. *Macromolecules* **2016**, *49*, 6285–6295.

(33) Hauenstein, O.; Agarwal, S.; Greiner, A. Bio-based polycarbonate as synthetic toolbox. *Nat. Commun.* **2016**, *7*, 11862.

(34) Byrne, C. M.; Allen, S. D.; Lobkovsky, E. B.; Coates, G. W. Alternating copolymerization of limonene oxide and carbon dioxide. *J. Am. Chem. Soc.* **2004**, *126*, 11404–11405.

(35) Carrodeguas, L. P.; Chen, T. T. D.; Gregory, G. L.; Sulley, G. S.; Williams, C. K. High elasticity, chemically recyclable, thermoplastics from bio-based monomers: carbon dioxide, limonene oxide and ε-decalactone. *Green Chem.* **2020**, *22*, 8298–8307.

(36) Jia, M.; Zhang, D.; Kort, G. W. de; Wilsens, C. H. R. M.; Rastogi, S.; Hadjichristidis, N.; Gnanou, Y.; Feng, X. All-Polycarbonate Thermoplastic Elastomers Based on Triblock Copolymers Derived from Triethylborane-Mediated Sequential Copolymerization of CO_2 with Various Epoxides. *Macromolecules* **2020**, *53*, 5297–5307.

(37) Zhang, Y.-Y.; Zhang, X.-H.; Wei, R.-J.; Du, B.-Y.; Fan, Z.-Q.; Qi, G.-R. Synthesis of fully alternating polycarbonate with low T_g from carbon dioxide and bio-based fatty acid. *RSC Adv* **2014**, *4*, 36183–36188.

(38) Johann, T.; Houck, H. A.; Dinh, T.; Kemmer-Jonas, U.; Du Prez, F. E.; Frey, H. Multi-olefin containing polyethers and triazolinediones: a powerful alliance. *Polym. Chem.* **2019**, *10*, 4699–4708.

(39) Alexandridis, P.; Lindman, B. *Amphiphilic block copolymers: Self-assembly and applications*, 1. ed.; Elsevier: Amsterdam, 2000.

(40) Li, Y.; Liu, S.; Zhao, X.; Wang, Y.; Liu, J.; Wang, X.; Lu, L. CO_2-based amphiphilic polycarbonate micelles enable a reliable and efficient platform for tumor imaging. *Theranostics* **2017**, *7*, 4689–4698.

(41) Sharifi, S.; Blanquer, S. B. G.; van Kooten, T. G.; Grijpma, D. W. Biodegradable nanocomposite hydrogel structures with enhanced mechanical properties prepared by photo-crosslinking solutions of poly(trimethylene carbonate)-poly(ethylene glycol)-poly(trimethylene carbonate) macromonomers and nanoclay particles. *Acta Biomater.* **2012**, *8*, 4233–4243.

(42) Wang, Y.; Xi, L.; Zhang, B.; Zhu, Q.; Su, F.; Jelonek, K.; Orchel, A.; Kasperczyk, J.; Li, S. Bioresorbable hydrogels prepared by photo-initiated crosslinking of diacrylated PTMC-PEG-PTMC triblock copolymers as potential carrier of antitumor drugs. *Saudi Pharm. J.* **2020**, *28*, 290–299.

(43) Brook, M. G. Thermoplastic hydrogels. *Brit. Poly. J.* **1990**, *23*, 257–259.

(44) Chang, H.; Li, C.; Huang, R.; Su, R.; Qi, W.; He, Z. Amphiphilic hydrogels for biomedical applications. *J. Mater. Chem. B* **2019**, *7*, 2899–2910.

(45) Kunze, L.; Tseng, S.-Y.; Schweins, R.; Sottmann, T.; Frey, H. Nonionic Aliphatic Polycarbonate Diblock Copolymers Based on CO_2, 1,2-Butylene Oxide, and mPEG: Synthesis, Micellization, and Solubilization. *Langmuir* **2019**, *35*, 5221–5231.

(46) Scharfenberg, M.; Wald, S.; Wurm, F. R.; Frey, H. Acid-Labile Surfactants Based on Poly(ethylene glycol), Carbon Dioxide and Propylene Oxide: Miniemulsion Polymerization and Degradation Studies. *Polymers* **2017**, *9*, 422.

(47) Hilf, J.; Schulze, P.; Frey, H. CO_2 -Based Non-ionic Surfactants: Solvent-Free Synthesis of Poly(ethylene glycol)- block -Poly(propylene carbonate) Block Copolymers. *Macromol. Chem. Phys.* **2013**, *214*, 2848–2855.

(48) Eastoe, J. Fluorinated surfactants in supercritical CO_2. *Current Opinion in Colloid & Interface Science* **2003**, *8*, 267–273.

(49) Song, P.; Shang, Y.; Chong, S.; Zhu, X.; Xu, H.; Xiong, Y. Synthesis and characterization of amino-functionalized poly(propylene carbonate). *RSC Adv.* **2015**, *5*, 32092–32095.

(50) Tong, Y.; Cheng, R.; Yu, L.; Liu, B. New strategies for synthesis of amino-functionalized poly(propylene carbonate) over SalenCo (III) Cl catalyst. *J. Polym. Sci.* **2020**, *58*, 1325–1337.

(51) Seong, J. E.; Na, S. J.; Cyriac, A.; Kim, B.-W.; Lee, B. Y. Terpolymerizations of CO_2 , Propylene Oxide, and Various Epoxides Using a Cobalt(III) Complex of Salen-Type Ligand Tethered by Four Quaternary Ammonium Salts. *Macromolecules* **2010**, *43*, 903–908.

ABSTRACT

Sustainability is becoming an increasingly important topic in our society, and the goal of a "circular economy" is also gaining more attention in the plastics industry. A significant aspect is the use of biodegradable plastics and renewable materials. This thesis focuses on biodegradable, CO_2-based polycarbonates based on renewable biobased materials such as terpenes. The biodegradability of polycarbonates, for example, offers the opportunity to establish novel non-ionic surfactants. Polycarbonates not only exhibit biodegradability but also possess exceptional biocompatibility. These attributes make them excellent potential materials for the biomedical field. Due to this the other target of this work is the development of polycarbonates in the biomedical field in the direction of hydrogels and water-soluble bactericides.

Chapter 1 briefly and concisely exemplifies the development in the field of polycarbonates based on CO_2 as a building block of polymer materials with increasingly complex structures. This chapter highlights the theoretical background of the synthesis of polycarbonates from CO_2: Addressing the corresponding mechanisms and the known catalysts as well as the used epoxide monomers. Moreover, **Chapter 1** illustrates an overview of different functional and biobased epoxides used in polycarbonate synthesis by focusing on terpene-based epoxides. Furthermore, it discusses the synthesis of amphiphilic structures based on CO_2 and epoxides in detail presenting two different synthesis routes: The synthesis by using PEG as macroinitiator and the synthesis of amphiphilic structures via post-modification reactions. **Chapter 1** includes in addition to the behavior of block copolymers in aqueous solution the behavior in the solid-state ("bulk"). Therefore the "Flory-Huggins theory" is explained and the phase diagram of di- and triblocks examined. An overview of CO_2-based TPEs closes the Chapter.

Chapter 2.1 introduces poly citronellol glycidyl ether carbonate (PCitroGEC) homopolymer acquired from citronellol. Citronellol is a monoterpene, which derives from roses and lemongrass. PCitroGEC is produced by using citronellol glycidyl ether and CO_2 through a catalytic reaction using a Co(Salen) catalyst system. The resulting polycarbonates are not only biobased and biodegradable but also have an exceptionally low glass transition temperature (T_g) of -55°C. Furthermore, the side chain of citronellol has a vinyl group. This group provides post-modification reactions such as TAD-click reactions. Using a bifunctional TAD-click reagent, a crosslinked gel was prepared from the PCitroGEC homopolymer in seconds.

In **Chapter 2.2**, the low T_g of PCitroGEC is employed to vary the T_g of common polycarbonates such as poly(propylene carbonate) (PPC) and poly(cyclohexene carbonate) (PCHC). In addition, this

chapter investigates the microstructure of CHO/CitroGE/CO_2 and PO/CitroGE/CO_2 copolymers. The Jaacks model was applied to identify the r-ratios determining statistical incorporation for the CHO/CitroGE/CO_2 copolymerization at 60°C and the PO/CitroGE/CO_2 copolymerizations at 20°C. However, for the CHO/CitroGE/CO_2 copolymerization at 30°C, a gradient structure was evident. The low T_g of PCitroGEC is not only advantageous in setting T_gs in copolymers. This low T_g is also beneficial for thermoplastic elastomer (TPE).

Chapter 3 illuminates the synthesis of several PLA-*b*-PCitroGEC-*b*-PLA triblocks. These triblocks exhibit two T_gs suggesting microphase segregation. These polymers expand elastically up to 400% with little permanent deformation and are fully biodegradable and biobased due to their polyester-polycarbonate structure. Combining good material properties such as elasticity and processability with biodegradability and organic derivation are fundamental requirements for new materials that take environmental considerations into account.

In addition to biodegradability, polycarbonates also have excellent biocompatibility. Moreover, degradation does not yield in acids as a degradation product, unlike the polyesters currently used in biomedicine. These properties qualify aliphatic polycarbonates as promising materials for use in the biomedical field.

Chapter 4 presents the application of CO_2-based aliphatic polycarbonates as hydrogels. In a straightforward "one-pot" synthesis, PCHC-*b*-PEG-*b*-PCHC triblock copolymers with molar masses between 16 000 to 25 000 g/mol were synthesized. Investigating the equilibrium swelling in aqueous solution and mechanical properties of the polymer's exceptional toughness up to 70 MN/mm^2 in the dry state and 43 MN/mm^2 in the water-swollen state (at a water absorption of 81 %) were determined. The triblocks were extended to multiblocks by using diisocyanates and the multiblocks showed even higher toughness due to their higher molar masses and the additional domain bridges. Lastly, processability by extruder was studied. The use of amino acids as additives minimizes the degradation of the polymer during extrusion. The equilibrium swelling in aqueous solution, toughness, and processability, as well as the biocompatibility and partial biodegradability of the material, qualify it as a suitable candidate for biomedical applications possibly in “tissue engineering”. Water-soluble bactericidal polymers are additionally of interest in the biomedical field. These often consist of polymers with charged side chains.

Chapter 5 displays a direct synthesis route with charged amino side chains resulting in aliphatic polycarbonates. The aim of this work was thus to avoid post modification reactions and to present an easy synthetic route. Due to the charged side chain, the determination of the molar masses

was challenging and not successful. However, water solubility and degradability in acid-aqueous environments were demonstrated.

Chapter 6 also examines water-soluble polycarbonates. The surfactants commonly used for CO_2-H_2O mixtures are fluorinated ones. Since both polycarbonates and siloxanes are "CO2-philic," combining the two in an amphiphilic polymer appeared to be a viable alternative for the fluorinated, persistent surfactants. Self-prepared mPEG-*b*-PAGEC diblock copolymers were hydrosilylated and the water-soluble diblocks were used as surfactants in a CO_2-H_2O emulsion. Shish-Yu Tseng and Prof. Thomas Sottmann (Universität Stuttgart) investigated the phase behavior of the diblocks in water/n-decane containing sodium chloride and in water/supercritical CO_2 ($scCO_2$). In the water/n-decane mixture, they showed good performance as surfactants. In the scCO2/water mixture, they did not achieve the effect of the fluorinated established surfactants but still showed activity, making them a potentially promising alternative.

Appendix **Chapter A1** also addresses the issue of surfactants. In this project, the interdisciplinary cooperation with the Sottmann group results in the investigation of the enhancement of efficiency by polymer-based surfactants of established surfactants in an oil-water emulsion. For this purpose, mPEG-*b*-PAlkGE (with long alkyl side chain) diblocks were produced via anionic polymerization and, for comparison, also mPEG-*b*-PAlkGEC (the CO_2-based analogs) via catalytic synthesis. Since anionic polymerization does not tolerate impurities, technical (commercially available, 90 % pure) long-chain alkyl glycidyl ethers could be used only for polycarbonates. Both the polymers based on technical alkyl glycidyl ether and polymers from self-produced and purified alkyl glycidyl ethers showed a sharp increase in efficiency when replacing only small amounts of the commonly used surfactant in the oil-water emulsion. A reduced surfactant requirement due to these "boosters" has significant positive economic and environmental impacts and is therefore relevant for the industry.

ZUSAMMENFASSUNG

Nachhaltigkeit wird in unserer Gesellschaft zunehmend thematisiert, und auch in der Kunststoffindustrie erlangt das Ziel einer „circular economy“ immer mehr Bedeutung. Eine wichtige Rolle spielt die Verwendung von biologisch abbaubaren Kunststoffen und nachwachsenden Rohstoffen. Diese Arbeit fokussiert sich auf die Synthese von biologisch abbaubaren, CO_2-basierten Polycarbonaten mit Schwerpunkt auf erneuerbare Rohstoffe wie Terpene. Die biologische Abbaubarkeit bietet beispielsweise die Chance zur Etablierung neuartiger nicht-ionischer Tenside. Polycarbonate sind jedoch nicht nur biologisch abbaubar, sondern weisen auch eine ausgezeichnete Biokompatibilität auf. Diese Eigenschaften machen sie zu hervorragenden potenziellen Materialien für den biomedizinischen Bereich. Aus diesem Grund liegt der zweite Schwerpunkt dieser Arbeit auf der Entwicklung von Polycarbonaten im biomedizinischen Bereich in Richtung Hydrogele und wasserlösliche Bakterizide.

Kapitel 1 veranschaulicht kurz und prägnant die Entwicklung im Gebiet von Polycarbonaten basierend auf CO_2 als Baustein von Polymermaterialien mit zunehmend komplexer Struktur. Es beleuchtet den theoretischen Hintergrund der Synthese von Polycarbonaten aus CO_2, sowohl die entsprechenden Mechanismen als auch die bekannten Katalysatoren und die eingesetzten Epoxid-Monomere werden thematisiert. Ein Überblick zu verschiedenen funktionellen und auch biobasierten Epoxiden, die in der Polycarbonatsynthese verwendet werden, wird gegeben. Es wird ein Schwerpunkt auf terpenbasierte Epoxide gelegt. Ferner wird ausführlich auf die Synthese amphiphiler Strukturen basierend auf CO_2 und Epoxiden eingegangen. Es werden zwei verschiedene Syntheserouten dargestellt: die Synthese durch Verwendung von PEG als Makroinitiator und die Synthese von amphiphilen Strukturen über polymeranaloge Reaktionen. Nicht nur das Verhalten von Blockcopolymeren in wässrigem Milieu wird näher beleuchtet, auch die Nanophasensegregation im festen Zustand („bulk“) wird detailliert beschrieben. Dabei wird die „Flory-Huggins-Theorie“ erläutert und das Phasendiagramm von Di- und Triblöcken erörtert. Danach wird ein Überblick zu CO_2-basierten TPEs präsentiert.

In **Kapitel 2.1 wird** Polycitronellolglycidylethercarbonat (PCitroGEC) als Homopolymer vorgestellt. Dieses basiert auf Citronellol, welches ein Monoterpen ist, das aus Rosen und Zitronengras gewonnen werden kann. PCitroGEC wird mittels Citronellolglycidylether und CO_2 durch eine katalytische Reaktion mithilfe eines Co(Salen) Katalysatorsystems hergestellt. Die entstandenen Polycarbonate sind nicht nur biobasiert und bioabbaubar, sondern haben auch noch eine

außergewöhnlich niedrige Glasübergangstemperatur (T_g) von -55 °C. Ferner besitzt die Seitenkette des Citronellols eine Vinyl-Gruppe. Diese eröffnet die Möglichkeit vieler weiterer polymeranaloger Reaktionen, beispielsweise durch die TAD-Click Reaktion. Mittels eines bifunktionellen TAD-click Reagenz quervernetzte das in THF gelöste PCitroGEC zu einem Organogel in Sekunden.

In **Kapitel 2.2** wird der niedrige T_g des PCitroGEC genutzt, um den T_g von konventionellen Polycarbonaten wie Polypropylencarbonat (PPC) und Polycyclohexencarbonat (PCHC) durch Copolymerisation zu variieren. Außerdem wurde die Mikrostruktur der CHO/CitroGE/CO_2 und PO/CitroGE/CO_2 Copolymere untersucht. Das Jaacks-Modell wurde zu Identifizierung der *r*-Parameter verwendet. Für die CHO/CitroGE/CO_2 Copolymerisation bei 60 °C und die PO/CitroGE/CO_2 Copolymerisationen bei 20°C konnte ein statistisches Einbauverhalten bestimmt werden. Bei der Copolymerisation von CHO/CitroGE/CO_2 bei 30 °C war jedoch eine Gradientenstruktur ersichtlich. Der niedrige T_g von PCitroGEC ist nicht nur bei der Einstellung von T_gs in Copolymeren von Vorteil. Dieser kann auch als „weicher", d.h. flexibler Mittelblock in einem thermoplastischen Elastomer (TPE) dienen.

In **Kapitel 3** wurden mehrere PLLA-*b*-PCitroGEC-*b*-PLLA Triblöcke hergestellt. Diese zeigten zwei T_gs, was eine Mikrophasenseperation nahelegt. Diese Triblöcke konnten in der Zugdehnung bis zu 400 % elastisch gedehnt werden, wobei nur eine geringe permanente Deformation beobachtet wurde. Die Materialien sind aufgrund ihrer Polyester-Polycarbonatstruktur sowohl bioabbaubar als auch biobasiert. Die Kombination guter Materialeigenschaften wie Elastizität und Verformbarkeit mit Bioabbaubarkeit und biologischem Ursprung sind grundlegende Voraussetzungen für neue Materialien, die Umweltgesichtspunkte berücksichtigen.

Polycarbonate besitzen neben der biologischen Abbaubarkeit auch noch eine ausgezeichnete Biokomptabilität. Außerdem liefert der Abbau keine Säuren als Abbauprodukt im Gegensatz zu den zurzeit verwendet Polyestern in der Biomedizin. Diese Eigenschaften qualifizieren aliphatische Polycarbonate als vielversprechende Materialien für die Verwendung im biomedizinischen Bereich.

Kapitel 4 stellt den Einsatz von aliphatischen Polycarbonaten auf CO_2-Basis für Hydrogele vor. In einer simplen „one-pot" Synthese wurden PCHC-*b*-PEG-*b*-PCHC Triblockcopolymere im Molekulargewichtsbereich von 16 000 bis 25 000 g/mol dargestellt. Die Polymere wurden hinsichtlich ihrer Wasseraufnahme und ihrer mechanischen Eigenschaft untersucht. Diese zeigten eine außergewöhnliche Zähigkeit von bis zu 70 MN/mm^2 im trockenen und 43 MN/mm^2 im Wasser-gequollenen Zustand (bei einer Wasseraufnahme von 81 %). Die Triblöcke wurden durch

Verwendung von Diisocyanaten zu Multiblöcken aufgebaut und wiesen durch die höheren molaren Massen und die zusätzlichen Domänenverbrückungen dann eine noch höhere Zähigkeit auf. Zuletzt wurde auch die Verarbeitbarkeit mittels Extruder untersucht. Durch Verwendung von Aminosäuren als Additiv konnte ein Abbau des Polymers bei der thermischen Verarbeitung minimiert werden. Die Wasseraufnahme, Zähigkeit und Verarbeitbarkeit, sowie die Biokompatibilität und partielle Bioabbaubarkeit des Materials macht es zu einem geeigneten Kandidaten für die Biomedizin, möglicherweise im „Tissue Engineering“. Wasserlösliche bakterizide Polymere können auch im biomedizinischen Bereich Anwendung finden. Diese bestehen meist aus Polymeren mit geladenen Seitenketten.

In **Kapitel 5** werden direkt aus Epoxiden mit geladener Aminoseitenkette über eine katalytische Reaktion mit CO_2 aliphatische Polycarbonate dargestellt. Ziel dieser Arbeit war es somit polymeranaloge Reaktionen zu vermeiden und eine einfache Syntheseroute einzuführen. Aufgrund der geladenen Seitenkette war die Bestimmung der molaren Massen herausfordernd und bis zum Schluss nicht erfolgreich. Jedoch konnte die Wasserlöslichkeit und Abbaubarkeit in saurem wässrigem Milieu nachgewiesen werden.

Kapitel 6 befasst sich auch mit wasserlöslichen Polycarbonaten. Die gängigen Tenside für CO_2-H_2O Gemische sind fluorbasiert. Da sowohl Polycarbonate als auch Siloxane „CO_2-phil“ sind, erschien die Kombination beider in einer amphiphilen Polymerstruktur als eine mögliche Alternative für die fluorbasierten, wegen ihrer hohen Persistenz in der Umwelt schädlichen Tenside. Selbst hergestellte mPEG-*b*-PAGEC Diblockcopolymere wurden hydrosilyliert und die wasserlöslichen Diblöcke wurden als Tenside in einer CO_2-H_2O Emulsion verwendet. Shish-Yu Tseng und Prof. Thomas Sottmann (Universität Stuttgart) untersuchten das Phasenverhalten der Diblöcke in Natriumchlorid-haltigem Wasser/n-Decan und in Wasser/superkritischem CO_2 ($scCO_2$). Im Wasser/n-Decan Gemisch zeigten sie eine gute Wirkung als Tensid. Im $scCO_2$/Wasser Gemisch erzielten sie nicht die Wirkung der fluorbasierten etablierten Tenside, wiesen aber dennoch eine Aktivität auf, was sie zu einer potenziell interessanten Alternative macht.

Im **Appendixkapitel A1** wird ebenfalls die Thematik der Tenside aufgegriffen. In diesem Projekt wurde interdisziplinär mit der Gruppe Sottmann kooperiert, um die Verstärkung der Effizienz etablierter Tenside in einer Öl-Wasser-Emulsion durch polymerbasierte Tenside zu untersuchen. Hierfür wurden mPEG-*b*-PAlkGE (mit langer Alkylseitenkette) Diblöcke über eine anionische Polymerisation und zum Vergleich auch mPEG-*b*-PAlkGEC (die CO_2 basierten Analoga) mittels katalytischer Synthese dargestellt. Da die anionische Polymerisation keine Verunreinigung

toleriert, konnten nur im Hinblick auf die Polycarbonate technische (kommerziell erwerbbar, 90 % rein) langkettige Alkylglycidylether verwendet werden. Sowohl die Polymere aus technischen Alkylgylcidylether als auch Polymere aus selbst hergestellten und aufgereinigten Alkylglycidylethern zeigten eine starke Effizienzsteigerung bei einem Austausch von nur geringen Mengen des üblich verwendeten Tensids in der Öl-Wasser Emulsion. Ein reduzierter Tensidbedarf durch diese „Booster“ hat erhebliche positive wirtschaftliche und ökologische Auswirkungen und ist auch somit für die industrielle Anwendung relevant.

Graphical Abstract

CHAPTER 2.1: Addressing a Key Challenge of CO_2-Based Polycarbonates: Low Glass Transition Capitalizing on Citronellol Glycidvl Ether

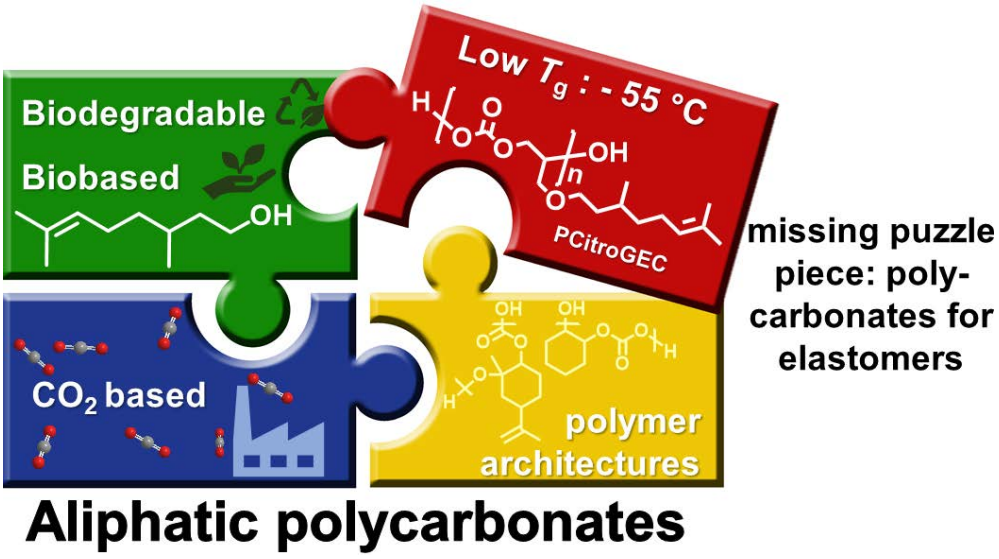

CHAPTER 2.2: Tailoring the Glass Transition Temperatures of the Established Aliphatic Polycarbonates PPC and PCHC Using Biobased Citronellol Glycidyl Ether: Kinetic Studies And Post-Modification

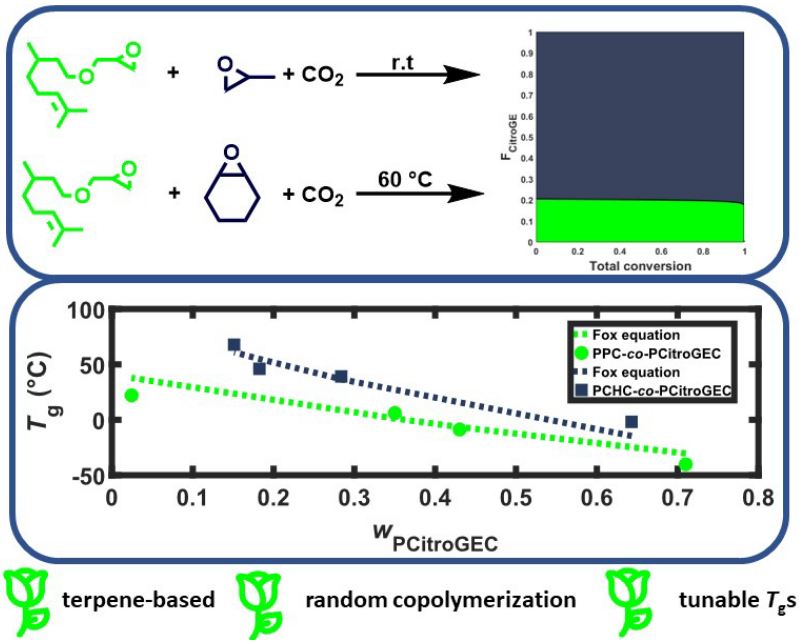

CHAPTER 3: Biobased Thermoplastic Elastomers Based on Citronellol Glycidyl Ether, CO_2 and Polylactide

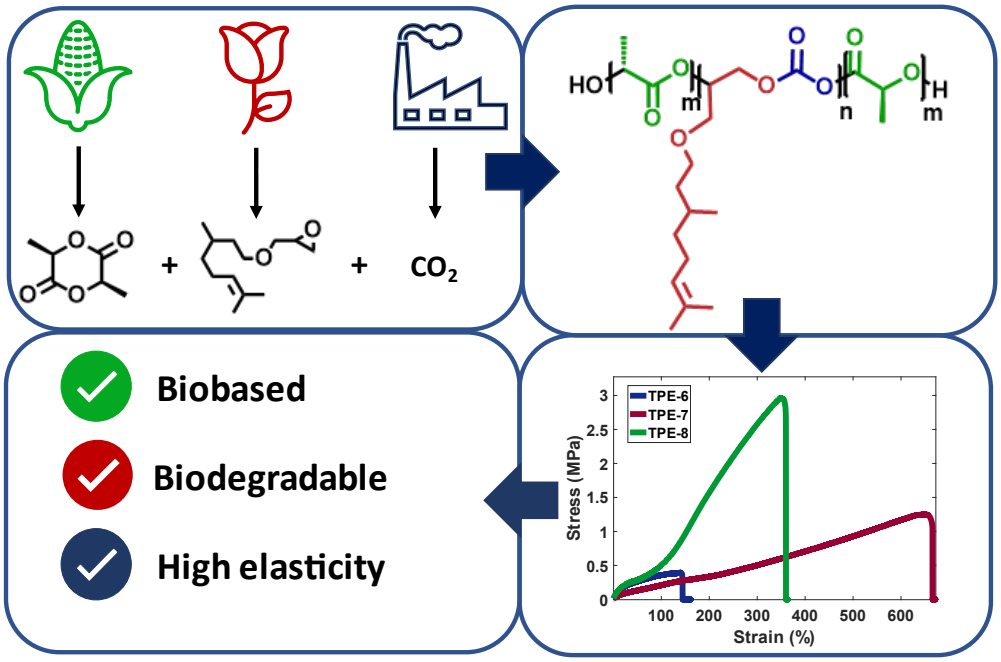

CHAPTER 4: Tough Hydrogels Based on Poly(ethylene oxide), Carbon Dioxide and Cyclohexene Oxide: Improvement of the Toughness via Polyurethane Multiblock Synthesis

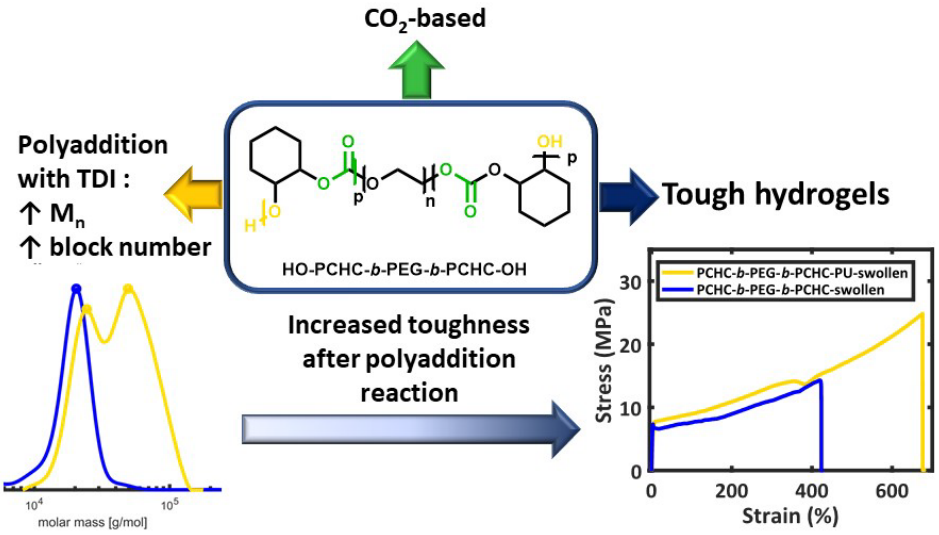

CHAPTER 5: Direct Synthesis of Cationic Polycarbonates from CO_2 and Methylated Glycidyl Amines

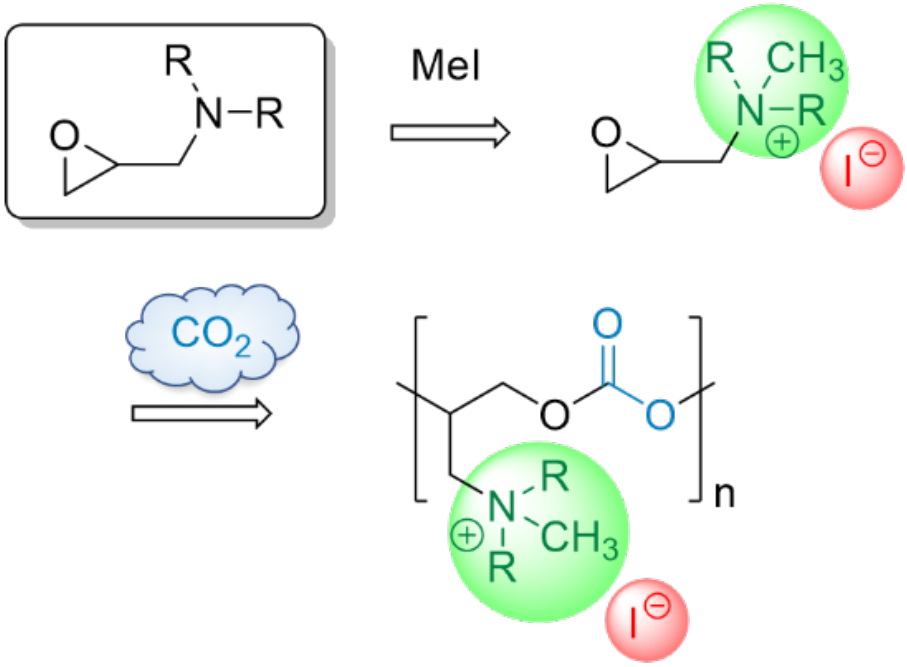

CHAPTER 6: Siloxane Functionalized Polyether-Polycarbonates with Amphiphilic Properties: A New Class of Surfactants

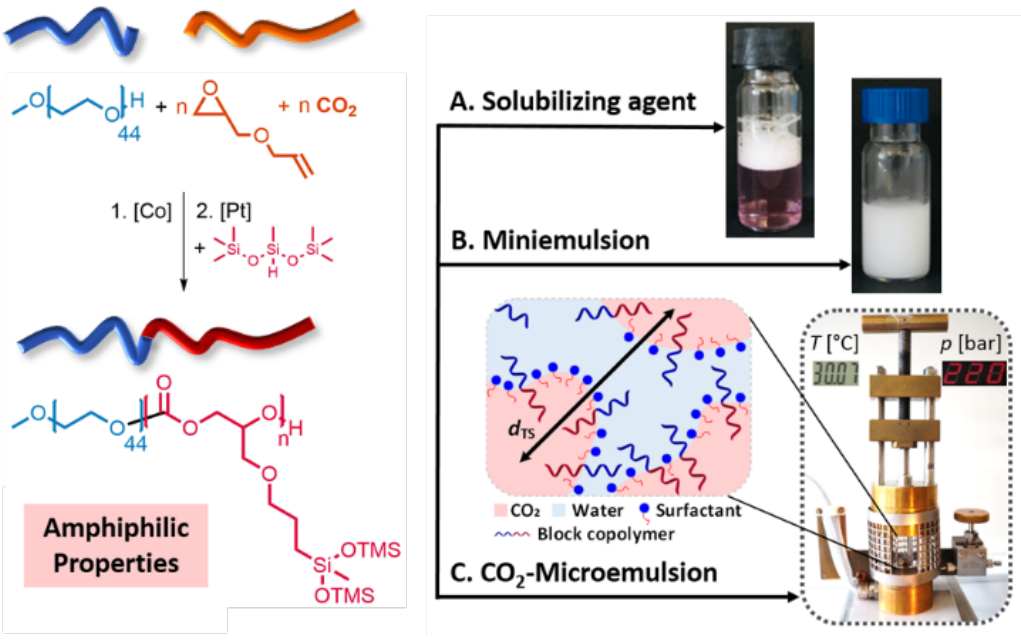

CHAPTER A1: Efficiency Boosting of Surfactants with Poly(ethylene oxide)-Poly(alkyl glycidyl ether)s – A New Class of Amphiphilic Polymers

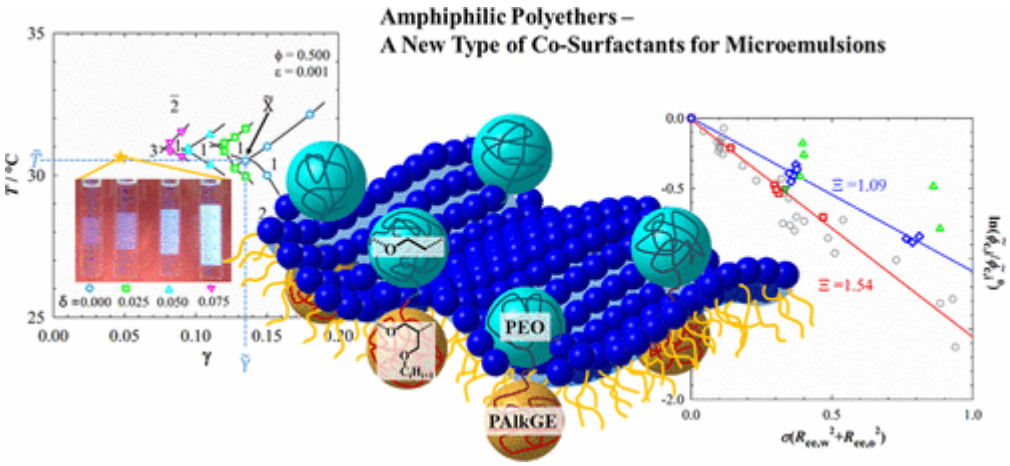

CHAPTER 1

Aliphatic Polycarbonates Based on CO_2: Tailoring Degradable Polymer Architectures.

CHAPTER 1

Aliphatic Polycarbonates Based on CO_2: Tailoring Degradable Polymer Architectures.

Christina Gardiner[a], Holger Frey[a*]

[a]Department of Chemistry, Johannes Gutenberg University, Duesbergweg 10-14, 55128 Mainz, Germany

ABSTRACT

Since 1969, when Inoue et al. introduced the copolymerization of CO_2 with epoxides resulting in an aliphatic polycarbonate, the interest in this topic has steadily increased. Initially, the focus was on the development of new catalyst systems, but in the last decade, the attention changed toward synthesizing new materials with well-defined polymer architectures based on the copolymerization of CO_2 and epoxides. This chapter focuses on the development towards value-added materials. First, we provided a short introduction to the mechanism and the theoretical background of "immortal polymerization". Moreover, we discussed the benefits and disadvantages of various frequently used epoxides, applying catalytic copolymerization with CO_2, and examined their use in different polymer structures. The centerpiece of this chapter is the application of amphiphilic block copolymers and thermoplastic elastomers based on CO_2.

INTRODUCTION

As carbon dioxide (CO_2) is a cheap, abundant, and potentially sustainable carbonyl resource, its utilization to generate value-added chemicals and polymeric materials has attracted much interest.[1,2] Carbon dioxide/epoxide copolymerization is an efficient way to use CO_2 as a C1 source in polymer manufacturing.[2,3] The use of this process to produce low-molecular-weight polycarbonate polyols is a commercially relevant route to new thermosets and polyurethanes. Covestro already uses polyols based on carbon dioxide as a starting material for polyurethane foams to design partly environment-friendly mattresses. Moreover, they generate new materials based on CO_2 for upholstered furniture and car interiors up to special adhesives for sports flooring underlays. Also, thermoplastic polyurethane (TPU) solutions are available for use in shoes, industrial tubing, and textile fibers, which are on the edge of market development.[4] All these materials show an aliphatic polycarbonate structure since they are generated from epoxides and CO_2.

Polycarbonates exhibit a -O-CO-O- repeating unit in the polymer backbone. Aliphatic polycarbonates (APCs) can be prepared via different routes. First, polycarbonates can be prepared via polycondensation reaction of dialkyl carbonates (i), second via the ring-opening polymerization (ii) of cyclic carbonates, and lastly through the copolymerization of carbon dioxide with epoxides (iii) (Scheme 1).[5]

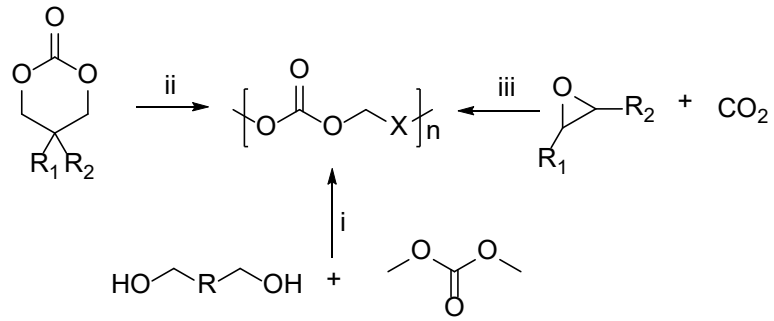

Scheme 1: Different synthesis routes to form aliphatic polycarbonates. X illustrates the variation of various alkyl groups. i) polycondensation of aliphatic polyols with dialkyl carbonates. ii) ROP of cyclic carbonates. iii) copolymerization of CO_2 with epoxides. Adopted from Scharfenberg et al.[5]

Since polycondensation reactions have the drawback of a low molar mass and high dispersity, and the ring-opening polymerization requires multi-step synthesis of the monomer to vary the sidechains, the copolymerization of CO_2 with epoxides is a valuable alternative.[5–9] A significant number of epoxides are already established in industry; a variety of other epoxides are available from natural product sources and usually require one-step synthesis.[5,10–13] In the next few sections, the copolymerization of epoxide with CO_2 will be discussed in more detail.

COPOLYMERIZATION OF CARBON DIOXIDE WITH EPOXIDES

In 1969, the first successful copolymerization of carbon dioxide with propylene oxide (PO) was carried out by Inoue et al.[14] In recent years it has become a promising method to obtain functional APCs directly from functionalized monomers since a large number of epoxide derivatives already exist and can be prepared in a few synthesis steps.[5]

Carbon dioxide

CO_2 is an advantageous C1 building block for the synthesis of macromolecules because of its non-existent flammability and toxicity.[1,15] However, it is also thermodynamically stable because the central carbon atom is in its highest oxidation state (+IV) and thus has a low energy level.[2,16] Although the molecule itself is nonpolar due to its linear arrangement, the respective orthogonal π-bonds between the oxygen atoms and the carbon atom are polar. This results in an electrophilic center that can be attacked in a nucleophilic manner and thus offers a possibility to chemically convert the inert molecule.[17] Catalysts are required, among other things, to reduce the high activation energy of CO_2 so that copolymerization with epoxides can take place.[18]

Mechanism: coordinative ring-opening polymerization

The ring-opening copolymerization of CO_2 with epoxides offers an attractive route to gain access to polycarbonates.[19] The driving force of the process is based on the cleavage of the C-O bond. Epoxides possess an E_t-value of 27.2 kcal/mol and are reactive enough to take part in copolymerization with CO_2.[20] Metal-based catalysts are desirable due to their adaptable oxidation-stated, bonding modes (e.g. variability of coordination number and capacity to form both σ and π bonds) and tunability of the ligands to regulate activity or selectivity.[1]

The catalytic systems that are used to copolymerize epoxides with carbon dioxide to aliphatic polycarbonates mostly consist of a Lewis base acting as a nucleophile with a Lewis acid species in form of a metal center (Scheme 2).[18,21–23] First, the epoxide is activated by the Metal (**1**).

Epoxides are generally weak ligands because the coordinating metal-oxygen bond is based on the transfer of electrons from one of the oxygens' free electron pairs. However, since the s-character of these electrons is relatively high, less electron density is donated overall, leading to a weak bond. Since the epoxide is in excess relative to the initiator, ligand substitution occurs statistically.[18] The free nucleophile, either the initiator or, after the first propagation cycle, the negatively charged chain end of a growing polymer, can now initiate the ring-opening of the epoxide activated by the preceding coordination (**2**). The bond between the resulting alkoxide (**2**) and the metal is stronger than that of the other ligands, which is why substitution does normally

not occur here. Otherwise, insertion of another epoxide molecule would occur directly, resulting in an unintended ether bond. Instead, the CO_2 molecule is inserted (**3**). For this, no preceding coordination of the carbon dioxide to the coordinatively saturated metal center is necessary.[24]

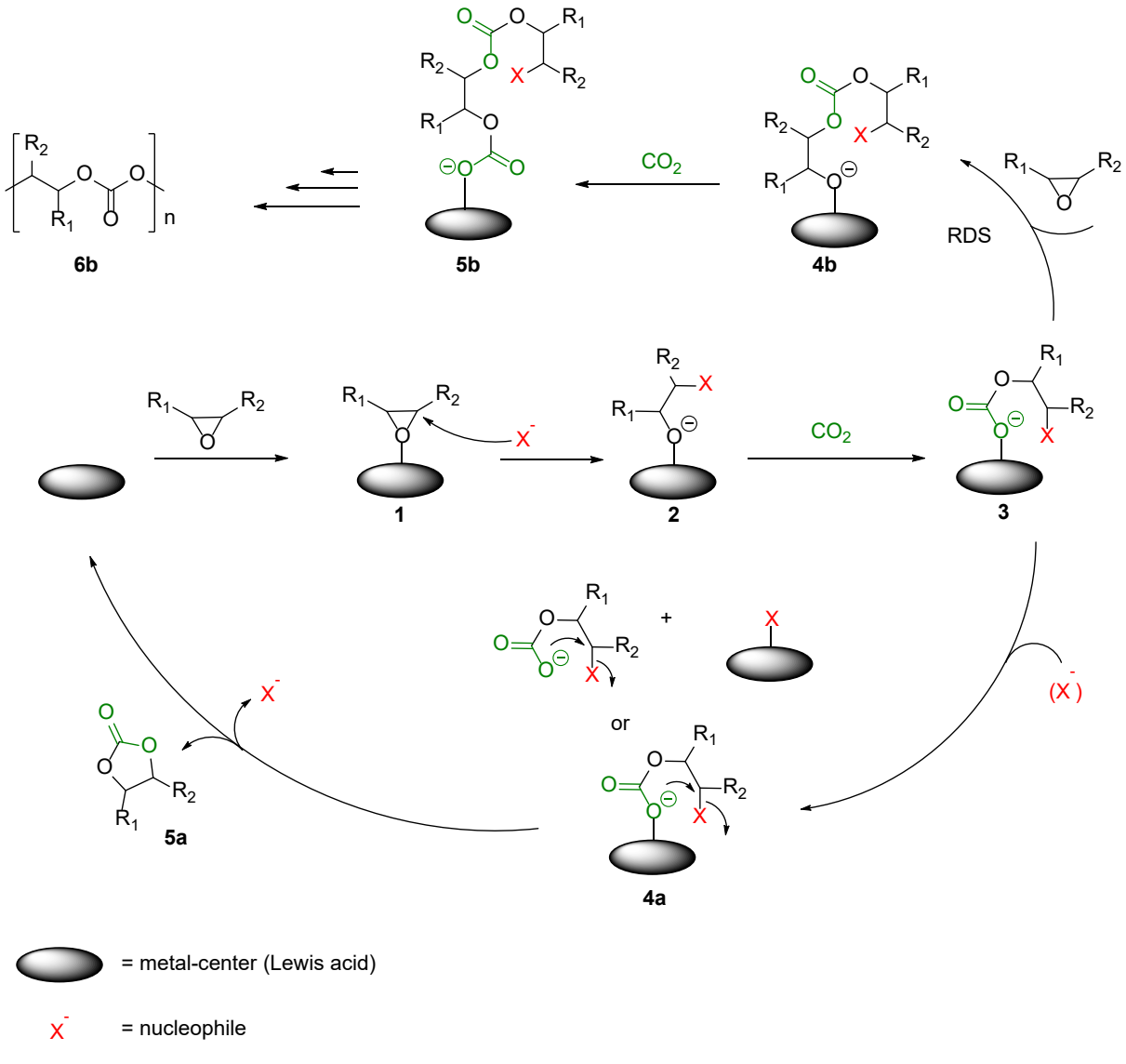

Scheme 2: Catalytic cycle for the copolymerization of epoxides and carbon dioxide using a Co(salen) catalyst system. In the case of the zinc catalyst system, the assumed mechanism is different.[18,21]

The speed of insertion is much more related to the nucleophilicity of the oxygen atom of the alkoxide and the steric availability of its free electron pairs than to the carbon atom of CO_2, which is a weak electrophile.[25] The resulting carbonate formed from the alkoxide is coordinated weakly to the metal (**3**), allowing it to be easily substituted by a new epoxide monomer and itself become the new nucleophile that attacks the newly coordinated epoxide (**4b**). The described ligand

exchange is the rate-determining step (RDS) of the polymerization. An alternating insertion of more epoxides and CO_2 molecules (**5b**) leads to polycarbonates (**6b**).

A side reaction besides the formation of ether linkages is the creation of cyclic carbonates (**5a**), which can emerge from the free carbonate chain ends (**4a**). The undesired degradation reaction, the backbiting, is thermodynamically preferred and thus more probable with increasing reaction time and temperature.[18] The properties of the metal at the center of the catalyst are very important for the mechanism to proceed correctly. For example, the metal should be electrophilic enough to activate the epoxide for ring-opening, but at the same time sufficiently nucleophilic for insertion of the very weakly electrophilic CO_2. In addition, the metal must be substitutionally inert to some degree so that the growing polymer chain does not dissociate too rapidly, thereby promoting the formation of cyclic carbonates.[26] Therefore, the salen complexes with Cr(III) and Co(III) are the most suitable, since both do not occupy antibonding d-orbitals, and the bonds to the ligands are not additionally weakened.[26]

Another aspect of the mechanism is the direction of the nucleophilic attack of the epoxide. Ring-opening of the epoxide can occur via various pathways according to the nature of the terminal groups. Electron donating or electron-withdrawing side groups affect the nucleophilic attack of the 3-membered cyclic monomer. An electron-donating methyl group of propylene oxide (PO) is preferably attacked at the carbon without a side group.[27] On the other hand epoxides with electron-withdrawing groups such as an aromatic phenyl will be attacked at the substituted carbon (Scheme 3).[28] It is important to note that such cleavages can occur simultaneously during a polymerization process. This leads to the production of regio-irregular architectures.[1,27]

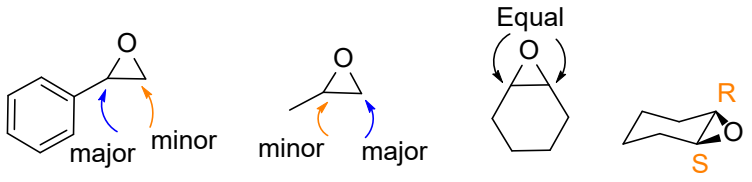

Scheme 3: Regioselectivity of the nucleophilic attack of epoxides with different substitutes.[22,28]

"Immortal polymerization" is the polymerization that provides polymers with a narrow molecular distribution, even in the occurrence of a chain transfer reaction, because of its reversibility, which leads to the regeneration of the polymers once dormant, that is, the immortal character of the polymers. As a result, immortal polymerization can afford polymers with controlled molecular weight.[29] In 1985, Inoue established this term for the copolymerization of CO_2 with epoxides in the presence of a chain transfer agent (CTA).[30] In this process, low polydispersity is achieved by chain transfer and thus has similarities to controlled radical polymerization. The addition of a

protic substance can lead to reversible deactivation of one polymer chain, as shown in Scheme 4, while the next one can be started. However, this dormant chain can again be reactivated, so that dormant and active polymers are in equilibrium. As a result, all chains grow at approximately similar rates. This phenomenon can also be observed in the copolymerization of CO_2 and epoxides.[31,32] Thus, water as a protic substance can also lead to such distributions. As commercially available pure carbon dioxide contains still small amounts of water, a bimodal distribution of polycarbonates is often detected. This can be circumvented by either extra drying of the carbon dioxide or using a catalyst system without an additional initiator. [33,34]

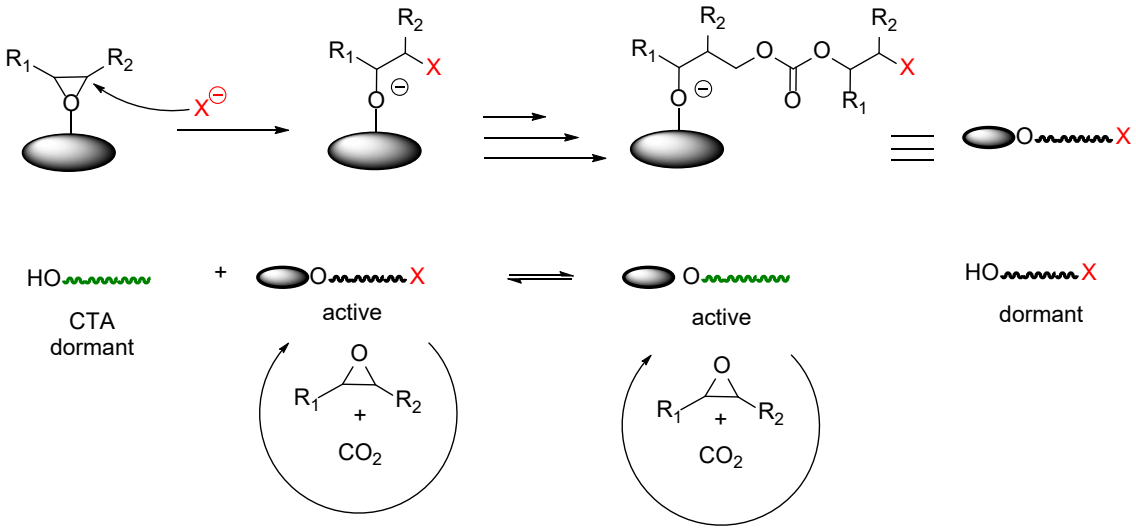

Scheme 4: "Immortal polymerization" via chain transfer reactions.[32]

Through "immortal polymerization", different structures of the polymers are accessible. Block copolymers can be formed using mono- and di-functional PEG/PS/PMMA homopolymers. Moreover, graft polymers can be synthesized using polymers with hydroxy functionalized sidechains.[31,32]

Catalyst

In recent years a variety of catalyst systems were developed to copolymerize CO_2 with epoxides. Heterogenic and homogenous catalyst systems were established with different characteristics.[28,35–41] A key objective of catalyst development was the generation of high molar masses and high content of carbonate linkages.[35,38,40,41] The homogenous Co-Salen catalyst system is known for a perfectly alternating insertion of carbon dioxide and epoxides leading to polycarbonates with more than 98% carbonate linkages (Figure 1).[42,43] Moreover, they exhibit remarkable regioselectivity for ring-opening of the epoxides, a high turnover frequency, and a wide scope of applications for different functionalized epoxides.[37,42–44] The disadvantage of the catalyst system is, that a Lewis base is required for the systems (like [PPN]Cl) (Figure 1), and

therefore an additional initiator Cl^- is then present, leading to lower molar masses and bifunctional distributions, since small amounts of water are still present in commercially available CO_2.[33,37] Moreover they are a huge amount of different catalyst system with a different metal center such as Cr, Mn, Al, Zn, etc. are known in the literature, but in this work, the focus is on the Co(salen) catalyst system.[36,45–47] Organo-based catalyst systems with triethyl borane and other borane-based catalyst systems are currently in focus of science, enable an anionic copolymerization, resulting in higher molar mass polymers.[48] Furthermore, different initiators can be used for the polymerizations, leading to monomodal distributions. A large variety of different epoxides can be copolymerized with CO_2 using this catalyst.[49–53] The drawback of the catalyst is that CO_2 must be inserted in the reaction mixture directly since ether defects are formed.[54]

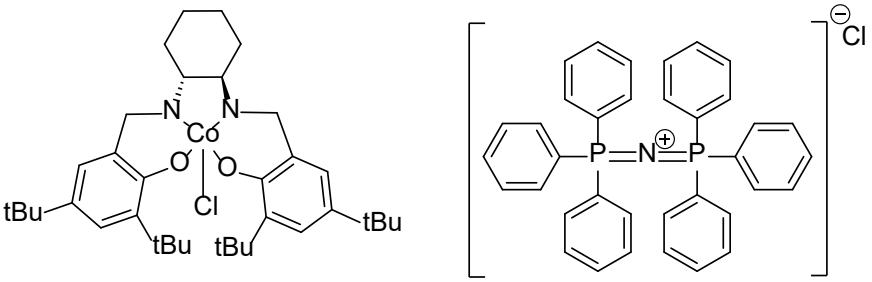

(*R*,*R*)-Co(salen)Cl [PPN]Cl

Figure 1: Chemical structure of the binary Co(salen) catalyst system. With Cl^- as a counterion.

Variety of Monomers

Various epoxides can be used for the synthesis of aliphatic polycarbonates. The most famous are propylene oxide (PO) and cyclohexene oxide (CHO). The corresponding polycarbonates are poly(propylene carbonate) (PPC) and poly(cyclohexene carbonate) (PCHC). PPC itself exhibits a median T_g of 40 °C.[55–57] Because of this intermediate T_g it cannot be used for elastomers (low T_g less than -20 °C is required) or as a thermoplastic material (high T_g over 100 °C is required). PPC is therefore often copolymerized with different monomers to improve the toughness or functionalization.[58–64] PCHC, however, displays a high T_g of 120 °C and is used as an outer glassy block in thermoplastic elastomers and as a thermoplastic material with a property profile similar to polystyrene.[48,65–67] Since the monomers are mostly based on fossil fuels, fully biobased polycarbonates are of interest. One source to obtain biobased monomers are terpenes extracted from plants.[68,69] In the field of polycarbonates, limonene oxide (LO) and menth-2-ene oxide (Men2O) have come into focus.[70–75] The resulting polycarbonates poly(limonene[34] carbonate) (PLimC) and poly(menth-2-ene carbonate) (PMen2C) show high T_gs above 100 °C, transparency, and high gas permeability.[74,76,77] Since PLimC exhibits a double bond, it lacks thermal processability. PMen2C, however, shows processability and exceptional thermal stability.[77] Both

polymers are biobased alternatives for PCHC and therefore biobased and biodegradable alternatives for thermoplastic materials. For elastic materials like thermoplastic elastomers (TPEs) or elastomers, aliphatic polycarbonates with T_gs below -20 °C are essential. Polycarbonates based on octene oxide (OO) (POC (T_g) = -24 °C) or 2-ethylhexyl glycidyl ether (EHGE) (PEGHEC (T_g) = -46 °C) show such a low glass transition temperature and are used for the soft middle block of TPEs.[48] However, both monomers are based on fossil fuels.

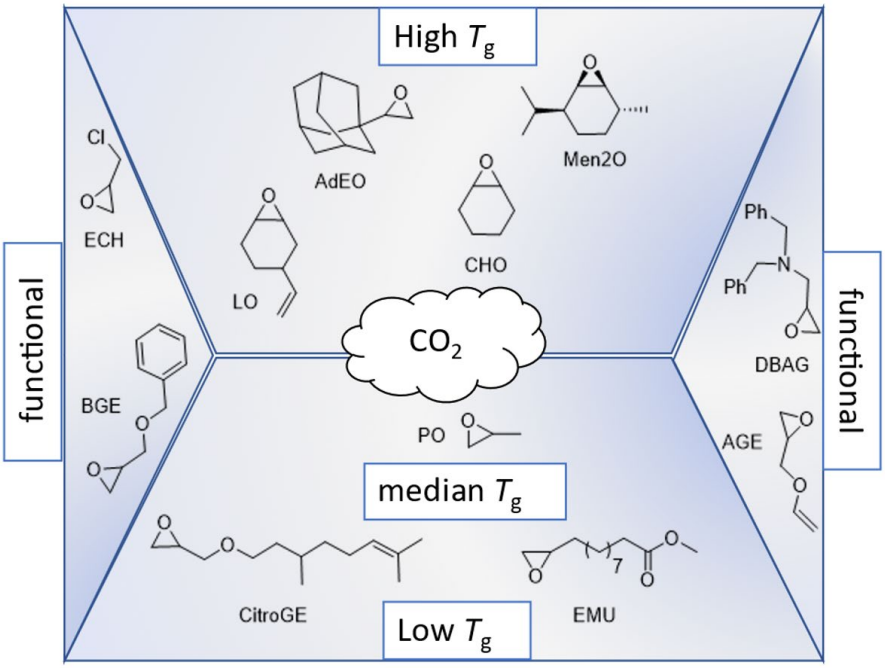

Figure 2: Overview of some epoxides used for the copolymerization with CO_2. In the middle, the monomers are shown which lead to polycarbonates with low (bottom) to high (top) T_g. On the outer sides, some functional epoxides are demonstrated.

A biobased alternative is the application of epoxides generated from fatty acids, e.g. epoxy methyl 10-undecenoate (EMU). The copolymerization of EMU with CO_2 leads to a polycarbonate with a low glass transition temperature of -44 °C. The resulting polycarbonate has not been employed in TPEs or other elastomers to date.[78] Terpenes offer a variety of potential monomer precursors.[68,69] One of these precursors is citronellol. Citronellol is abundant in lemongrass and roses and can be converted to citronellol glycidyl ether (CitroGE) via a phase transfer reaction.[79] The resulting polycarbonate shows a low T_g of -55 °C. This biobased non-food polycarbonate is additionally a biobased alternative for the soft middle block of TPES. Poly citronellol glycidyl ether carbonate (PCitroGEC) shows as a middle inner block in a PLA-*b*-PCitroGEC-*b*-PLA triblock copolymer with excellent elasticity up to 400 % elongation at break.[80] However, a variety of epoxides can be generated from terpenes. Terpenes can not only be derived from biomass like orange peels or

pines, they can also be synthesized biochemically using different bacteria and yeasts.[68,81,82] This provides some major advantages since microbial production hosts can accomplish terpenoid biosynthesis from simple carbon sources due to endogenous metabolic pathways, which produce the universal precursors for all terpenoids, isopentenyl diphosphate (IPP), and dimethylallyl diphosphate (DMAPP). Recent technologies for genome editing exploit metabolic engineering of microbial hosts for recombinant terpenoid production.[81–83] The universal precursors IPP and DMAPP are then used by the organism to develop structures like alpha-pinene, limonene, and citronellol. Since all terpenes and terpenoids are based on these precursors they follow the isoprene rule (C5 rule), which groups the numbers of linked isoprene units resulting in hemiterpenes (1 isoprene unit), monoterpenes (2 isoprene units), sesquiterpenes (3 isoprene units), etc. [81,82]

Terpene-based polycarbonates often exhibit an ene moiety such as poly(limonene carbonate) and citronellol glycidyl ether carbonate. But not just terpene-based polycarbonates carry a functionality at the side chain: Allyl glycidyl ether (AGE) is often used for the copolymerization with CO_2, leading to poly(allyl glycidyl ether) (PAGEC).[84–86] The ene moiety is then mostly transformed in a post-modification process via thiol-ene click reactions to different functionalities like amine groups or acidic groups.[84–87] The group of Guang-Peng used PAGEC as the middle block and converted the ene moieties to hydroxy groups. These hydroxy groups could then interact with boronic ester leading to a self-healing material.[67] The positively charged amino group was introduced via thiol-ene click to an ene moiety like in poly limonene oxide to yield water-soluble and antibacterial materials.[11] The group of Darensbourg introduced a BOC-protected amino group using the thiol-ene click reaction in a PPC-*co*-PAGEC copolymer. The deprotection of the amine with HCl led to a quaternary ammonium cation as side moiety and therefore to amphiphilic polymers.[84] Our group introduced hydroxyl groups in the side chains of polycarbonates using epoxides with protected hydroxyl groups, such as benzyl glycidyl ethers (BGE) and ethoxy ethyl glycidyl ether (EEGE), resulting in poly(1,2-glycerol carbonates). These polymers swell in water and methanol and degrade in an aqueous acidic environment.[88,89] Moreover, protected amino groups in the sidechains of the epoxides offer a synthesis route of amino-based polycarbonates.[63,64] Song et al. copolymerized PO with a benzyl-protected amino glycidol, *N,N*-dibenzyl amino glycidyl (DBAG), resulting in a polycarbonate with amine sidechains after deprotection. Besides, they investigated the hydrophilicity of the polymers (Figure 2).[63]

POLYMER STRUCTURES

Sophisticated applications necessitate a combination of specific properties. Therefore, some approaches to synthesize "hybrids" have been taken. A facile route is to blend two different polymers, the second is to form copolymers. Copolymer structures are classified into statistical copolymers, block copolymers, and graft copolymers.[90] The following section focuses on terpolymerization and formation of linear block copolymers in the field of polycarbonates based on CO_2.

Terpolymerization

The copolymerization of epoxies and CO_2 itself is an almost ideal alternating copolymerization. This means that epoxide incorporation is immediately followed by CO_2 incorporation, resulting in a polycarbonate structure. Without this alternating incorporation, ether defects would occur.[18,23,24,45] In addition to this ideal alternating copolymerization, random copolymerization of different epoxides can take place using CO_2 and two different epoxides in a one-pot synthesis. A random copolymer is one in which the monomer residues are arranged statistically in the polymer molecule. In summary, terpolymerization of CO_2 and two other epoxides is always based on alternating and random copolymerization since after a CO_2 insertion an epoxide insertion fallowed. Thus, it is a copolymerization of at least 3 monomers.[5,91,92] This method is often used to introduce functional monomers in statistical variation or to adjust the thermal properties of polymers.[90] PPC exhibits an intermediate glass transition temperature of 40 °C. Copolymerizing it with CHO led to higher T_gs.[92–95] Darensbourg et al. demonstrated that at 25 °C PO was preferably incorporated compared to CHO, at 40 °C a polymer with more equal distribution could be generated.[92] Using hexene oxide (HO) as a comonomer in a terpolymerization reaction with PO and CO_2, the T_g of PPC is lowered by up to -2 °C (64 mol% of HO).[95] However, the use of biobased epoxides to lower the T_g of PPC is not known in the literature. Reiter et al. copolymerized CO_2 with LO and PO or CHO, respectively. This terpolymerization offers the ability to adjust the glass transition temperatures and the transparencies.[96] Wang and coworkers copolymerized CO_2/PO/Me_3MO (2-((2-(2-(2-methoxyethoxy)ethoxy)ethoxy)methyl) oxirane) generating a water-soluble polycarbonate and therefore a better acid-degradable polymer because of its hydrophilicity.[97] As discussed in the section "monomers" a copolymerization with protected amino-functionalized epoxides with PO and CO_2 led to a random distribution of the functionalities and more hydrophilic polycarbonates.[63,64]

Block copolymerization

Another form of macromolecular architecture is block copolymers. These macromolecules consist of chemically different, terminally-linked segments. Block copolymers offer unique possibilities such as the creation of thermoplastic elastomers or amphiphilic polymers[90] and can be classified into diblocks (AB), triblocks (ABA), and multiblocks(e.g. ABC, ABCD, $(AB)_n$).[90,98,99] Moreover you can differ between linear, graft, star-and cyclic block copolymers.[99] Those systems usually (with sufficient P_n) exhibit two phases termed microphase separation (since the segments are still connected chemically a macro-phase separation can not occur). The incompatibility of the chemically connected homopolymers forms often micelles or hydrogels in solution.[90] Moreover, using immiscible polymers, one with a low T_g (B) and one with a high T_g (A) in combination as ABA triblock, results in a thermoplastic elastomer. In the next part, these two important applications of block copolymers are more specified.

Amphiphilic polymers

Amphiphilic polymers describe macromolecules that exhibit both hydrophobic and hydrophilic units.[100] The incompatibility of the hydrophilic and the hydrophobic part leads to microphase separation in water, resulting in an assembly of the hydrophobic segments in form of nanoscopic structures of different morphologies.[101] Amphiphilic polymers are used as drug carriers and gene vectors in the biomedical field[102–105] and can be categorized as block, random, gradient, graft, star polymer, and dendrimer.[100,101] In this chapter the focus will be on amphiphilic block copolymers.

The water-soluble amphiphilic block copolymer self-assembles in water to micelles and other structures and can be used as surfactants because of their capability to interact with hydrophobic media like oil and hydrophilic media like water. An important value to determine the efficiency of surfactants is the critical micellar concentration (CMC).[106–108] CMC defines the concentration of surfactants above which micelles are formed. The CMC can be determined by a tensiometer using the change of the surface tension.[106–108] Recently, the group of Feng introduced a copolymerization of ethylene oxide (EO) with CO_2. The resulting polyethylene carbonate with ether defects (PECEO) was then used as macroinitiator for PEO resulting in a PEO-*b*-PECEO-*b*-PEO triblock copolymer. This triblock copolymer shows CMC values of 37-55 mg/L.[54] One route to synthesize surfactants based on CO_2 is to use hydrophilic macroinitiators like mPEG or PEG as chain transfer agents and polymerize hydrophobic polycarbonate onto them (Scheme 5). The group of Frey introduced mPEG-*b*-PPC and PPC-*b*-PEG-*b*-PPC di- and triblock copolymers as surfactants. These were shown to act as emulsifiers in a miniemulsion reaction and be degradable in acidic medium. Since the polymers form micelles in water, the degradation needs harsh conditions

(concentrated HCl).[109,110] Furthermore, Kunze et al. synthesized mPEG-*b*-PBC diblock copolymers and investigated the micellization behavior and the solubilization of the polymers.[111] Augustin et al. also applied PEG as the hydrophilic part of a star polymer. Therefore, vinyl cyclohexene dioxide (VCD) was utilized to generate a polycarbonate core. Ethylene oxide (EO) was polymerized onto the hydroxy end groups of the core leading to a (PVCDC)-$(PEO)_n$ star polymer. The advantage of this resulting surfactant is the hydrolyzable core.[112] Moreover, CO_2-based surfactants are available via click reactions (Scheme 5). Liu et al. copolymerized VCO/CHO/CO2 in a one-pot reaction resulting in a PCHC-*co*-PVCHC polymer. Subsequently, a thiol-ene click reaction was accomplished to convert the vinyl functionalities of the PVCHC to a charged PCHC (CPCHC). These charged polymers show then an amphiphilic character and have been used as biodegradable surfactants for an oil-in-water mini-emulsion. Furthermore, they were converted into degradable nanoparticles, and properties such as loading capacity, drug release, and cytotoxicity have been revealed.[110,113]

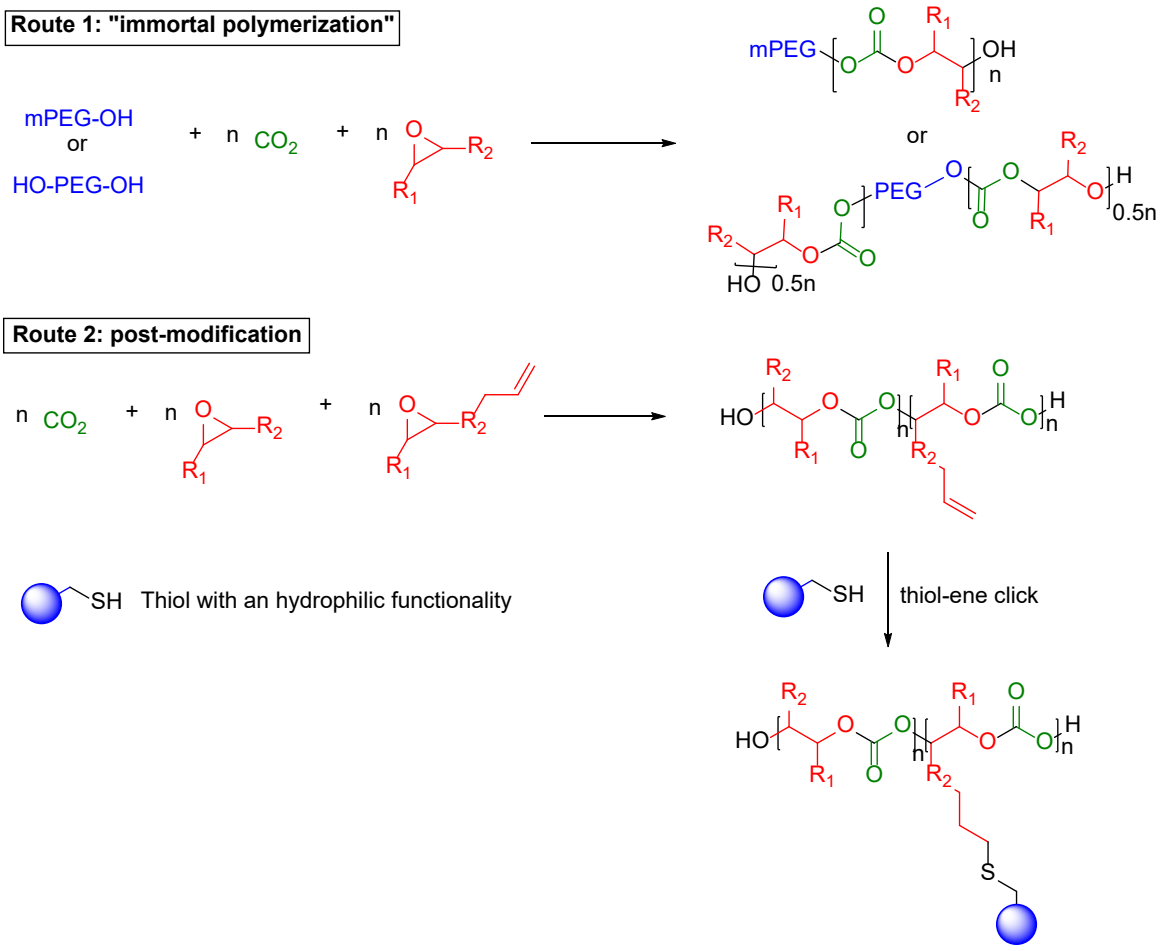

Scheme 5: Overview of different routes to synthesize amphiphilic polycarbonate surfactants based on CO_2. Route 1 demonstrates the use of the "immortal polymerization" using mPEG or PEG as CTA (top). Route 2 shows the copolymerization of aliphatic or cyclic epoxides with epoxide with vinyl functionality and CO_2 to yield through thiol-ene click reaction surfactants based on CO_2 (bottom).

The group of Meng copolymerized maleic anhydride (MA) with PO and CO_2 using zinc adipate (ZnAA) as a catalyst to yield a polycarbonate-polyester copolymer. The molecular chain sequence structure of these terpolymers was demonstrated to be a gradient-based on ^{1}H NMR investigation combined with *in situ* infrared technology monitoring of the reaction process. The sulfonation of ethylenic double bonds in the maleic building structure of the unsaturated polyester unit via sodium hydrogen sulfite leads to biodegradable PPCMA. The surface tension of the aqueous solution of the polymer with 56.8% hydrophilic segments exhibits a CMC of 47.5 mN m^{-1} .[114] Darensbourg et al. also used the thiol-ene click to introduce multiple hydroxy or acid functionalities to the side chain of poly(2-vinyloxirane carbonate) (PVIC) leading to a water-soluble polymer after deprotonation by aqueous ammonium hydroxide ($NH_4OH(aq)$).[115] Li et al. designed a CO_2-based amphiphilic polycarbonate with improved hydrophilicity and processability as an efficient platform for tumor imagining. PAGEC-*b*-PPC-*b*-PAGEC, synthesized in a sequential addition of the monomers, served as starting material. Next, the triblock copolymer was connected with Boc-protected cysteine. After deprotection of the Boc group, an amphiphilic triblock copolymer was obtained. Subsequently, the resulting APCs were labeled with gadolinium to provide APC-DTPA/Gd after reacting with diethyleneetriaminopentaacetic acid (DTPA) dianhydride as the chelating agent. CMC values of 32.56 mg/L (APC) and 53.86 mg/L (APC-DTA/Gd) were determined.[116]

Besides surfactants hydrogels can also be formed using amphiphilic triblock copolymers with an inner hydrophilic block. Hydrogels are a 3D network of hydrophilic polymer chains, that have the ability to absorb water (without dissolving) while preserving their mechanical integrity through chemically or physically crosslinking.[117,118] Physically crosslinked hydrogels can be transformed by heat or solvents, which allows for recycling and processability and are therefore called thermoplastic hydrogels .[118] Physical crosslinking can be powered by hydrophobic, ionic, or H-bonding forces or due to entanglement of high molecular weight polymers. During swelling their properties change for instance in hardness, permeability, and transparency. Since they can imitate the characteristics of living tissues but are still thermally deformable they are an ideal candidate for use in tissue engineering, wound dressing, and as contact lenses.[117] Hydrogels based on CO_2 and epoxides are not known in the literature since they usually exhibit a hydrophobic character. Nevertheless, triblock copolymers with a hydrophilic mid-block and glassy outer blocks can form hydrogels in water. Biocompatible polymers with such structures are established in literature and mostly depend on poly(ethylene glycol) (PEG) as a mid-block. Polyesters such as polycaprolactone and polylactide are applied as outer glassy blocks, but their acidic degradation products present a major disadvantage.[119–123,124,125] These acids can harm the living environment of the tissue and lead

to necrosis.[126–128] Aliphatic polycarbonates on the other hand have no acidic degradation products and present exceptional biocompatibility and biodegradability.[129,130] Considering all aspects of amphiphilic CO_2-based polymers there is a huge variety of potential applications in biomedical fields which could also be extended by the synthesis of new thermoplastic hydrogels or new variants of micelles for drug delivery systems.

Thermoplastic elastomers

Thermoplastic elastomers (TPES) are rubber-like materials with the capability to melt and be processed in this state. The combination of features of thermoset rubbers and thermoplastic materials in microphase separated structures leads to wide use in almost all areas of plastics.[90,131]

Microphase separation in bulk

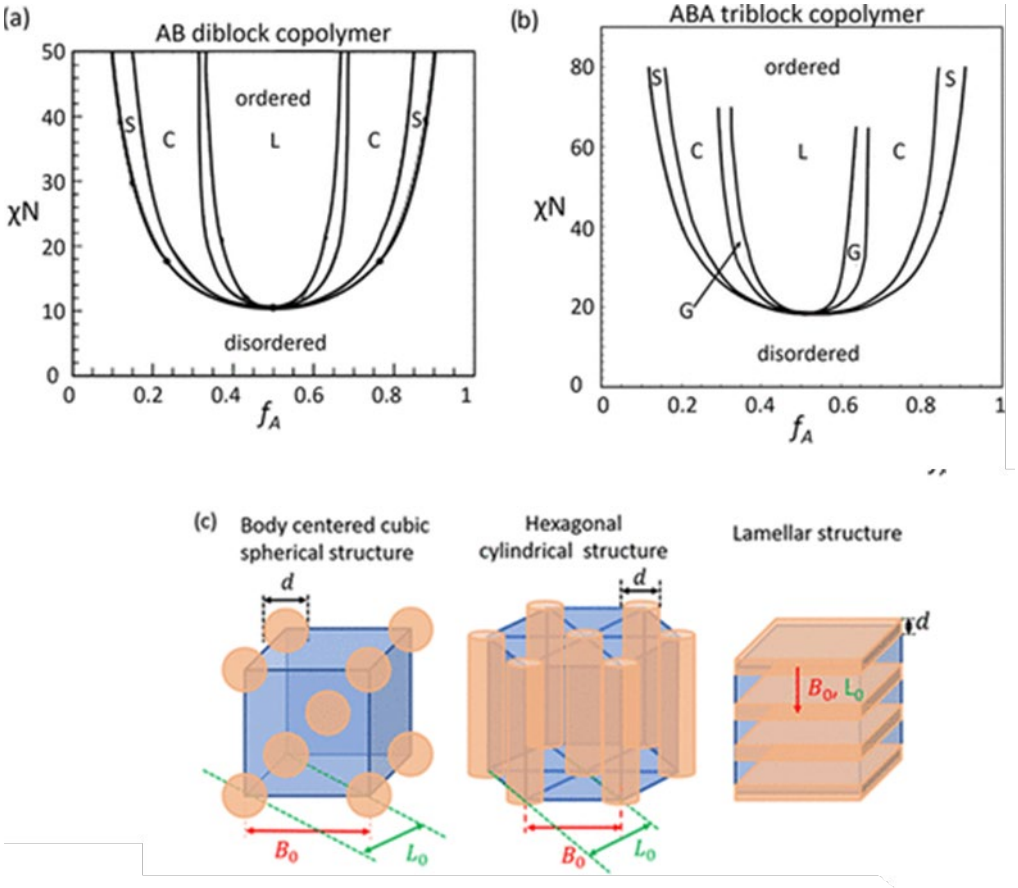

Figure 3: Theoretically calculated phase diagrams based on the mean-field theory of (a) AB diblock[132] and (b) ABA triblock copolymers.[133] "S" show the spherical, "C" the hexagonal cylindrical, "G" the gyroid, and "L" the lamellar microstructure. (c) 3D visualization of the different microstructures. The long-range-order distance L_0, quantifiable in SAXS, the crystallographic vector of the unit cell B_0, and the diameter d of the soft phase are marked. Reprinted (adapted) with permission. Hirschberg, V.; Faust, L.; Rodrigue, D.; Wilhelm, M. Effect of Topology and Molecular Properties on the Rheology and Fatigue Behavior of Solid Polystyrene/Polyisoprene Di- and Triblock Copolymers. *Macromolecules* 2020, *53*, 5572–5587. Copyright 2020 American Chemical Society.[131]

To understand why thermoplastic elastomers, combine the elasticity of rubber with the ability to be proceed through heat or solvents like thermoplastic materials the microphase separation requires closer examination. Blends of two polymers lead to macro phase separation. Phase separation is a thermodynamic process.[134] The process is powered by the repulsion of the different polymers. Since block copolymers of the different polymers are chemically linked a macro phase separation such as in blend can not occur.[90,134,135]

Instead of macro phase separation, a microphase separation takes place. The polymers arrange themselves in different segments driven by the reduction of segmental contacts. This microphase separation can be explained by the Flory Huggins theory using the Gibbs free energy (ΔG_m) as thermodynamic variable.[136–139] ΔG_m depends on the interactions of the copolymerized monomers. The monomer-to-monomer interaction parameter is called the mixing (Flory-Huggins) parameter (χ). χ together with the degree of polymerization (N) and the volume fraction of each block ($f_{A,B}$) influence, in turn, the mixing or separation of the segments.[140,141] It could be proven, that under the order-disorder temperature (T_{ODT}) using an equal volume fraction of A and B in case of the diblocks at $N\chi > 10$,[142] in case of the triblocks at $N\chi > 18$[133] microphase separation occurs (Figure 3). The $N\chi$ is higher in ABA triblock copolymers since the phase separation is hindered by entropic constraints of both blocks.[143] The microphase separation is driven by the free Gibbs enthalpy, which attempts to minimize the interfacial energy. This leads to spherical (S), hexagonal (H), cylindrical (C), or lamellar (L) microdomains (depending on the volume fraction of each block). The distance of two A-A microdomains is illustrated by the diameter (d). The long-distance order (L_o) is illustrated in Figure 3 in green showing the distance between the different spheres (S), hexagonal packed cylinders (C), gyroids (G), or lamella (L). Comparison of the phase diagram of the diblock copolymers´ with the phase diagram of the triblock copolymers shows that the diblock copolymers phase diagram is symmetrical, and the triblock copolymer phase diagram shifted toward larger volume fractions of A.

The strength of the phase separation is influenced by the $N\chi$ value. For instance, for diblock copolymer with a weak segregation limit such as $N\chi \approx 10$ leads to a single peak in the small-angle X-ray scattering (SAXS). An increase of $N\chi$ results in sharper phase separation.[144] For an AB diblock the blocks distinguish in individual microdomains. However, due to its structure ABA triblock can form a loop conformation (both blocks are within the same A microdomain) or a bridge conformation (both blocks are connected to different A microdomains separated by the B domain). Due to this bridging and looping of the B block of the triblock, the mechanical toughness of triblock copolymers is enhanced against diblock copolymers (Figure 4). [132]

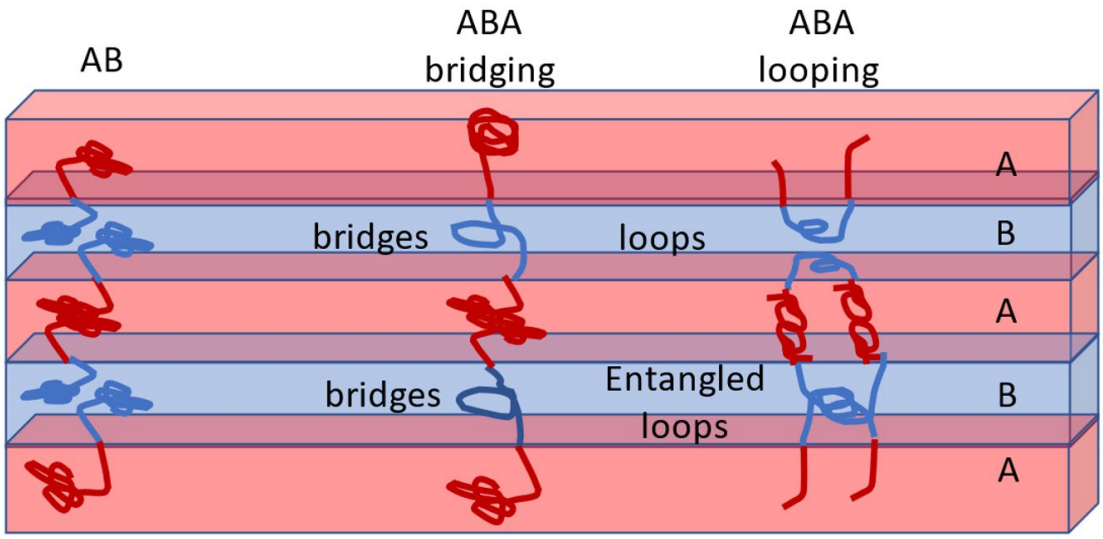

Figure 4: Comparison of the different conformations in AB di- and ABA triblock copolymers. ABA triblock copolymers can form bridges, loops, and entangled loops.

Thermoplastic elastomers in the polycarbonate field based on CO_2

Since Inoue et al. established the copolymerization of epoxides with CO_2 the focus was mainly to improve the catalyst systems.[14,21,22,34,145] In the last few years, however, the focus changed to the development of new polymer structures based on CO_2 for new materials. [5,54,71,73,76,77] Jia et al. introduced in 2020 an all-polycarbonate TPE with poly octene carbonate (POC, T_g = -24 °C) as an inner soft block and PCHC (T_g= 120 °C) as glassy outer blocks. These polymers show elastic behavior and consist completely of polycarbonates based on CO_2. However, the used epoxides are derived from fossil fuels. The different morphologies of the resulting PCHC-*b*-POC-*b*-PCHC triblock copolymers were analyzed via AFM.[48] In 2019, Yang et al. showed that a tandem strategy using AGE together with CO_2 resulted in PAGEC. PAGEC (B) was then combined with PCHC (A) to form an ABA triblock. This does not initially lead to thermoplastic elastomers. However, conversion of the ene groups of PAGEC to hydroxyl groups via a thiol-ene click reaction resulted in curable thermoplastic elastomers as boronic esters were blended with these polymers.[146] The combination of polyesters with polycarbonates provides an additional route to TPEs. The group of Williams synthesized in 2020 a PCHC-*b*-PDL-*b*-PCHC (PDL = poly decalactone) triblock copolymer in a one-pot reaction using a switchable catalyst. These new materials expand the properties of PCHC and, more precisely, they show good thermal stability ($T_{d,5}$ ~ 280 °C), high toughness (112 MJ m^{-3}), and very high elongation at break (>900%).[147] In the same year the authors presented the biobased alternative using LO instead of CHO for the outer blocks leading to polymers with high elasticity (elongation at break = 400 %).[71] Neumann et al. copolymerized in 2021 LO/CO_2 with

lactide in a one-pot reaction applying [(BDI)Zn-(μ-OAc)] as a catalyst resulting in a PLimC-*b*-PLA diblock copolymer. They investigated the microphase separation of these polymers using transmission electronic microscopy (TEM). Polymers with 72 000 g/mol already showed two T_gs and phase separation in the TEM pictures. Besides they presented a PLimC-*b*-P(diHLA)-*b*-PLimC triblock copolymer. Dihexyllactide (diHLA) was synthesized in a one-step reaction using 2-hydroxyoctanoic acid. The resulting triblock polymers were elastic according to the authors, but no mechanical characterization was performed to date.[148] The same group studied 2019 the morphologies of PCHC-*b*-PLimC block copolymers. Although both blocks were polycarbonates a microphase separation was detectable via TEM and SAXS measurements. Cylindrical, lamellar, and hexagonally perforated lamellar microstructures were observed.[149]

CONCLUSION AND PERSPECTIVES

In this chapter, the development of CO_2-based polycarbonates towards tailor-made materials was demonstrated. Functionalized aliphatic polycarbonates based on carbon dioxide and tailored epoxide building blocks represent a resource-saving opportunity for a broad range of materials and applications that require both biodegradability and biocompatibility.[91,150] They offer prospects for, e.g. drug delivery and tissue engineering due to their biodegradability.[109,113–116] Moreover, it could be demonstrated, that using different polymer structures yields different characteristics of the polycarbonates.[48,66,110,111] Amphiphilic block copolymers result in partly or fully biodegradable surfactants.[109–111,114,115] Additionally, it was shown, that in the field of widely used TPEs the aliphatic polycarbonates are also a promising alternative to established systems like SIS and SBS.[48,134,146] This alternative does not only reduce the use of fossil resources but also produces biodegradable materials.[151–153] Biodegradability is an important property of future materials, like plastic pollution in the landfills increases.[5,150,153] Furthermore, the focus shifts in science and industry towards biobased polymers. In the field of polycarbonates, this aspect is increasingly coming into the focus. Terpenes offer a great biobased non-food source and are easily modifiable to epoxides. In this chapter LO, Men2O were already shown to be used as terpene-based epoxides. The application of the resulting polycarbonates entails antibacterial coatings, glazing materials, and thermoplastic elastomers, but there are hundreds more of different terpenes which could be used as starting material and therefore offer potentially new properties for biobased polycarbonates.[69–76,81–83,148]

REFERENCES

(1) Huang, J.; Worch, J. C.; Dove, A. P.; Coulembier, O. Update and Challenges in Carbon Dioxide-Based Polycarbonate Synthesis. *ChemSusChem* **2020**, *13*, 469–487.

(2) Sakakura, T.; Choi, J.-C.; Yasuda, H. Transformation of carbon dioxide. *Chem. Rev.* **2007**, *107*, 2365–2387.

(3) Zheng, J.; Suh, S. Strategies to reduce the global carbon footprint of plastics. *Nat. Clim. Chang.* **2019**, *9*, 374–378.

(4) Turning waste into added value: CO_2 technology. https://solutions.covestro.com/en/highlights/articles/theme/product-technology/turning-waste-into-added-value-CO_2-technology (accessed October 9, 2021).

(5) Scharfenberg, M.; Hilf, J.; Frey, H. Functional Polycarbonates from Carbon Dioxide and Tailored Epoxide Monomers: Degradable Materials and Their Application Potential. *Adv. Funct. Mater.* **2018**, *28*, 1704302.

(6) Carothers, W. H.; van Natta, F. J. STUDIES ON POLYMERIZATION AND RING FORMATION. III. GLYCOL ESTERS OF CARBONIC ACID. *J. Am. Chem. Soc.* **1930**, *52*, 314–326.

(7) Wenxiang Zhu; Xi Huang; Chuncheng Li; Yaonan Xiao; Dong Zhang; Guohu Guan. High-molecular-weight aliphatic polycarbonates by melt polycondensation of dimethyl carbonate and aliphatic diols: synthesis and characterization. *Polym. Int.* **2011**, *60*, 1060–1067.

(8) Feng, J.; Zhuo, R.-X.; Zhang, X.-Z. Construction of functional aliphatic polycarbonates for biomedical applications. *Prog. Polym. Sci* **2012**, *37*, 211–236.

(9) Tempelaar, S.; Mespouille, L.; Coulembier, O.; Dubois, P.; Dove, A. P. Synthesis and post-polymerisation modifications of aliphatic poly(carbonate)s prepared by ring-opening polymerisation. *Chem. Soc. Rev.* **2013**, *42*, 1312–1336.

(10) Hilf, J.; Frey, H. Propargyl-functional aliphatic polycarbonate obtained from carbon dioxide and glycidyl propargyl ether. *Macromol. Rapid Commun.* **2013**, *34*, 1395–1400.

(11) Hauenstein, O.; Agarwal, S.; Greiner, A. Bio-based polycarbonate as synthetic toolbox. *Nat. Commun.* **2016**, *7*, 11862.

(12) Poland, S. J.; Darensbourg, D. J. A quest for polycarbonates provided via sustainable epoxide/CO_2 copolymerization processes. *Green Chem.* **2017**, *19*, 4990–5011.

(13) Taherimehr, M.; Pescarmona, P. P. Green polycarbonates prepared by the copolymerization of CO_2 with epoxides. *J. Appl. Polym. Sci.* **2014**, *131*.

(14) Inoue, S.; Koinuma, H.; Tsuruta, T. Copolymerization of carbon dioxide and epoxide with organometallic compounds. *Makromol. Chem.* **1969**, *130*, 210–220.

(15) Liu, Q.; Wu, L.; Jackstell, R.; Beller, M. Using carbon dioxide as a building block in organic synthesis. *Nat. Commun.* **2015**, *6*, 5933.

(16) Janes, T.; Yang, Y.; Song, D. Chemical reduction of CO_2 facilitated by C-nucleophiles. *Chem. Commun.* **2017**, *53*, 11390–11398.

(17) Xu, Y.; Lin, L.; Xiao, M.; Wang, S.; Smith, A. T.; Sun, L.; Meng, Y. Synthesis and properties of CO_2-based plastics: Environmentally-friendly, energy-saving and biomedical polymeric materials. *Prog. Polym. Sci* **2018**, *80*, 163–182.

(18) Darensbourg, D. J. Copolymerization of Epoxides and CO_2 : Polymer Chemistry for Incorporation in Undergraduate Inorganic Chemistry. *J. Chem. Educ.* **2017**, *94*, 1691–1695.

(19) Beckman, E. J. Making Polymers from Carbon Dioxide. *Science* **1999**, *283*, 946–947.

(20) Bird, C. W.; Katritzky, A. R.; Rees, C. W.; Scriven, E. F. V., Eds. *Comprehensive heterocyclic chemistry II: A review of the literature 1982 - 1995; the structure, reactions, synthesis, and uses of heterocyclic compounds*, 1. ed.; Pergamon: Oxford, 1996.

(21) Pescarmona, P. P.; Taherimehr, M. Challenges in the catalytic synthesis of cyclic and polymeric carbonates from epoxides and CO_2. *Catal. Sci. Technol.* **2012**, *2*, 2169.

(22) Taherimehr, M.; Al-Amsyar, S. M.; Whiteoak, C. J.; Kleij, A. W.; Pescarmona, P. P. High activity and switchable selectivity in the synthesis of cyclic and polymeric cyclohexene carbonates with iron amino triphenolate catalysts. *Green Chem.* **2013**, *15*, 3083.

(23) Darensbourg, D. J.; Moncada, A. I. Mechanistic insight into the initiation step of the coupling reaction of oxetane or epoxides and CO_2 catalyzed by (salen)CrX complexes. *Inorg. Chem.* **2008**, *47*, 10000–10008.

(24) Darensbourg, D. J.; Lee, W.-Z.; Phelps, A. L.; Guidry, E. Kinetic Study of the Insertion and Deinsertion of Carbon Dioxide into fac -(CO) 3 (dppe)MnOR Derivatives. *Organometallics* **2003**, *22*, 5585–5588.

(25) Darensbourg, D. J. Making plastics from carbon dioxide: salen metal complexes as catalysts for the production of polycarbonates from epoxides and CO_2. *Chem. Rev.* **2007**, *107*, 2388–2410.

(26) *Manganese Salan Complexes As Catalysts For Hydrosilylation Of Aldehydes And Ketones*, 2019.

(27) Ren, W.-M.; Yue, T.-J.; Zhang, X.; Gu, G.-G.; Liu, Y.; Lu, X.-B. Stereoregular CO_2 Copolymers from Epoxides with an Electron-Withdrawing Group: Crystallization and Unexpected Stereocomplexation. *Macromolecules* **2017**, *50*, 7062–7069.

(28) Lu, X.-B.; Ren, W.-M.; Wu, G.-P. CO_2 copolymers from epoxides: catalyst activity, product selectivity, and stereochemistry control. *Acc. Chem. Res.* **2012**, *45*, 1721–1735.

(29) Inoue, S. Immortal polymerization: The outset, development, and application. *J. Polym. Sci. A Polym. Chem.* **2000**, *38*, 2861–2871.

(30) *Photochemical Reactions of Stereoisomeric 7, 7, 8, 8-Tetramethylbicyclo [4.2. 0] octan-2-ones Richard J. Batten, Howard AJ Carless*, 1985.

(31) Cyriac, A.; Lee, S. H.; Varghese, J. K.; Park, E. S.; Park, J. H.; Lee, B. Y. Immortal CO_2 /Propylene Oxide Copolymerization: Precise Control of Molecular Weight and Architecture of Various Block Copolymers. *Macromolecules* **2010**, *43*, 7398–7401.

(32) Zhang, Y.-Y.; Yang, G.-W.; Wang, Y.; Lu, X.-Y.; Wu, G.-P.; Zhang, Z.-S.; Wang, K.; Zhang, R.-Y.; Nealey, P. F.; Darensbourg, D. J.*; et al.* Synthesis of CO_2 -Based Block Copolymers via Chain Transfer Polymerization Using Macroinitiators: Activity, Blocking Efficiency, and Nanostructure. *Macromolecules* **2018**, *51*, 791–800.

(33) Jia, M.; Hadjichristidis, N.; Gnanou, Y.; Feng, X. Monomodal Ultrahigh-Molar-Mass Polycarbonate Homopolymers and Diblock Copolymers by Anionic Copolymerization of Epoxides with CO_2. *ACS Macro Lett.* **2019**, *8*, 1594–1598.

(34) Kember, M. R.; Williams, C. K. Efficient magnesium catalysts for the copolymerization of epoxides and CO_2; using water to synthesize polycarbonate polyols. *J. Am. Chem. Soc.* **2012**, *134*, 15676–15679.

(35) Coates, G. W.; Moore, D. R. Discrete metal-based catalysts for the copolymerization of CO_2 and epoxides: discovery, reactivity, optimization, and mechanism. *Angew. Chem. Int. Ed. Engl.* **2004**, *43*, 6618–6639.

(36) Klaus, S.; Lehenmeier, M. W.; Anderson, C. E.; Rieger, B. Recent advances in CO_2/epoxide copolymerization—New strategies and cooperative mechanisms. *Coord. Chem. Rev.* **2011**, *255*, 1460–1479.

(37) Lu, X.-B.; Wang, Y. Highly active, binary catalyst systems for the alternating copolymerization of CO_2 and epoxides under mild conditions. *Angew. Chem. Int. Ed. Engl.* **2004**, *43*, 3574–3577.

(38) Zhang, Y.-Y.; Yang, G.-W.; Wu, G.-P. A Bifunctional β-Diiminate Zinc Catalyst with CO_2 /Epoxides Copolymerization and RAFT Polymerization Capacities for Versatile Block Copolymers Construction. *Macromolecules* **2018**, *51*, 3640–3646.

(39) Klaus, S.; Lehenmeier, M. W.; Herdtweck, E.; Deglmann, P.; Ott, A. K.; Rieger, B. Mechanistic insights into heterogeneous zinc dicarboxylates and theoretical considerations for CO_2-epoxide copolymerization. *J. Am. Chem. Soc.* **2011**, *133*, 13151–13161.

(40) Lan, J.; Qu, Y.; Zhang, X.; Ma, H.; Xu, P.; Sun, J. A novel water-stable MOF Zn(Py)(Atz) as heterogeneous catalyst for chemical conversion of CO_2 with various epoxides under mild conditions. *J. CO_2 Util.* **2020**, *35*, 216–224.

(41) Parmar, B.; Patel, P.; Pillai, R. S.; Tak, R. K.; Kureshy, R. I.; Khan, N.-U. H.; Suresh, E. Cycloaddition of CO_2 with an Epoxide-Bearing Oxindole Scaffold by a Metal-Organic Framework-Based Heterogeneous Catalyst under Ambient Conditions. *Inorg. Chem.* **2019**, *58*, 10084–10096.

(42) Peretti, K. L.; Ajiro, H.; Cohen, C. T.; Lobkovsky, E. B.; Coates, G. W. A highly active, isospecific cobalt catalyst for propylene oxide polymerization. *J. Am. Chem. Soc.* **2005**, *127*, 11566–11567.

(43) Darensbourg, D. J. Making plastics from carbon dioxide: salen metal complexes as catalysts for the production of polycarbonates from epoxides and CO_2. *Chem. Rev.* **2007**, *107*, 2388–2410.

(44) Chisholm, M. H.; Navarro-Llobet, D. NMR Assignments of Regioregular Poly(propylene oxide) at the Triad and Tetrad Level. *Macromolecules* **2002**, *35*, 2389–2392.

(45) Moore, D. R.; Cheng, M.; Lobkovsky, E. B.; Coates, G. W. Mechanism of the alternating copolymerization of epoxides and CO_2 using beta-diiminate zinc catalysts: evidence for a bimetallic epoxide enchainment. *J. Am. Chem. Soc.* **2003**, *125*, 11911–11924.

(46) Darensbourg, D. Catalysts for the reactions of epoxides and carbon dioxide. *Coord. Chem. Rev.* **1996**, *153*, 155–174.

(47) Li, F.; Xiao, L.; Xia, C.; Hu, B. Chemical fixation of CO_2 with highly efficient ZnCl2/[BMIm]Br catalyst system. *Tetrahedron Lett.* **2004**, *45*, 8307–8310.

(48) Jia, M.; Zhang, D.; Kort, G. W. de; Wilsens, C. H. R. M.; Rastogi, S.; Hadjichristidis, N.; Gnanou, Y.; Feng, X. All-Polycarbonate Thermoplastic Elastomers Based on Triblock Copolymers Derived from Triethylborane-Mediated Sequential Copolymerization of CO_2 with Various Epoxides. *Macromolecules* **2020**, *53*, 5297–5307.

(49) Chen, Z.; Yang, J.-L.; Lu, X.-Y.; Hu, L.-F.; Cao, X.-H.; Wu, G.-P.; Zhang, X.-H. Triethyl borane-regulated selective production of polycarbonates and cyclic carbonates for the coupling reaction of CO_2 with epoxides. *Polym. Chem.* **2019**, *10*, 3621–3628.

(50) Zhang, D.-D.; Feng, X.; Gnanou, Y.; Huang, K.-W. Theoretical Mechanistic Investigation into Metal-Free Alternating Copolymerization of CO_2 and Epoxides: The Key Role of Triethylborane. *Macromolecules* **2018**, *51*, 5600–5607.

(51) Chidara, V. K.; Boopathi, S. K.; Hadjichristidis, N.; Gnanou, Y.; Feng, X. Triethylborane-Assisted Synthesis of Random and Block Poly(ester-carbonate)s through One-Pot Terpolymerization of Epoxides, CO_2 , and Cyclic Anhydrides. *Macromolecules* **2021**, *54*, 2711–2719.

(52) Andrea, K. A.; Kerton, F. M. Triarylborane-Catalyzed Formation of Cyclic Organic Carbonates and Polycarbonates. *ACS Catal.* **2019**, *9*, 1799–1809.

(53) Patil, N. G.; Boopathi, S. K.; Alagi, P.; Hadjichristidis, N.; Gnanou, Y.; Feng, X. Carboxylate Salts as Ideal Initiators for the Metal-Free Copolymerization of CO_2 with Epoxides: Synthesis of Well-Defined Polycarbonates Diols and Polyols. *Macromolecules* **2019**, *52*, 2431–2438.

(54) Jia, M.; Zhang, D.; Gnanou, Y.; Feng, X. Surfactant-Emulating Amphiphilic Polycarbonates and Other Functional Polycarbonates through Metal-Free Copolymerization of CO_2 with Ethylene Oxide. *ACS Sustain. Chem. Eng.* **2021**, *9*, 10370–10380.

(55) Luinstra, G. A.; Borchardt, E. Material Properties of Poly(Propylene Carbonates). In *Synthetic biodegradable polymers*; Rieger, B., Amann, M., Eds.; Advances in Polymer Science 245; Springer: Heidelberg, 2012; pp 29–48.

(56) Ree, M.; Bae, J. Y.; Jung, J. H.; Shin, T. J. A new copolymerization process leading to poly(propylene carbonate) with a highly enhanced yield from carbon dioxide and propylene oxide. *J. Polym. Sci. A Polym. Chem.* **1999**, *37*, 1863–1876.

(57) Zhu, Q.; Meng, Y.; Tjong, S.; Zhao, X.; Chen, Y. Thermally stable and high molecular weight poly(propylene carbonate)s from carbon dioxide and propylene oxide. *Polym. Int.* **2002**, *51*, 1079–1085.

(58) Chen, S.; Xiao, M.; Sun, L.; Meng, Y. Study on Thermal Decomposition Behaviors of Terpolymers of Carbon Dioxide, Propylene Oxide, and Cyclohexene Oxide. *Int. J. Mol. Sci.* **2018**, *19*, 3723.

(59) Gao, L. J.; Xiao, M.; Wang, S. J.; Meng, Y. Z. Thermally stable poly(propylene carbonate) synthesized by copolymerizing with bulky naphthalene containing monomer. *J. Appl. Polym. Sci.* **2008**, *108*, 1037–1043.

(60) Honda, M.; Ebihara, T.; Ohkawa, T.; Sugimoto, H. Alternating terpolymerization of carbon dioxide, propylene oxide, and various epoxides with bulky side groups for the tuning of thermal properties. *Polym. J.* **2021**, *53*, 121–127.

(61) Liu, S.; Xiao, H.; Huang, K.; Lu, L.; Huang, Q. Terpolymerization of Carbon Dioxide with Propylene Oxide and ε-Caprolactone: Synthesis, Characterization and Biodegradability. *Polym. Bull.* **2006**, *56*, 53–62.

(62) Liu, Y.; Huang, K.; Peng, D.; Wu, H. Synthesis, characterization and hydrolysis of an aliphatic polycarbonate by terpolymerization of carbon dioxide, propylene oxide and maleic anhydride. *Polymer* **2006**, *47*, 8453–8461.

(63) Song, P.; Shang, Y.; Chong, S.; Zhu, X.; Xu, H.; Xiong, Y. Synthesis and characterization of amino-functionalized poly(propylene carbonate). *RSC Adv.* **2015**, *5*, 32092–32095.

(64) Tong, Y.; Cheng, R.; Yu, L.; Liu, B. New strategies for synthesis of amino-functionalized poly(propylene carbonate) over SalenCo (III) Cl catalyst. *J. Polym. Sci.* **2020**, *58*, 1325–1337.

(65) Koning, C.; Wildeson, J.; Parton, R.; Plum, B.; Steeman, P.; Darensbourg, D. Synthesis and physical characterization of poly(cyclohexane carbonate), synthesized from CO_2 and cyclohexene oxide. *Polymer* **2001**, *42*, 3995–4004.

(66) Sulley, G. S.; Gregory, G. L.; Chen, T. T. D.; Peña Carrodeguas, L.; Trott, G.; Santmarti, A.; Lee, K.-Y.; Terrill, N. J.; Williams, C. K. Switchable Catalysis Improves the Properties of CO_2-Derived Polymers: Poly(cyclohexene carbonate-b-ε-decalactone-b-cyclohexene carbonate) Adhesives, Elastomers, and Toughened Plastics. *J. Am. Chem. Soc.* **2020**, *142*, 4367–4378.

(67) Yang, G.-W.; Wu, G.-P. High-Efficiency Construction of CO_2 -Based Healable Thermoplastic Elastomers via a Tandem Synthetic Strategy. *ACS Sustain. Chem. Eng.* **2019**, *7*, 1372–1380.

(68) Zhu, Y.; Romain, C.; Williams, C. K. Sustainable polymers from renewable resources. *Nature* **2016**, *540*, 354–362.

(69) Della Monica, F.; Kleij, A. W. From terpenes to sustainable and functional polymers. *Polym. Chem.* **2020**, *11*, 5109–5127.

(70) Byrne, C. M.; Allen, S. D.; Lobkovsky, E. B.; Coates, G. W. Alternating copolymerization of limonene oxide and carbon dioxide. *J. Am. Chem. Soc.* **2004**, *126*, 11404–11405.

(71) Carrodeguas, L. P.; Chen, T. T. D.; Gregory, G. L.; Sulley, G. S.; Williams, C. K. High elasticity, chemically recyclable, thermoplastics from bio-based monomers: carbon dioxide, limonene oxide and ε-decalactone. *Green Chem.* **2020**, *22*, 8298–8307.

(72) Martín, C.; Kleij, A. W. Terpolymers Derived from Limonene Oxide and Carbon Dioxide: Access to Cross-Linked Polycarbonates with Improved Thermal Properties. *Macromolecules* **2016**, *49*, 6285–6295.

(73) Neumann, S.; Leitner, L.-C.; Schmalz, H.; Agarwal, S.; Greiner, A. Unlocking the Processability and Recyclability of Biobased Poly(limonene carbonate). *ACS Sustain. Chem. Eng.* **2020**, *8*, 6442–6448.

(74) Parrino, F.; Fidalgo, A.; Palmisano, L.; Ilharco, L. M.; Pagliaro, M.; Ciriminna, R. Polymers of Limonene Oxide and Carbon Dioxide: Polycarbonates of the Solar Economy. *ACS Omega* **2018**, *3*, 4884–4890.

(75) Stößer, T.; Li, C.; Unruangsri, J.; Saini, P. K.; Sablong, R. J.; Meier, M. A. R.; Williams, C. K.; Koning, C. Bio-derived polymers for coating applications: comparing poly(limonene carbonate) and poly(cyclohexadiene carbonate). *Polym. Chem.* **2017**, *8*, 6099–6105.

(76) Hauenstein, O.; Agarwal, S.; Greiner, A. Bio-based polycarbonate as synthetic toolbox. *Nat. Commun.* **2016**, *7*, 11862.

(77) Wambach, A.; Agarwal, S.; Greiner, A. Synthesis of Biobased Polycarbonate by Copolymerization of Menth-2-ene Oxide and CO_2 with Exceptional Thermal Stability. *ACS Sustain. Chem. Eng.* **2020**, *8*, 14690–14693.

(78) Zhang, Y.-Y.; Zhang, X.-H.; Wei, R.-J.; Du, B.-Y.; Fan, Z.-Q.; Qi, G.-R. Synthesis of fully alternating polycarbonate with low T g from carbon dioxide and bio-based fatty acid. *RSC Adv* **2014**, *4*, 36183–36188.

(79) Johann, T.; Houck, H. A.; Dinh, T.; Kemmer-Jonas, U.; Du Prez, F. E.; Frey, H. Multi-olefin containing polyethers and triazolinediones: a powerful alliance. *Polym. Chem.* **2019**, *10*, 4699–4708.

(80) Gardiner, C.; Schüttner, S.; Petrov, F.; Floudas, G.; Frey, H. Biobased thermoplastic elastomers based on citronellol glycidyl ether, CO_2 and polylactide. *to be submitted* **2021**.

(81) Rubulotta, G.; Quadrelli, E. A. Terpenes: A Valuable Family of Compounds for the Production of Fine Chemicals. *Horizons in Sustainable Industrial Chemistry and Catalysis*; Studies in Surface Science and Catalysis; Elsevier, 2019; pp 215–229.

(82) Mosquera, M. E. G.; Jiménez, G.; Tabernero, V.; Vinueza-Vaca, J.; García-Estrada, C.; Kosalková, K.; Sola-Landa, A.; Monje, B.; Acosta, C.; Alonso, R.*; et al.* Terpenes and Terpenoids: Building Blocks to Produce Biopolymers. *Sustain. Chem.* **2021**, *2*, 467–492.

(83) Moser, S.; Pichler, H. Identifying and engineering the ideal microbial terpenoid production host. *Appl. Microbiol. Biotechnol.* **2019**, *103*, 5501–5516.

(84) Wang, Y.; Fan, J.; Darensbourg, D. J. Construction of Versatile and Functional Nanostructures Derived from CO_2 -based Polycarbonates. *Angew. Chem.* **2015**, *127*, 10344–10348.

(85) Luo, W.; Deng, K.; Wang, S.; Ren, S.; Han, D.; Wang, Y.; Xiao, M.; Meng, Y. A Novel Gel Polymer Electrolyte by Thiol-Ene Click Reaction Derived from CO_2 -Based Polycarbonate for Lithium-Ion Batteries. *Adv. Polym. Technol.* **2020**, *2020*, 1–12.

(86) Bhat, G. A.; Rashad, A. Z.; Folsom, T. M.; Darensbourg, D. J. Placing Single-Metal Complexes into the Backbone of CO_2 -Based Polycarbonate Chains, Construction of Nanostructures for Prospective Micellar Catalysis. *Organometallics* **2020**, *39*, 1612–1618.

(87) Bhat, G. A.; Rashad, A. Z.; Darensbourg, D. J. Synthesis of terpyridine-containing polycarbonates with post polymerization providing water-soluble and micellar polymers and their metal complexes. *Polym. Chem.* **2020**, *11*, 4699–4705.

(88) Geschwind, J.; Frey, H. Poly(1,2-glycerol carbonate): A Fundamental Polymer Structure Synthesized from CO_2 and Glycidyl Ethers. *Macromolecules* **2013**, *46*, 3280–3287.

(89) Hilf, J.; Phillips, A.; Frey, H. Poly(carbonate) copolymers with a tailored number of hydroxyl groups from glycidyl ethers and CO_2. *Polym. Chem.* **2014**, *5*, 814–818.

(90) Noshay, A.; McGrath, J. E. *Block Copolymers: Overview and Critical Survey*; Elsevier Science: Burlington, 1977.

(91) Darensbourg, D. J.; Yeung, A. D. A concise review of computational studies of the carbon dioxide–epoxide copolymerization reactions. *Polym. Chem.* **2014**, *5*, 3949–3962.

(92) Darensbourg, D. J.; Poland, R. R.; Strickland, A. L. (Salan)CrCl, an effective catalyst for the copolymerization and terpolymerization of epoxides and carbon dioxide. *J. Polym. Sci. A Polym. Chem.* **2012**, *50*, 127–133.

(93) Ren, W.-M.; Zhang, X.; Liu, Y.; Li, J.-F.; Wang, H.; Lu, X.-B. Highly Active, Bifunctional Co(III)-Salen Catalyst for Alternating Copolymerization of CO_2 with Cyclohexene Oxide and Terpolymerization with Aliphatic Epoxides. *Macromolecules* **2010**, *43*, 1396–1402.

(94) Shi, L.; Lu, X.-B.; Zhang, R.; Peng, X.-J.; Zhang, C.-Q.; Li, J.-F.; Peng, X.-M. Asymmetric Alternating Copolymerization and Terpolymerization of Epoxides with Carbon Dioxide at Mild Conditions. *Macromolecules* **2006**, *39*, 5679–5685.

(95) Seong, J. E.; Na, S. J.; Cyriac, A.; Kim, B.-W.; Lee, B. Y. Terpolymerizations of CO_2, Propylene Oxide, and Various Epoxides Using a Cobalt(III) Complex of Salen-Type Ligand Tethered by Four Quaternary Ammonium Salts. *Macromolecules* **2010**, *43*, 903–908.

(96) Reiter, M.; Vagin, S.; Kronast, A.; Jandl, C.; Rieger, B. A Lewis acid β-diiminato-zinc-complex as all-rounder for co- and terpolymerisation of various epoxides with carbon dioxide. *Chem. Sci.* **2017**, *8*, 1876–1882.

(97) Gu, L.; Qin, Y.; Gao, Y.; Wang, X.; Wang, F. Hydrophilic CO_2 -based biodegradable polycarbonates: Synthesis and rapid thermo-responsive behavior. *J. Polym. Sci. A Polym. Chem.* **2013**, *51*, 2834–2840.

(98) Lazzari, M.; Torneiro, M. A Global View on Block Copolymers. *Polymers* **2020**, *12*, 869.

(99) Feng, H.; Lu, X.; Wang, W.; Kang, N.-G.; Mays, J. W. Block Copolymers: Synthesis, Self-Assembly, and Applications. *Polymers* **2017**, *9*, 494.

(100) Alexandridis, P.; Lindman, B. *Amphiphilic block copolymers: Self-assembly and applications*, 1. ed.; Elsevier: Amsterdam, 2000.

(101) Xiong, X.-B.; Binkhathlan, Z.; Molavi, O.; Lavasanifar, A. Amphiphilic block co-polymers: preparation and application in nanodrug and gene delivery. *Acta Biomater.* **2012**, *8*, 2017–2033.

(102) Lv, S.; Wu, Y.; Cai, K.; He, H.; Li, Y.; Lan, M.; Chen, X.; Cheng, J.; Yin, L. High Drug Loading and Sub-Quantitative Loading Efficiency of Polymeric Micelles Driven by Donor-Receptor Coordination Interactions. *J. Am. Chem. Soc.* **2018**, *140*, 1235–1238.

(103) Li, J.; Huo, M.; Wang, J.; Zhou, J.; Mohammad, J. M.; Zhang, Y.; Zhu, Q.; Waddad, A. Y.; Zhang, Q. Redox-sensitive micelles self-assembled from amphiphilic hyaluronic acid-deoxycholic acid conjugates for targeted intracellular delivery of paclitaxel. *Biomaterials* **2012**, *33*, 2310–2320.

(104) Gu, L.; Faig, A.; Abdelhamid, D.; Uhrich, K. Sugar-based amphiphilic polymers for biomedical applications: from nanocarriers to therapeutics. *Acc. Chem. Res.* **2014**, *47*, 2867–2877.

(105) Cai, K.; He, X.; Song, Z.; Yin, Q.; Zhang, Y.; Uckun, F. M.; Jiang, C.; Cheng, J. Dimeric drug polymeric nanoparticles with exceptionally high drug loading and quantitative loading efficiency. *J. Am. Chem. Soc.* **2015**, *137*, 3458–3461.

(106) Fuguet, E.; Ràfols, C.; Rosés, M.; Bosch, E. Critical micelle concentration of surfactants in aqueous buffered and unbuffered systems. *Analytica Chimica Acta* **2005**, *548*, 95–100.

(107) Leibler, L.; Orland, H.; Wheeler, J. C. Theory of critical micelle concentration for solutions of block copolymers. *The Journal of Chemical Physics* **1983**, *79*, 3550–3557.

(108) Williams, R. J.; Phillips, J. N.; Mysels, K. J. The critical micelle concentration of sodium lauryl sulphate at 25° C. *Trans. Faraday Soc.* **1955**, *51*, 728–737.

(109) Scharfenberg, M.; Wald, S.; Wurm, F. R.; Frey, H. Acid-Labile Surfactants Based on Poly(ethylene glycol), Carbon Dioxide and Propylene Oxide: Miniemulsion Polymerization and Degradation Studies. *Polymers* **2017**, *9*, 422.

(110) Hilf, J.; Schulze, P.; Frey, H. CO_2 -Based Non-ionic Surfactants: Solvent-Free Synthesis of Poly(ethylene glycol)- block -Poly(propylene carbonate) Block Copolymers. *Macromol. Chem. Phys.* **2013**, *214*, 2848–2855.

(111) Kunze, L.; Tseng, S.-Y.; Schweins, R.; Sottmann, T.; Frey, H. Nonionic Aliphatic Polycarbonate Diblock Copolymers Based on CO_2, 1,2-Butylene Oxide, and mPEG: Synthesis, Micellization, and Solubilization. *Langmuir* **2019**, *35*, 5221–5231.

(112) Augustine, D.; Hadjichristidis, N.; Gnanou, Y.; Feng, X. Hydrophilic Stars, Amphiphilic Star Block Copolymers, and Miktoarm Stars with Degradable Polycarbonate Cores. *Macromolecules* **2020**, *53*, 895–904.

(113) Liu, G.-L.; Wu, H.-W.; Lin, Z.-I.; Liao, M.-G.; Su, Y.-C.; Chen, C.-K.; Ko, B.-T. Synthesis of functional CO_2 -based polycarbonates via dinuclear nickel nitrophenolate-based catalysis for degradable surfactant and drug-loaded nanoparticle applications. *Polym. Chem.* **2021**, *12*, 1244–1259.

(114) Liu, Y.; Deng, K.; Wang, S.; Xiao, M.; Han, D.; Meng, Y. A novel biodegradable polymeric surfactant synthesized from carbon dioxide, maleic anhydride and propylene epoxide. *Polym. Chem.* **2015**, *6*, 2076–2083.

(115) Darensbourg, D. J.; Tsai, F.-T. Postpolymerization Functionalization of Copolymers Produced from Carbon Dioxide and 2-Vinyloxirane: Amphiphilic/Water-Soluble CO_2 -Based Polycarbonates. *Macromolecules* **2014**, *47*, 3806–3813.

(116) Li, Y.; Liu, S.; Zhao, X.; Wang, Y.; Liu, J.; Wang, X.; Lu, L. CO_2-based amphiphilic polycarbonate micelles enable a reliable and efficient platform for tumor imaging. *Theranostics* **2017**, *7*, 4689–4698.

(117) Chang, H.; Li, C.; Huang, R.; Su, R.; Qi, W.; He, Z. Amphiphilic hydrogels for biomedical applications. *J. Mater. Chem. B* **2019**, *7*, 2899–2910.

(118) Brook, M. G. Thermoplastic hydrogels. *Brit. Poly. J.* **1990**, *23*, 257–259.

(119) Gong, C.; Shi, S.; Wu, L.; Gou, M.; Yin, Q.; Guo, Q.; Dong, P.; Zhang, F.; Luo, F.; Zhao, X.*; et al.* Biodegradable in situ gel-forming controlled drug delivery system based on thermosensitive PCL-PEG-PCL hydrogel. Part 2: sol-gel-sol transition and drug delivery behavior. *Acta Biomater.* **2009**, *5*, 3358–3370.

(120) Ma, G.; Miao, B.; Song, C. Thermosensitive PCL-PEG-PCL hydrogels: Synthesis, characterization, and delivery of proteins. *J. Appl. Polym. Sci.* **2010**, *37*, NA-NA.

(121) Zhang, Y.; Wu, X.; Han, Y.; Mo, F.; Duan, Y.; Li, S. Novel thymopentin release systems prepared from bioresorbable PLA-PEG-PLA hydrogels. *International journal of pharmaceutics* **2010**, *386*, 15–22.

(122) Cui, H.; Shao, J.; Wang, Y.; Zhang, P.; Chen, X.; Wei, Y. PLA-PEG-PLA and its electroactive tetraaniline copolymer as multi-interactive injectable hydrogels for tissue engineering. *Biomacromolecules* **2013**, *14*, 1904–1912.

(123) Cohn, D.; Hotovely-Salomon, A. Biodegradable multiblock PEO/PLA thermoplastic elastomers: molecular design and properties. *Polymer* **2005**, *46*, 2068–2075.

(124) Manavitehrani, I.; Fathi, A.; Wang, Y.; Maitz, P. K.; Dehghani, F. Reinforced Poly(Propylene Carbonate) Composite with Enhanced and Tunable Characteristics, an Alternative for Poly(lactic Acid). *ACS applied materials & interfaces* **2015**, *7*, 22421–22430.

(125) Fu, K.; Pack, D. W.; Klibanov, A. M.; Langer, R. Visual evidence of acidic environment within degrading poly(lactic-co-glycolic acid) (PLGA) microspheres. *Pharmaceutical Research* **2000**, *17*, 100–106.

(126) Tinsley-Bown, A.; Fretwell, R.; Dowsett, A.; Davis, S.; Farrar, G. H. Formulation of poly(d,l-lactic-co-glycolic acid) microparticles for rapid plasmid DNA delivery. *Journal of Controlled Release* **2000**, *66*, 229–241.

(127) Walter, E.; Moelling, K.; Pavlovic, J.; Merkle, H. P. Microencapsulation of DNA using poly(dl-lactide-co-glycolide): stability issues and release characteristics. *Journal of Controlled Release* **1999**, *61*, 361–374.

(128) Yoon, S. J.; Kim, S. H.; Ha, H. J.; Ko, Y. K.; So, J. W.; Kim, M. S.; Yang, Y. I.; Khang, G.; Rhee, J. M.; Lee, H. B. Reduction of inflammatory reaction of poly(d,l-lactic-co-glycolic Acid) using demineralized bone particles. *Tissue engineering. Part A* **2008**, *14*, 539–547.

(129) Zhang, Z.; Kuijer, R.; Bulstra, S. K.; Grijpma, D. W.; Feijen, J. The in vivo and in vitro degradation behavior of poly(trimethylene carbonate). *Biomaterials* **2006**, *27*, 1741–1748.

(130) Brannigan, R. P.; Dove, A. P. Synthesis, properties and biomedical applications of hydrolytically degradable materials based on aliphatic polyesters and polycarbonates. *Biomaterials science* **2016**, *5*, 9–21.

(131) Hirschberg, V.; Faust, L.; Rodrigue, D.; Wilhelm, M. Effect of Topology and Molecular Properties on the Rheology and Fatigue Behavior of Solid Polystyrene/Polyisoprene Di- and Triblock Copolymers. *Macromolecules* **2020**, *53*, 5572–5587.

(132) Matsen, M. W.; Thompson, R. B. Equilibrium behavior of symmetric ABA triblock copolymer melts. *The Journal of Chemical Physics* **1999**, *111*, 7139–7146.

(133) Abu-Sharkh, B.; AlSunaidi, A. Morphology and Conformation Analysis of Self-Assembled Triblock Copolymer Melts. *Macromol. Theory Simul.* **2006**, *15*, 507–515.

(134) Spontak, R. J.; Patel, N. P. Thermoplastic elastomers: fundamentals and applications. *Current Opinion in Colloid & Interface Science* **2000**, *5*, 333–340.

(135) Legge, N. R. Thermoplastic Elastomers. *Rubber Chemistry and Technology* **1987**, *60*, 83–117.

(136) BATES, F. S. Polymer-polymer phase behavior. *Science (New York, N.Y.)* **1991**, *251*, 898–905.

(137) *The Physics of Block Copolymers Oxford Univ*, 1998.

(138) Goldacker, T.; Abetz, V.; Stadler, R.; Erukhimovich, I.; Leibler, L. Non-centrosymmetric superlattices in block copolymer blends. *Nature* **1999**, *398*, 137–139.

(139) Zhang, Y.; Wiesner, U. Rheology of lamellar polystyrene-block-polyisoprene diblock copolymers. *Macromol. Chem. Phys.* **1998**, *199*, 1771–1784.

(140) Heck, M.; Schneider, L.; Müller, M.; Wilhelm, M. Diblock Copolymers with Similar Glass Transition Temperatures in Both Blocks for Comparing Shear Orientation Processes with DPD Computer Simulations. *Macromol. Chem. Phys.* **2018**, *219*, 1700559.

(141) Langela, M.; Wiesner, U.; Spiess, H. W.; Wilhelm, M. Microphase Reorientation in Block Copolymer Melts As Detected via FT Rheology and 2D SAXS. *Macromolecules* **2002**, *35*, 3198–3204.

(142) Khandpur, A. K.; Foerster, S.; Bates, F. S.; Hamley, I. W.; Ryan, A. J.; Bras, W.; Almdal, K.; Mortensen, K. Polyisoprene-Polystyrene Diblock Copolymer Phase Diagram near the Order-Disorder Transition. *Macromolecules* **1995**, *28*, 8796–8806.

(143) Oelschlaeger, C.; Gutmann, J. S.; Wolkenhauer, M.; Spiess, H.-W.; Knoll, K.; Wilhelm, M. Kinetics of Shear Microphase Orientation and Reorientation in Lamellar Diblock and Triblock Copolymer Melts as Detected via FT-Rheology and 2D-SAXS. *Macromolecular Chemistry and Physics* **2007**, *208*, 1719–1729.

(144) Hadjichristidis, N.; Hirao, A.; Tezuka, Y.; Du Prez, F. *Complex macromolecular architectures: Synthesis, characterization, and self-assembly*, 1. ed.; Wiley (Asia): Singapore, 2011.

(145) Kember, M. R.; Buchard, A.; Williams, C. K. Catalysts for CO_2/epoxide copolymerisation. *Chem. Commun. (Camb)* **2011**, *47*, 141–163.

(146) Yang, G.-W.; Wu, G.-P. High-Efficiency Construction of CO_2 -Based Healable Thermoplastic Elastomers via a Tandem Synthetic Strategy. *ACS Sustain. Chem. Eng.* **2019**, *7*, 1372–1380.

(147) Sulley, G. S.; Gregory, G. L.; Chen, T. T. D.; Peña Carrodeguas, L.; Trott, G.; Santmarti, A.; Lee, K.-Y.; Terrill, N. J.; Williams, C. K. Switchable Catalysis Improves the Properties of CO_2-Derived Polymers: Poly(cyclohexene carbonate-b-ε-decalactone-b-cyclohexene carbonate) Adhesives, Elastomers, and Toughened Plastics. *J. Am. Chem. Soc.* **2020**, *142*, 4367–4378.

(148) Neumann, S.; Däbritz, S. B.; Fritze, S. E.; Leitner, L.-C.; Anand, A.; Greiner, A.; Agarwal, S. Sustainable block copolymers of poly(limonene carbonate). *Polym. Chem.* **2021**, *12*, 903–910.

(149) Bailer, J.; Feth, S.; Bretschneider, F.; Rosenfeldt, S.; Drechsler, M.; Abetz, V.; Schmalz, H.; Greiner, A. Synthesis and self-assembly of biobased poly(limonene carbonate)- block -poly(cyclohexene carbonate) diblock copolymers prepared by sequential ring-opening copolymerization. *Green Chem.* **2019**, *21*, 2266–2272.

(150) Darensbourg, D. J. Comments on the depolymerization of polycarbonates derived from epoxides and carbon dioxide: A mini review. *Polym. Degrad. Stab.* **2018**, *149*, 45–51.

(151) Bentley, R. W. Global oil & gas depletion: an overview. *Energy Policy* **2002**, *30*, 189–205.

(152) Liu, Q.; Wu, L.; Jackstell, R.; Beller, M. Using carbon dioxide as a building block in organic synthesis. *Nat. Commun.* **2015**, *6*, 5933.

(153) Mwanza, B. G.; Mbohwa, C. Major Obstacles to Sustainability in the Plastic Industry. *Procedia Manuf.* **2017**, *8*, 121–128.

CHAPTER 2.1

Addressing a Key Challenge of CO_2-Based Polycarbonates: Low Glass Transition Capitalizing on Citronellol Glycidyl Ether

CHAPTER 2.1

Addressing a Key Challenge of CO_2-Based Polycarbonates: Low Glass Transition Capitalizing on Citronellol Glycidyl Ether

Christina Gardiner[a], Tobias Johann[a], Andreas Hanewald[b], Holger Frey[a,*]

[a] Institute of Organic Chemistry, Duesbergweg 10-14, Johannes Gutenberg University Mainz, 55128 Mainz, Germany.

[b] Department of Physics at Interfaces, Ackermannweg 10, Max Planck Institute for Polymer Research, 55128 Mainz, Germany.

To be submitted.

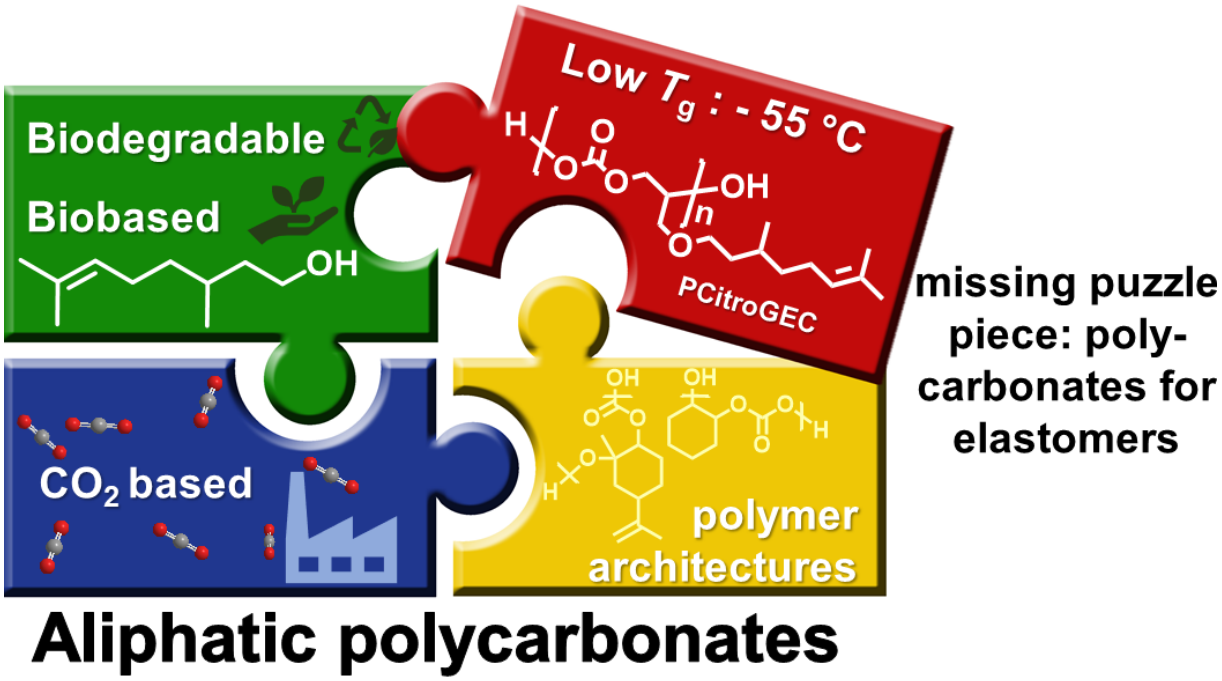

ABSTRACT

A new type of bio-based aliphatic polycarbonate based on CO_2 with an exceptionally low glass transition temperature of T_g = -55 °C is introduced, which is relevant for (thermoplastic) elastomers based on aliphatic polycarbonates. A variety of copolymers was synthesized *via* cobalt-salen catalysis from citronellol glycidyl ether (CitroGE) and carbon dioxide. In-depth characterization based on NMR, IR-spectroscopy, MALDI-ToF and SEC revealed apparent molar masses of 4 600 to 18 000 g/mol, which are underestimated due to the long side chains. Furthermore, ABA triblock copolymers consisting of a flexible PCitroGEC midblock and poly cyclohexyl carbonate A-blocks were prepared that form stable free-standing films. In exploratory experiments the α, ω-hydroxyl-functional PCitroGEC homopolymers were additionally employed as flexible chain extenders in an addition reaction with MDI. Moreover, the ene-moiety of the citronellol sidechains enables fast TAD-click modification of the polymers.

INTRODUCTION

In recent years polycarbonates directly synthesized from CO_2 have gained enormous attention due to the excellent availability of CO_2 as a C_1 substrate.[1] In several recent reviews the progress in this growing field was highlighted, particularly in the context of sustainable and degradable polymers.[2–5] Recent progress was achieved by employing bio-based epoxides in combination with CO_2 to generate potentially sustainable and biodegradable polymer materials.[6–14] Besides homopolymers based on polycarbonates also block copolymers and several polymer architectures have been introduced in recent years.[15–20] For many applications, such as thermoplastic elastomers (TPEs), ABA block structures are desirable, combining a "hard" A block (high T_g) and a highly flexible B midblock (low T_g).[21]However, a key obstacle for application of polycarbonates as crosslinked elastomers or as a "soft" segment for a variety of applications is the intermediate glass transition temperature of almost all currently known polycarbonate structures. Several high T_g materials have been introduced with a T_g in a range of 110-120 °C, e.g. poly(cyclohexene oxide carbonate) (PCHC), poly(limonene oxide carbonate) (PLimC) that are considered to possess similarity to polystyrene in their property profile.[20,22,23] Current state-of-the art polycarbonates aiming at low T_gs are the often-used poly(propylene carbonate) (T_g: 28°C) and poly(octene carbonate) (POC) (T_g: -24°C). [24] In a recent work, Jia et al. show ABA triblock copolymers with POC as flexible inner B block and PCHC as a glassy outer A block. The resulting polymers show elastomeric behavior. Additionally they introduced a new polycarbonate from 2-ethylhexyl glycidyl ether with a T_g of -46 °C.[24] Zhang et al. presented a fully biobased aliphatic polycarbonate based on fatty acid with a low T_g of -40 °C.[25] Apart from these polymers no fully aliphatic particularly terpene based polycarbonate structures with a low glass transition below -40 °C have been reported to date. Such structures would be crucial to realize elastomer properties in the typical desired service temperature range. Hence, highly flexible polycarbonates with a glass transition temperature below -40 °C have to be identified to enable the preparation of polycarbonate-based elastomers, TPEs or use as soft segments for polycarbonate-based polyurethanes.

The catalytic synthesis of polycarbonates based on CO_2 relies on the copolymerization with epoxide derivatives. In this work we introduce citronellol glycidyl ether (CitroGE) as a bio-based epoxide monomer for the synthesis of poly(citronellol glycidyl ether carbonate) (PCitroGEC, Scheme 1).

RESULTS AND DISCUSSION

Polymer synthesis and characterization

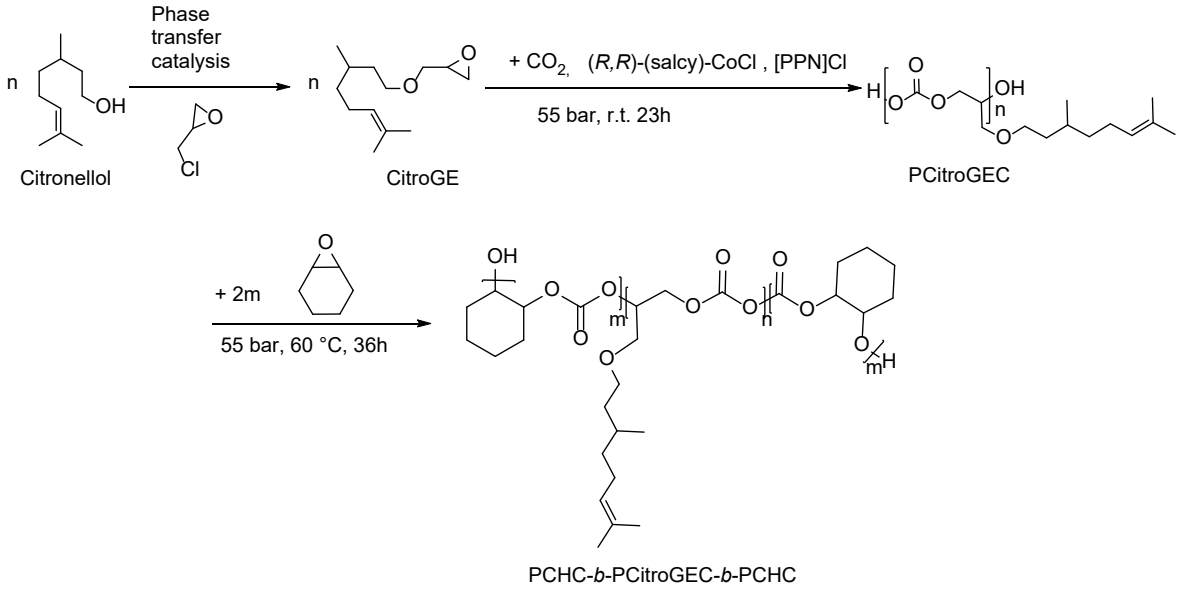

Scheme 1. Synthesis of aliphatic poly(citronellol glycidyl ether carbonate) and PCHC-*b*-PCitroGEC-*b*-PCHC triblock copolymer in a one pot reaction.

Citronellol glycidyl ether can be prepared from citronellol, a mono-terpene that is abundant in plants like roses and lemon grass.[26] CitroGE was prepared according to work previously published by our group.[26,27] All copolymerizations of CO_2 and CitroGE have been performed *via* the established process for the copolymerization of epoxides with CO_2, using (*R,R*)-(salcy)-Co(III)Cl (Co(Salen)Cl) and bis(triphenylphosphine)iminium chloride ([PPN]Cl) as a catalyst system.[28] Successful polymerization with quantitative conversion of CitroGE was confirmed *via* NMR, IR, SEC and MALDI-ToF (Figures S 2-S 14, Table 1). Undesired formation of the thermodynamically favored cyclic carbonates was virtually suppressed by employing low temperatures (r.t) and reaction times of 17-20h. A low content of cyclic carbonates can be confirmed in the IR spectrum of the crude homopolymer. Residual cyclic carbonates can be separated by precipitation in methanol (Figure S 9).

Any metathesis or radical reaction of the double bonds induced by the catalyst was excluded by verifying the integrals of the signals of the ^{1}H NMR spectrum (Figure S 2). This demonstrates the compatibility of the monomer and the Co-Salen catalyst system.

Table 1. Overview of the synthesized homo-PCitroGEC, the PCHC-PCitroGEC block copolymers and the PCitroGEC polyurethanes sample. A complete overview of the synthesized polymers is shown in the Supp. Info. (Table S 1).

Composition	M_n[a]	$Đ$ [a]	yield	T_g/T_m[b]
	g/mol		%	°C
$PCitroGEC_{18}$	4 660	1.09	97	-57/-
$PCitroGEC_{19}$	4 800	1.17	100	-55/-
$PCitroGEC_{20}$	5 000	1.09	100	-57/-
$PCitroGEC_{23}$	5 900	1.11	100	-55/-
$PCitroGEC_{72}$	18 650	1.15	70	-51/-
PCHC-*b*- PCitroGEC -*b*-PCHC	5 100[c]/6 750	1.13/1.17	68	-20/-
$PCitroGEC_{0.5}$ -*co*-$PCHC_{0.5}$	9 500	1.34	93	-2/-
$PCitroGEC_{19}$-MDI-PU	12 080	2.39	100	-40/-34

[a] measured by SEC (Eluent: DMF, standard: PEG). [b] Determined by DSC with a heating rate of 20 °C/min. [c] Molar mass of the PCitroGEC block.

Polymers in the molar mass range of 4 600 – 18 000 g/mol (SEC) (Table 1) with low dispersity of 1.09-1.15 were obtained. The formation of higher molar masses is difficult, which can be explained by the fact that 0.2 mol% of the binary catalyst system is required for activation, which in turn leads to increasing initiation by the chloride of the [PPN]Cl catalyst. Furthermore, we also observed initiation by water traces contained in carbon dioxide. These effects lead to lowering of the molar mass. Experiments with a lower amount of the catalyst and the co-catalyst were conducted, albeit resulting in lower conversion. Therefore, no higher molar masses were obtained (Table S 1, sample 6), which implies that a minimum of 0.2 mol% of the catalyst must be used for the reaction. In order to obtain a higher molar mass of the PCitroGEC a method by Hauenstein et al. was applied (Table S 1, sample 7).[23] The monomer CitroGE was treated with methyl iodide and sodium hydride before employing it in the copolymerization with carbon dioxide. Impurities like hydroxyl groups are masked and cannot act as additional initiators. This leads to double molar mass of the polymer shown in Table 1 and in the SEC trace which is shown in Figure S 26a. To demonstrate that the eluent and the standard have an large impact of the evaluated molar mass, the molar mass for sample 7 was also determined by using THF as eluent and polystyrene (PS) as standard (which is used mostly in the literature for aliphatic polycarbonates).[15,23,24] The resulting molar mass of 42 000 g/mol is illustrated in Figure S 26b. Utilizing different SEC reveals a significant change in the measured molar masses and the modality of the polymers.

Absolute determination of the molar mass *via* NMR end group analysis was not possible, hence SEC analysis was used to estimate the molar mass. Additionally, the molar masses were estimated by using mass spectrometry (MALDI-ToF) for PCitroGEC$_{18}$. The MALDI-ToF spectrum in Figure 1 confirms the structure of the fractionated high molar mass distribution part (~11 000 g/mol) of the PCitroGEC$_{18}$ homopolymer with two hydroxyl end groups and also shows that SEC molar masses (Table 1) are underestimated due to the large side chains. Using these telechelic polymers with two hydroxyl end groups as macroinitiators, triblock copolymers may be synthesized, e.g. by using different lactones as monomers. The mass differences between the signals of 256.36 g/mol (yellow arrow) can be assigned to the molar mass of the repeating unit of the CitroGE/CO_2 repeating unit, confirming the alternating epoxide and CO_2 incorporation. The MALDI-ToF spectra (Figure S 12 and Figure 1) show the different species assigned to the respective distributions. Distribution A) (Figure 1) exhibits the double molar mass (M_n = 11 000 g/mol) of the distributions B, C and D (Figure 1 and Figure S 12). This indicates that the series (A) is initiated by the bifunctional CitroGEC-diol (resulting from hydrolysis with water) (Scheme S 1, A). Figure S 12 shows the low molar mass distribution with half the molar mass (6 000 g/mol), suggesting that these chains were initiated by the chloride of the co-catalyst, which was then substituted with a hydroxyl group (Scheme S 1, B) or the chloride was eliminated *via* the ionization process (Scheme S 1, C)[29]. From the MALDI-ToF we conclude, that both water traces[30,31] and the chloride of the cobalt salen catalyst system can initiate the polymer chains. The chloride can act as a monofunctional initiator and water as a bifunctional initiator, resulting in two distributions (Figure 1, Figure S 12, Scheme S 1). Kember et al. also discussed the initiation of the polymerization by the anion of the catalyst and by water traces.[15] Additionally in a recent work by Jia et al. the initiation by water traces was suppressed by drying CO_2 with tri isobutyl aluminum, which confirms the hypothesis of initiation from residual water traces.[32] Wu et al. further confirmed this mechanism and discussed the bis-hydroxyl end-functional polymers.[31]

To further verify the hypothesis that the higher molar mass distributions are initiated by water traces, a drop of water was deliberately added to the reaction. The resulting monomodal distribution is shown in Figure S 13 at a molar mass of 2 850 g/mol and with a PDI of 1.07. The lower molar mass can be explained by the additional amount of water. Additionally, a MALDI-ToF spectrum was recorded. The distribution A is assigned to the polymers with α,ω–hydroxyl end groups (Figure S 14, A, Scheme S 1, A). The distribution C is assigned to polymers with an ene and a hydroxyl end group (Figure S 14, C, Scheme S 1, C). These results confirm the hypothesis that water-traces lead to the higher molar mass distribution of the synthesized PCitroGEC (Figure 1).

Because of the higher amount of traces of water in the reaction mixture, nearly all polymers are initiated by water and not by the catalyst, which results in an almost monomodal distribution and lower molar mass. Nevertheless, a small amount of the polymer initiated by the chloride of the [PPN]Cl is detectable (Figure S 14).

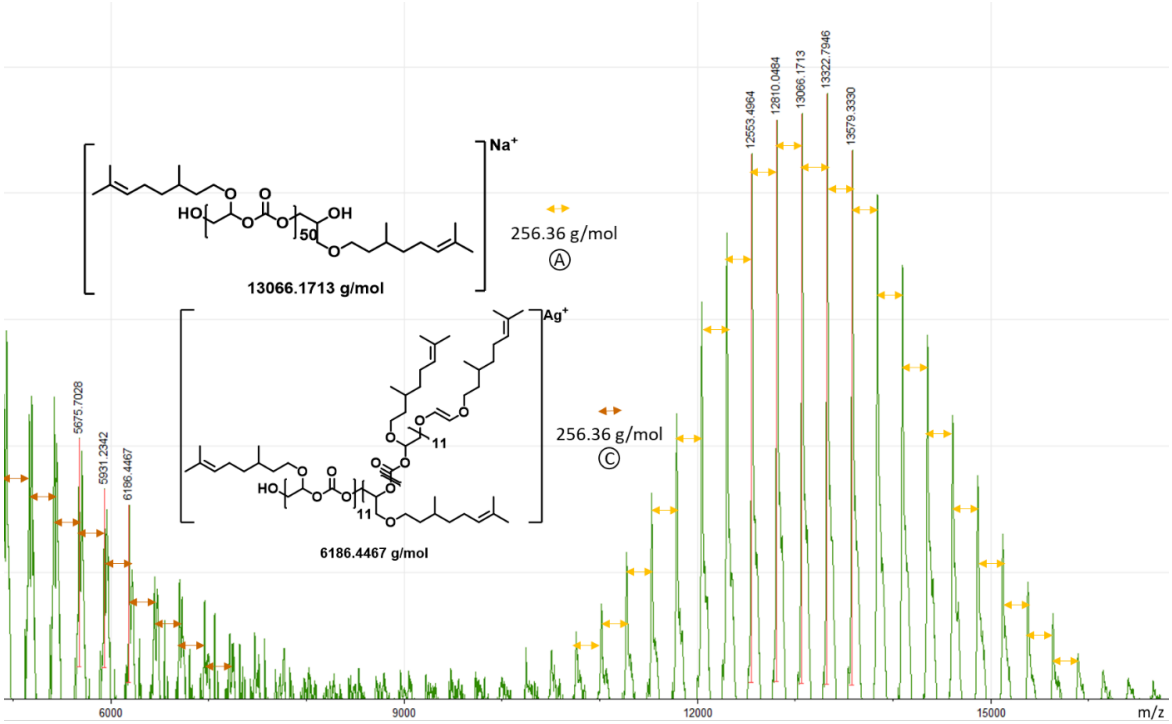

Figure 1: MALDI-ToF MS of PCitroGEC$_{18}$ (DCTB, NaTFA), reflecting the high molar mass distribution of the fractionated sample (the low molar mass distribution part is shown in the Supp. Inf.).

Thermal characterization

Thermal characterization of PCitroGEC *via* DSC reveals an exceptionally low glass transition temperature of the homopolymers of T_g -51 to -57°C (Table 1, Figure S 15). It is an intriguing question, why the T_g of these aliphatic polycarbonates is by far lower than for mostly all related CO_2-based polycarbonate structures reported to date. We tentatively ascribe this flexibility to the following structural characteristics: (i) the aliphatic C_{10} side chain is branched, which impedes ordering and crystallization and (ii) the double bond stereochemistry additionally disturbs ordering. Considering these structural characteristics, the citronellol-based side chain is similar to an oligoisoprene structure, leading to high flexibility and thus low T_g values. An increasing molar mass of PCitroGEC leads to a slightly higher T_g of -51 °C.

PCHC-PCitroGEC copolymers

PCHC-*b*-PCitroGEC-*b*-PCHC triblock copolymers

The low glass transition temperature paves the way for elastomers and block copolymers based on polycarbonates. As a proof of principle, we also synthesized a PCHC-*b*-PCitroGEC-*b*-PCHC triblock copolymer by addition of cyclohexene oxide (CHO) after full conversion of CitroGE in a one pot reaction. One advantage of this synthesis protocol is that no purification of the PCitroGEC block is required. Another feature of the one-pot synthesis is that no homo-PCHC (poly(cyclohexene carbonate)) is formed, because an equilibrium of PCitroGEC initiated by water or the chloride counter ion of the catalyst already exists. This equilibrium leads to a mixture of PCitroGEC-*b*-PCHC di- and PCHC-*b*-PCitroGEC-*b*-PCHC triblock copolymers. The successful polymerization of poly(cyclohexene carbonate) (PCHC) onto activated chain ends of PCitroGEC is proven by the lack of PCitroGEC homopolymer evidenced by DOSY NMR (Figure 2). Together with the absence of PCHC homopolymer (Figure S 17) this confirms the successful formation of the block copolymer. A complete assignment of the NMR signals is shown in the Supporting Information (Figures S 8). This copolymer shows an intermediate glass transition temperature in between PCHC (T_g =120 °C) [22,23] and the PCitroGEC homopolymer (T_g = -55 °C) (Table 1, Figure S 18) at -20 °C (Table 1, Figure S18).This indicates miscibility, since the molar mass of the polymer is not sufficient for microphase separation.[33]

To characterize the mechanical properties of this copolymer a flexible film was prepared *via* solvent evaporation (Figure S 18, (2)). Tensile testing revealed highly stretchable films with a total applicable strain of more than 1200% (Figure S 18, Table S 2). This flexibility can be explained by the higher amount of flexible PCitroGEC in the block copolymer than the rigid PCHC (PCitroGEC = 5 100 g/mol, PCHC = 1 650 g/mol, Table 1). The copolymer films showed merely 2% elastic deformation (ε_{yield}, Table S 2). The low stress ($\leq$ 350 KPa) shows the soft, plastic character (Figure S 18), similar to other polymers with flexible side chains.[34] To further enhance mechanical properties, higher molecular masses of the hard and soft blocks are desired. Work in this direction is in progress.

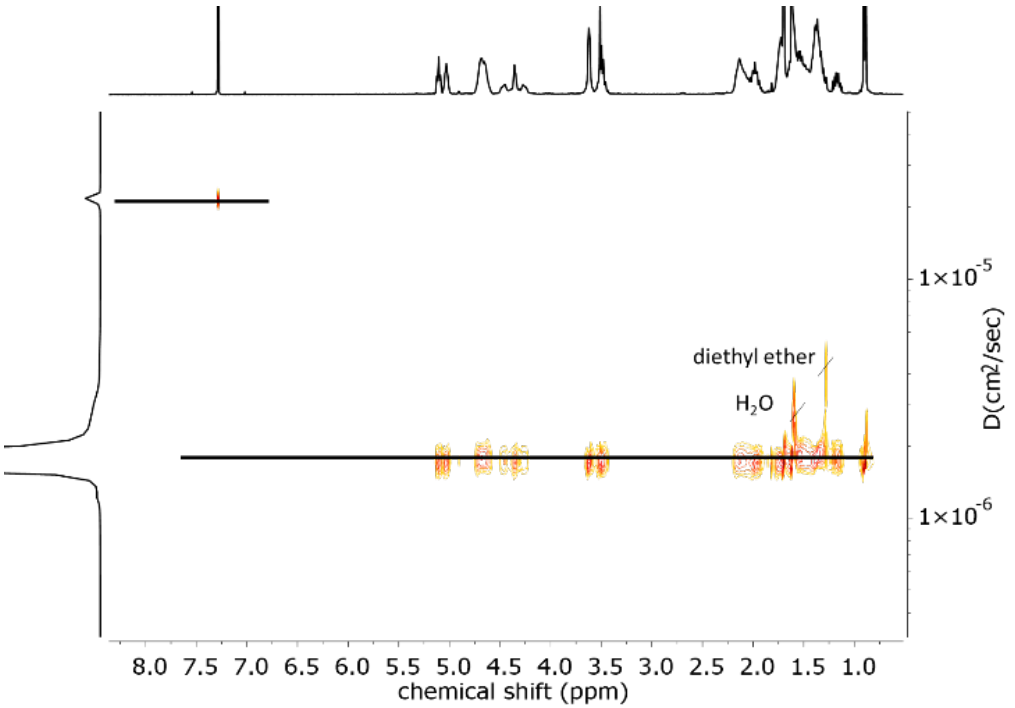

Figure 2: ^{1}H DOSY NMR (400 MHz, $CDCl_3$) of PCHC-*b*- PCitroGEC-*b*-PCHC triblock polymer synthesized in a one-pot reaction.

PCHC-*co*-PCitroGEC terpolymer

To demonstrate the use of the low T_g of the polymer a terpolymer of PCHC and PCitroGEC was synthesized. A polymer with 50 mol% PCHC and 50 mol% PCitroGEC was prepared. The successful terpolymerization was confirmed by NMR and SEC (Figures S 19 and S 20). 50 mol% of PCitroGEC in PCHC decreases the T_g from 120 °C to -2 °. This indicates, that the PCitroGEC could also be used to tailor the T_g of wide used polycarbonates like PCHC.

Post-modifications

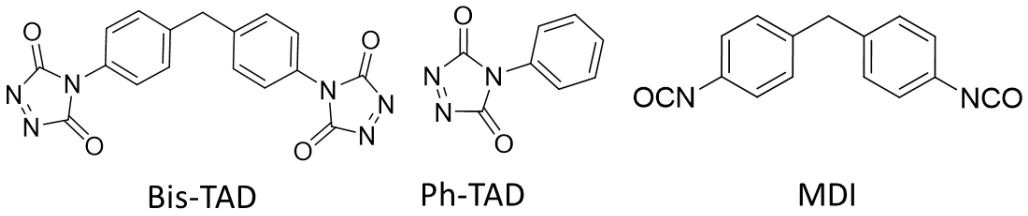

Scheme 2: Structures of the compounds used for post modifications.

Besides the low T_g a peculiar feature of PCitroGEC is its susceptibility to further post-polymerization of the double bond. In recent years, modification of ene-moieties *via* activated (di)enophiles, such as triazolindiones (TADs) has been investigated.[26,35] As a proof of concept the

ene moieties of PCitroGEC$_{20}$ were modified *via* Alder-ene reaction with 4-phenyl-(1,2,4-triazolin-3,5-dione) (Ph-TAD) (Scheme 2), resulting in altered solubility behavior. Additionally, the T_g increased from -57 °C to 24 °C (Figure S 16, S 24-25). These characteristic changes are explained both by hydrogen bonding between the urazole groups and the steric demand of the urazole groups that reduce the flexibility of the polymer.[36]

Using the same modification, crosslinked polymers are available *via* bifunctional 4'-(4,4'-diphenylmethylene)-bis-(1,2,4-triazolin-3,5-dione) (Bis-TAD) (Scheme 2) . The colorless PCitroGEC solution (Figure 3, (1)). and the red solution of Bis-TAD (Figure 3, (2)) formed a colorless organogel within seconds after mixing (Figure 3, (3)).

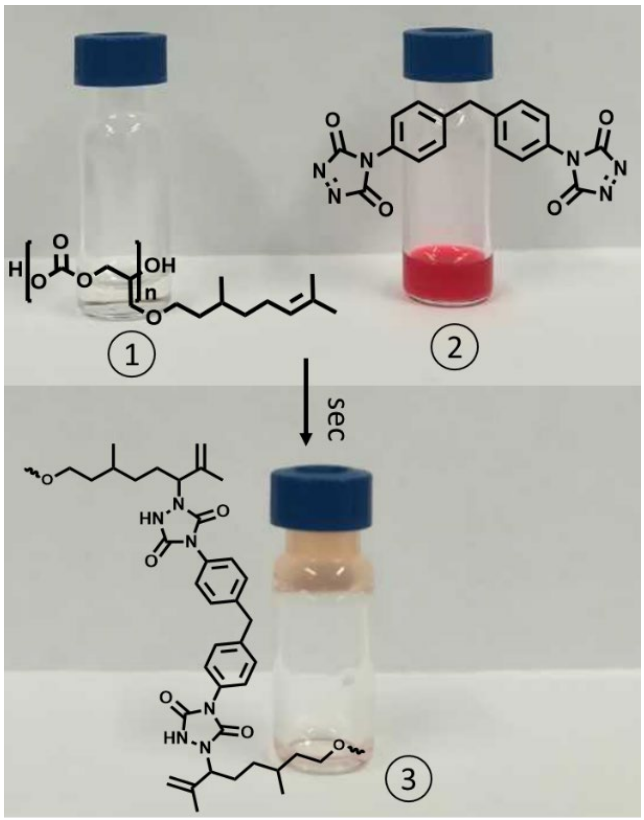

Figure 3: Reaction of PCitroGEC (1) in THF with Bis-TAD (2) in THF resulting in a crosslinked organogel (3).

Using the ene moiety for further post-modification enables tailoring of the polymers. Flexible polyols (like e.g. PPO, T_g = -70 °C)[37] are common industrial precursors for the preparation of polyurethane soft foams. Poly(propylene carbonate) (T_g = 28 °C)[38] is also used in industry as a rather flexible segment in polyurethanes, but there is a lack of polycarbonates with higher flexibility than PPC. To further explore their applicability in this direction, PCitroGEC

homopolymers that exhibit both an α and ω hydroxyl group were coupled *via* addition with 4,4′-methylenebis (phenyl isocyanate) (MDI) (Scheme 2), affording linear polyurethanes with tripled molar mass (12 000 g/mol) of the precursors (Figures S 21, S 22). This polymer does not just show a low T_g at -40 °C. Additionally a melting point at -34 °C can be detected. This small melting point could be caused by the urethane linkage crystallization due to the hydrogen bonds.

CONCLUSION

In summary, aliphatic polycarbonates with a low T_g below - 50 °C are obtained by copolymerization of the partially biobased CitroGE monomer with CO_2, using the common Co-salen catalyst system. This polymer opens manifold perspectives due to the low T_g as well as the ene moiety. The α, ω -hydroxyl groups qualify the material as a bifunctional initiator for different lactones and as a chain extender for diisocyanates, forming polyurethane-based thermoplastic elastomers. A PCHC-*b*-PCitroGEC-*b*-PCitroGEC triblock copolymer was synthesized in a one pot-reaction by sequential monomer addition, using PCitroGEC as an initiator. This polymer showed merely one T_g. The PCitroGEC homopolymer was also utilized as a flexible, biobased polyol alternative of widely used polyethers in a linear polyurethane synthesis. Besides the modification *via* hydroxyl groups, the ene moieties in the side chains were demonstrated to permit additional functionalization. Crosslinked polymers can be formed within several seconds *via* bis-functional TAD reagents. PCitroGEC represents a valuable, partially biobased polycarbonate based on CO_2 with unprecedented flexibility in this class of materials.

EXPERIMENTAL SECTION

Materials

All solvents and reagents were utilized as obtained, unless otherwise stated. Cyclohexene oxide (CHO) was distilled over CaH_2 under reduced pressure prior to use. Carbon dioxide (>99.999%) was purchased from Westfalen AG (Münster, Germany). 4,4'-methylene bis (phenyl isocyanate) (MDI) was obtained from Acros Organics (Pittsburgh, PA, USA). Bis(triphenylphosphine)iminium chloride ([PPN]Cl) was received from abcr GmbH. (*R,R*)-(salcy)-Co(III)Cl was prepared as described by Scharfenberg et al.[1] All solvents were received from Sigma Aldrich, Fischer Chemical (Pittsburgh, PA, USA) and Honeywell (Morris Plaines, NJ, USA) and used without further purification. All reagents were purchased from Sigma Aldrich, Arcos Organics (Pittsburgh, PA, USA), Alfa Aesar (Kandel, Germany) or TCI (Oxford, UK). Deuterated solvents were obtained from Deutero GmBH (Kastellaun, Germany).

Characterization

Nuclear magnetic resonance (NMR)Analysis: ^{1}H NMR spectra at 300 MHz and ^{13}C NMR spectra at 75 MHz were recorded on a Bruker Avance III HD 300 (5 mm BBFO-Head with *z*-gradient) at 23 °C. ^{1}H NMR spectra at 400 MHZ and ^{13}C NMR spectra at 100 MHz were recorded on a Bruker Avance III HD 400 (5 mm BBFO Smartprobe with *z*-gradient) at 23 °C. The spectra are referenced internally to residual proton signal of the deuterated solvent.

Size exclusion chromatography (SEC): SEC was accomplished in DMF (1 mL/min, 50 °C) containing 1 g/L lithium bromide as an additive, using an Agilent 1100 series SEC system equipped with a HEMA 300/100/40 Å column cascade, UV (254 nm) and RI detector. Calibration was performed using poly(ethylene glycol) (PEG) standards obtained from Polymer Standard Service (PSS). SEC measurement were accomplished in THF (1 mL/min, 30°C) on a SDV column set from PSS (SDV 103, SDV 105, SDV 106), equipped with a UV (254 nm) and RI detector Calibration was carried out using polystyrene standards (PSS). Recycling SEC measurements were carried out in $CHCl_3$ (3.5 mL/min, 30°C) on a Jaigel-4H column set from Japan Analytical Industry equipped with UV (254 nm) and RI detector. Calibration was carried out using polystyrene standards (PSS).

Matrix-assisted laser desorption and ionization time-of-flight mass spectrometry (MALDI-ToF): Mass spectra were measured on a MALDI ToF MS Autoflex Max by Bruker. The samples were prepared as a 1 mg/mL solution in dichloromethane. As a matrix *trans*-2-[3-(4-*tert*-Butylphenyl)-

2-methyl-2-propenyliden] malononitrile (DCTB) with NaTFA was used. The measurement was performed in linear modus. The data were analyzed by the *mmass 5.5.0* software.

Infrared spectroscopy (IR): FT-IR spectra were recorded using an iS10 FT-IR spectrometer (Thermo Scientific, Waltham, MA, USA) equipped with a diamond ATR unit.

Dynamic scanning calorimetry (DSC): DSC curves were recorded using a Perkin-Elmer DSC 7 CLN2 instrument in the temperature range of -95°C–200°C or -95 °C–40 °C at heating rates of 20K/min under nitrogen atmosphere.

Tensile Testing: Tensile tests were accomplished by a material testing machine Z005 (Zwick/Roell, Germany). Tensile tests were performed by exposing the stamped polymer stripes to a uniaxial tension. Samples with thicknesses around 0.3 mm were strained at a rate of 20 mm/min at room temperatures. A predefined load of 0.1 N was used. Dependencies of stress versus draw ratio were measured. All films were prepared by slow evaporation from a chloroform solution followed by full removal of the solvent under reduced pressure.

Synthesis

Monomer synthesis

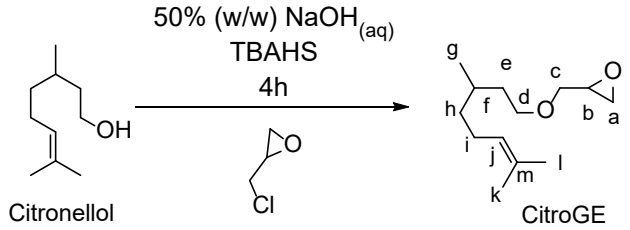

Scheme 3: Synthesis of CitroGE.

Citronellol glycidyl ether (CitroGE) (IUPAC: 2-(((3,7-dimethyloct-6-en-1-yl)oxy)methyl)oxirane) was prepared according to literature[2,3] on a scale of 0.1 mol citronellol. 40% of CitroGE as a colorless liquid was obtained after distillation under high vacuum ($1 \bullet 10^{-3}$ mbar, 80 °C). Before use CitroGE was dried with benzene in an azeotropic distillation. Sample 7 (Table S 1) was treated with methyl iodide and sodium hydride before use. [4]

^{1}H NMR (300 MHz, $CDCl_3$) δ = 5.10 – 5.03 (m, 1H, j), 3.70 – 3.65 (m, 1H, c), 3.57 – 3.42 (m, 2H, d), 3.38 – 3.31 (m, 1H, c'), 3.14 – 3.08 (m, 1H, b), 2.79 – 2.55 (m, 2H, a), 2.04 – 1.85 (m, 2H, i), 1.65 (s, 3H, k), 1.57 (s, 3H, l), 1.42 -1.09 (m, 5H, e+f+h), 0.87 (d, 3H,g) ppm.

Polymer synthesis

Synthesis of PCitroGEC, and PCHC-b-PCitroGEC-b-PCHC polymers

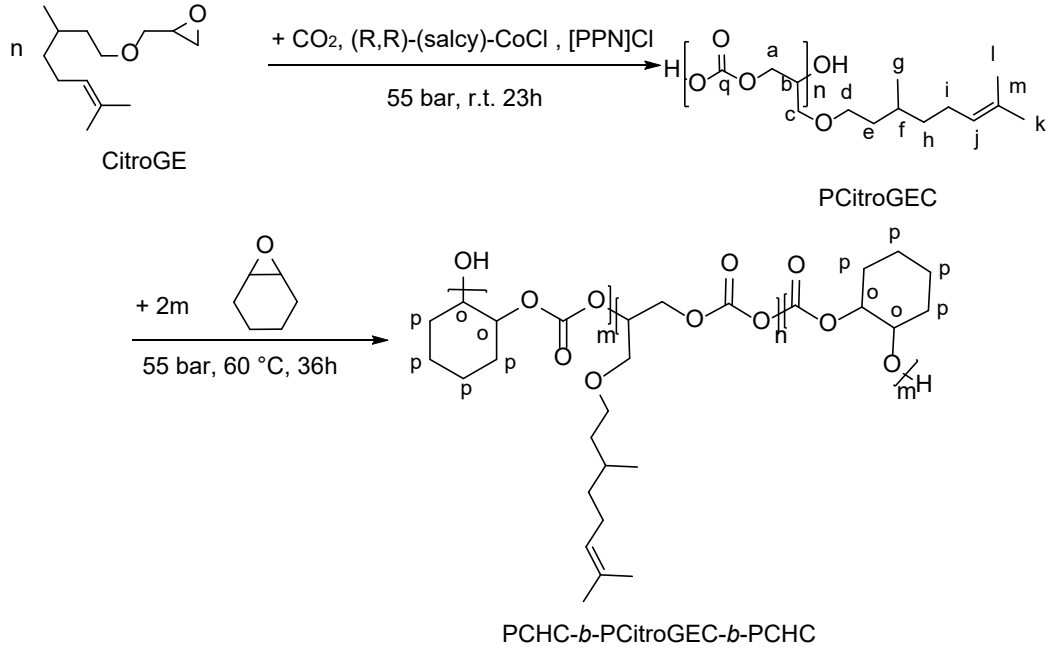

Scheme 4: Synthesis of PCitroGEC homopolymer and PCHC-*b*-PCitroGEC-*b*-PCHC block copolymer.

General procedure illustrated for the synthesis of PCHC-*b*-PCitroGEC-*b*-PCHC (7).

Synthesis: A 100 mL Roth autoclave was dried at 40 °C under reduced pressure. Citronellol glycidyl ether (CitroGE) (0.5 mL, 2.0 mmol), (*R,R*)-(salcy)-CoCl (3.9 mg, 0.006 mmol) and [PPN]Cl (3.4 mg, 0.006 mmol) was filled in the autoclave equipped with a stirring-bar in an inert argon-atmosphere. The reaction mixture was stirred at a carbon dioxide pressure of 55 bar at 20 °C for 23 h. Then CO_2 was released, and the autoclave was filled with argon. A sample was taken under argon atmosphere and CHO (0.9 mL, 8.8 mmol) was injected to the polymer mixture, and the autoclave was refilled with CO_2. The reaction mixture was stirred at a carbon dioxide pressure of 55 bar at 60 °C for additional 36 h.

Purification: The crude product was dissolved in DCM, and the catalyst was deactivated with 1 mL of a solution of 5%$_{vol}$ HCl (aq) in methanol. The product was precipitated in ice-cold methanol as a non-solvent. The precipitated product was collected by centrifugation at 4500 rpm at 0°C for 10 min. The colorless, rubbery solid was then dried under reduced pressure for 24h. A yield of 68 % polymer was obtained.

PCitroGEC homopolymers were purified in analogy to the triblock copolymers. Additionally we used different mol% (regarding to the monomer) to receive different molar masses of the polymers. The used amount of (*R,R*)-(salcy)-CoCl and [PPN]Cl is shown in mol% in Table S 1. In case of sample 1 a drop of water (15.94 mg, 0.93 mmol, 2.15 mol%) was added to the reaction mixture.

PCitroGEC$_{18}$ (Table S 1, sample 2):

^{1}H NMR (300 MHz, $CDCl_3$): δ = 5.16 – 5.06 (m, 1H, j),5.06 – 4.98(m, 1H, b), 4.52 – 4.20 (m, 2H, a), 3.62 (d, 2H, c) 3.55 – 3-43 (m, 2H, d), 2.09 – 1.88 (m, 2H, i), 1.69 (s, 3H, k), 1.61 (s, 3H, l), 1.60 – 1.08 (m, 5H, e+f+h), 0.84 (d, 3H, g) ppm.

^{13}C NMR (75 MHz, $CDCl_3$): δ = 154.36 (Q), 131.26 (M), 124.87 (J), 74.50 (B), 70.28 (D), 68.48 (C), 66.26 (A), 37.36 (E), 36.52 (H), 29.64 (F), 25.84 (I), 25.56 (K), 19.65 (G), 17.78 (L) ppm.

M_n (SEC, DMF, PEG calibration) = 4600 g / mol; $Đ$ (SEC, DMF, PEG calibration) = 1.09.

T_g: -57 °C.

***PCHC-b-PCitroGEC-b-PCHC (Table S 1, sample 7)**:*

^{1}H NMR (300 MHz, $CDCl_3$): δ = 5.16 – 5.06 (m, 1H, j), 4.68 (t, 4H, o), 4.52 – 4.20 (m, 2H, b), 3.62 (d, 2H, c) 3.55 – 3-43 (m, 2H, d), 2.40-2.08 (m, 16H, p), 2.09 – 1.88 (m, 2H, i), 1.69 (s, 3H, k), 1.61 (s, 3H, l), 1.60 – 1.08 (m, 5H, e+f+h), 0.84 (d, 3H, g) ppm.

M_n (SEC, DMF, PEG calibration) = 6750 g / mol; $Đ$ (SEC, DMF, PEG calibration) = 1.17.

T_g: -20 °C.

Post-polymerization modification reactions

Synthesis of PCitroGEC$_{19}$-MDI-PU (Table S 1, sample 8)

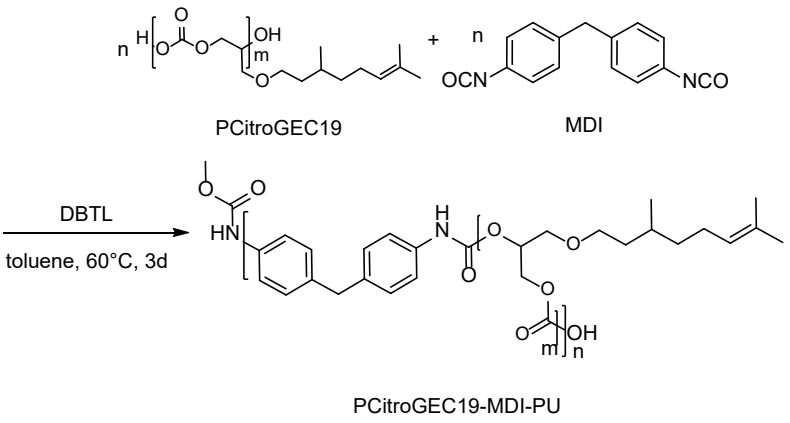

Scheme 5: Polyaddition of PCitroGEC$_{19}$ and MDI.

In a solution of dried PCitroGEC$_{19}$ (0.2 g, 0.042 mmol, 1 eq, (Table S 1, sample 6) in 1 mL dried toluene MDI (0.010 g, 0.042 mmol, 1 eq) was dissolved under an argon atmosphere. A drop of dibutyltin dilaurate (DBTL) was added to the solution and the reaction mixture was stirred and heated to 60 °C for 3 days. After the reaction, the polymer mixture was precipitated in methanol and dried under vacuum.

M_n (SEC, DMF, PEG calibration) = 12 080 g/mol; $Đ$ (SEC, DMF, PEG calibration) = 2.39.

T_g: -40 °C (DSC).

T_m: -34 °C , ΔH_m: 11.86 J/g (DSC).

Modification of PCitroGEC by Phenyl-TAD (Table S1, sample 9)

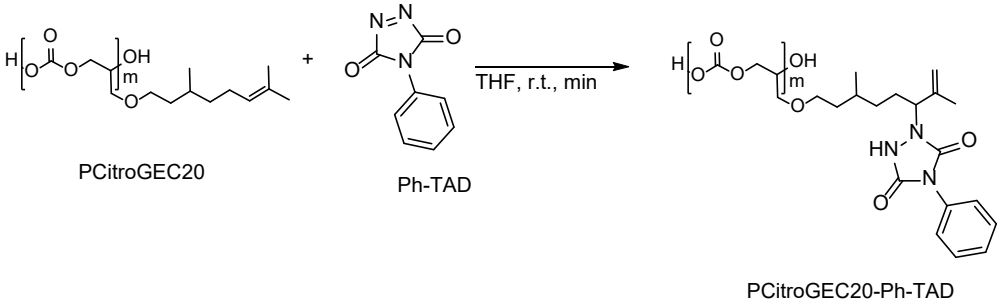

Scheme 6: Reaction of Ph-TAD with PCitroGEC$_{20}$.

PCitroGEC$_{20}$ (30 mg, 0.006 mmol, (Table S 1, sample 4)) was dissolved in 0.5 mL THF. Phenyl-(1,2,4-triazolin-3,5-dione) (Ph-TAD) (27 mg, 0.154 mmol) was dissolved in 1.5 mL THF. The Ph-TAD solution was added dropwise to a stirred PCitroGEC$_{20}$ solution until no imminent color change was detectable anymore. The polymer was precipitated in cold methanol. The product was dried under vacuum. Due to the insolubility of the product in DMF, the SEC characterization for this sample was performed *via* SEC in THF.

M_n (SEC, THF, PS calibration) = 15 100 g/mol; $Đ$ (SEC, THF, PS calibration) = 1.17

T_g: 24 °C

Crosslinking of PCitroGEC with Bis-TAD

4'-(4,4'-diphenylmethylene)-bis-(1,2,4-triazolin-3,5-dione) (Bis-TAD) was prepared according to literature[5] on a scale of 2 g. A pink crystalline powder was obtained (Figure S 23).

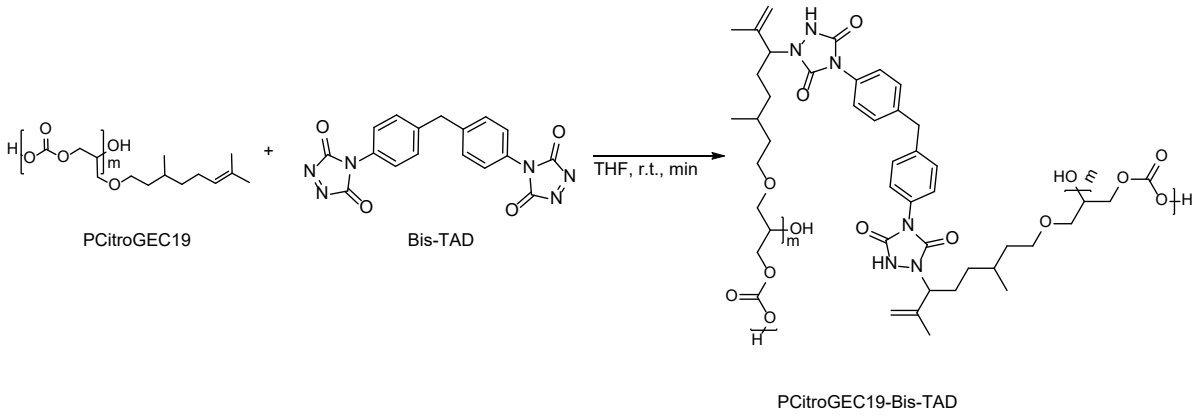

Scheme 7: Crosslinking of PCitroGEC$_{19}$ with Bis-TAD.

PCitroGEC$_{19}$ (34 mg, 0.007 mmol(Table S 1, sample 3)) was dissolved in 0.1 mL THF. Bis-TAD (20 mg, 0.055 mmol) was also dissolved in 0.1 mL THF. The Bis-TAD solution was added to the PCitoGEC$_{19}$ solution and the mixture was shaken three times. Within less than 30 seconds a gel was formed, and the mixture turned increasingly colorless.

ACKNOWLEDGMENT

The authors thank Dr. Kaloian Koynov for tensile test measurements, Monika Schmelzer for SEC measurements, Dr. Elena Berger-Nicoletti for MALDI-ToF measurements, Marcel Fickenscher for design proposals and Philip Dreier and Marvin Steube for valuable discussions.

REFERENCES

(1) Hepburn, C.; Adlen, E.; Beddington, J.; Carter, E. A.; Fuss, S.; Mac Dowell, N.; Minx, J. C.; Smith, P.; Williams, C. K. The technological and economic prospects for CO_2 utilization and removal. Nature 2019, 575, 87–97.

(2) Darensbourg, D. J. Making plastics from carbon dioxide: salen metal complexes as catalysts for the production of polycarbonates from epoxides and CO_2. *Chem. Rev.* **2007**, *107*, 2388–2410.

(3) Coates, G. W.; Moore, D. R. Discrete metal-based catalysts for the copolymerization of CO_2 and epoxides: discovery, reactivity, optimization, and mechanism. *Angew. Chem. Int. Ed. Engl.* **2004**, *43*, 6618–6639.

(4) Kember, M. R.; Buchard, A.; Williams, C. K. Catalysts for CO_2/epoxide copolymerisation. *Chem. Commun. (Camb)* **2011**, *47*, 141–163.

(5) Luinstra, G. Poly(Propylene Carbonate), Old Copolymers of Propylene Oxide and Carbon Dioxide with New Interests: Catalysis and Material Properties. *Polymer Revs.* **2008**, *48*, 192–219.

(6) Hauenstein, O.; Rahman, M. M.; Elsayed, M.; Krause-Rehberg, R.; Agarwal, S.; Abetz, V.; Greiner, A. Biobased Polycarbonate as a Gas Separation Membrane and “Breathing Glass” for Energy Saving Applications. *Adv. Mater. Technol.* **2017**, *2*, 1700026.

(7) Li, C.; Sablong, R. J.; Koning, C. E. Synthesis and characterization of fully-biobased α,ω-dihydroxyl poly(limonene carbonate)s and their initial evaluation in coating applications. *Eur. Polym.* **2015**, *67*, 449–458.

(8) Li, C.; van Berkel, S.; Sablong, R. J.; Koning, C. E. Post-functionalization of fully biobased poly(limonene carbonate)s: Synthesis, characterization and coating evaluation. *Eur. Polym.* **2016**, *85*, 466–477.

(9) Cui, S.; Qin, Y.; Li, Y. Sustainable Approach for the Synthesis of Biopolycarbonates from Carbon Dioxide and Soybean Oil. *ACS Sustainable Chem. Eng.* **2017**, *5*, 9014–9022.

(10) Martín, C.; Kleij, A. W. Terpolymers Derived from Limonene Oxide and Carbon Dioxide: Access to Cross-Linked Polycarbonates with Improved Thermal Properties. *Macromolecules* **2016**, *49*, 6285–6295.

(11) Byrne, C. M.; Allen, S. D.; Lobkovsky, E. B.; Coates, G. W. Alternating copolymerization of limonene oxide and carbon dioxide. *J. Am. Chem. Soc.* **2004**, *126*, 11404–11405.

(12) Firdaus, M.; Montero de Espinosa, L.; Meier, M. A. R. Terpene-Based Renewable Monomers and Polymers via Thiol–Ene Additions. *Macromolecules* **2011**, *44*, 7253–7262.

(13) Zhi, Y.; Shan, X.; Shan, S.; Jia, Q.; Ni, Y.; Zeng, G. Synthesis and thermal degradation kinetics of new terpolymer of carbon dioxide, cyclohexene oxide and alpha-pinene oxide. *J. CO_2 Util.* **2017**, *22*, 299–306.

(14) Song, Y.; Ji, X.; Dong, M.; Li, R.; Lin, Y.-N.; Wang, H.; Wooley, K. L. Advancing the Development of Highly-Functionalizable Glucose-Based Polycarbonates by Tuning of the Glass Transition Temperature. *J. Am. Chem. Soc.* **2018**, *140*, 16053–16057.

(15) Kember, M. R.; Copley, J.; Buchard, A.; Williams, C. K. Triblock copolymers from lactide and telechelic poly(cyclohexene carbonate). *Polym. Chem.* **2012**, *3*, 1196.

(16) Reiter, M.; Kronast, A.; Kissling, S.; Rieger, B. In Situ Generated ABA Block Copolymers from CO_2 , Cyclohexene Oxide, and Poly(dimethylsiloxane)s. *ACS Macro Lett.* **2016**, *5*, 419–423.

(17) Scharfenberg, M.; Seiwert, J.; Scherger, M.; Preis, J.; Susewind, M.; Frey, H. Multiarm Polycarbonate Star Polymers with a Hyperbranched Polyether Core from CO_2 and Common Epoxides. *Macromolecules* **2017**, *50*, 6577–6585.

(18) Geschwind, J.; Wurm, F.; Frey, H. From CO_2 -Based Multifunctional Polycarbonates With a Controlled Number of Functional Groups to Graft Polymers. *Macromol. Chem. Phys.* **2013**, *214*, 892–901.

(19) Yang, G.-W.; Wu, G.-P. High-Efficiency Construction of CO_2 -Based Healable Thermoplastic Elastomers via a Tandem Synthetic Strategy. *ACS Sustainable Chem. Eng.* **2019**, *7*, 1372–1380.

(20) Sulley, G. S.; Gregory, G. L.; Chen, T. T. D.; Peña Carrodeguas, L.; Trott, G.; Santmarti, A.; Lee, K.-Y.; Terrill, N. J.; Williams, C. K. Switchable Catalysis Improves the Properties of CO_2-Derived Polymers: Poly(cyclohexene carbonate-b-ε-decalactone-b-cyclohexene carbonate) Adhesives, Elastomers, and Toughened Plastics. *J. Am. Chem. Soc.* **2020**, *142*, 4367–4378.

(21) Wang, W.; Lu, W.; Goodwin, A.; Wang, H.; Yin, P.; Kang, N.-G.; Hong, K.; Mays, J. W. Recent advances in thermoplastic elastomers from living polymerizations: Macromolecular architectures and supramolecular chemistry. *Prog. Polym. Sci.* **2019**, *95*, 1–31.

(22) Allen, S. D.; Byrne, C. M.; Coates, G. W. Carbon Dioxide as a Renewable C1 Feedstock: Synthesis and Characterization of Polycarbonates from the Alternating Copolymerization of Epoxides and CO_2. In *Feedstocks for the future: Renewables for the production of chemicals and materials*; Bozell, J. J., Ed.; ACS Symposium Series 921; American Chemical Society: Washington, D.C, 2006; pp 116–129.

(23) Hauenstein, O.; Reiter, M.; Agarwal, S.; Rieger, B.; Greiner, A. Bio-based polycarbonate from limonene oxide and CO_2 with high molecular weight, excellent thermal resistance, hardness and transparency. *Green Chem.* **2016**, *18*, 760–770.

(24) Jia, M.; Zhang, D.; Kort, G. W. de; Wilsens, C. H. R. M.; Rastogi, S.; Hadjichristidis, N.; Gnanou, Y.; Feng, X. All-Polycarbonate Thermoplastic Elastomers Based on Triblock Copolymers Derived from Triethylborane-Mediated Sequential Copolymerization of CO_2 with Various Epoxides. *Macromolecules* **2020**, *53*, 5297–5307.

(25) Zhang, Y.-Y.; Zhang, X.-H.; Wei, R.-J.; Du, B.-Y.; Fan, Z.-Q.; Qi, G.-R. Synthesis of fully alternating polycarbonate with low T_g from carbon dioxide and bio-based fatty acid. *RSC Adv* **2014**, *4*, 36183–36188.

(26) Johann, T.; Houck, H. A.; Dinh, T.; Kemmer-Jonas, U.; Du Prez, F. E.; Frey, H. Multi-olefin containing polyethers and triazolinediones: a powerful alliance. *Polym. Chem.* **2019**, *10*, 4699–4708.

(27) Mouzin, G.; Cousse, H.; Rieu, J.-P.; Duflos, A. A Convenient One-Step Synthesis of Glycidyl Ethers. *Synthesis* **1983**, *1983*, 117–119.

(28) Scharfenberg, M.; Hofmann, S.; Preis, J.; Hilf, J.; Frey, H. Rigid Hyperbranched Polycarbonate Polyols from CO_2 and Cyclohexene-Based Epoxides. *Macromolecules* **2017**, *50*, 6088–6097.

(29) Yang, G.-W.; Xu, C.-K.; Xie, R.; Zhang, Y.-Y.; Zhu, X.-F.; Wu, G.-P. Pinwheel-Shaped Tetranuclear Organoboron Catalysts for Perfectly Alternating Copolymerization of CO_2 and Epichlorohydrin. *J. Am. Chem. Soc.* [Online early access]. DOI: 10.1021/jacs.0c12425. Published Online: Feb. 16, 2021.

(30) Darensbourg, D. J.; Wu, G.-P. A one-pot synthesis of a triblock copolymer from propylene oxide/carbon dioxide and lactide: intermediacy of polyol initiators. *Angew. Chem. Int. Ed. Engl.* **2013**, *52*, 10602–10606.

(31) Wu, G.-P.; Darensbourg, D. J. Mechanistic Insights into Water-Mediated Tandem Catalysis of Metal-Coordination CO_2 /Epoxide Copolymerization and Organocatalytic Ring-Opening Polymerization: One-Pot, Two Steps, and Three Catalysis Cycles for Triblock Copolymers Synthesis. *Macromolecules* **2016**, *49*, 807–814.

(32) Jia, M.; Hadjichristidis, N.; Gnanou, Y.; Feng, X. Monomodal Ultrahigh-Molar-Mass Polycarbonate Homopolymers and Diblock Copolymers by Anionic Copolymerization of Epoxides with CO_2. *ACS Macro Lett.* **2019**, *8*, 1594–1598.

(33) Fredrickson, G. H.; Liu, A. J.; Bates, F. S. Entropic Corrections to the Flory-Huggins Theory of Polymer Blends: Architectural and Conformational Effects. *Macromolecules* **1994**, *27*, 2503–2511.

(34) Daniel, W. F. M.; Burdyńska, J.; Vatankhah-Varnoosfaderani, M.; Matyjaszewski, K.; Paturej, J.; Rubinstein, M.; Dobrynin, A. V.; Sheiko, S. S. Solvent-free, supersoft and superelastic bottlebrush melts and networks. *Nature materials* **2016**, *15*, 183–189.

(35) Vlaminck, L.; Bruycker, K. de; Türünç, O.; Du Prez, F. E. ADMET and TAD chemistry: a sustainable alliance. *Polym. Chem.* **2016**, *7*, 5655–5663.

(36) Bica, C. I. D.; Burchard, W.; Stadler, R. Dilute solution properties of polybutadiene modified by 4-phenyl-1,2,4-triazoline-3,5-dione. *Macromol. Chem. Phys.* **1996**, *197*, 3407–3426.

(37) Herzberger, J.; Niederer, K.; Pohlit, H.; Seiwert, J.; Worm, M.; Wurm, F. R.; Frey, H. Polymerization of Ethylene Oxide, Propylene Oxide, and Other Alkylene Oxides: Synthesis, Novel Polymer Architectures, and Bioconjugation. *Chem. Rev.* **2016**, *116*, 2170–2243.

(38) Thorat, S. D.; Phillips, P. J.; Semenov, V.; Gakh, A. Physical properties of aliphatic polycarbonates made from CO_2 and epoxides. *J. Appl. Polym. Sci.* **2003**, *89*, 1163–1176.

SUPPORTING INFORMATION

Addressing a Key Challenge of CO_2-Based Polycarbonates: Low Glass Transition Capitalizing on Citronellol Glycidyl Ether

Christina Gardiner[a], Tobias Johann[a], Andreas Hanewald[b], Holger Frey[a,*]

[a] Institute of Organic Chemistry, Duesbergweg 10-14, Johannes Gutenberg University Mainz, 55128 Mainz, Germany

[b] Department of Physics at Interfaces, Ackermannweg 10, Max Planck Institute for Polymer Research, 55128 Mainz, Germany

Table of Content

1. Monomer characterization

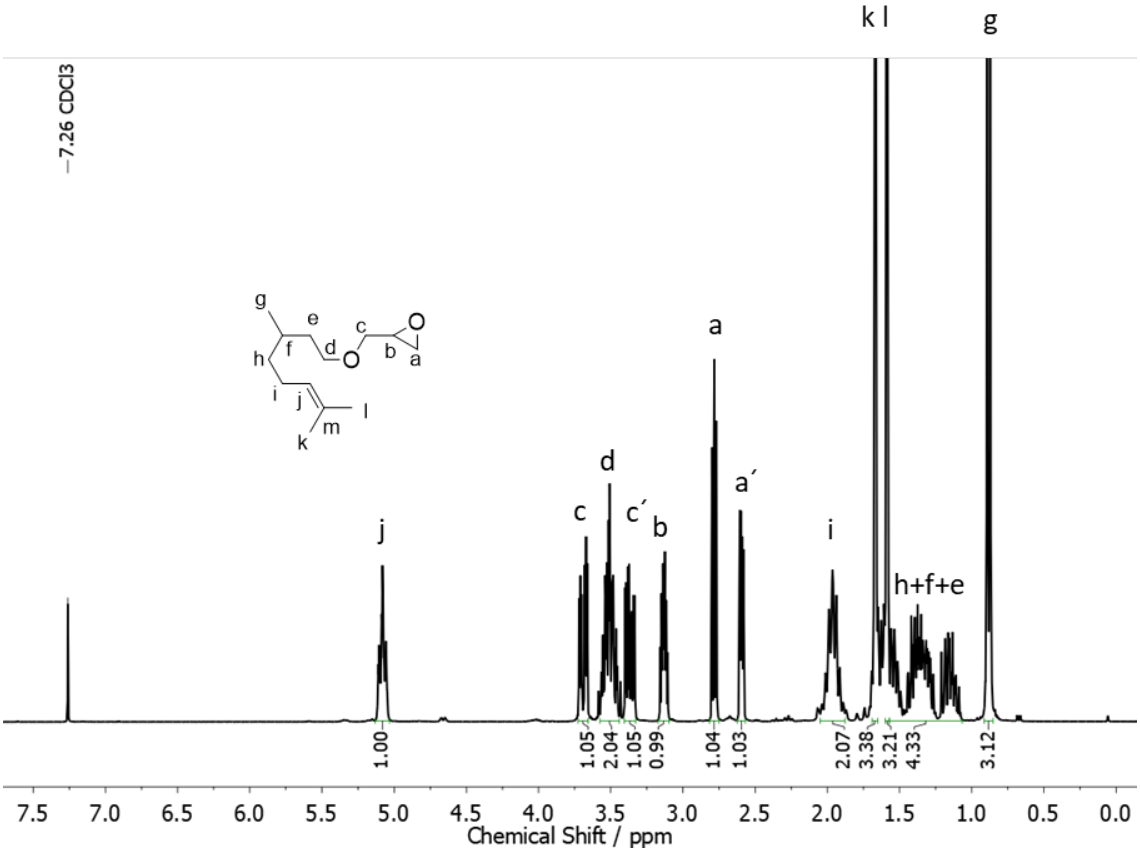

Figure S 1: ^{1}H NMR spectrum (300 MHz, $CDCl_3$) of CitroGE after distillation.

2. Polymer characterization

Table S 1: Overview of the synthesized homo-PCitroGEC and the PCHC-*b*-PCitroGEC-*b*-PCHC triblock copolymer and modified PCitroGEC homopolymers.

sample	composition	Catalyst	M_n[a]	$Đ$	yield	Conversion[b] (CitroGE/CHO)	T_g	Δcp
		mol%	g/mol		%	%	°C	J/g*°C
1	$PCitroGEC_{11}$	0.6+drop H_2O	2 800	1.07	31	97/-	-55	1.569
2	$PCitroGEC_{18}$	0.6	4 600	1.09	97	97/-	-57	0.997
3	$PCitroGEC_{19}$	0.5	4 800	1.17	100	100/-	-55	0.943
4	$PCitroGEC_{20}$	0.4	5 000	1.09	100	100/-	-57	0.917
5	$PCitroGEC_{23}$	0.2	5 900	1.11	100	100/-	-55	1.004
6	$PCitroGEC_{19}$	0.15	4 800	1.13	51	75/-	-59	15.909
7	$PCitroGEC_{72}$	0.2[d]	18 650	1.15	70	80/-	-51	0.694
8	PCHC-*b*-PCitroGEC-*b*-PCHC	0.3	5 100[c]/6 750	1.13[c]/1.17	68	97/75	-20	0.577
9	$PCitroGEC_{0.5}$-*co*-$PCHC_{0.5}$	0.2	9 570	1.34	93	94/92	-2	0.282
10	$PCitroGEC_{19}$-MDI-PU	-	12 080	2.39	100	75/-	-40	1.043
11	$PCitroGEC_{20}$-Ph-TAD	-	9280*,[c]/15130*	1.18[c]/1.18	100	100/-	24	0.465

[a]measured by SEC (Eluent: DMF, standard: PEG). [b]Determined by ^1H NMR (300 MHz, $CDCl_3$). [C] Mn/ PDI belonging to the PCitroGEC block/part.[d]impurities in the CitroGE monomer were masked by methyl iodide before use. *measured by SEC (Eluent: THF, standard: PS).

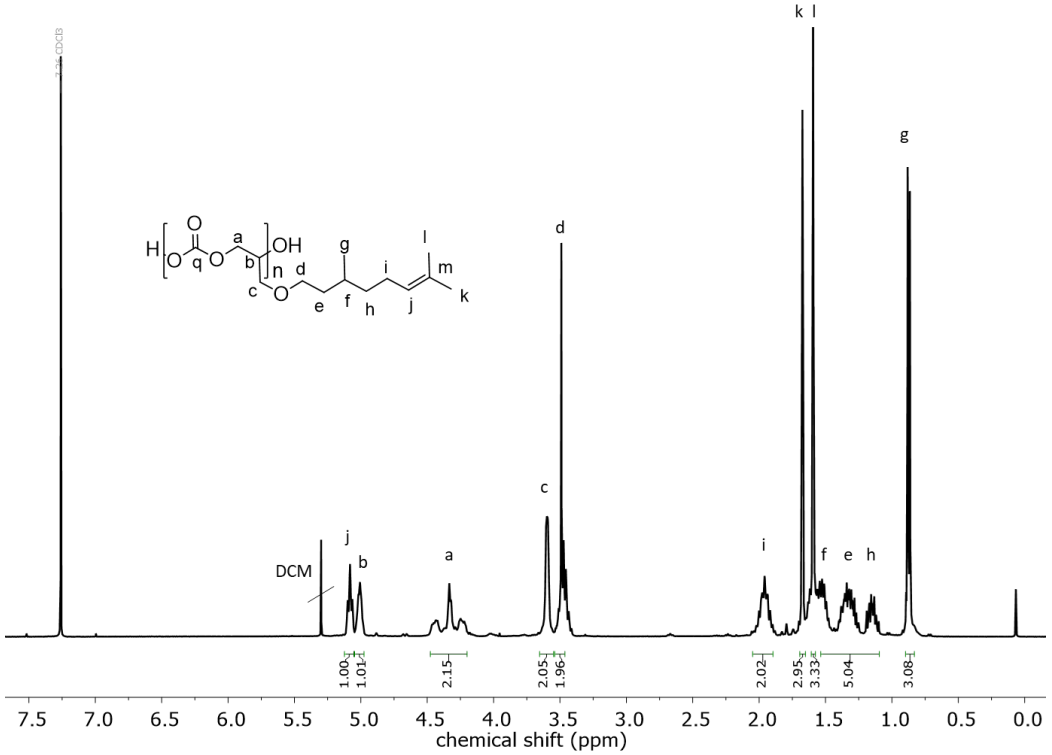

Figure S 2: ^{1}H NMR spectrum (300 MHz, $CDCl_3$) of $PCitroGEC_{18}$ (Table S 1, sample 2), indicating the compatibility of the ene double bond with the catalyst system.

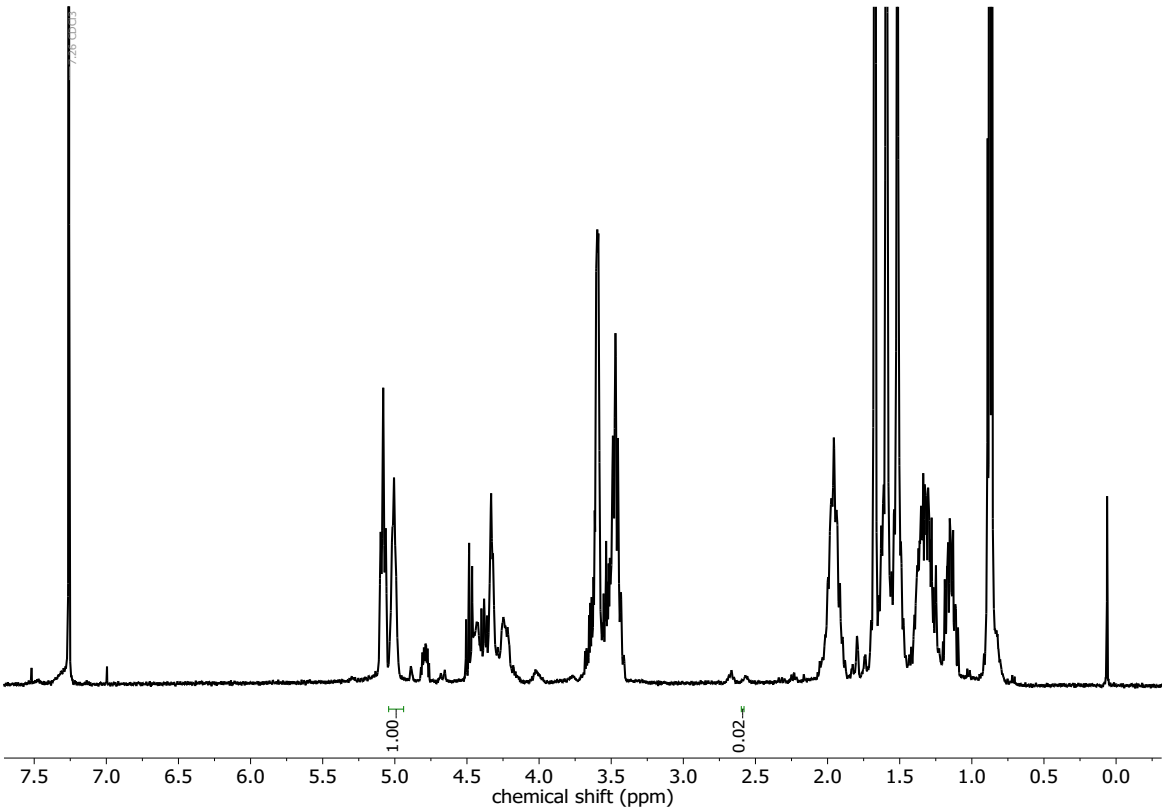

Figure S 3: ^{1}H NMR spectrum (300 MHz, $CDCl_3$) of crude $PCitroGEC_{18}$ (Table S 1, sample 2), showing almost full conversion of the monomer CitroGE by the very small intensity of the epoxide signals at 3.13, 2.81 and 2.62 ppm.

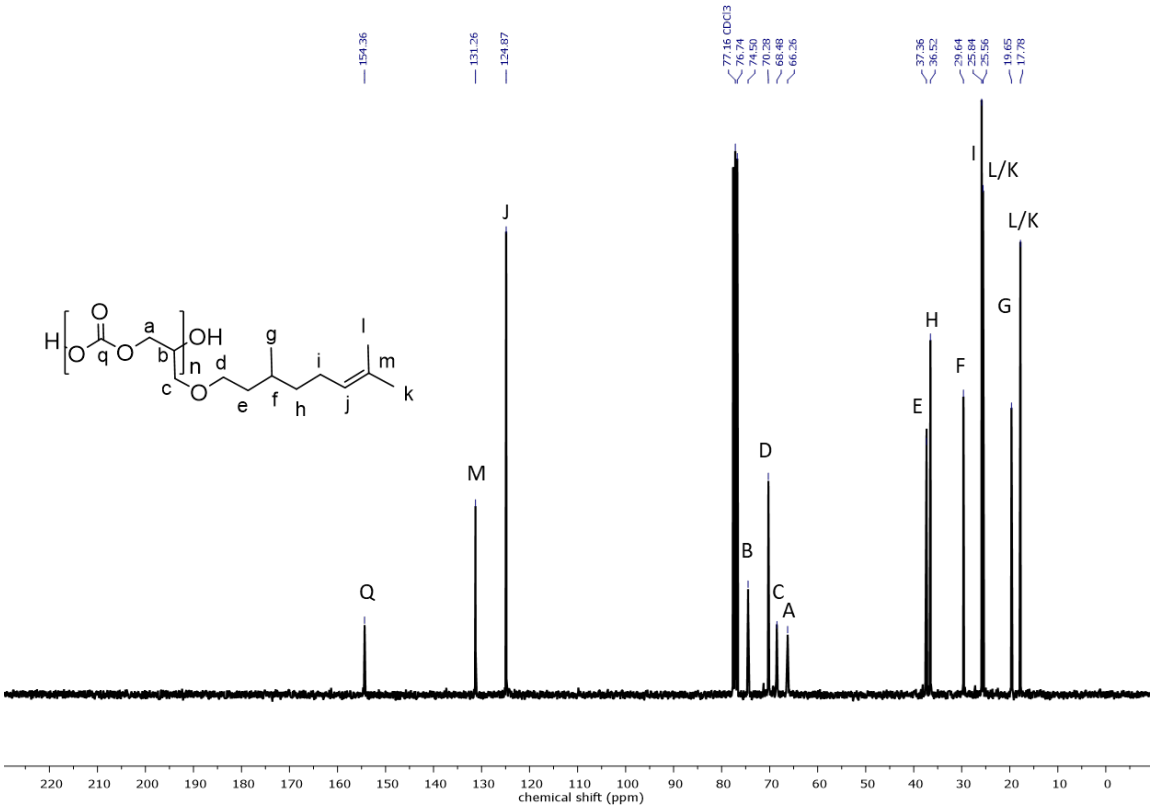

Figure S 4: ^{13}C NMR spectrum (75 MHz, $CDCl_3$) of $PCitroGEC_{18}$ (Table S 1, sample 2), showing the formation of polycarbonate structure, based on the signal of the carbonyl carbon at 154.36 ppm.

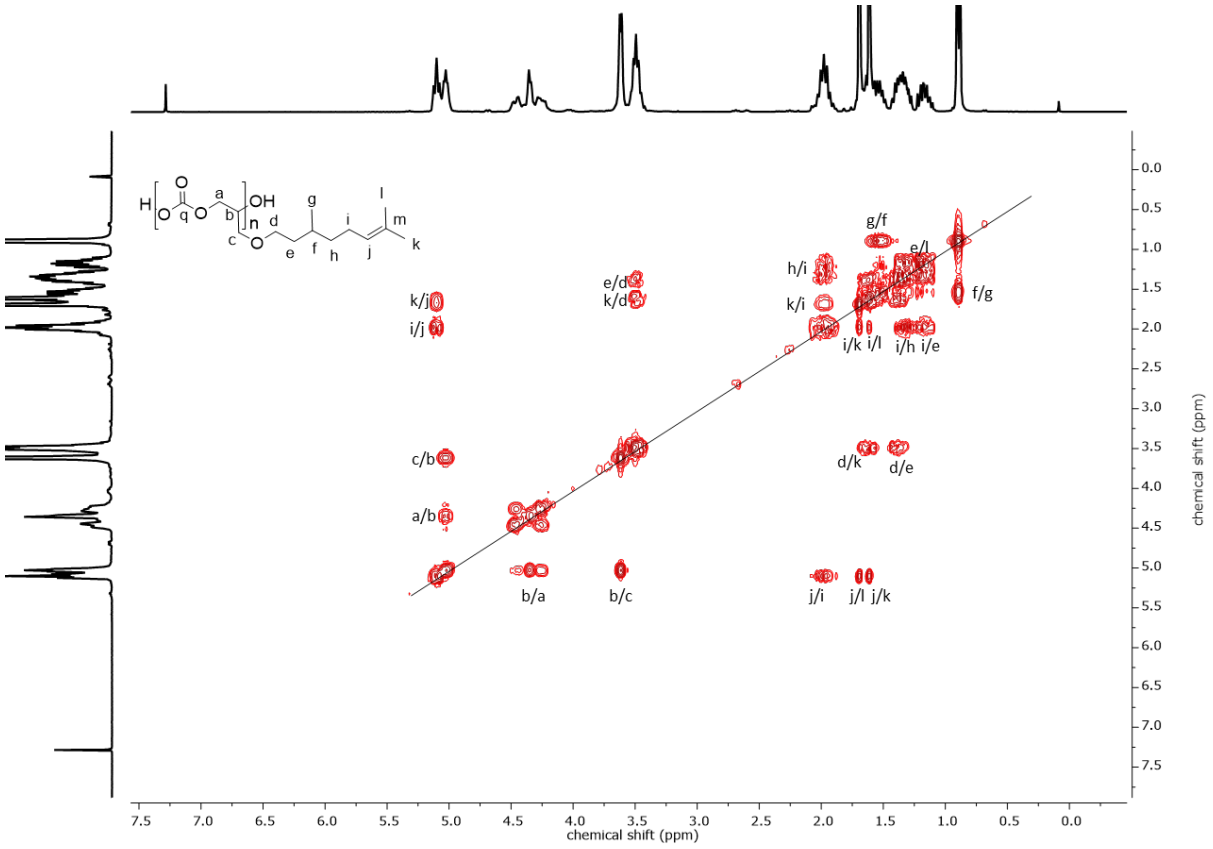

Figure S 5: ^{1}H-^{1}H COSY NMR (300 MHz, $CDCl_3$) spectrum of $PCitroGEC_{18}$ (Table S 1, sample 2) .

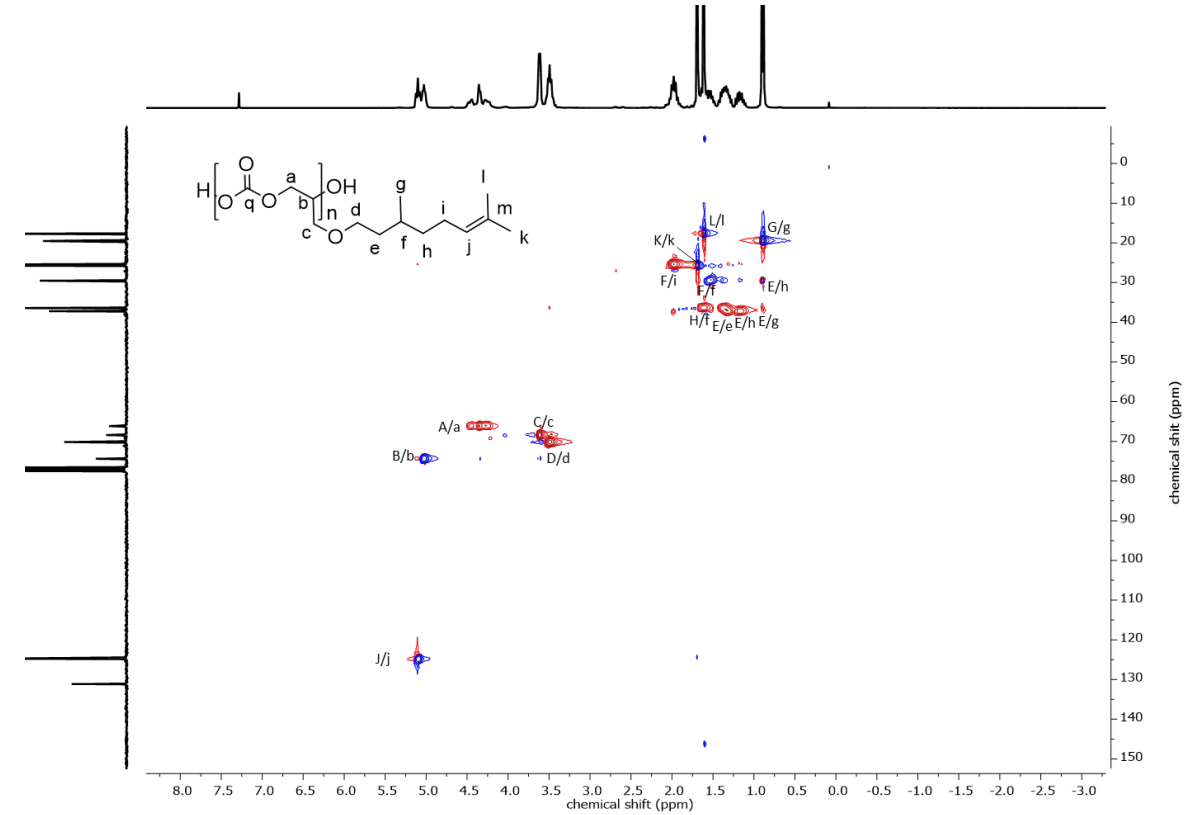

Figure S 6: ^{1}H-^{13}C HSQC NMR spectrum (300 MHz/75 MHz, $CDCl_3$) of $PCitroGEC_{18}$ (Table S 1, sample 2)

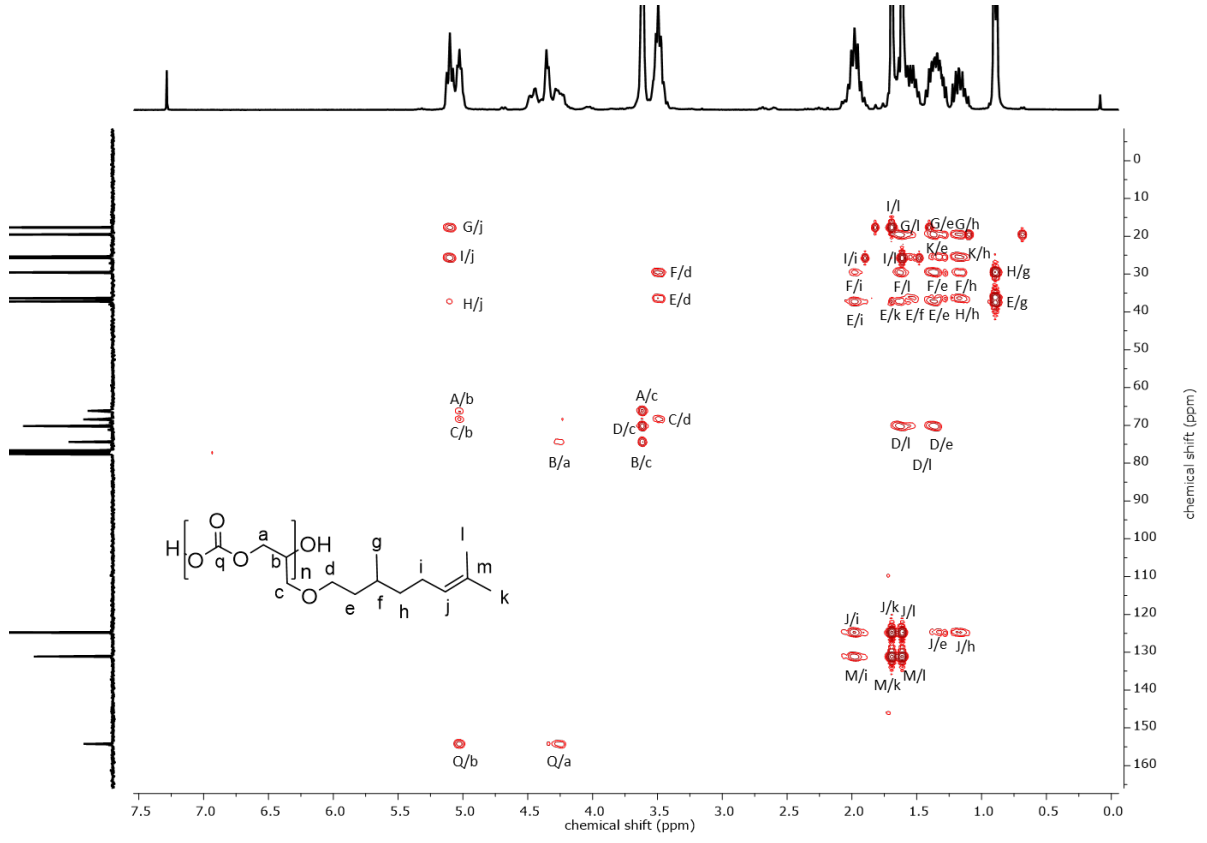

Figure S 7: ^{1}H-^{13}C HMBC NMR spectrum (300 MHz/75 MHz, $CDCl_3$) spectrum of $PCitroGEC_{18}$ (Table S 1, sample 2) .

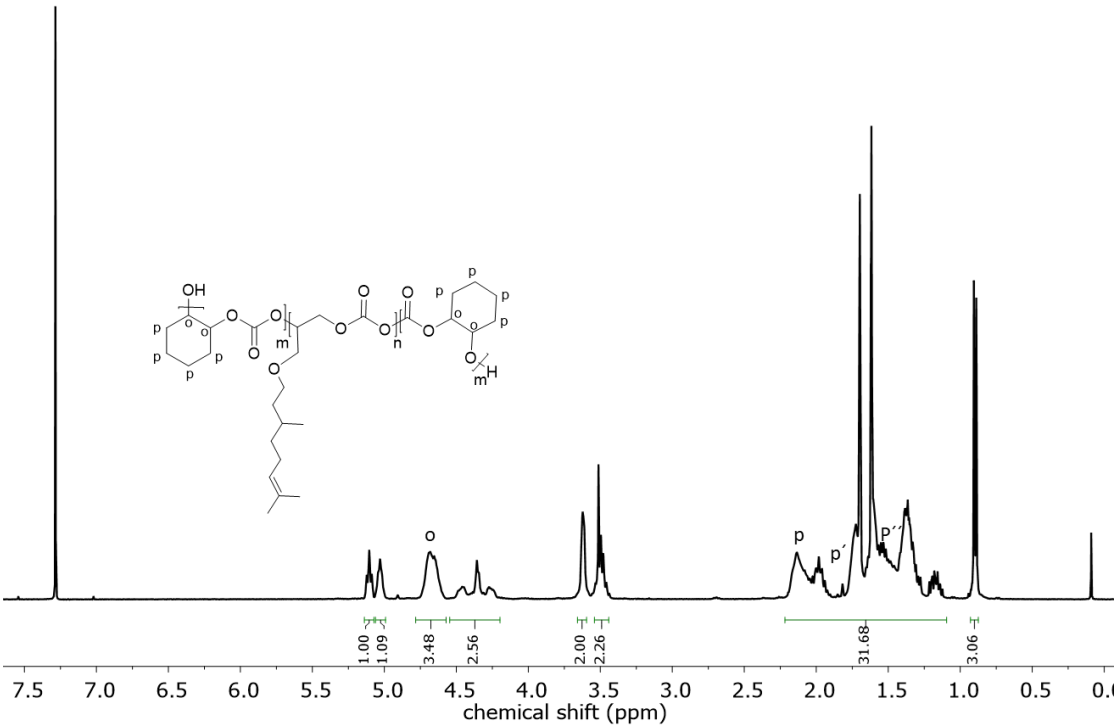

Figure S 8: ^{1}H NMR spectrum (300 MHz, $CDCl_3$) of PCHC-*b*-PCitroGEC-*b*-PCHC (Table S 1, sample 8) .

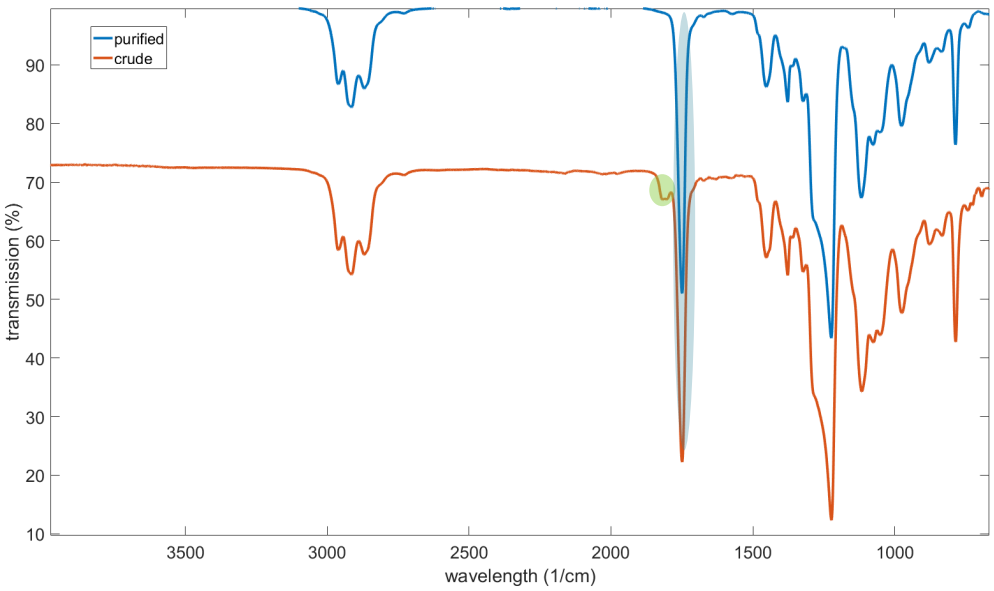

Figure S 9: IR spectrum of crude and purified PCitroGEC18 (Table S 1, sample 2) . Orange: crude homopolymer. Blue: purified homopolymer after precipitation in methanol. Highlighted in green at 1819 cm^{-1}: carbonyl bands of cyclic carbonates that occur as a side product. Highlighted in blue at 1740 cm^{-1}: carbonyl bands of the PCitroGEC.

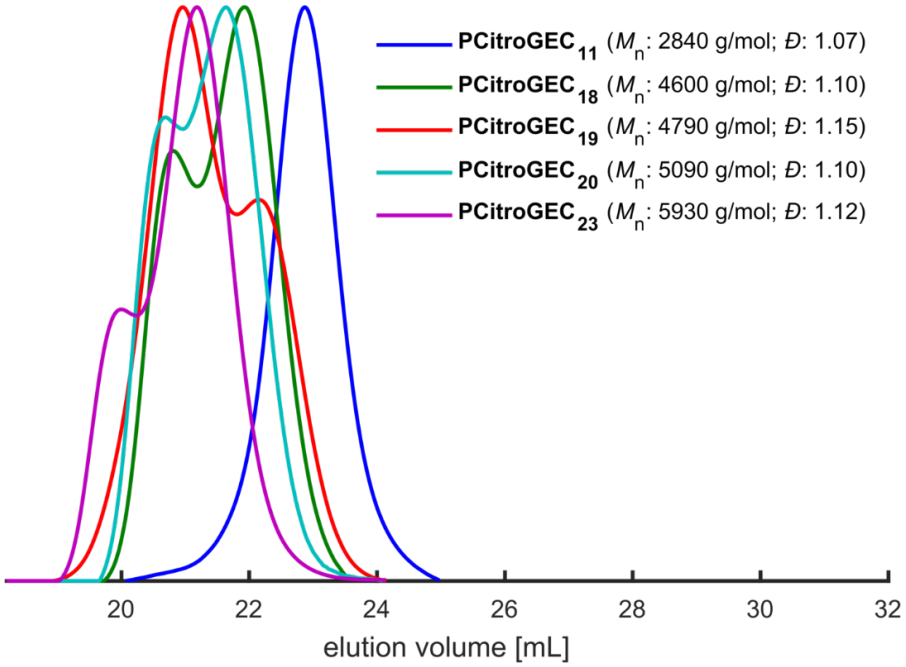

Figure S 10: SEC traces (DMF, PEG calibration, RI detector) of PCitroGEC homopolymers.

To further elucidate the bimodal distribution (Figure S10) that is known in literature[6,7], MALDI-ToF analysis was performed. Therefore the two distributions of the polymer $PCitroGEC_{18}$ (Table S 1, sample 2)) were separated using a preparative SEC. Fraction 1 (blue) and Fraction 6 (purple) (Figure S 11) were characterized via MALDI-ToF measurements.

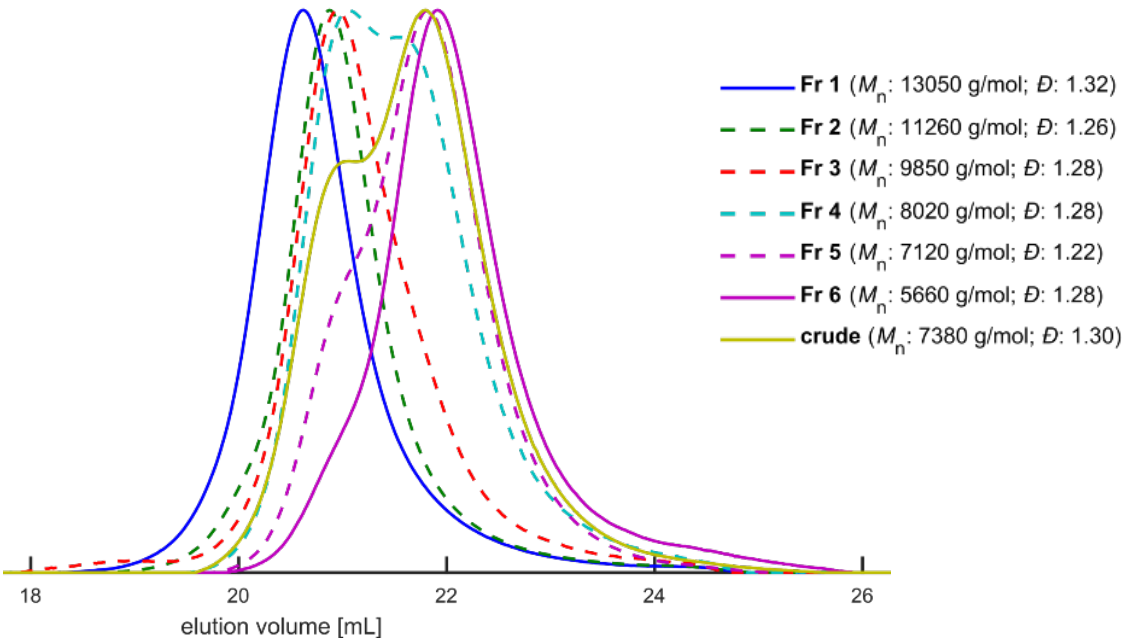

Figure S 11: SEC-traces of $PCitroGEC_{18}$ (Table S 1, sample 2) fractions before (crude) and after separation by a preparative SEC (Eluent: $CHCl_3$, Standard: PS). Fr 1 and Fr 6 show the best separation.

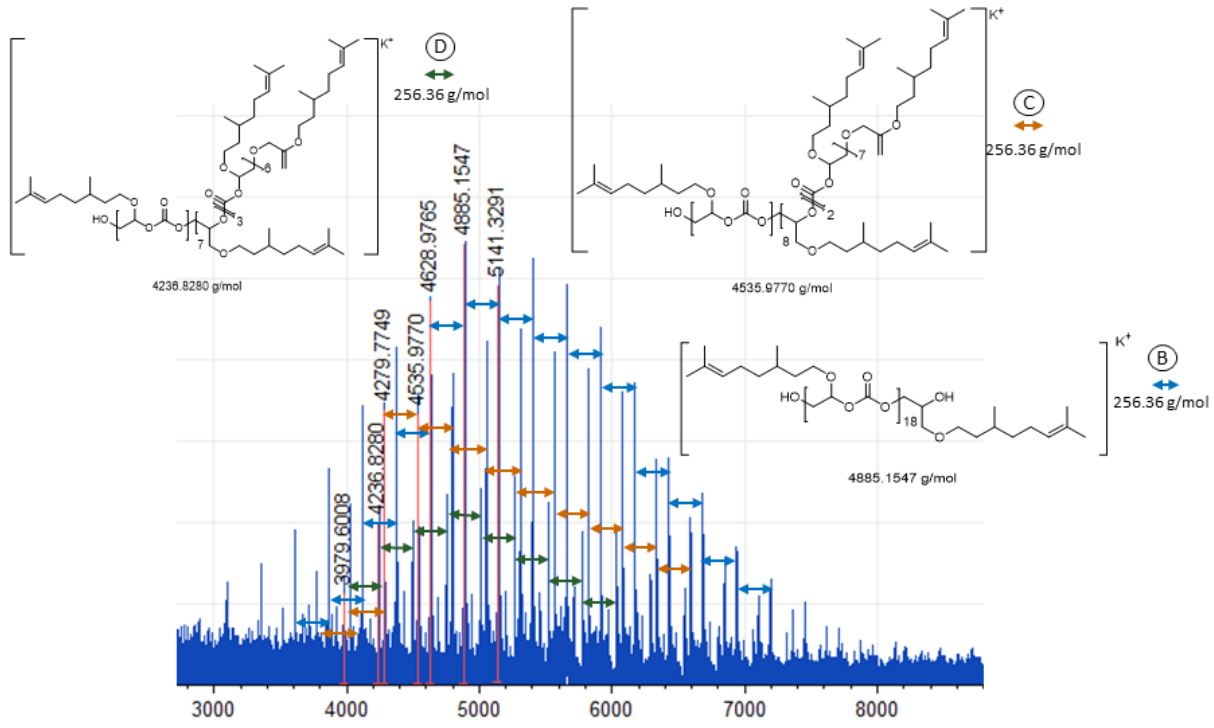

Figure S 12: MALDI-ToF spectrum of fraction 6 of PCitroGEC18(Table S 1, sample 2) .

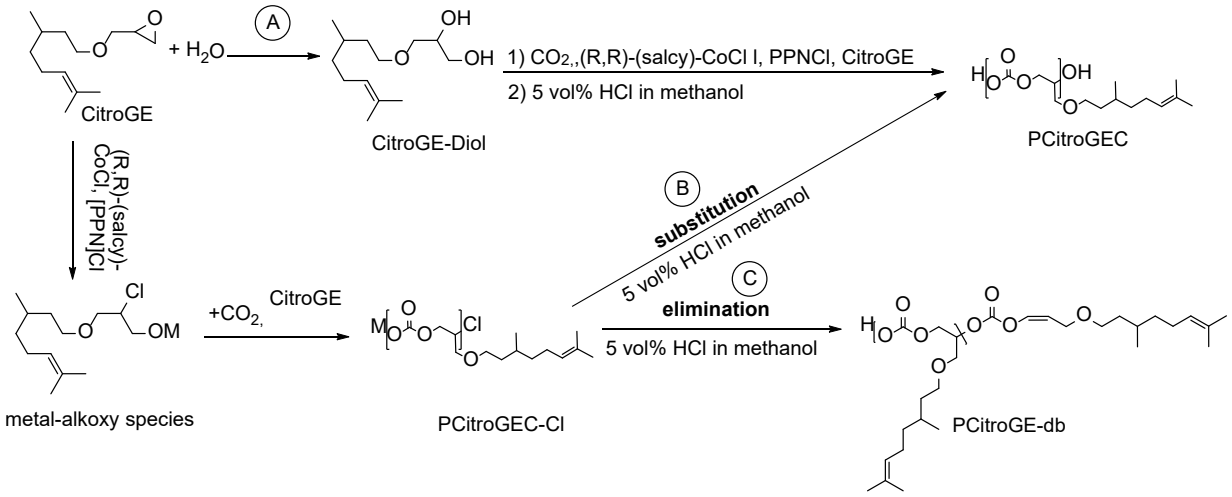

Scheme S 1: Routes to the different species of the distributions shown in the MALDI-ToF spectrum (Figure S 11). A) This route shows the hydrolysis of CitroGE via water. The formed bifunctional CitroGE-diol is then activated by the Co-salen catalyst system and both hydroxyl groups initiate then the polymer chains. B+C) Additionally a CitroGE could be activated directly by the Co-salen catalyst system, resulting in a metal-Alkoxy species (O-M). This Species reacts then with carbon dioxide and CitroGE in a coordination-insertion process to a polycarbonate with Cl as an end group (PCitroGEC-Cl). Using 5 vol% HCl in methanol for hydrolysis of the catalyst leads to a substitution (B) or to an elimination (C) of the chloride end group. B) results in α,ω hydroxyl-PCitroGEC and C) in a hydroxyl and a double bond end capped PCitroGE (PCitro-db).

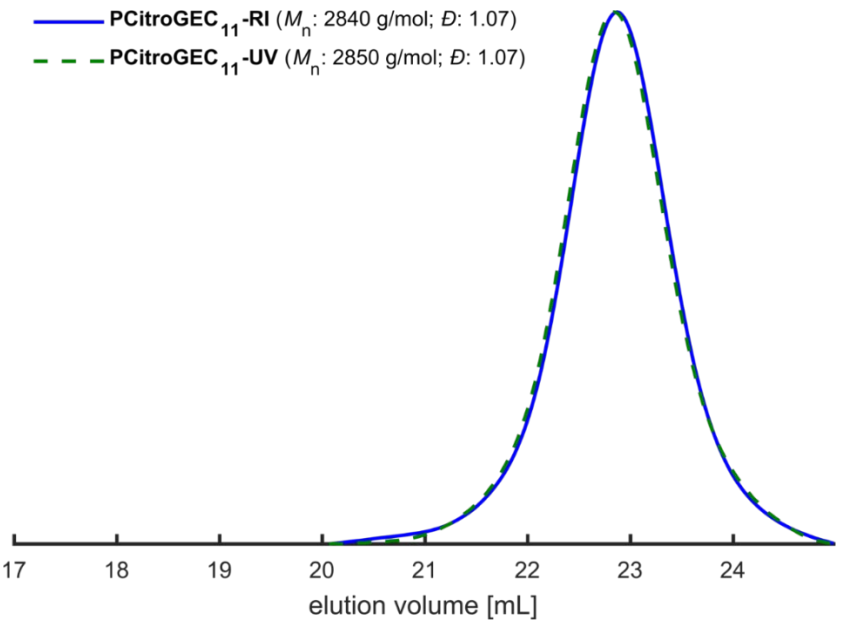

Figure S 13: SEC traces (DMF, PEG calibration, RI/UV detector) of PCitroGEC11 (using additional water) (Table S 1, sample 1).

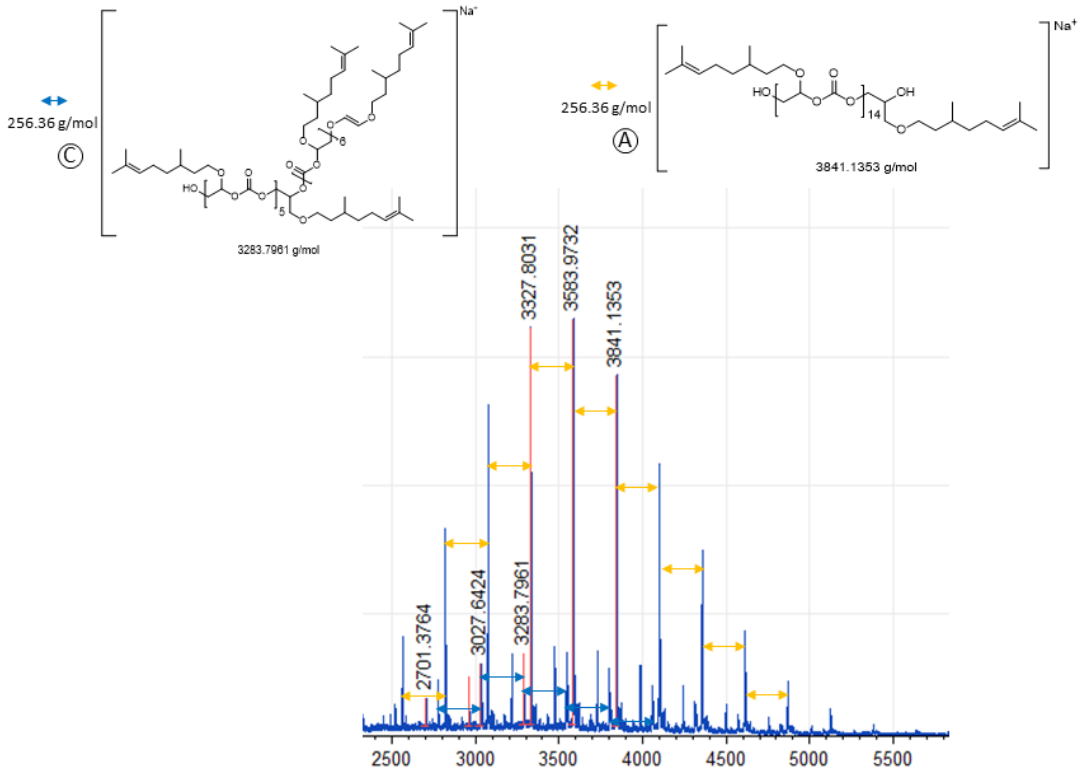

Figure S 14: MALDI-ToF spectrum of water initiated PCitroGEC$_{11}$ (using additional water) (Table S 1, sample 1).

Note: Since bifunctional CitroGEC-diol coexists with the monofunctional CitroGEC-ol, a sequential monomer addition of CHO leads to a mixture of di- and triblock copolymers. To simplify the discussion, the term “triblock copolymers” was used to describe this mixture in the main text.

3. Thermal characterization

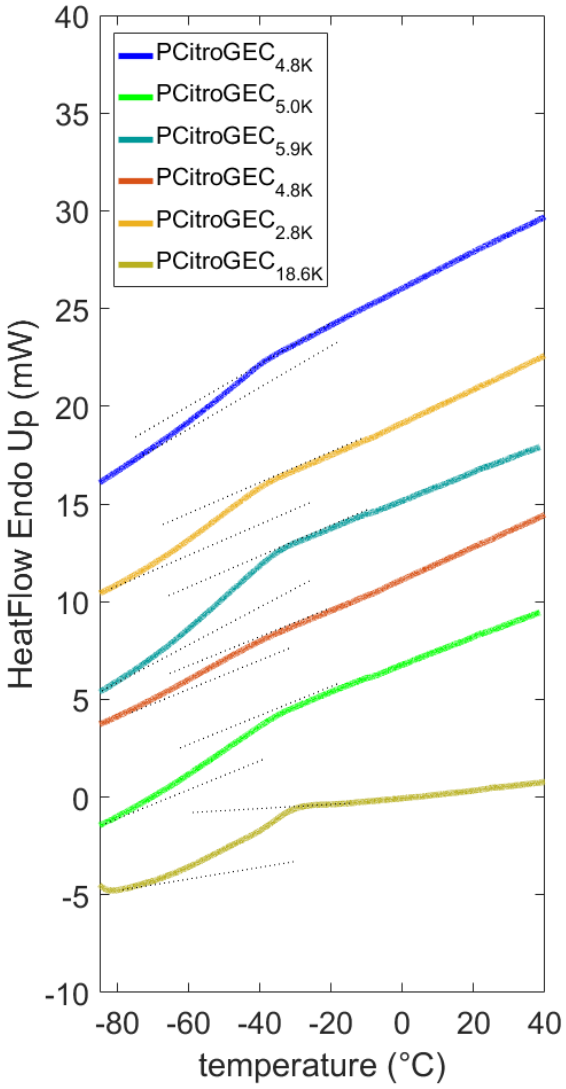

Figure S 15: DSC-diagrams of homo-PCitroGEC samples (HR:20 °C/min).

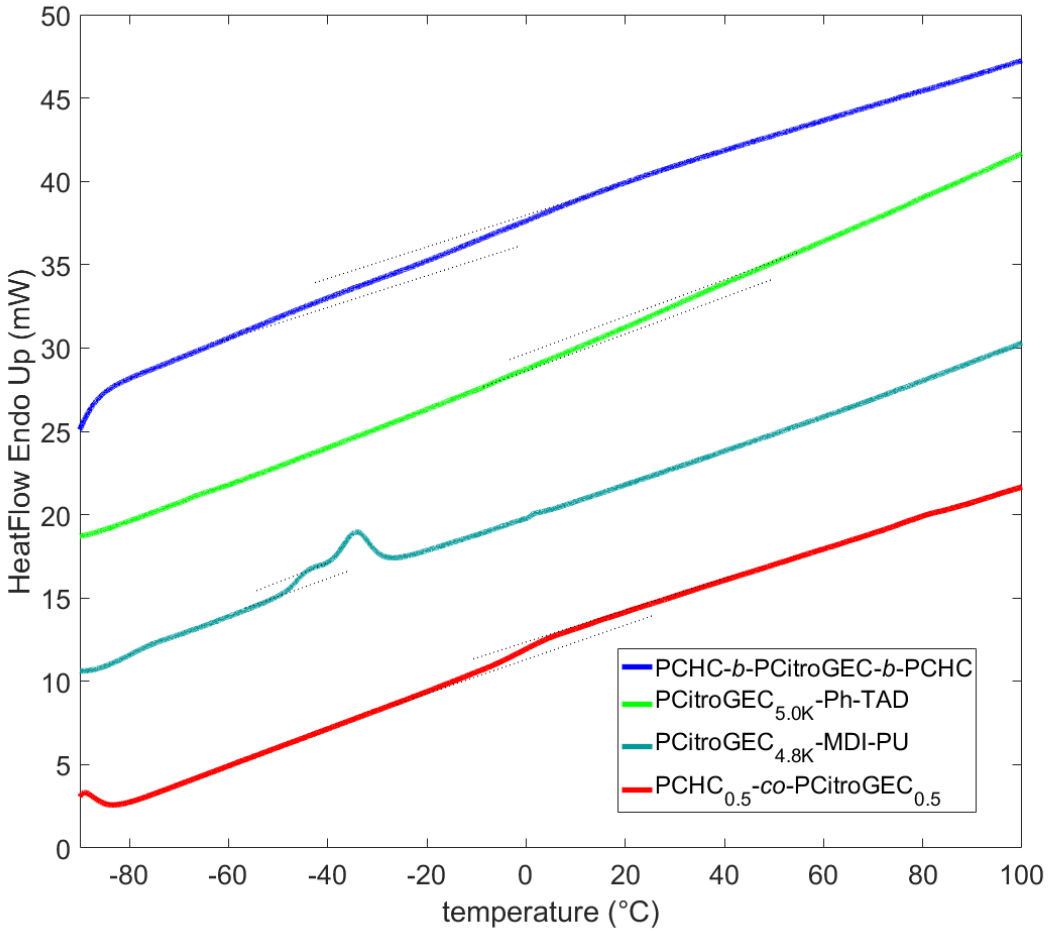

Figure S 16: DSC-diagrams of modified PCitroGEC polymer samples (HR: 20 °C/min).

4. Post-Modifications

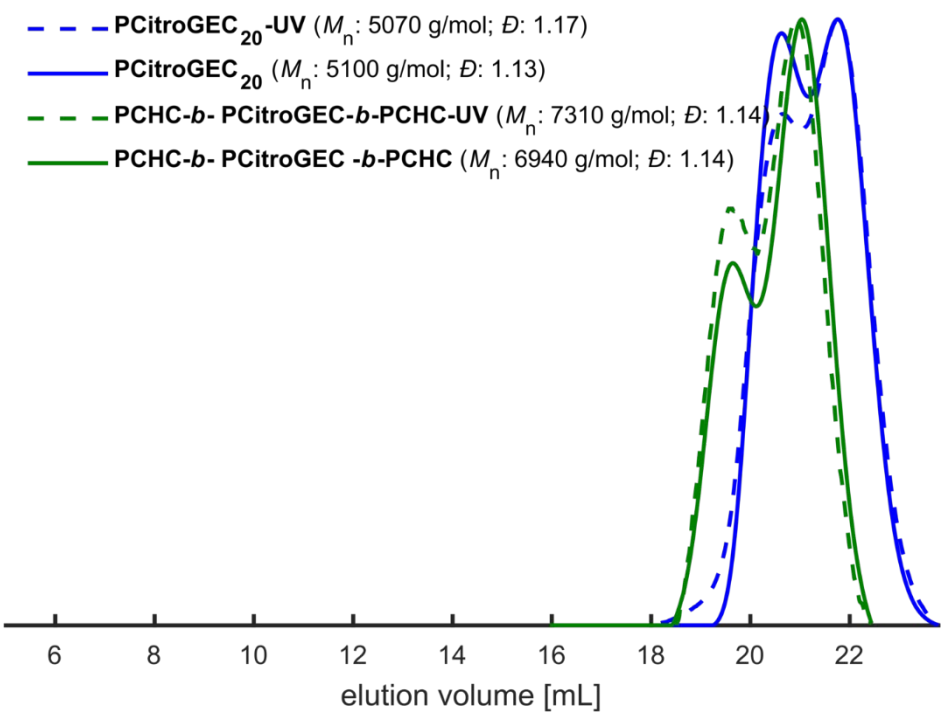

Figure S 17: SEC traces (DMF, PEG calibration, RI & UV detector) of PCitroGEC$_{20}$ (sample before CHO addition) and PCHC-*b*-PCitroGEC-*b*-PCHC (Table S 1, sample 8). A shift to lower elution volume and therefore to higher molar masses is detectable for the PCHC-*b*-PCitroGEC-*b*-PCHC compared to the PCitroGEC initiator. This confirms successful polymerization onto the activated chain ends of PCitroGEC. Additionally, the UV and the IR signal of the SEC traces match, which excludes the formation of homo PCHC (via UV non-detectable).

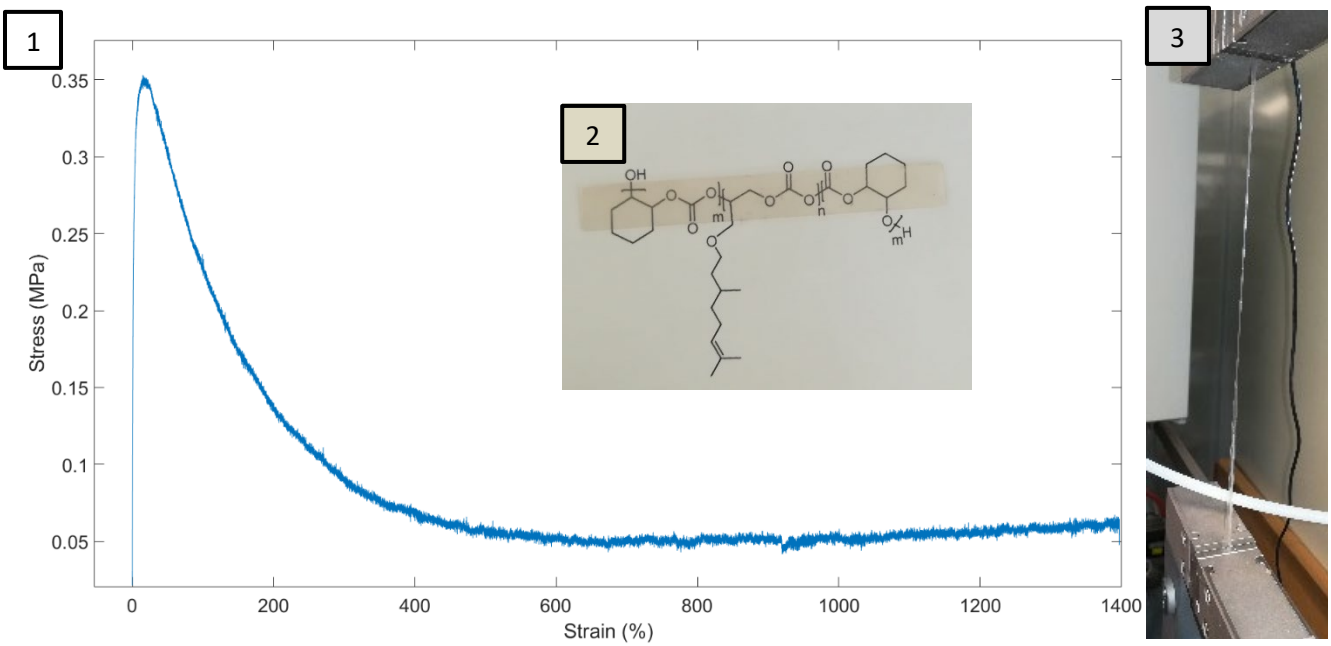

Figure S 18: 1) Stress-Strain curve of the PCHC-*b*- PCitroGEC -*b*-PCHC triblock copolymer (Table S 1, sample 7). 2) Transparent film sample of the PCHC-*b*- PCitroGEC -*b*-PCHC triblock copolymer before testing (Table S 1, sample 7). 3) Stretched film of the PCHC-*b*- PCitroGEC -*b*-PCHC triblock copolymer (Table S 1, sample 7).

Table S 2: Overview of the mechanical properties of the PCHC-*b*- PCitroGEC -*b*-PCHC triblock copolymer (Table S 1, sample 8). (n = 2, average ± SD).

E^a	σ_{break}	ε_{break}	$\sigma_{yield}{}^b$	ε_{yield}	$W_{tensile}$
MPa	**Mpa**	**%**	**MPa**	**%**	**MN/m^2**
0.112±0.02	0.042±0.005	1301±90	0.21±0.05	2.3±0.3	0.8±0.4

[a]Calculated by using the slope of the initial part of the curve. Considering the tensile stress–strain data at small strains no linear elastic behavior above about 2% strain was detectable. Observing the limited range of linear elasticity in this triblock copolymer, we still relate the initial stress–strain slope with the Young's modulus.

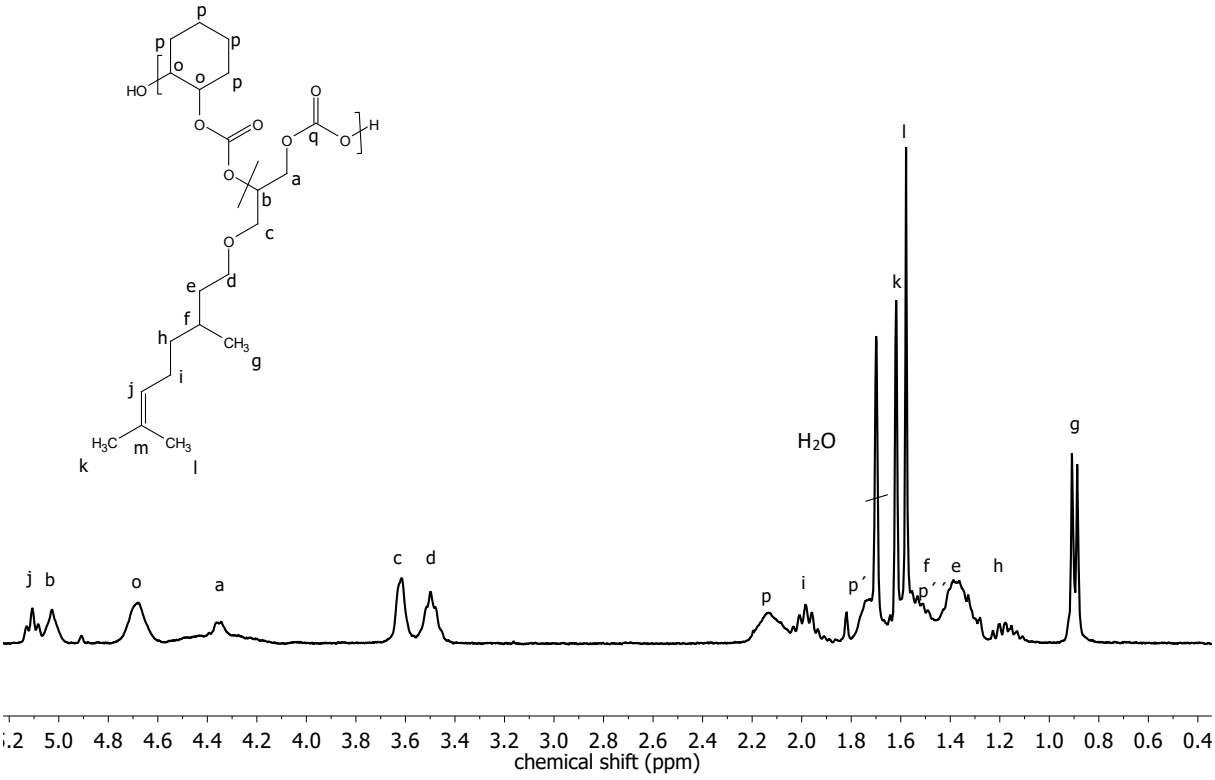

Figure S 19: ^{1}H NMR spectrum (300 MHz, $CDCl_3$) of PCitroGEC0.5-*co*-PCHC$_{0.5}$ (table S 1, sample 9).

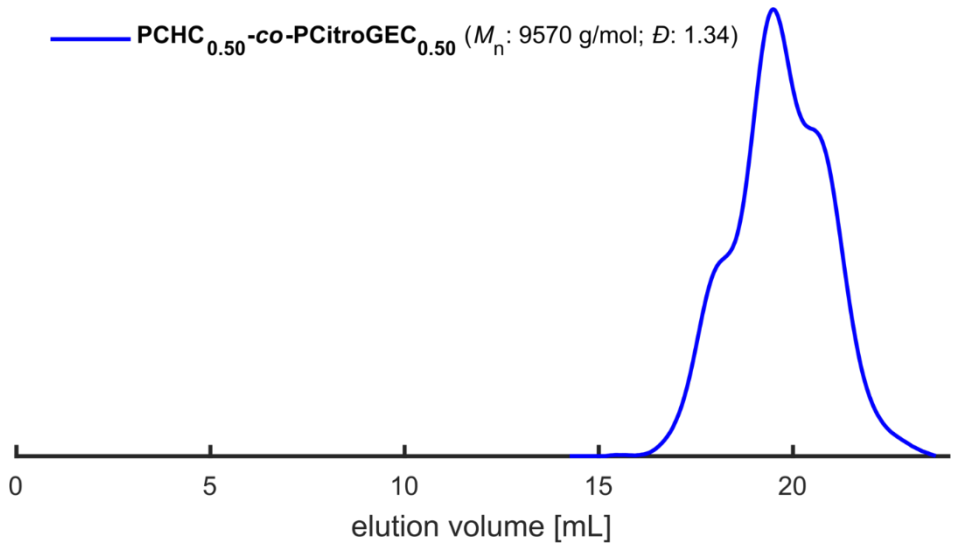

Figure S 20: SEC traces (DMF, PEG calibration, RI detector) of PCitroGEC$_{0.5}$ -*co*-PCHC$_{0.5}$ (Table S 1, sample 9).

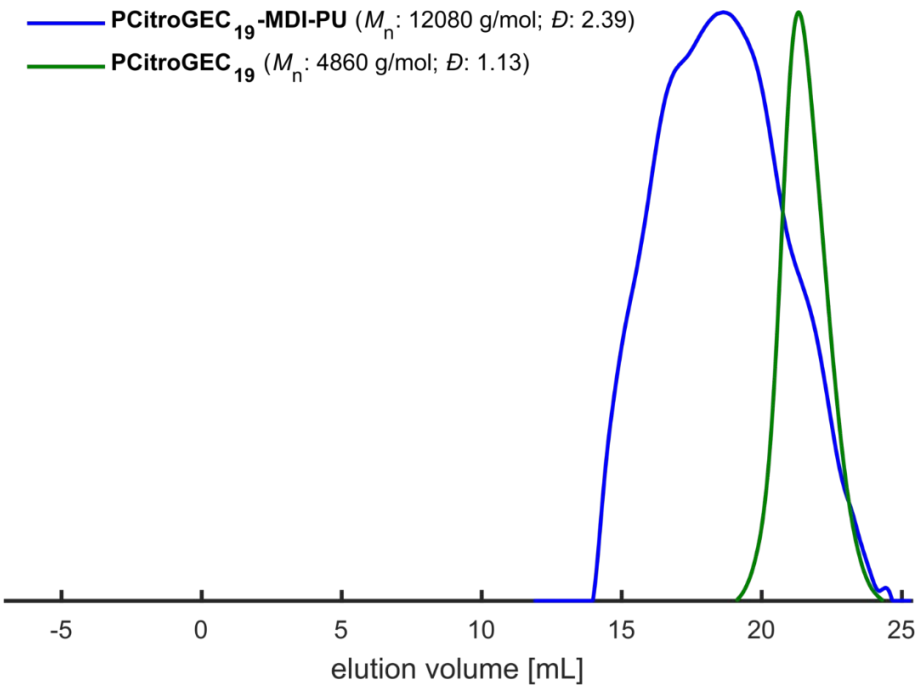

Figure S 21: SEC traces (DMF, PEG calibration, RI detector) of PCitroGEC$_{19}$ (Table S 1, sample 6) (green) and PCitroGEC$_{19}$-MDI-PU (Table S 1, sample 10) (blue).

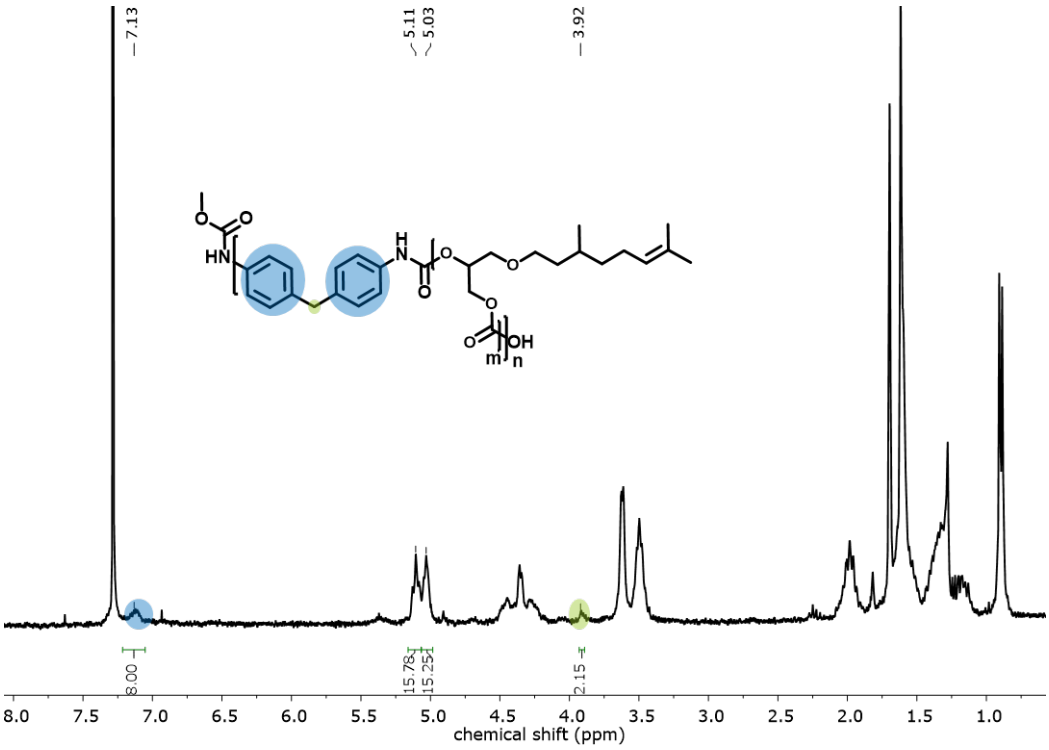

Figure S 22: ^{1}H NMR spectrum (300 MHz, $CDCl_3$) of PCitroGEC$_{19}$-MDI-PU (Table S 1, sample 10). The aromatic protons of MDI are highlighted in blue, and the aliphatic protons of MDI are highlighted in green.

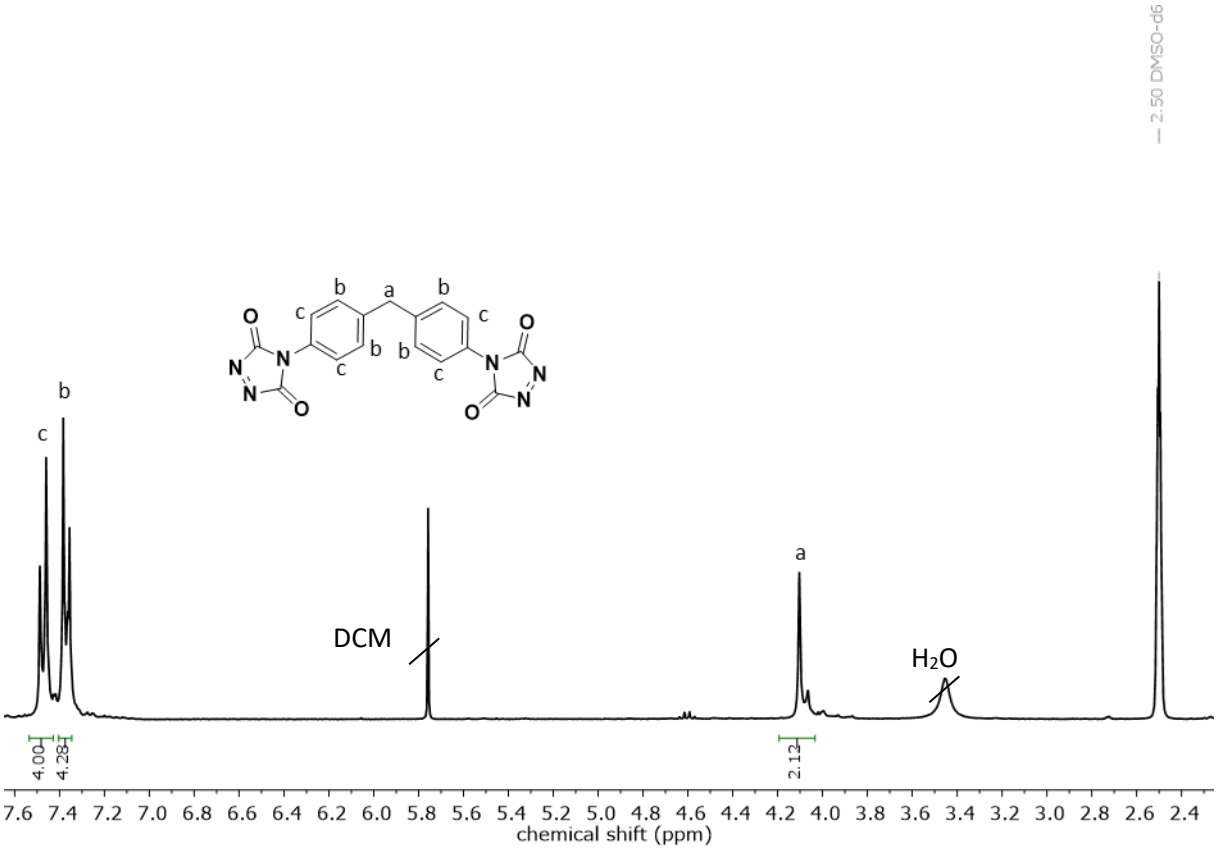

Figure S 23: ^{1}H NMR spectrum of Bis-TAD (DMSO-d_6, 300 MHz).

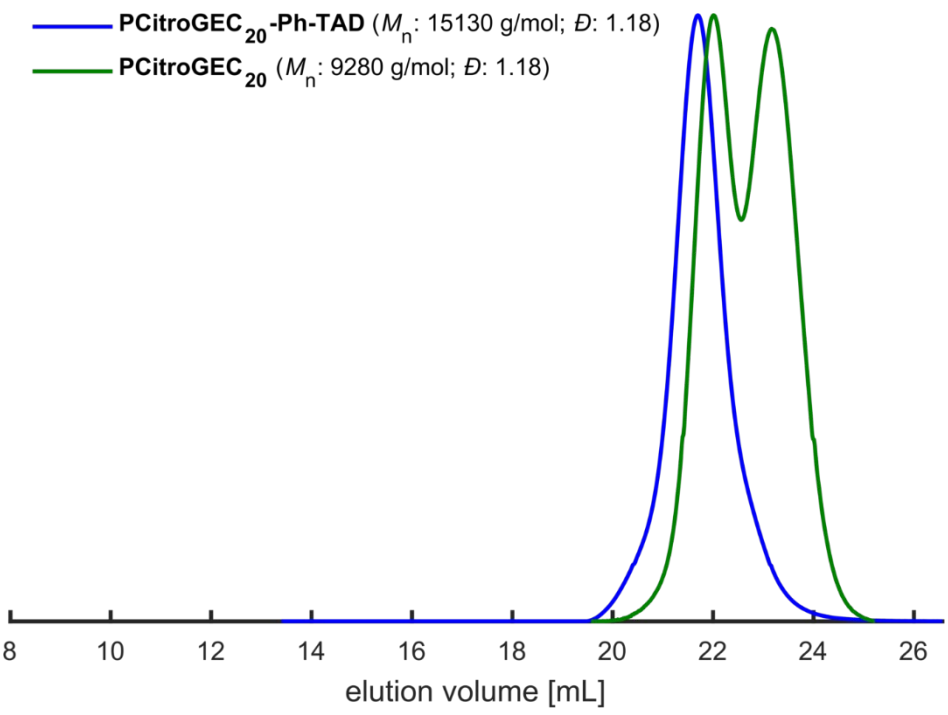

Figure S 24: SEC traces (THF, PS calibration, RI detector) of PCitroGEC$_{20}$ (Table S 1, sample 4) (green) and PCitroGEC$_{20}$-Ph-TAD (Table S 1, sample 11) (blue).

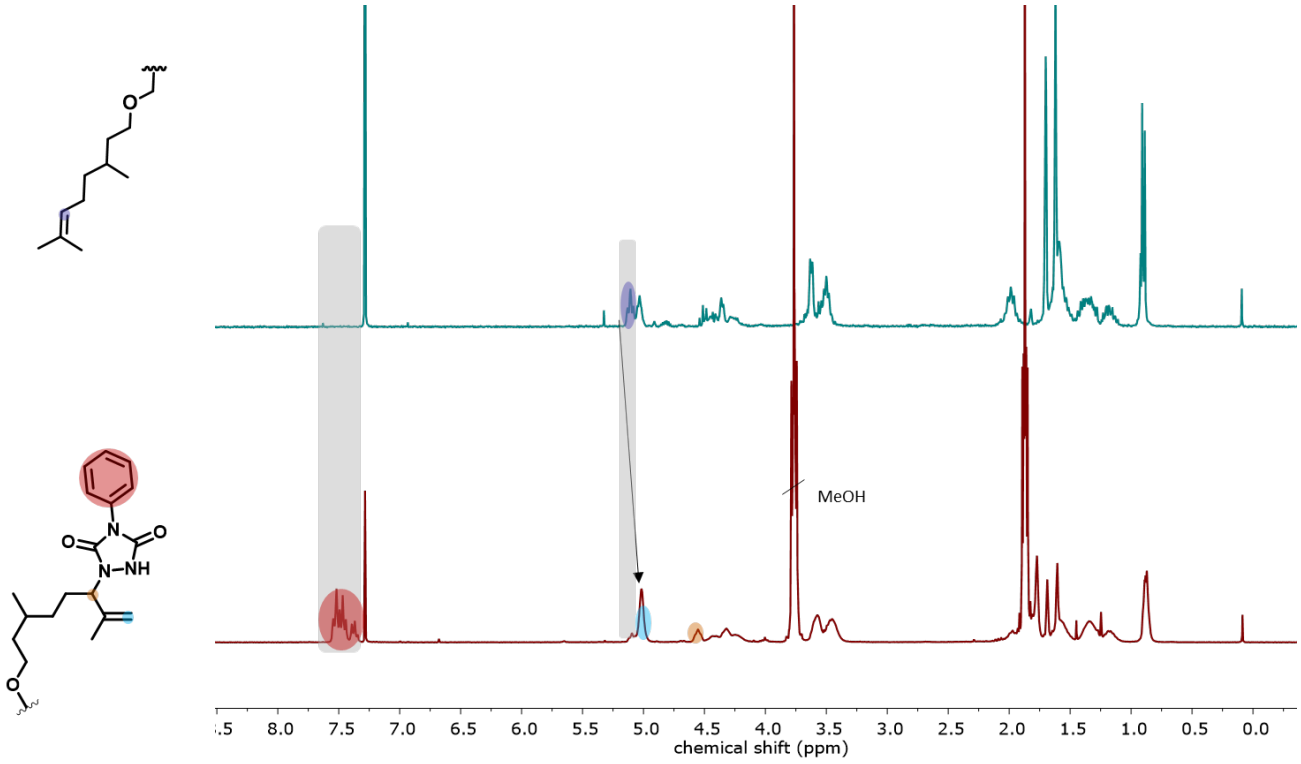

Figure S 25: Stacked ^{1}H NMR spectrum of PCitroGEC$_{20}$ (Table S 1, sample 4) (turquoise) and PCitroGEC$_{20}$-Ph-TAD (Table S 1, sample 11) (red).

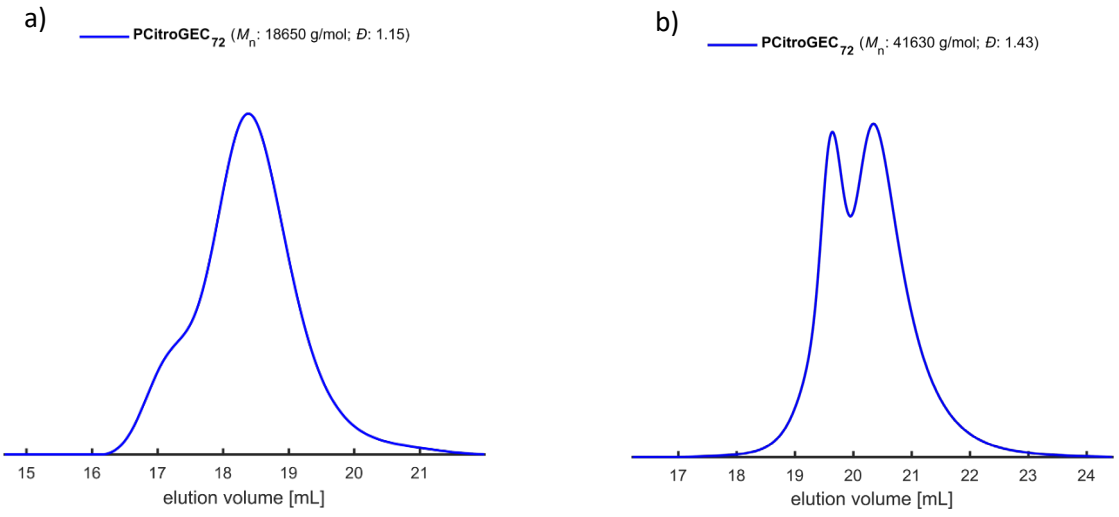

Figure S 26: a) SEC traces (DMF, PEG calibration, RI detector) of masked PCitroGEC$_{72}$ homopolymer (table S 1, sample 7). b) SEC traces (THF, PS calibration, RI detector) of masked PCitroGEC homopolymer (table S 1, sample 7).

REFERENCES

(1) Scharfenberg, M.; Hofmann, S.; Preis, J.; Hilf, J.; Frey, H. Rigid Hyperbranched Polycarbonate Polyols from CO_2 and Cyclohexene-Based Epoxides. *Macromolecules* **2017**, *50*, 6088–6097.

(2) Johann, T.; Houck, H. A.; Dinh, T.; Kemmer-Jonas, U.; Du Prez, F. E.; Frey, H. Multi-olefin containing polyethers and triazolinediones: a powerful alliance. *Polym. Chem.* **2019**, *10*, 4699–4708.

(3) Mouzin, G.; Cousse, H.; Rieu, J.-P.; Duflos, A. A Convenient One-Step Synthesis of Glycidyl Ethers. *Synthesis* **1983**, *1983*, 117–119.

(4) Hauenstein, O.; Reiter, M.; Agarwal, S.; Rieger, B.; Greiner, A. Bio-based polycarbonate from limonene oxide and CO_2 with high molecular weight, excellent thermal resistance, hardness and transparency. *Green Chem.* **2016**, *18*, 760–770.

(5) Vlaminck, L.; Bruycker, K. de; Türünç, O.; Du Prez, F. E. ADMET and TAD chemistry: a sustainable alliance. *Polym. Chem.* **2016**, *7*, 5655–5663.

(6) Kember, M. R.; Copley, J.; Buchard, A.; Williams, C. K. Triblock copolymers from lactide and telechelic poly(cyclohexene carbonate). *Polym. Chem.* **2012**, *3*, 1196.

(7) Jia, M.; Hadjichristidis, N.; Gnanou, Y.; Feng, X. Monomodal Ultrahigh-Molar-Mass Polycarbonate Homopolymers and Diblock Copolymers by Anionic Copolymerization of Epoxides with CO_2. *ACS Macro Lett.* **2019**, *8*, 1594–1598.

CHAPTER 2.2

Tailoring the Glass Transition Temperatures of the Established Aliphatic Polycarbonates PPC and PCHC Using Biobased Citronellol Glycidyl Ether: Kinetic Studies and Post-Modification

CHAPTER 2.2

Tailoring the Glass Transition Temperatures of the Established Aliphatic Polycarbonates PPC and PCHC Using Biobased Citronellol Glycidyl Ether: Kinetic Studies and Post-Modification.

Christina Gardiner[a], Holger Frey[a*]

[a]Department of Chemistry, Johannes Gutenberg University, Duesbergweg 10-14, 55128 Mainz, Germany.

To be submitted.

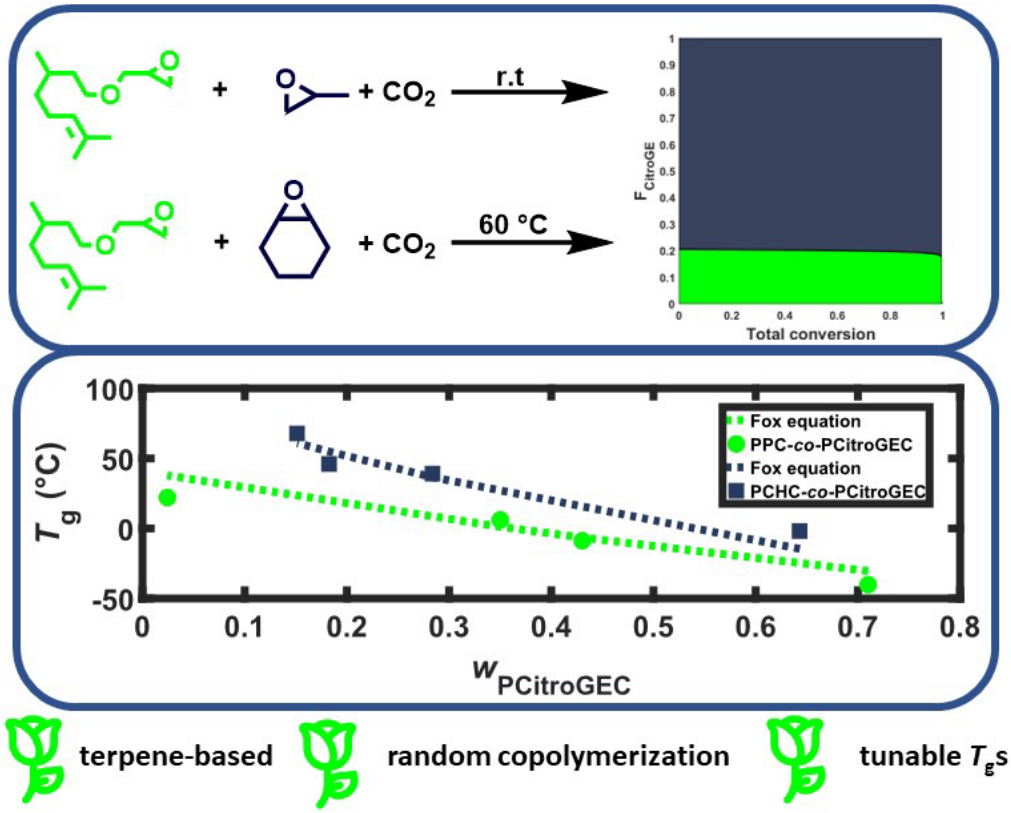

ABSTRACT

The terpene-based citronellol glycidyl ether (CitroGE) was investigated as a comonomer in the statistical terpolymerization with carbon dioxide (CO_2) and propylene oxide (PO) or cyclohexene oxide (CHO) *via* catalytic polymerization, applying (*R,R*)-Co(salen)Cl (CoSalenCl) and bis(triphenylphosphine (iminium chloride)) (PPN[Cl]) as a binary catalyst system. A series of copolymers with varied molar content of CitroGE (1-50 mol%) was synthesized, reaching molecular weights up to 13 900 g/mol. The kinetics studies demonstrate a random copolymerization of PO/CitroGE/CO_2 (20 °C) and of CHO/CitroGE/CO_2 (60 °C) with reactivity ratios of $r_{CitroGE}$ = 1.2152, r_{PO} = 0.8888 and $r_{CitroGE}$ = 1.0326, r_{CHO} = 0.9966, respectively (CO_2 is not considered in this calculation, because its copolymerization is alternating with the catalyst employed). Changing the reaction temperature from 60 °C to 30 °C in the CHO/CitroGE/CO_2 copolymerization results in a gradient microstructure. The thermal properties of the copolymers were investigated *via* differential scanning calorimetry (DSC) showing the tunability of the glass transition temperatures (T_gs), using CitroGE as copolymer. A linear decrease of the T_g with higher content of PCitroGEC was detectable, leading to PPC copolymers with T_gs in the range of of -40 to +22 °C, and to PCHC copolymers with T_gs between -2 and +68 °C. Furthermore, the thiol-ene click for post-modification reactions was established, utilizing the ene moiety of the PCitroGEC sidechain.

INTRODUCTION

CO_2 is a useful C1 source, because it is non-flammable, non-toxic, readily available, inexpensive and sustainable.[1,2] In 1969 Inoue et al. published the first synthesis of aliphatic polycarbonates using carbon dioxide and epoxides as monomers.[3] Since then, the focus was on the optimization of the catalyst systems, but it shifted in the last few years towards the synthesis of new materials with versatile features, for instance aqueous solubility and improved processability.[4–6] One method to tune the properties of the well-known poly(cyclohexene carbonate) (PCHC) and poly(propylene carbonate) (PPC) is the copolymerization with various monomers.[7] Propylene oxide is inexpensive and readily available, but the resulting polycarbonate PPC exhibits an intermediate glass transition temperature (T_g) of 40 °C.[8] To adjust the thermal characteristics of PPC, PO was copolymerized with CHO (PCHC, T_g = 120 °C) and CO_2, leading to aliphatic polycarbonates with one T_g.[9–13] Reiter et al. demonstrated the copolymerization of the biobased alternative limonene oxide (LO) with PO to yield higher T_gs of the PPC.[14] Seong at al. showed that by using hexene oxide as an additional monomer, the T_g could be lowered linearly in the terpolymerization.[15] Chukanova et al. additionally investigated the kinetic behavior of the PO/HO/CO_2 copolymerization.[16] Moreover, the group of Qi demonstrated the effect of a low T_g using an epoxide with a long alkyl side chain in aliphatic polycarbonates.[17] To the best of our knowledge, no terpolymerization is known using a biobased monomer to lower T_gs of well-known polycarbonates like PPC and PCHC. Citronellol glycidyl ether (CitroGE) can be used in copolymerizations to decrease the T_g of PCHC and PPC. CitroGE is prepared from citronellol, a monoterpene that is abundant in plants like roses and lemongrass and exhibits a branched C10 alkyl chain with a double bond (Scheme 1). This long alkyl chain enables to lower the T_gs in the resulting polycarbonates. Furthermore, we investigated the microstructure of these terpolymers. In literature, aliphatic polycarbonates based on CO_2 mostly show a gradient- microstructure.[18,19] Honda et al. recently found a random copolymer structure using PO, CO_2, and styrene oxide (SO) in a terpolymerization with (TPP)CoCl/DMAP as a catalyst system.[20] A random copolymer structure is crucial for post-modification reactions, because the functionalities are evenly distributed in the polymer chains. Citronellol exhibits an ene moiety, which enables post-modifications like TAD click, thiol-ene click, and radical-crosslinking reactions. This work aims at demonstrating the adaptation of T_gs of well-known aliphatic polycarbonates such as PPC and PCHC and to demonstrate that the introduced double bonds can be used for further post-modification leading to new properties.

RESULTS AND DISCUSSION

Polymer synthesis and characterization

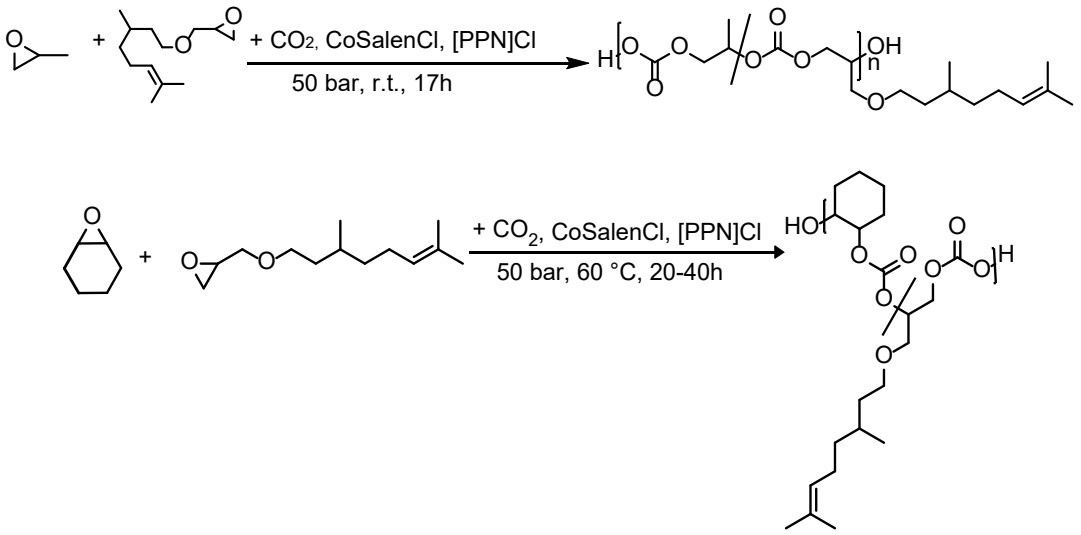

Scheme 1: Terpolymerization of PO/CitroGE/CO_2 (top) and CHO/CitroGE/CO_2 (down) using a binary CoSalen catalyst system.

Citronellol glycidyl ether was prepared according to the established route of Mouzin et al., using epichlorohydrin and citronellol in a phase transfer reaction.[21,22] PO or CHO were copolymerized with CO_2 and CitroGE, applying (*R,R*)-Co(salen)Cl (CoSalenCl) and bis(triphenylphosphine(iminium chloride) (PPN[Cl]) (Figure 1) as binary catalyst system. The CoSalen catalyst systems are widely used in the synthesis of aliphatic polycarbonates, due to the perfectly alternating incorporation of carbon dioxide and epoxides.[23,24] This inhibits the formation of undesired ether linkages, which are often formed in side reactions of the synthesis of APC *via* the copolymerization of epoxides and carbon dioxide.

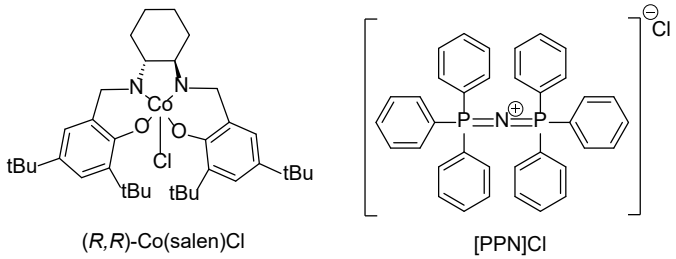

Figure 1: Chemical structure of the binary catalyst system used.

All synthesized polymers show no signals in addition to the ether signal of the side chain of PCitroGEC (3.62 ppm and 3.55 – 3-43 ppm) between 3.0 ppm and 3.5 ppm in the ^{1}H NMR spectra (Figure S 2,

Figure S 7). This confirms that all polymers contain >99 % carbonate linkages in the main chain, as targeted.

Table 1: Overview of the synthesized ter- and homopolymers. All polymers were synthesized using 0.1 mol% of the catalyst system.

sample	Composition[b]	CitroGE[theo]	PC|CC[b]	M_n[a]	$Đ$[a]	yield	conversion[b]	T_g[c]
		mol%		g/mol		%	%	°C
	PCitroGEC	100	92|8	18 650	1.15	70	80	-51
1	$PPC_{0.50}$-*co*-$PCitroGEC_{0.50}$	50	86|14	6 100	1.46	20	74(PO), 100 (CitroGE)	-40
2	$PPC_{0.76}$-*co*-$PCitroGEC_{0.24}$	20	97|3	9 500	1.32	35	100	-9
3	$PPC_{0.82}$-*co*-$PCitroGEC_{0.18}$	10	96|4	13 700	1.50	65	100	6
4	$PPC_{0.99}$-*co*-$PCitroGEC_{0.01}$	2	84|16	9 600	1.23	60	93(PO), 100(CitroGE)	22
	PPC[d]	0	-	13 900	1.61	-	-	41
5	$PCHC_{0.5}$-*co*-$PCitroGEC_{0.5}$	50	99|1	9 570	1.34	93	94(CHO);92(CitroGE)	-2
6	$PCHC_{0.82}$-*co*-$PCitroGEC_{0.18}$	20	95|5	12 000	1.36	94	94(CHO);88(CitroGE)	39
7	$PCHC_{0.89}$-*co*-$PCitroGEC_{0.11}$	17	95|5	12 750	1.37	100	100	56
8	$PCHC_{0.91}$-*co*-$PCitroGEC_{0.09}$	10	87|13	1 2860	1.37	90	94(CHO)/100(CitroGE)	68
	PCHC	0	100|0	10 200	1.36	70	70	94

[a]measured by SEC (Eluent: DMF, standard: PEG). [b]Determined by ^{1}H NMR (300 MHz, $CDCl_3$). [c] Measured by DSC with a heating rate of 20 K/min.[d] Value taken from Kunze et al. (Eluent: DMD, standard: PS).[25] The indices of the composition show the mol fraction of the units in the polymer.

NMR characterization confirms the incorporation of CitroGEC and the stability of the ene moiety in the presence of the binary CoSalen catalyst system (Figure S 2- S 11). Moreover, the formation of carbonate linkages can be verified by ^{13}C NMR. All polymers show a signal at 154 ppm (Figure S 3 and Figure S 8), which belongs assigned to the carbonyl carbon. Additionally, the signals at 124 ppm and 131 ppm can be assigned to the carbons next to the ene moiety of the PCitroGEC units in PPC-*co*-PCitroGEC and PCHC-*co*-PCitroGEC copolymers. All carbon signals were assigned using 2D NMR spectroscopy shown in the Supp. Inf. part (Figures S 2- S 11). A typical side reaction is the depolymerization of the polymer chains, leading to stable cyclic carbonates. This could be observed by checking the IR spectrum of the crude product (Figure S 12). The crude products exhibit a weak signal at 1800 cm^{-1}, attributed to the typical C=O vibration of cyclic carbonate structures, and an intense signal at 1743 cm^{-1} caused by the C=O vibration of the polycarbonate structure. The formed cyclic carbonates were completely removed by precipitation of the crude polymer solution in ice-cold methanol, as evidenced by Figure S 12. The cyclic carbonate content was determined by ^{1}H NMR spectroscopy of the crude products (Figure S 13). The results are presented in Table 1 and show a low extent of cyclic carbonates of 1-16%. This low amount of undesired cyclic carbonates can be attributed

to the mild reaction conditions, i. e. low temperatures (PO/CitroGE/CO_2: 20°C; CHO/CitroGE/CO_2: 60°C) and short reaction times (PO/CitroGE/CO_2: 17h; CHO/CitroGEC/CO_2: 20-40 h). The synthesized polymers were obtained in yields between 20 and 100%. The removal of the catalyst by precipitation was more difficult with the PPC copolymers, because they were more viscous than the PCHC copolymers and precipitated less readily in methanol due to the lower glass transition temperature. This leads to lower yields in the case of the PPC copolymers (Table 1). Terpolymerization of CHO/CitroGE/ CO_2 and PO/CitroGE/CO_2 was accomplished in an autoclave at 50 bar. Polymer with molecular weights between 6 000 and 14 000 g/mol (SEC: eluent: DMF, standard: PEG) with 1-50 mol% of PCitroGEC were obtained. All SEC traces show a bimodal distribution caused by the initiation of water traces in CO_2 and the initiation by the chloride ion of the [PPN]Cl (Figure S 14, S 15).[26] The PCHC copolymers with 50 and 11 mol% CitroGE incorporation exhibit a third high molar mass mode (Figure S 15). Crosslinking of the polymers can be excluded, since the signals of the double bond protons show a consistent integral value (Figure S 7). One assumption could be that the polymers form agglomerates. To test this hypothesis, different concentrations of the polymers will have to be investigated by SEC. ^{1}H NMR DOSY spectra were recorded as well to verify the successful terpolymerizations. **Fehler! Verweisquelle konnte nicht gefunden werden.** shows the ^{1}H NMR DOSY spectrum of $PCHC_{0.89}$-*co*-$PCitroGEC_{0.11}$, Figure S6 of $PPC_{0.82}$-*co*-$PCitroGEC_{0.18}$. All signals of the polymers exhibit the same diffusion coefficient, indicating successful terpolymerization in both cases.

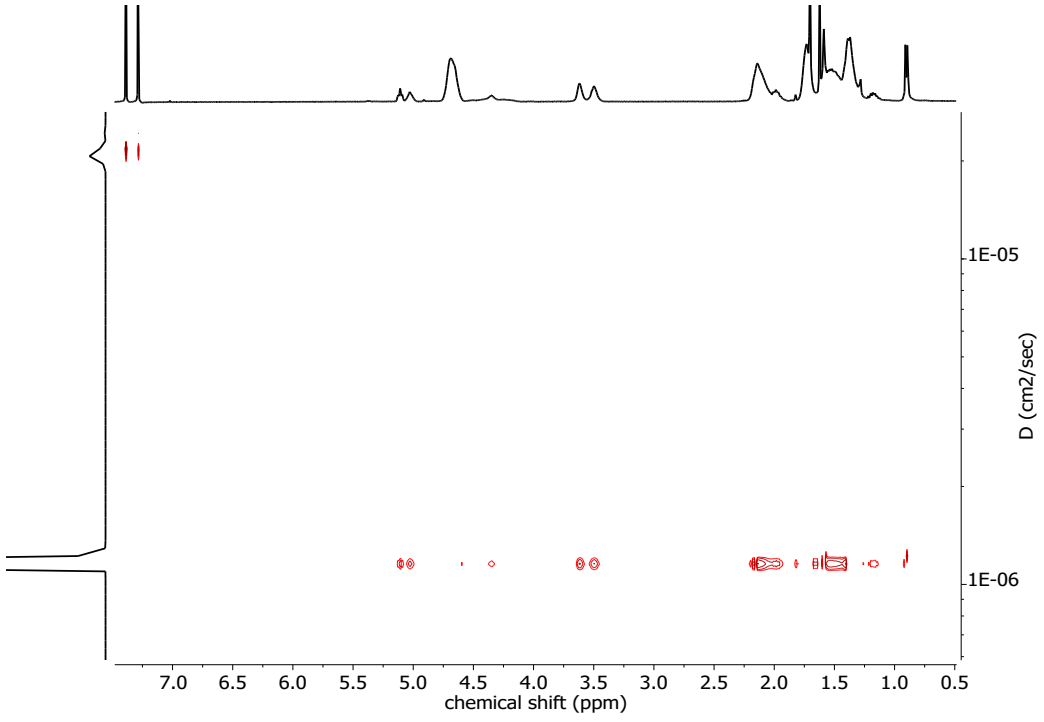

Figure 2: ^{1}H DOSY NMR (400 MHz, $CDCl_3$) of $PCHC_{0.89}$-*co*-$PCitroGEC_{0.11}$ (Table 1, sample 7).

To further confirm the successful terpolymerization of the monomers, MALDI-ToF characterization was conducted. Since accurate mass determination and resolution of isobaric ions using MALDI-ToF are reliable only for oligomer samples below *m/z* 3000, low molar mass terpolymers were synthesized and characterized by MALDI-ToF (Table S 1).[27] Figure S 16 shows the MALDI-ToF spectrum of $PPC_{0.82}$-*co*-$PCitroGEC_{0.18}$ with a molar mass of 1 600 g/mol (SEC: eluent: DMF, standard: PEG). Both repeating units ($M_{CitroGE+CO2}$ = 256 g/mol; M_{PO+CO2} = 104 g/mol) can be identified (Figure S 16 b). In case of $PCHC_{0.75}$-*co*-$PCitroGEC_{0.25}$ (Table S 1, 1500 g/mol) the repeating units ($M_{CitroGE+CO2}$ = 256 g/mol; $M_{CHO+CO2}$ = 142 g/mol) can be detected as well, verifying the formation of a copolymer (Figure S 16 d). These successful terpolymerizations of PO/CitroGE/CO_2 and CHO/CitroGE/CO_2 are not only valuable for tailoring the T_gs of well-known PPC and PCHC polycarbonates, but they also enable post-modification reactions and incorporation of functionalities through the reactive double bond of CitroGE.

Kinetic studies

Kinetic studies were conducted to investigate the microstructure of the copolymers. For this purpose, an autoclave with an external outlet was constructed (Figure S 18). The external outlet is connected to the inner part of the autoclave *via* a cannula. Because of the pressure of 50 bar inside the autoclave, opening the external outlet permitted direct sampling without releasing CO_2 and without opening of the autoclave. This method permits to follow the reaction events under the actual reaction conditions. All samples were immediately measured by ^{1}H NMR spectroscopy to monitor the polymerization. The copolymerization with PO was conducted at 20 °C, and for CHO at 60 °C with 0.1 mol% of the catalyst system in bulk. Homopolymerization of PO or CHO with the CoSalen catalyst system using the same temperatures results in higher conversion and lower amount of cyclic carbonates (same reaction conditions as used for the synthesized polymers (Table 1)). 20 mol% of CitroGE was used for the kinetic studies. Sampling was carried out after different periods (Figures S 20+21). The ^{1}H NMR spectra of the samples are given in Figure S 20 and S 21 in a superimposed mode, with decreasing epoxide protons used for *in situ* calculation of the monomer concentration.

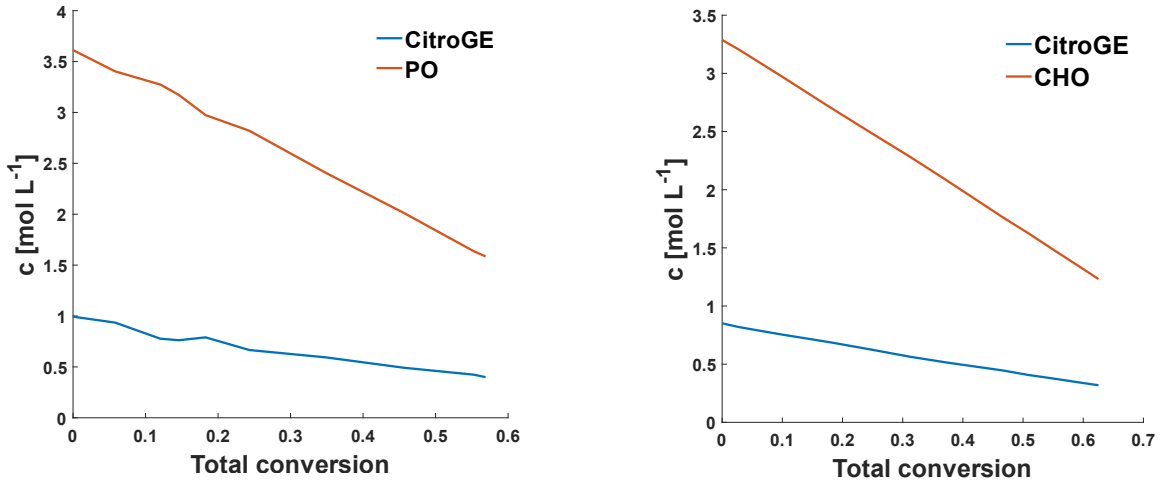

Figure 3: Normalized monomer concentration plotted vs total conversion determined *via* ^{1}H NMR spectroscopy (300 MHz, $CDCl_3$). Copolymerization of CitroGE/PO/CO_2 at room temperature (left). Copolymerization of CitroGE/CHO/CO_2 at 60°C (right).

To evaluate reactivity ratios (r) for both comonomer systems, the Jaacks fit method[28] (since CO_2 copolymerizes in an alternating manner with epoxides, the reactivity ratio of CO_2 was neglected) was utilized (Figure 4). The Jaacks method was preferred, since it involves the use of a large excess of one monomer (PO or CHO) relative to the other one (CitroGE).[29] For PO/CitroGE/CO_2, reactivity ratios of $r_{CitroGE}$ = 1.2151 and r_{PO} = 0.8888 were determined, which indicate an almost ideally random microstructure.

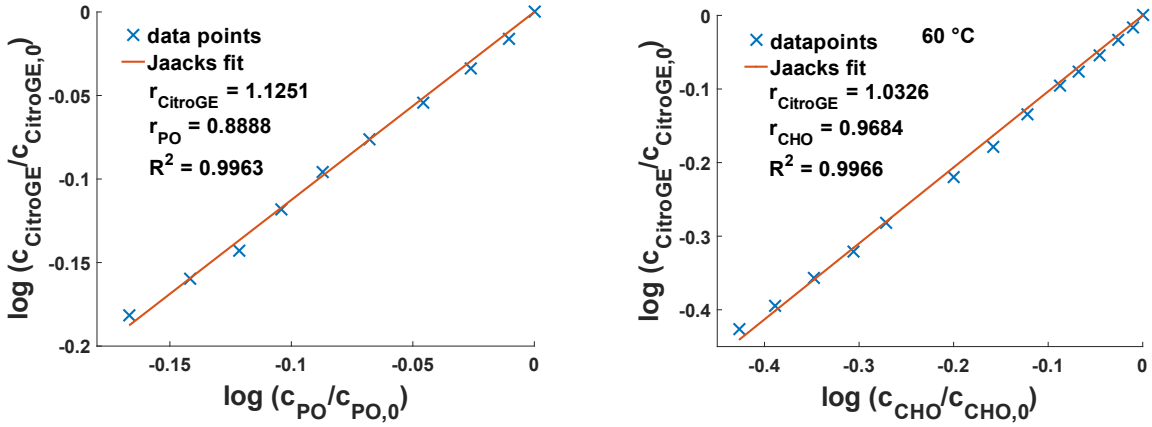

Figure 4: Measured data points (blue cross) and Jaacks-fit for the copolymerization of CitroGE and PO at room temperature (left) and CitroGE and CHO at 60 °C (right) with reactivity ratios determined by the fitting procedure.

To calculate the incorporation preferences, the normalized monomer concentration was plotted against the total monomer conversion, shown in Figure 3. An equal consumption rate of CitroGE and PO or CHO is detected. Moreover, the copolymerization of CHO/CitroGE/CO_2 at 60 °C shows reactivity ratios of $r_{CitroGE}$ = 1.0326 and r_{CHO} = 0.9966, which again indicates a random distribution of CitroGE in

the resulting terpolymer. For better visualization of the distribution in the terpolymers, a simulation of the distribution of CitroGE ($F_{CitroGE}$) plotted versus the total conversion is illustrated in Figure 5. In order to elucidate the influence of temperature on the microstructure of the CHO/CitroGE/CO_2 copolymerization, we conducted a kinetic study at 30 °C (under otherwise identical conditions). The results are shown in Figures S 24 and 25 using again the Jaacks method to determine the reactivity parameters. The CHO/CitroGE/CO_2 copolymerization at 30 °C exhibits reactivity ratios of $r_{CitroGE}$ = 3.0633 and r_{CHO} = 0.3264, indicating favored incorporation of CitroGE, which results in a gradient structure (Figure S 25). This change in the microstructure implies that higher activation energy is required for the CHO compared to the CitroGE monomer resulting in different microstructures using different reaction temperatures.[30] Moreover, this copolymerization was tracked *via* SEC, showing an increase in molar mass with longer reaction times. This leads to a bimodal distribution of PCHC-*co*-PCitroGEC with M_n of 27 800 g/mol and dispersity of 1.41 after 23.5 h (Figure S 26).

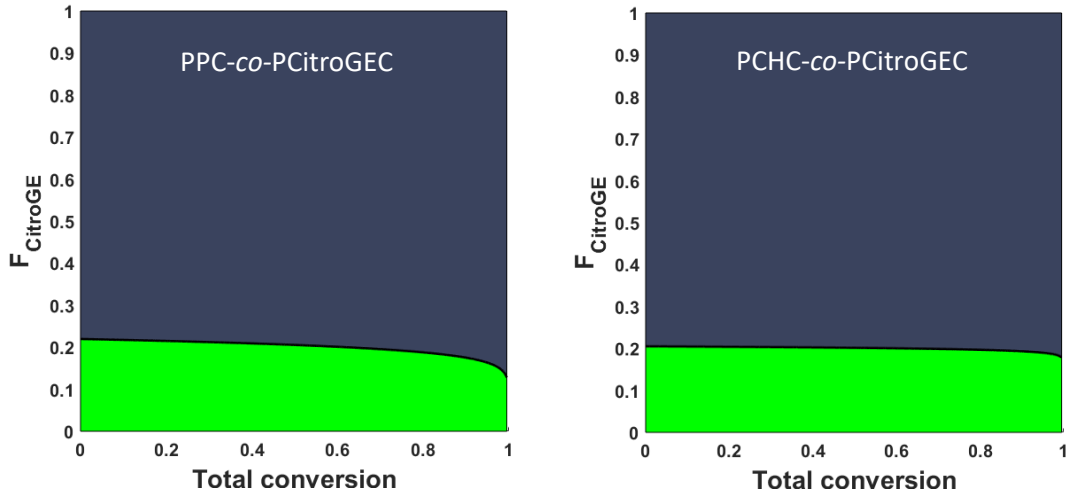

Figure 5: Simulation of the distribution of CitroGE in PPC-*co*-PCitroGEC at 20 °C (left) and of CitroGE in PCHC-*co*-PCitroGE at 60°C (right). This simulation is based on the reactivity ratios determined by the Jaacks-fit for a mixture with 20 mol % of CitroGE. The green area relates to CitroGE, and the grey to PO and CHO, respectively.

Thermal characterization

To further investigate the properties of the synthesized terpolymers, differential scanning calorimetry (DSC)characterization was carried out. The resulting data are summarized in Table 1. The fox equation was utilized for estimation of the plotted glass transition temperatures (T_g) of both types of copolymers.[31]

$$\frac{1}{T_g} = \frac{w_1}{T_{g,1}} + \frac{w_2}{T_{g,2}} \quad (1)$$

w_1 equals the weight fraction of PCitroGEC and w_2 of PCHC or PPC. $T_{g,1}$ relates to the T_g of PCitroGEC homopolymer (Table 1) and $T_{g,2}$ to the PCHC and PPC homopolymers (Table 1), respectively. The copolymers exhibit glass transition temperatures in the range of -40 – +22°C (PPC-*co*-PCitroGEC series) and -2 – +68°C (PCHC-*co*-PCitroGEC series). Clearly, with increasing content of PCitroGEC units, the T_g decreases (Figure 6, Figure S 17+S 18) because of the aliphatic branched C_{10} side chain of PCitroGEC, which leads to higher mobility and flexibility and thus to lower T_g. The T_g observed for the copolymers is in good agreement with the predicted trends applying the Fox equation (1) (Figure 6). Moreover, the PPC-*co*-PCitroGEC with 50 mol% of PCitroGEC displays a T_g of -40 °C. This polymer can be used for crosslinked elastomers, since low T_g is required in this area.[32–34] This sample shows that the terpolymerization with CitroGE/CO_2 with widely used monomers like PO can lead to the desired new structures, since normal PPC exhibits a intermediate T_g of 41 °C (Table 1). PCHC homopolymer itself reveals a high T_g of 94 °C (10 200 g/mol (SEC: eluent: DMF, standard: PEG) (Table 1) and can be viewed as a CO_2-based alternative for polystyrene (PS), which displays a T_g of 100 °C.[35] Lowering the T_g of PCHC using CitroGE leads to intermediate T_gs of -2 – +68 °C, which limits their use as a structural material, but may be relevant for other applications.

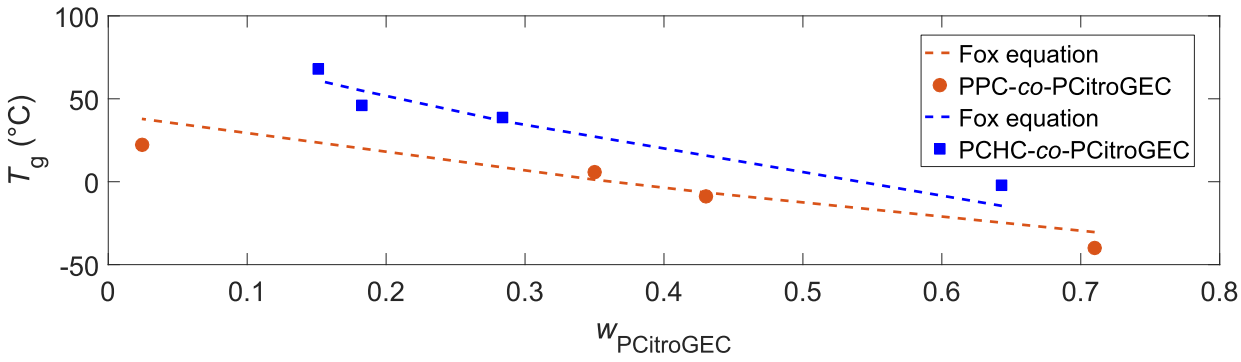

Figure 6: Glass transition temperatures (T_gs) plotted vs the weight fraction of incorporated PCitroGEC and plotted Fox equation. The orange circles show the T_gs of the PPC-*co*-PCitroGEC terpolymers the blue squares the T_gs of the PCHC-*co*-PCitroGEC terpolymers. The dashed lines show the resulting T_gs of the Fox equation.

To sum up, the copolymerization of CHO/CitroGE/CO_2 and the resulting T_gs provide useful insights into the reaction behavior of the two monomers. A linear decrease of the T_g with higher content of PCitroGEC is observable, which is in line with a statistical distribution of the PCitroGEC units.[36]

Post-modification

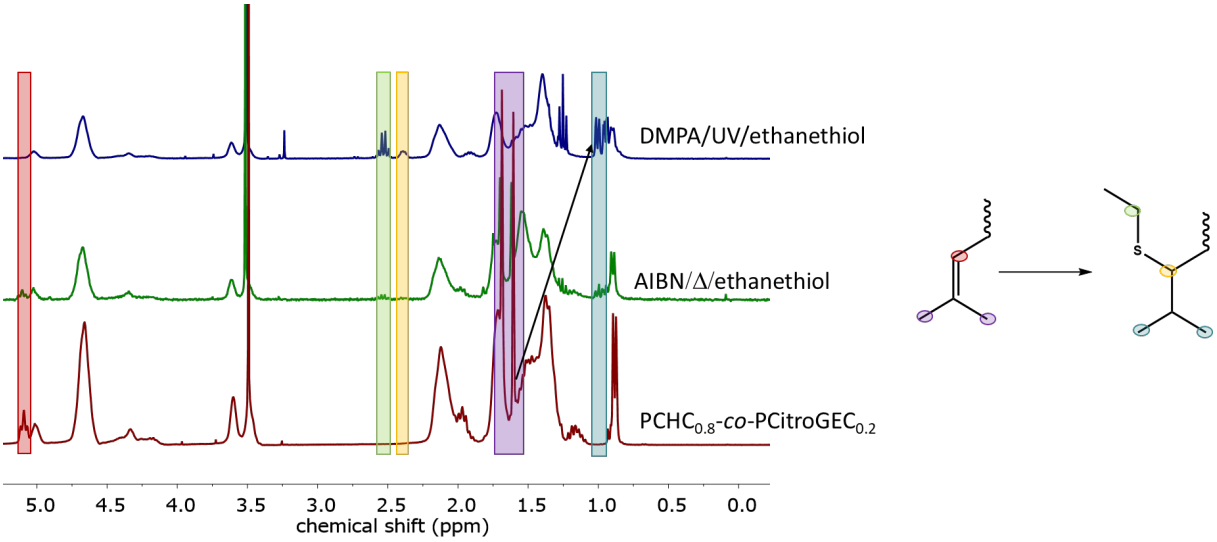

Figure 7: Stacked ^{1}H NMR spectra of PCHC$_{0.8}$-*co*-PCitroGEC$_{0.2}$ (red), PCHC$_{0.8}$-*co*-PCitroGEC$_{0.2}$ reacts with AIBN and ethanethiol at 80 °C (green) and PCHC$_{0.8}$-*co*-PCitroGEC$_{0.2}$ reacts with DMPA and ethanethiol in UV light (blue). The arrow shows the shift of the signals of the CH$_3$-groups to a higher field after the functionalization.

In previous work, we already demonstrated the post-modification of the ene moiety of the citronellol side chain *via* TAD-click chemistry.[22,37] Moreover, we could prove the stability of the aliphatic carbonates also for TAD-click reactions.[37] To expand the range of useful post-modifications, we performed thiol-ene click reactions with PCHC$_{0.8}$-*co*-PCitroGEC$_{0.2}$ (sample of the kinetic study) under different conditions. First, we used AIBN (azobisisobutyronitrile) as a thermal initiator and ethanethiol at 80 °C in dry dichloromethane. Secondly, DMPA (2,2-Dimethoxy-2-phenylacetophenone) and UV light were utilized with ethanethiol to modify the double bond. The first reactions with AIBN and 80 °C resulted in a partial conversion of the ene moiety, indicated by a signal at 5.02 ppm. This can be assigned to the ene moiety. (Figure 7, green ^{1}H NMR, the signal is highlighted with red). The experiment with DMPA and UV light was successful, in this case no signal for the double bond was quantifiable (Figure 7, blue ^{1}H NMR, red highlighted), indicating full conversion. Furthermore, new signals corresponding to the protons next to the established thiol ether can be identified at 2.50 ppm which are highlighted in green and yellow. Additionally, a shift of the CH$_3$ groups (purple) next to the ene moiety from 1.60 ppm to higher fields (1.00 ppm) confirmed complete conversion of the ene moiety to the thiol ether. This model experiment in addition to previous experiments[22,37] shows that the double bond of the CitroGE side chain enables various post-modification reactions, permitting to adapt the properties of homo- and copolymers for different applications.

CONCLUSION

Successful copolymerization of CitroGE/PO/CO_2 and CitroGE/CHO/CO_2 using the CoSalenCl catalyst system has been demonstrated. Systematically varied comonomer fractions of the terpene-based CitroGE were incorporated in the polycarbonate copolymers, resulting in a decrease of T_g with higher content of CitroGE. For instance, a PPC copolymer with 50 mol% of PCitroGEC displays a T_g of -40 °C. Polymers with low T_gs in this range are promising for the synthesis of elastomers.[33,34] This shows that the terpolymerization results in useful materials, since PPC itself reveals an intermediate T_g of 41 °C.[25] Furthermore, kinetic studies were conducted to get an insight into the microstructure of the copolymers. These studies revealed a random microstructure for PO/CitroGE/CO_2 terpolymerization at 20°C and for CHO/CitroGE/CO_2 at 60 °C a random microstructure. Utilizing the Jaacks method, reactivity ratios of $r_{CitroGE}$ = 1.2152 and r_{PO} = 0.8888 for the PO/CitroGE/CO_2 copolymerization at 20 °C and $r_{CitroGE}$ = 1.0326 and r_{CHO} = 0.9966 for the CHO/CitroGE/CO_2 copolymerization at 60°C were determined. The copolymerization of CHO/CitroGE/CO_2 at 30 °C reveals a gradient structure with reactivity ratios of $r_{CitroGE}$ = 3.0633 and r_{CHO} = 0.3264. Probably because CHO has a higher activation energy than CitroGE. Finally, we could demonstrate that the ene moiety of the PCitroGE chain is not just advantageous for TAD-click reactions[22] but also thiol-ene click reactions are feasible using DMPA and UV light.

EXPERIMENTAL SECTION

Materials

Solvents and reagents were applied as obtained unless otherwise stated. Cyclohexene oxide (CHO) and Propylene oxide (PO) was distilled over CaH_2 under reduced pressure before use. Carbon dioxide (>99.999%) was achieved from Westfalen AG (Münster, Germany). Bis(triphenylphosphine)iminium chloride ([PPN]Cl) was received from abcr GmbH. (*R,R*)-(salcy)-Co(III)Cl was prepared as described by Ford et al.[38] All solvents were purchased from Sigma Aldrich, Fischer Chemical (Pittsburgh, PA, USA), and Honeywell (Morris Plaines, NJ, USA) and used without further purification. All reagents were acquired from Sigma Aldrich, Arcos Organics (Pittsburgh, PA, USA), Alfa Aesar (Kandel, Germany), or TCI (Oxford, UK). Deuterated solvents were purchased from Deutero GmBH (Kastellaun, Germany).

Characterization

NMR Analysis. ^{1}H NMR spectra at 300 MHz and ^{13}C NMR spectra at 75 MHz were recorded on a Bruker Avance III HD 300 (5 mm BBFO-Head with *z*-gradient) at 23 °C. ^{1}H NMR spectra at 400 MHZ and ^{13}C NMR spectra at 100 MHz were recorded on a Bruker Avance III HD 400 (5 mm BBFO Smartprobe with *z*-gradient) at 23 °C. The spectra are referenced internally to the residual proton signal of the deuterated solvent.

Size exclusion chromatography (SEC). SEC was completed in DMF (1 mL/min, 50 °C) containing 1 g/L lithium bromide as an additive, using an Agilent 1100 series SEC system equipped with a HEMA 300/100/40 Å column cascade, UV (254 nm), and RI detector. Calibration was accomplished using poly(ethylene glycol) (PEG) standards acquired from Polymer Standard Service (PSS).

Differential scanning calorimetry (DSC). DSC curves were recorded using a Perkin-Elmer DSC 7 CLN2 instrument in the temperature range of -95°C– +180°C or -95 °C– +60 °C with heating rates of 20K/min under nitrogen atmosphere. Glass transition temperatures (T_g) were determined using Pyris™ software.

Infrared spectroscopy. FT-IR spectra were recorded using an iS10 FT-IR spectrometer (Thermo Scientific, Waltham, MA, USA) equipped with a diamond ATR unit.

Matrix-Assisted Laser Desorption Ionization Time of Flight Mass Spectrometry (MALDI-ToF). Mass spectra were measured on a MALDI ToF MS Autoflex Max by Bruker. The samples were prepared as a 1 mg/mL solution in dichloromethane. As a matrix, *trans*-2-[3-(4-*tert*-Butylphenyl)-2-methyl-2-

propenyliden] malononitrile (DCTB) with NaTFA was used. The measurement was performed in linear or reflector mode. The data were analyzed by the *mmass 5.5.0* software.

Kinetic studies. Samples were taken after different periods (Figure S 20+21) *via* the cannula connected directly to the reaction mixture (Figure S 19). The concentration of the monomers at different time spots was calculated using ^{1}H NMR (300 MHz, $CDCl_3$). The normalized concentrations were used to calculate the shown data. Data were evaluated by using NIRVAL Software from Tobias Johann, Marvin Steube und Holger Frey.[30] The reactivity ratio of the monomer in excess is obtained from the linear logarithmic plot of comonomer conversions:

$$r_1 = \frac{ln\frac{c_{1,0}}{c_i}}{n\frac{c_{2,0}}{c_2}} \quad (1)$$

where $c_{i,0}$, c_i are the initial concentration of monomer i and concentration of unreacted monomer i after a given polymerization time, respectively.[39]

Synthesis

Monomer synthesis

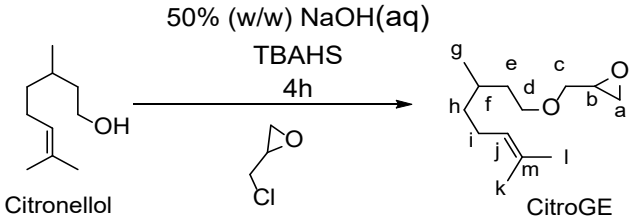

Citronellol glycidyl ether (CitroGE) (IUPAC: 2-(((3,7-dimethyloct-6-en-1-yl)oxy)methyl)oxirane) was prepared according to literature[21,22] on a scale of 0.1 mol citronellol. 40% of CitroGE as a colorless liquid was obtained after distillation under a high vacuum (1x10^{-3} mbar, 80 °C). Before use, CitroGE was dried with benzene in an azeotropic distillation.

^{1}H NMR (300 MHz, $CDCl_3$) δ = 5.10 – 5.03 (m, 1H, j), 3.70 – 3.65 (m, 1H, c), 3.57 – 3.42 (m, 2H, d), 3.38 – 3.31 (m, 1H, c'), 3.14 – 3.08 (m, 1H, b), 2.79 – 2.55 (m, 2H, a), 2.04 – 1.85 (m, 2H, i), 1.65 (s, 3H, l), 1.57 (s, 3H, k), 1.42 -1.09 (m, 5H, e+f+h), 0.87 (d, 3H,g) ppm.

Polymer synthesis

Synthesis of PPC-co-PCitroGEC

General procedure illustrated for the synthesis of $PPC_{0.82}$-*co*-$PCitroGEC_{0.18}$ (Table 1, sample 4).

Synthesis: A 100 mL Roth autoclave was dried at 40 °C under reduced pressure. Citronellol glycidyl ether (CitroGE) (0.5 mL, 2.16 mmol), propylene oxide (PO)(1.36 mL, 19.50 mmol), (*R,R*)-(salcy)-CoCl (13.8 mg, 0.022 mmol) and [PPN]Cl (12.4 mg, 0.022 mmol) were filled in the autoclave equipped with a stirring-bar in an inert argon atmosphere. The reaction mixture was stirred at a carbon dioxide pressure of 55 bar at room temperature for 17 h.

Different ratios of PO and CitroGE were used to prepare polymers with various contents of PCitroGEC.

Purification: The crude product was dissolved in dichloromethane (DCM), and the catalyst was deactivated with 1 mL of a solution of $5\%_{vol}$ HCl (aq) in methanol. The product was precipitated in ice-cold methanol as a non-solvent. The precipitated product was collected by centrifugation at 4500 rpm at 0°C for 10 min. The process was repeated an additional time to increase purity. The light yellow, viscous product was then dried under reduced pressure for 24h. A yield of 65 % polymer was obtained.

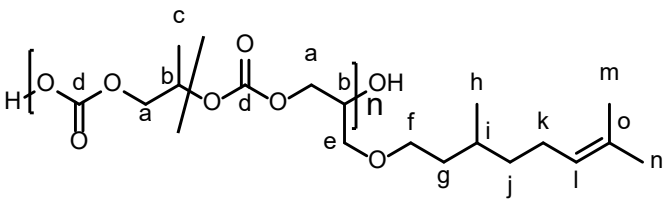

^{1}H NMR (300 MHz, $CDCl_3$) δ = 5.00 (t, 1H, l), 4.96 – 4.83 (m, 7H, b), 4.41 – 3.92 (m, 14 H, a), 3.5 (d, 2H, e), 3.38 (h, 2H, f), 2.00 – 1.73 (m, 2H, k), 1.58 (s, 3H, m), 1.50 (s, 3 H, n), 1.47 – 0.97 (m, 23H, i+g+c+j), 0.78 (d, 3H, h) ppm.

^{13}C NMR (75 MHz, $CDCl_3$): δ = 154.24 (D), 131.16 (O), 124.75 (L), 74.39 (B), 72.39 (B), 70.14 (F), 69.20 (A), 69.01 (E), 37.21 (G), 36.30 (J), 29.50 (I), 25.73 (L), 25.44 (M/N), 19.54 (H), 17.67 (M/N), 16.25 (C) ppm.

M_n (SEC, DMF, PEG calibration) = 13 700 g/mol; $Đ$ (SEC, DMF, PEG calibration) = 1.50.

T_g: 6 °C.

Synthesis of PCHC-co-PCitroGEC

General procedure illustrated for the synthesis of $PCHC_{0.89}$-*co*-$PCitroGEC_{0.11}$ (Table 1, sample 8).

Synthesis: A 100 mL Roth autoclave was dried at 40 °C under reduced pressure. Citronellol glycidyl ether (CitroGE) (0.6 mL, 2.43 mmol), cyclohexene oxide (CHO) (1.1 mL, 10.87 mmol), (*R,R*)-(salcy)-CoCl (10.3 mg, 0.016 mmol) and [PPN]Cl (9.3 mg, 0.016 mmol) were filled in the autoclave equipped with a stirring-bar in an inert argon atmosphere. The reaction mixture was stirred at a carbon dioxide pressure of 55 bar at 60 °C for 47 h.

Different ratios of CHO and CitroGE were applied to create polymers with a variety of content of PCitroGEC.

Purification: The crude product was dissolved in DCM, and the catalyst was deactivated with 1 mL of a solution of 5%$_{vol}$ HCl (aq) in methanol. The product was precipitated in ice-cold methanol as a non-solvent. The precipitated product was collected by centrifugation at 4500 rpm at 0°C for 10 min. The process was repeated an additional time to increase purity. The colorless, solid product was then dried under reduced pressure for 24h. A yield of 100% polymer was obtained.

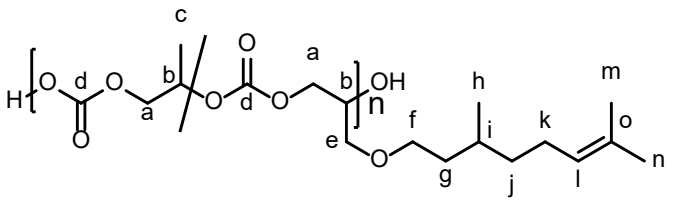

^{1}H NMR (300 MHz, $CDCl_3$) δ = 5.16 – 5.07 (m, 1H, n), 5.03 (s, 1H, f), 4.69 (m, 9H, a), 4.59 – 4.11 (m, 2H, e), 3.69 – 3.56 (m, 2H, g), 3.55 – 4.42 (m, 2H, h), 2.41 (s, 9H, b), 2.00 (q, 2H, m) 1.98 – 1.06 (m, 39H, c+q+p+j+i+l), 0.90 (dd, 3H, h) ppm.

^{13}C NMR (75 MHz, $CDCl_3$): δ = 153.82 (D), 131.15 (O), 124.78 (N), 76.69 (A), 74.01 (F), 70.12 (H), 67.51 (G), 65.43 (E), 37.26 (I), 36.45 (L), 29.64 (J), 29.54 (B), 25.75 (M), 25.46 (P/Q), 23.51 (C), 19.51 (K), 17.67 (P/Q)ppm.

M_n (SEC, DMF, PEG calibration) = 12750 g/mol; $Đ$ (SEC, DMF, PEG calibration) = 1.37.

T_g: 56 °C.

Post-modification reactions

Thiol-ene-click reaction with DMPA/UV

The $PCHC_{0.8}$-*co*-$PCitroGEC_{0.2}$ (polymer resulting from the kinetic studies at 60 °C) (0.2 g, 0.046 mmol, ethanethiol (0.11 mL, 1.58 mmol), DMPA (0.11 g, 0.046 mmol) were dissolved in a minimal amount of DCM. The reaction mixture was purged 5 – 10 min with argon. After the purging, the mixture was irradiated for 4h with a 365 nm UV lamp. The polymer was precipitated in methanol and then in acetonitrile.

Thiol-ene-click reaction with AIBN/80 °C

The $PCHC_{0.8}$-*co*-$PCitroGEC_{0.2}$ (polymer resulting from the kinetic studies at 60 °C) (0.2 g, 0.046 mmol, ethanethiol (0.11 mL, 1.58 mmol), AIBN (0.0076 g, 0.046 mmol) were dissolved in a minimal amount of DCM. The reaction mixture was purged 5 – 10 min with argon. After the purging, the mixture was heated at 80 °C for 4h. The polymer was precipitated in methanol and then in acetonitrile.

ACKNOWLEDGMENTS

We thank Monika Schmelzer for the SEC measurements and Elena Dr.Berger Nicoletti for the MALDI-ToF measurements. Philipp Holzmüller and Kevin Woods for the critical reading of this work.

REFERENCES

(1) Artz, J.; Müller, T. E.; Thenert, K.; Kleinekorte, J.; Meys, R.; Sternberg, A.; Bardow, A.; Leitner, W. Sustainable Conversion of Carbon Dioxide: An Integrated Review of Catalysis and Life Cycle Assessment. *Chem. Rev.* **2018**, *118*, 434–504.

(2) Sakakura, T.; Choi, J.-C.; Yasuda, H. Transformation of carbon dioxide. *Chem. Rev.* **2007**, *107*, 2365–2387.

(3) Inoue, S.; Koinuma, H.; Tsuruta, T. Copolymerization of carbon dioxide and epoxide. *J. Polym. Sci. B Polym. Lett.* **1969**, *7*, 287–292.

(4) Scharfenberg, M.; Hilf, J.; Frey, H. Functional Polycarbonates from Carbon Dioxide and Tailored Epoxide Monomers: Degradable Materials and Their Application Potential. *Adv. Funct. Mater.* **2018**, *28*, 1704302.

(5) Welle, A.; Kröger, M.; Döring, M.; Niederer, K.; Pindel, E.; Chronakis, I. S. Electrospun aliphatic polycarbonates as tailored tissue scaffold materials. *Biomaterials* **2007**, *28*, 2211–2219.

(6) Zhang, Y.-Y.; Wei, R.-J.; Zhang, X.-H.; Du, B.-Y.; Fan, Z.-Q. Efficient solvent-free alternating copolymerization of CO_2 with 1, 2-epoxydodecane and terpolymerization with styrene oxide via heterogeneous catalysis. *J. Polym. Sci. A Polym. Chem.* **2015**, *53*, 737–744.

(7) Geschwind, J.; Wurm, F.; Frey, H. From CO 2 -Based Multifunctional Polycarbonates With a Controlled Number of Functional Groups to Graft Polymers. *Macromol. Chem. Phys.* **2013**, *214*, 892–901.

(8) Qin, Y.; Wang, X. Carbon dioxide-based copolymers: environmental benefits of PPC, an industrially viable catalyst. *Biotechnol. J.* **2010**, *5*, 1164–1180.

(9) Ren, W.-M.; Zhang, X.; Liu, Y.; Li, J.-F.; Wang, H.; Lu, X.-B. Highly Active, Bifunctional Co(III)-Salen Catalyst for Alternating Copolymerization of CO_2 with Cyclohexene Oxide and Terpolymerization with Aliphatic Epoxides. *Macromolecules* **2010**, *43*, 1396–1402.

(10) Li, H.; Niu, Y. Alternating copolymerization of CO_2 with propylene oxide and terpolymerization with aliphatic epoxides by bifunctional cobalt Salen complex. *Polym. J.* **2011**, *43*, 121–125.

(11) Darensbourg, D. J.; Poland, R. R.; Strickland, A. L. (Salan)CrCl, an effective catalyst for the copolymerization and terpolymerization of epoxides and carbon dioxide. *J. Polym. Sci. A Polym. Chem.* **2012**, *50*, 127–133.

(12) Quan, Z.; Min, J.; Zhou, Q.; Xie, D.; Liu, J.; Wang, X.; Zhao, X.; Wang, F. Synthesis and properties of carbon dioxide – epoxides copolymers from rare earth metal catalyst. *Macromol. Symp.* **2003**, *195*, 281–286.

(13) Shi, L.; Lu, X.-B.; Zhang, R.; Peng, X.-J.; Zhang, C.-Q.; Li, J.-F.; Peng, X.-M. Asymmetric Alternating Copolymerization and Terpolymerization of Epoxides with Carbon Dioxide at Mild Conditions. *Macromolecules* **2006**, *39*, 5679–5685.

(14) Reiter, M.; Vagin, S.; Kronast, A.; Jandl, C.; Rieger, B. A Lewis acid β-diiminato-zinc-complex as all-rounder for co- and terpolymerisation of various epoxides with carbon dioxide. *Chem. Sci.* **2017**, *8*, 1876–1882.

(15) Seong, J. E.; Na, S. J.; Cyriac, A.; Kim, B.-W.; Lee, B. Y. Terpolymerizations of CO_2 , Propylene Oxide, and Various Epoxides Using a Cobalt(III) Complex of Salen-Type Ligand Tethered by Four Quaternary Ammonium Salts. *Macromolecules* **2010**, *43*, 903–908.

(16) Chukanova, O. M.; Korenkov, K. O.; Garifullin, N. O.; Sheverdenkina, O. G.; Sedov, I. V. Kinetics of Carbon Dioxide Terpolymerization with Propylene Oxide and Hexene Oxide. *Kinet. Catal.* **2020**, *61*, 569–574.

(17) Zhang, Y.-Y.; Zhang, X.-H.; Wei, R.-J.; Du, B.-Y.; Fan, Z.-Q.; Qi, G.-R. Synthesis of fully alternating polycarbonate with low T g from carbon dioxide and bio-based fatty acid. *RSC Adv* **2014**, *4*, 36183–36188.

(18) Wu, G.-P.; Xu, P.-X.; Zu, Y.-P.; Ren, W.-M.; Lu, X.-B. Cobalt(III)-complex-mediated terpolymerization of CO_2 , styrene oxide, and epoxides with an electron-donating group. *J. Polym. Sci. A Polym. Chem.* **2013**, *51*, 874–879.

(19) Liu, Y.; Ren, W.-M.; He, K.-K.; Lu, X.-B. Crystalline-gradient polycarbonates prepared from enantioselective terpolymerization of meso-epoxides with CO_2. *Nat. Commun.* **2014**, *5*, 5687.

(20) Honda, M.; Ebihara, T.; Ohkawa, T.; Sugimoto, H. Alternating terpolymerization of carbon dioxide, propylene oxide, and various epoxides with bulky side groups for the tuning of thermal properties. *Polym. J.* **2021**, *53*, 121–127.

(21) Mouzin, G.; Cousse, H.; Rieu, J.-P.; Duflos, A. A Convenient One-Step Synthesis of Glycidyl Ethers. *Synthesis* **1983**, *1983*, 117–119.

(22) Johann, T.; Houck, H. A.; Dinh, T.; Kemmer-Jonas, U.; Du Prez, F. E.; Frey, H. Multi-olefin containing polyethers and triazolinediones: a powerful alliance. *Polym. Chem.* **2019**, *10*, 4699–4708.

(23) Coates, G. W.; Moore, D. R. Discrete metal-based catalysts for the copolymerization of CO_2 and epoxides: discovery, reactivity, optimization, and mechanism. *Angew. Chem. Int. Ed. Engl.* **2004**, *43*, 6618–6639.

(24) Decortes, A.; Castilla, A. M.; Kleij, A. W. Salen-complex-mediated formation of cyclic carbonates by cycloaddition of CO_2 to epoxides. *Angew. Chem. Int. Ed. Engl.* **2010**, *49*, 9822–9837.

(25) Kunze, L.; Wolfs, J.; Verkoyen, P.; Frey, H. Crystalline CO_2 -Based Aliphatic Polycarbonates with Long Alkyl Chains. *Macromol. Rapid Commun.* **2018**, *39*, e1800558.

(26) Jia, M.; Hadjichristidis, N.; Gnanou, Y.; Feng, X. Monomodal Ultrahigh-Molar-Mass Polycarbonate Homopolymers and Diblock Copolymers by Anionic Copolymerization of Epoxides with CO_2. *ACS Macro Lett.* **2019**, *8*, 1594–1598.

(27) Nakamura, S.; Fouquet, T.; Sato, H. Molecular Characterization of High Molecular Weight Polyesters by Matrix-Assisted Laser Desorption/Ionization High-Resolution Time-of-Flight Mass Spectrometry Combined with On-plate Alkaline Degradation and Mass Defect Analysis. *J. Am. Soc. Mass Spectrom* **2019**, *30*, 355–367.

(28) Blankenburg, J.; Maciol, K.; Hahn, C.; Frey, H. Poly(ethylene glycol) with Multiple Aldehyde Functionalities Opens up a Rich and Versatile Post-Polymerization Chemistry. *Macromolecules* **2019**, *52*, 1785–1793.

(29) Jaacks, V. A novel method of determination of reactivity ratios in binary and ternary copolymerizations. *Makromol. Chem.* **1972**, *161*, 161–172.

(30) Steube, M.; Johann, T.; Plank, M.; Tjaberings, S.; Gröschel, A. H.; Gallei, M.; Frey, H.; Müller, A. H. E. Kinetics of Anionic Living Copolymerization of Isoprene and Styrene Using in Situ NIR Spectroscopy: Temperature Effects on Monomer Sequence and Morphology. *Macromolecules* **2019**, *52*, 9299–9310.

(31) FOX, T. G. Influence of Diluent and of Copolymer Composition on the Glass Temperature of a Polymer System. *Bull. Am. Phys. Soc.* **1956**, *1*, 123.

(32) Javadinejad, S.; Eslamian, S.; Ostad-Ali-Askari, K.; Nekooei, M.; Azam, N.; Talebmorad, H.; Hasantabar-Amiri, A.; Mousavi, M. Relationship Between Climate Change, Natural Disasters, and Resilience in Rural and Urban Societies. In *Handbook of Climate Change Resilience*; Leal Filho, W., Ed.; Springer International Publishing: Cham, 2020; pp 607–631.

(33) Bogoslovov, R. B.; Roland, C. M.; Gamache, R. M. Impact-induced glass transition in elastomeric coatings. *Appl. Phys. Lett.* **2007**, *90*, 221910.

(34) Bandzierz, K.; Reuvekamp, L.; Dryzek, J.; Dierkes, W.; Blume, A.; Bielinski, D. Influence of Network Structure on Glass Transition Temperature of Elastomers. *Materials (Basel, Switzerland)* **2016**, *9*, 607.

(35) Rieger, J. The glass transition temperature of polystyrene. *J. Therm. Anal.* **1996**, *46*, 965–972.

(36) Sperling, L. H.; Fay, J. J. Factors which affect the glass transition and damping capability of polymers. *Polym. Adv. Technol.* **1991**, *2*, 49–56.

(37) Gardiner, C.; Johann, T.; Hanewald A.; Frey, H. Addressing a key challenge of CO_2-based polycarbonates: low glass transition capitalizing on citronellol glycidyl ether. *to be submitted* **2021**.

(38) Ford, D. D.; Nielsen, L. P. C.; Zuend, S. J.; Musgrave, C. B.; Jacobsen, E. N. Mechanistic basis for high stereoselectivity and broad substrate scope in the (salen)Co(III)-catalyzed hydrolytic kinetic resolution. *J. Am. Chem. Soc.* **2013**, *135*, 15595–15608.

(39) Ydens, I.; Degée, P.; Haddleton, D. M.; Dubois, P. Reactivity ratios in conventional and nickel-mediated radical copolymerization of methyl methacrylate and functionalized methacrylate monomers. *Eur. Polym. J.* **2005**, *41*, 2255–2263.

SUPPORTING INFORMATION

Tailoring the glass transition temperatures of the established aliphatic polycarbonates PPC and PCHC using biobased citronellol glycidyl ether: kinetic studies and post-modification.

Christina Gardiner[1], Holger Frey[1*]

[1]Department of Chemistry, Johannes Gutenberg University, Duesbergweg 10-14, 55128 Mainz, Germany

Table of content

1. Monomer characterization

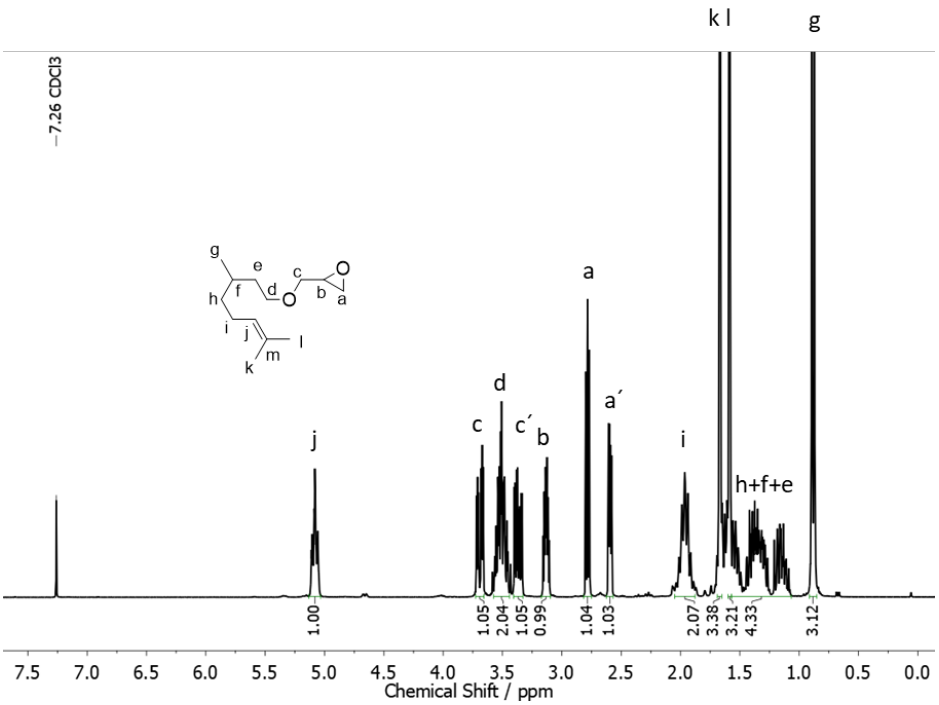

Figure S 1: ^{1}H NMR spectrum (300 MHz, $CDCl_3$) of CitroGE after distillation.

2. Polymer characterization

Table S 1: Overview of the low molar mass terpolymers. The polymerizations were conducted using 1.5 mol% (PPC-*co*-PCitroGEC) and 8 mol% (PCHC-*co*-PCitroGEC) of the catalyst system.

sample	Composition[b]	M_n[a]	$Đ$[a]	yield	conversion[b]	T_g[c]
		g/mol		%	%	°C
10	$PPC_{0.82}$-*co*-$PCitroGEC_{0.18}$	1600	1.12	50	100	-21
11	$PCHC_{0.75}$-*co*-$PCitroGEC_{0.25}$	1500	1.09	17	100	26

[a] measured by SEC (Eluent: DMF, standard: PEG). [b] Determined by ^{1}H NMR (300 MHz, $CDCl_3$). [c] Measured by DSC with a heating rate of 20 K/min.

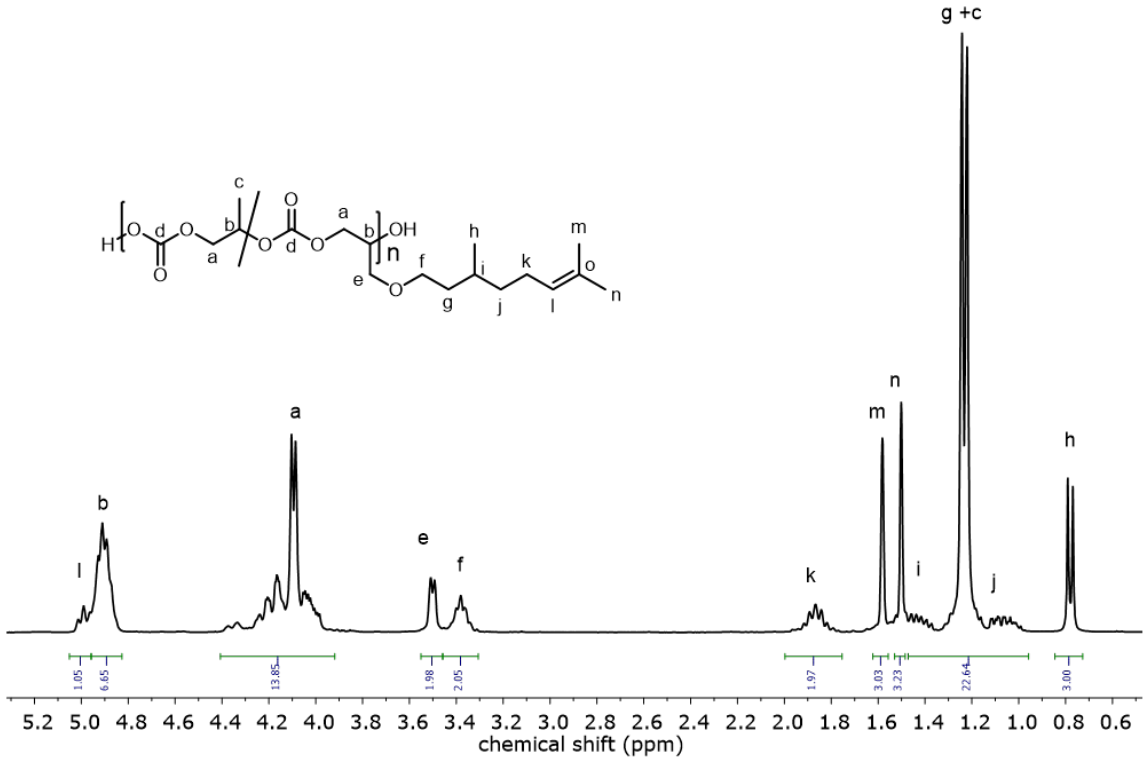

Figure S 2: ^{1}H NMR spectrum (300 MHz, $CDCl_3$) of $PPC_{0.82}$-*co*-$PCitroGEC_{0.18}$ (Table 1, sample 3).

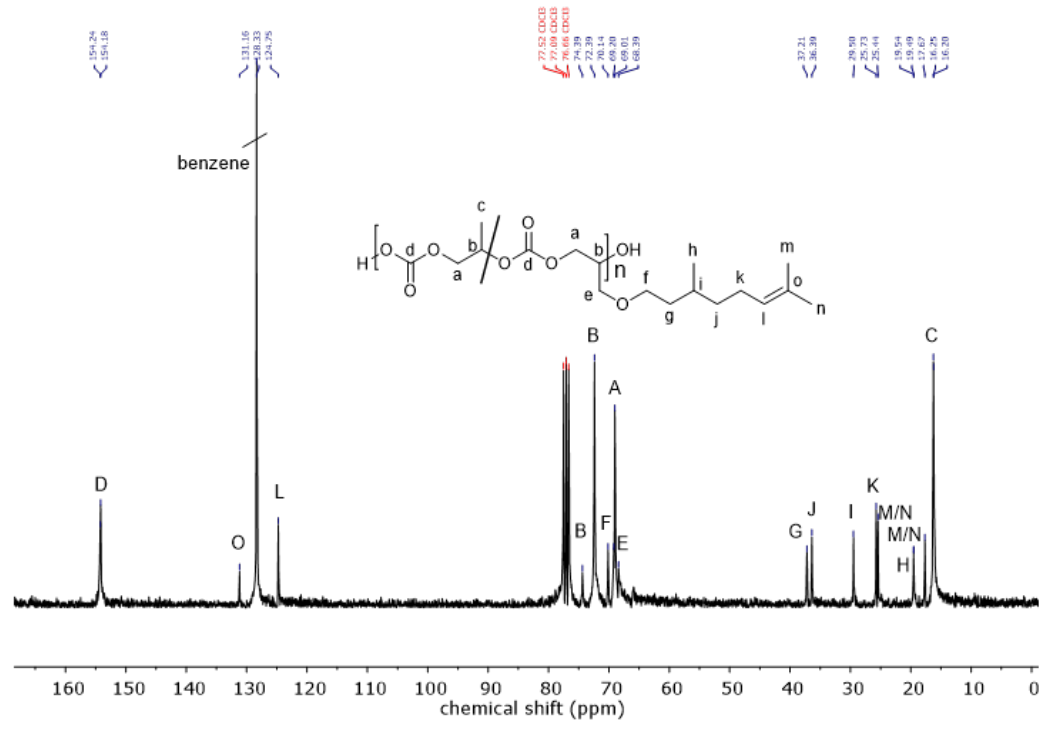

Figure S 3: ^{13}C NMR spectrum (75 MHz, $CDCl_3$) of $PPC_{0.82}$-*co*-$PCitroGEC_{0.18}$ (Table 1, sample 3), showing the newly formed polycarbonate structure, based on the signal of the carbonyl carbon at 154.24 ppm.

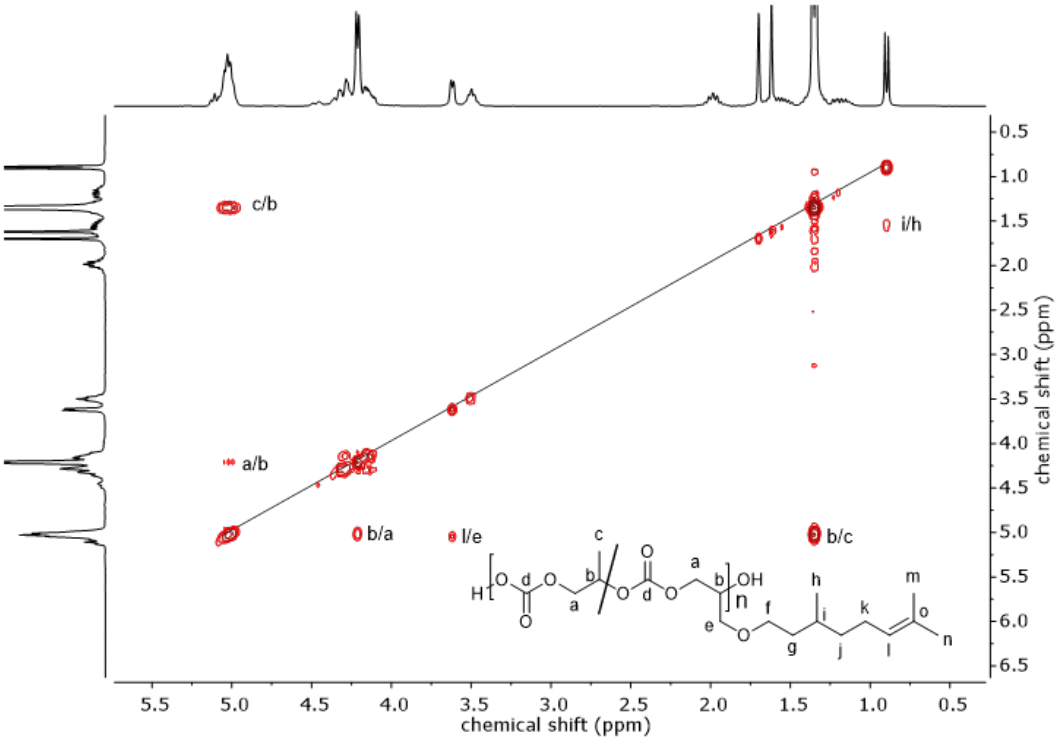

Figure S 4: ^{1}H ^{1}H COSY NMR (300 MHz, $CDCl_3$) spectrum of $PPC_{0.82}$-*co*-$PCitroGEC_{0.18}$ (Table 1, sample 3).

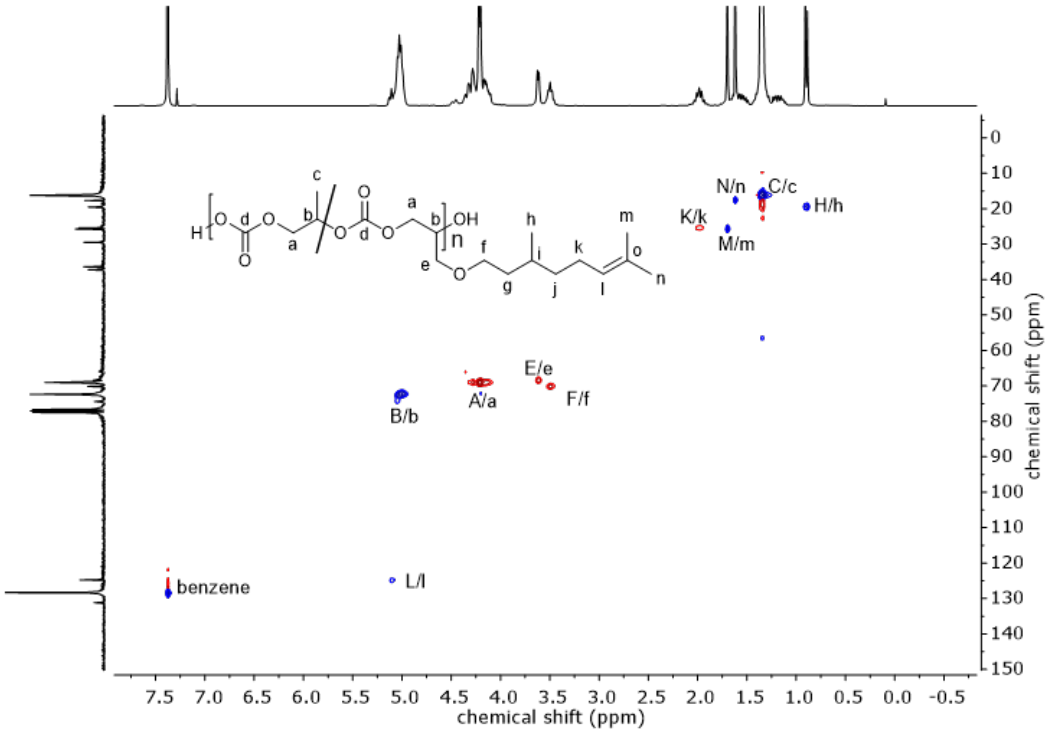

Figure S 5: ^{1}H ^{13}C HSQC NMR spectrum (300 MHz/75 MHz, $CDCl_3$) of $PPC_{0.82}$-*co*-$PCitroGEC_{0.18}$ (Table 1, sample 4).

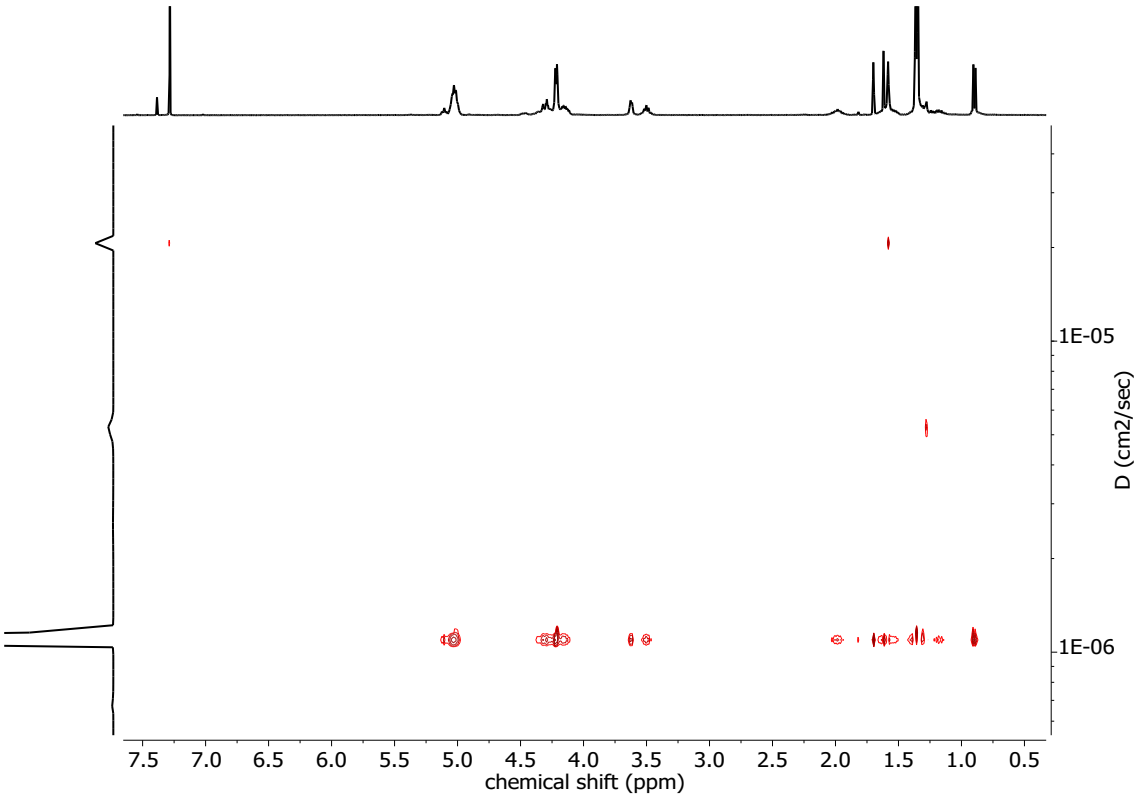

Figure S 6: ^{1}H NMR DOSY (400 MHz, $CDCl_3$) of $PPC_{0.82}$-*co*-$PCitroGEC_{0.18}$ terpolymer (Table 1, sample 3).

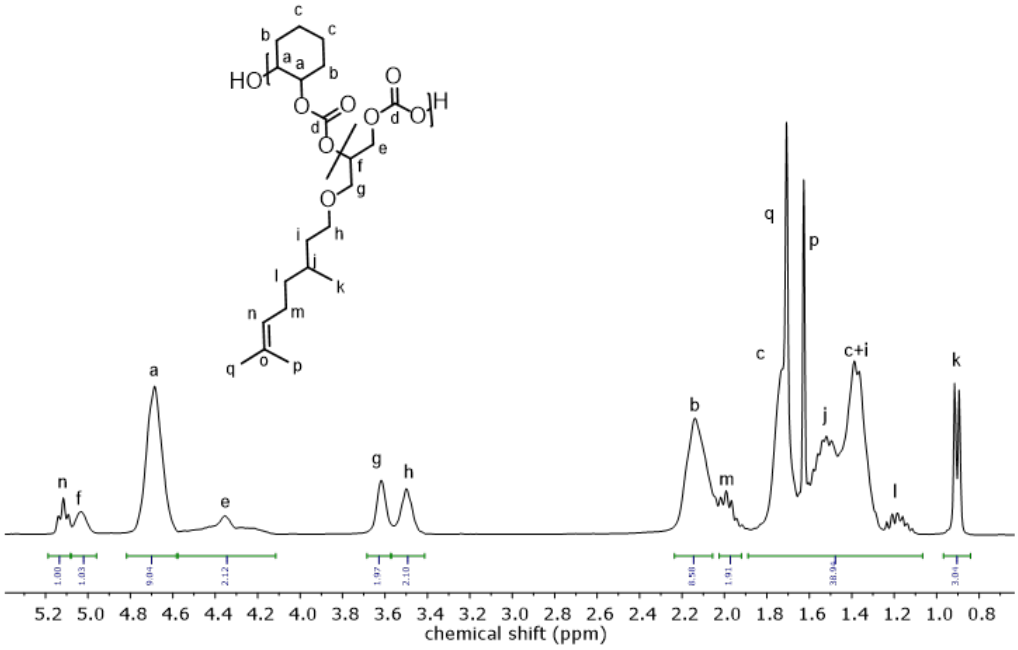

Figure S 7: ^{1}H NMR spectrum (300 MHz, $CDCl_3$) of $PCHC_{0.89}$-*co*-$PCitroGEC_{0.11}$ (Table 1, sample 7).

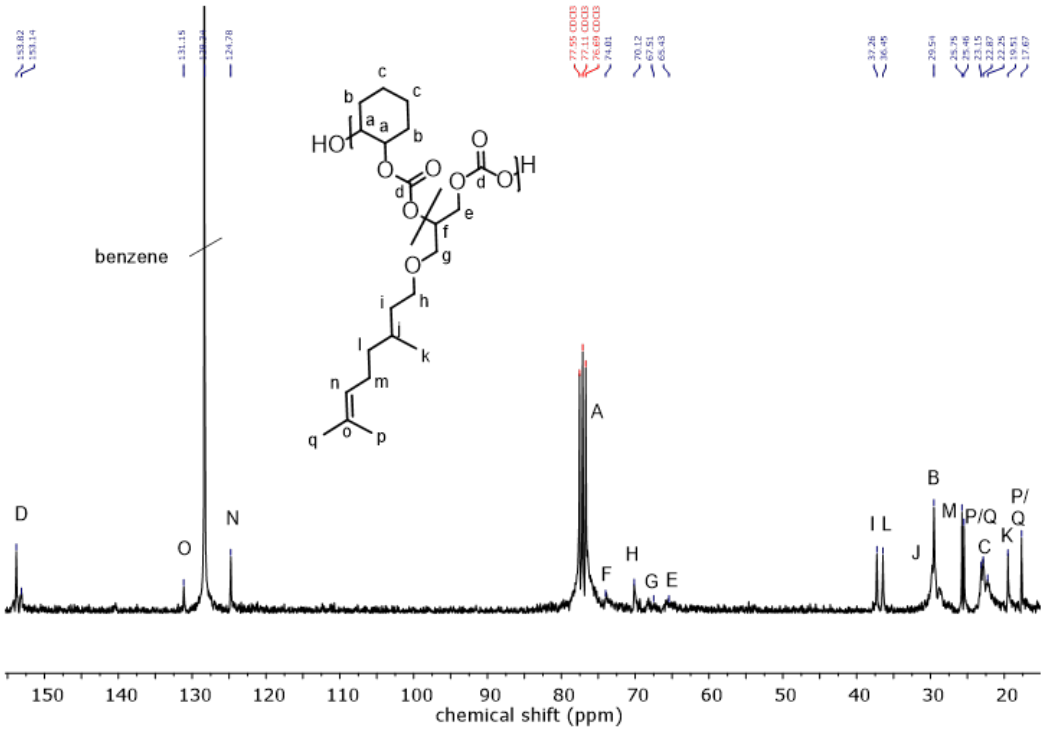

Figure S 8: ^{13}C NMR spectrum (75 MHz, $CDCl_3$) of $PCHC_{0.89}$-*co*-$PCitroGEC_{0.11}$ (Table 1, sample 7), showing the newly formed polycarbonate structure, based on the signal of the carbonyl carbon at 153.82 ppm.

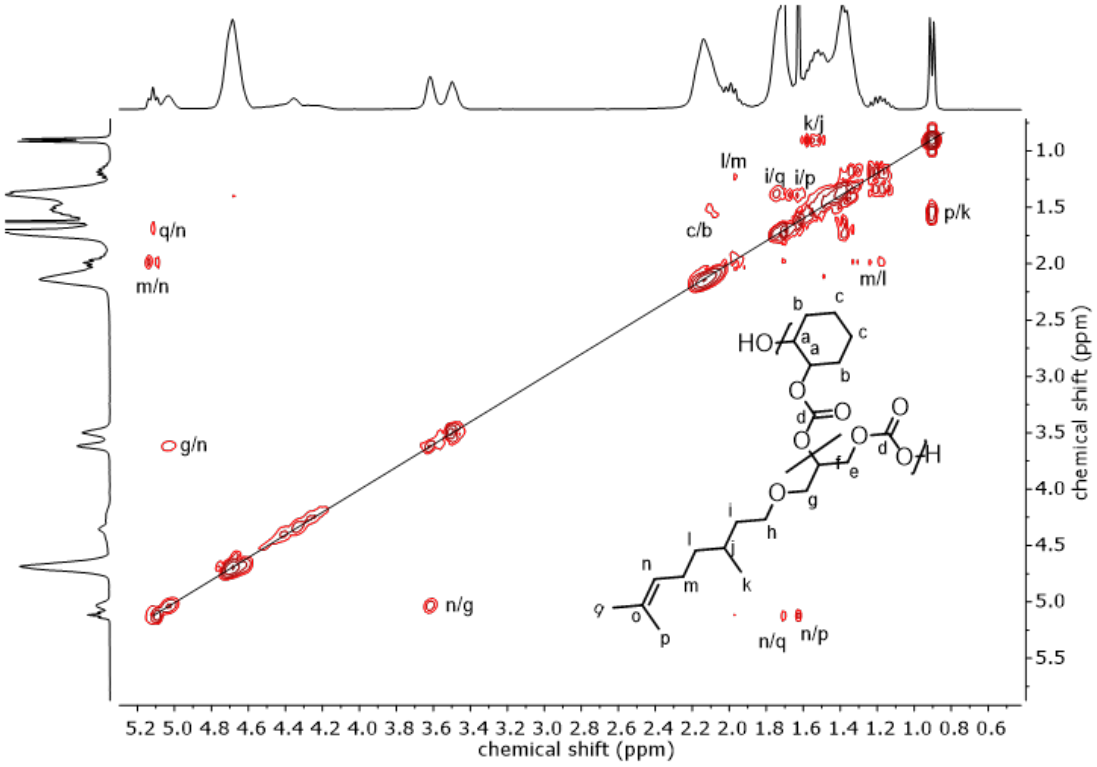

Figure S 9: ^{1}H ^{1}H COSY NMR (300 MHz, $CDCl_3$) spectrum of $PCHC_{0.89}$-*co*-$PCitroGEC_{0.11}$ (Table 1, sample 7).

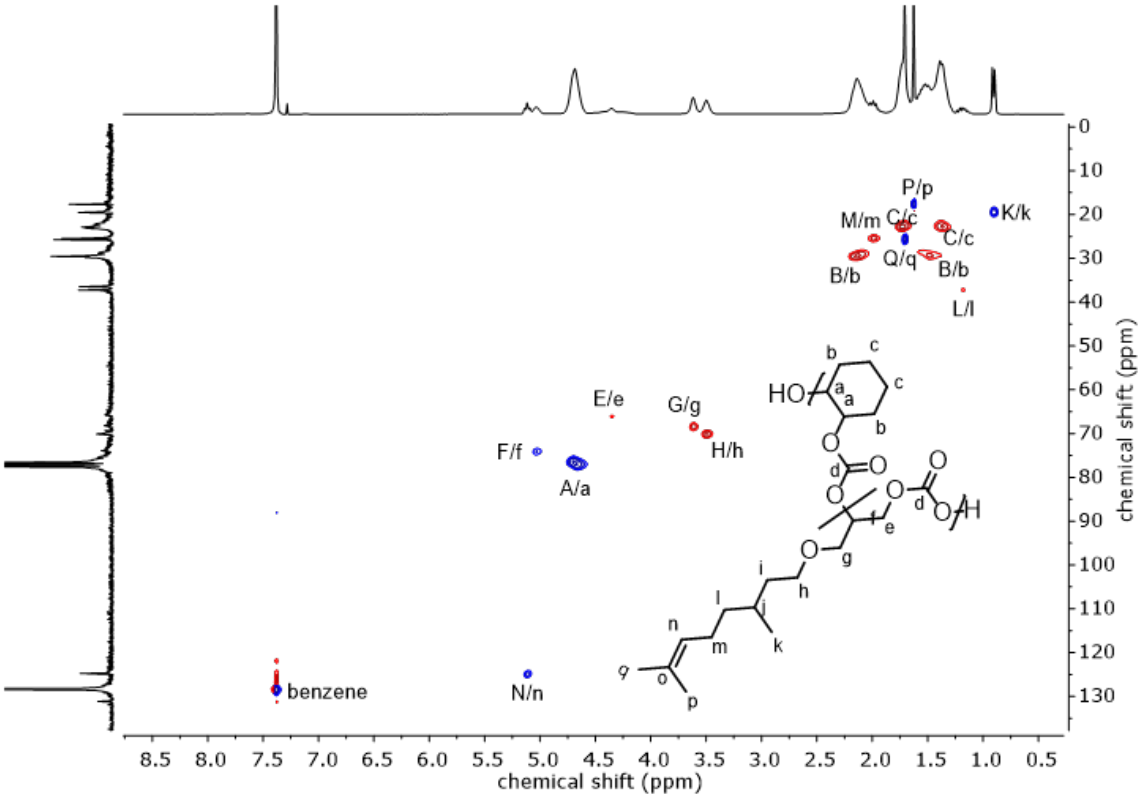

Figure S 10: ^{1}H ^{13}C HSQC NMR spectrum (300 MHz/75 MHz, $CDCl_3$) of $PCHC_{0.89}$-*co*-$PCitroGEC_{0.11}$ (Table 1, sample 7).

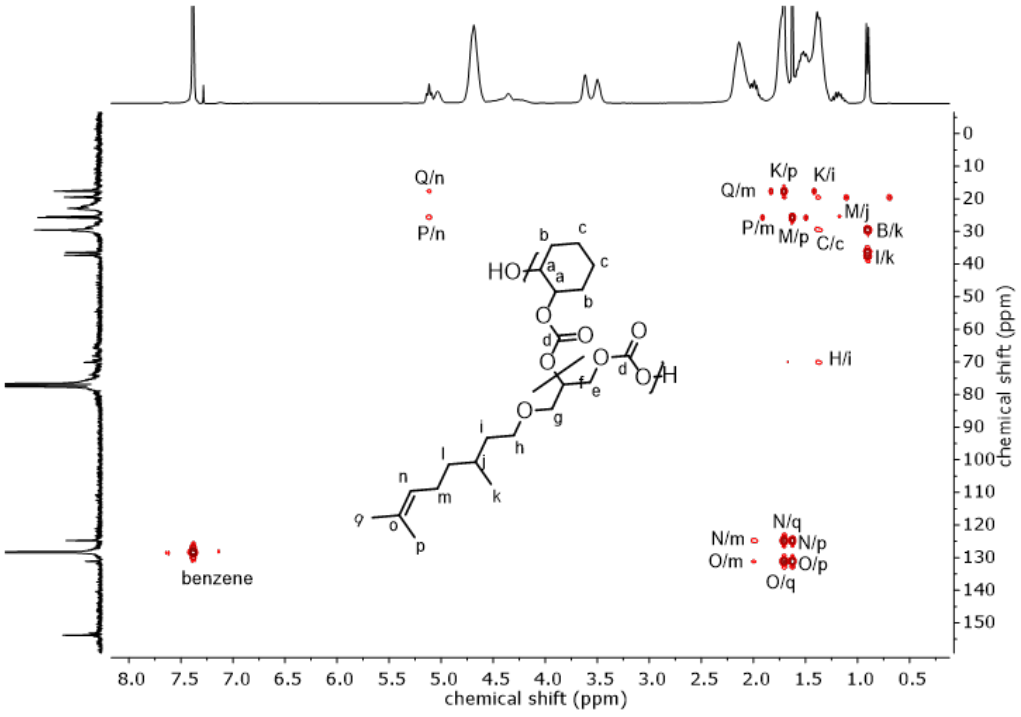

Figure S 11: ^{1}H ^{13}C HMBC NMR spectrum (300 MHz/75 MHz, $CDCl_3$) spectrum of $PCHC_{0.89}$-*co*-$PCitroGEC_{0.11}$ (Table 1, sample 8).

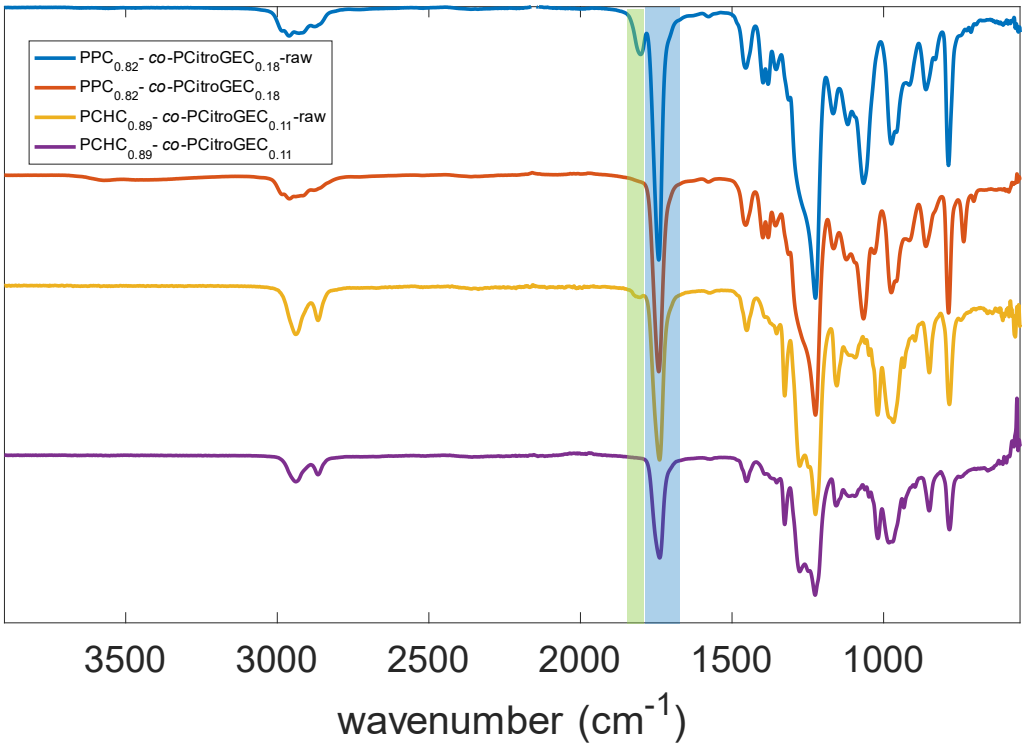

Figure S 12: IR spectra of the crude $PPC_{0.82}$-co-$PCitroGEC_{0.18}$ (blue), precipitated $PPC_{0.82}$-co-$PCitroGEC_{0.18}$ (orange), crude $PCHC_{0.89}$-co-$PCitroGEC_{0.11}$ (yellow) and precipitated $PCHC_{0.89}$-co-$PCitroGEC_{0.11}$ (purple) copolymer. The signal of the cyclic carbonates at 1800 cm^{-1} is highlighted in green and the signal of the polycarbonate C=O vibration (1743 cm^{-1}) in blue.

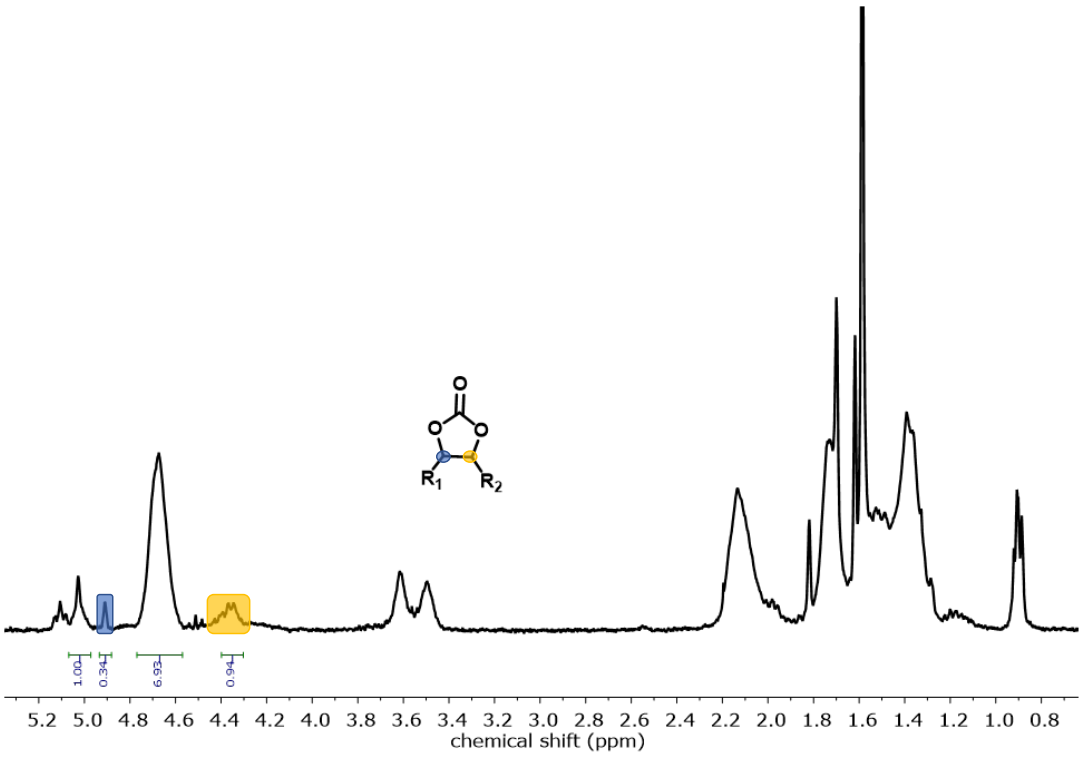

Figure S 13: ^1H NMR (300 MHz, $CDCl_3$) of the crude product of $PCHC_{0.89}$-*co*-$PCitroGEC_{0.11}$ (Table 1, sample 7). The protons of the cyclic carbonates are highlighted in blue and in yellow.

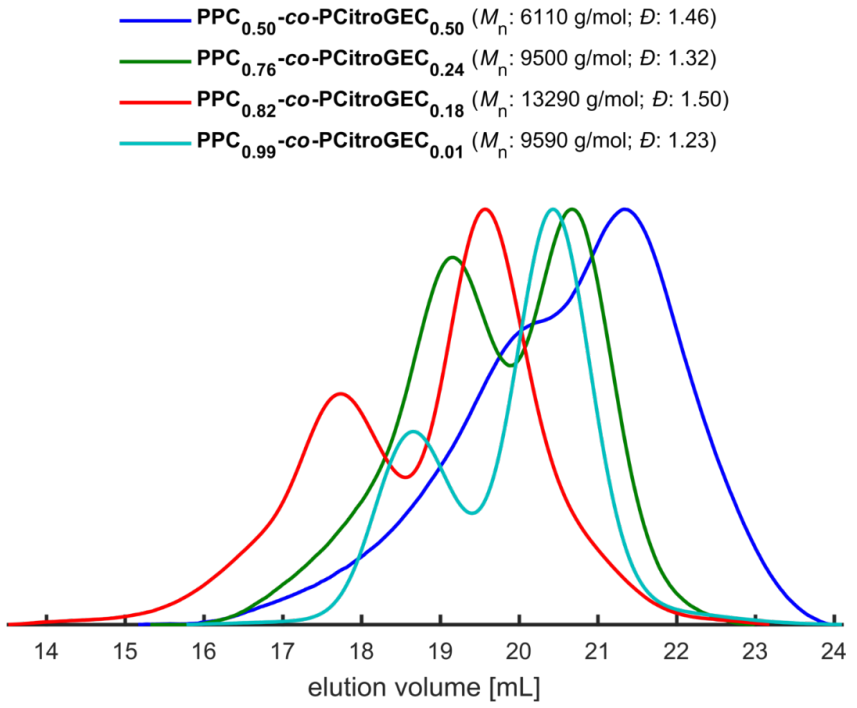

Figure S 14: SEC curves of the PPC-*co*-PCitroGEC terpolymers (eluent: DMF, standard: PEG).

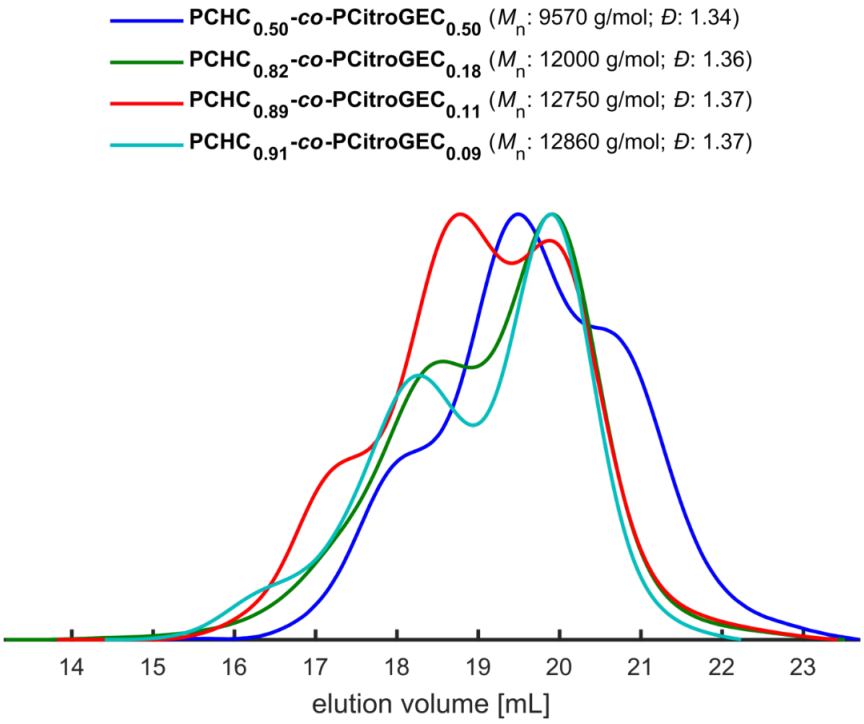

Figure S 15: SEC curves of the PCHC-*co*-PCitroGEC terpolymers (eluent: DMF, standard: PEG).

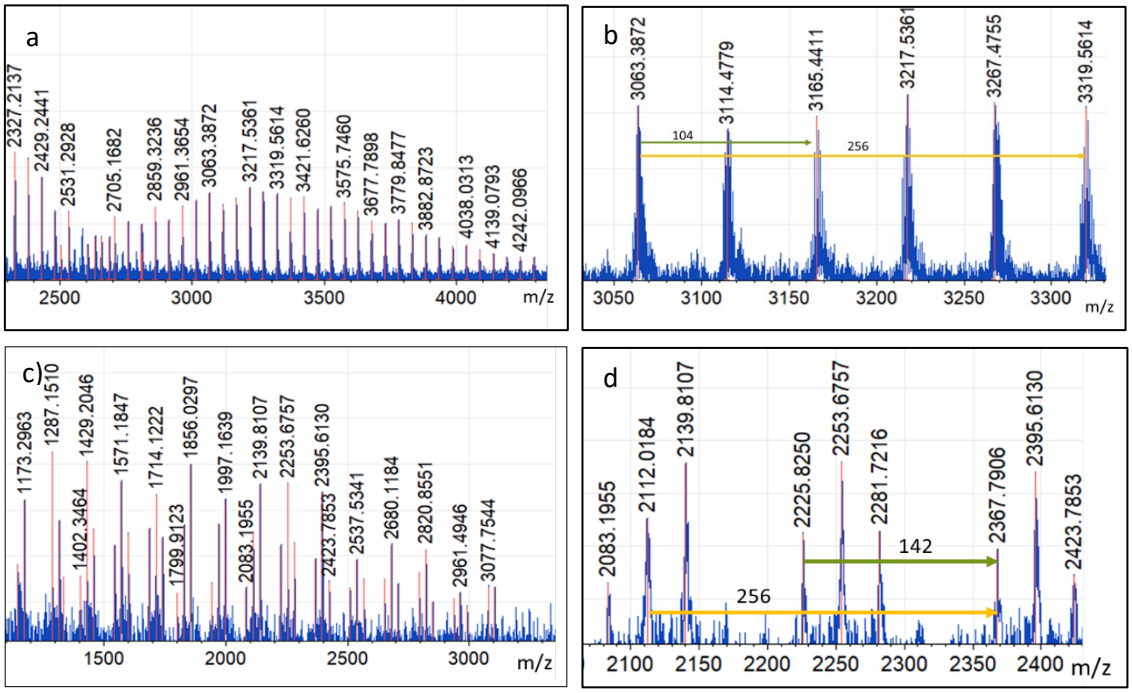

Figure S 16: MALDI -ToF spectrum of $PPC_{0.82}$-co-$PCitroGEC_{0.18}$ (a) and the zoom in of the MALDI-ToF (b). The repeating unit PPC (104 g/mol) is shown with the green arrow, the repeating unit of PCitroGEC with the yellow arrow. MALDI -ToF spectrum of $PCHC_{0.75}$-*co*-$PCitroGEC_{0.25}$ (c) and the zoom in of the MALDI-ToF (d). The repeating unit PCHC (142 g/mol) is shown with the green arrow, the repeating unit of PCitroGEC with the yellow arrow.

3. Thermal characterization

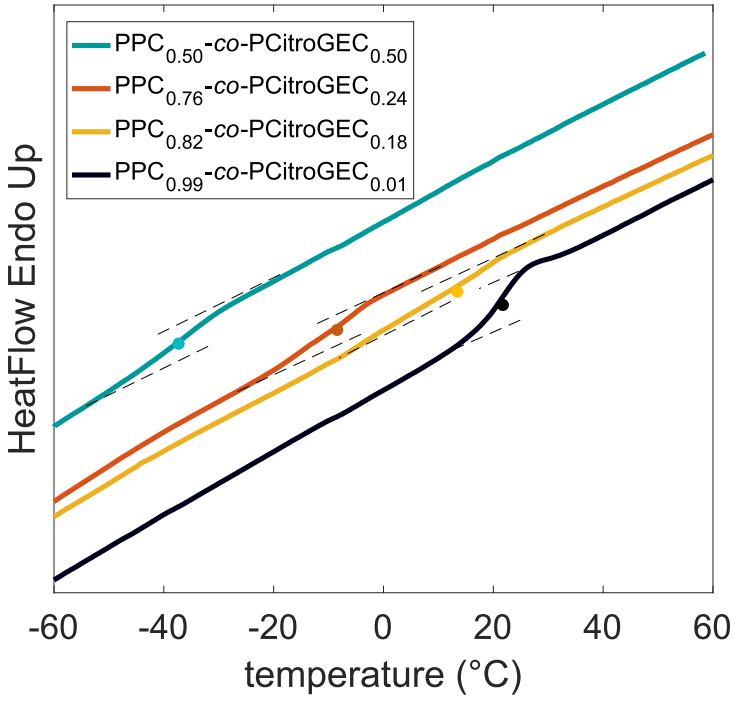

Figure S 17: DSC curves of the PPC-*co*-PCitroGEC terpolymers (heating rate: 20K/min). With a higher content of PCitroGEC the T_gs decrease. The dots show the T_gs of the polymers.

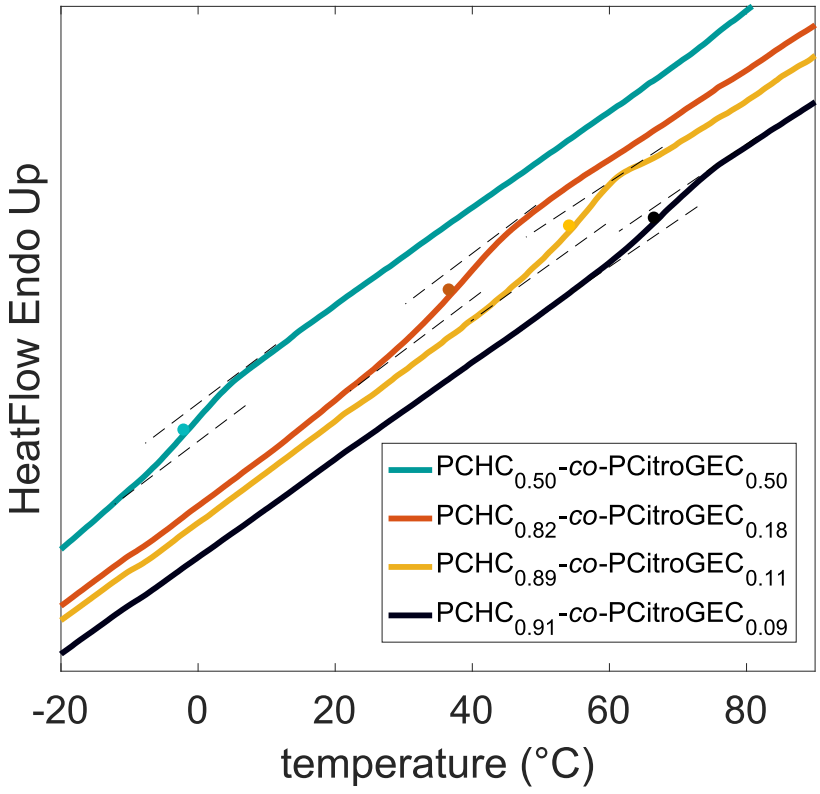

Figure S 18: DSC curves of the PCHC-*co*-PCitroGEC terpolymers (heating rate: 20K/min). With a higher content of PCitroGEC the T_gs decrease. The dots show the T_gs of the polymers.

4. Kinetic studies

Figure S 19: Image of the autoclave used for the kinetic studies.

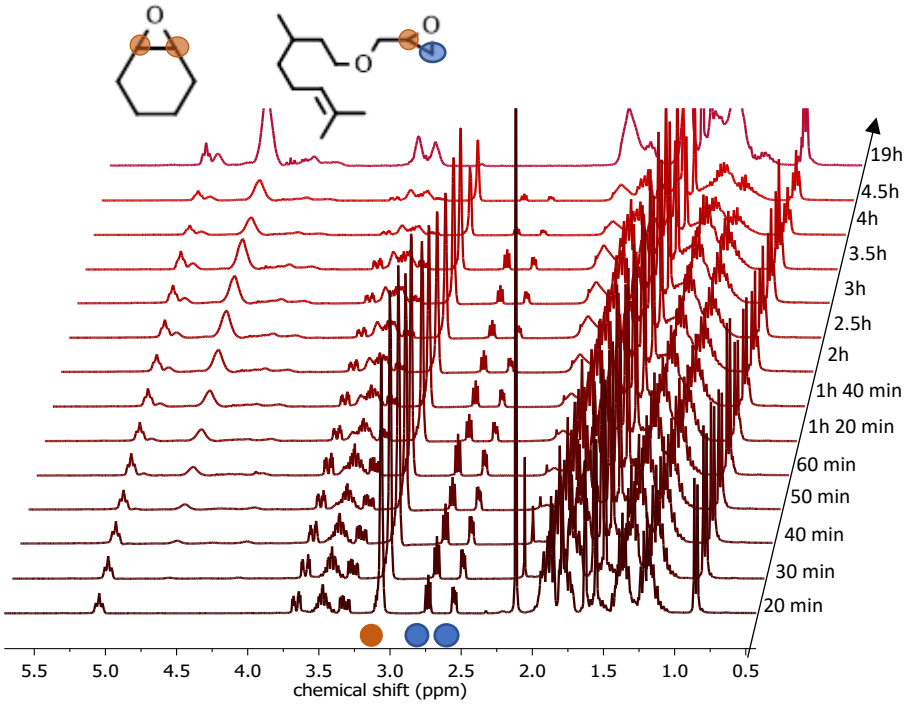

Figure S 20: Stacked ^{1}H NMR spectra (300 MHz, $CDCl_3$) for copolymerization of CHO and CitroGE (20 mol%) with CO_2 at 60 °C at 50 bar using 0.1 mol% of the CoSalen catalyst system. Samples were taken after different periods. After 4.5 h the data collection was stopped since the polymerization mixture was too viscous to pass the cannula. The decreasing signals of the CHO protons and the CitroGE Proton (orange) and the protons of CitroGE (blue) were used for evaluation.

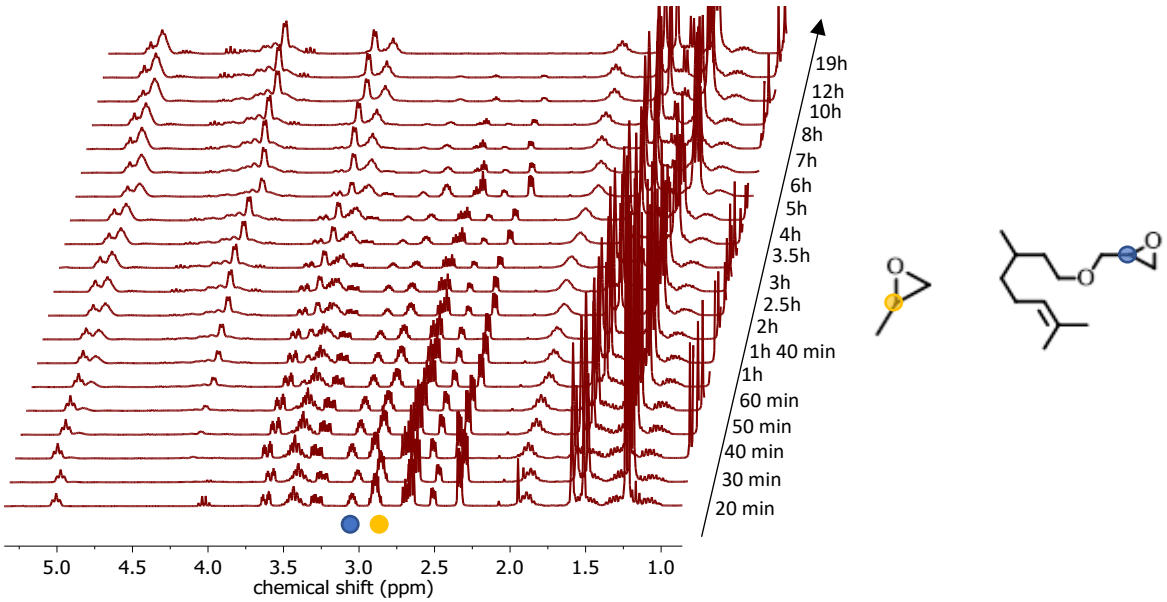

Figure S 21: Stacked ^{1}H NMR spectra (300 MHz, $CDCl_3$) for copolymerization of PO and CitroGE (20 mol%) with CO_2 at room temperature at 50 bar using 0.1 mol% of the CoSalen catalyst system. Samples were taken after different periods. After 13 h the data collection was stopped since the polymerization mixture was too viscous to pass the cannula. The decreasing signals of the PO protons (yellow) and the CitroGE protons (blue) were used for evaluation.

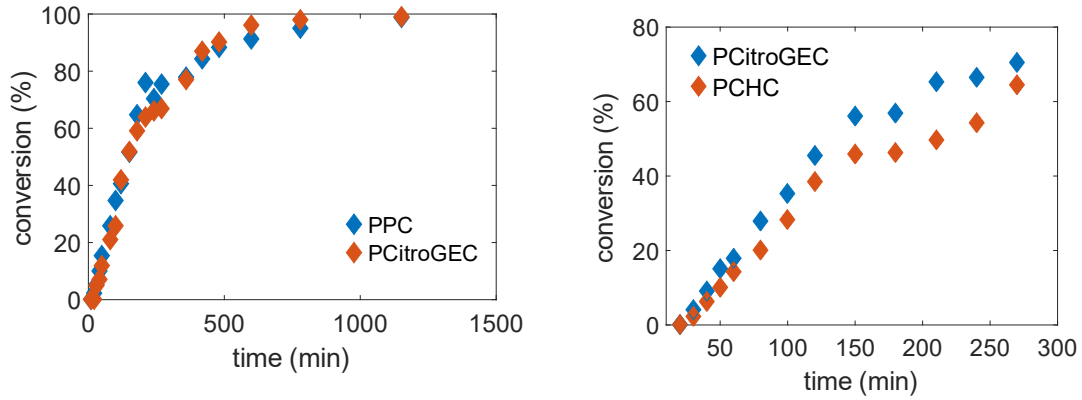

Figure S 22: Conversion in % plotted vs the time in min determined via ^{1}H NMR spectroscopy (300 MHz, $CDCl_3$) at room temperature for the copolymerization of PO/CitroGE/CO_2 (left) and at 60 °CHO/CitroGE/CO_2 (right).

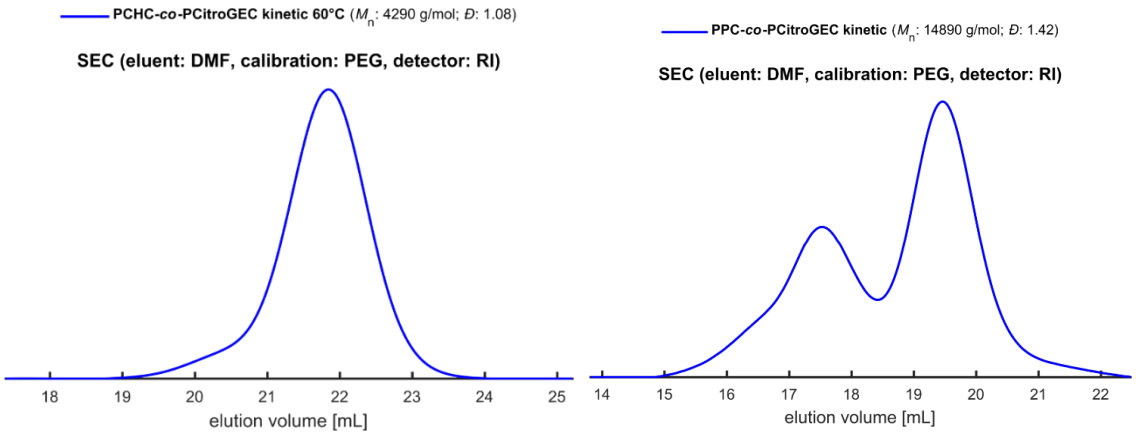

Figure S 23: SEC trace (eluent: DMF, standard: PEG) of PCHC-*co*-PCitroGEC copolymer (left) and PPC-*co*-PCitroGEC (right) from kinetics studies.

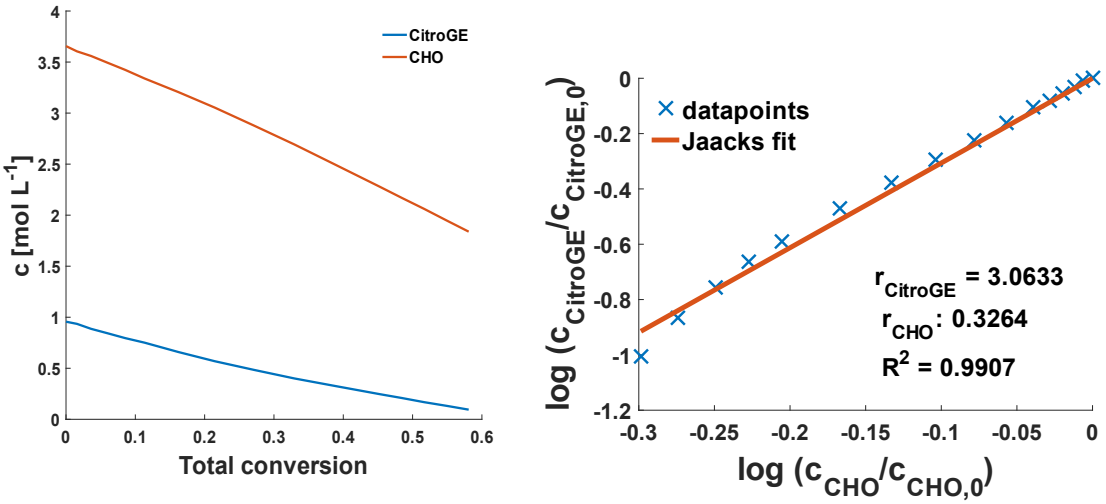

Figure S 24: Normalized monomer concentration plotted vs the total conversion determined via ^{1}H NMR spectroscopy (300 MHz, $CDCl_3$) for the copolymeriation of CitroGE/CHO/CO_2 30 °C (left). Measured data points (blue cross) and Jaacks-fit for the copolymerization of CitroGE and CHO at 30 °C with reactivity ratios determined by the fitting procedure (left)..

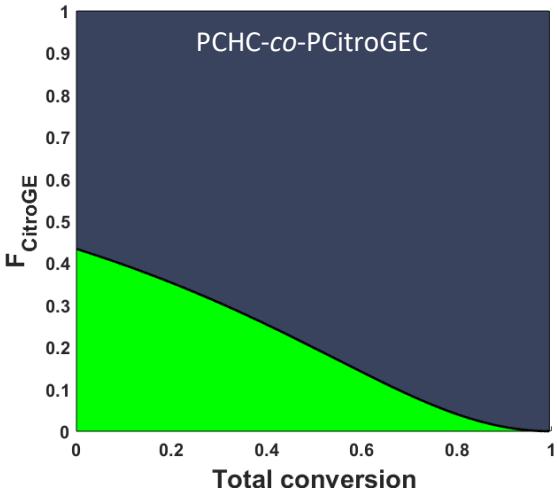

Figure S 25: Simulation of the distribution of CitroGE ($F_{CitroGE}$) in PCHC-*co*-PCitroGEC at 30 °C. This simulation is based on the reactivity ratios determined by the Jaacks-fit for a mixture with 20 mol % of CitroGE. The green area relates to CitroGE and the grey to CHO.

Table S 2: Overview of the different reactivity ratios (r) and their error (r err) (determined using the Jaacks fit) with different monomers (M) at different temperatures (T)).

M_1	M_2	T (°C)	r_1	r_1 err	r_2	r_2 err	r_1*r_2	r_1*r_2 err	ResNorm
CitroGE	PO	r.t.	1.1251	0.0287	0.8888	0.0227	1	0.0.0361	0.9963
CitroGE	CHO	60	1.0326	0.0222	0.9684	0.0208	1	0.0303	0.9966
CitroGE	CHO	30	3.0633	0.1092	0.3264	0.0116	1	0.0504	0.9907

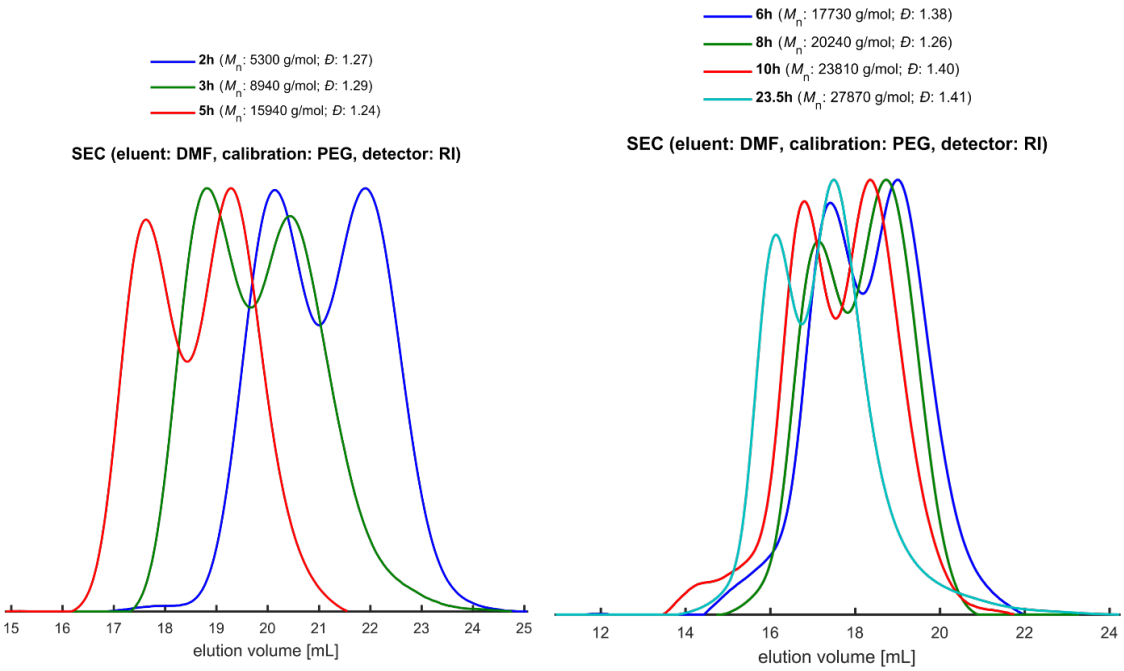

Figure S 26: SEC traces of the samples taken after different periods of the copolymerization of CHO/CitroGE/CO_2 at 30 °C.

CHAPTER 3

Biobased Thermoplastic Elastomers Based on Citronellol Glycidyl Ether, CO_2 and Polylactide

CHAPTER 3

Biobased Thermoplastic Elastomers Based on Citronellol Glycidyl Ether, CO_2 and Polylactide

Christina Gardiner[a], Sandra Schüttner[a], Frédéric Petrov[a], George Floudas[b], Holger Frey[a*]

[a]Department of Chemistry, Johannes Gutenberg University, Duesbergweg 10-14, 55128 Mainz, Germany.

[b]Department of Physics, University of Ioannina, P.O. Box 1186, 45110 Ioannina, Greece.

To be submitted.

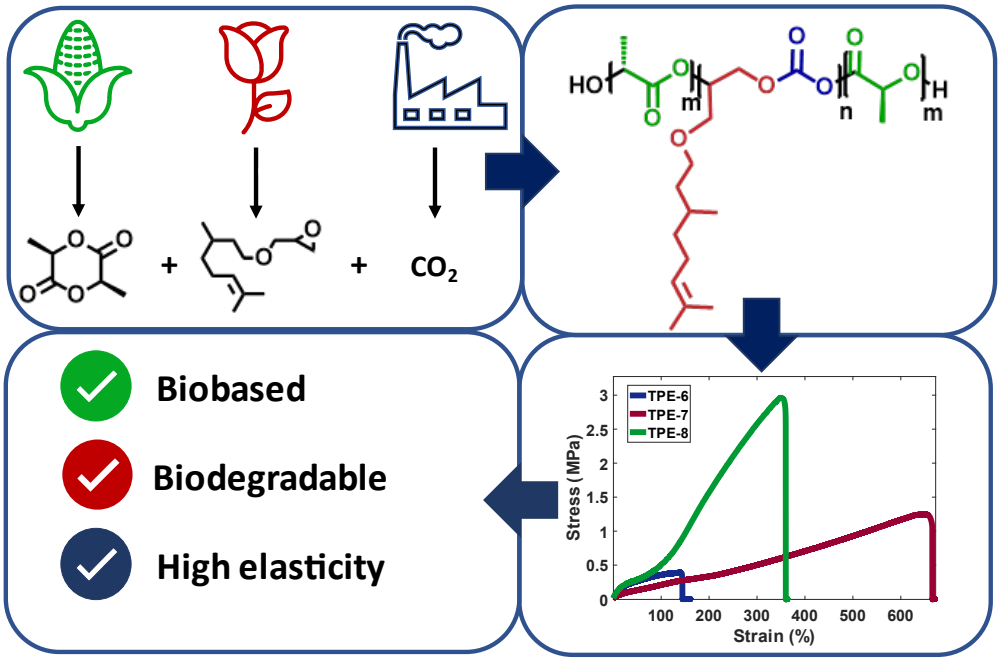

ABSTRACT

An important component of potentially sustainable materials are biodegradable and bio-based feedstocks. This work presents the synthesis of PLLA-*b*-PCitroGEC-*b*-PLLA triblock copolymers as degradable thermoplastic elastomers, featuring biodegradability while being sourced from bio-renewable feedstocks. The cyclic ester L,L-Lactide (LLA) is produced by fermentation of corn or sugar on a large scale, while citronellol can be extracted from rose or lemongrass. Poly(citronellol glycidyl ether carbonate) (PCitronGEC) was formed by catalytic copolymerization of CO_2 and citronellol glycidyl ether using (*R,R*)-(salcy)-Co(III)Cl (CoSalenCl) and bis(triphenylphosphine)iminium chloride ([PPN]Cl) as a catalyst system. The resulting PCitroGEC macroinitiators (in the range of 11 000 – 26 000 g/mol) were used in a DBU-catalyzed ring opening polymerization (ROP) of L-lactide, resulting in a series of promising PLLA-*b*-PCitroGEC-*b*-PLLA triblock copolymer structures (18 000 – 41 000 g/mol). NMR and IR spectroscopy as well as SEC analysis support the successful synthesis of the novel triblock copolymer system. Molar masses range between 18 000 and 41 000 g/mol, while the molar fraction of the "soft" PCitroGEC soft block was varied between 22 to 60 mol%. As all triblock copolymers exhibit two glass transition temperatures (T_gs). Small angle X-ray scattering (SAXS) revealed micro-phase separation for all synthesized TPEs, which was reflected in tensile test results. All polymers with a PCitroGEC content exceeding 31 mol% show elasticity, with elongation at break up to 600% and almost no plastic deformation. Furthermore, they exhibit low *E*-moduli of 0.15-1.0 MPa, rendering the PLLA-*b*-PCitroGEC-*b*-PLLA triblock copolymers suitable for potential use in soft tissue engineering.

INTRODUCTION

Thermoplastic elastomers (TPEs) are biphasic polymer materials of high industrial and academic interest, as they exhibit the processability of thermoplastics and the elasticity of vulcanized rubber.[1–4] Common TPEs are based on an ABA triblock copolymer structure, which combines a microphase separated elastomeric middle B-block with "hard" A-blocks.[1,3,4] The hard blocks exhibit a high glass transition temperature (T_g) and create a physically crosslinked, three-dimensional nanodomain network within the low T_g rubbery matrix. The resulting dimensional stability provides creep resistance, while the soft segments lead to elasticity without the need for chemical vulcanization. The mechanical properties derived from the covalent linkage between the immiscible blocks can be compared to vulcanized rubber, while maintaining thermally reversible crosslinking. Hence, TPEs are excellent materials for industrial thermoplastic processing such as melt extrusion and inject molding.[1,3,5–7]

Nevertheless, the majority of commercial TPEs like SIS or SBS are produced from fossil resources, and lack degradability.[7–10] To reduce the overall environmental footprint, a transition to a more sustainable approach for polymer synthesis is important. The identification and assessment of sustainable feedstock-based monomer precursors provides considerable potential for the manufacture of sustainable materials and products. [6,11–15] Additionally, utilizing and fixating greenhouse gases such as carbon dioxide (CO_2) in polymer materials provides a promising opportunity. CO_2 represents a cheap, renewable carbon source and acts as a clean C1 building block in polycarbonate synthesis. Additionally, it is readily available, non-toxic and the resulting polycarbonates are biocompatible as well as biodegradable.[13–19]

In 1969, Inoue et al. discovered the synthesis of aliphatic polycarbonates based on CO_2, however, interest in polycarbonate-based TPEs has only emerged in recent years.[20] Jia et al. published a CO_2-based TPE based on poly(cyclohexene carbonate) (PCHC) as outer hard blocks and poly(octene carbonate) (POC) as flexible midblock, showing elastomeric behavior.[21] Although polycarbonates allow for T_g modulation over a wide temperature range, all-carbonate triblock copolymer TPEs only show microphase separation for high molar masses.[21] Consequently, high molar masses or deployment of invariable blocks are required to facilitate phase separation. Furthermore, Yang et al. developed a TPE *via* post-polymerization modification of a PCHC-*b*-PAGEC-*b*-PCHC triblock copolymer, generating a hydroxyl-functional midblock. The reaction of the hydroxyl groups with boronic esters results in a physically crosslinked network, leading to a phase separated, elastic polymer.[22] In 2020, Williams and coworkers employed a switchable catalyst, leading to PCHC-*b*-PDL-*b*-PCHC (PDL = polydecalactone) triblock copolymer in a one-pot reaction. These new materials feature good thermal stability ($T_{d,5}$ ~

280 °C), high toughness (112 MJ m^{-3}) and very high elongation at break (>900%).[23] Within the same year, the authors also presented a biobased alternative using LO instead of CHO for the outer blocks, leading to polymers with high elasticity (elongation at break = 400 %).[24]

Terpenes and terpenoids are attracting growing attention as polymeric building blocks. Their structural diversity renders them suitable for various polymerization techniques, ranging from catalytic, radical to carbanionic and oxyanionic polymerization.[6,11,14,25,26] Particularly, cyclic terpenoids featuring a *p*-menthane scaffold, such as limonene oxide (LO) and menthene oxide (MEO), present a bio-derived alternative for cyclohexene oxide and are well-established in polycarbonate synthesis with CO_2. [24,25,27–29] Limonene is abundant in orange peels and the corresponding LO is already commercially available.[11,27] The resulting aliphatic polycarbonates exhibit high glass transition temperature (over 120 °C), stiffness and can be used for glassy outer blocks in TPEs.[30,31] Polycarbonates with a low T_g under -40 °C could act as a middle soft block. Zhang *et al.* provide a fully biobased polycarbonate based on fatty acid with a low T_g of -44 °C.[32] Moreover, we recently introduced poly(citronellol glycidyl ether carbonate) (PCitroGEC), prepared from CO_2 and citronellol glycidyl ether.[33] This terpenoid-based polycarbonate reveals a low T_g of -55 °C and could be used as a biobased, biodegradable elastic (soft) midblock for TPEs.[33]

In this context, Agarwal and coworkers introduced a double degradable diblock copolymer, consisting of a poly-L,L-lactide acid (PLLA) and a poly limonene oxide carbonate (PLimOC) block.[30] The chemically disparate blocks exhibit phase separation and a variation of morphologies, indicating a high χ parameter even with low molar mass of 70 kg/mol. Furthermore, they formed a TPE using a hexyl substituted lactide (diHLA) and limonene oxide, resulting in a PLimOC-*b*-P(diHLA)-*b*-PlimOC triblock copolymer. Although this triblock copolymers showed elastomeric behavior, no mechanical characterization data have been published.[27]

Herein, we present a novel type of ABA triblock copolymers as a bio-based, biodegradable and biocompatible TPE. We combined low T_g PCitroGE as a soft middle block with glassy PLLA end blocks in a sequential, catalytic synthesis process. The investigation of thermal and mechanical properties of the triblock copolymers reveals two T_gs and elastic behavior respectively, indicating a microphase segregation.

RESULTS AND DISCUSSION

Polymer synthesis and characterization

Synthesis of the PCitroGEC macroinitiator

The soft middle block PCitroGEC was synthesized using CitroGE and CO_2 as monomers in a catalytic ring opening copolymerization with (*R,R*)-(salcy)-Co(III)Cl (CosalenCl) and bis(triphenylphosphine)-iminium chloride ([PPN]Cl) as a catalyst system. The glycidyl ether CitroGE was prepared in a phase transfer reaction of epichlorohydrin with citronellol.[34] Citronellol itself is abundant in lemongrass and roses and is a biobased monoterpenoid.[26] The long alkyl side chain possesses an alkene ("ene") moiety, which enables further post-polymerization modification to tailor the polymer properties.[26]

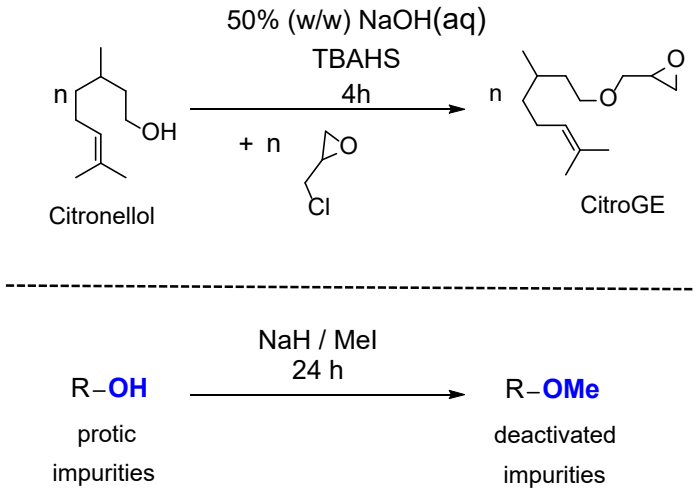

Scheme 1: Synthesis pathway of CitroGE *via* phase transfer catalysis, including methylation of protic impurities as a purification step.

Successful polymerization showing quantitative conversion of CitroGE was confirmed *via* NMR, SEC, and IR analysis (Table 1, Figure S 2-8). The formation of thermodynamically favored cyclic carbonates was suppressed by employing room temperature (r.t.) and reaction times of 20 h. IR spectroscopy still reveals a small amount of cyclic carbonates in the crude product, which were removed by multiple precipitation in ice-cold methanol (Figure S 11). The amount of the cyclic carbonates was quantified using ^{1}H NMR analysis of the crude products (Figure S 10). High amounts of catalyst result in an increase of the cyclic carbonates as a by-product (Table 1). The integrals of the ^{1}H NMR spectrum verify the absence of any potential metathesis or radical reaction of the double bonds caused by the catalyst (Figure S 2). Moreover, the ^{13}C NMR spectrum reveals the formation of a carbonate structure. The signal at 155.40 ppm in the ^{13}C NMR spectrum is ascribed to the carbonate carbon (Figure S 3). Since CoSalen catalyst systems are known for the alternative incorporation of CO_2 and epoxides, no further ether signals (except for the monomer ether signals at 3.63 and 3.49 ppm) were identified by ^{1}H NMR

spectroscopy (Figure S 2). To overcome molar mass limitations caused by monomer impurities, CitroGE was treated with methyl iodide and sodium hydride before use in the copolymerization reaction (Scheme 1).[27] In a series of experiments the molar mass could be increased with this treatment from 6 000 g/mol to 19 000 g/mol using the same amount of the catalyst (Figure S 9). CO_2 was dried over molecular sieves (technical CO_2 gas still contains water impurities)[35] to obtain higher molar masses and reduce water initiation. The pre-treatment of the monomers led to molar masses between 11 000 to 26 000 g/mol, using DMF as eluent and PEG as standard (Figure S 7). Since no end group analysis is possible for these polymers, SEC analysis was used to estimate the molar mass. The PCitroGEC homopolymers were also measured by THF-SEC with PS as standard, resulting in molar masses of up to 41 000 g/mol (Figure S 7 and S 8). After comparing the results of the THF-SEC and the DMF-SEC analysis, the absolute molar mass of the PCitroGE macroinitiators for the triblock copolymer synthesis were estimated by multiplying DMF-SEC values by 1.5. Despite drying of CO_2, bimodal SEC traces confirm water initiation (Figure S 7 and Figure S 8).

Molar masses were varied using different amounts (mol%) of the catalyst system (0.15 - 0.4 mol%). High catalyst amounts present during the polymerization led to lower molar masses due to the presence of chloride ions in the cocatalyst acting as an initiating species (Table 1). The lowest amount of catalyst required to start the polymerization is 0.15 mol%, resulting in the highest molar masses. However, water impurities in CO_2 gas and the resulting fluctuation in water initiation significantly influence the achievable molar masses, ranging from 20 000 g/mol to 26 000 g/mol for 0.15 mol% (Table 1). Based on the DMF-SEC traces (DMF, PEG, Figure S7), it can be estimated that in the case of $PCitroGEC_{11K}$, 40% of the PCitroGEC chains are initiated by water and 60% by chloride. However, these two different initiations do not have a major impact on the resulting triblock copolymers. In a previous work, we have shown that hydroxy end groups are predominately are formed after a workup with 5 vol% HCl in methanol. This leads to catalyst deactivation and a substitution reaction of the chloride by a hydroxy ion. Elimination may also occur, resulting in the formation of an ene moiety as an end group (small amounts of this species were detected in the MALDI-ToF).[33] Small amounts of this monofunctional PCitroGEC result in PCitroGEC-*b*-PLLA diblock copolymer formation during PLLA-*b*-PCitroGEC-*b*-PLLA triblock copolymer synthesis, but no significant effect on mechanical properties is expected. Steube et al. demonstrated high elongations at break (700 ± 55%) with a blend of 40 wt% diblock in a hexablock copolymer. The pure hexablock copolymer exhibited an elongation at break of 800 ± 96 %.[4]

Table 1: Overview of the PCitroGEC homopolymers.

sample	compostion[b]	catalyst mol%	conversion[a] %	CC[a] %	M_n[b] kg/mol	$Đ$[b]	M_n[c] kg/mol	$Đ$[c]	T_g °C
PCitroGEC-1	$PCitroGEC_{11K}$	0.4	98	22	11	1.24	-	-	-65
PCitroGEC-2	$PCitroGEC_{20K}$	0.15	98	2	20	1.23	32	1.26	-62
PCitroGEC-3	$PCitroGEC_{24K}$	0.21	99	1	24	1.27	39	1.43	-57
PCitroGEC-4	$PCitroGEC_{26K}$	0.2	99	3	26	1.23	41	1.24	-62

[a]Calculated using ^{1}H NMR spectroscopy. [b]Determined via SEC using DMF as eluent and PEG as standard. [c] Determined via SEC using THF as eluent and PS as standard. CC illustrated the cyclic carbonates in %.

Synthesis of the triblock copolymer

After the successful synthesis of the PCitroGE macroinitiators, they were employed in the ROP of LLA, using 1,8-diazabicyclo[5.4.0]undec-7-ene (DBU) as a catalyst. Although $Sn(Oct)_2$ is an industrially relevant catalyst for the synthesis of PLLA, DBU provides notable advantages as an organocatalyst. With regard to potential transesterification reactions and the degradability of PCitroGE, mild reaction conditions (r.t., short reactions times), low cost and excellent polymerization control make DBU a superior choice in comparison to the established Sn catalyst systems.[36]

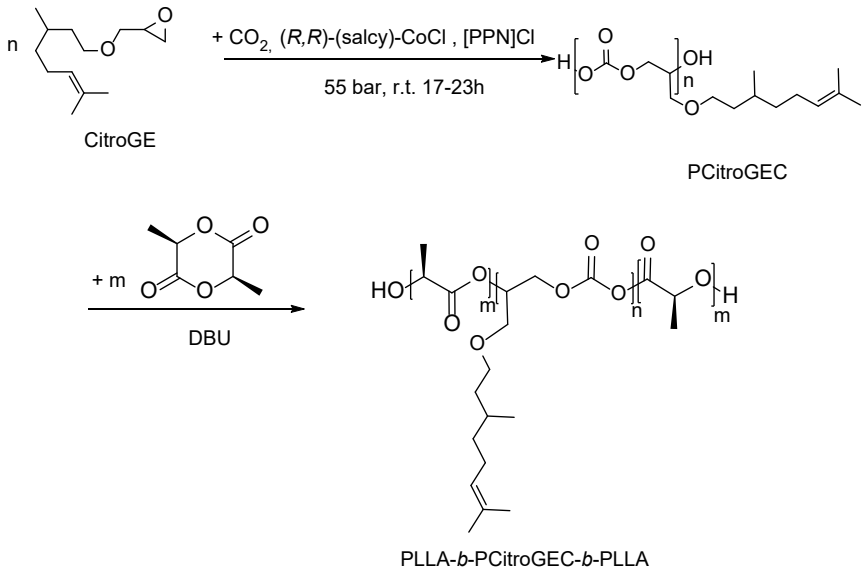

Scheme 2: Synthesis sequence of the PLLA-*b*-PCitroGEC-*b*-PLLA triblock copolymers.

The targeted application as a bioderived, biodegradable TPE requires nanophase segregation of the polymer blocks in bulk, ideally resulting in a spherical morphology of the hard phase for the desired mechanical properties of TPEs.[1,37] Molar masses of macroinitiators were only gauged by SEC measurements ($M_{n,calculated}$=M_n (SEC,DMF)·1.5) due to missing end groups. Therefore, the final triblock

copolymer composition might vary from the targeted composition. As molar mass limitations occur for the PCitroGE synthesis, varying the degree of polymerization (P_n) of PLLA enables tailoring the material properties. Hence, as the macroinitiators varied in molar mass, we present four series of TPEs, starting from an identical macroinitiator in each series. Molar masses were determined via SEC and range between 18 000 g/mol and 41 000 g/mol, exhibiting dispersities (*Đ)* of 1.25 to 1.38 (Figure S 19). Moreover, molar compositions were determined via ^{1}H NMR spectroscopy (Table 2) and lie in the range of 22 and 60 mol% of PCitroGE. Successful polymerisation can be confirmed as the distinct methine group of PLLA is visible at 5.15 ppm. The characteristic peak for the PLLA methyl group is overlapping with methyl signals of the citronellol side chain (1.62 – 1.45 ppm) (Figure S 12). Additionally, the polycarbonate-polyester structure features two different carbonyl groups, which are distinguished in ^{13}C NMR spectroscopy as a peak at 169.73 ppm (PLLA) and 154.33 ppm (PCitroGE) (Figure S 13). No other carbonyl peaks are observed, which confirms that no side reactions occurred in the second polymerization step. SEC analysis and DOSY spectroscopy evidence block copolymer synthesis rather than blending of the two homopolymers of PCitroGE and PLLA (Figure S18). All SEC traces show a clear shift to smaller elution volumes and therefore indicate an increase in molar mass (Figure 1 + Figure S 19).

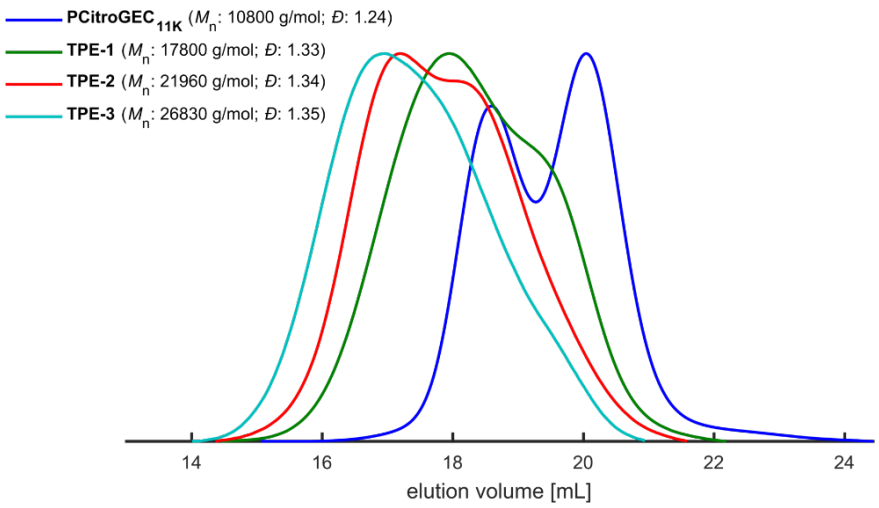

Figure 1: SEC elution traces of PLLA-*b*-PCitroGEC-*b*-PLLA triblock copolymers TPE-1, TPE-2 and TPE-3. The triblock copolymers are presented together with their PCitroGE macroinitiator and the shift of triblock copolymer traces towards smaller elution volumes prove successful polymerization.

Table 2: Overview of the synthesized PLLA-*b*-PCitroGEC-*b*-PLLA triblock copolymers

sample	composition	$M_{n,\ PCitroGEC}$ (kg/mol)	$M_{n,\ total}$ (kg/mol)	$Đ$	morphology (SAXS)	$T_{g,1}$ °C	$T_{g,2}$ °C
TPE-1	$PLLA_{0.29}$-*b*-$PCitroGEC_{0.42}$-*b*-$PLLA_{0.29}$ -18K	11	18	1.33	LAM/~Dis	-48	44
TPE-2	$PLLA_{0.35}$-*b*-$PCitroGEC_{0.31}$-*b*-$PLLA_{0.35}$ -22K	11	22	1.34	CYL	-36	49
TPE-3	$PLLA_{0.39}$-*b*-$PCitroGEC_{0.22}$-*b*-$PLLA_{0.39}$ -27K	11	27	1.35	Spheres	-38	50
TPE-4	$PLLA_{0.20}$-*b*-$PCitroGEC_{0.60}$-*b*-$PLLA_{0.20}$ -25K	20	25	1.28	CYL	-55	47
TPE-5	$PLLA_{0.31}$-*b*-$PCitroGEC_{0.38}$-*b*-$PLLA_{0.31}$ -28K	20	28	1.38	CYL/LAM	-48	47
TPE-6	$PLLA_{0.24}$-*b*-$PCitroGEC_{0.53}$-*b*-$PLLA_{0.24}$ -33K	24	33	1.35	CYL/LAM	-41	44
TPE-7	$PLLA_{0.29}$-*b*-$PCitroGEC_{0.42}$-*b*-$PLLA_{0.29}$ -40K	24	40	1.30	~LAM	-36	48
TPE-8	$PLLA_{0.35}$-*b*-$PCitroGEC_{0.31}$-*b*-$PLLA_{0.35}$ -38K	24	38	1.32	LAM/CYL	-38	48
TPE-9	$PLLA_{0.30}$-*b*-$PCitroGEC_{0.41}$-*b*-$PLLA_{0.30}$ -39K	26	39	1.33	HPC	-40	51
TPE-10	$PLLA_{0.33}$-*b*-$PCitroGEC_{0.34}$-*b*-$PLLA_{0.33}$ -41K	26	41	1.33	HPC	-48	50

[a]Calculated using ^{1}H NMR spectroscopy. [b]Determined via SEC using DMF as eluent and PEG as standard. [c]Determined by DSC with a heating rate of 10 °C/min.

Thermal characterization

Thermal behavior was investigated by DSC measurements. All triblock copolymers exhibit two T_gs, indicating phase separation of the elastic PCitroGE and glassy PLLA domains (Figure S 20 – S 23). The PLLA blocks exhibits a T_g in the range of 44 to 51 °C, which is slightly lower than the T_g of PLLA homopolymer (55-60 °C).[38] In contrast, all T_g values for the PCitroGE blocks are higher than those of the corresponding macroinitiator (Table 1+2). We assume partly miscible phases, resulting in approaching T_g values for both blocks. Surprisingly, the melting point (T_m) of PLLA is only (weakly) observable in the first heating curve for some samples (Figure S 24). Although PLLA is a semicrystalline polymer, it is known for its slow crystallization. Not only does the thermal history impact PLLA crystallization behaviour, but the cooling and heating rates during DSC measurement play a key role. Pyda et. al show that the tendency for PLLA crystallization upon reheating depends on the heating rate. PLLA crystallization undergoes reorganization, melting and recrystallization between glass transition and final melting.[39,40] Hence, low heating and cooling rates facilitate PLLA crystallization and explains the different heating curves in Figure S 24. Furthermore, partial miscibility of the covalently bound

polymer blocks can be ascribed a plasticizing effect as it impedes crystallinity and results in amorphous PLLA.

Nevertheless, a profound understanding of the phase separation behavior requires structural investigation *via* small angle x-ray scattering (SAXS), which reveals the distinct morphology in case of phase separation.

Morphology

The thermal characterization indicates a phase separation, due to the occurrence of two T_gs. To investigate the microstructure of the phase-separated triblock copolymers, small angle X-ray scattering (SAXS) measurements were performed. The SAXS patterns of selected samples are shown in Figure 2 and Figures S 25 – S 27. First, the TPE with $PCitroGEC_{11k}$ as a middle block was investigated. The smallest triblock copolymer (18 000 g/mol), TPE-1, with 42 mol% of PCitroGEC reveals Bragg reflections with relative q values of 1:2, corresponding to a lamellar (LAM) structure to the border of a disordered microstructure. TPE-2 (22 000 g/mol) with a PCitroGEC molar fraction of 0.31 exhibits Bragg reflections with relative q values of 1:2:3 and $1:3^{1/2}:7^{1/2}$, corresponding to an ill-defined cylindrical nanophase separated structure. TPE-3 (27 000 g/mol, 22 mol% of PCitroGEC) show a spherical microstructure (Figure S 25). The resulting microstructures are in line with expectation, as spheres occur in microphase separated polymers at 20 vol% of one polymer block (or 80 vol% of the other polymer, respectively). Hexagonally packed cylinders (HPC) can be observed at 30-40 vol% (or 60-70 vol%), while lamellar structures form around 40-60 vol% of the microphase separated blocks.[37] Since the density of PCitroGEC is not available, the exact volume fraction of PCitroGEC can not be calculated. To compare the results with theory, the molar fraction of PCitroGEC is applied.

The SAXS patterns of the TPEs generated from the $PCitroGEC_{20K}$ homopolymer are presented in Figure S 26. TPE-4 with 60 mol% of PCitroGEC shows weak Bragg reflections with relative q values 1: $3^{1/2}:7^{1/2}$, assigned to an ill-defined cylindrical microstructure. TPE-5 with a lower content of 38 mol% of PCitroGEC reveals Bragg reflections with q values of 1:2:3 typical of lamellae(LAM) and q values of 1: $3^{1/2}:7^{1/2}$ corresponding to cylinders. This polymer shows an ill-defined microphase separation, leading to a mixture of lamellas and cylinders. Since the border between LAM and HPC is around 40 % volume fraction, this again fits well with phase-separation theory.[37]

Figure 2 illustrates the SAXS patterns of the triblock copolymers generated from the $PCitroGEC_{24K}$. TPE-6 with the highest content of 53 mol% of PCitroGEC reveals Bragg reflections with q values of 1:2:3:4 and $1:7^{1/2}$. This pattern corresponds to a mixture of cylinders (CYL) and lamellae(LAM). TPE-7 with 42 mol% PCitroGEC shows a Bragg reflection with q values of 1:2:3 relating to a lamellar microstructure.

TPE-8 with 31 mol% demonstrates a Bragg reflection with q values of 1:2:3:4 and $1:7^{1/2}$ corresponding to a mixture of LAM and CYL.

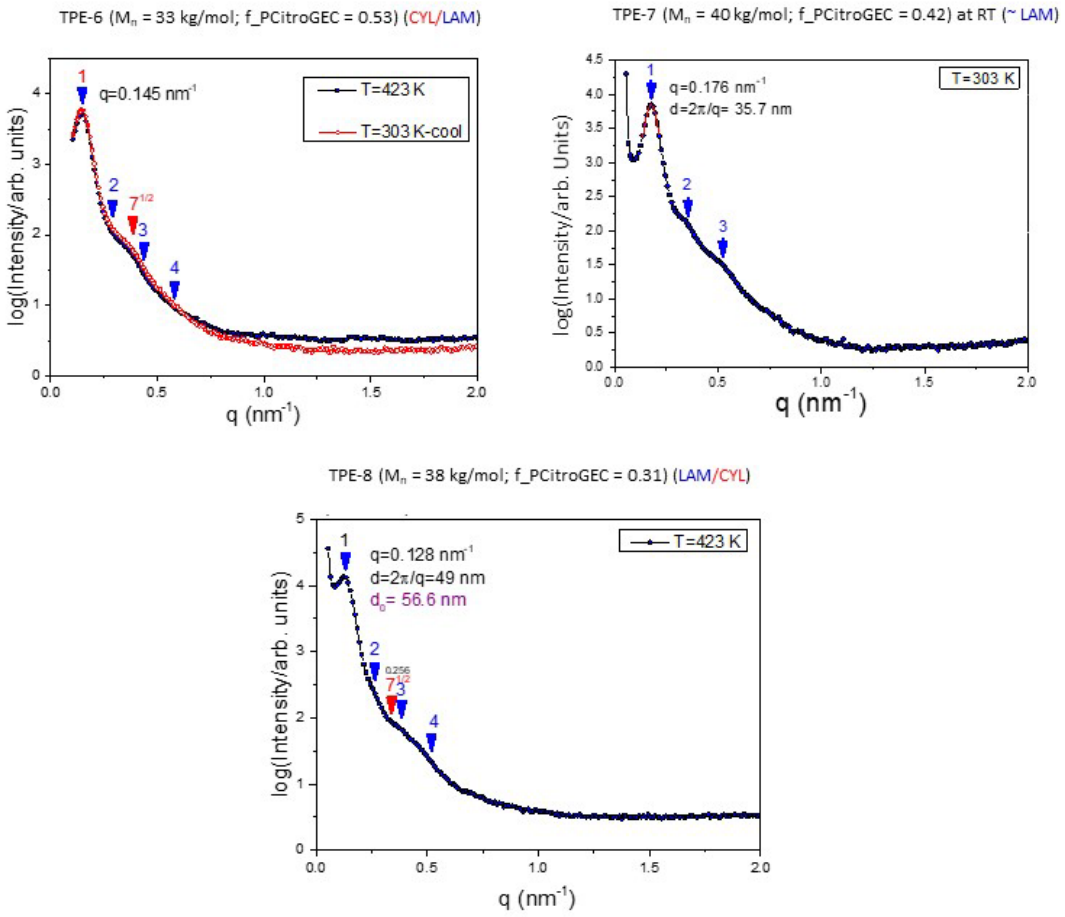

Figure 2: SAXS patterns for the triblock copolymers with PCitroGEC$_{24K}$ as middle block (TPE-6, TPE-7, and TPE-8). Blue arrows give the position of the Bragg peaks corresponding to the lamellar morphology. Red arrows indicate the position of the Bragg peaks corresponding to the cylindrical morphology.

The SAXS patterns of the TPEs with the longest middle PCitroGEC block of 24 000 g/mol are illustrated in Figure S 27. TPE-9 with 41 mol% of PCitroGEC content shows a SAXS pattern with q values of 1: $3^{1/2}$:$7^{1/2}$ corresponding to hexagonally packed cylinder (HPC). TPE-10 with 34 mol% PCitroGEC content reveals a pattern with q values of 1:$3^{1/2}$:$7^{1/2}$:$12^{1/2}$ corresponding again to HPC. Weak Bragg reflections are also detectable with q values of 1:2:3 relating to LAM. But the reflections corresponding to the HPC are more intense, revealing this as the main microstructure. All results are listed in Table 2.

All triblocks show ill-defined nanophase separated microstructures except for TPE-9 and TPE-10, featuring the highest molar masses. This leads to the suggestion that the molar mass of TPE-9 and TPE-10 are just within the range, in which the corresponding blocks start microphase separation.

Mechanical characterization

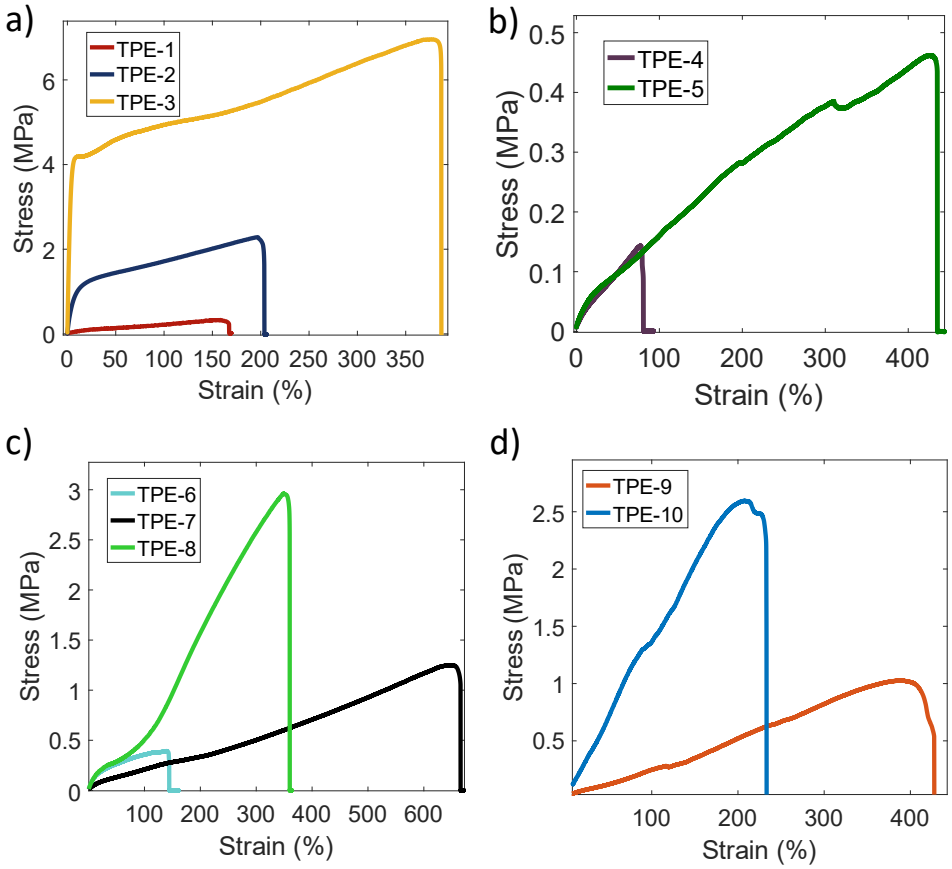

Figure 3: Stress-strain curves of the PLLA-*b*-PCitroGEC-*b*-PLLA triblock copolymers. a) ABA triblock copolymers with PCitroGEC$_{11K}$ as B middle block. b) ABA triblock copolymers with PCitroGEC$_{20K}$ as B middle block. c) ABA triblock copolymers with PCitroGEC$_{24K}$ as B middle block. d) ABA triblock copolymers with PCitroGEC$_{26K}$ as B middle block.

Stress-strain measurements were conducted to analyze the mechanical properties of the polymers. In all cases 2-3 samples were characterized with respect to their stress-strain behavior. Comparing the polymers with PCitroGEC$_{11K}$ as a middle block (Figure 3, a)), it is detectable, that with a higher content of PLLA "hard" domains, both *E*-modulus (*E*) and stiffness increase. Furthermore, the elongation at break (ε_{break}) and the toughness ($W_{tensile}$) increase with higher content of PLLA due to the higher stiffness. Comparing these results with the determined microstructures (Table 2), the increase in stiffness can also be explained. TPE-1 with the lowest molar mass exhibits (Table 3) the lowest elongation at break at around 164 %. TPE-1 shows a lamellar microstructure at the border to a disordered structure. As TPE-2 and 3 feature higher molar masses, the corresponding microstructure is revealed as reverse cylinders and spheres of the flexible PCitroGEC domains, leading to stiffer materials because the PCitroGEC chains are restricted in their mobility.[37] TPE-1 with the highest amount of PCitroGEC of 42 mol% shows elastic behavior(Figure 3, a)). The films were slightly elongated after break at maximum strain, indicating a small hysteresis. No yield point is detectable. The triblock

copolymers with lower PLLA content of 31 and 22 mol% (TPE-2 and TPE-3) exhibit a yield point at around 7% elongation (Table 3). At the yield point, the elastic deformation changes to plastic deformation. Since the plastic deformation begins after 7% elongation, TPE-2 and TPE-3 can be considered as rather ductile materials (Figure 3, a)). Once again, this can be ascribed to the microstructure, in which the flexible PCitroGEC build spherical or cylindrical domains. Hence, stretching is limited, resulting in a more ductile material.

Table 3: Overview of the mechanical properties of the PLLA-*b*-PCitroGEC-*b*-PLLA triblock copolymers.

Sample	Composition[a]	E	ε_{break}	σ_{break}	ε_{yield}	σ_{yield}	$W_{tensile}$
		MPa	%	MPa	%	MPa	MN/mm²
TPE-1	$PLLA_{0.29}$-*b*-$PCitroGEC_{0.42}$-*b*-$PLLA_{0.29}$-18K	0.41±0.07	164±15	0.37±0.05	-	-	0.37±0.08
TPE-2	$PLLA_{0.35}$-*b*-$PCitroGEC_{0.31}$-*b*-$PLLA_{0.35}$-22K	15±2	180±50	2.3±0.3	7.7±0.9	0.97±0.05	3±1
TPE-3	$PLLA_{0.39}$-*b*-$PCitroGEC_{0.22}$-*b*-$PLLA_{0.39}$-27K	100±10	352±46	7.5±0.5	6±2	4.4±0.6	22±3
TPE-4	$PLLA_{0.20}$-*b*-$PCitroGEC_{0.60}$-*b*-$PLLA_{0.20}$-25K	0.151±0.005	80±10	0.16±0.05	-	-	0.07±0.04
TPE-5	$PLLA_{0.31}$-*b*-$PCitroGEC_{0.38}$-*b*-$PLLA_{0.31}$-28K	0.20±0.06	420±20	0.6±0.2	-	-	1.7±0.5
TPE-6	$PLLA_{0.24}$-*b*-$PCitroGEC_{0.53}$-*b*-$PLLA_{0.24}$-33K	1.1±0.5	160±30	0.5±0.1	-	-	0.6±0.3
TPE-7	$PLLA_{0.29}$-*b*-$PCitroGEC_{0.42}$-*b*-$PLLA_{0.29}$-40K	0.188±0.004	650±20	1.26±0.08	-	-	4.1±0.1
TPE-8	$PLLA_{0.35}$-*b*-$PCitroGEC_{0.31}$-*b*-$PLLA_{0.35}$-38K	0.81±0.04	350±10	2.90±0.05	-	-	5.1±0.1
TPE-9	$PLLA_{0.30}$-*b*-$PCitroGEC_{0.41}$-*b*-$PLLA_{0.30}$-39K	0.24±0.01	316±80	0.8±0.2	-	-	1.6±0.8
TPE-10	$PLLA_{0.33}$-*b*-$PCitroGEC_{0.34}$-*b*-$PLLA_{0.33}$-41K	1.0±0.1	190±30	1.9±0.8	-	-	2±1

[a]The indices show the molar fraction calculated *via* NMR. The numbers e.g. 19K demonstrate the molar mass examined by SEC. All values regarding the mechanical properties were determined using 2-3 film samples of the polymer.

TPE-4 and TPE-5 based on the $PCitroGEC_{20k}$ middle block also showed higher toughness and elongation at break, with higher content of PLLA (Figure 3, c)). TPE-4 exhibits 60 mol% and TPE-5 38 mol% of the PCitroGEC block. Nevertheless, TPE-4 shows slightly more softness (Table 3) with reference to the *E*-modulus due to the higher amount of flexible PCitroGEC. Comparing the triblock copolymers with $PCitroGEC_{24K,}$ a trend in toughness is once more detectable (Figure 3, c)). With a higher amount of PLLA, the toughness increases (Table 3). TPE-6 (53 mol% PCitroGEC) and TPE-8 (31 mol% CitroGEC) show both a lower elongation at break than TPE-7 with 42 mol% PCitroGEC. This can be explained by their determined microstructures (Table 2). TPE-7 shows an ill-defined lamellar nanophase separated microstructure and TPE-6 and TPE-8 show a CYL/LAM And a Lam/CYL mixture. This mixture could have an effect of the elongation at break. TPE-9 and TPE-10 were prepared using $PCitroGEC_{26}$ as a macroinitiator. Both polymers show a toughness of around 2 MN/mm². Since PLLA is stiffer than

PCitroGEC, the triblock with 41 mol% PCitroGEC exhibits a lower *E*-modulus than the triblock with 34 mol%. Interestingly, TPE-10 with higher content of PLLA shows a lower elongation at break (Figure 3, d)). Checking the determined microstructures of the samples, they reveal hexagonally packed cylinders (HPC) for TPE 9 and HPCs for TPE-10. The SAXS pattern of TPE-10 demonstrates a slight mixture of LAM. This mixture of LAM with HPC could explain why TPE 10 exhibit a higher stiffness and a lower elongation at break.

All polymers with 40-60 mol% of flexible PCitroGEC show a low *E*-moduli of 0.15 to 1.0 MPa and elongations of break up to 600 %. A comparison of the results with those of Jia et al. shows that they are in the same range, although the PCHC-*b*-POC-*b*-PCHC triblock copolymers exhibit a much higher molar mass. They synthesized PCHC-*b*-POC-*b*-PCHC triblock copolymers with molar masses of 353 000 to 372 000 g/mol and 19-25 wt% of the hard PCHC block. These materials show similar low *E*-moduli of 1.43 to 2.5 MPa and elongation at break of 331 to 1052 %. [21]

All polymers show elastic behavior with exception of the triblock copolymers with PCitroGEC content of less than 31 mol% (TPE-2, TPE-3). However, due to the slightly elongated films after break at maximum strain, a small hysteresis was detectable (Figure S 28). In addition, all polymers featuring elastic behavior show low *E*-moduli of 0.15 to 1.0 MPa, comparable to human soft tissue as cartilage and vascular elastin (*E* 0.3-10 MPa), and makes them applicable for soft tissue engineering.[41–44] Similar *E*-moduli are required to reduce the mismatch between the natural soft tissue and the material used for the implant.[43,44] Furthermore they show high elasticity with an elastic elongation up to 600 %. This characteristic is also important for tissue engineering materials since they are not allowed to change their form.

CONCLUSIONS

We introduced PLLA-*b*-PCitroGEC-*b*-PLLA triblock copolymers., which are composed of renewable monomers derived from terpenes and starch as starting materials. We showed a straightforward synthesis using catalytic-polymerization to copolymerize CO_2 with CitroGE, which leads to a flexible macroinitiator with exceptionally low T_g of -55°C. The PLLA-*b*-PCitroGEC-*b*-PLLA triblock copolymer was successfully synthesized by utilizing DBU-catalyzed ROP of LLA. Two T_gs were detected for all polymers, suggesting microphase separation of the chemically dissimilar block types. Surprisingly, PLLA's crystallization is impeded due partial phase miscibility as well its thermal history, resulting in the absence of a T_m. SAXS measurements confirmed microphase separation for all TPEs. Nevertheless, all TPEs show ill-defined microstructures except the TPEs based on $PCitroGEC_{26K}$ with the highest molar masses. The molar masses of these triblock copolymers are just in the range where microphase separation occurs. Stress-Strain measurements were conducted. These measurements demonstrate

the elasticity (elongation up to 600 %) of these polycarbonate-polyester TPEs with nearly no plastic deformation. Furthermore, they revealed a low *E*-modulus of 0.15-1.0 MPa (TPE with elastic behavior). This elastic behavior combined with the known biocompatibility and biodegradability renders the PLLA-*b*-PCitroGEC-*b*-PLLA triblock copolymers suitable as potential materials in soft tissue engineering and regenerative medicine.

EXPERIMENTAL SECTION

Materials

The solvents and reagents were applied as acquired, unless otherwise stated. Carbon dioxide (>99.999%) was bought from Westfalen AG (Münster, Germany). Bis(triphenylphosphine)iminium chloride ([PPN]Cl) was received from abcr GmbH. (*R,R*)-(salcy)-Co(III)Cl was prepared as described by Ford *et al*.[45] . L,L-Lactid (LLA) was provided by BASF SE and recrystallized in toluene before use. All solvents were purchased from Sigma Aldrich, Fischer Chemical (Pittsburgh, PA, USA), and Honeywell (Morris Plaines, NJ, USA) and used without further purification. All reagents were acquired from Sigma Aldrich, Arcos Organics (Pittsburgh, PA, USA), Alfa Aesar (Kandel, Germany), or TCI (Oxford, UK). Deuterated solvents were purchased from Deutero GmBH (Kastellaun, Germany).

Characterization

NMR Analysis. ^{1}H NMR spectra at 300 MHz and ^{13}C NMR spectra at 75 MHz were recorded on a Bruker Avance III HD 300 (5 mm BBFO-Head with *z*-gradient) at 23 °C. ^{1}H NMR spectra at 400 MHZ and ^{13}C NMR spectra at 100 MHz were recorded on a Bruker Avance III HD 400 (5 mm BBFO Smartprobe with *z*-gradient) at 23 °C. The spectra are referenced internally to the residual proton signal of the deuterated solvent.

Size exclusion chromatography (SEC). SEC was completed in DMF (1 mL/min, 50 °C) containing 1 g/L lithium bromide as an additive, using an Agilent 1100 series SEC system equipped with a HEMA 300/100/40 Å column cascade, UV (254 nm), and RI detector. Calibration was accomplished using poly (ethylene glycol) (PEG) standards acquired from Polymer Standard Service (PSS). SEC measurements were accomplished in THF (1 mL/min, 30°C) on a SDV column set from PSS (SDV 103, SDV 105, SDV 106), equipped with a UV (254 nm) and RI detector. Calibration was carried out using polystyrene standards (PSS).

Differential scanning calorimetry (DSC). DSC curves were recorded using a Perkin-Elmer DSC 7 CLN2 instrument in the temperature range of -95°C–180°C or -95 °C–50 °C, at heating rates of 10K/min under nitrogen atmosphere. Glass transition temperatures (T_g) were determined using Pyris™ software.

Fourier-Transformations-Infrared spectroscopy. FT-IR spectra were recorded using a *Nicolet* iS10 FT-IR spectrometer (Thermo Scientific, Waltham, MA, USA) equipped with a diamond ATR unit.

Tensile test. Tensile tests were realized by a material testing machine Z005 (Zwick/Roell, Germany). Tensile tests were accomplished by exposing the stamped polymer stripes (5 mm x 45 mm) to uniaxial tension. Samples with thicknesses around 0.3 – 0.6 mm were strained with a rate of 20 mm/min at

room temperatures. A predefined load of 0.02 N was applied. Stress-strain measurements were carried out 3 times for each copolymer. All films were prepared by slow evaporation from a chloroform solution followed by full removal of the solvent under reduced pressure. The E-modulus (*E*) was determined by calculating the slope of the stress-strain curves before the yield point. The yield point of the films were calculated by the intersection of the tangents of the elastic field and the plastic field before the strain hardening. The toughness is displayed by the area under the strain stress curves. The elongation at break (ε_{break}) and stress at break(σ_{break}) is the point, where film rupture occurs. are damaged.

X-Ray Scattering. Small-angle X-ray scattering (SAXS) measurements were made using CuKα radiation (Rigaku MicroMax 007 X-ray generator, Osmic Confocal Max-Flux curved multilayer optics). 2D diffraction patterns were recorded on an Mar345 image plate detector. Intensity distributions as a function of the modulus of the total scattering vector, q = (4π/λ) sin(2θ/2), where 2θ is the scattering angle, were obtained by radial averaging of the 2D datasets. Samples in the form of thick films (~0.5 mm) were prepared by slow solvent casting (chloroform). Temperature-dependent measurements of 1 hour long were made by heating the films subsequent cooling aiming at identifying the different equilibrium morphologies.

Synthesis

Monomer synthesis

Synthesis of CitroGE[26]

Citronellol (20 mL, 0.11 mol, 1 eq.) and tetrabutylammonium hydrogen sulfate (TBAHS, 1.61 g, 0.40 mmol, 0.04 eq.) were dissolved in an aqueous sodium hydroxide solution (50 wt%) stirred vigorously at room temperature. The mixture was cooled to 0 °C and then epichlorohydrin (45 mL, 0.57 mol,5.18 eq.) was added within 30 min. After stirring for 3.5 h at room temperature, the reaction solution was added to ice water, extracted three times with diethyl ether, and washed with saturated sodium chloride solution to neutrality. The organic phases were combined and dried with sodium sulfate. The solvent was removed under pressure and the residue was fractionally distilled. Citronellol glycidyl ether was obtained as a colorless liquid. Yield: 44 % (10.39 g, 48.93 mmol).

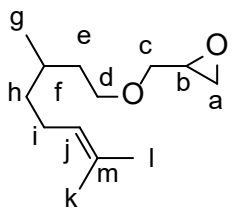

^{1}H NMR (300 MHz, $CDCl_3$) δ = 5.13 – 5.05. (m, 1H, j), 3.77 – 3.61 (m, 1H, c), 3.62 – 3.42 (m, 2H, d), 3.42 – 3.31 (m, 1H, c'), 3.20 – 3.06 (m, 1H, b), 2.83 – 2.55 (m, 2H, a), 2.09 – 1.86 (m, 2H, i), 1.68 (s, 3H, l), 1.61 (s, 3H, k), 1.63 -1.07 (m, 5H, e+f+h), 0.89 (d, 3H,g) ppm.

Polymer synthesis

Synthesis of PCitroGEC

As an example, PCitroGEC-4 was used. The other PCitroGEC homopolymers were synthesized in the same manner using different amounts of catalyst system (Table 1).

A 150 mL Roth autoclave was dried at 40 °C under reduced pressure. Citronellol glycidyl ether (CitroGE) (2.2 mL, 1.89 mmol), (*R,R*)-(salcy)-CoCl (11.7 mg, 0.018 mmol) and [PPN]Cl (10.5 mg, 0.0018 mmol) was filled in the autoclave equipped with a stirring-bar in an inert argon atmosphere. The reaction mixture was stirred at a carbon dioxide pressure of 55 bar at 20 °C for 17 h. CO_2 was then released; the crude product was dissolved in DCM and the catalyst was deactivated with 2 mL of a solution of 5%$_{vol}$ HCl (aq) in methanol. The product was precipitated twice in ice-cold methanol as a non-solvent. The precipitated product was collected by centrifugation at 4500 rpm at 0°C for 10 min. The colorless viscous polymer was then dried under reduced pressure for 24h. A yield of 57 % polymer was obtained.

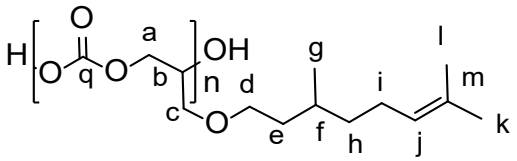

^{1}H NMR (300 MHz, $CDCl_3$): δ = 5.16 – 5.06 (m, 1H, j),5.06 – 4.98(m, 1H, b), 4.52 – 4.29 (m, 2H, a), 3.63 (d, 2H, c) 3.56 – 3-40 (m, 2H, d), 2.10 – 1.85 (m, 2H, i), 1.70 (s, 3H, k), 1.62 (s, 3H, l), 1.65 – 1.10 (m, 5H, e+f+h), 0.91(d, 3H, g) ppm.

^{13}C NMR (75 MHz, $CDCl_3$): δ = 154.40 (Q), 131.24 (M), 124.86 (J), 74.48 (B), 70.26 (D), 68.44 (C), 66.14 (A), 37.35 (E), 36.51 (H), 29.63 (F), 25.84 (I), 25.56 (K), 19.64 (G), 17.77 (L) ppm.

M_n (SEC, DMF, PEG calibration) = 26 000 g / mol; *Đ* (SEC, DMF, PEG calibration) = 1.23.

M_n (SEC, THF, PS calibration) = 41 000 g / mol; *Đ* (SEC, THF, PS calibration) = 1.24.

$T_{g,1}$: -55 °C.

Synthesis of PLA-b-PCitroGEC-b-PLA

The ROP of L,L-Lactid (LLA) using the organocatalyst 1,8-diazabicyclo[5.4.0]undec-7-ene (DBU) is described exemplarily for TPE-2 and was performed according to established literature procedures, applying minor changes.[46] The macroinitiator PCitroGE and LLA were respectively dissolved in benzene and freeze-dried *in vacuo* to remove residual water. DBU was dried over CaH_2 before use. All chemicals were transferred into a glovebox (MBRAUN, UNILAB, < 0.1 ppm of O_2 and < 0.1 ppm of H_2O) to perform the triblock copolymer synthesis. The macroinitiator (0.4148 g, 0.025 mmol, 1 eq.) and LLA (0.415 g, 2.88 mmol, 114.5 eq.) were dissolved in 1.66 mL dichloromethane (5,32 mL / 1 g LLA) in a screw cap vial. Subsequently, 0.45 mL of a DBU (0.01 mol% of LLA) stock solution (0.0001 mL / mL DCM) was added to initiate the polymerization. The solution was stirred for 50 min at room temperature and quenched by adding benzoic acid. The resulting triblock copolymer was precipitated three times in methanol and dried *in vacuo*. A viscous liquid was obtained in yields of 77%.

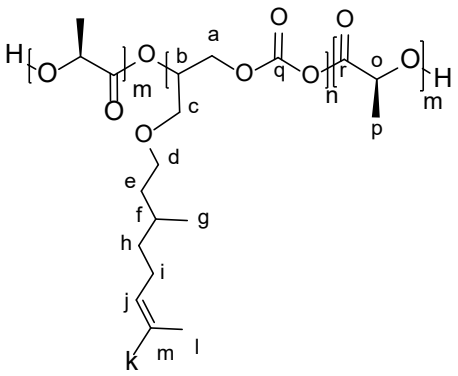

^{1}H NMR (400 MHz, $CDCl_3$): δ = 5.15 (q, 1H, o), 5.10 – 5.03 (m, 1H, j), 5.03 – 4.92 (m, 1H, b), 4.51 – 4.16 (m, 1H, a), 3.63 – 3.53 (m, 2H, c), 3.52 – 3.40 (m, 2H, d), 2.05 – 1.87 (m, 2H, i), 1.66 (s, 3H, k), 1.62 – 1.45 (m, 7H, p+l+f), 1.42 – 1.20 (m, 2H, e), 1.20 – 1.05 (m, 2H, h), 0.86 (d, 3H, g) ppm.

^{13}C NMR (75 MHz, $CDCl_3$): δ = 169.73 (R), 154.33 (Q), 131.25 (M), 124.84 (J), 74.47 (B), 70.25 (D), 69.11 (O), 68.46 (C), 66.15 (A), 37.33 (E), 36.48 (H), 29.58 (F), 25.84 (I), 25.53 (K), 19.63 (G), 17.77 (L), 16.75 (P) ppm.

M_n (SEC, DMF, PEG calibration) = 23 000 g / mol; $Đ$ (SEC, DMF, PEG calibration) = 1.31.

$T_{g,1}$: -59 °C (PCitroGE) $T_{g,2}$: 55 °C (PLLA)

ACKNOWLEGMENTS

The authors thank Monika Schmelzer for the SEC measurements and Andreas Hanewald for the assistance regarding the strain-stress-measurements.

REFERENCES

(1) Spontak, R. J.; Patel, N. P. Thermoplastic elastomers: fundamentals and applications. *Curr. Opin. Colloid Interface Sci.* **2000**, *5*, 333–340.

(2) Kear, K. E. *Developments in thermoplastic elastomers*; Report / Rapra Technology Ltd 166; Rapra Technology: Shrewsbury, 2003.

(3) Holden, G. Thermoplastic Elastomers. *Rubber Technology*; Springer, Boston, MA, 1987; pp 465–481.

(4) Steube, M.; Plank, M.; Gallei, M.; Frey, H.; Floudas, G. Building Bridges by Blending: Morphology and Mechanical Properties of Binary Tapered Diblock/Multiblock Copolymer Blends. *Macromol. Chem. Phys.* **2021**, *222*, 2000373.

(5) *Rubber Technology*; Springer, Boston, MA, 1987.

(6) Wahlen, C.; Frey, H. Anionic Polymerization of Terpene Monomers: New Options for Bio-Based Thermoplastic Elastomers. *Macromolecules* **2021**, *54*, 7323–7336.

(7) Wang, W.; Lu, W.; Goodwin, A.; Wang, H.; Yin, P.; Kang, N.-G.; Hong, K.; Mays, J. W. Recent advances in thermoplastic elastomers from living polymerizations: Macromolecular architectures and supramolecular chemistry. *Progress in Polymer Science* **2019**, *95*, 1–31.

(8) Bolton, J. M.; Hillmyer, M. A.; Hoye, T. R. Sustainable Thermoplastic Elastomers from Terpene-Derived Monomers. *ACS Macro Lett.* **2014**, *3*, 717–720.

(9) Ding, W.; Wang, S.; Yao, K.; Ganewatta, M. S.; Tang, C.; Robertson, M. L. Physical Behavior of Triblock Copolymer Thermoplastic Elastomers Containing Sustainable Rosin-Derived Polymethacrylate End Blocks. *ACS Sustainable Chem. Eng.* **2017**, *5*, 11470–11480.

(10) Gregory, G. L.; Sulley, G. S.; Carrodeguas, L. P.; Chen, T. T. D.; Santmarti, A.; Terrill, N. J.; Lee, K.-Y.; Williams, C. K. Triblock polyester thermoplastic elastomers with semi-aromatic polymer end blocks by ring-opening copolymerization. *Chemical science* **2020**, *11*, 6567–6581.

(11) Della Monica, F.; Kleij, A. W. From terpenes to sustainable and functional polymers. *Polym. Chem.* **2020**, *11*, 5109–5127.

(12) Noppalit, S.; Simula, A.; Ballard, N.; Callies, X.; Asua, J. M.; Billon, L. Renewable Terpene Derivative as a Biosourced Elastomeric Building Block in the Design of Functional Acrylic Copolymers. *Biomacromolecules* **2019**, *20*, 2241–2251.

(13) Hepburn, C.; Adlen, E.; Beddington, J.; Carter, E. A.; Fuss, S.; Mac Dowell, N.; Minx, J. C.; Smith, P.; Williams, C. K. The technological and economic prospects for CO2 utilization and removal. *Nature* **2019**, *575*, 87–97.

(14) Zhu, Y.; Romain, C.; Williams, C. K. Sustainable polymers from renewable resources. *Nature* **2016**, *540*, 354–362.

(15) Hasan, M. M. F.; Rossi, L. M.; Debecker, D. P.; Leonard, K. C.; Li, Z.; Makhubela, B. C. E.; Zhao, C.; Kleij, A. Can CO 2 and Renewable Carbon Be Primary Resources for Sustainable Fuels and Chemicals? *ACS Sustainable Chem. Eng.* **2021**, *9*, 12427–12430.

(16) Scharfenberg, M.; Hilf, J.; Frey, H. Functional Polycarbonates from Carbon Dioxide and Tailored Epoxide Monomers: Degradable Materials and Their Application Potential. *Adv. Funct. Mater.* **2018**, *28*, 1704302.

(17) Artz, J.; Müller, T. E.; Thenert, K.; Kleinekorte, J.; Meys, R.; Sternberg, A.; Bardow, A.; Leitner, W. Sustainable Conversion of Carbon Dioxide: An Integrated Review of Catalysis and Life Cycle Assessment. *Chem. Rev.* **2018**, *118*, 434–504.

(18) Sakakura, T.; Choi, J.-C.; Yasuda, H. Transformation of carbon dioxide. *Chem. Rev.* **2007**, *107*, 2365–2387.

(19) Xu, Y.; Zhou, F.; Zhou, D.; Mo, J.; Hu, H.; Lin, L.; Wu, J.; Yu, M.; Zhang, M.; Chen, H. *Degradation Behaviors of Biodegradable Aliphatic Polyesters and Polycarbonates* 14; American Scientific Publishers, 2020.

(20) Inoue, S.; Koinuma, H.; Tsuruta, T. Copolymerization of carbon dioxide and epoxide with organometallic compounds. *Makromol. Chem.* **1969**, *130*, 210–220.

(21) Jia, M.; Zhang, D.; Kort, G. W. de; Wilsens, C. H. R. M.; Rastogi, S.; Hadjichristidis, N.; Gnanou, Y.; Feng, X. All-Polycarbonate Thermoplastic Elastomers Based on Triblock Copolymers Derived from Triethylborane-Mediated Sequential Copolymerization of CO2 with Various Epoxides. *Macromolecules* **2020**, *53*, 5297–5307.

(22) Yang, G.-W.; Wu, G.-P. High-Efficiency Construction of CO 2 -Based Healable Thermoplastic Elastomers via a Tandem Synthetic Strategy. *ACS Sustainable Chem. Eng.* **2019**, *7*, 1372–1380.

(23) Sulley, G. S.; Gregory, G. L.; Chen, T. T. D.; Peña Carrodeguas, L.; Trott, G.; Santmarti, A.; Lee, K.-Y.; Terrill, N. J.; Williams, C. K. Switchable Catalysis Improves the Properties of CO2-Derived Polymers: Poly(cyclohexene carbonate-b-ε-decalactone-b-cyclohexene carbonate) Adhesives, Elastomers, and Toughened Plastics. *J. Am. Chem. Soc.* **2020**, *142*, 4367–4378.

(24) Carrodeguas, L. P.; Chen, T. T. D.; Gregory, G. L.; Sulley, G. S.; Williams, C. K. High elasticity, chemically recyclable, thermoplastics from bio-based monomers: carbon dioxide, limonene oxide and ε-decalactone. *Green Chem.* **2020**, *22*, 8298–8307.

(25) Martín, C.; Kleij, A. W. Terpolymers Derived from Limonene Oxide and Carbon Dioxide: Access to Cross-Linked Polycarbonates with Improved Thermal Properties. *Macromolecules* **2016**, *49*, 6285–6295.

(26) Johann, T.; Houck, H. A.; Dinh, T.; Kemmer-Jonas, U.; Du Prez, F. E.; Frey, H. Multi-olefin containing polyethers and triazolinediones: a powerful alliance. *Polym. Chem.* **2019**, *10*, 4699–4708.

(27) Hauenstein, O.; Reiter, M.; Agarwal, S.; Rieger, B.; Greiner, A. Bio-based polycarbonate from limonene oxide and CO 2 with high molecular weight, excellent thermal resistance, hardness and transparency. *Green Chem.* **2016**, *18*, 760–770.

(28) Byrne, C. M.; Allen, S. D.; Lobkovsky, E. B.; Coates, G. W. Alternating copolymerization of limonene oxide and carbon dioxide. *J. Am. Chem. Soc.* **2004**, *126*, 11404–11405.

(29) Wambach, A.; Agarwal, S.; Greiner, A. Synthesis of Biobased Polycarbonate by Copolymerization of Menth-2-ene Oxide and CO 2 with Exceptional Thermal Stability. *ACS Sustainable Chem. Eng.* **2020**, *8*, 14690–14693.

(30) Neumann, S.; Däbritz, S. B.; Fritze, S. E.; Leitner, L.-C.; Anand, A.; Greiner, A.; Agarwal, S. Sustainable block copolymers of poly(limonene carbonate). *Polym. Chem.* **2021**, *12*, 903–910.

(31) Li, C.; Johansson, M.; Buijsen, P.; Dijkstra, G.; Sablong, R. J.; Koning, C. E. Limonene-derived polycarbonates as biobased UV-curable (powder) coating resins. *Prog. Org. Coat.* **2021**, *151*, 106073.

(32) Zhang, Y.-Y.; Zhang, X.-H.; Wei, R.-J.; Du, B.-Y.; Fan, Z.-Q.; Qi, G.-R. Synthesis of fully alternating polycarbonate with low T g from carbon dioxide and bio-based fatty acid. *RSC Adv.* **2014**, *4*, 36183–36188.

(33) Gardiner, C.; Johann, T.; Hanewald, A.; Frey, H. Addressing a key challenge of CO2-based polycarbonates: low glass transition capitalizing on citronellol glycidyl ether. *to be submitted* **2021**.

(34) Mouzin, G.; Cousse, H.; Rieu, J.-P.; Duflos, A. A Convenient One-Step Synthesis of Glycidyl Ethers. *Synthesis* **1983**, *1983*, 117–119.

(35) Jia, M.; Hadjichristidis, N.; Gnanou, Y.; Feng, X. Monomodal Ultrahigh-Molar-Mass Polycarbonate Homopolymers and Diblock Copolymers by Anionic Copolymerization of Epoxides with CO 2. *ACS Macro Lett.* **2019**, *8*, 1594–1598.

(36) Dove, A. P. Organic Catalysis for Ring-Opening Polymerization. *ACS Macro Lett.* **2012**, *1*, 1409–1412.

(37) Hirschberg, V.; Faust, L.; Rodrigue, D.; Wilhelm, M. Effect of Topology and Molecular Properties on the Rheology and Fatigue Behavior of Solid Polystyrene/Polyisoprene Di- and Triblock Copolymers. *Macromolecules* **2020**, *53*, 5572–5587.

(38) Dove, A. P. Controlled ring-opening polymerisation of cyclic esters: polymer blocks in self-assembled nanostructures. *Chemical communications (Cambridge, England)* **2008**, 6446–6470.

(39) Pyda, M.; Bopp, R.; Wunderlich, B. Heat capacity of poly(lactic acid). *The Journal of Chemical Thermodynamics* **2004**, *36*, 731–742.

(40) Lim, L.-T.; Auras, R.; Rubino, M. Processing technologies for poly(lactic acid). *Progress in Polymer Science* **2008**, *33*, 820–852.

(41) Gosline, J.; Lillie, M.; Carrington, E.; Guerette, P.; Ortlepp, C.; Savage, K. Elastic proteins: biological roles and mechanical properties. *Phil. Trans. R. Soc. Lond. B* **2002**, *357*, 121–132.

(42) Dutta, D.; Lee, K.-W.; Allen, R. A.; Wang, Y.; Brigham, J. C.; Kim, K. Non-invasive assessment of elastic modulus of arterial constructs during cell culture using ultrasound elasticity imaging. *Ultrasound in Medicine & Biology* **2013**, *39*, 2103–2115.

(43) Laasanen, M. S.; Saarakkala, S.; Töyräs, J.; Hirvonen, J.; Rieppo, J.; Korhonen, R. K.; Jurvelin, J. S. Ultrasound indentation of bovine knee articular cartilage in situ. *Journal of Biomechanics* **2003**, *36*, 1259–1267.

(44) Kurkijärvi, J. E.; Nissi, M. J.; Kiviranta, I.; Jurvelin, J. S.; Nieminen, M. T. Delayed gadolinium-enhanced MRI of cartilage (dGEMRIC) and T2 characteristics of human knee articular cartilage: topographical variation and relationships to mechanical properties. *Magn. Reson. Med.* **2004**, *52*, 41–46.

(45) Ford, D. D.; Nielsen, L. P. C.; Zuend, S. J.; Musgrave, C. B.; Jacobsen, E. N. Mechanistic basis for high stereoselectivity and broad substrate scope in the (salen)Co(III)-catalyzed hydrolytic kinetic resolution. *J. Am. Chem. Soc.* **2013**, *135*, 15595–15608.

(46) Lohmeijer, B. G. G.; Pratt, R. C.; Leibfarth, F.; Logan, J. W.; Long, D. A.; Dove, A. P.; Nederberg, F.; Choi, J.; Wade, C.; Waymouth, R. M.*; et al.* Guanidine and Amidine Organocatalysts for Ring-Opening Polymerization of Cyclic Esters. *Macromolecules* **2006**, *39*, 8574–8583.

SUPPORTING INFORMATION

Biobased Thermoplastic Elastomers Based on Citronellol Glycidyl Ether, CO_2 and Polylactide

Christina Gardiner[a], Sandra Schüttner[a], Frédéric Petrov[a], George Floudas[b] Holger Frey[a*]

[a]Department of Chemistry, Johannes Gutenberg University, Duesbergweg 10-14, 55128 Mainz, Germany

[b]Department of Physics, University of Ioannina, P.O. Box 1186, 45110 Ioannina, Greece.

Table of content

1. Monomer characterization

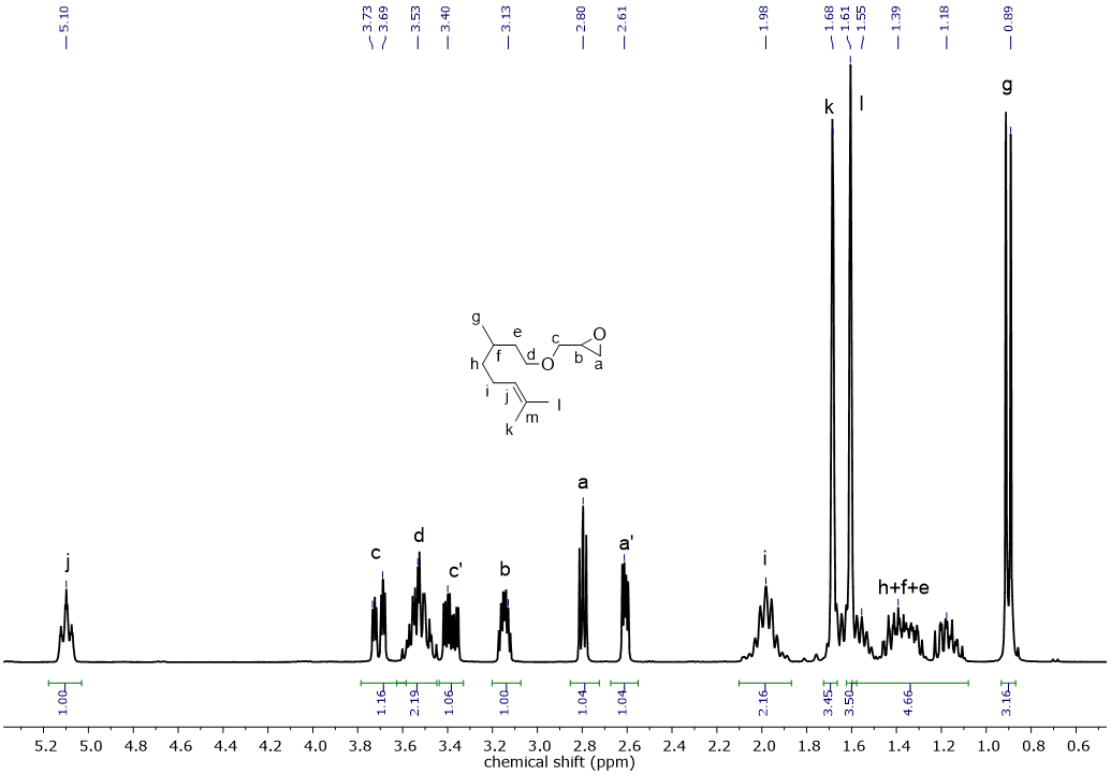

Figure S 1: ^{1}H NMR spectrum (300 MHz, $CDCl_3$) of CitroGE after distillation.

2. Polymer characterization

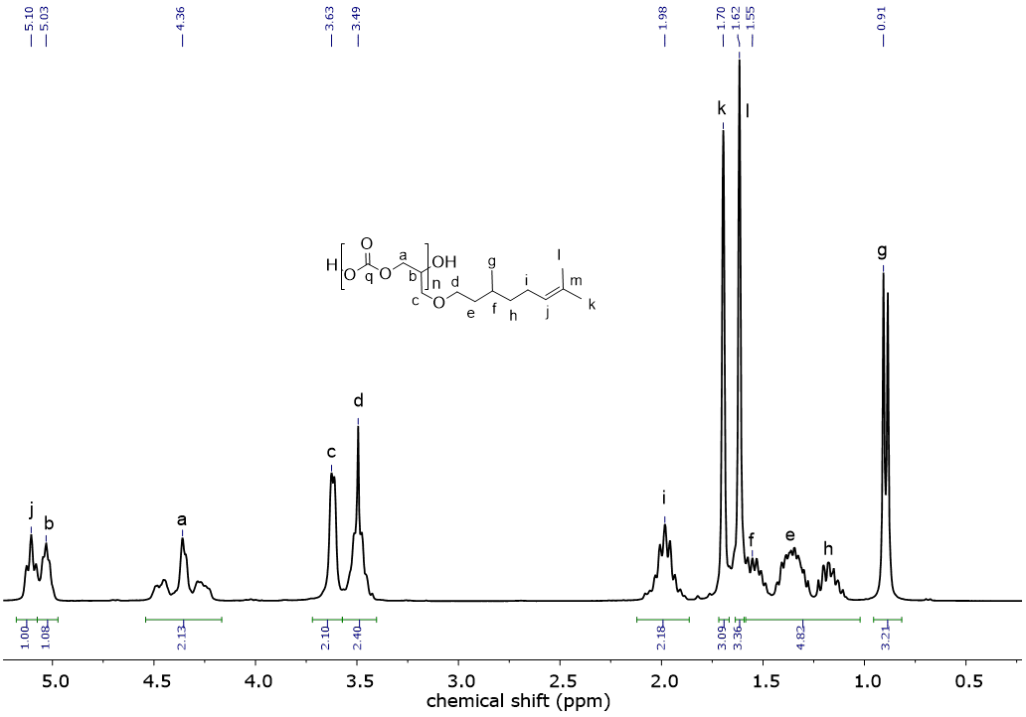

Figure S 2: ^{1}H NMR spectrum (300 MHz, $CDCl_3$) of $PCitroGEC_{26K}$ homopolymer.

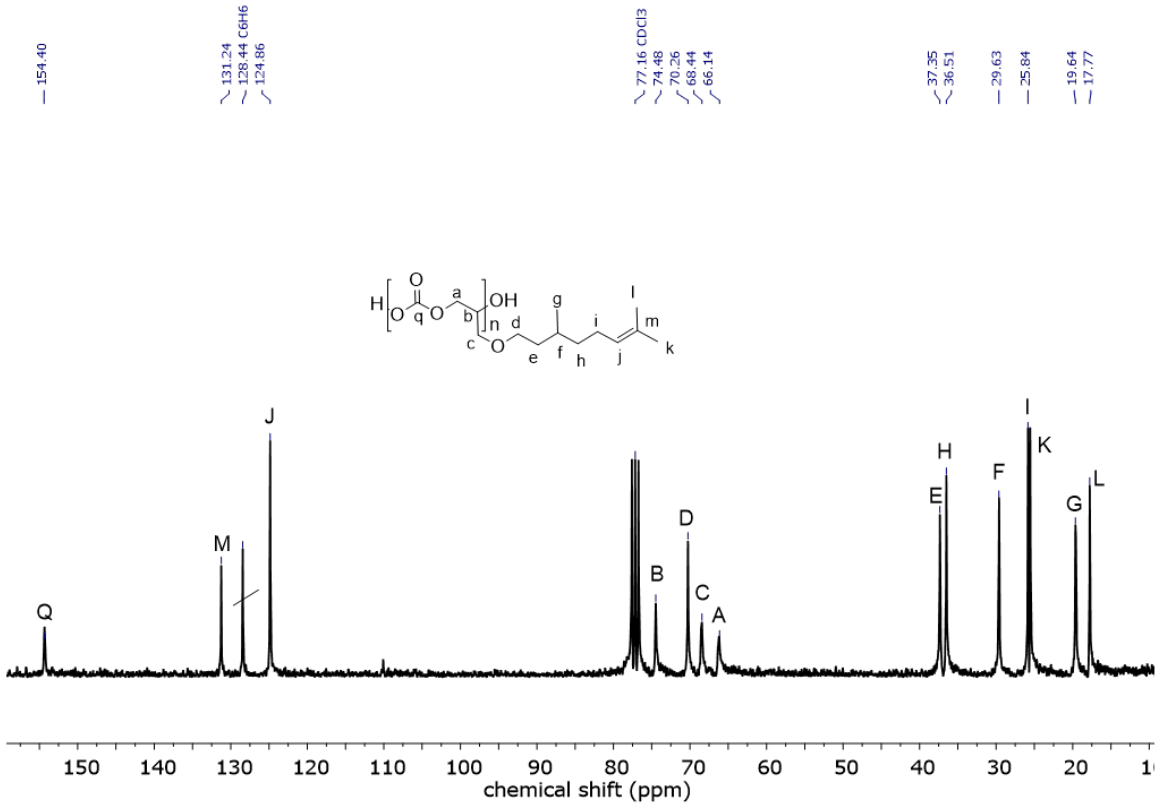

Figure S 3: ^{13}C NMR spectrum (75 MHz, $CDCl_3$) of PCitroGEC$_{26K}$ homopolymer, showing the formation of polycarbonate structure, based on the signal of carbonyl carbon at 154.40 ppm.

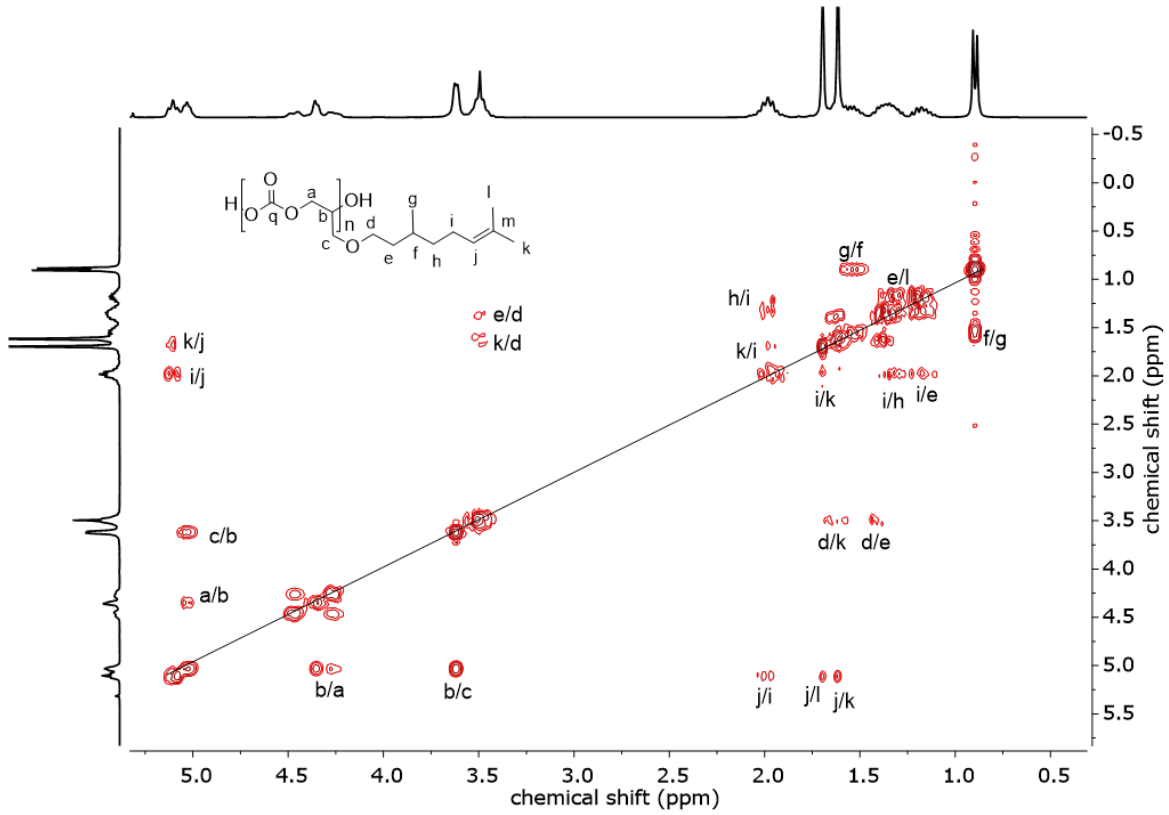

Figure S 4: ^{1}H-^{1}H COSY NMR (300 MHz, $CDCl_3$) spectrum of PCitroGEC$_{26K}$ homopolymer.

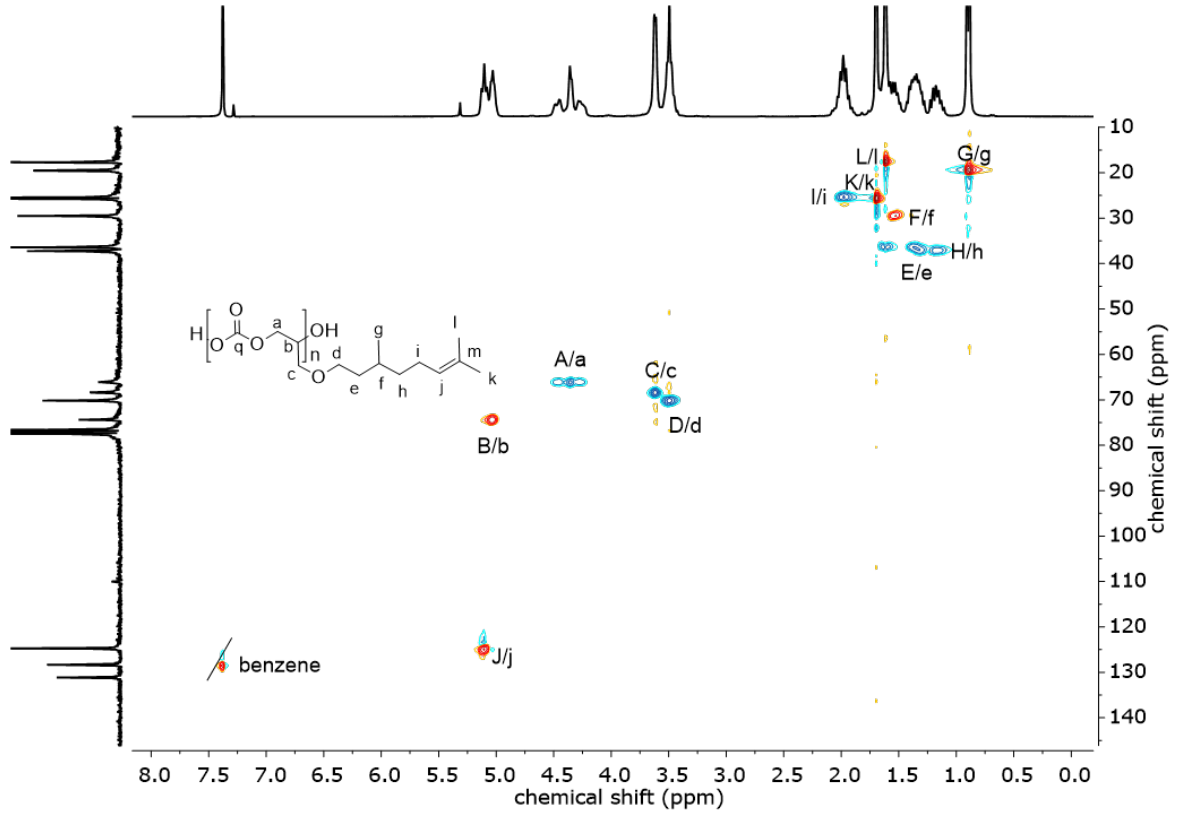

Figure S 5: ^{1}H-^{13}C HSQC NMR spectrum (300 MHz/75 MHz, $CDCl_3$) of $PCitroGEC_{26K}$.

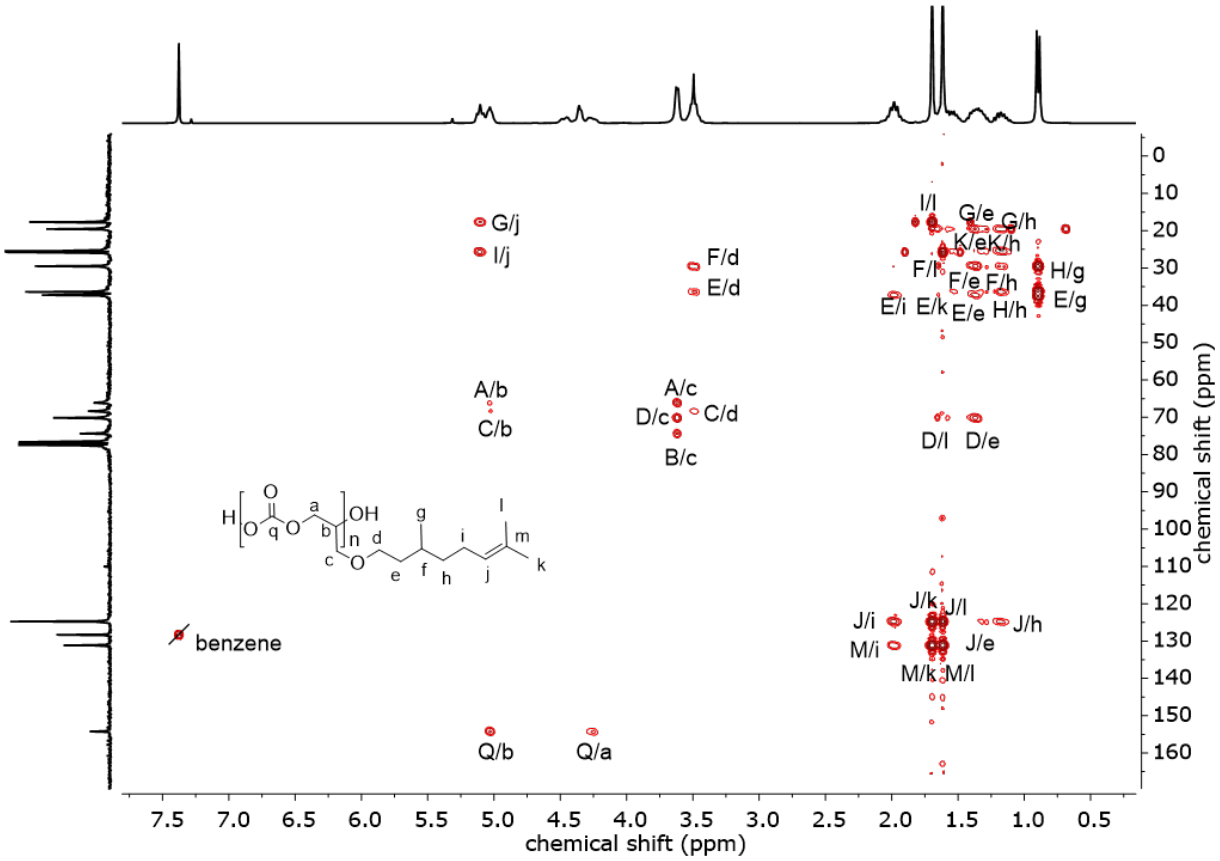

Figure S 6: ^{1}H-^{13}C HMBC NMR spectrum (300 MHz/75 MHz, $CDCl_3$) of $PCitroGEC_{26K}$.

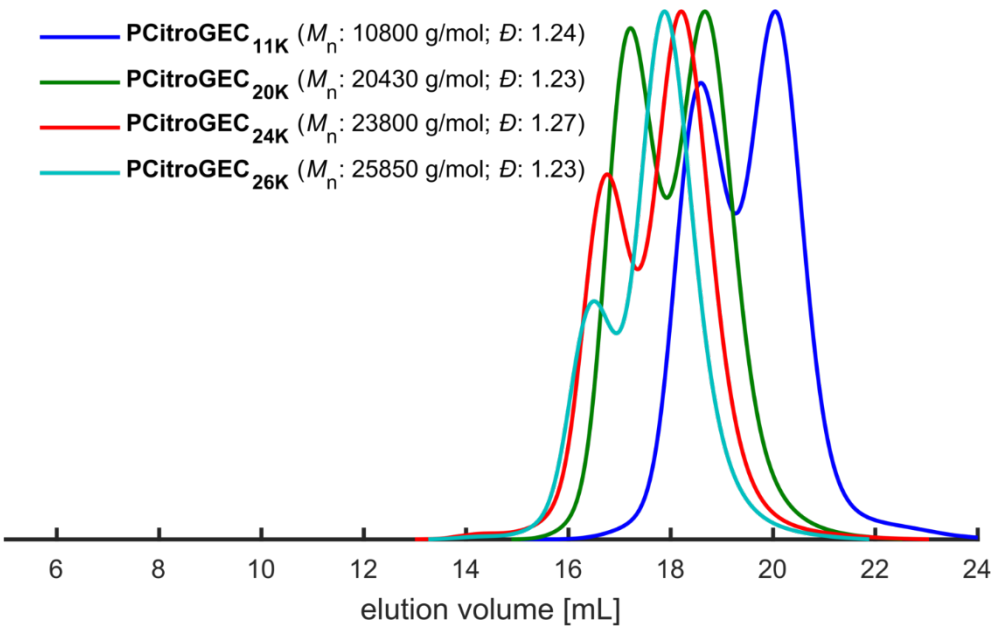

Figure S 7: SEC traces of the PCitroGEC macroinitiators (eluent: DMF, standard: PEG).

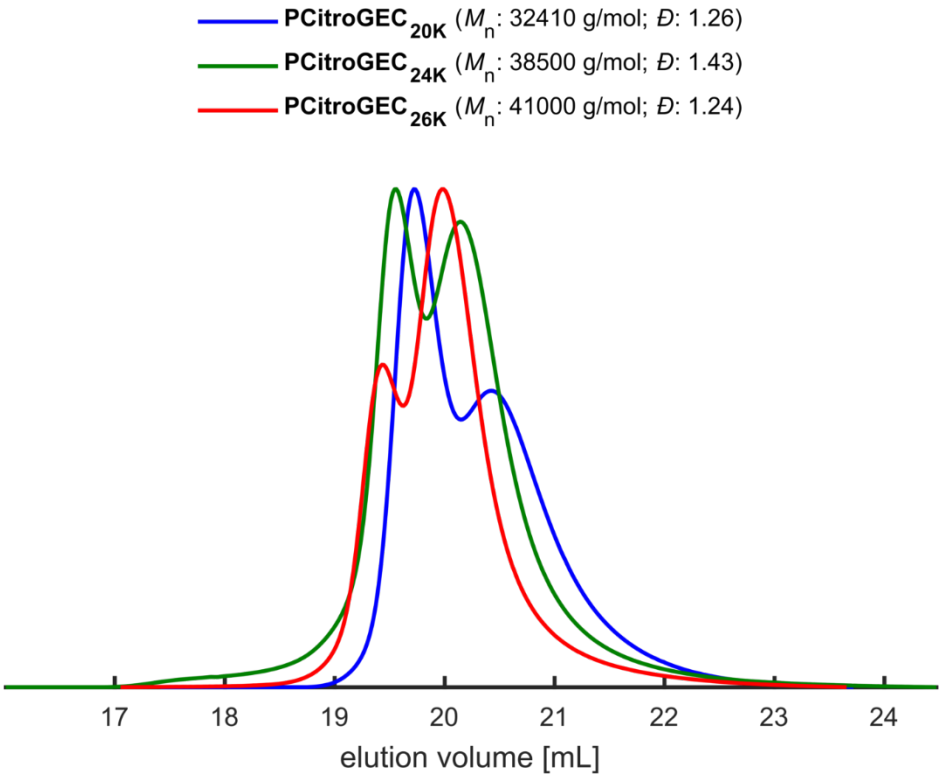

Figure S 8: SEC trace of PCitroGEC macroinitiators (eluent: THF, standard: PS).

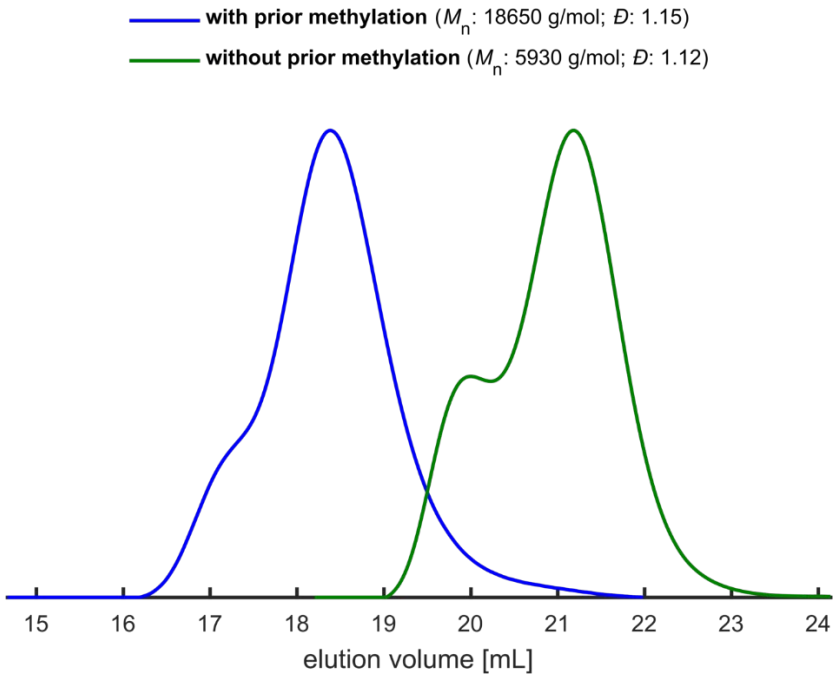

Figure S 9: SEC trace of PCitroGEC using 0.2 mol% of the catalyst without prior methylation of CitroGE (green) and with prior methylation of CitroGE (blue) (eluent: DMF, standard: PEG).

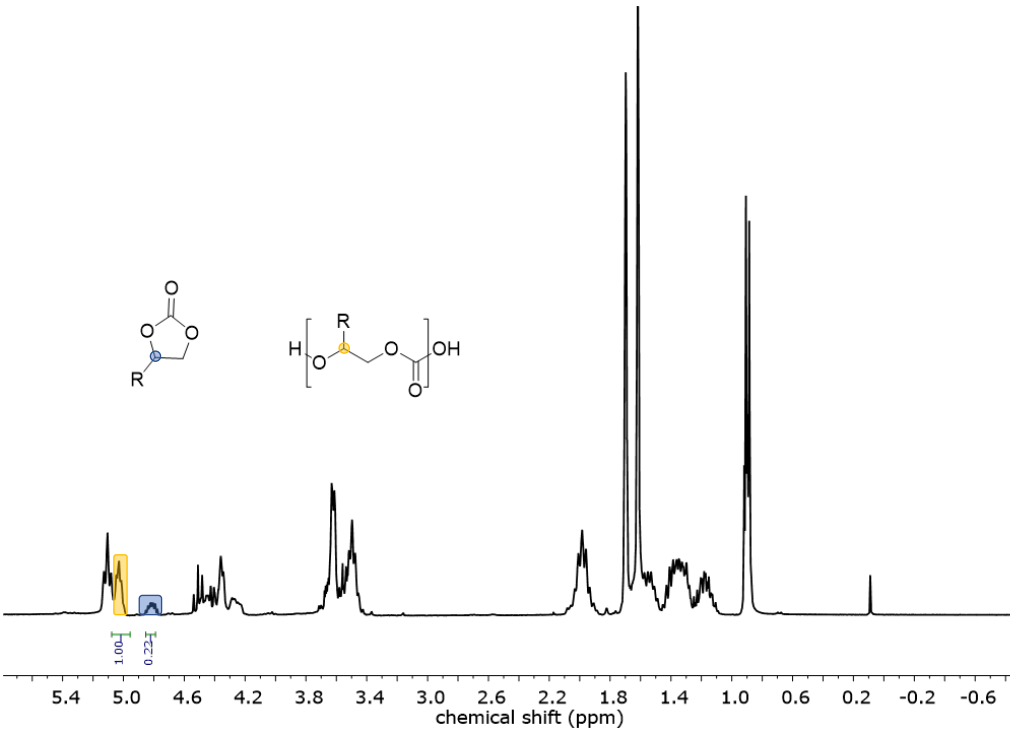

Figure S 10: ^{1}H NMR spectrum (300 MHz, $CDCl_3$) of the crude product of $PCitroGEC_{11K}$. In yellow the proton signal of the polycarbonate, in blue, the proton of the cyclic carbonate is illustrated. Using these integrals of the signals, the molar fraction of cyclic carbonates can be calculated.

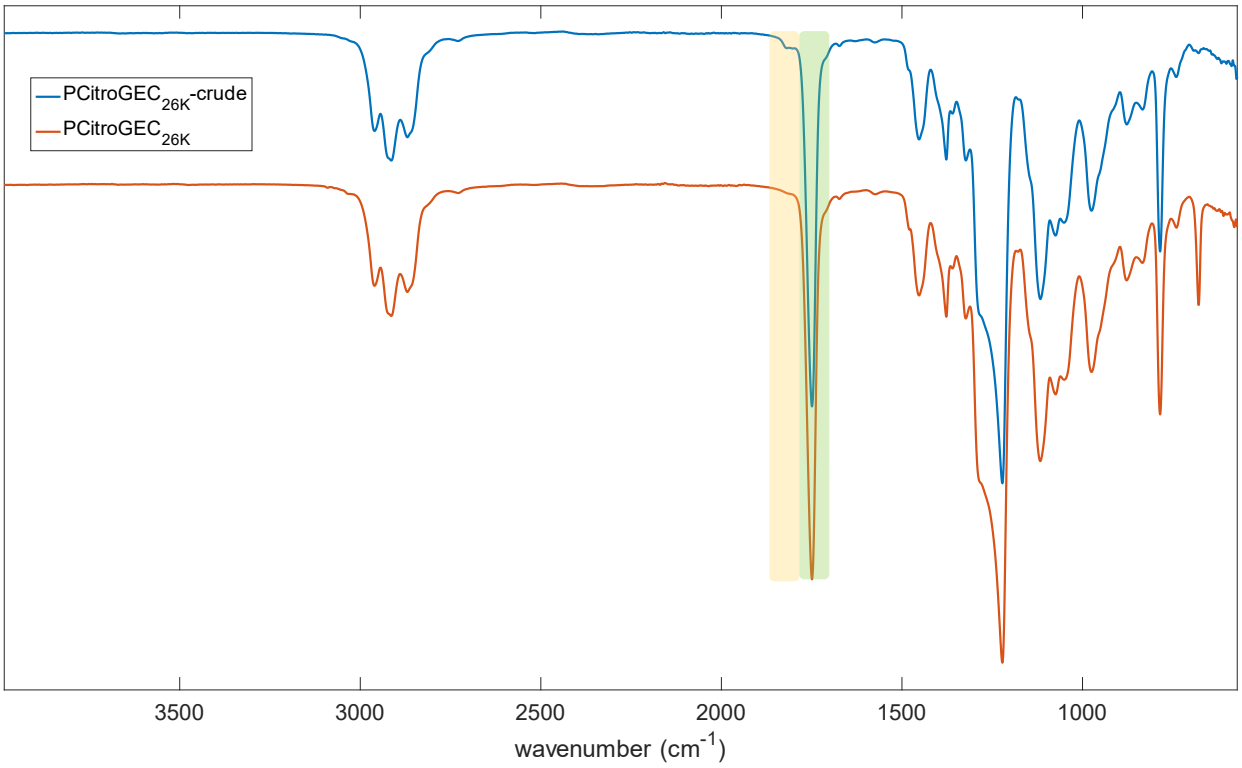

Figure S 11: IR spectra of PCitroGEC$_{26k}$. In blue is the crude product of the polymer illustrated showing the intensive band of the polycarbonate at 1749 cm^{-1} (highlighted in green) and the weak band of the cyclic carbonates at 1800 cm^{-1} (highlighted in yellow). In orange is the IR spectrum of PCitroGEC$_{26K}$ after precipitation is shown. No band of cyclic carbonates is detectable here.

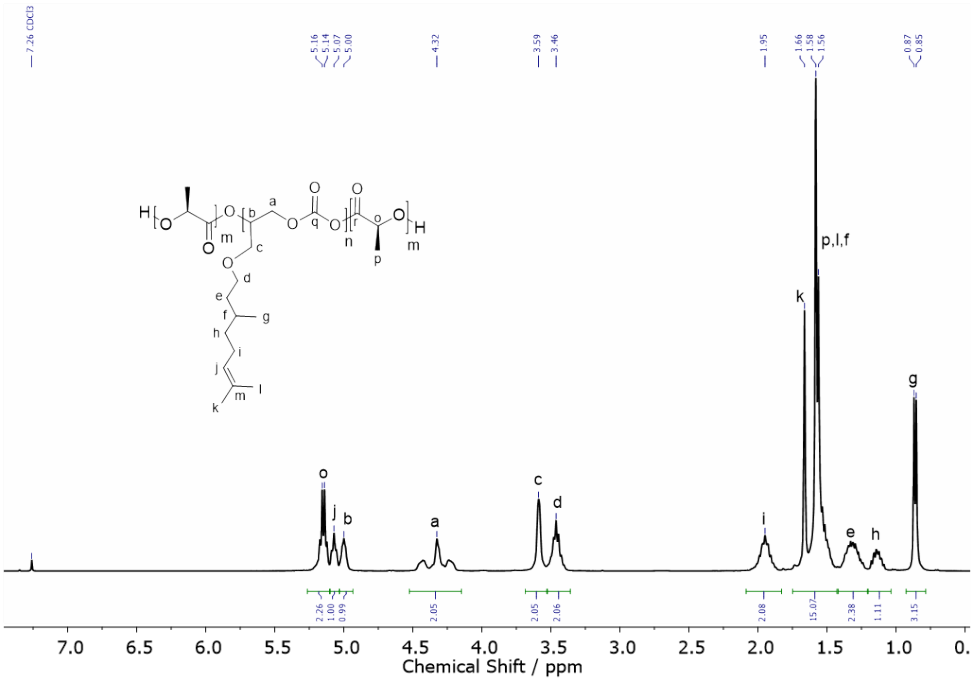

Figure S 12: ^{1}H NMR spectrum (400 MHz, $CDCl_3$) of TPE-2 (PLLA$_{0.35}$-*b*-PCitroGEC$_{0.31}$-*b*-PLLA$_{0.35}$).

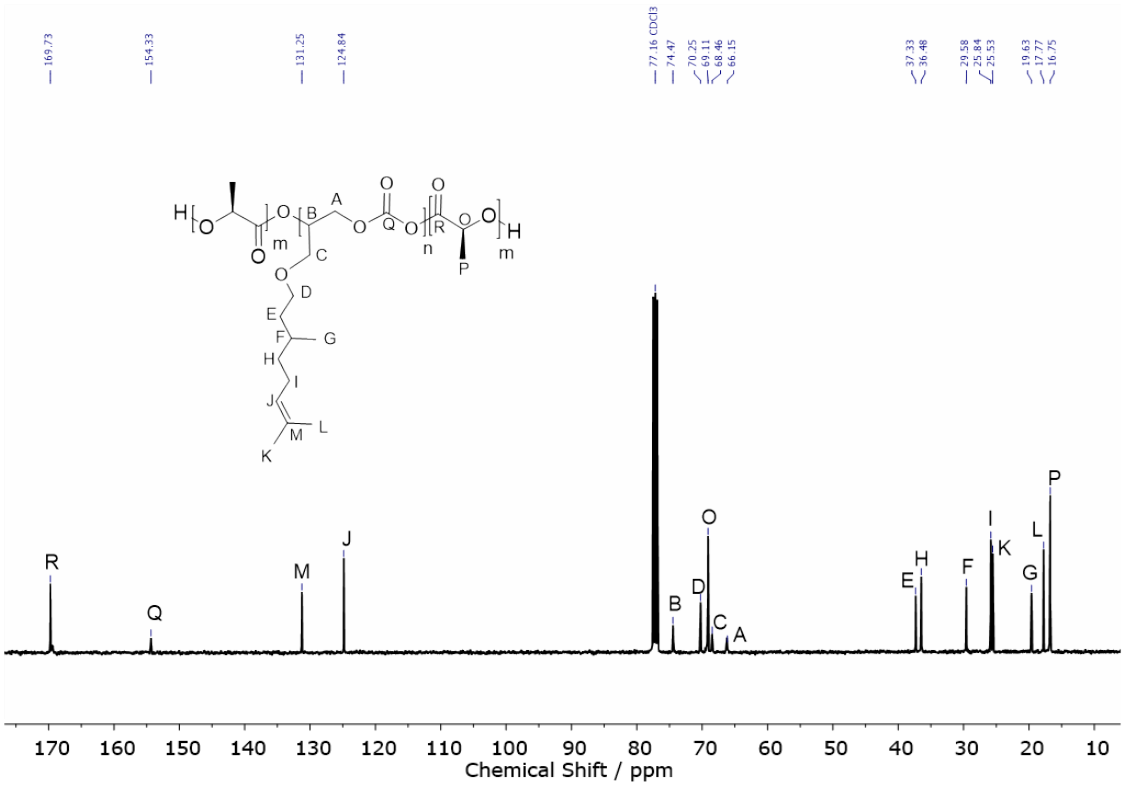

Figure S 13: ^{13}C NMR spectrum (75 MHz, $CDCl_3$) of TPE-2 ($PLLA_{0.35}$-*b*-$PCitroGEC_{0.31}$-*b*-$PLLA_{0.35}$).

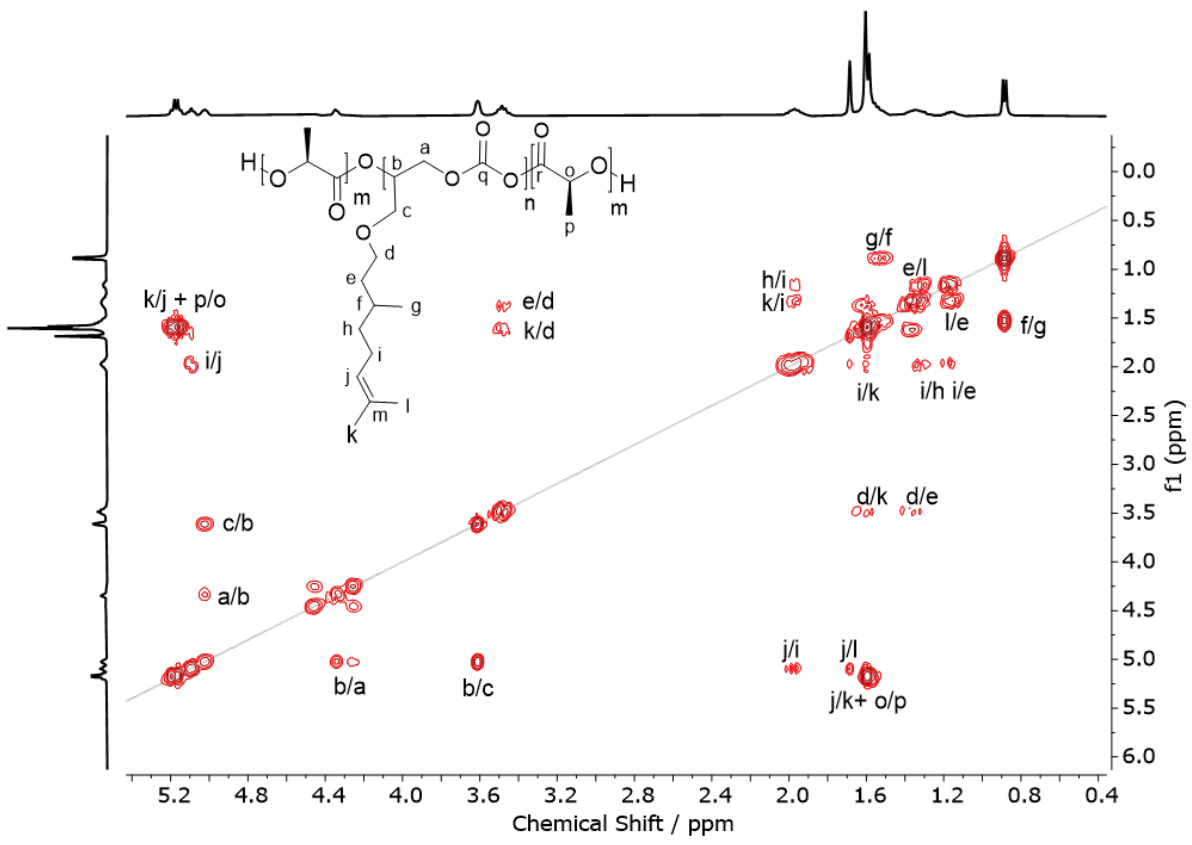

Figure S 14: ^{1}H-^{1}H COSY NMR spectrum (400 MHz, $CDCl_3$) of TPE-2 ($PLLA_{0.35}$-*b*-$PCitroGEC_{0.31}$-*b*-$PLLA_{0.35}$).

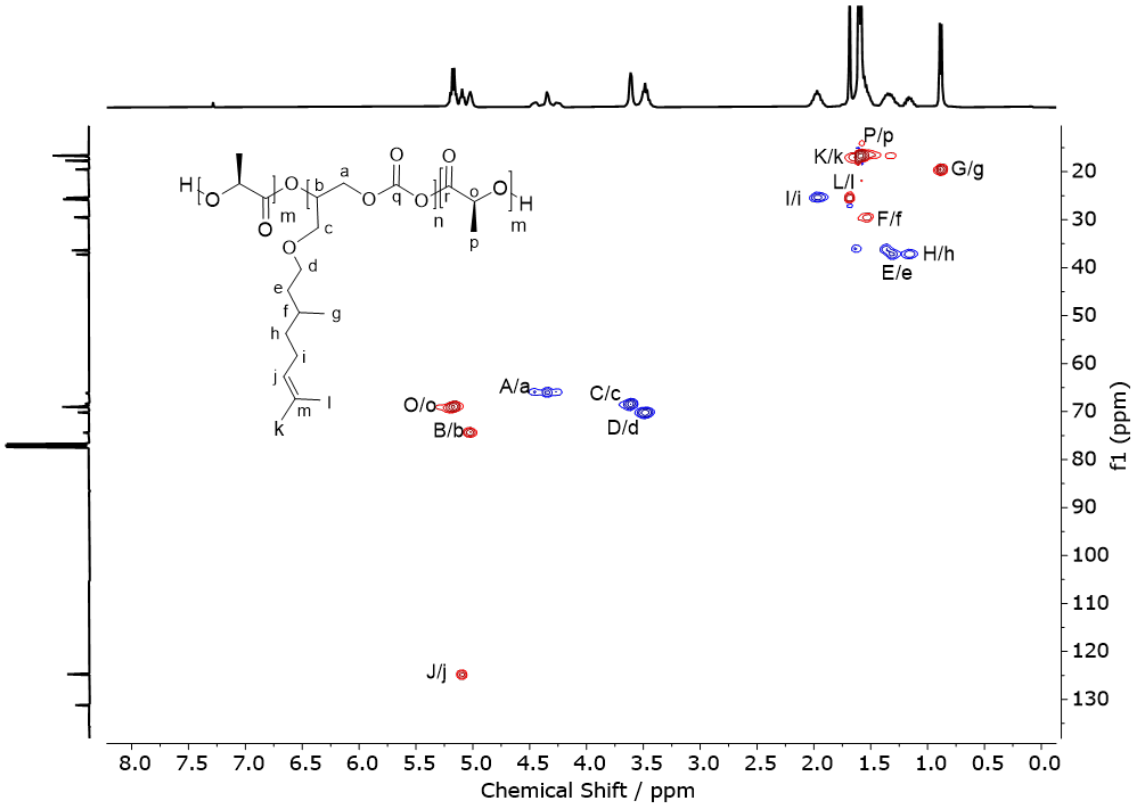

Figure S 15: ^{1}H-^{13}C HSQC NMR spectrum (400 MHz/75 MHz, $CDCl_3$) of TPE-2 ($PLLA_{0.35}$-*b*-$PCitroGEC_{0.31}$-*b*-$PLLA_{0.35}$).

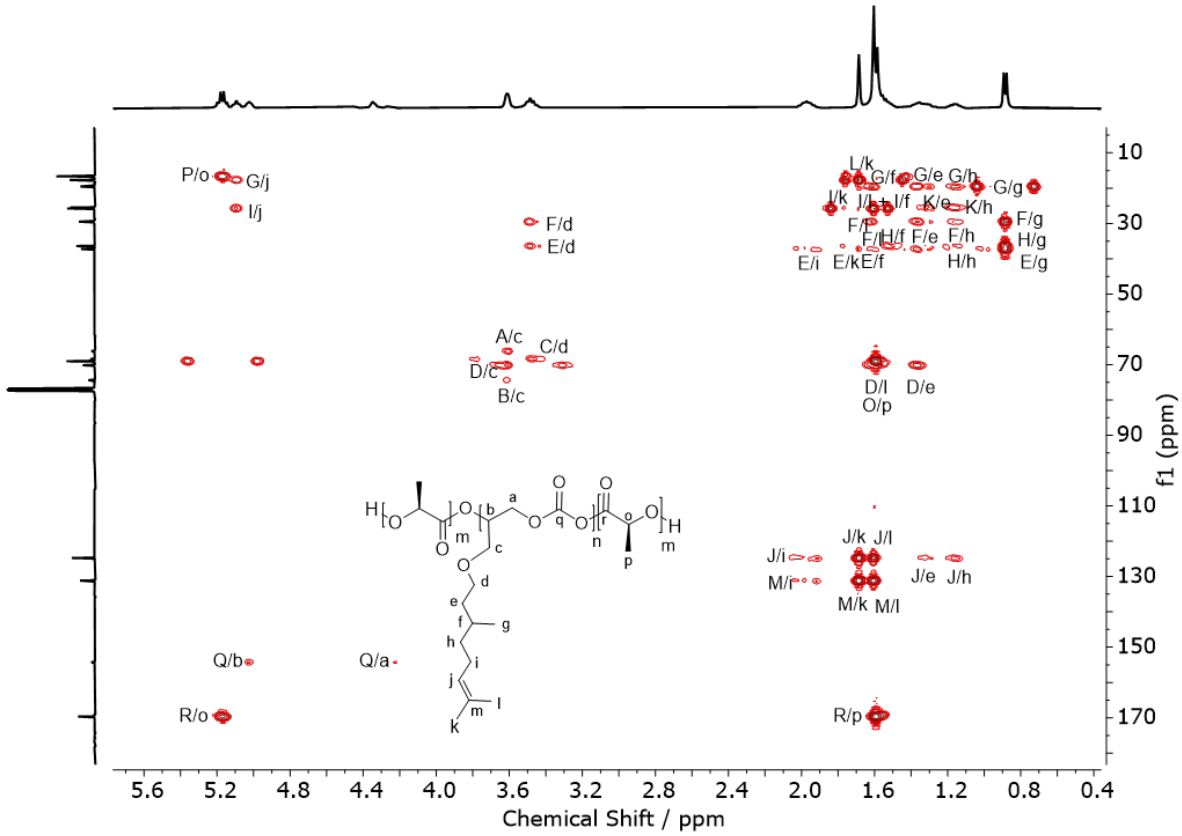

Figure S 16: ^{1}H-^{13}C HMBC NMR spectrum (400 MHz/75 MHz, $CDCl_3$) of TPE-2 ($PLLA_{0.35}$-*b*-$PCitroGEC_{0.31}$-*b*-$PLLA_{0.35}$).

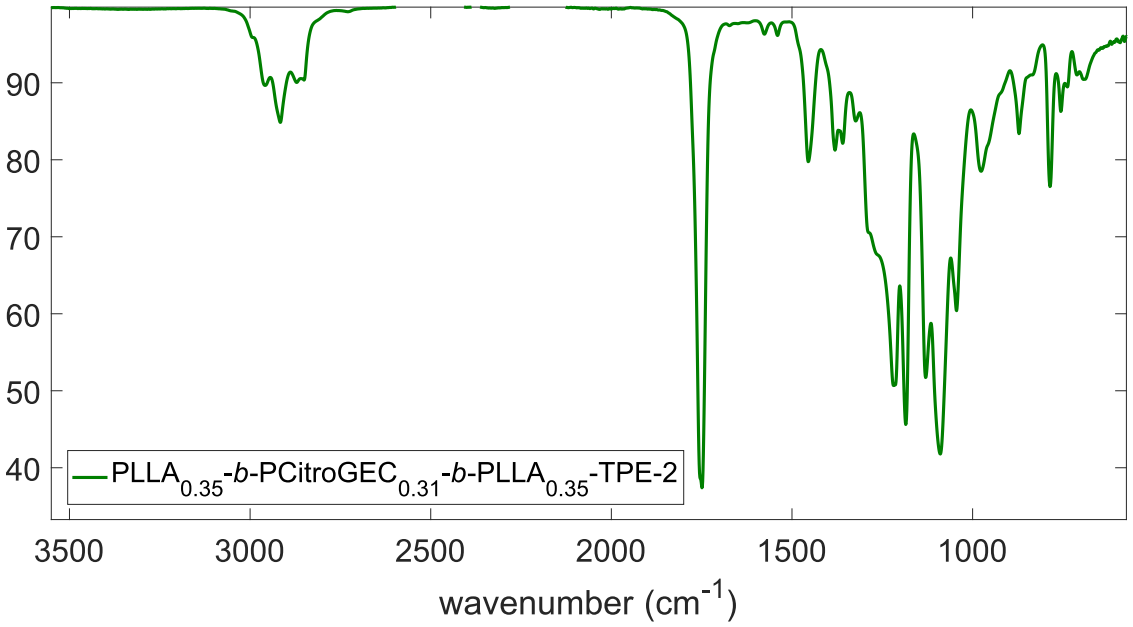

Figure S 17: IR spectrum of TPE-2 ($PLLA_{0.34.5}$-*b*-$PCitroGEC_{0.31}$-*b*-$PLLA_{0.34.5}$).

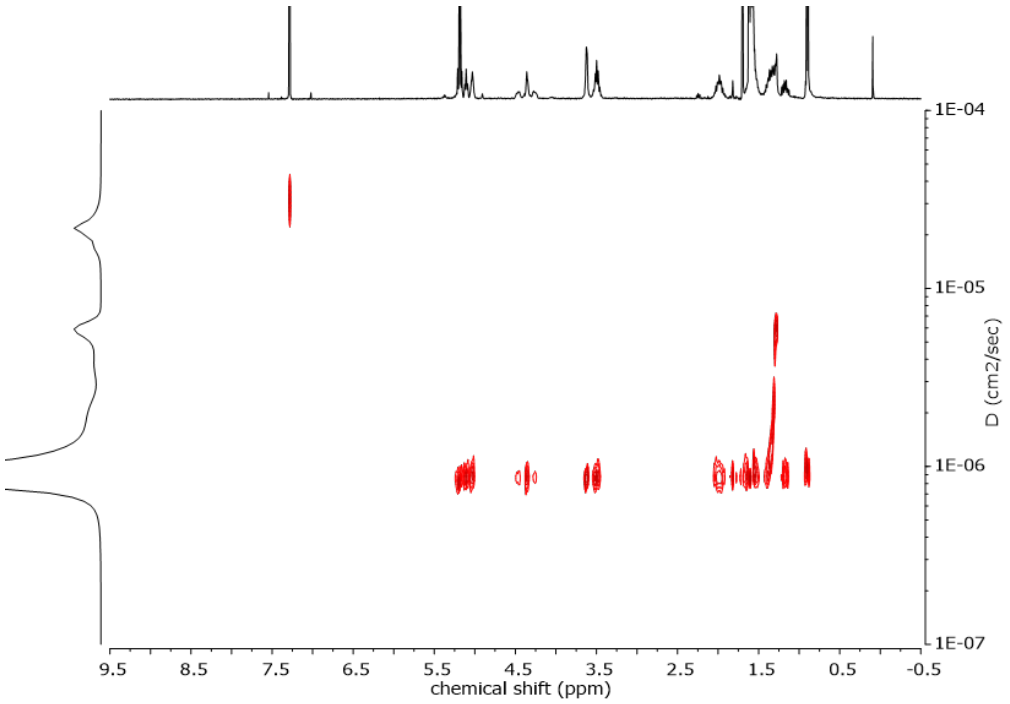

Figure S 18: DOSY NMR spectrum (400 MHz/75 MHz, $CDCl_3$) of TPE-2 ($PLLA_{0.34.5}$-*b*-$PCitroGEC_{0.31}$-*b*-$PLLA_{0.34.5}$).The signal at 7.2 ppm with a higher diffusion coefficient belongs to the $CDCl_3$ solvent. The other signals at 1.45 ppm feature a higher diffusion coefficient and can be attributed to solvent impurities.

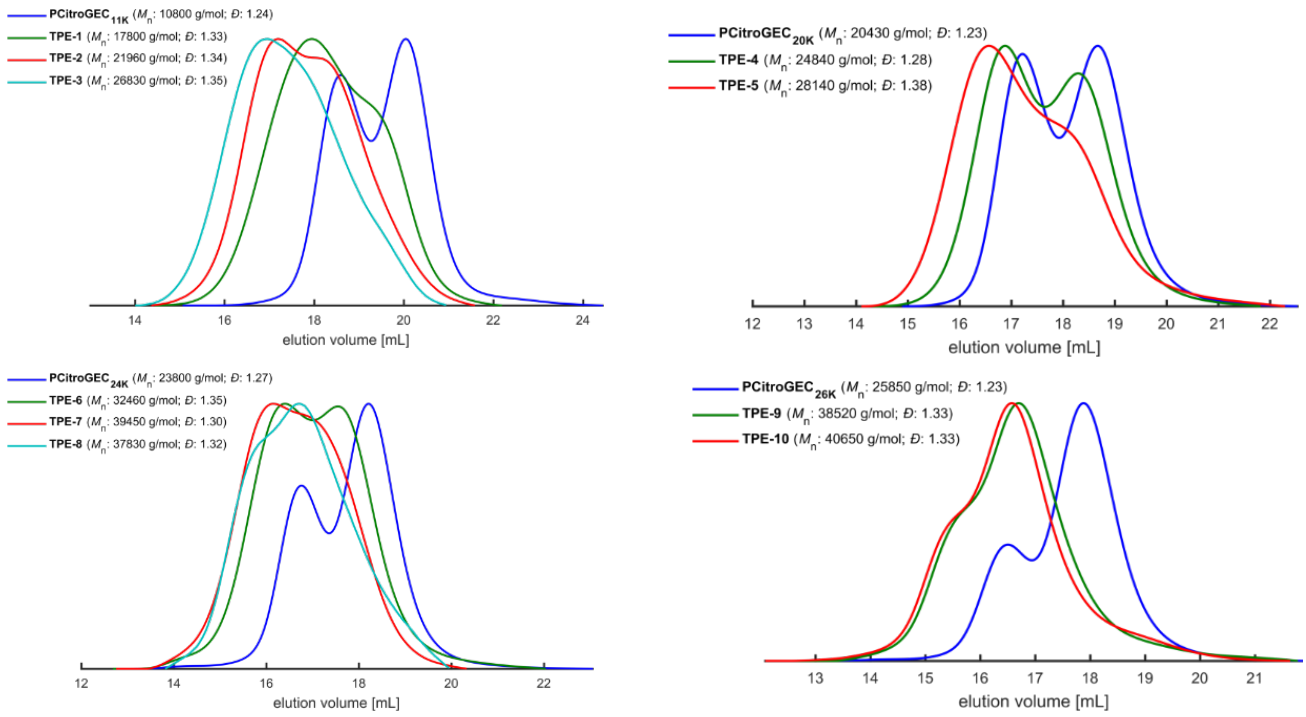

Figure S 19: SEC traces of the ABA triblock copolymers (eluent: DMF, standard: PEG). All triblock copolymers are presented together with their initial PCitroGEC macroinitiator to highlight the shift to higher molar masses.

3. Thermal characterization

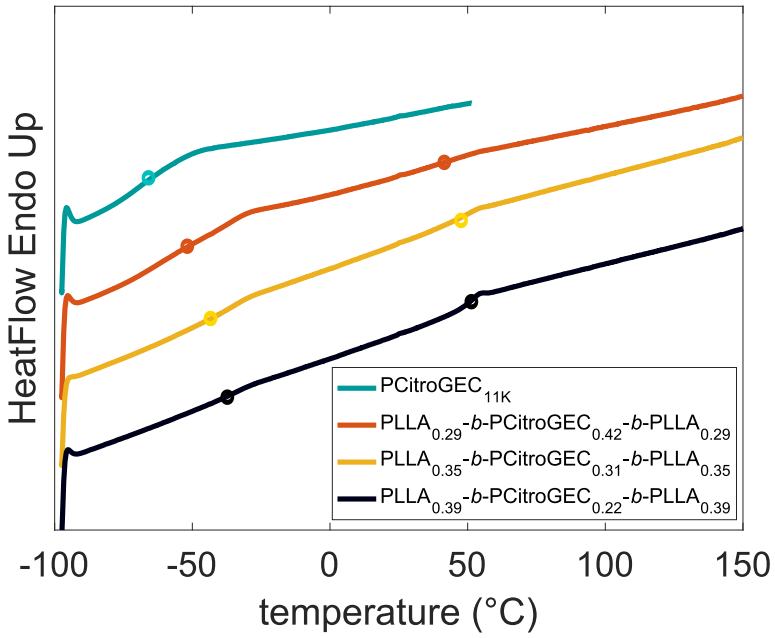

Figure S 20: DSC curves of the PCitroGEC$_{11K}$ homopolymer and the corresponding triblock copolymers.

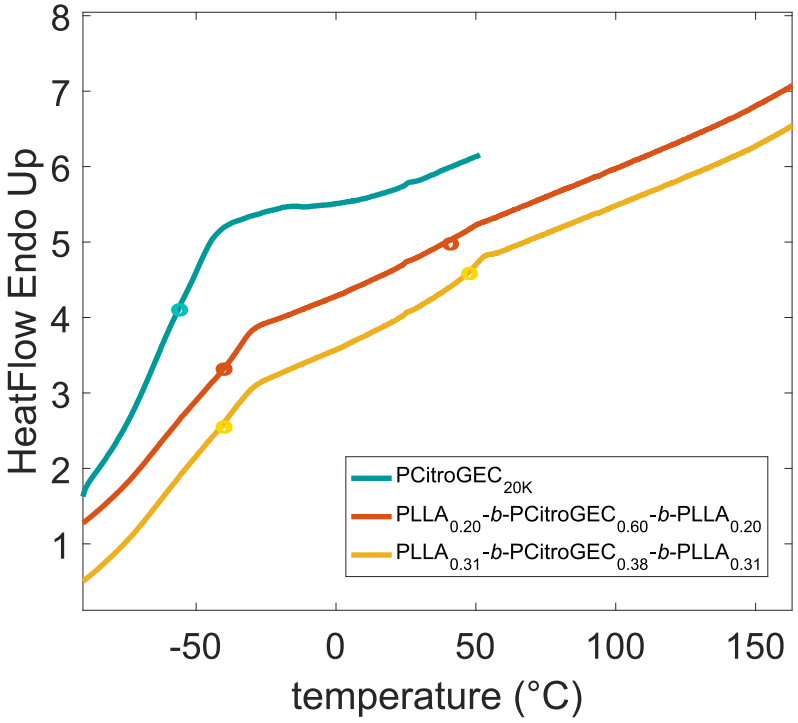

Figure S 21: DSC curves of the PCitroGEC$_{20K}$ homopolymer and the corresponding triblock copolymers.

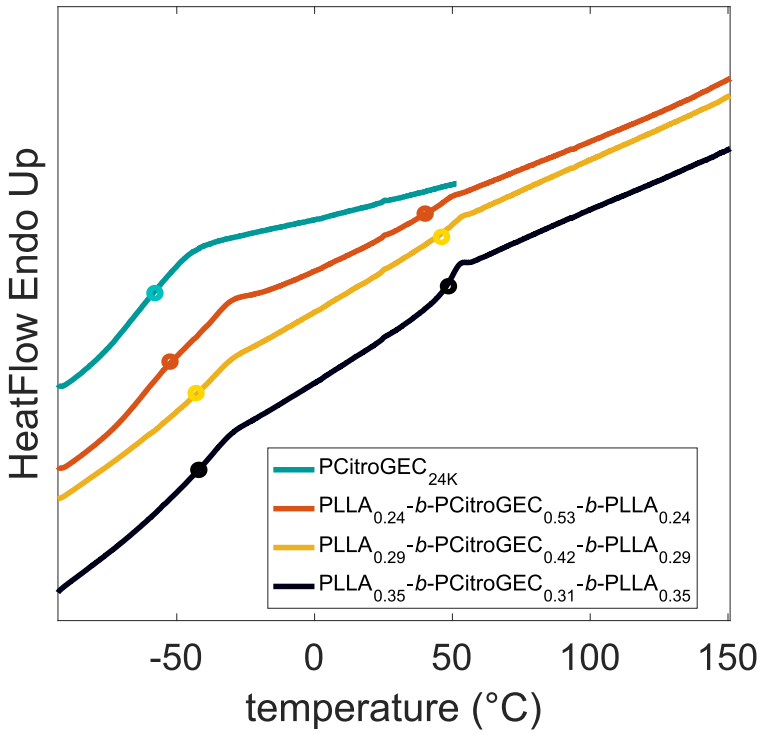

Figure S 22: DSC curves of the PCitroGEC$_{24K}$ homopolymer and the corresponding triblock copolymers.

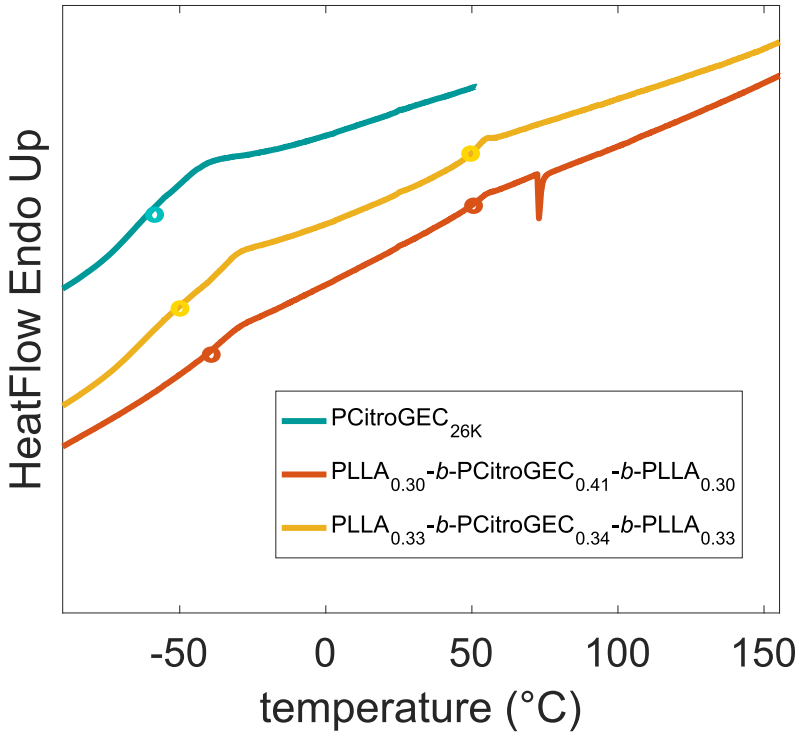

Figure S 23: DSC curves of the PCitroGEC$_{26K}$ homopolymer and the corresponding triblock copolymers.

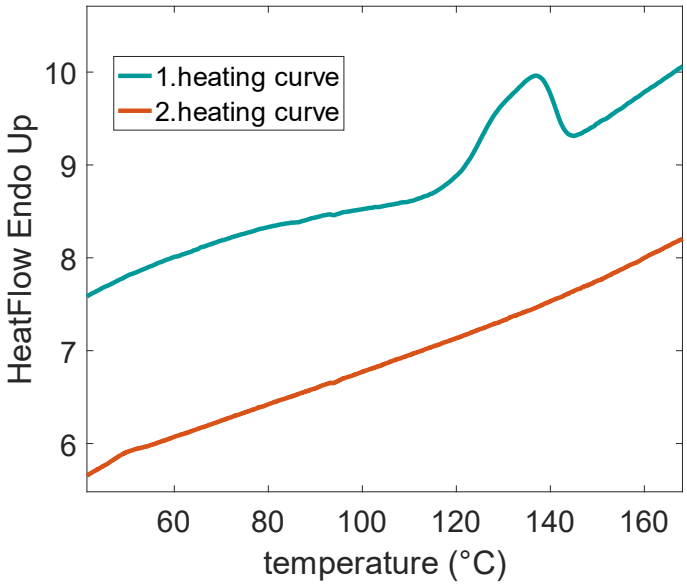

Figure S 24: DSC curves of the first and the second heating curve of TPE-6. The first heating curve shows a melting peak T_m of 136 °C, whereas no melting peak is observed in the second heating run.

4. Morphology

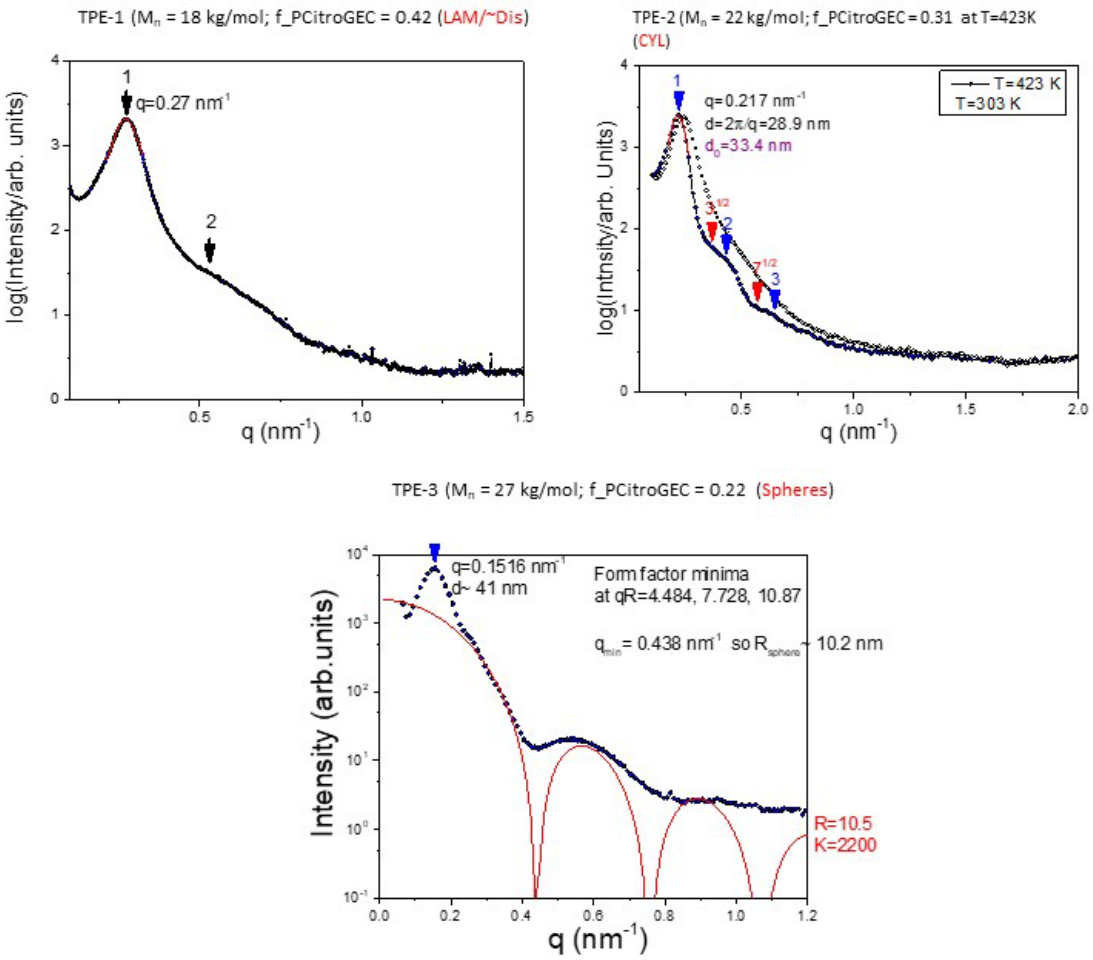

Figure S 25: SAXS patterns for the triblock copolymers PCitroGEC$_{11K}$ as middle block (TPE-1, TPE-2 and TPE-3). Arrows give the position of the Bragg peaks.

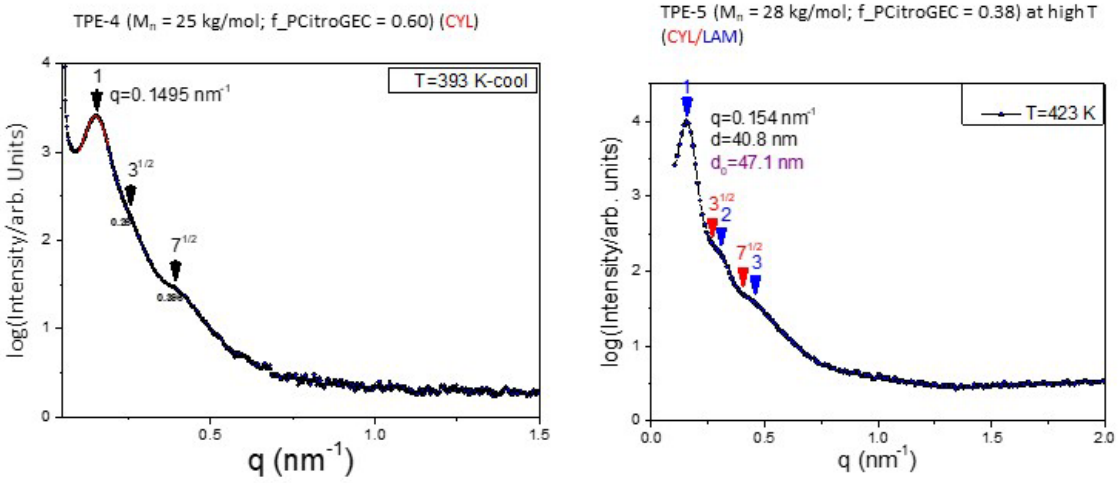

Figure S 26: SAXS patterns for the triblock copolymers with PCitroGEC$_{20K}$ as middle block (TPE-4 and TPE-5). Arrows give the position of the Bragg peaks.

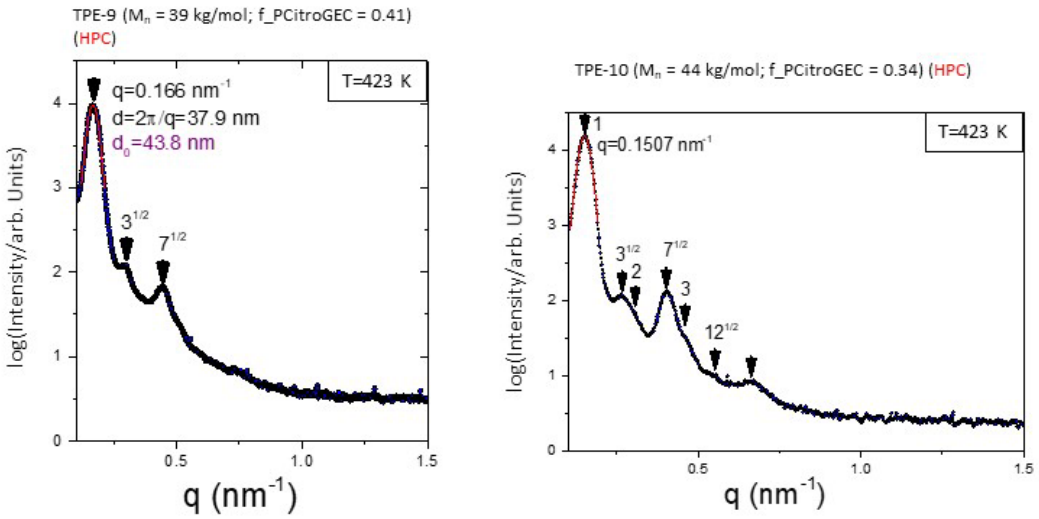

Figure S 27: SAXS patterns for the triblock copolymers PCitroGEC$_{26K}$ as middle block (TPE-9 and TPE-10). Arrows give the position of the Bragg peaks.

5. Mechanical characterization

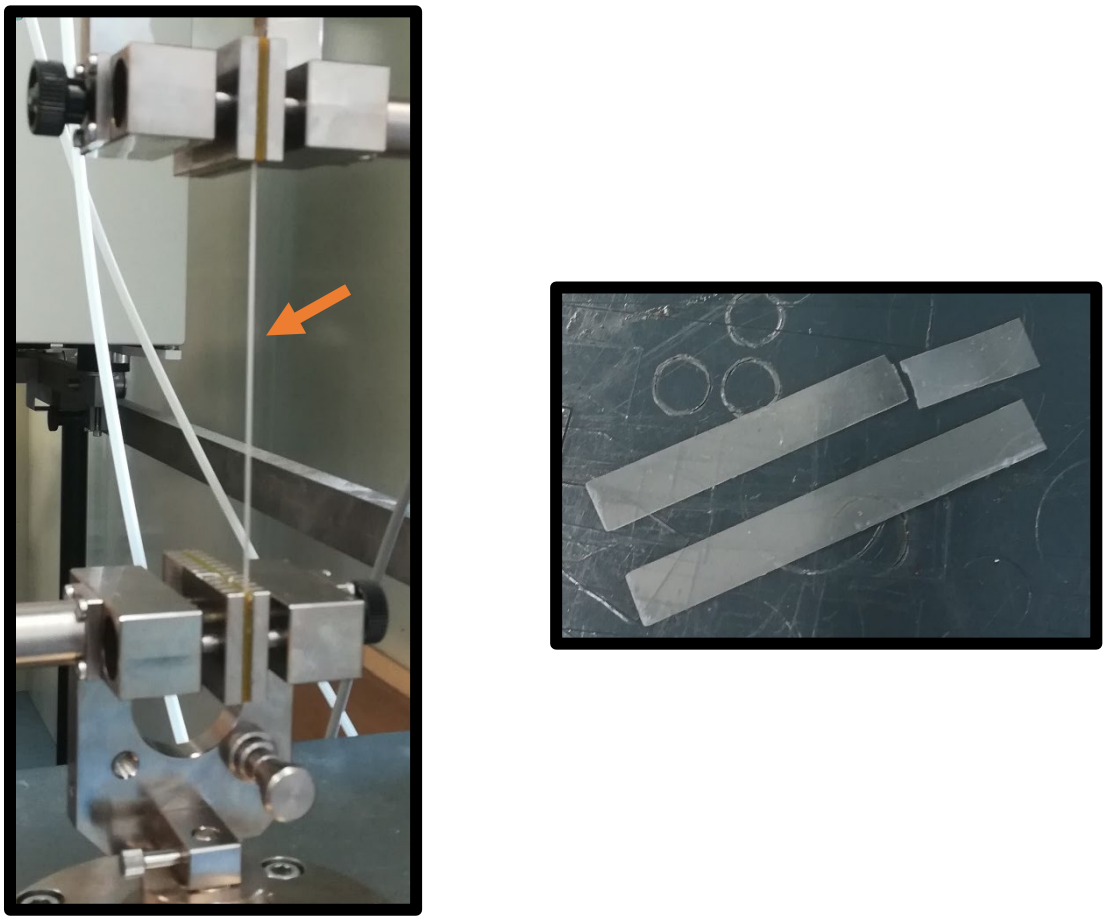

Figure S 28: Picture of the strained film of TPE-1 (left). Picture of the strained (torn) and the unstrained film of TPE-1 (right).

CHAPTER 4

Tough Hydrogels Based on Poly(ethylene oxide), Carbon Dioxide and Cyclohexene Oxide: Improvement of the Toughness via Polyurethane Multiblock Synthesis

CHAPTER 4

Tough Hydrogels Based on Poly(ethylene oxide), Carbon Dioxide and Cyclohexene Oxide: Improvement of the Toughness via Polyurethane Multiblock Synthesis

Christina Gardiner[a], Kaloian Koynov[b] and Holger Frey[a]*

[a] Institute of Organic Chemistry, Johannes Gutenberg University Mainz, Duesbergweg 10-14, 55128 Mainz, Germany.

[b]Max Planck Institute for Polymer Research, Ackermannweg 10, 55128 Mainz, Germany.

To be submitted.

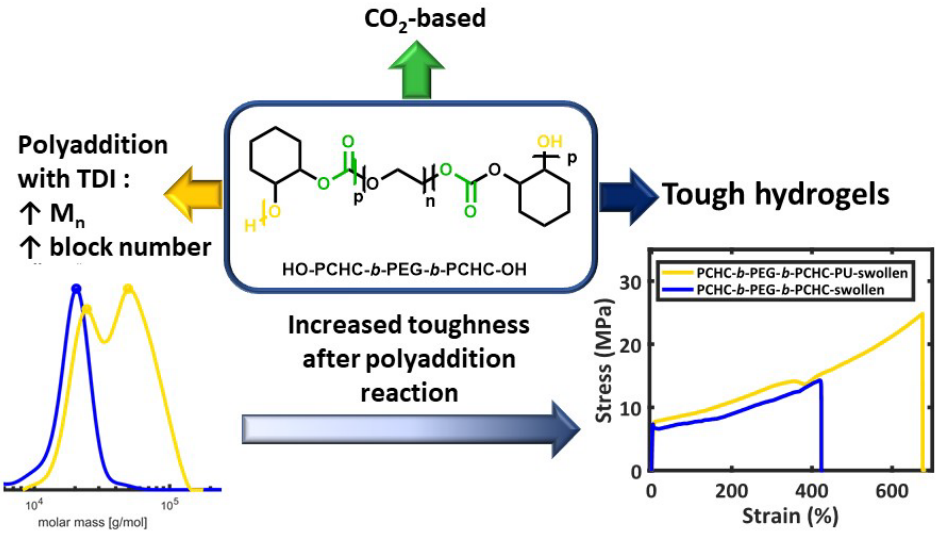

ABSTRACT

The disadvantage of CO_2-based poly(cyclohexene carbonate) (PCHC) is the brittleness of this amorphous polymer, however, desirable properties such as flexibility and water absorption can be achieved for different copolymers. The combination of the FDA-approved hydrophilic polyethylene glycol (PEG) with the hydrophobic PCHC in a PCHC-*b*-PEG-*b*-PCHC triblock copolymer is promising for hydrophilic thermoplastic hydrogels in the biomedical field. The advantage of polycarbonates compared with established polyesters used in the biomedical field are the non-acidic degradation products of the polymers. We synthesized several novel ABA triblock copolymers with different block length of PCHC. Molar masses between 16 and 25 kg/mol and narrow molar mass distributions with dispersity (*Đ)* of 1.07-1.21 were achieved. We demonstrate the influence of PCHC on the mechanical and thermal behavior of the synthesized triblock copolymers. Equilibrium swelling in aqueous solution of the materials and their processability were investigated. Furthermore, an increase in toughness was reached by forming multiblock copolymers with higher molar masses (30 – 37 kg/mol) using the PCHC-*b*-PEG-*b*-PCHC triblock copolymers and toluene diisocyanate (TDI) as a chain extender. The obtained materials form transparent films with up to 260% equilibrium swelling in aqueous solution (stable after swelling) and a toughness (tensile test, equilibrium water-swelling) up to 97 MN/mm^2.

INTRODUCTION

Hydrogels are crosslinked hydrophilic polymers which are insoluble in water. They mimic natural tissue and are used widely in biomedical applications due to their hydrophilicity and resulting soft consistency.[1,2,3] Although hydrogels are mostly prepared by covalent crosslinking of hydrophilic biopolymers (alginate, galantine or collagen) or synthetic polymers, such as polyethylene glycol, poly acrylic acid and poly(vinyl alcohol). Physical crosslinking of hydrogels represent a reversible alternative to permanent covalent crosslinking.[4–6] Materials that can be processed in the dry state and then swollen in aqueous environment are termed thermoplastic hydrogels.[7] The shape of these materials are able to be changed by heat or solvents, which allows for recycling and processability.[7] Physical crosslinking can be achieved by hydrophobic, ionic or H-bonding forces or due to multiple entanglements of high molecular weight polymers. Triblock copolymers with a hydrophilic mid-block and glassy outer blocks can form these thermoplastic hydrogels. Biocompatible polymers with such structures are known in literature and mostly consist of poly(ethylene glycol) (PEG) as a mid-block. Polyesters such as polycaprolactone and polylactide are used as outer glassy blocks, but their acidic degradation products can pose a major drawback.[8–12,13,14] These acids can lead to necrosis.[15–17] Aliphatic polycarbonates on the other hand have no acidic degradation products and feature excellent biocompatibility and biodegradability.[18,19]

Poly(cyclohexene carbonate) (PCHC) (T_g =117 °C) can be used as a sustainable, carbon dioxide based alternative to polyesters.[20] It can be prepared *via* catalytic copolymerization of cyclohexene oxide (CHO) and carbon dioxide.[21] Winkler et al. showed that cyclohexene oxide can be derived from 1,4-cyclohexadiene (CHD), the latter produced from renewable resources *via* self-metathesis of plant oil derivatives.[22] Carbon dioxide is known as a non-flammable, non-toxic, renewable and sustainable C_1 resource. Additionally, it is a waste product found in blast furnace combustion reactions. The general use of carbon dioxide is limited due to its high thermodynamic stability and low reactivity.[23,24] Since the development of the immortal carbon dioxide/epoxide polymerization by Inoue et al. in 1969, carbon dioxide has been used as a monomer in polymerizations. In recent years, polymer architectures based on CO_2 have received increasing attention and are studied by an increasing number of groups.[21,23,25–31] Cyriac et al. introduced block copolymers based on carbon dioxide, synthesized using chain transfer agents (CTAs) with hydroxyl or acid end groups.[27] Zhang et al. demonstrated examples of triblocks combining a central PEG-sequence with PCHC, albeit thermal and mechanical properties of the synthesized polymers were not measured or discussed. Additionally, the molecular weight achieved was limited.[32]

Aliphatic polycarbonates based on carbon dioxide have been utilized as a surfactant[31,33,34], as polyols for polyurethanes[35–38] or for elastomers.[39] To the best of our knowledge, there is no publication of supramolecular hydrogels based on carbon dioxide in the literature.

PCHC itself is a brittle polymer with a strain at break at 1.7±0.6% and an *E*-Modulus of 3 600±100 MPa.[40]

We hypothesize that the combination of PCHC and PEG in a triblock copolymer may reduce the crystallinity of the PEG block, resulting in an enhanced toughness compared to brittle PCHC and PEG. Processability is improved by lower crystallinity and thus lower brittleness. In this way, we want to produce a processable material that can swell after processing in an aqueous environment leading to a thermoplastic hydrogel.

In this work, we report the synthesis of PCHC-*b*-PEG-*b*-PCHC triblock copolymers. Several block copolymers with ABA structures were prepared *via* a one pot reaction directly from carbon dioxide and cyclohexene oxide, relying on a straightforward synthesis. PEG was applied as a difunctional chain transfer agent. The synthesized polymers were characterized with respect to their thermal behaviour in bulk, their mechanical properties both in swollen and dry state and their equilibrium swelling capacity as a physically crosslinked network. We aim to investigate the properties of PCHC as an environmentally friendly alternative to other high glass transition blocks for thermoplastic hydrogels[7] based on polyesters.

RESULTS AND DISCUSSION

Polymer synthesis

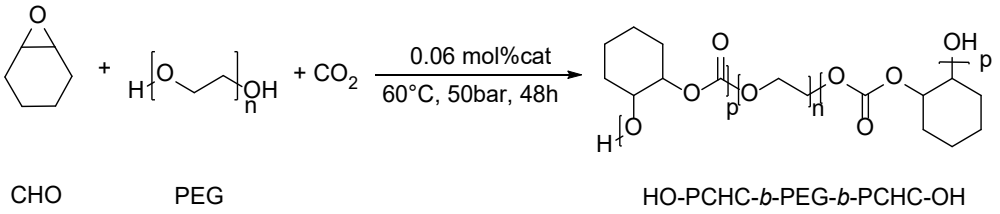

Scheme 1: PCHC-*b*-PEG-*b*-PCHC triblock copolymer synthesis.

PCHC-*b*-PEG-*b*-PCHC triblock copolymers were synthesized *via* an immortal polymerization using PEG_{227} as chain transfer agent (CTA) and cyclohexene oxide (CHO) and carbon dioxide (CO_2) as monomers. The immortal polymerization is a controlled reaction and relies on equilibrium between dormant and active species. A protic chain transfer agent such as PEG can protonate the active PCHC homopolymer (initiated by the Cl^- of [PPN]Cl), resulting in a dormant a PCHC

homopolymer. This activates the PEG and allows the PCHC to polymerize onto the PEG chain. Due to the equilibrium between the dormant and active species of the PCHC homopolymer or the PCHC-*b*-PEG-*b*-PCHC triblock copolymer, the reaction proceeds in a controlled manner, leading to low dispersities.[27] The catalyst system (R,R)-(salcy)-CoCl and bis(triphenylphosphine)iminium chloride ([PPN]Cl] was chosen due to the perfectly alternating incorporation of carbon dioxide and CHO. This catalyst system excludes the occurrence of ether defects, which could be formed as side reactions in the catalytic polymerization.[41,42] This is supported by the ^{1}H NMR spectrum (Figure S 1) (no poly(cyclohexene oxide) signals at 3.46 ppm).[43] Another potential side reaction is the formation of cyclic carbonates. Since cyclohexene oxide is a rigid monomer, formation of the thermodynamically favored cyclic carbonates is suppressed. FT-IR spectroscopy (Figure S 7) demonstrate the absence of side products, e.g., five membered cyclic carbonates. Exclusively the carbonyl stretch vibration of the aliphatic polycarbonates at 1738 cm^{-1} was detected. An additional carbonyl band indicative of the cyclic carbonates at around 1800 cm^{-1} is not visible. To remove the catalyst and the generated homopolymer PCHC, the crude polymer solution was flushed over neutral aluminum oxide and precipitated in cold diethyl ether. This work up results in monomodal weight distributions exhibiting dispersities (*Đ*) of 1.07-1.21 (Figure 1, Figure S 8).

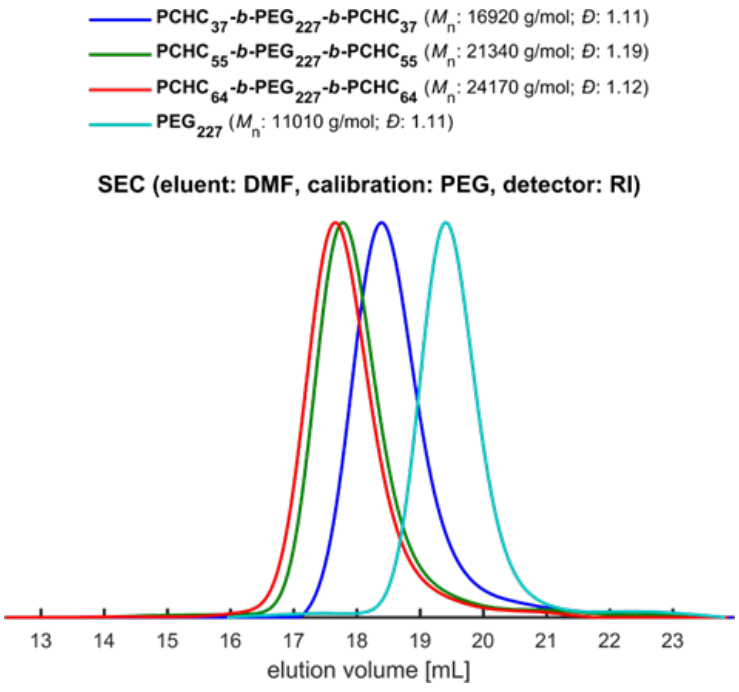

Figure 1: SEC traces of the PCHC-*b*-PEG-*b*-PCHC triblock copolymers (eluent: DMF, standard: PEG).

Targeting higher PCHC block length resulted in higher molar masses of the additionally formed PCHC homopolymer. As the length of the PCHC blocks increases, the number of repeating units of the PCHC homopolymers increases (the ratio between initiator and monomer decreases). The

higher molar mass PCHC homopolymers are difficult to remove from the reaction mixture by precipitation. Hence, polymers with a higher amount of PCHC and consequently higher molar mass PCHC homopolymer contamination had to be precipitated three times in diethyl ether and still featured increased dispersity values compared to polymers with a lower PCHC amount. Adjusting the amount of monomer and PEG macroinitiator, the PCHC block length was varied. The polymers were characterized *via* NMR, IR and SEC. Using the signal of the PEG backbone in the ^{1}H NMR spectra, molar masses of the triblock copolymers were calculated (Figure S 1). All molar masses are shown in Table 1. Furthermore, the molar masses were determined using SEC with DMF as an eluent and PEG as standard (Figure 1, Figure S8 , Table 1). The number-average molar mass (M_n) of NMR and SEC differs as PCHC exhibits a different hydrodynamic radius compared to the PEG standard. The successful synthesis of block copolymers and the separation of the homopolymer PCHC was verified by ^{1}H NMR-DOSY spectroscopy (Figure S 6). All signals (3.66 ppm (PEG) and the CH (4.67 ppm) and CH (2.26-1.27 ppm) (PCHC)) demonstrate the same diffusion coefficient.

Table 1: Overview of the synthesized PCHC-*b*-PEG-*b*-PCHC triblock copolymers and PCHC-*b*-PEG-*b*-PCHC-PU multiblock copolymers.

sample	composition[a]	PCHC	equilibrium swelling[d]	M_n[a]	M_n[b]	$Đ$[b]	Yield[e]	T_{g1}[c]	T_{g2}[c]	T_m[c]	ΔH_m[c]	X_{PEG}[d]
		vol%	%	g/mol	g/mol		%	°C	°C	°C	J/g	%
1	$PCHC_{24}$-*b*-PEG_{227}-*b*-$PCHC_{24}$	43	309	16 800	16 250	1.07	26	-55	-	41	26	13
2	$PCHC_{37}$-*b*-PEG_{227}-*b*-$PCHC_{37}$	51	180	20 500	16 900	1.11	27	-54	-	44	33	17
3	$PCHC_{55}$-*b*-PEG_{227}-*b*-$PCHC_{55}$	63	81	25 600	21 234	1.18	50	- 60	116	46	9	4.7
4	$PCHC_{64}$-*b*-PEG_{227}-*b*-$PCHC_{64}$	66	79	28 200	24 170	1.15	32	-51	116	44	5	2.6
5	$PCHC_{70}$-*b*-PEG_{227}-*b*-$PCHC_{70}$	68	65	30 390	21 230	1.10	38	-56	117	43	2	1.0
6	$PCHC_{90}$-*b*-PEG_{227}-*b*-$PCHC_{90}$	74	34	35 560	19 350	1.24	70	-51	56	27	0.6	0.08
7	$PCHC_{127}$-*b*-PEG_{227}-*b*-$PCHC_{127}$	79	32	45 370	25 707	1.21	71	-	118	-	-	-
8	$PCHC_{50}$-*b*-PEG_{227}-*b*-$PCHC_{50}$-PU	60	88	-	34 490	1.33	100	-59	-	40	2	0.7
9	$PCHC_{60}$-*b*-PEG_{227}-*b*-$PCHC_{60}$-PU	65	127	-	32 240	1.60	79	-57	-	43	5	1.5
10	$PCHC_{68}$-*b*-PEG_{227}-*b*-$PCHC_{68}$-PU	67	81	-	37 210	2.55	100	-54	-	28	2	0.5
11	$PCHC_{90}$-*b*-PEG_{227}-*b*-$PCHC_{90}$-PU	74	80	-	30 480	1.67	90	-51	51	26	0.4	0.08
12	$PCHC_{131}$-*b*-PEG_{227}-*b*-$PCHC_{131}$-PU	80	57	-	30 630	1.79	85	-56	104	-	-	-

[a]Determined by ^{1}H NMR (300 MHz, CDCl3). [b]measured by SEC (Eluent: DMF, standard: PEG).[c] Measured by DSC with a heating rate of 10 K/min. [d]Calculated by using the equitation in the experimental section..

The monomodal distribution and the shift of the SEC curve to higher molecular weights in Figure 1 and Figure S 8 suggests a successful block copolymer synthesis.). The yield of the triblock

synthesis varied between 26 and 71 %. Low yields of the triblock copolymers after purification in some cases can be explained by incomplete monomer conversion. Additionally, a small amount of generated homopolymer PCHC was removed by a neutral aluminum oxide column.

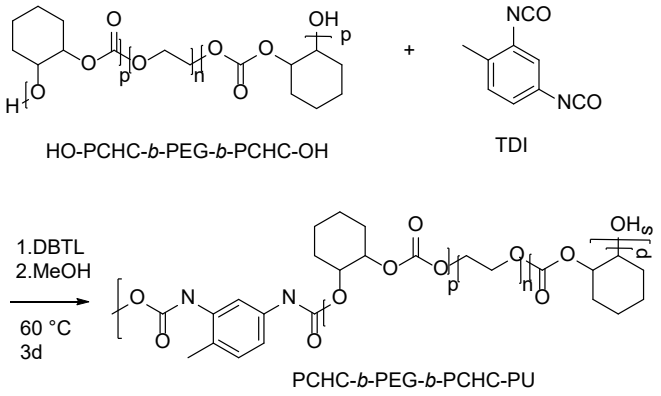

Scheme 2: Synthesis of the PCHC-*b*-PEG-*b*-PCHC-PU multiblock copolymers.

To enhance the toughness of the PCHC-*b*-PEG-*b*-PCHC triblock copolymers, the purified and dried triblock copolymers were reacted with toluene diisocyanate (TDI) to generate multiblock copolymers in a polyaddition reaction using DBTL (dibutyl tin dilaurate) as a catalyst. This technique was used to obtain a higher M_n of the triblock copolymers and to incorporate additional loops and bridges by the "soft" segments in case of a phase separation to improve the mechanical toughness of the polymers. To evaluate the most suitable chain extender for high M_n, a model triblock copolymer ($PCHC_{50}$-*b*-PEG_{227}-*b*-$PCHC_{50}$) was applied in the polyaddition. The comparison of the two commercially available and reactive diisocyanates, toluene diisocyanate (TDI) and methylene diphenyl diisocyanate (MDI), revealed higher Mn and the expected mixture of the tri-, penta- and heptablocks when applying TDI. The use of MDI was observed to lead to pentablock formation only (Figure S 11). During the polyaddition reaction it was crucial that 1.1 eq TDI was used. Higher excess of TDI caused end-capping of the triblock copolymers, which impeded the polyaddition process (Figure S 12). No shift in the SEC curves to higher molar masses was identified, and the UV detector yielded the same monomodal trace as the prepolymer after polyaddition (Figure S 12). The best-suited amount of TDI and a reaction time of 3 days led to double or triple molar masses of the primary polymers (Figure S 13). In Figure 2 the molar mass distribution of the $PCHC_{68}$-*b*-PEG_{227}-*b*-$PCHC_{68}$-PU multiblock copolymer is displayed in comparison to the triblock precursor. In Figure 2 the observed distribution after chain extension supports the coexistence of the tri- (max. 24 100 g/mol), penta- (max. 58 700 g/mol) and heptablock (max. 173 200 g/mol). This confirms reaction of the isocyanate with the hydroxy groups of the triblock copolymers. The observed broadening of the distribution is unavoidable due to the step growth

reaction. Nevertheless, good mechanical properties can be expected despite the dispersity increase. Steube et al. studied blending of diblock copolymers with multiblock copolymers and revealed that the blending does not destroy the mechanical properties, e.g blending 60 % diblocks (P(I-co-S)) with 40 % hexablock copolymer (P(I-co-S)3) results still a material with 400 % elongation at break and reasonable strength and toughness.[44] Additional SEC data of multiblock copolymers are shown in the Supporting Information in Figure S 13. Characterization data of all multiblock structures prepared are given in Table 1. The aromatic protons of TDI are observable in the ^{1}H NMR spectrum, but the integration of the aromatic signals at 7.02 and 8.85 is difficult due to the low signal-to-noise ratio. The molar ratio of the triblock copolymers in comparison to TDI leads to a low signal intensity of TDI (Figure S 9).

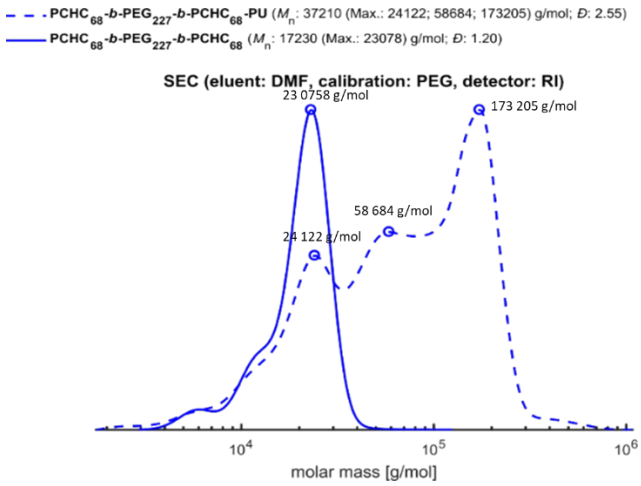

Figure 2: SEC traces of the PCHC$_{68}$-*b*-PEG$_{227}$-*b*-PCHC$_{68}$-PU multiblock copolymers (eluent: DMF, standard: PEG, detector RI), dashed line. The maxima (Max.) of the different modes are highlighted with blue dots.

Thermal characterization

To further investigate the triblock and multiblock copolymers with respect to their thermal behavior and potential nanophase separation, DSC measurements were conducted (Figure S 14, results Table 1). The samples 3-6 in Table 1 showed two glass transitions (T_gs) and a melting point. The two Tgs indicate microphase separation of the copolymers. In case of the triblock copolymers with 63 – 68 vol% PCHC, the two Tgs belong to the PEG block (-60 to -56 °C) and the PCHC block (116-117 °C), respectively. In case of the PCHC$_{90}$-*b*-PEG$_{227}$-*b*-PCHC$_{90}$ triblock copolymer (sample 6) the T_g attributed to PCHC is lowered to 56 °C. The PEG block appears to feature a very low amount of crystalline domains in the triblock copolymers (Table 1, sample 6, ΔH_m= 0.6 J/g). In addition, a lower T_g and a lower melting point of 56 °C and 27 °C, respectively, can be observed. These two features indicate a partial mixing of the PEG blocks with the PCHC blocks. Regarding the PEG crystallization of the copolymers, samples 3-4 must be highlighted. These polymers show a low

crystallinity of 1.0 to 4.7 %. This low crystallinity of the 10 kg/mol midblock can be explained by the rigid PCHC outer blocks, which inhibit the crystallization of the central PEG block. The DSC data suggest that increasing amounts of PCHC inhibit the crystallization progressively, and sample $PCHC_{127}$-*b*-PEG_{227}-*b*-$PCHC_{127}$ (highest amount of PCHC with 79 vol%) shows neither a melting point for the PEG block nor the T_g of PEG.

Sample 1 and 2 are low in PCHC content, which results in polymers with only a T_m and T_g of the PEG block, albeit a glass transition for PCHC is not observed. Comparing the melting point and melting enthalpy of pure PEG_{227} (T_m = 67 °C; , ΔHm = 162 J/g) (heating rate 10 K/min) and the triblock copolymers with low amount of PCHC, the triblock copolymers show lower T_m of 41-44 °C and ΔH_m (26-33 J/g). This indicates that crystallization is also inhibited by the PCHC segments, although not as strongly as in the samples 3-6.

Evaluating the thermal behavior of the multiblock copolymers, a significant change is noticeable. The multiblock copolymers with 60 – 67 vol % of PCHC show no second T_g when compared to the triblock with the same amount of PCHC. This can be explained by a decrease in phase separation due to the higher number of blocks.[45,46] All multiblock copolymers exhibit a low or non-existent crystallinity for the PEG block. The weak melting points are in the same temperature range as the values of the triblock precursors. Higher PCHC content lowers the Tm and eventually leads to its disappearance in sample 12 with 80 vol% PCHC.

Equilibrium swelling in aqueous solution

Since the polymers are made for application in self assembled hydrogels, the equilibrium swelling in aqueous solution of the polymers is a key parameter. Since the hydrogels become mechanically weaker with increasing equilibrium swelling, generally materials with equilibrium swelling of less than 400% are applied.[7] For the measurement, a dry film of the polymer was weighed and put in MilliQ water at 37 °C, until an equilibrium of the swelling in aqueous solution was obtained. The weight of the swollen film was determined, and the equilibrium swelling in aqueous solution calculated (equation 2, experimental). The results are summarized in Table 1.

Higher amounts of PEG led to an increased equilibrium swelling in case of the triblock copolymers. Sample 1 with the highest PEG content (43 vol% of PCHC) exhibits an equilibrium swelling in aqueous solution of 309 %. The lowest equilibrium swelling of 32% is found in sample 7 (79 vol% of PCHC). As expected, the equilibrium swelling is directly correlated to the volume fraction of PEG in the materials.

With regard to the multiblock copolymers, sample 9 ($PCHC_{60}$-*b*-PEG_{227}-*b*-$PCHC_{60}$-PU) represents an exception as it consists of a lower PEG content than sample 8 ($PCHC_{50}$-*b*-PEG_{227}-*b*-$PCHC_{50}$-PU), but shows higher equilibrium swelling in aqueous solution. This unusual equilibrium swelling behavior might be ascribed to different domain formation due to the multiblock system.[45] The equilibrium swelling of the polymers, albeit without dissolution supports the physical crosslinking of the PCHC blocks *via* hydrophobic interactions, since all polymers swell in water. Furthermore it is in line with the values of thermoplastic hydrogels in the literature.[7]

Mechanical properties

To study moduli and toughness of the tri and multiblock copolymers, tensile tests were conducted with polymer films prepared *via* solvent evaporation. Dogbone-shaped specimens were cut out and stress-strain measurements at room temperature were performed. Dry and swollen films (dry films were kept in MilliQ water until swelling equilibrium had been reached) were tested.

Table 2: Overview of the mechanical properties of the PCHC-*b*-PEG- *b*-PCHC triblock copolymers and the PCHC-*b*-PEG-*b*-PCHC-PU multiblock copolymers in dry and swollen state.

sample[b]	PCHC	composition[a]	E	σ_{break}	ε_{break}	σ_{yield}	ε_{yield}	$W_{tensile}$
	vol%		MPa	MPa	%	MPa	%	MN/mm²
3	63	$PCHC_{55}$-*b*-PEG_{227}-*b*-$PCHC_{55}$	390±80	20±3	660±80	10.7±0.7	3.9±0.8	69±18
4	66	$PCHC_{64}$-*b*-PEG_{227}-*b*-$PCHC_{64}$	330±5	19±2	660±36	9.9±1.3	3.3±0.6	69±6
5	68	$PCHC_{70}$-*b*-PEG_{227}-*b*-$PCHC_{70}$	454±15	19±6	583±122	12.2±0.4	3.00±0.05	67±21
6	74	$PCHC_{90}$-*b*-PEG_{227}-*b*-$PCHC_{90}$	880±230	19±6	4.4±1.25	20±5	2.66±0.03	0.7±0.2
7	79	$PCHC_{127}$-*b*-PEG_{227}-*b*-$PCHC_{127}$	1600±30	29±1	4±1	30±1	2.00±0.06	1.1±0.3
3-s	63	$PCHC_{55}$-*b*-PEG_{227}-*b*-$PCHC_{55}$	330±90	14±2	424±84	6.7±0.3	4±2	43±11
4-s	66	$PCHC_{64}$-*b*-PEG_{227}-*b*-$PCHC_{64}$	280±90	15±4	415±113	6.44±0.06	2.7±0.2	43±16
5-s	68	$PCHC_{70}$-*b*-PEG_{227}-*b*-$PCHC_{70}$	390±70	10.2±0.5	189±16	8.5±0.2	2.67±0.06	17±2
6-s	74	$PCHC_{90}$-*b*-PEG_{227}-*b*-$PCHC_{90}$	1287±400	23±6	5.5±0.2	28±8	2.31±0.01	1.2±0.3
7-s	79	$PCHC_{127}$-*b*-PEG_{227}-*b*-$PCHC_{127}$	1400±30	26±2	3.0±0.3	27.0±0.4	2.03±0.01	0.56±0.06
8	60	$PCHC_{50}$-*b*-PEG_{227}-*b*-$PCHC_{50}$-PU	335±45	26±4	855±75	10±1	3.6±0.6	107±16
9	65	$PCHC_{60}$-*b*-PEG_{227}-*b*-$PCHC_{60}$-PU	192±18	29±3	910±60	6.4±02	3.9±0.4	111±13
10	67	$PCHC_{68}$-*b*-PEG_{227}-*b*-$PCHC_{68}$-PU	568±54	24±5	595±80	16±2	3.4±0.4	93±25
11	74	$PCHC_{90}$-*b*-PEG_{227}-*b*-$PCHC_{90}$-PU	1032±135	24±3	4±1	25±4	2.9±0.2	1.3±0.8
12	80	$PCHC_{131}$-*b*-PEG_{227}-*b*-$PCHC_{131}$-PU	1690±104	25±8	3±1	34±1	2.09±0.05	0.9±0.4
8-s	60	$PCHC_{50}$-*b*-PEG_{227}-*b*-$PCHC_{50}$-PU	200±36	26±6	687±49	6±1	3.7±0.4	97±17
9-s	65	$PCHC_{60}$-*b*-PEG_{227}-*b*-$PCHC_{60}$-PU	222±78	17±1	483±12	6±1	4.1±0.6	50±4
10-s	67	$PCHC_{68}$-*b*-PEG_{227}-*b*-$PCHC_{68}$-PU	539±50	12±2	45±16	11.8±0.3	2.3±0.1	5±2
11-s	74	$PCHC_{90}$-*b*-PEG_{227}-*b*-$PCHC_{90}$-PU	1011±421	25±2	3.4±0.3	-	-	0.61±0.06
12-s	80	$PCHC_{131}$-*b*-PEG_{227}-*b*-$PCHC_{131}$-PU	1383±70	24±2	3.6±0.3	27±1	2.2±0.1	0.72±0.05

[a]Determined by ^{1}H NMR (300 MHz, CDCl3). All tensile test results were measured with rate of 20 mm/min at room temperatures. The parameters were evaluated by averaging the results at 4-6 measurements. [b]The Index s show, that the polymer was in water-swollen state.

Typical stress-strain curves of the dry and swollen films are shown in Figure 3 and Figures S 15-17, and the corresponding mechanical properties evaluated from 4-6 measurements are summarised in Table 2. For the dry films, Figure S 15 and the results in Table 2 demonstrate that triblock

copolymers with 63-68 vol% of PCHC have the highest elongation at break about 660% and the highest toughness of 68 MN/mm^2. PCHC-*b*-PEG-*b*-PCHC triblock copolymers with a higher amount of 74-79 vol% of PCHC show strongly reduced toughness of only 1 MN/mm^2 and elongation at break of 3-5 % only (Figure 5). This sudden drop in the toughness can be explained by the occurrence of phase separation in case of lower vol% of 63-68% PCHC (indicated by 2 T_gs). Nanophase segregation of PCHC domains is essential for supramolecular crosslinking. As already discussed with the thermal characterization, sample 6 (74 vol% PCHC) also exhibits two T_gs with a decreased second T_g at 56 °C, indicating partial mixing of PCHC and PEG domains. This mixing of the domains leads to a drop in the toughness. In the case of sample 7, with 79 vol% of PCHC, the low toughness and the low elongation at break can be ascribed to the strong PCHC character. Only the T_g of the PCHC is detected in this sample and the PCHC-like behaviour is underlined by the brittleness, resulting in the low elongation at break of 4±1%.

The toughness increases as a consequence of the polyaddition of the triblock copolymers and TDI to PCHC-*b*-PEG-*b*-PCHC-PU multiblock copolymers. This can be explained by the fact, that higher molar masses and additional bridges between PCHC domains are achieved *via* the polyaddition reaction and therefore higher toughness.[47,48] Multiblock copolymers with 60 – 67 vol% PCHC exhibited an enormous toughness of 93 – 111 MN/mm^2 in dry state (comparable to isoprene/styrene multiblocks)[46] (sample 8-10, Table 2, Figure S 17, Figure 5). Low strength triblock copolymers feature no improved toughness as multiblock copolymers are formed (Table 2, sample 11-12). This can be explained by a lack of phase separation already in the triblock structures employed. The difference between the strength of the multiblock and triblock copolymers in dry state is illustrated in Figure 5a.

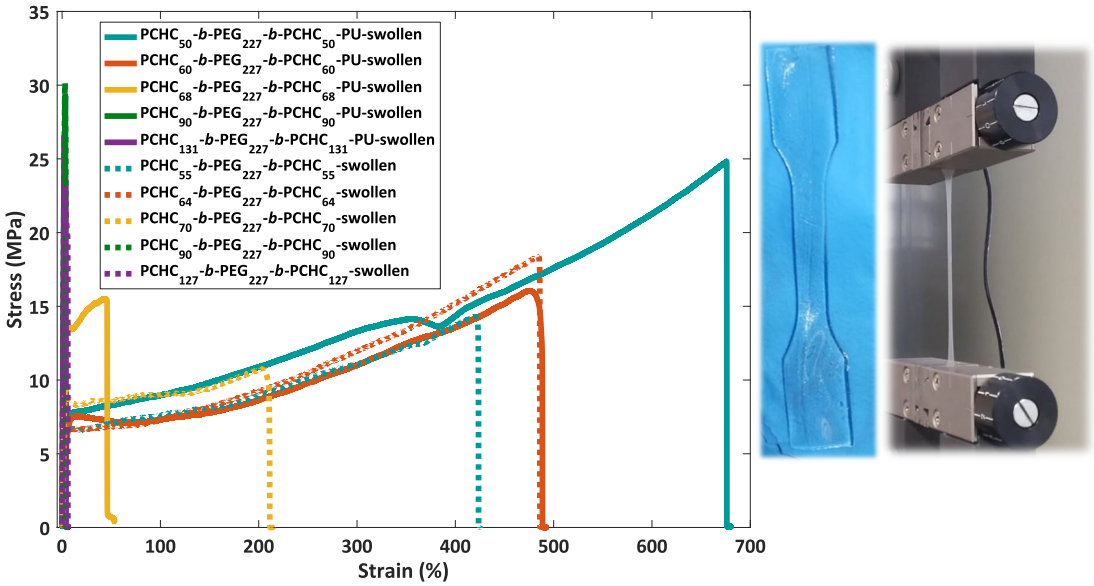

Figure 3: Stress-strain curves of the PCHC-*b*-PEG-*b*-PCHC triblock copolymers and the PCHC-*b*-PEG-*b*-PCHC-PU multiblock copolymers in the swollen state (left). A sample of the water-swollen film in dog bone shape (middle). The strained water-swollen film (right).

The stress-strain curves of the dry films were then compared with the swollen films of the PCHC-*b*-PEG-*b*-PCHC triblock copolymers. The results reveal generally lower values of elongation at break and toughness for the swollen films (Table 2, Figure S 15). In dry films, the non-crystalline PEG chains are entangled and more resistant to plastic deformation. In the swollen state the PEG chains are more disentangled due to the interaction with water molecules and additional more diluted resulting in an lowered strength.[49] In the case of samples 3 and 4, elongation at break is around 430 % with a toughness of 43 MN/mm^2 (Table 2, Figure S1 5 Figure 5).

A similar trend is also detectable in case of the multiblock copolymers in swollen state (Figure 3). The (PCHC$_{50}$-*b*-PEG$_{227}$-*b*-PCHC$_{50}$)-PU multiblock copolymer shows an elongation at break of 687±49 % in the swollen state, and the corresponding triblock copolymer (PCHC$_{55}$-*b*-PEG$_{227}$-*b*-PCHC$_{55}$, sample 3s) shows half elongation at break of 424±84%. This leads also to a difference of 30 MN/mm^2 in the copolymers' toughness (Table 2, Figure 5b). All other polymers with higher PCHC content show no increase in toughness for the multiblock copolymers in the swollen state. Sample 9, with 65 vol% PCHC and M_n of 32 240 g/mol exhibits the same strength as its corresponding triblock copolymer in the swollen state (Table 1, Table 2, Figure 5b). Figure 5b demonstrates that with a higher PCHC content, the effect of the higher molar masses on the toughness of the multiblock copolymers decreases, as the values of toughness of the tri and multiblock copolymers converge. This can be explained by the fact that phase separation no longer occurs at higher PCHC contents.

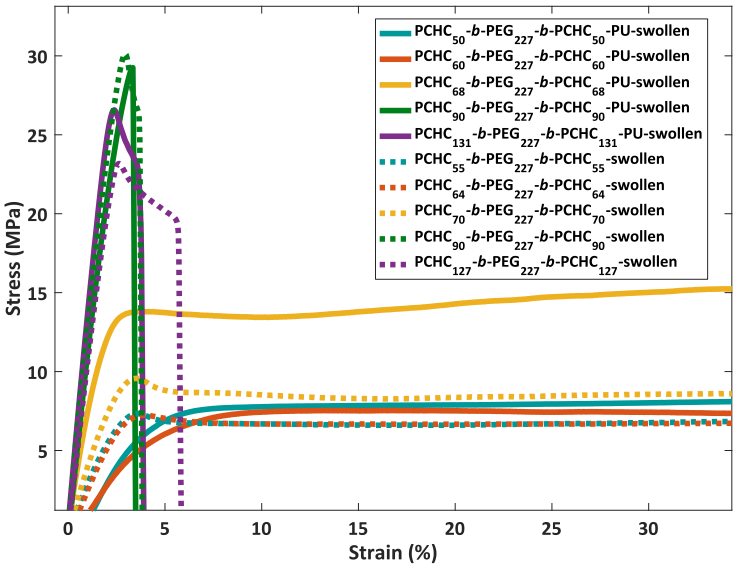

Figure 4: Zoom in of the Stress-strain curves to illustrate the yield point of the PCHC-*b*-PEG-*b*-PCHC triblock copolymer an the PCHC-*b*-PEG-*b*-PCHC-PU multiblock copolymers in the swollen state.

Comparing the mechanical properties of the multiblock copolymers in the dry and swollen state (Figure 5 c, Figure S 16), leads to similar results as the comparison of the triblock copolymers in the dry and swollen state. The water-swollen films are weaker than the dry samples. This could again be related to the hypothesis that the PEG chains are disentangled by water molecules and are also more diluted than in the dry state.[49]

The *E*-modulus (*E*) of the polymers increased with a higher PCHC content in the triblock and multiblock copolymers in both the dry and swollen state (Table 2). Furthermore, the stress at break (σ_{break}) has a value between 14 and 30 MPa. The yield elongation of the polymer films is low (2– 4 %) (Table 2, Figure 4).This result demonstrates that these copolymers have a limited elasticity with an enhanced plastic behaviour. Furthermore, polymers with a lower PCHC content have a higher yield elongation. The stress at the yield point is between 6 and 34 MPa. Polymers with higher content of PCHC showed a higher stress at the yield point. This can be ascribed to the increased stiffness of PCHC in comparison to PEG. Additionally, all swollen polymers show a lower stress at the yield point, illustrating their softness in the swollen state (Table 2). The yield points are exemplified in Figure 4 for the water-swollen polymers

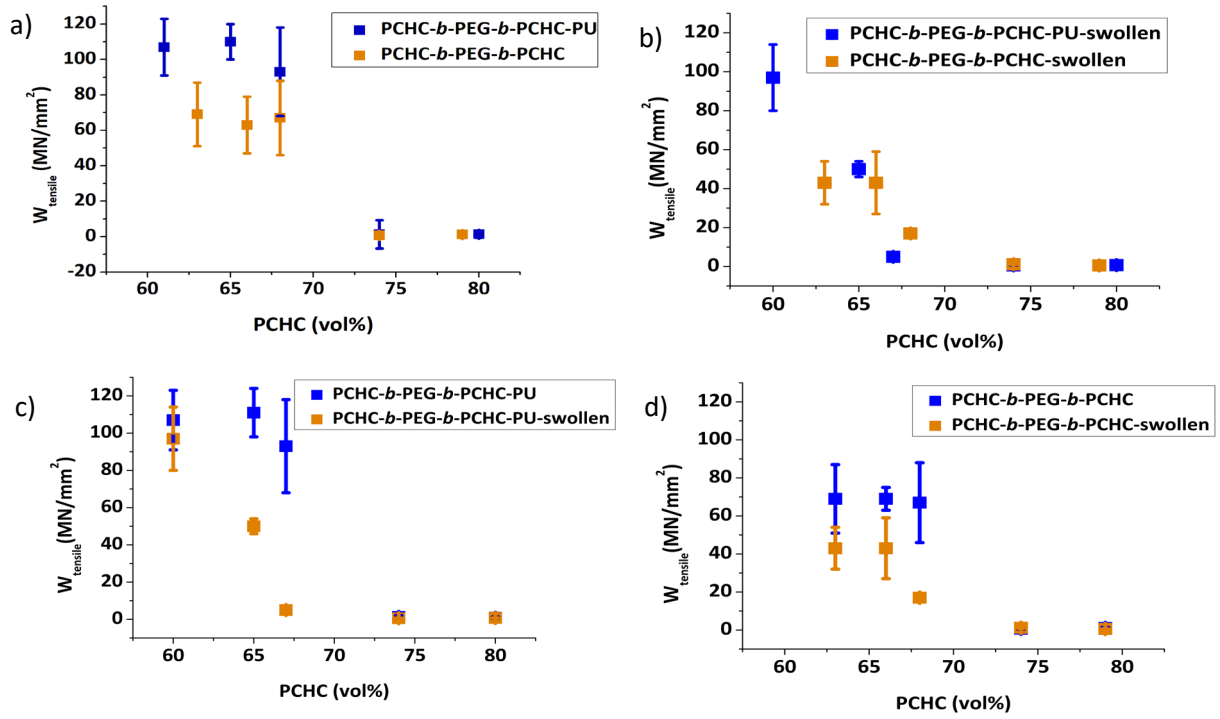

Figure 5: Toughness in MN/mm² against PCHC content in vol% of the tri- and multiblock copolymers. a) comparison of the PCHC-*b*-PEG-*b*-PCHC triblock copolymers with the PCHC-*b*-PEG-*b*-PCHC-PU multiblock copolymers in dry state. b) comparison of the PCHC-*b*-PEG-*b*-PCHC triblock copolymers with the PCHC-*b*-PEG-*b*-PCHC-PU multiblock copolymers in swollen state. c) comparison the PCHC-*b*-PEG-*b*-PCHC-PU multiblock copolymers in dry and swollen state. d) comparison the PCHC-*b*-PEG-*b*-PCHC triblock copolymers in dry and swollen state.

Summarizing the main aspects of the mechanical analysis, the increase of molar masses *via* polyaddition reaction leads to stronger materials both in the dry and swollen state, with polymers containing between 63 and 68 vol% of PCHC showing the highest toughness.

Lower amounts of PCHC result in higher crystallinity of PEG, which leads to more brittle polymers (no films of the polymers could be fabricated). On the other hand, a higher content of PCHC (> 68vol%) results in a brittle material showing the brittle character of pure PCHC. This highlights the limits for such kind of block copolymers

Extrusion

The thermal processability of these tough materials was demonstrated by extrusion of different PCHC-*b*-PEG-*b*-PCHC triblock copolymers to evaluate extrusion temperature and speed. Based on the previous test, an extrusion temperature of 140 °C and an extrusion speed of 140 min^{-1} was chosen. $PCHC_{115}$-*b*-PEG_{227}-*b*-$PCHC_{115}$ was extruded as a model compound without any additives, using a mini-extruder, resulting in a slightly yellowish transparent filament (Figure S 18). The degradation occurring by the extrusion process was quantified *via* SEC analysis (Figure S 19), which

reveals a degradation of the triblock copolymer. The molar mass of the polymer drops from 18 000 g/mol to 13 000 g/mol. Moreover, the distribution broadened from a polydispersity value of 1.17 to 1.31 and the highest mode shifted significantly to higher elution volume and therefore to lower molar masses (Figure S 19). Kernbichel et al. demonstrate a decrease in depolymerisation using Irganox® as antioxidant in the extrusion of PCHC and PLimC.[50] Blending $PCHC_{131}$-*b*-PEG_{227}-*b*-$PCHC_{131}$ with 500 ppm Irganox® resulted in a reduced degradation. Although a decrease in the molar mass could still be detected, the shift to higher elution volumes was significantly smaller (Figure S 21). Irganox® itself is not biobased and not biocompatible.[51] On the contrary Yun et al. demonstrated the effectiveness of biobased and biocompatible amino acids as additives. A 2 wt% blend of *L*-aspartic acid with PPC resulted in minor degradation. They suggest somehow a kind of end capping of the PPC by the amino acid inhibiting the "unzipping" degradation of PPC.[52] We could also observe that blending of the triblock copolymers with 4 wt% of *L*-asparagine leads to an inhibiting of the degradation as only a decrease of molar mass from 18 000 g/mol to 17 000 g/mol was visible (Figure S 23). The drawback of this method is a change of colour of the resulting filament from colourless to slightly brownish (Figure S 22).

CONCLUSION

We show a straight-forward synthesis of PCHC-*b*-PEG-*b*-PCHC triblock copolymers based on PEG as a macroinitiator. Polymers with a content of 63-68 vol% PCHC exhibit high toughness of 69 MN/mm^2 in the dry and 40 MN/mm^2 in the water-swollen state. Moreover, the toughness of the materials could be expanded by using TDI as a chain extender to obtain higher molar mass multiblock structures. PCHC-*b*-PEG-*b*-PCHC-PU multiblock copolymers with 60-67 vol% PCHC show a toughness of $93 - 111$ MN/mm^2. The strongest polymer $PCHC_{50}$-*b*-PEG_{227}-*b*-$PCHC_{50}$-PU exhibited a toughness of 107±16 MN/mm^2 (at dry state) and of 97±17 MN/mm^2 (water-swollen state). Furthermore, the processability *via* extrusion using *L*-asparagine as additive could be demonstrated. The known biocompatibility of polycarbonates and PEG, the biodegradability (without acidic degradation products) of polycarbonates combined with this toughness and the availability of equilibrium swelling in aqueous solution renders these polymers promising materials for biomedical applications, e.g. in tissue engineering.

EXPERIMENTAL SECTION

Materials

All solvents and reagents were utilized as obtained, unless otherwise stated. Cyclohexene oxide (Acros Organics, Pittsburgh, PA, USA or Alfa Aesar, Kandel, Germany) was distilled over CaH_2 under reduced pressure prior to use. Carbon dioxide (>99.99%) was purchased from Westfalen AG (Münster, Germany). Bis(triphenylphosphine)iminium chloride ([PPN]Cl) was received from abcr GmbH. (R,R)-(salcy)-Co(III)Cl was prepared as described by Ford et al.[53] All solvents were received from Sigma Aldrich, Fischer Chemical (Pittsburgh,PA,USA) and Honeywell (Morris Plaines, NJ, USA) and used without further purification. All other reagents were purchased from Sigma Aldrich or Arcos Organics (Pittsburgh, PA, USA). Deuterated solvents were obtained from Deutero GmbH (Kastellaun, Germany).

Characterization

NMR analysis. ^{1}H and ^{13}C NMR spectra were documented on Bruker 400 spectrometer (Bruker Corporation, Billerica, MA, USA), operated at 300 MHz, 400 MHz and 75 MHz, respectively, at 23 °C and the chemical shifts are given in parts per million (ppm). All spectra are referenced to residual solvent signal.

Size exclusion chromatography. For size exclusion chromatography (SEC) measurements in DMF (containing 0.25 g/L of lithium bromide as an additive) an Agilent 1100 Series system (Agilent Technologies, Santa Clara, CA, USA) was used as integrated instrument, including a PSS HEMA 300/100/40 column (Mainz, Germany, MZ Analysetechnik), a RI and an UV detector. Calibration was performed by using poly (ethylene glycol) standards delivered by Polymer Standards Service (Mainz, Germany). Toluene was used as a reference for the baseline.

DSC analysis. DSC curves were recorded using a Perkin-Elmer DSC 7 CLN2 instrument in the temperature range of -95°C-200°C at heating rates of 10 K/min under nitrogen. The amount of crystallinity was measured with the equitation below:

$$\boldsymbol{X_{\mathrm{c\ PEG}}}(\%) = \frac{\boldsymbol{\Delta H^{1}_{\mathrm{m\ PCHC-}b\mathrm{-PEG-}b\mathrm{-PCHC}}}}{\boldsymbol{\Delta H^{2}_{\mathrm{m\ PEG}}}} \textbf{ x 100 x } \frac{\boldsymbol{M_{\mathrm{n\ PEG}}}}{\boldsymbol{M_{\mathrm{n\ PCHC-}b\mathrm{-PEG-}b\mathrm{-PCHC}}}} \quad (1)$$

$$\boldsymbol{\Delta H^{2}_{m\ PEG}} \textbf{=189,8 J/g}$$

where $\boldsymbol{\Delta H^{1}_{\mathrm{m\ PCHC-}b\mathrm{-PEG-}b\mathrm{-PCHC}}}$ represents experimental enthalpy of melting of the triblock copolymer while $\Delta H^{2}_{m\,PEG}$ shows theoretical enthalpy of melting of 100% crystalline PEG homopolymers. $M_{\mathrm{n\ PCHC}}$, $M_{\mathrm{n\ PEG}}$ and $M_{\mathrm{n\ PCHC\text{-}b\text{-}PEG\text{-}b\text{-}PCHC}}$ represent M_{n} values evaluated from the integral ratio of the ^{1}H NMR peaks for each homopolymer and triblock copolymer.

FT-IR analysis. FT-IR spectra were recorded using a iS10 FT-IR spectrometer (Thermo Scientific, Waltham, MA, USA) equipped with a diamond ATR unit.

Tensile test. Tensile tests were performed on a material testing machine Z005 (Zwick/Roell, Germany). Bone shaped samples were stamped from polymer films prepared by slow evaporation from a chloroform solution followed by a full removal of the solvent under reduced pressure. The film thickness was around 0.2mm. The samples were subjected to a predefined load of 0.1 N and then strained with rate of 20 mm/min at room temperatures. Stress-strain dependences were measured 4-6 times for each polymer. The elastic modulus (*E*) was determined by calculating the slope of the stress-strain curves before the yield point. The yield point of the films was determined by the intersection of the tangents to the initial elastic part of the curve and to the plastic deformation part before the strain hardening. The toughness was calculated as the area under the strain stress curves. The elongation at break ($\varepsilon_{\mathrm{break}}$) and stress at break($\sigma_{\mathrm{break}}$) were estimated from the point of rupture.

Equilibrium swelling in aqueous solution. The equilibrium swelling in aqueous solution of the PCHC-*b*-PEG-*b*-PCHC films were determined after an equilibrium swelling by exposing to an excess of water at 37 °C. The following equation was used to calculate the equilibrium swelling in aqueous solution:

$$\mathbf{equilibrium\ swelling} = \frac{\boldsymbol{m_{\mathrm{swollen}} - m_{\mathrm{dry}}}}{\boldsymbol{m_{\mathrm{dry}}}} \mathbf{x\ 100} \qquad (2)$$

where m_{dry} and m_{swollen} are the mass of the dry film and that after after equilibrium swelling, respectively.

Extrusion. The extrusion was accomplished by the HAAKE MiniLab II (ThermoFisher Scientic) a twin screw extruder. The polymers were blended with the additives (Irganox® (500 ppm), *L*-asparagine (4 wt%)) prior before the extrusion. All triblock polymers were used as powder. Ca. 2.5 g of the triblock copolymers were extruded in each extrusion process. The extrusion temperature exhibits 140 °C the extrusion rate 140 min^{-1}.

Polymer Synthesis

Triblock copolymer synthesis

PEG was dried by azeotropic distillation with benzene under reduced pressure. A 100 mL Roth autoclave was dried at 40 °C under reduced pressure.

PEG_{227} (2.0 g, 0.2 mmol,1 eq), cyclohexene oxide (CHO) (4.0 mL, 40 mmol, 200 eq), (*R,R*)-(salcy)-CoCl (15.3 mg, 0.024 mmol, 0.12 eq) and [PPN]Cl (13,7mg, 0.024 mmol, 0.12 eq) was filled in the autoclave, equipped with a stir bar, in an inert argon-atmosphere. The reaction mixture was stirred at a carbon dioxide pressure of 50 bar at 50 °C for 23-48 h. The crude product was dissolved in DCM and the catalyst was deactivated with 10 mL of a solution of 5%vol HCl in methanol at 60 °C. The product was precipitated by using ice-cold diethyl ether as non-solvent. The precipitated product, which was collected by centrifugation at 4500 rpm at 0°C for 10 min, was dissolved again in 4 mL DCM. A neutral aluminium oxide column and 400 mL THF as eluent was used for the further purification of the product to eliminate the catalyst. The THF was evaporated by using reduced pressure and the product was dissolved again and precipitated in ice-cold diethyl ether. The colourless solid was then dried under reduced pressure at 40°C for 24h. This preparation shows the synthesis of sample 3, $PCHC_{55}$-*b*-PEG_{227}-*b*-$PCHC_{55}$ (yield 50%). The other PCHC-*b*-PEG-*b*-PCHC (sample 1-7) triblock copolymers were prepared in a similar procedure using different amount of CTA and cyclohexene oxide.

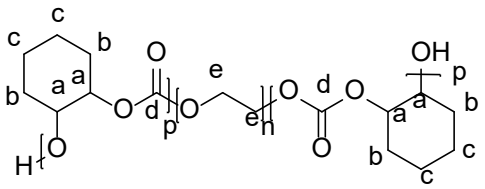

^{1}H NMR (400 MHz, Chloroform-d): δ [ppm] = 4.62 (s, CH PCHC), 3.61 (s, CH_2 polyether), 2.08 (m, CH_2 PCHC), 1.67 (m, CH_2 PCHC), 1.43-1.33 (m, CH_2 PCHC).

^{13}C NMR (75 MHz, Chloroform-d): δ [ppm] = 154.79 (C=O), 78.41 (CH PCHC), 71.11 (CH_2 polyether), 30.68 (CH_2 PCHC), 23.88 (CH_2 PCHC).

Multiblock copolymer synthesis

The $PCHC_{50}$-*b*-PEG_{227}-*b*-$PCHC_{50}$ triblock copolymer (1.5 g, 0.061 mmol, 1 eq) was dried by azeotropic distillation with benzene under reduce pressure. One drop of DBTL and 3 mL dried toluene were added to the dried triblock copolymer and the reaction mixture was stirred at 60 °C.

After the addition of TDI (9.65 µL, 0.067 mmol, 1.1 eq) the reaction mixture was stirred at 60 °C for 4 days. After 2 days, 2 mL dried toluene was added due to increased viscosity of the mixture. The polymer mixture was quenched with a few drops of methanol, solved in DCM and precipitated in cold diethyl ether.

ACKNOWLEDGEMENTS

The authers thank Andreas Hanewald for technical assitance using the tensile test machine and Monika Schmelzer for GPC measurments. The authors thank Sandra Schüttner and Mathew Evans for the critical reading of the manuscript.

REFERENCES

(1) Hoffman, A. S. Hydrogels for biomedical applications. *Adv. Drug Deliv. Rev.* **2002**, *54*, 3–12.

(2) Caló, E.; Khutoryanskiy, V. V. Biomedical applications of hydrogels: A review of patents and commercial products. *Eur. Polym. J.* **2015**, *65*, 252–267.

(3) Fischenich, K. M.; Lewis, J. T.; Bailey, T. S.; Haut Donahue, T. L. Mechanical viability of a thermoplastic elastomer hydrogel as a soft tissue replacement material. *J. Mech. Behav. Biomed. Mater.* **2018**, *79*, 341–347.

(4) Cho, C.-S.; Jeong, Y.-I.; Kim, S.-H.; Nah, J.-W.; Kubota, M.; Komoto, T. Thermoplastic hydrogel based on hexablock copolymer composed of poly(γ-benzyl l -glutamate) and poly(ethylene oxide). *Polymer* **2000**, *41*, 5185–5193.

(5) Dai, X.; Zhang, Y.; Gao, L.; Bai, T.; Wang, W.; Cui, Y.; Liu, W. A Mechanically Strong, Highly Stable, Thermoplastic, and Self-Healable Supramolecular Polymer Hydrogel. *Adv. Mater.* **2015**, *27*, 3566–3571.

(6) Wright, E. R.; McMillan, R. A.; Cooper, A.; Apkarian, R. P.; Conticello, V. P. Thermoplastic Elastomer Hydrogels via Self-Assembly of an Elastin-Mimetic Triblock Polypeptide. *Adv. Funct. Mater.* **2002**, *12*, 149–154.

(7) Brook, M. G. Thermoplastic hydrogels. *Brit. Poly. J.* **1990**, *23*, 257–259.

(8) Gong, C.; Shi, S.; Wu, L.; Gou, M.; Yin, Q.; Guo, Q.; Dong, P.; Zhang, F.; Luo, F.; Zhao, X.*; et al.* Biodegradable in situ gel-forming controlled drug delivery system based on thermosensitive PCL-PEG-PCL hydrogel. Part 2: sol-gel-sol transition and drug delivery behavior. *Acta Biomaterialia* **2009**, *5*, 3358–3370.

(9) Ma, G.; Miao, B.; Song, C. Thermosensitive PCL-PEG-PCL hydrogels: Synthesis, characterization, and delivery of proteins. *J. Appl. Polym. Sci.* **2010**, *37*, NA-NA.

(10) Zhang, Y.; Wu, X.; Han, Y.; Mo, F.; Duan, Y.; Li, S. Novel thymopentin release systems prepared from bioresorbable PLA-PEG-PLA hydrogels. *Int. J. Pharm.* **2010**, *386*, 15–22.

(11) Cui, H.; Shao, J.; Wang, Y.; Zhang, P.; Chen, X.; Wei, Y. PLA-PEG-PLA and its electroactive tetraaniline copolymer as multi-interactive injectable hydrogels for tissue engineering. *Biomacromolecules* **2013**, *14*, 1904–1912.

(12) Cohn, D.; Hotovely-Salomon, A. Biodegradable multiblock PEO/PLA thermoplastic elastomers: molecular design and properties. *Polymer* **2005**, *46*, 2068–2075.

(13) Manavitehrani, I.; Fathi, A.; Wang, Y.; Maitz, P. K.; Dehghani, F. Reinforced Poly(Propylene Carbonate) Composite with Enhanced and Tunable Characteristics, an Alternative for Poly(lactic Acid). *ACS Appl. Mater. Interfaces* **2015**, *7*, 22421–22430.

(14) Fu, K.; Pack, D. W.; Klibanov, A. M.; Langer, R. Visual evidence of acidic environment within degrading poly(lactic-co-glycolic acid) (PLGA) microspheres. *Pharm. Res.* **2000**, *17*, 100–106.

(15) Tinsley-Bown, A.; Fretwell, R.; Dowsett, A.; Davis, S.; Farrar, G. H. Formulation of poly(d,l-lactic-co-glycolic acid) microparticles for rapid plasmid DNA delivery. *J. Control. Release* **2000**, *66*, 229–241.

(16) Walter, E.; Moelling, K.; Pavlovic, J.; Merkle, H. P. Microencapsulation of DNA using poly(dl-lactide-co-glycolide): stability issues and release characteristics. *J. Control. Release* **1999**, *61*, 361–374.

(17) Yoon, S. J.; Kim, S. H.; Ha, H. J.; Ko, Y. K.; So, J. W.; Kim, M. S.; Yang, Y. I.; Khang, G.; Rhee, J. M.; Lee, H. B. Reduction of inflammatory reaction of poly(d,l-lactic-co-glycolic Acid) using demineralized bone particles. *Tissue Eng.* **2008**, *14*, 539–547.

(18) Zhang, Z.; Kuijer, R.; Bulstra, S. K.; Grijpma, D. W.; Feijen, J. The in vivo and in vitro degradation behavior of poly(trimethylene carbonate). *Biomaterials* **2006**, *27*, 1741–1748.

(19) Brannigan, R. P.; Dove, A. P. Synthesis, properties and biomedical applications of hydrolytically degradable materials based on aliphatic polyesters and polycarbonates. *Biomater. Sci.* **2016**, *5*, 9–21.

(20) Thorat, S. D.; Phillips, P. J.; Semenov, V.; Gakh, A. Physical properties of aliphatic polycarbonates made from CO2 and epoxides. *J. Appl. Polym. Sci.* **2003**, *89*, 1163–1176.

(21) Shi, L.; Lu, X.-B.; Zhang, R.; Peng, X.-J.; Zhang, C.-Q.; Li, J.-F.; Peng, X.-M. Asymmetric Alternating Copolymerization and Terpolymerization of Epoxides with Carbon Dioxide at Mild Conditions. *Macromolecules* **2006**, *39*, 5679–5685.

(22) Winkler, M.; Romain, C.; Meier, M. A. R.; Williams, C. K. Renewable polycarbonates and polyesters from 1,4-cyclohexadiene. *Green Chem.* **2015**, *17*, 300–306.

(23) Sakakura, T.; Choi, J.-C.; Yasuda, H. Transformation of carbon dioxide. *Chem. Rev.* **2007**, *107*, 2365–2387.

(24) Aresta, M.; Dibenedetto, A. Utilisation of CO_2 as a chemical feedstock: opportunities and challenges. *Dalton Trans.* **2007**, 2975–2992.

(25) Inoue, S.; Koinuma, H.; Tsuruta, T. Copolymerization of carbon dioxide and epoxide with organometallic compounds. *Makromol. Chem.* **1969**, *130*, 210–220.

(26) Cheng, M.; Moore, D. R.; Reczek, J. J.; Chamberlain, B. M.; Lobkovsky, E. B.; Coates, G. W. Single-Site β-Diiminate Zinc Catalysts for the Alternating Copolymerization of CO_2 and Epoxides: Catalyst Synthesis and Unprecedented Polymerization Activity. *J. Am. Chem. Soc.* **2001**, *123*, 8738–8749.

(27) Cyriac, A.; Lee, S. H.; Varghese, J. K.; Park, E. S.; Park, J. H.; Lee, B. Y. Immortal CO_2 /Propylene Oxide Copolymerization: Precise Control of Molecular Weight and Architecture of Various Block Copolymers. *Macromolecules* **2010**, *43*, 7398–7401.

(28) Darensbourg, D. J. Making plastics from carbon dioxide: salen metal complexes as catalysts for the production of polycarbonates from epoxides and CO_2. *Chem. Rev.* **2007**, *107*, 2388–2410.

(29) Hauenstein, O.; Reiter, M.; Agarwal, S.; Rieger, B.; Greiner, A. Bio-based polycarbonate from limonene oxide and CO_2 with high molecular weight, excellent thermal resistance, hardness and transparency. *Green Chem.* **2016**, *18*, 760–770.

(30) Scharfenberg, M.; Hilf, J.; Frey, H. Functional Polycarbonates from Carbon Dioxide and Tailored Epoxide Monomers: Degradable Materials and Their Application Potential. *Adv. Funct. Mater.* **2018**, *28*, 1704302.

(31) Scharfenberg, M.; Wald, S.; Wurm, F. R.; Frey, H. Acid-Labile Surfactants Based on Poly(ethylene glycol), Carbon Dioxide and Propylene Oxide: Miniemulsion Polymerization and Degradation Studies. *Polymers* **2017**, *9*, 422.

(32) Zhang, Y.-Y.; Yang, G.-W.; Wang, Y.; Lu, X.-Y.; Wu, G.-P.; Zhang, Z.-S.; Wang, K.; Zhang, R.-Y.; Nealey, P. F.; Darensbourg, D. J.*; et al.* Synthesis of CO_2 -Based Block Copolymers via Chain Transfer Polymerization Using Macroinitiators: Activity, Blocking Efficiency, and Nanostructure. *Macromolecules* **2018**, *51*, 791–800.

(33) Hilf, J.; Schulze, P.; Frey, H. CO_2 -Based Non-ionic Surfactants: Solvent-Free Synthesis of Poly(ethylene glycol)- block -Poly(propylene carbonate) Block Copolymers. *Macromol. Chem. Phys.* **2013**, *214*, 2848–2855.

(34) Kunze, L.; Tseng, S.-Y.; Schweins, R.; Sottmann, T.; Frey, H. Nonionic Aliphatic Polycarbonate Diblock Copolymers Based on CO2, 1,2-Butylene Oxide, and mPEG: Synthesis, Micellization, and Solubilization. *Langmuir : the ACS journal of surfaces and colloids* **2019**, *35*, 5221–5231.

(35) Hilf, J.; Schulze, P.; Seiwert, J.; Frey, H. Controlled synthesis of multi-arm star polyether-polycarbonate polyols based on propylene oxide and CO2. *Macromol. Rapid. Commun.* **2014**, *35*, 198–203.

(36) Orgilés-Calpena, E.; Arán-Aís, F.; Torró-Palau, A. M.; Orgilés-Barceló, C. Novel polyurethane reactive hot melt adhesives based on polycarbonate polyols derived from CO_2 for the footwear industry. *Int. J. Adhes. Adhes.* **2016**, *70*, 218–224.

(37) Wang, Y.; Darensbourg, D. J. Carbon dioxide-based functional polycarbonates: Metal catalyzed copolymerization of CO_2 and epoxides. *Coord. Chem. Rev.* **2018**, *372*, 85–100.

(38) Xu, S.; Zhang, M. Synthesis and characterization of a novel polyurethane elastomer based on CO_2 copolymer. *J. Appl. Polym. Sci.* **2007**, *104*, 3818–3826.

(39) Xu, J.; Feng, E.; Song, J. Renaissance of Aliphatic Polycarbonates: New Techniques and Biomedical Applications. *J. Appl. Polym. Sci.* **2014**, *131*.

(40) Koning, C.; Wildeson, J.; Parton, R.; Plum, B.; Steeman, P.; Darensbourg, D. Synthesis and physical characterization of poly(cyclohexane carbonate), synthesized from CO_2 and cyclohexene oxide. *Polymer* **2001**, *42*, 3995–4004.

(41) Lu, X.-B.; Darensbourg, D. J. Cobalt catalysts for the coupling of CO_2 and epoxides to provide polycarbonates and cyclic carbonates. *Chem. Soc. Rev.* **2012**, *41*, 1462–1484.

(42) Cohen, C. T.; Thomas, C. M.; Peretti, K. L.; Lobkovsky, E. B.; Coates, G. W. Copolymerization of cyclohexene oxide and carbon dioxide using (salen)Co(III) complexes: synthesis and characterization of syndiotactic poly(cyclohexene carbonate). *Dalton Trans.* **2006**, 237–249.

(43) Yahiaoui, A.; Belbachir, M.; Soutif, J. C.; Fontaine, L. Synthesis and structural analyses of poly (1, 2-cyclohexene oxide) over solid acid catalyst. *Mater. Lett.* **2005**, *59*, 759–767.

(44) Steube, M.; Plank, M.; Gallei, M.; Frey, H.; Floudas, G. Building Bridges by Blending: Morphology and Mechanical Properties of Binary Tapered Diblock/Multiblock Copolymer Blends. *Macromol. Chem. Phys.* **2021**, *222*, 2000373.

(45) Zielinski, J. M.; Spontak, R. J. Confined single-chain model of microphase-separated multiblock copolymers. 1. (AB)n copolymers. *Macromolecules* **1992**, *25*, 653–662.

(46) Steube, M.; Johann, T.; Galanos, E.; Appold, M.; Rüttiger, C.; Mezger, M.; Gallei, M.; Müller, A. H. E.; Floudas, G.; Frey, H. Isoprene/Styrene Tapered Multiblock Copolymers with up to Ten Blocks: Synthesis, Phase Behavior, Order, and Mechanical Properties. *Macromolecules* **2018**, *51*, 10246–10258.

(47) Fennell, B.; Hill, R. G. The influence of poly(acrylic acid) molar mass and concentration on the properties of Polyalkenoate cements Part III Fracture toughness and toughness. *J. Mater. Sci.* **2001**, *36*, 5185–5192.

(48) Schollenberger, C. S.; Dinbergs, K. Thermoplastic Polyurethane Elastomer Molecular Weight-Property Relations. Further Studies. *J. Elastomers Plast.* **1979**, *11*, 58–91.

(49) Johnson, B.; Beebe, D.; Crone, W. Effects of swelling on the mechanical properties of a pH-sensitive hydrogel for use in microfluidic devices. *Mater. Sci. Eng.* **2004**, *24*, 575–581.

(50) Kernbichl, S.; Rieger, B. Aliphatic polycarbonates derived from epoxides and CO_2: A comparative study of poly(cyclohexene carbonate) and poly(limonene carbonate). *Polymer* **2020**, *205*, 122667.

(51) Bernard, M.; Jubeli, E.; Bakar, J.; Tortolano, L.; Saunier, J.; Yagoubi, N. Biocompatibility assessment of cyclic olefin copolymers: Impact of two additives on cytotoxicity, oxidative stress, inflammatory reactions, and hemocompatibility. *J. Biomed. Mater. Res* **2017**, *105*, 3333–3349.

(52) Yun, X.; Wu, J.; Wang, Y.; Zhao, Z.; Jin, Y.; Dong, T. Effects of l -aspartic acid and poly(butylene succinate) on thermal stability and mechanical properties of poly(propylene carbonate). *J. Appl. Polym. Sci.* **2016**, *133*, n/a-n/a.

(53) Ford, D. D.; Nielsen, L. P. C.; Zuend, S. J.; Musgrave, C. B.; Jacobsen, E. N. Mechanistic basis for high stereoselectivity and broad substrate scope in the (salen)Co(III)-catalyzed hydrolytic kinetic resolution. *J. Am. Chem. Soc.* **2013**, *135*, 15595–15608.

SUPPORTING INFORMATION

Though Hydrogels Based on Poly(ethylene oxide), Carbon Dioxide and Cyclohexene Oxide: Improvement of the Toughness via Polyurethanes Multiblock Synthesis

Christina Gardiner[a],Kaloian Koynov[b] and Holger Frey[a*]

[a] Institute of Organic Chemistry, Johannes Gutenberg University Mainz ,Duesbergweg 10-14, 55128 Mainz,Germany.

[b] Max Planck Institute for Polymer Research,Ackermannweg 10, 55128 Mainz, Germany.

Table of Content

1. Polymer characterization

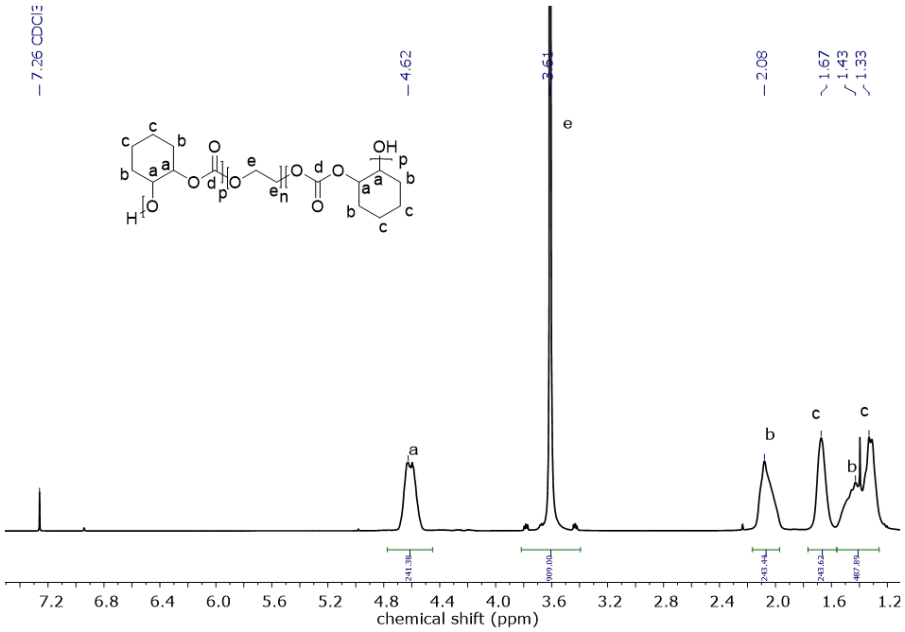

Figure S 1: ^{1}H NMR spectrum (400 MHz, $CDCl_3$) of $PCHC_{55}$-*b*-PEG_{227}-*b*-$PCHC_{55}$ triblock copolymer (sample 3).

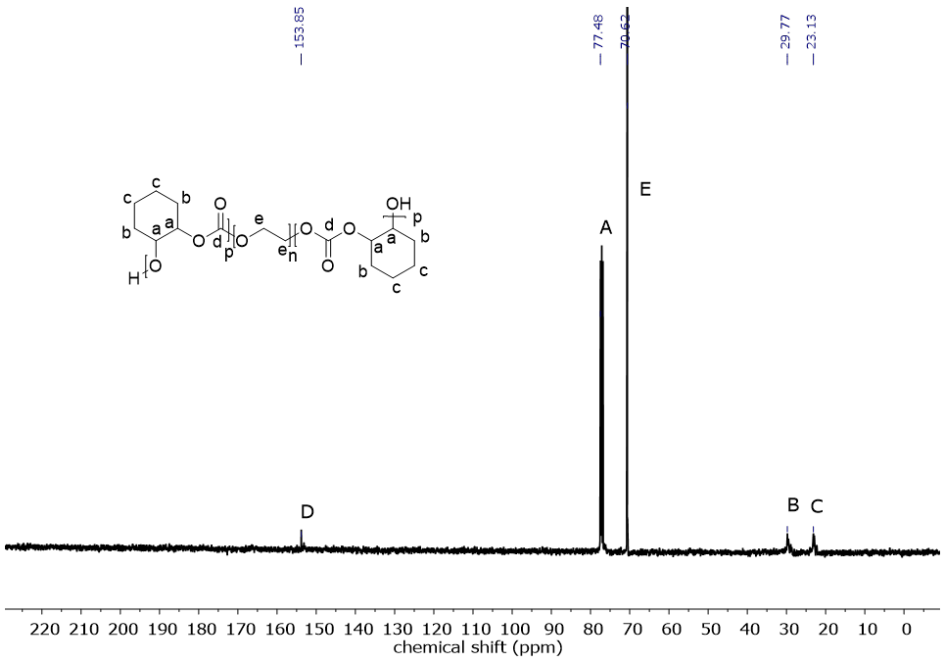

Figure S 2: ^{13}C NMR spectrum (75 MHz, $CDCl_3$) of $PCHC_{55}$-*b*-PEG_{227}-*b*-$PCHC_{55}$ triblock copolymer (sample 3), showing the formation of polycarbonate structure, based on the signal of the carbonyl carbon at 153.85 ppm.

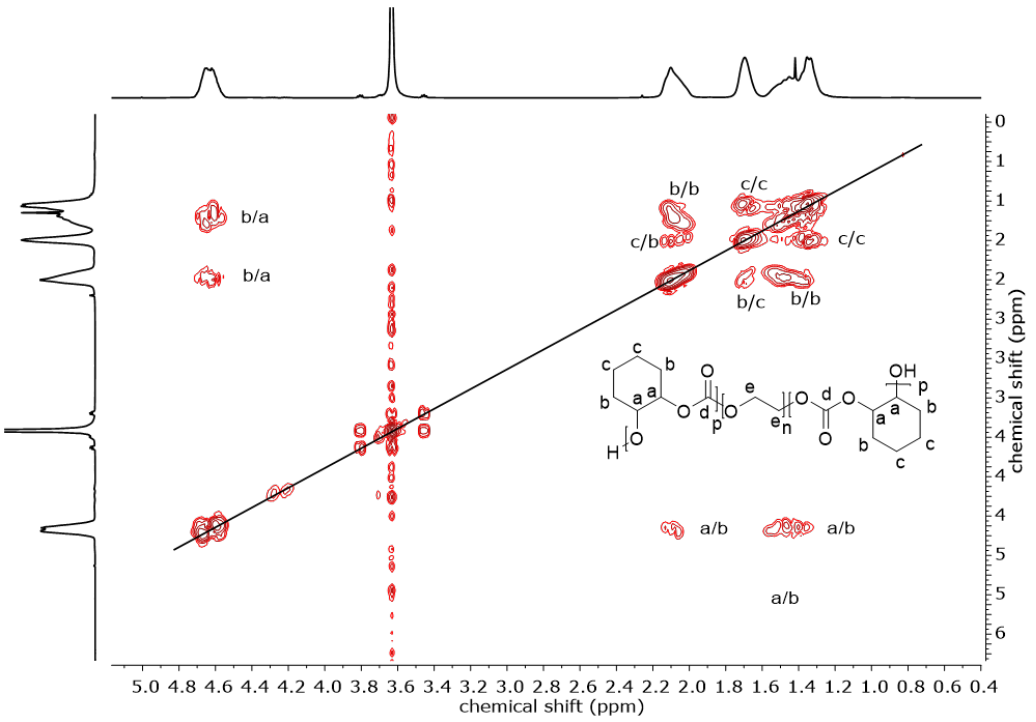

Figure S 3: ^{1}H-^{1}H COSY NMR (400 MHz, $CDCl_3$) spectrum of $PCHC_{55}$-*b*-PEG_{227}-*b*-$PCHC_{55}$ triblock copolymer (sample 3).

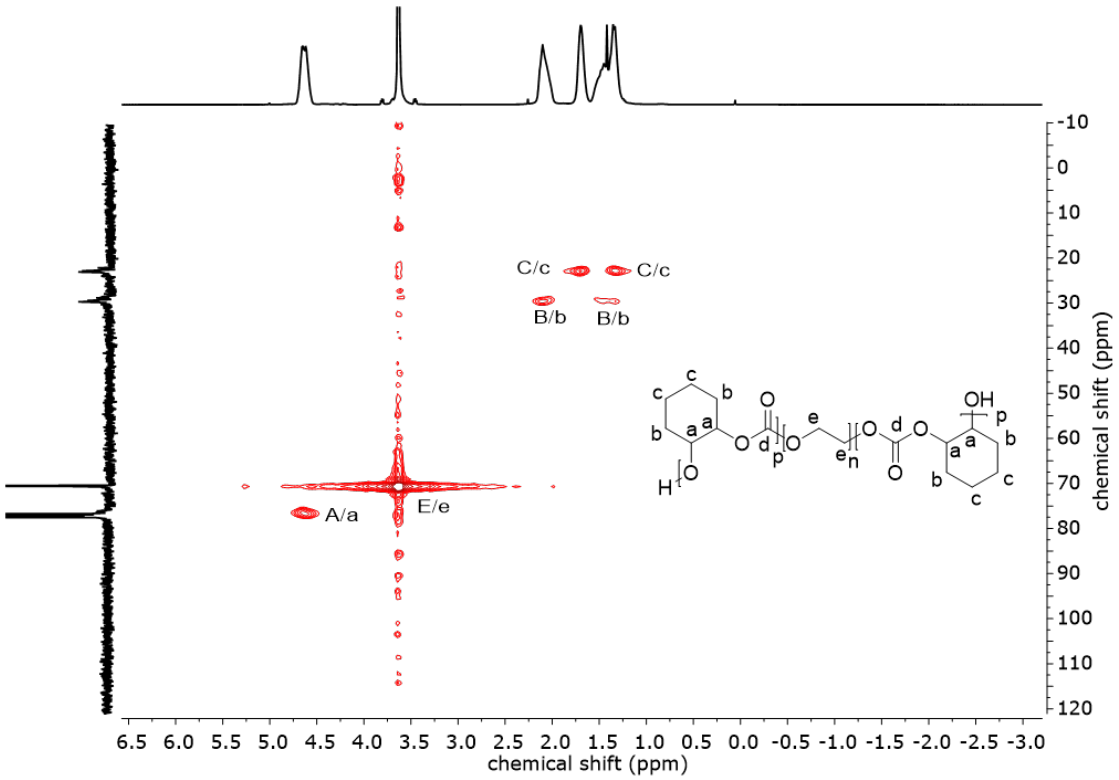

Figure S 4: ^{1}H-^{13}C HSQC NMR spectrum (400 MHz/75 MHz, $CDCl_3$) of $PCHC_{55}$-*b*-PEG_{227}-*b*-$PCHC_{55}$ triblock copolymer (sample 3).

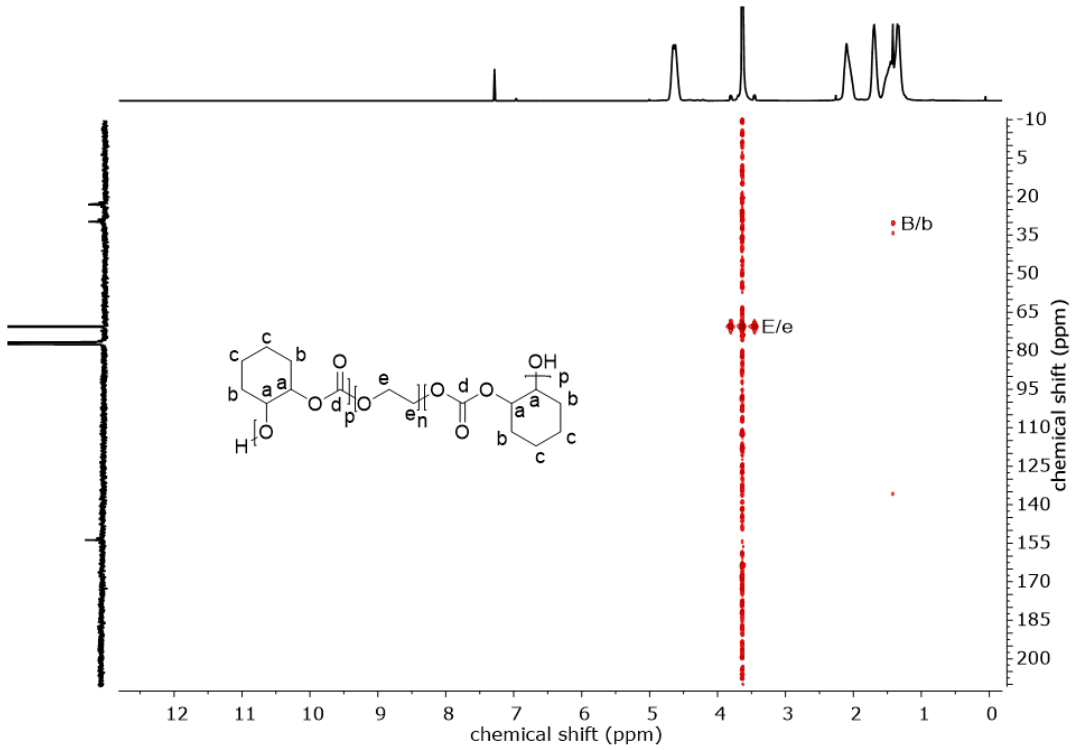

Figure S 5: ^{1}H-^{13}C HMBC NMR spectrum (400 MHz/75 MHz, $CDCl_3$) spectrum of $PCHC_{55}$-*b*-PEG_{227}-*b*-$PCHC_{55}$ triblock copolymer (sample 3).

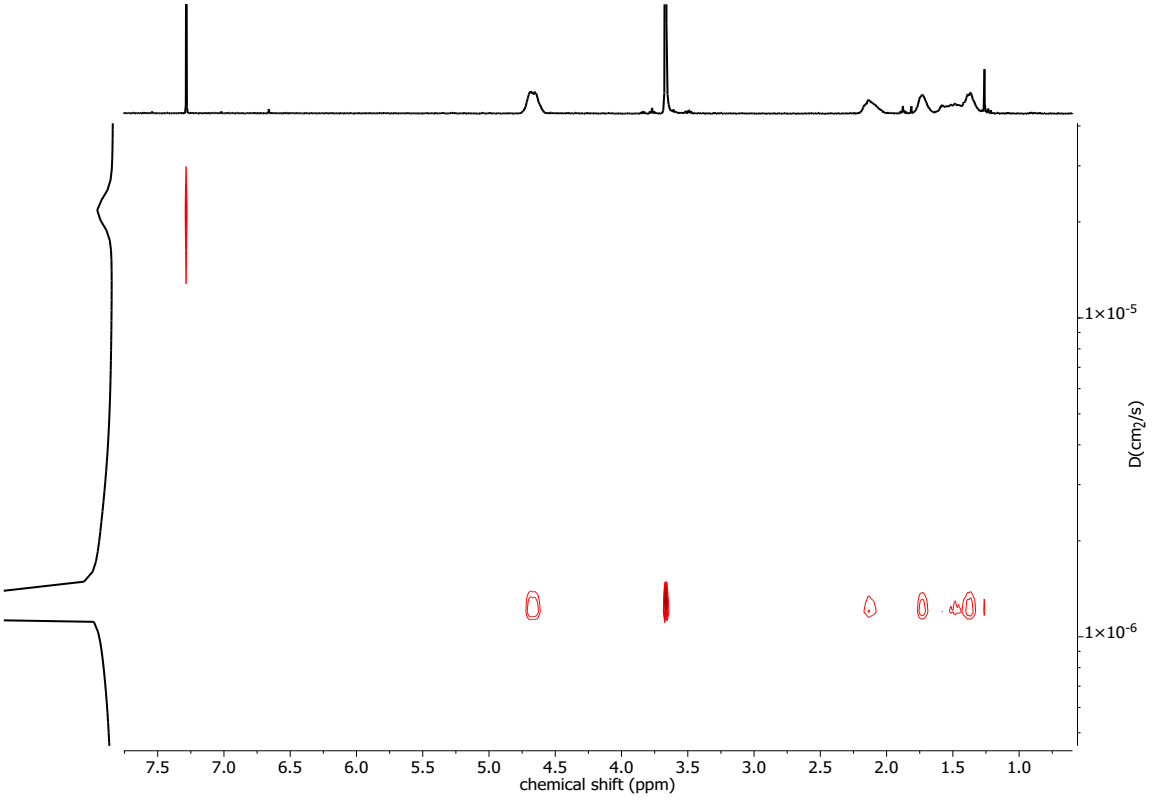

Figure S 6: ^{1}H DOSY NMR (400 MHz, $CDCl_3$) of the $PCHC_{55}$-*b*-PEG_{227}-*b*-$PCHC_{55}$ triblock copolymer (sample 3) synthesized in a one-pot reaction.

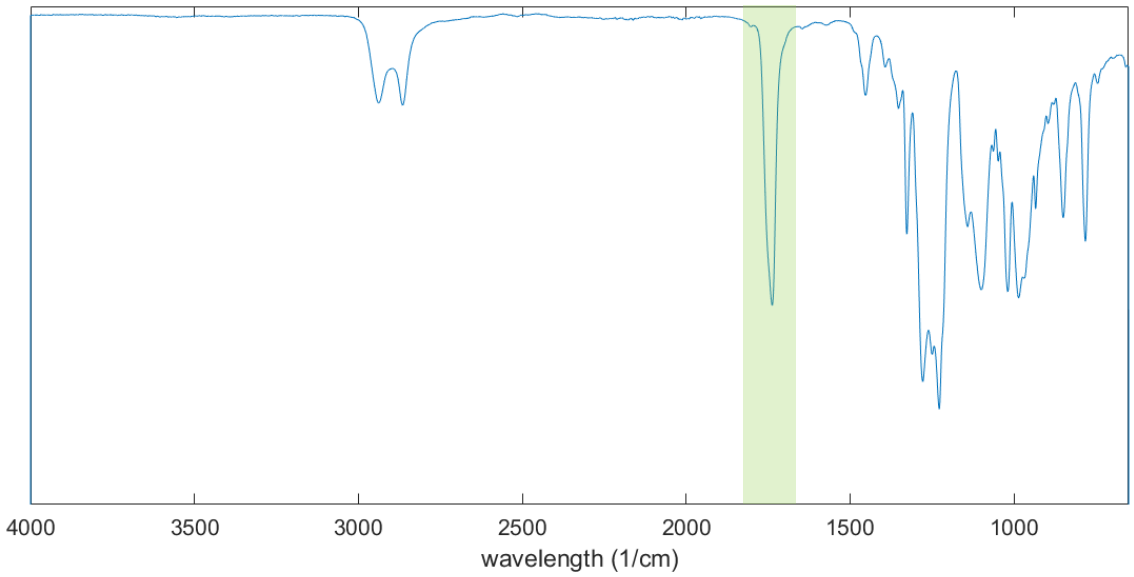

Figure S 7: FT-IR spectrum of $PCHC_{55}$-*b*-PEG_{227}-*b*-$PCHC_{55}$ triblock copolymer (sample 3) with the characteristic signal at 1738 1/cm(highlighted in green) for the C=O vibration of polycarbonates.

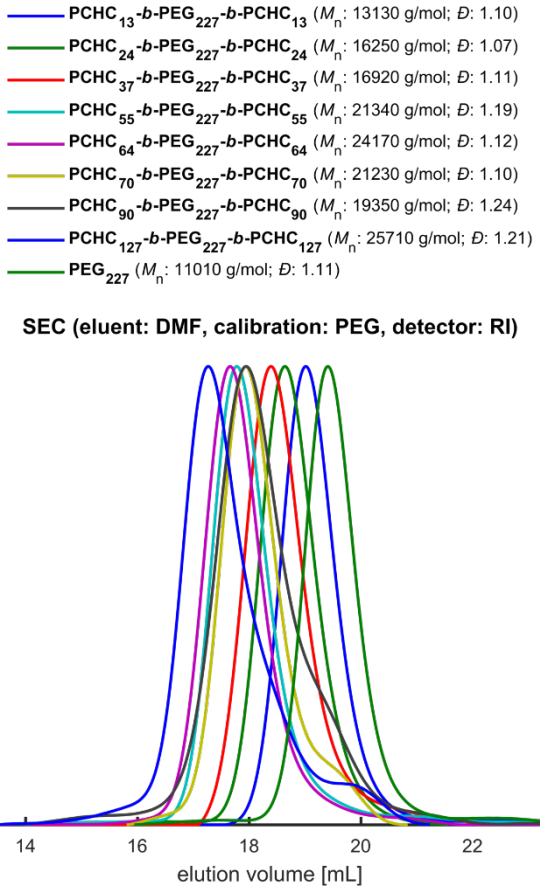

Figure S 8: SEC traces of the PCHC-*b*-PEG-*b*-PCHC triblock copolymers (eluent: DMF, calibration: PEG).

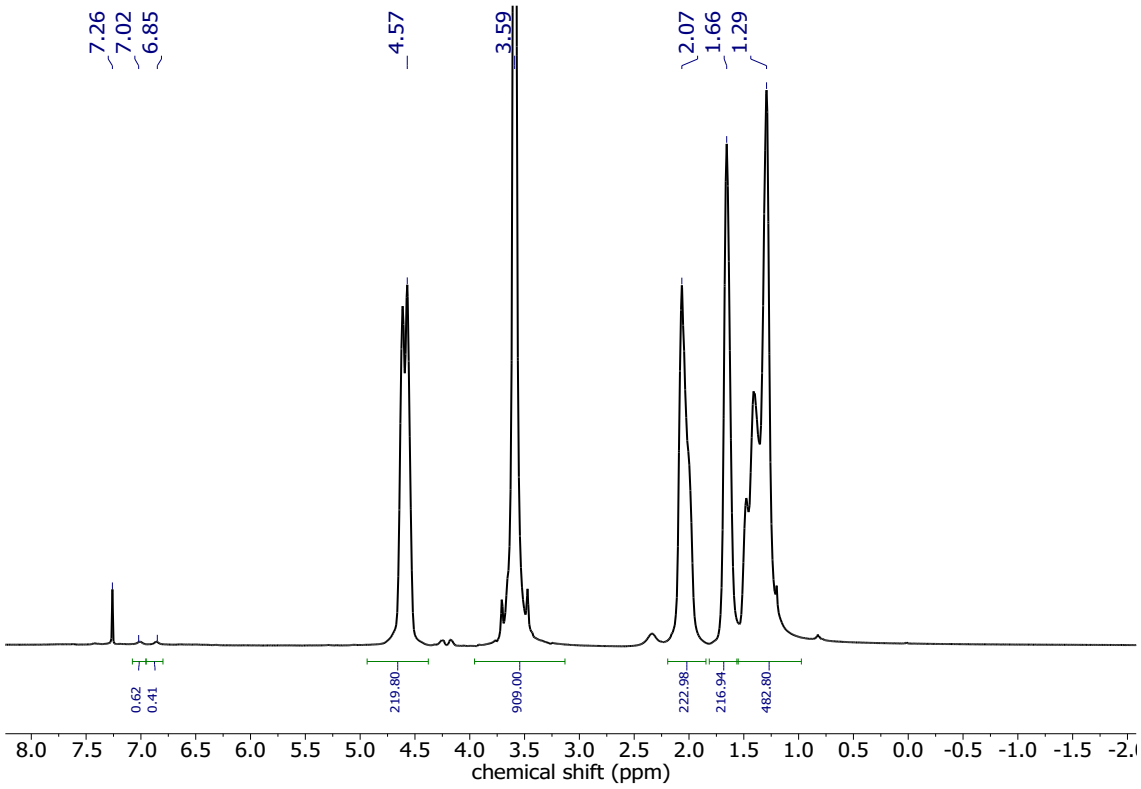

Figure S 9: ^{1}H NMR spectrum (400 MHz, $CDCl_3$) of $PCHC_{50}$-*b*-PEG_{227}-*b*-$PCHC_{50}$-PU multiblock copolymer (sample 8).

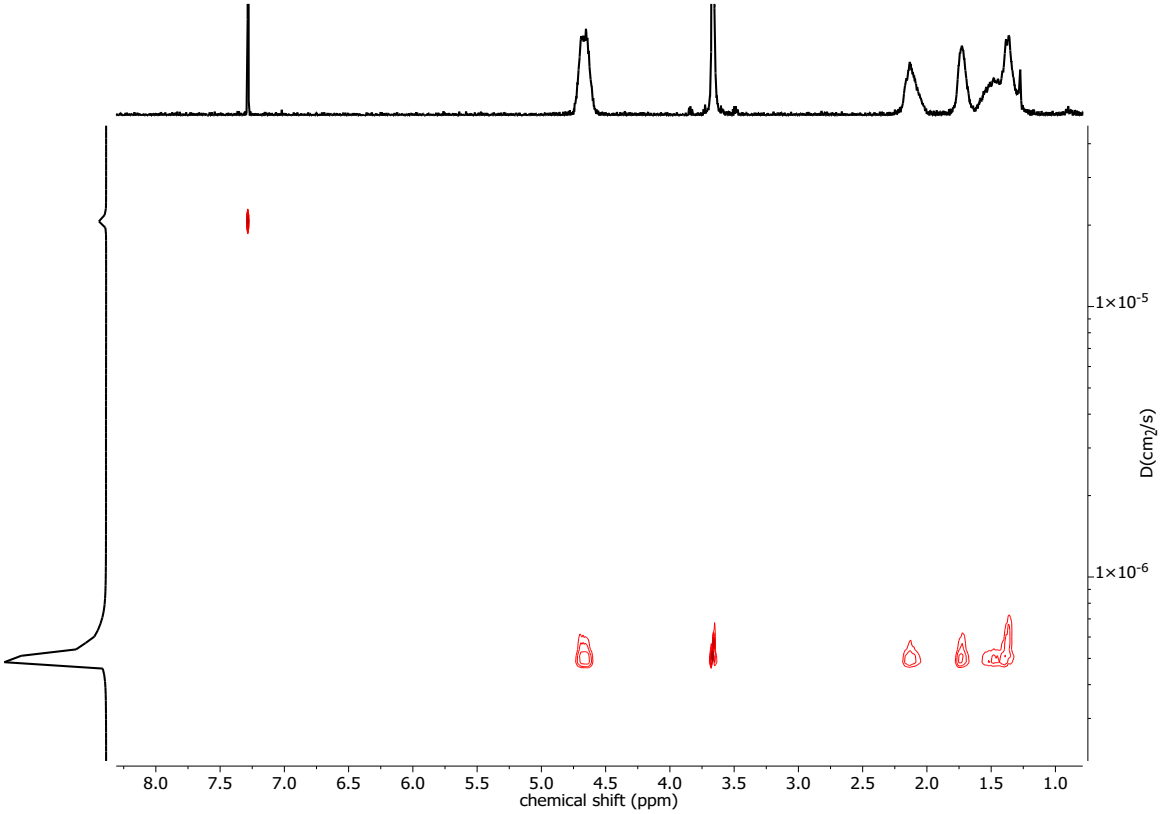

Figure S 10: ^{1}H DOSY NMR (400 MHz, $CDCl_3$) of PCHC-*b*-PEG-*b*-PCHC-PU multiblock copolymer synthesized in a one-pot reaction.

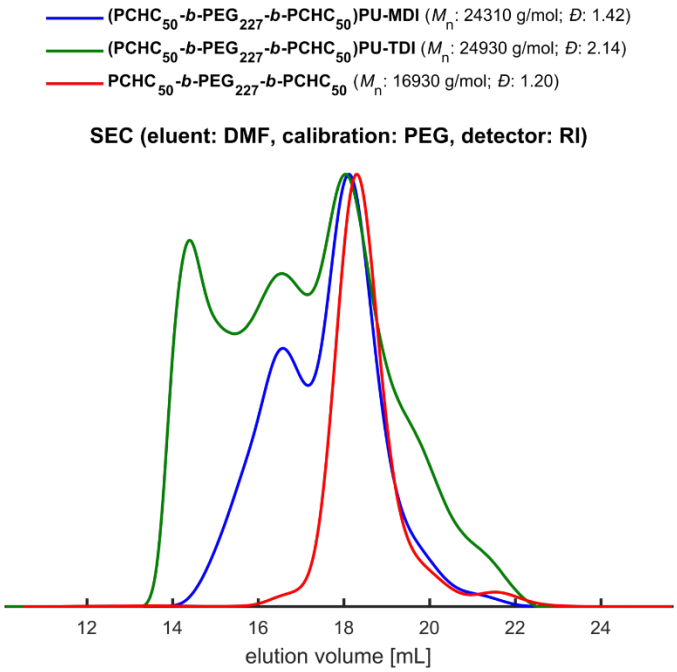

Figure S 11: SEC curves of the model experiment PCHC-*b*-PEG-*b*-PCHC-PU multiblock copolymers using MDI (blue) or TDI (green) as chain extender.

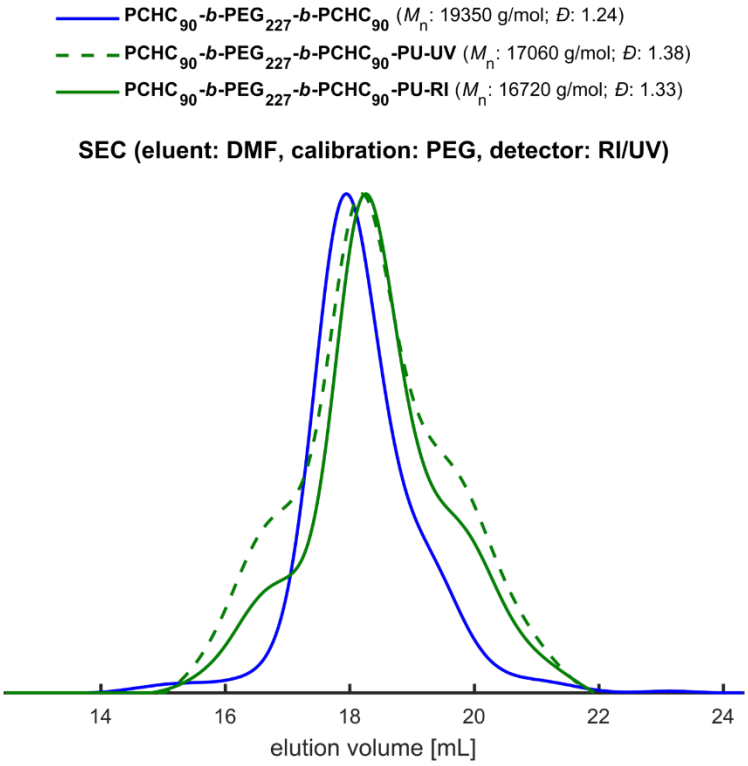

Figure S 12: Resulting SEC curve using a higher amount than 1.1 eq of TDI.

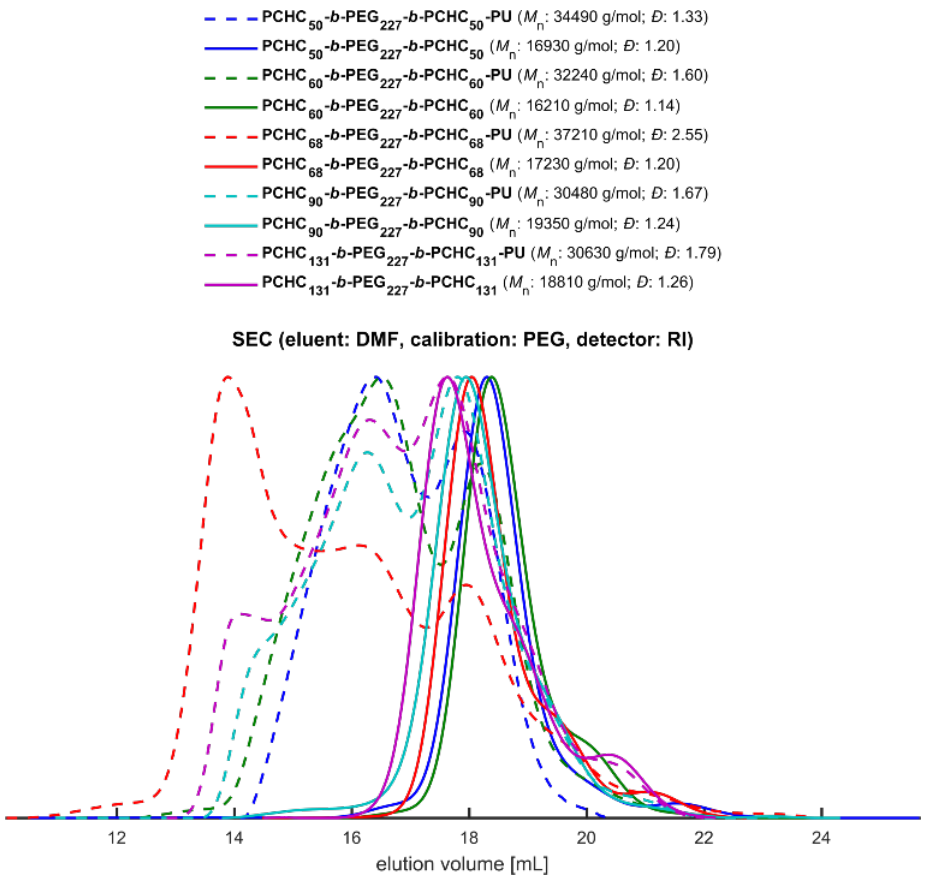

Figure S 13: SEC curves of the PCHC-*b*-PEG-*b*-PCHC-PU multiblock copolymers (dotted lines) in comparison to their prepolymers (solid line) (eluent: DMF, calibration: PEG).

2. Thermal characterization

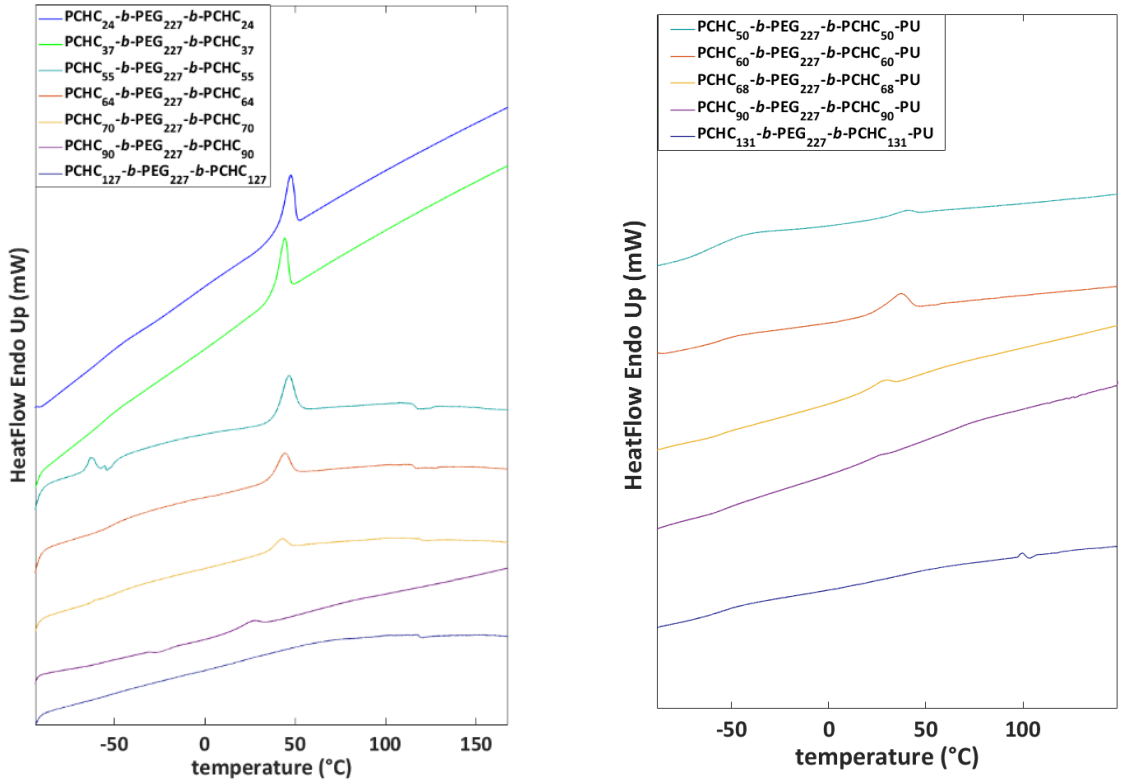

Figure S 14: DSC curves of the PCHC-*b*-PEG-*b*-PCHC triblock copolymers (left) and the PCHC-*b*-PEG-*b*-PCHC-PU multiblock copolymers (right).

3. Mechanical characterization

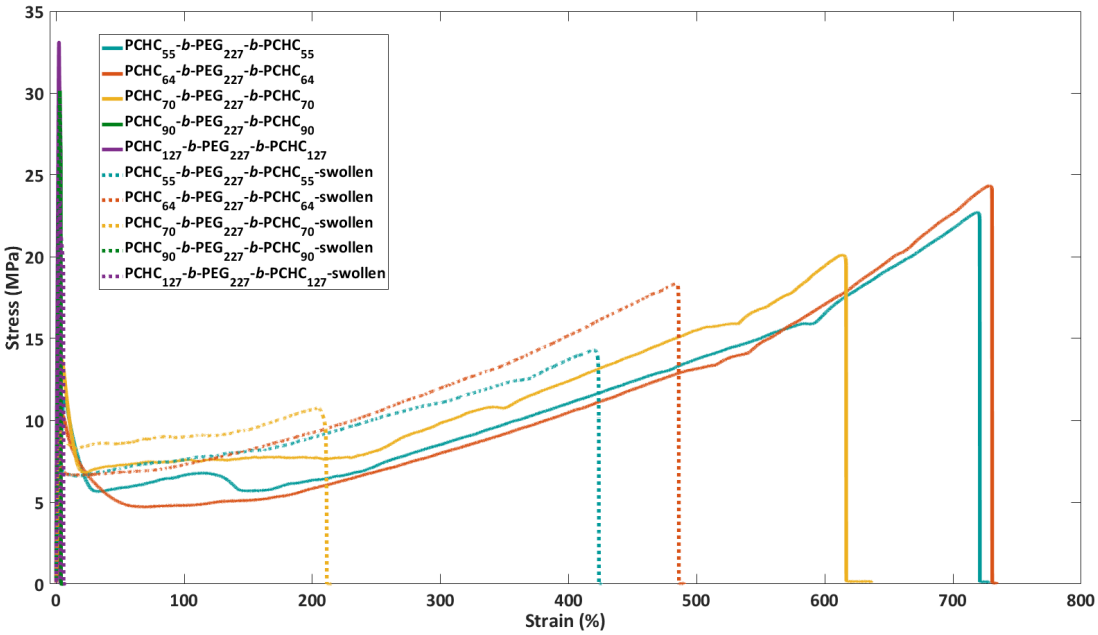

Figure S 15: Stress-strain curves of the PCHC-*b*-PEG-*b*-PCHC triblock copolymers in dry and water-swollen state.

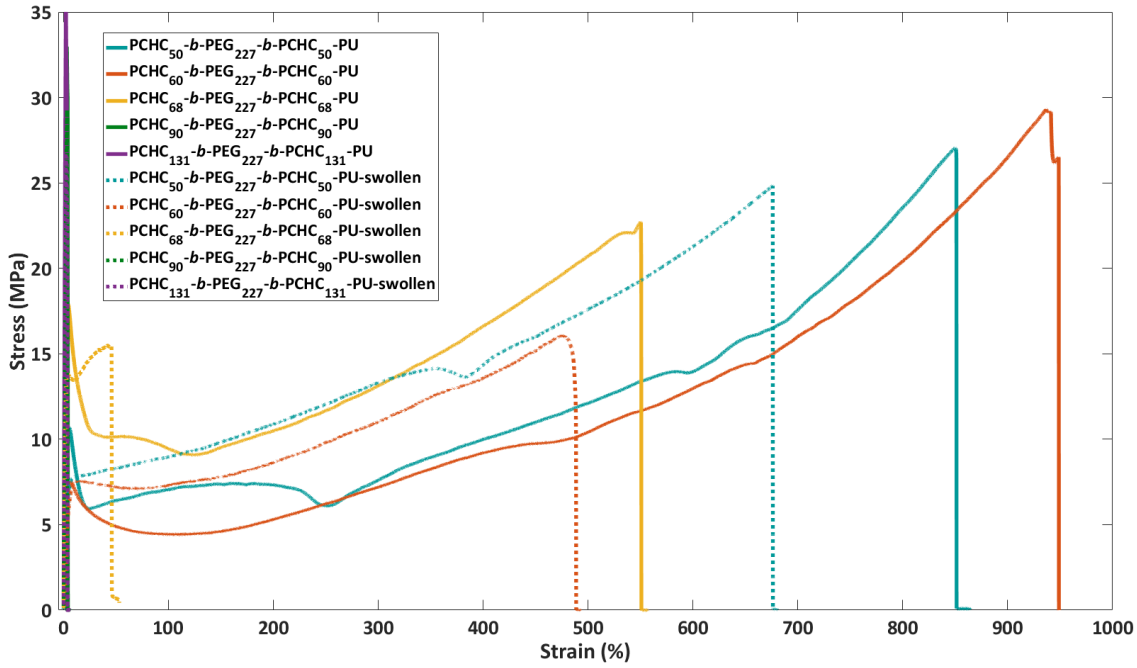

Figure S 16: Stress-strain curves of the PCHC-*b*-PEG-*b*-PCHC-PU multiblock copolymers in dry and water-swollen state.

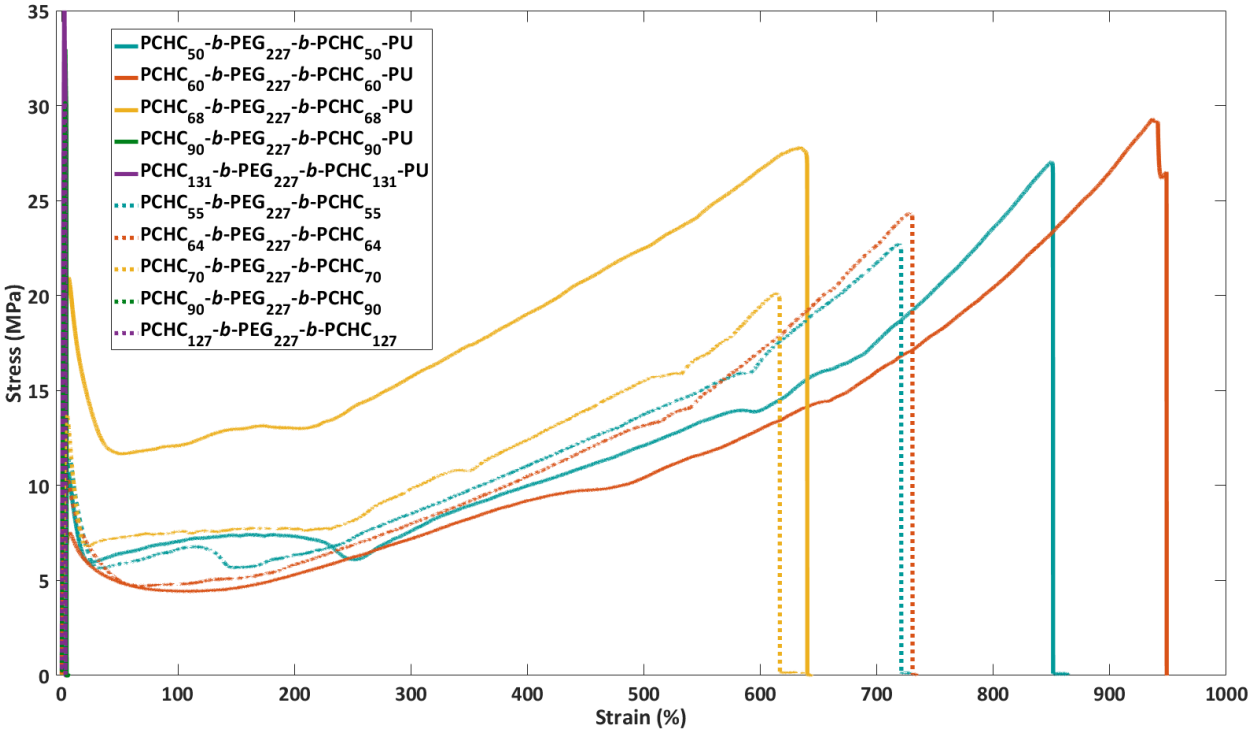

Figure S 17: Stress-strain curves of the PCHC-*b*-PEG-*b*-PCHC triblock copolymer and PCHC-*b*-PEG-*b*-PCHC-PU multiblock copolymers in dry state.

4. Extrusion

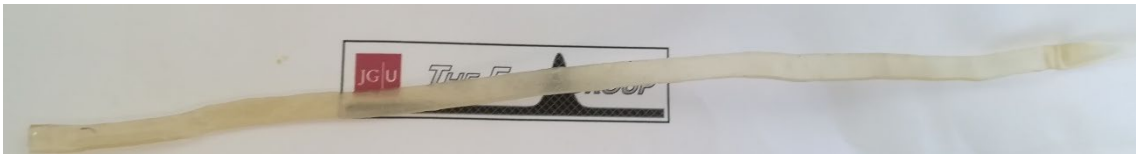

Figure S 18: Extruded filament at 140 °C with 140 min^{-1} without any additives.

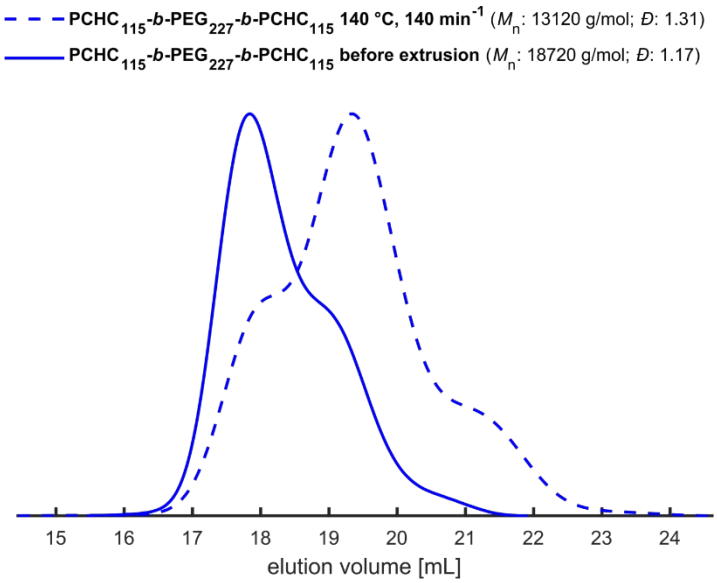

Figure S 19: SEC curves of PCHC$_{115}$-*b*-PEG$_{227}$-*b*-PCHC$_{115}$ before extrusion (straight line) and after extrusion (dashed lines) (eluent: DMF, standard: PEG).

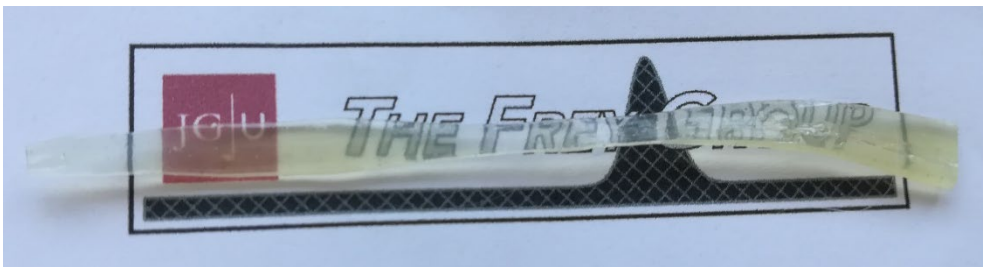

Figure S 20: Extrudate filament at 140 °C with 140 min^{-1} extrusion speed with 500 ppm Irganox®.

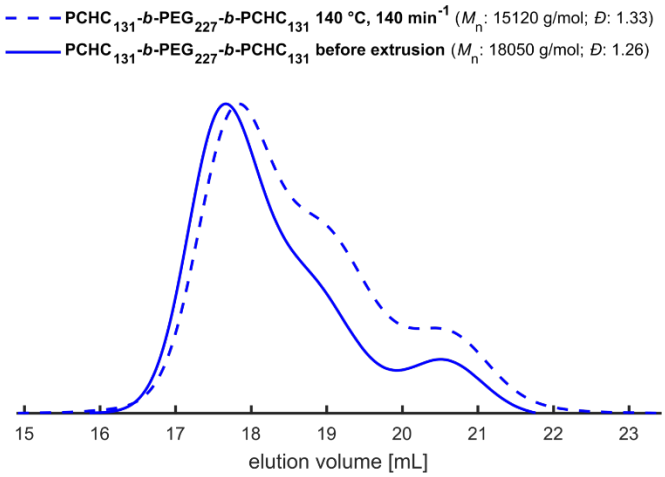

Figure S 21: SEC curves of $PCHC_{131}$-*b*-PEG_{227}-*b*-$PCHC_{131}$ blended with 500 ppm Irganox® before extrusion (straight line) and after extrusion (dashed lines) (eluent: DMF, standard: PEG).

Figure S 22: Extrudate filament at 140 °C with 140 min^{-1} extrusion speed with 4 wt% of asparagine.

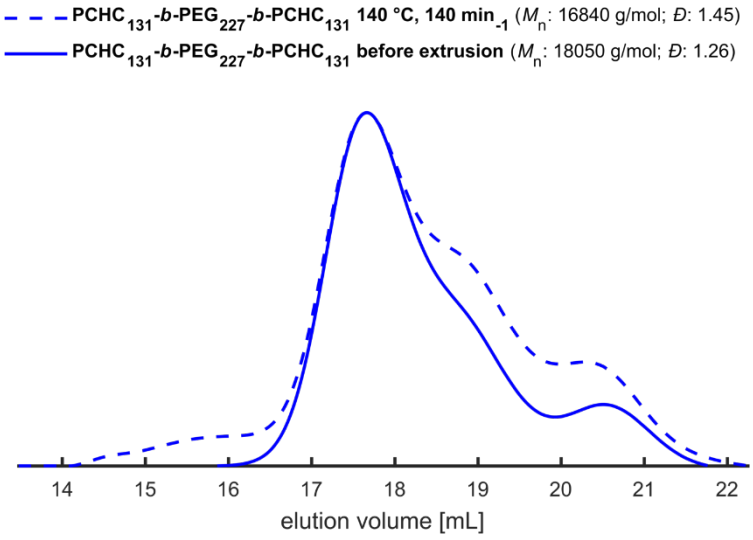

Figure S 23: SEC curves of $PCHC_{131}$-*b*-PEG_{227}-*b*-$PCHC_{131}$ blended with 4 wt% asparagine before extrusion (straight line) and after extrusion (dashed lines) (eluent: DMF, standard: PEG).

CHAPTER 5

Direct Synthesis of Cationic Polycarbonates from CO_2 and Methylated Glycidyl Amines

CHAPTER 5

Direct Synthesis of Cationic Polycarbonates from CO_2 and Methylated Glycidyl Amines

Christina Gardiner[a], Caroline Bockhard[a], Holger Frey[a*]

[a]Department of Chemistry, Johannes Gutenberg University, Duesbergweg 10-14, 55128 Mainz, Germany

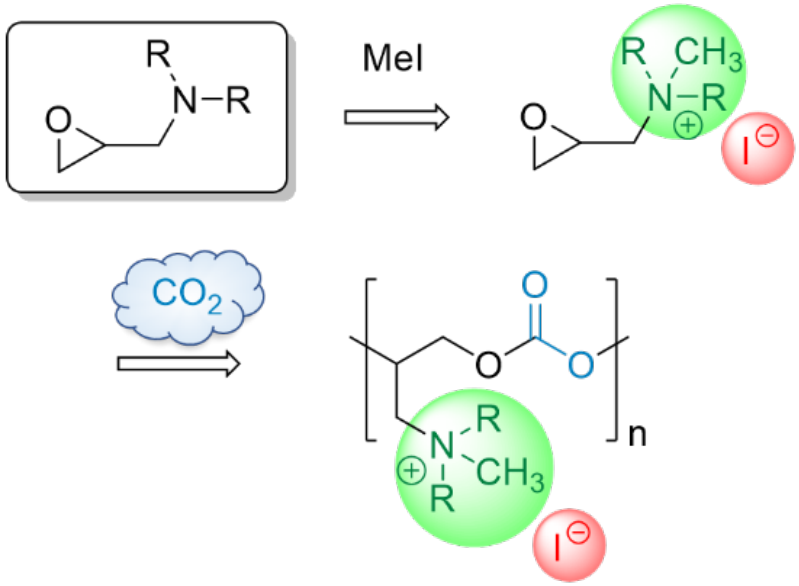

ABSTRACT

Direct copolymerizations of cationic glycidyl amines with CO_2 was achieved, using a binary cobalt salen catalyst system; polycarbonates with quaternary ammonium groups as a side group were successfully synthesized. This was confirmed by NMR, IR, and SEC analysis. The determination of the molar mass of the polymers was challenging due to the interactions of the cationic side groups with the column material. The change of the counterions from I^- to TFA^- (matching the counterion of the salt used as an additive in the HFIP eluent) results in a lower interaction and therefore in more probable molar masses. The thermal properties of the polymers were determined *via* DSC, revealing T_gs of 0 °C (P(PiGA[I])C)) and 10 °C (P(DEGA[I])C)). The polymers with TFA as a counterion showed lower T_gs of -14 to -30 °C. Moreover, a weak melting point at 63 °C (probably caused by H-bonding between the cationic moiety and the carbonyl of the backbone) was detectable, in all polymers with TFA as counterion.

INTRODUCTION

The majority of polymers that are used in everyday life obtain their carbon building blocks from fossil fuels.[1] For polycarbonates, however, the use of CO_2 is a more resource-friendly and inexpensive alternative. Due to the combustion processes in industry, carbon dioxide is an easily accessible compound that is available in large quantities.[2] Therefore, the development of new synthesis routes and materials involving the non-toxic C1 building block is a promising project to utilize CO_2. For example, the synthesis of aliphatic polycarbonates from epoxides with CO_2 is a promising alternative to complete fossil-based polymer synthesis. In addition to the attractive synthesis from carbon dioxide, their biodegradability and biocompatibility also qualify them as potential materials for life sciences such as cationic polyelectorlytes.[3–8]. Cationic polyelectrolytes carry positive charges in their backbone or side chain.[9] Because of their positive charge, they can form electrostatic complexes with anionic biomolecules, nucleic acids, and proteins. This makes them particularly interesting for potential applications in gene delivery or drug delivery systems.[10] Their antimicrobial and antioxidant behavior qualify them for therapeutic applications.[10] The antibacterial behavior is related to the Coulomb interaction between the positive charge of the polymers and the negatively charged cell membrane proteins of the bacterial cells. In the case of Gram-positive bacteria, the polymers interact with teichoic acid and in the case of Gram-negative bacteria with phospholipids of the outer membrane.[11] The interaction allows the polymers to penetrate the outer lipid layer and thus destroys the membrane, leading to the death of the bacterium. They are also used as flocculants for water treatment.[12] For most cationic polyelectrolytes, the cationic charge is introduced *via* quaternary ammonium compounds, as these are known for their stability and easy preparation.[13]

Cationic polyelectrolytes can be synthesized *via* two routes, either v*ia* post-polymerization modification of uncharged polymers or *via* direct polymerization of cationic monomers. The direct variant is almost exclusively carried out *via* radical polymerization, since the charge of the monomers has the least influence there.[13,14] The disadvantage to this polymerization method, however, is that the resulting polymers exhibit a nonpolar backbone, which is not biodegradable. In case of the post-polymerization modification route, polar amino-functional polyethers were synthesized *via* anionic ring-opening polymerization (AROP) and then converted to cations by quaternization of the amino group.[15] However, polyethers are also not biodegradable. Polycarbonates on the other hand are both biodegradable and biocompatible, making them ideal candidates as a basis for cationic polyelectrolytes.[4,8]

Positively charged polycarbonates have also been obtained mostly *via* post-polymerization modification to date. The polycarbonates are usually prepared from cyclic carbonates with good leaving groups. A quaternary ammonium function can then be integrated into the side chain *via* a substitution reaction.[16,17] For polycarbonates produced from CO_2 and epoxides, monomers with a double bond, such as limonene oxide, are used. An amino function can be incorporated into the side chain of the double bond *via* a thiol-ene-click reaction, which in turn can be quaternized.[18] Direct polymerization of glycidyl amines and subsequent quaternization has not yet been achieved by this polymerization route, since amines deactivate the necessary catalysts by coordination. In general, the problem with the preparation of quaternary ammonium salts on the side chains of polycarbonates is that full conversion is often not achieved.[19] So far, cationic polyelectrolytes based on polycarbonates have only been prepared by subsequent modification of the already polymerized aliphatic polycarbonates (APC).[19] Direct polymerization of cationic monomers to positively charged polycarbonates is known to date in only two cases. On the one hand, cationic cyclic carbonates were successfully polymerized *via* ROP, and on the other hand, Lena Kunze from the Frey group was able to copolymerize methylated amino glycidyl ethers with CO_2 as part of her dissertation.[19,20]

The aim of this work is the direct synthesis and characterization of aliphatic polycarbonates with a positively charged side chain.

RESULTS AND DISCUSSION

Monomer synthesis and characterization

For the synthesis of amino-functional polycarbonates, both glycidyl amines and glycidyl amino ethers can be used. These two substance classes are also utilized for the synthesis of multifunctional polyethers.[21,22] Amino-based polyethers are mainly applied as drug transport systems and as pH- and temperature-dependent coatings.[23,24] Both the glycidyl amines and the glycidyl amino ethers are prepared from epichlorohydrin, which can be converted to the desired product in a nucleophilic substitution reaction. Amines as nucleophiles lead to glycidyl amines and amino alcohols to glycidyl amino ethers.[23,25] In this work, glycidyl amines were used to synthesize polycarbonates since Kunze et al. already synthesized polycarbonates based on glycidyl amino ethers with a low bactericidal effect.[20] Piperidinyl glycidyl amine (PiGA) and *N,N*-diethyl glycidyl amine (DEGA) were used as monomers. Both show a similar structure, PiGA shows a cyclic sidechain and DEGA two aliphatic groups (Figure1).[23,24] Thus, it can be compared whether the

structure of the ammonium salt (aliphatic or cyclic) influences the polymerization and the polymer properties.

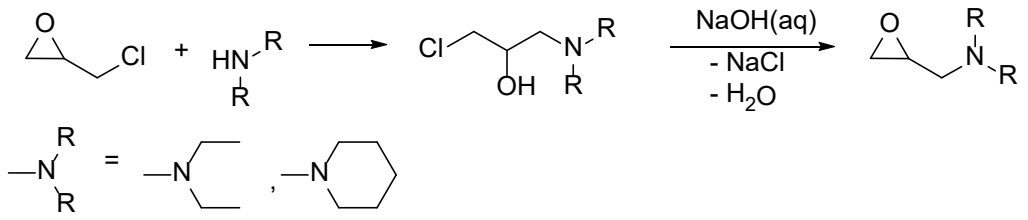

Scheme 1: Synthesis of the glycidyl amines.

The synthesis of the glycidyl amines was carried out according to Herzberger *et al*.[23,26] In this process, epichlorohydrin reacts with the corresponding secondary amine in a basic environment (Scheme 1). The ^{1}H NMR spectra of PIGA and DEGA reveal a successful synthesis of both monomers since all signals could be assigned and show the right proton amount (Figure S 1+3). The effective quaternization of the two glycidyl amines *via* methylation using methyl iodide is confirmed *via* the NMR analysis (Figure S 2+4).

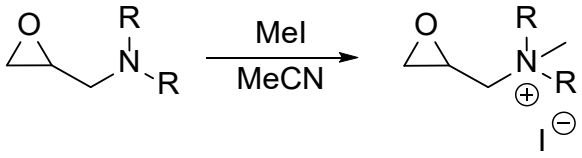

Scheme 2: Quaternization of the glycidyl amines.

Since the methylated glycidyl amines are not soluble in $CDCl_3$, the NMR spectra were measured in DMSO-*d6*. Due to the quaternization of the amine, the signals in the ^{1}H NMR shifted to lower fields (Figure S 2+4). To demonstrate that the shift is not influenced using DMSO-*d6* instead of $CDCL_3$, a ^{1}H NMR spectrum of PiGA was recorded in DMSO-d*6* revealing the same shift to lower field after quaternization (Figure S 5). Moreover, a new singlet at 3.06 ppm is detectable belonging to the introduced methyl group (Figure S 2+4).

Polymer synthesis and characterization

To synthesize polycarbonates from the previously prepared cationic monomers, PiGA[I] and DEGA[I] were copolymerized with CO_2 as shown in Scheme 3. A binary catalyst system, (*R,R*)-Co(Salen)Cl was used together with [PPN]Cl as cocatalyst (Scheme S 1).

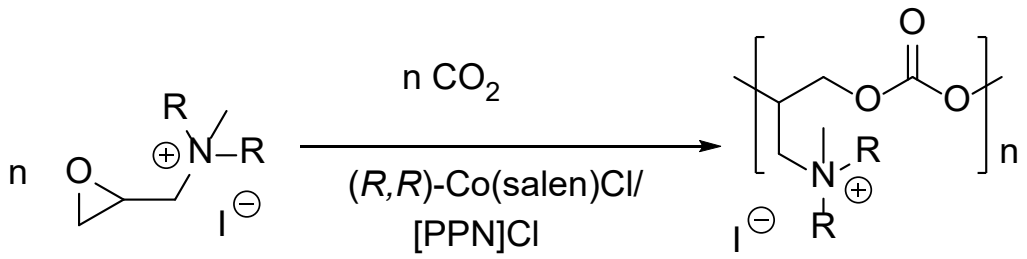

Scheme 3: Polymerization of PiGA[I] with CO_2

Before polymerization, the solubility of the monomers was tested. The quaternary monomers are soluble in acetonitrile (ACN), dichloromethane (DCM), and dimethylformamide (DMF). Since Kunze et al. used DCM as solvent in the copolymerization of amino glycidyl ethers, we also used DCM in the first experiments, which resulted in 26% P(PiGA[I]C) and 23% P(DEGA[I]C) conversion. This was caused by the low solubility of the resulting polymers in DCM.

Table 1: Overview of the P(PiGA[I]C) homopolymers.

sample	solvent	catalyst[a]	*T*	conversion[b]	yield[c]	M_n[d]	P_n[d]	$Đ$[d]
		mol%	°C	%	%	g/mol		
P1	DCM	0.6	30	26	25	1 570	5	1.06
P2	DCM	0.4	30	23	25	1 550	5	1.06
P3	DMF	0.6	30	88	89	1 420	4	1.06
P4	DMF	0.7	30	88	90	1 310	4	1.07
P5	DMF	0.4	30	83	81	790	2	1.13
P6	ACN	0.4	30	15	20	940	3	1.12
P7	DMF	0.3	30	39	45	1 280	4	1.07
P8	DMF	0.2	30	75	78	2 510	8	1.08
P9	DMF	0.1	30	35	42	840	2	1.14
P8	DMF	0.2	30	75	75	2 510	8	1.08
P10	DMF	0.2	50	92	95	5 90	2	1.16

[a]Related to the amount of PiGA[I]. [b]Calculated by ^{1}H NMR. [d]Measured *via* SEC (eluent: HFIP, standard: PMMA).

The polymerization rate is diminished significantly, if the monomer and growing polymer chain are in different phases. The polymerization in ACN did not improve conversions, but the polymerization in DMF enhanced the conversion to 80%. The conversion of the polymerizations can be calculated using ^{1}H NMR spectra, which are listed in Tables 1 and 2. For the calculation, the signal of the proton next to the carbonate moiety (c) and the epoxide signals at 2.91 ppm and 2.71 ppm were used (Figure S 6). The polymerization of DEGA[I] with CO_2 and PiGA[I] with CO_2 was

carried out at 30 °C for 70 h. Table 2 shows the conversion rates, the number averages of the molar masses (M_n), the degree of polymerization (P_n), and the dispersity ($Đ$), which were measured by SEC. The ^{13}C NMR spectra reveal a signal A at 153.89 ppm indicating the incorporation of the carbon dioxide in P(PiGA[I]C) and P(DEGA[I]C), correspondingly (Figure S 8+15).Cyclic carbonates can be formed as a side reaction of the polymerization instead of the polymer. However, the formation of the undesired by-products could be suppressed by the low reaction temperature of 30 °C (as shown in the IR spectrum (Figure S 12)). The band at 1791 cm^{-1} is typical for the carbonate group of the polymer backbone. Commonly, polycarbonates exhibit a wavenumber of 1750 cm^{-1}.[27] However, the charged side chain can cause a shift of the band to higher wavenumbers, as also shown in the work of Kunze.[20] Following her work, it is also assumed in this case that due to the quaternary ammonium salt the carbonate band of the polymers is located at 1790 cm^{-1}, which is not caused by cyclic carbonates. The carbonate band of the cycles is usually observed at above 1800 cm^{-1}.[7,28] A further increase in reaction temperature from 30 °C to 50 °C (sample 10) did not lead to cyclic carbonates (Figure S 13). The molar masses were determined *via* SEC with HFIP as eluent and PMMA as standard (Figure S 19 and S 20). Potassium trifluoroacetate was added to the eluent to minimize interactions between packing material and sample. The degrees of polymerization determined in this way ranged from 2 to 8, and no correlation between molar masses and catalyst concentration was found. It was expected that the molar masses would increase with decreasing catalyst concentration since a small number of polymer chains can be started due to fewer catalyst complexes and chloride ions of the cocatalyst, which serve as initiators of polymerization. However, this assumption could not be validated for either P(PiGA[I]C) or P(DEGA[I]C). Also, the measured molar masses are smaller than expected and more in line with those of oligomers. However, it is important to note that the synthesized polymers are cations. Due to the positive charge on the side chain, interactions with the column material can occur, increasing the elution time and resulting in a molar mass distribution at lower masses. The shift of the SEC curves to the side reinforces this thesis (Figure S 19+20). In a repeat measurement of P17, it was shown that the measurements are not reproducible (Figure 1).

Table 2: Overview of the P(DEGA[I]C) homopolymers.

sample	solvent	catalyst[a]	conversion[b]	yield	M_n[d]	P_n[d]	$Đ$[d]
		mol%	%	%	g/mol		
P11	DMF	0.6	94	93	920	3	1.11
P12	DMF	0.4	90	87	750	2	1.14
P13	DMF	0.3	90	91	1 310	4	1.06
P14	DMF	0.2	83	87	1 200	4	1.07
P15	DMF	0.6	89	93	750	2	1.15
P16	DMF	0.4	85	82	690	2	1.15
P17	DMF	0.1	91	92	660	2	1.15

[a]Related to the amount of PiGA[I]. [b]Calculated by ^{1}H NMR. [d]Measured *via* SEC (eluent: HFIP, standard: PMMA).

This also confirms the hypothesis that unpredictable interaction between polymer and column greatly reduces the validity of GPC measurements. Difficulties in determining the molecular weight of cationic polyelectrolytes *via* SEC are also frequently reported in the literature. [29–31]

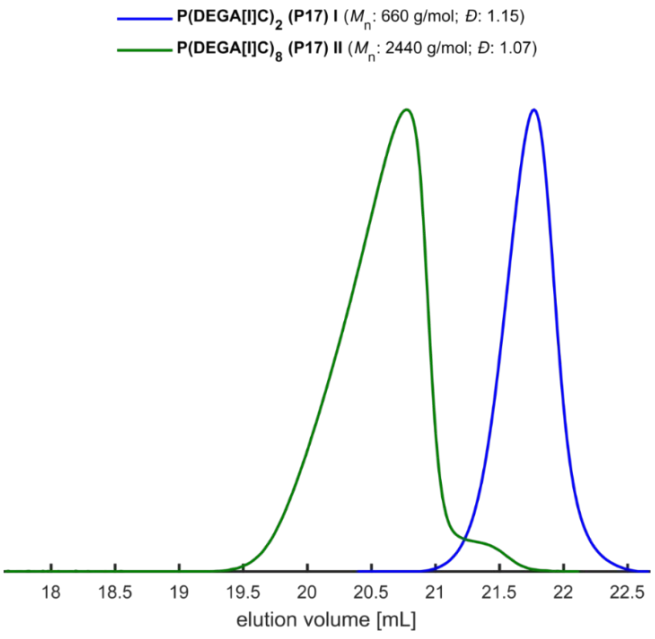

Figure 1: SEC curves (eluent: HFIP, standard: PMMA) of the same polymer P17 in different measurements. The blue SEC curve shows the first measurement. The green SEC curve shows the second measurement.

However, in 2013, Matyjaszewski et al. found a minimizing effect using a salt with the same counterion as the polymer in the eluent. This improves the flow behavior through the column due to interactions between the column and the free ions instead of polymeric (poly)cations.[29] Since

it was difficult to replace the salt with lithium iodide in the available GPCs, the iodide of the polymers was replaced with trifluoroacetate (TFA) and KTFA was used as an additive for the eluent.

For this purpose, the polymer and silver trifluoroacetate were each dissolved separately in water and then both solutions were combined. The insoluble silver iodide precipitated according to the HSAB principle as a yellow precipitate, which could be separated from the polymer solution by filtration. After the removal of the water, a viscous polymer was obtained.

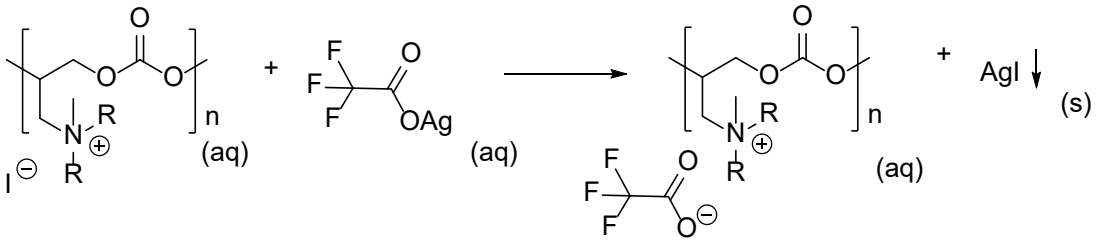

Scheme 4: Anion exchange of P(PiGA[I]C) or P(DEGA[I]C) to P(PiGA[TFA]C) or P(DEGA[TFA]C), respectively.

Successful ion exchange was confirmed by recording ^{19}F NMR spectra (Figure S 21+22), where for both P(PiGA[TFA]C) and P(DEGA[TFA]C) the singlet at -74 ppm can be assigned to the $-CF_3$ group of the trifluoroacetate. SEC measurements were conducted with these polymers. The results are listed in Table 3 and compared with the results of the polymers with iodide as a counterion. The average molar masses for the polymers with TFA are approx. 1 000 g/mol higher than with iodide, and it can be assumed that the interaction between the column and cationic polyelectrolytes could be reduced. However, a repeat measurement also showed that the molar masses differ, although the difference was 540 g/mol with TFA, which is significantly less than with iodide, where the difference was 1780 g/mol. However, the deviation indicates that the interactions cannot be completely prevented. Nevertheless, the GPC measurements with TFA lead to more reasonable results. Only a slight correlation between catalyst concentration and molar mass can be seen. The samples that were modified with a higher concentration of Co(Salen)Cl and [PPN]Cl have lower molar masses, but the difference is only in the order of 60-280 g/mol, which may also be in the range of the measurement error that was also found in the repeat measurement. Furthermore, since no absolute method confirms the molar masses measured by SEC, it is not possible to make a definite statement about the order of magnitude of the molar mass.

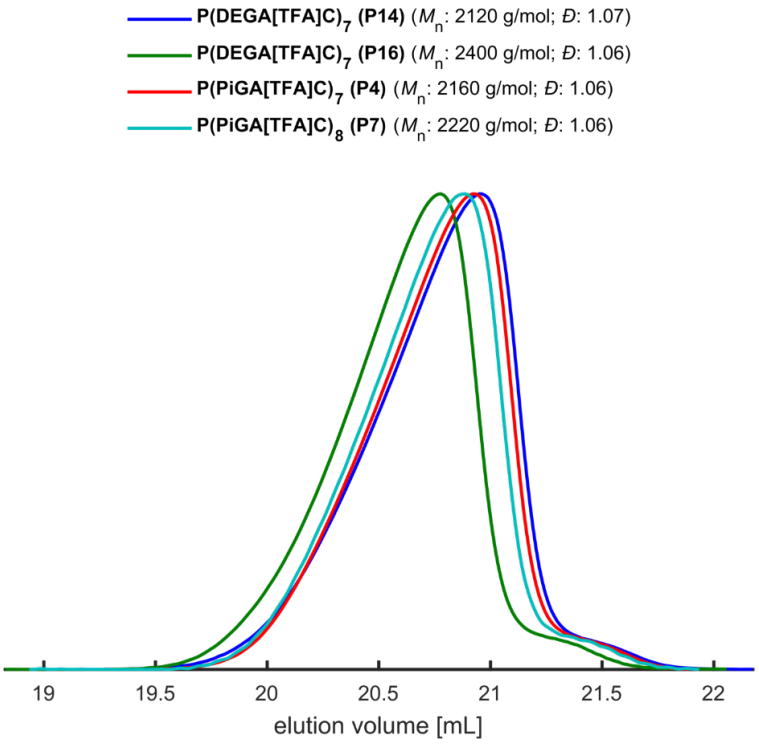

Figure 2: SEC curve of the polymers with TFA as counter ion (eluent: HFIP, standard: PMMA).

Table 3: Overview of the polymers with TFA as counterion.

sample	catalyst[a]	M_n[I][d]	P_n[d]	$Đ$[d]	M_n[TFA][d]	P_n[d]	$Đ$[d]
	mol%	g/mol			g/mol		
P4 (PiGA)	0.7	1 310	4	1.07	2 120	7	1.06
P7 (PiGA)	0.3	1 280	4	1.07	2 400	8	1.06
P14 (DEGA)	0.2	1 200	4	1.07	2 220	7	1.07
P16 (DEGA)	0.4	690	2	1.15	2 160	7	1.06

[a]Related to the amount of PiGA[I]. [d]Measured *via* SEC (eluent: HFIP, standard: PMMA).

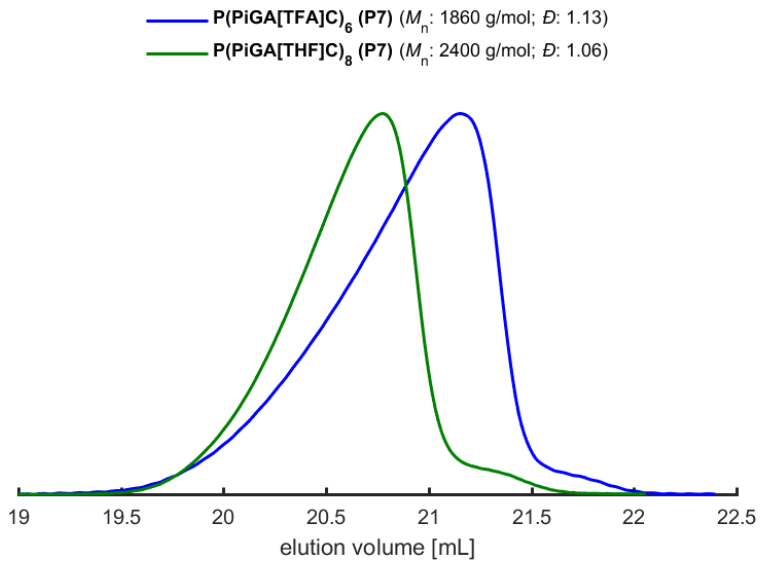

Figure 3: SEC curves (eluent: HFIP, standard: PMMA) of P(PiGA[TFA]C) (P7) at different measurements.

Further investigations using vapor pressure osmometry (VPO) (Figure S 23–25) or MALDI-ToF spectrometry (Figure S 26–28) led to no successful determination of the molar masses of the polymers.

Thermal characterization

Differential scanning calorimetry (DSC) measurements were performed to determine glass transition temperatures (T_g) and melting points (T_m). The results of the measurements are listed in Table 4. The specimens P1, P2, and P6 are polymers of PiGA[I] and CO_2 and differ only in their molar masses. Therefore, it is also reasonable that the glass temperatures vary only by a few degrees. For P4, unlike the other two, no clear melting point was evident. However, the melting points at P(PiGA[I]C) were also only observed in the first heating curve (Figure S31+32). Kunze et al. observed the same phenomenon in the thermal behavior of poly(methyl dibutyl amino ethanol glycidyl ether iodide carbonates) P(MeDButEAGE[I]C). These cationic polyelectrolytes showed T_ms between 97 and 104 °C in the first heating curve, but no recrystallization occurred upon cooling (even at heating rates of 1 K/min), and the no melting point in the second heating. In addition, they performed XRD measurements that revealed a high degree of crystallinity in their structures. They hypothesized that the melting point in the first heating curve was due to the H-bonding between the carbonyl group and the catatonically charged groups.[20] The lack of recrystallization after cooling and the absence of a melting point in the second heating curve support this

hypothesis and indicate a low-order amorphous polymer. The amorphous region results from the flexible backbone known for aliphatic polycarbonates.[7,16]

Table 4: Thermal properties of the synthesized polymers with iodide as counterion.

sample	M_n	T_g[a]	T_m[b]	ΔH_m[b]
	g/mol	°C	°C	J/g
P1 P(PiGA[I]C)	1570	0	114	51
P2 P(PiGA[I]C)	1550	-1	114	54
P4 P(PiGA[I]C)	1310	1	-	-
P11 P(DEGA[I]C)	920	-14	-	-
P12 P(DEGA[I]C)	750	-11	-	-
P14 P(DEGA[I]C)	1200	-7	-	-

Heating rate of 10 K/min. [a]Second heating curve. [b]First heating curve

In the case of the polymers from DEGA[I] and CO_2 T_gs in a range of -7 to .14 °C were determined. However, in contrast to P(PiGA[I]C,) no melting point was detected in any of the measurements, which means that it has no crystalline components and is thus purely amorphous and probably the interaction of the Carbonyl and the cationic moiety is somehow hindered. The T_{gs} of P(PiGA[I]C) are higher than that of P(DEGA[I]C) due to the more flexible side chains of the ethyl groups (Figure S 29+32). The ring in P(PiGA[I]C) in the side chain limits the flexibility thus decreasing slightly the free volume of the polymer. This increases the glass transition temperature.

To investigate the influence of the counterion on the thermal properties of the polymer, DSC measurements of the polymers with TFA as counterion were performed. The results of the measurements are documented in Table 5. Significant changes in the thermal properties were observed. While for P(PiGA[I]C) only one melting point occurs in the first heating curve and none could be measured for P(DEGA[I]C), for both polymers with TFA as counterion the melting points in the first and second heating curves are measurable (Figure S 30+33). These occur at 61-63 °C, 50 °C below that of P(PiGA[I]C) and show a low degree of melting enthalpy (ΔH_m) of 2-4 J/g. This again leads to the hypothesis that the melting points are caused by the interaction of the carbonyl and the cationic moieties.[20] Since TFA^- is bigger than I^- the H-bonding interaction is interrupted resulting in lower ΔH_ms.[20] Their melting points are well below 100 °C, so the polymers with TFA can be classified as polyionic liquids, which could explain the change in their nature from a powder

to an oily solid.[32] The low melting enthalpy of 2-4 J/g implies only very small crystallinity, while the enthalpy of P(PiGA[I]C) at 51-54 J/g suggests much larger fractions in ordered state.

Table 5: Thermal properties of the synthesized polymers with TFA as counterion.

sample	M_n g/mol	T_g[a] °C	T_m[b] °C	ΔH_m[b] J/g
P4 P(PiGA[TFA]C)	2120	-45	63	4
		-29	63	3
P7 P(PiGA[TFA]C)	2400	-14	62	2
P14 P(DEGA[TFA]C)	2220	-30	63	4
P16 P(DEGA[TFA]C)	2160	-29	61	2

Heating rate of 10 K/min. [a]Second heating curve. [b]First heating curve.

The glass transition temperatures of the polymers with different counterions also vary significantly. The replacement of the iodide with TFA results in decreased T_gs. The decrease in T_g observed for the polymers with TFA is related to the size of the anion. TFA has a larger ionic radius than iodide, which enhances the free volume of the polymers and results in a decrease in the glass transition temperature.[33] In the case of P(DEGA[TFA]C), the glass transition temperatures are very close to each other, while those of P(PiGA[TFA]C) exhibit a 30 °C difference. The reasons for this difference are unclear. When P4 was measured again, a T_g at -29 °C was determined. Due to the deviations of the T_g, further measurements of polymers from PiGA and with TFA as anion are necessary.

Water solubility

To show that the cationic polyelectrolytes are soluble in water, a ^{1}H NMR spectrum of P(PiGA[I]C) in D_2O was recorded (Figure 4). The integrals are based on the normalization of signal c to 1.00. Signal b partially overlaps with the solvent signal, so integration of this signal does not yield a useful result. All signals seen in the ^{1}H NMR spectra recorded in DMSO-*d6* can also be found in D_2O (Figure 4 and Figure S 7).

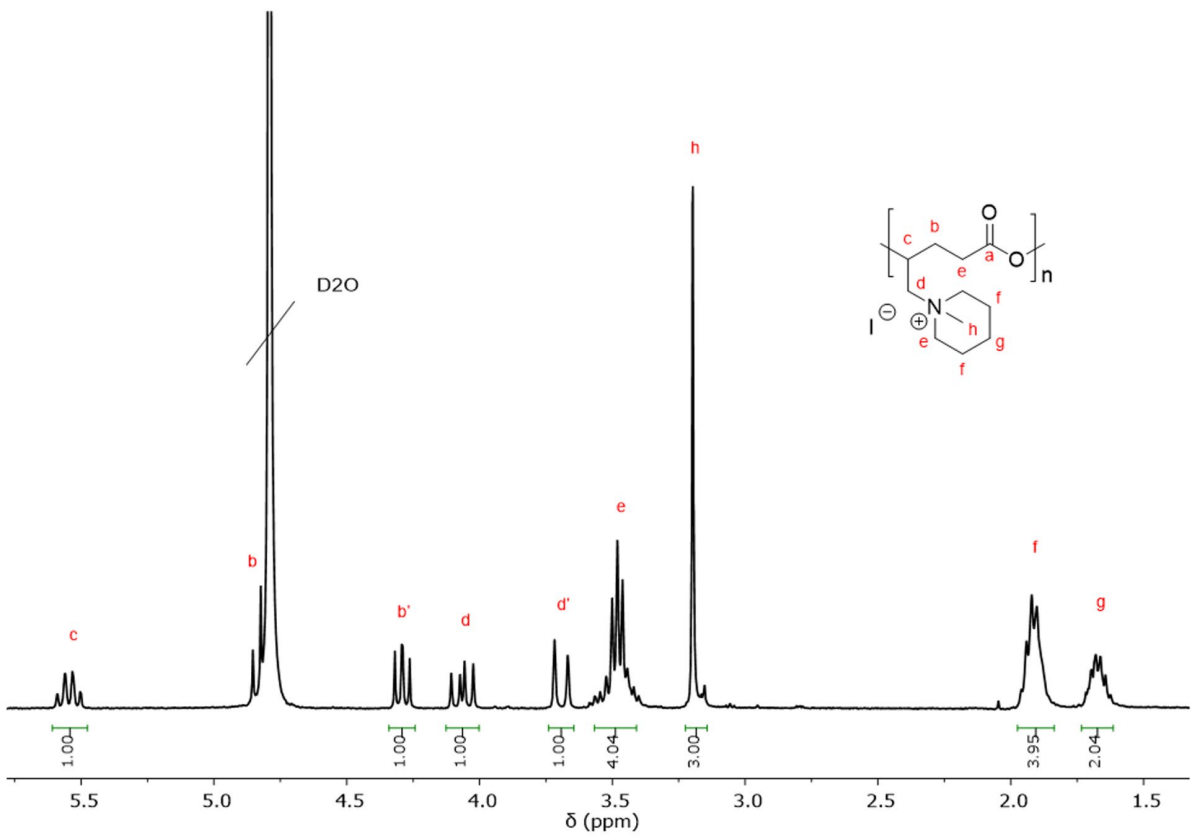

Figure 4: ^{1}H NMR spectrum (D_2O, 300 MHz) von P(PiGA[I]C) to show the water solubility.

Degradation in an acidic environment

To observe the degradation of the prepared polycarbonates in an acidic environment, 0.35 mL of concentrated DCl solution (36%) was added to a polymer sample of P(DEGA[I]C) (P13) dissolved in 0.35 mL of deuterated water. The degradation of the polycarbonate in the acidic environment is shown in Scheme 5. *Via* backbiting, a cyclic carbonate (A) was cleaved from the polymer chain. The cyclic carbonate reacts by hydrolysis to a diol (B), releasing CO_2. This stepwise deconstruction could also be detected in P13. Approximately 1 h after the addition of the deuterated hydrochloric acid, gas evolution could be observed, revealing the release of CO_2 during a successful degradation reaction. 96 h after the addition of the acid, a ^{1}H NMR spectrum was recorded (Figure 5).

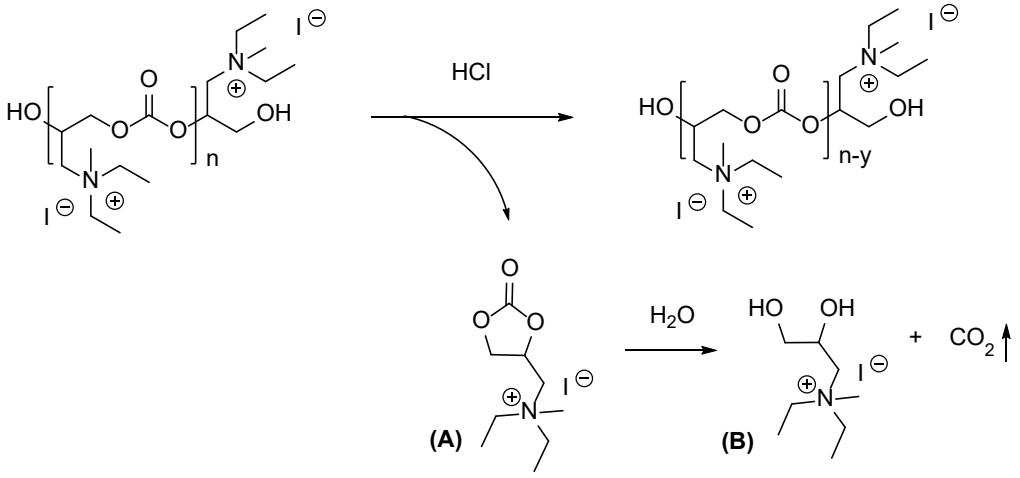

Scheme 5: Degradation reaction of P(DEGA[I]C) in an acidic environment under formation of cyclic carbonates (A), which reacts to diols (B) with elimination of CO_2.

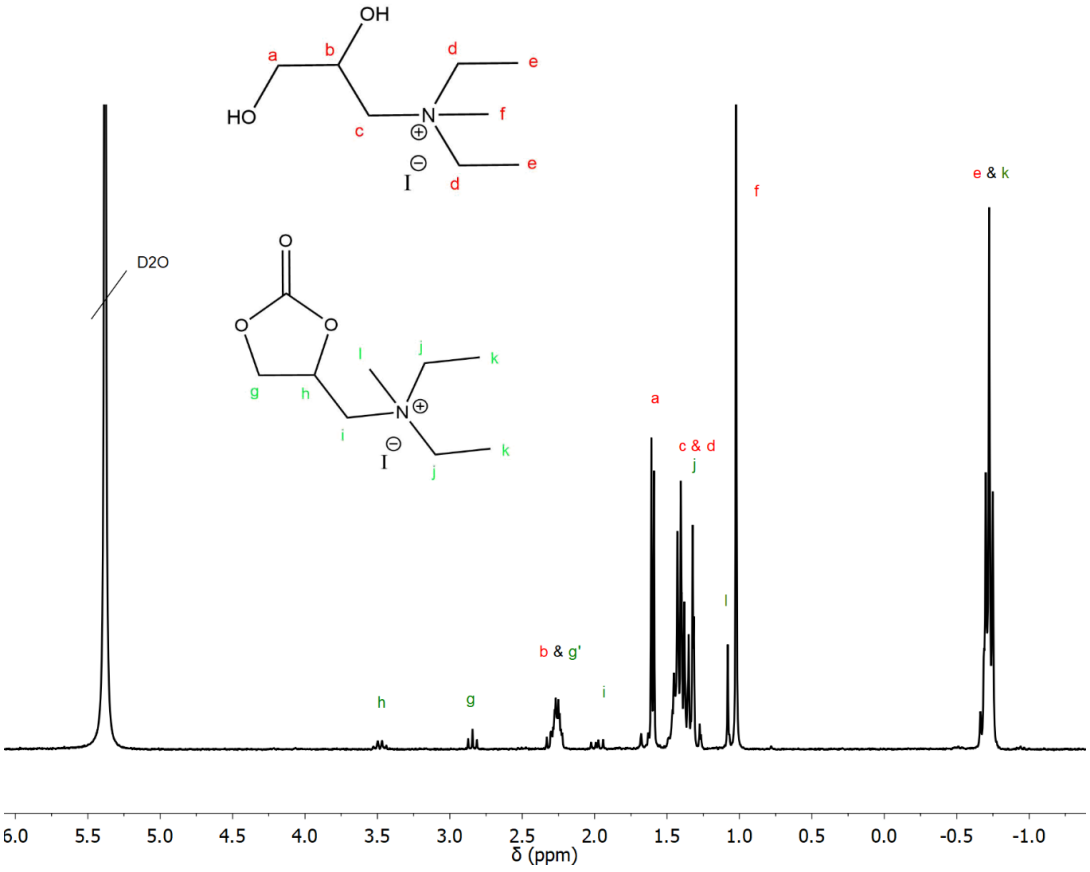

Figure 5: ^{1}H NMR spectrum (D_2O/DCl, 300Hz) of the degraded P13, recorded 96 h after addition of DCl (36%, 0.35 mL).

In Figure 5, most of the signals can be assigned to diols (signals a-f). The signals g-l belong to the remaining cyclic carbonates that have not yet been converted to diols. The signals are shifted by

the low pH, which is why the signals of the methyl group show a negative chemical shift (-0.75 ppm). The fact that the signals of the cyclic carbonates are not those of the polycarbonate is shown by the comparison of a ^{1}H NMR spectrum recorded immediately after addition of the DCl with the ^{1}H NMR spectrum after 96 h (Figure S 30). Although the resolution of the D_2O signal of the spectrum after one minute is not as good as in the spectrum after 96 h, a change in the chemical shift of the carbonate signals can still be observed. Due to the formation of the cyclic product, the signals of the corresponding protons are high field shifted. After 96 h, no signals appear in the region of the polycarbonates, but only in the region of the cycles and the diols.

CONCLUSION

The aim of this work was to directly synthesize aliphatic polycarbonates with a charged side chain from cationic glycidyl amines and CO_2. Literature-known glycidyl amines selected for this purpose, piperidine glycidyl amine and *N,N*-diethyl glycidyl amine were successfully prepared and subsequently quantitatively methylated.[23,24] It was shown that the cationic monomers could be copolymerized directly in a coordinative ring-opening polymerization with CO_2. Thus, a successful alternative to post-polymerization modifications was presented.

The polymers were characterized by IR and NMR spectroscopy revealing a successful synthesis of polycarbonates. Several methods were used to determine the average molecular masses, but vapor pressure osmometry and MALDI-ToF-MS did not yield usable results. Even *via* SEC measurements, plausible molecular weights could only be obtained after an exchange of the counterion from iodide to trifluoroacetate, which, however, could not be verified by any absolute method so far. The thermal properties of the cationic polyelectrolytes were determined by DSC measurements. While for P(PiGA[I]C) both a glass transition and a melting point could be detected exclusively in the first heating curve, P(DEGA[I]C) showed only a glass transition but no melting point. For the polymers with TFA as counterion, a melting point and a glass transition could be observed for both cationic polyelectrolytes. The melting point of P(PiGA[TFA]C) and P(DEGA[TFA]C) has been observed in both the first and second heating curves, but each has lower ΔH_m than the polymers with iodide. These melting points could be caused by H-bonding interactions of the carbonyl function with the cationic moiety rather than by ordering and crystallization.[20] In addition, it has been revealed that the prepared polycarbonates can degrade in an acidic environment under the formation of diols, presumably *via* formation of cyclic carbonates as intermediates. This again proofs of the successful synthesis of polycarbonates

instead of cyclic carbonates. However, it cannot be excluded that oligomers and not polymers were synthesized.

Outlook

In this work, it was demonstrated that the cationic monomers can be polymerized directly into polycarbonates avoiding post-polymerization modifications. However, the determination of the molar mass was a major challenge. Until now, reasonable molar mass distributions could only be measured by anion exchange to match the salt of the SEC eluent. To simplify this step as well and to be able to completely circumvent post-polymerization modifications, an exchange of the ion would already be possible in the monomer. Polymerization with TFA instead of iodide must be investigated. So far, the antibacterial efficiency has not been investigated on both Gram-positive and Gram-negative bacterial strains. The results of these investigations are necessary to discuss possible applications for the synthesized cationic polycarbonates. It would be useful to test both polymers with iodide and with TFA as counterion to understand the influence of the anion on potential antibacterial properties. If it is found that the cationic polymers can destroy the cell membranes of bacteria, they could conceivably be used as a water-soluble bactericide in the medical field, among other applications.

Experimental Section

Materials

All solvents and reagents were applied as acquired unless otherwise stated. Carbon dioxide (>99.999%) was achieved from Westfalen AG (Münster, Germany). Bis(triphenylphosphine)iminium chloride ([PPN]Cl) was received from abcr GmbH. (*R,R*)-(salcy)-Co(III)Cl was prepared as described by Ford *et al*.[34] All solvents were purchased from Sigma Aldrich, Fischer Chemical (Pittsburgh, PA, USA), and Honeywell (Morris Plaines, NJ, USA) and used without further purification. All reagents were acquired from Sigma Aldrich, Arcos Organics (Pittsburgh, PA, USA), Alfa Aesar (Kandel, Germany), or TCI (Oxford, UK). Deuterated solvents were purchased from Deutero GmBH (Kastellaun, Germany).

Characterization

NMR Analysis. ^{1}H NMR spectra at 300 MHz and ^{13}C NMR spectra at 75 MHz were recorded on a Bruker Avance III HD 300 (5 mm BBFO-Head with *z*-gradient) at 23 °C. The spectra are referenced internally to the residual proton signal of the deuterated solvent.

Size exclusion chromatography (SEC). SEC measurements were completed over a PFG column (particle size: 7 µm, porosity: 100 and 1000 Å) and with a JASCO G 1362A RID RI detector. Hexafluoro isopropanol (HFIP) with potassium trifluoroacetate (3 g/L) was used as the flow medium. The flow rate was 0.8 mL/min at a temperature of 40 °C. A toluene standard was added to the samples as a reference, and the calculation was of the molecular weight was based on a PMMA standard from Polymer Standards Services GmbH (PSS). The SEC curves shown were generated using *MatLab*.

Differential scanning calorimetry (DSC). A Perkin Elmer 8500 thermal analysis system with Elmer Thermal Analysis Controller TAC7/DX was used for the DSC measurements. The temperature range in which the polymers were analyzed was -95 °C to 170 °C for P(PiGA[I]C)/P(DEGA[I]C) and -100 °C - +100 °C for P(PiGA[TFA]C)/P(DEGA[TFA]C), and the measurements were performed in two cycles. The temperature program for the measurements is given below:

1. heating from 30 °C to 170 °C (iodide)/ from 30 °C to 100 °C (TFA) at 10 C/min.

2. hold temperature at 170 °C (iodide)/ 100 °C (TFA) for 1 min.

3. cool from 170 °C to -95 °C (iodide)/ from 100 °C to -100 °C (TFA) at 10 C/min.

4. hold temperature at -95 °C (iodide)/ -100 °C (TFA) for 1 min.

5. heat up from -95 °C to 170 °C (iodide)/ from -100 °C to 100 °C (TFA) at 10 °C/min. Glass transition temperatures (T_g) were determined using Pyris™ software.

Fourier-Transformations-Infrared spectroscopy. FT-IR spectra were recorded using a *Nicolet* iS10 FT-IR spectrometer (Thermo Scientific, Waltham, MA, USA) equipped with a diamond ATR unit.

Matrix-Assisted Laser Desorption Ionization Time of Flight Mass Spectrometry (MALDI-ToF). Mass spectra were measured on a MALDI ToF MS Autoflex Max by Bruker. The samples were prepared as a 1 mg/mL solution in methanol. The matrix consisted in each case of dithranol or α-cyano-4-hydroxycinnamic acid (CHCA) without the addition of salts. Data were analyzed using Bruker Daltonics flexAnalysis. Dr. Elena Berger-Nicoletti conducted the measurements. The data were analyzed by the *mmass 5.5.0* software.

Vapor pressure osmometry (VPO). Vapor pressure osmometry measurements were carried out with a Knauer K-7000 vapor pressure osmometer in methanol at 45 °C. Concentrations of 10, 20, 30 and 40 mg/g were selected. Benzil was used as an external standard. Dr. Elena Berger-Nicoletti was responsible for carrying out and evaluating the measurements

Synthesis

Monomer synthesis

Synthesis of PiGA

A small excess of epichlorohydrin (30.5 mL, 389 mmol, 1.20 eq) and water (0.876 mL, 48.6 mmol, 0.150 eq) were added to piperidine (32.1 mL, 324 mmol, 1.00 eq) at 0 °C. The reaction time was extended to 20 h at r.t. Subsequently, the reaction mixture was extracted with an aqueous K_2CO_3 solution (20 wt%, 50mL) and sodium hydroxide solution was added (36 wt%, 30mL). After a reaction time of 20 h at r.t., the solid formed was separated from the solution *via* centrifugation. After the addition of 100 mL diethyl ether and 100 mL water, the organic phase was separated from the aqueous phase *via* a separating funnel. To isolate the product, the aqueous phase was extracted with diethyl ether (3x50 mL), the total organic phases were dried over MgSO4 and the

solvent was removed *via* rotary distillation. The crude product was fractional vacuum distillated. The yield was 13.9 g of a colorless liquid, thus 30.3% of the theory. T_b = 68-80 °C (p = 1x10^{-3} mbar).

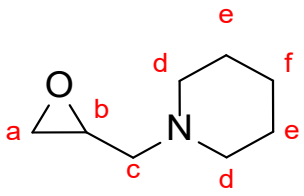

^{1}H NMR (300 MHz, $CDCl_3$): δ [ppm] 3.09 (dtd, J = 6.6, 3.9, 2.7 Hz, 1H, b), 2.76 (dd, J = 5.0, 4.1 Hz, 1H, a), 2.65 (dd, J = 13.3, 3. 7 Hz, 1H, c), 2.58 - 2.37 (m, 5H, d+a'), 2.26 (dd, J = 13.3, 6.6 Hz, 1H, c'), 1.66 - 1.54 (m, 4H, e), 1.37 - 1.48 (m, 2H, f).

^{13}C NMR (75 MHz, $CDCl_3$): δ [ppm] 61.80 (C), 55.00 (D), 50.38 (B), 45.16 (A), 25.84 (E), 24.10 (F).

Synthesis of DEGA

The procedure was analogous to the synthesis of PiGA. 32.1 mL dimethylamine (377 mmol, 1.00 eq), 35.5 mL epichlorohydrin (452 mmol, 1.20 eq), and 1.02 mL water (56.6 mmol, 0.150 eq) were used. The yield was 15.2 g of a colorless liquid, which is 31.0% of the theory. T_b = 29-32 °C (2.9x10^{-3} mbar).

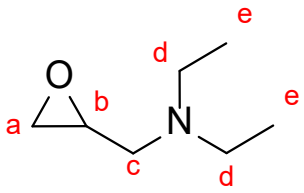

^{1}H NMR (300 MHz, $CDCl_3$): δ [ppm] 2.96 (dtd, J = 6.5, 3.9, 2.7 Hz, 1H, b), 2.70 - 2.62 (m, 2H, a+c), 2.62 - 2.44 (m, 4H, d), 2.44 - 2.30 (m, 2H, a'+c'), 0.95 (t, J = 7.2 Hz, 6H, e).

^{13}C NMR (75 MHz, $CDCl_3$): δ [ppm] 55.72 (C), 50.86 (B), 47.39 (D), 45.17 (A), 11.57 (E).

Methylation of PiGA

For methylation, PiGA (10.3 mL, 70.8 mmol, 1.00 eq) was dissolved in 40 mL acetonitrile in a 100 mL round bottom flask. The solution was cooled with an ice bath, sealed *via* a septum, and fitted with an argon balloon. Methyl iodide (4.85 mL, 77.9 mmol, 1.10 eq) was added with a syringe and

stirred with a stirrer overnight at r.t. The solvent and the excess methyl iodide were evaporated. 19.3 g of a colorless crystalline solid could be isolated, corresponding to 96.5% yield of the theory.

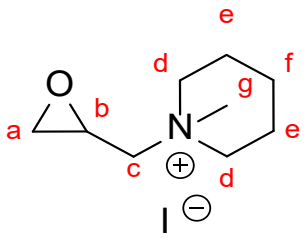

^{1}H NMR (300 MHz, DMSO-*d6*): δ [ppm] 3.87 (dd, J = 14.0, 2.0 Hz, 1H, c), 3.53 (ddt, J = 8.8, 4.5, 2.3 Hz, 1H, b), 3.48 - 3.36 (m, 4H, d), 3.23 (dd, J = 14.1, 8. 6 Hz, 1H, c'), 3.15 (s, 3H, g), 2.93 (dd, J = 5.0, 4.4 Hz, 1H, a), 2.70 (dd, J = 5.0, 2.5 Hz, 1H, a'), 1.82 (p, J = 5.9 Hz, 4H, e), 1.44 - 1.63 (m, 2H, f).

^{13}C NMR (75 MHz, DMSO-*d6*): δ [ppm] 64.27 (C), 60.48 (D), 48.26 (G), 44.40 (A), 44.05 (B), 20.31 (F), 19.16 (E).

Methylation of DEGA

The procedure was analogous to the synthesis of PiGA[I]. 6.20 mL of DEGA (46.4 mmol, 1.00 eq) and 3.18 mL of methyl iodide (51.1 mmol, 1.10 eq) were used. 12.2 g of a colorless crystalline solid was obtained, corresponding to a 97.2% theoretical yield.

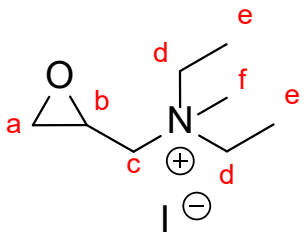

^{1}H NMR (300 MHz, DMSO-*d6*): δ [ppm] 3.85 (dd, J = 14.2, 2.1 Hz, 1H, c), 3.56 - 3.36 (m, 5H, b+d), 3.15 (dd, J = 14.3, 8. 5 Hz, 1H, c'), 3.06 (s, 3H, f), 2.95 - 2.87 (m, 1H, a), 2.71 (dd, J = 5.0, 2.5 Hz, 1H, a'), 1.23 (td, J = 7.3, 1.5 Hz, 6H, e).

^{13}C NMR (75 MHz, DMSO-*d6*): δ [ppm] 62.50 (C), 56.43 (D), 47.20 (G), 44.61 (A), 44.08 (B), 7.70 (E).

Polymer synthesis

Synthesis of P(PiGA[I]C)

The synthesis was carried out according to the instructions of Kunze.[20] For this purpose, PiGA[I] was dried over benzene; all other substances were stored under exclusion of water and oxygen, so further drying was not necessary. In an autoclave dried under vacuum and equipped with a stirring bar, PiGA[I] (0.490 g, 1.74 mmol, 1.00 eq), (*R,R*)-Co(salen)Cl (1, 11-7.79 mg, $1.74x10^{-3}$-$12.2x10^{-3}$ mmol, 0.001-0.007 eq), (1.00-7.00 mg $1.74x10^{-3}$-$12.2x10^{-3}$ mmol, 0.001-0.007 eq) and 0.5 mL solvent were added. The reaction vessel was placed under a CO_2 pressure of 50 bar and stirred at 30 °C for 70 h. The reaction was stopped. After the finished reaction time, the crude product was dissolved in acetonitrile and a few drops of HCl (5 vol%) in THF solution were added to deactivate the catalyst. The completely dissolved product was precipitated twice in diethyl ether. In the second precipitation step, an addition of one milliliter of methanol was necessary to dissolve the polymer. The yield was between 25-90%.

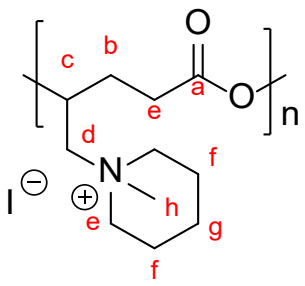

^{1}H NMR (300 MHz, DMSO-*d6*): *δ* [ppm] 5.50 (p, *J* = 8.5 Hz, 1H, c), 4.72 (t, *J* = 8.6 Hz, 1H, b), 4.20 (t, *J* = 8.2 Hz, 1H, b‘), 4.09 (dd, *J* = 14.8, 9.3 Hz, 1H, d), 3.75 (dd, *J* = 14.8, 1.1 Hz, 1H, d‘), 3.54 – 3.37 (m, 4H, e), 3.14 (s, 3H, h), 1.82 (p, *J* = 5.2 Hz, 4H, f), 1.82 (p, *J* = 5.2 Hz, 4H, g).

^{13}C NMR (75 MHz, DMSO-*d6*): *δ* [ppm] 153.90 (A), 70.33 (C), 66.95 (B), 63.07 (D), 61.14 (E), 48.82 (H), 20.28 (G), 19.13 (F).

Synthesis of P(DEGA[I]C)

The procedure was analogous to the synthesis procedure for P(PiGA[I]C). For this purpose, DEGA[I] (0.49 g, 1.81 mmol, 1.00 eq) was reacted together with the catalyst system of (*R,R*)-Co(salen)Cl (1.16-6.94 mg, 1.81x10-3-10.9x10-3 mmol, 0.001-0.006 eq) and (1.04-6.23 mg 1.81x10-3-10.9x10-3 mmol, 0.001-0.007 eq) in 0.5 mL DMF. The yield was 87-93%.

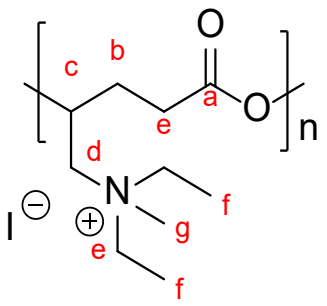

^{1}H NMR (300 MHz, DMSO-*d6*): δ [ppm] 5.44 (p, J = 8.1 Hz, 1H, c), 4.72 (t, J = 8.6 Hz, 1H, b), 4.18 (dd, J = 8.7, 7.8 Hz, 1H, b‘), 3.94 (dd, J = 14.9, 9.3 Hz, 1H, d), 3.67 (dd, J = 15.0, 1.1 Hz, 1H, d‘), 3.47 – 3.35 (m, 4H, e), 3.03 (s, 3H, g), 1.24 (t, J = 7.2 Hz, 6H, f).

^{13}C NMR (75 MHz, DMSO-*d6*): δ [ppm] 153.89 (A), 70.43 (C), 66.94 (B), 61.27 (D), 56.83 (E), 47.34 (G), 7.56 (F).

Exchange of the counterion in P(PiGA[I]C)

To exchange the iodide to trifluoroacetate, 0.200 g P(PiGA[I]C) (0.609 mmol, 1 eq) was dissolved in 3 mL water and 0.156 g AgTFA (0.609 mmol, 1 eq) in 1 mL water. When the two solutions are combined, a yellow solid (AgI) precipitates, which was removed from the solution by filtration. Subsequently, the water was removed by freeze-drying. An oily, clear solid with a slight blue coloration remained.

Degradation in an acidic environment

For degradation, P(DEGA[I]C) (13.1 mg) was dissolved in 350 µL D_2O, and 350 µL DCl/D2O (33%) was added in an NMR tube. Immediately after the addition of DCl, a ^{1}H NMR spectrum was recorded. After 96 h, a ^{1}H NMR spectrum was recorded again, and the degradation was terminated.

ACKNOWLEDGMENTS

The authors thank Dr. Elena Berger-Nicoletti for MALDI-ToF measurements and VPO measurements.

REFERENCES

(1) Xu, Y.; Lin, L.; Xiao, M.; Wang, S.; Smith, A. T.; Sun, L.; Meng, Y. Synthesis and properties of CO_2-based plastics: Environmentally-friendly, energy-saving and biomedical polymeric materials. *Prog. Polym. Sci.* **2018**, *80*, 163–182.

(2) Huang, C.-H.; Tan, C.-S. A Review: CO_2 Utilization. *Aerosol Air Qual. Res.* **2014**, *14*, 480–499.

(3) Feng, J.; Zhuo, R.-X.; Zhang, X.-Z. Construction of functional aliphatic polycarbonates for biomedical applications. *Prog. Polym. Sci.* **2012**, *37*, 211–236.

(4) Frère, A.; Kawalec, M.; Tempelaar, S.; Peixoto, P.; Hendrick, E.; Peulen, O.; Evrard, B.; Dubois, P.; Mespouille, L.; Mottet, D.*; et al.* Impact of the structure of biocompatible aliphatic polycarbonates on siRNA transfection ability. *Biomacromolecules* **2015**, *16*, 769–779.

(5) Xu, Y.; Zhou, F.; Zhou, D.; Mo, J.; Hu, H.; Lin, L.; Wu, J.; Yu, M.; Zhang, M.; Chen, H. *Degradation Behaviors of Biodegradable Aliphatic Polyesters and Polycarbonates* 14; American Scientific Publishers, 2020.

(6) Yu, W.; Maynard, E.; Chiaradia, V.; Arno, M. C.; Dove, A. P. Aliphatic Polycarbonates from Cyclic Carbonate Monomers and Their Application as Biomaterials. *Chem. Rev.* [Online early access]. DOI: 10.1021/acs.chemrev.0c00883. Published Online: Feb. 16, 2021.

(7) Scharfenberg, M.; Hilf, J.; Frey, H. Functional Polycarbonates from Carbon Dioxide and Tailored Epoxide Monomers: Degradable Materials and Their Application Potential. *Adv. Funct. Mater.* **2018**, *28*, 1704302.

(8) Artham, T.; Doble, M. Biodegradation of aliphatic and aromatic polycarbonates. *Macrolol. Biosci.* **2008**, *8*, 14–24.

(9) Ramos, J.; Forcada, J.; Hidalgo-Alvarez, R. Cationic polymer nanoparticles and nanogels: from synthesis to biotechnological applications. *Chem. Rev.* **2014**, *114*, 367–428.

(10) Samal, S. K.; Dash, M.; van Vlierberghe, S.; Kaplan, D. L.; Chiellini, E.; van Blitterswijk, C.; Moroni, L.; Dubruel, P. Cationic polymers and their therapeutic potential. *Chem. Soc. Rev.* **2012**, *41*, 7147–7194.

(11) Bobbarala, V. Concepts, Compounds and the Alternatives of Antibacterials; BoD – Books on Demand, 2015.

(12) Isik, M.; Fernandes, A. M.; Vijayakrishna, K.; Paulis, M.; Mecerreyes, D. Preparation of poly(ionic liquid) nanoparticles and their novel application as flocculants for water purification. *Polym. Chem.* **2016**, *7*, 1668–1674.

(13) Jaeger, W.; Bohrisch, J.; Laschewsky, A. Synthetic polymers with quaternary nitrogen atoms—Synthesis and structure of the most used type of cationic polyelectrolytes. *Prog. Polym. Sci.* **2010**, *35*, 511–577.

(14) Qian, W.; Texter, J.; Yan, F. Frontiers in poly(ionic liquid)s: syntheses and applications. *Chem. Soc. Rev.* **2017**, *46*, 1124–1159.

(15) Reuss, V. S.; Werre, M.; Frey, H. Thermoresponsive copolymers of ethylene oxide and N,N-diethyl glycidyl amine: polyether polyelectrolytes and PEGylated gold nanoparticle formation. *Macromol. Rapid Commun.* **2012**, *33*, 1556–1561.

(16) Antimicrobial cationic polycarbonates, 2017.

(17) Lee, A. L. Z.; Yang, C.; Gao, S.; Wang, Y.; Hedrick, J. L.; Yang, Y. Y. Biodegradable Cationic Polycarbonates as Vaccine Adjuvants. *ACS Appl. Mater. Interfaces* **2020**, *12*, 52285–52297.

(18) Hauenstein, O.; Agarwal, S.; Greiner, A. Bio-based polycarbonate as synthetic toolbox. *Nat. Commun.* **2016**, *7*, 11862.

(19) Yuen, A. Y.; Lopez-Martinez, E.; Gomez-Bengoa, E.; Cortajarena, A. L.; Aguirresarobe, R. H.; Bossion, A.; Mecerreyes, D.; Hedrick, J. L.; Yang, Y. Y.; Sardon, H. Preparation of Biodegradable Cationic Polycarbonates and Hydrogels through the Direct Polymerization of Quaternized Cyclic Carbonates. *ACS Biomater. Sci. Eng.* **2017**, *3*, 1567–1575.

(20) Lena Kunze. Synthesis of Aliphatic Polycarbonate-Architectures: From Elastomers and Surfactants to Ionic Polymers: Can Cationic Epoxides be Polymerized by Ring-Opening?, 2018.

(21) Lee, A.; Lundberg, P.; Klinger, D.; Lee, B. F.; Hawker, C. J.; Lynd, N. A. Physiologically relevant, pH-responsive PEG-based block and statistical copolymers with N,N-diisopropylamine units. *Polym. Chem.* **2013**, *4*, 5735–5742.

(22) Wilms, V. S.; Frey, H. Aminofunctional polyethers: smart materials for applications in solution and on surfaces. *Polym. Int.* **2013**, *62*, 849–859.

(23) Herzberger, J.; Kurzbach, D.; Werre, M.; Fischer, K.; Hinderberger, D.; Frey, H. Stimuli-Responsive Tertiary Amine Functional PEGs Based on N , N -Dialkylglycidylamines. *Macromolecules* **2014**, *47*, 7679–7690.

(24) Blankenburg, J.; Wagner, M.; Frey, H. Well-Defined Multi-Amino-Functional and Stimuli-Responsive Poly(propylene oxide) by Crown Ether Assisted Anionic Ring-Opening Polymerization. *Macromolecules* **2017**, *50*, 8885–8893.

(25) Mouzin, G.; Cousse, H.; Rieu, J.-P.; Duflos, A. A Convenient One-Step Synthesis of Glycidyl Ethers. *Synthesis* **1983**, *1983*, 117–119.

(26) Hovland, R.; Gløgård, C.; Aasen, A. J.; Klaveness, J. Gadolinium DO3A derivatives mimicking phospholipids; preparation and in vitro evaluation as pH responsive MRI contrast agents. *J. Chem. Soc., Perkin Trans. 2* **2001**, 929–933.

(27) Kim, I.; Yi, M. J.; Lee, K. J.; Park, D.-W.; Kim, B. U.; Ha, C.-S. Aliphatic polycarbonate synthesis by copolymerization of carbon dioxide with epoxides over double metal cyanide catalysts prepared by using ZnX2 (X=F, Cl, Br, I). *Catalysis Today* **2006**, *111*, 292–296.

(28) He, H.; Zhong, M.; Adzima, B.; Luebke, D.; Nulwala, H.; Matyjaszewski, K. A simple and universal gel permeation chromatography technique for precise molecular weight characterization of well-defined poly(ionic liquid)s. *J. Am. Chem. Soc.* **2013**, *135*, 4227–4230.

(29) Hann, N. D. Effects of lithium bromide on the gel-permeation chromatography of polyester-based polyurethanes in dimethylformamide. *J. Polym. Sci. Polym. Chem. Ed.* **1977**, *15*, 1331–1339.

(30) Zagar, E.; Zigon, M. Dilute solution behaviour of hexamethylene diisocyanate-based carboxylated polyurethanes and related ionomers in tetrahydrofuran. *Polymer* **1999**, *40*, 2727–2735.

(31) Yuan, J.; Antonietti, M. Poly(ionic liquid)s: Polymers expanding classical property profiles. *Polymer* **2011**, *52*, 1469–1482.

(32) Wang, H.; Zhang, X.; Wu, Q.; Cao, F.; Yang, D.; Shang, Y.; Ning, Z.; Zhang, W.; Zheng, W.; Yan, Y.*; et al.* Trifluoroacetate induced small-grained CsPbBr3 perovskite films result in efficient and stable light-emitting devices. *Nat. Commun.* **2019**, *10*, 665.

(33) Ford, D. D.; Nielsen, L. P. C.; Zuend, S. J.; Musgrave, C. B.; Jacobsen, E. N. Mechanistic basis for high stereoselectivity and broad substrate scope in the (salen)Co(III)-catalyzed hydrolytic kinetic resolution. *J. Am. Chem. Soc.* **2013**, *135*, 15595–15608.

SUPPORTING INFORMATION

Direct Synthesis of Cationic Polycarbonates from CO_2 and Methylated Glycidyl Amines

Christina Gardiner[a], Caroline Bockhard[a], Holger Frey[a*]

[a]Department of Chemistry, Johannes Gutenberg University, Duesbergweg 10-14, 55128 Mainz, Germany

Table of content

1. Monomer synthesis

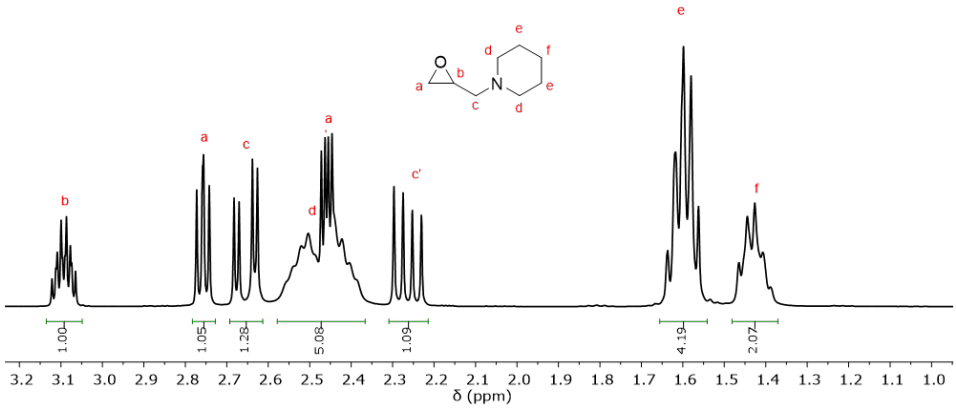

Figure S 1: ^{1}H NMR spectrum ($CDCl_3$, 300 MHz) of PiGA after distillation.

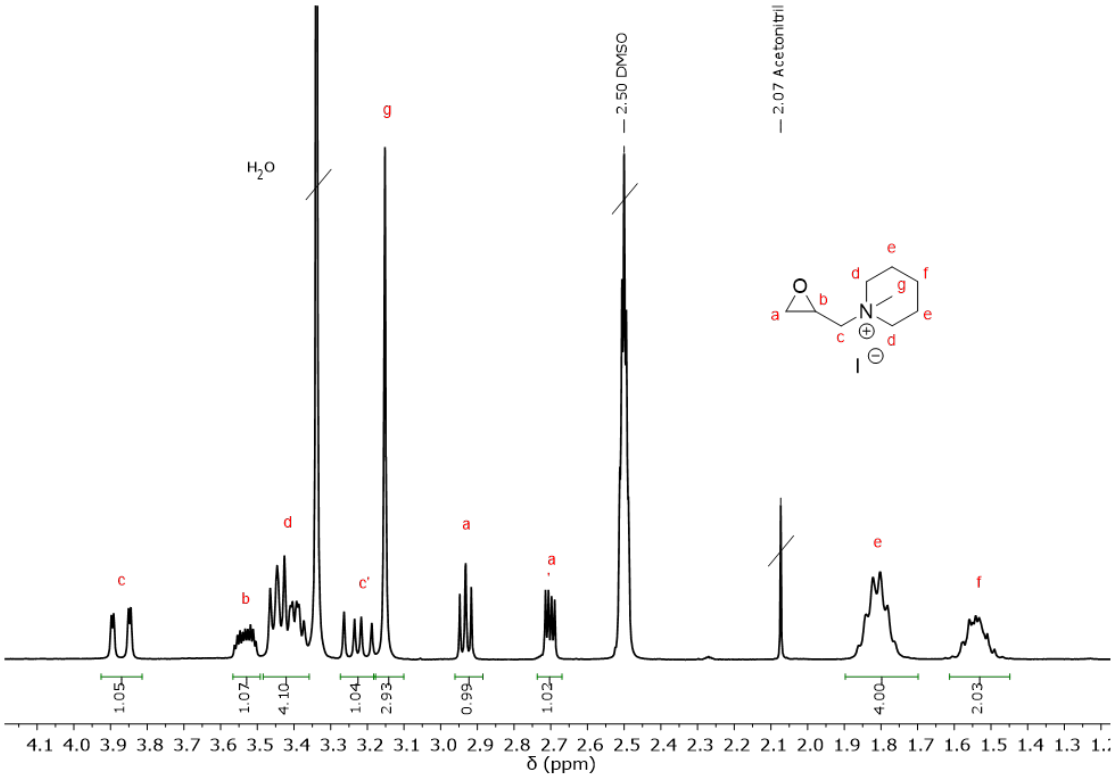

Figure S 2: ^{1}H NMR spectrum (DMSO-*d6*, 300 MHz) of PiGA[I].

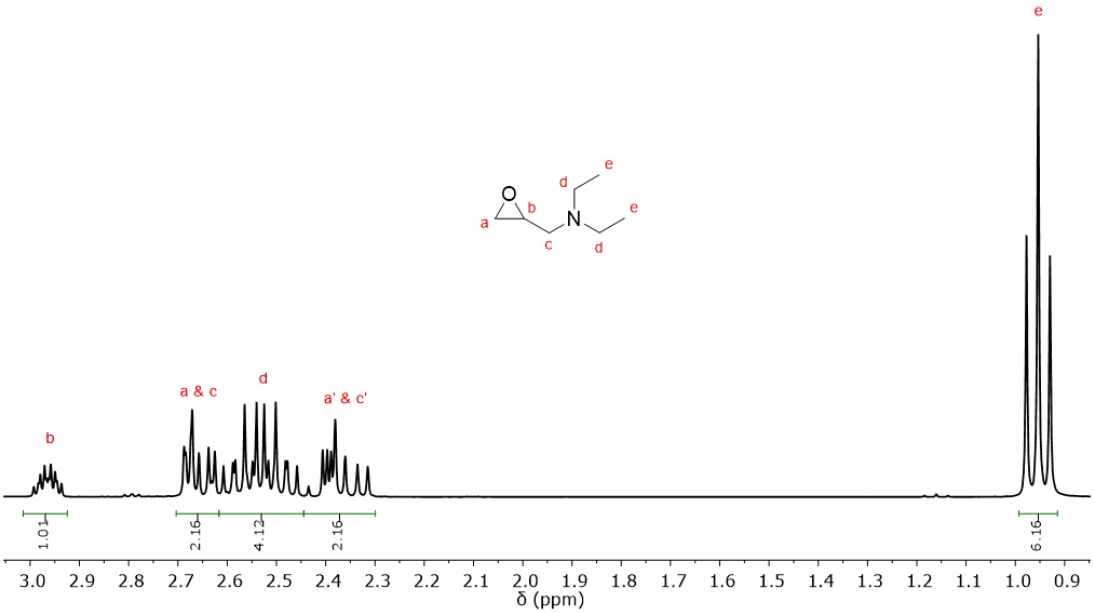

Figure S 3: ^{1}H NMR spectrum ($CDCl_3$, 300 MHz) of DEGA after distillation.

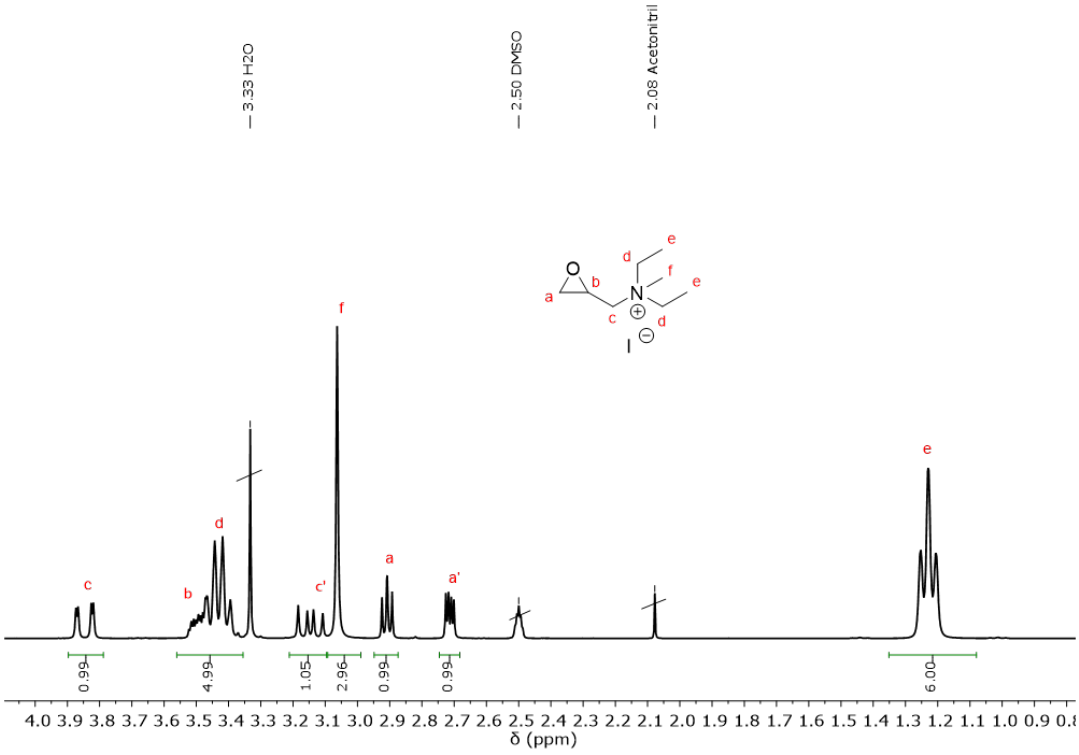

Figure S 4: ^{1}H NMR spectrum (DMSO-*d6*, 300 MHz) of DEGA[I].

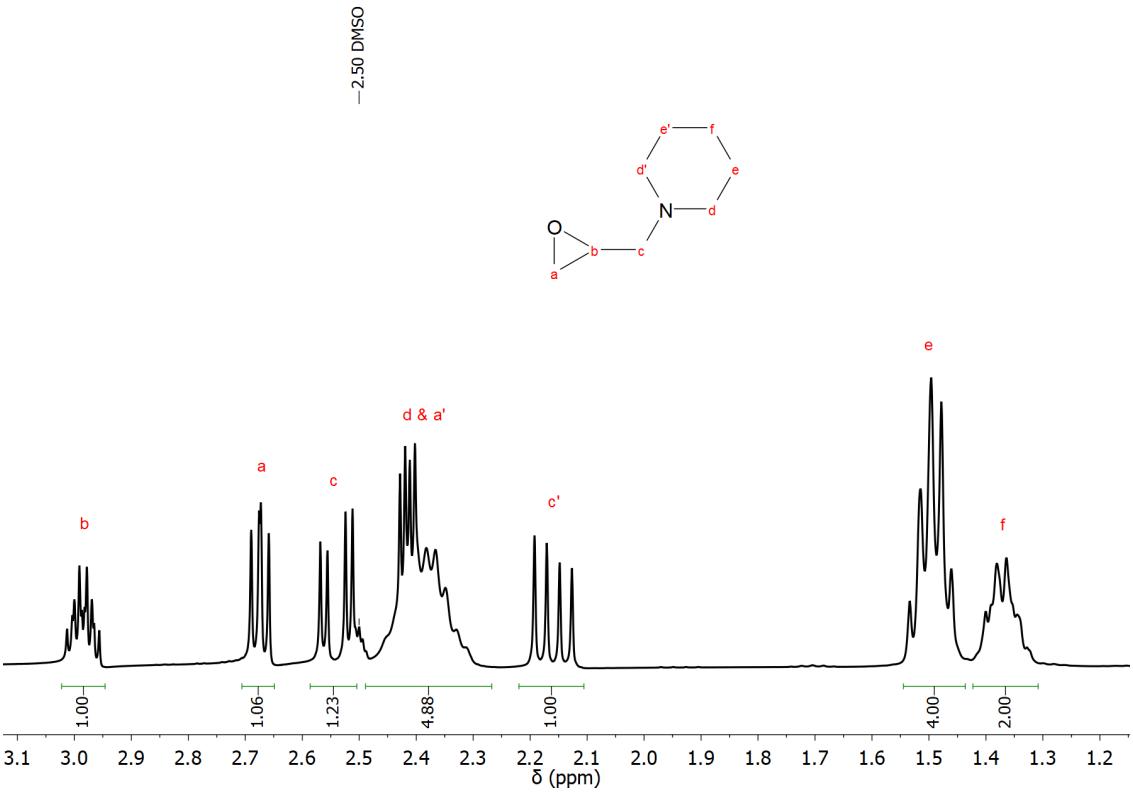

Figure S 5: ^{1}H NMR spectrum (DMSO-*d6*, 300 MHz) of PiGA.

2. Polymer synthesis

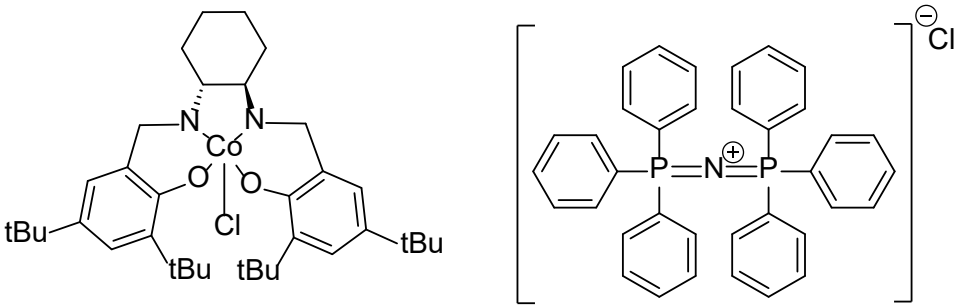

(*R,R*)-Co(salen)Cl [PPN]Cl

Scheme S 1: Chemical structure of the binary catalyst system.

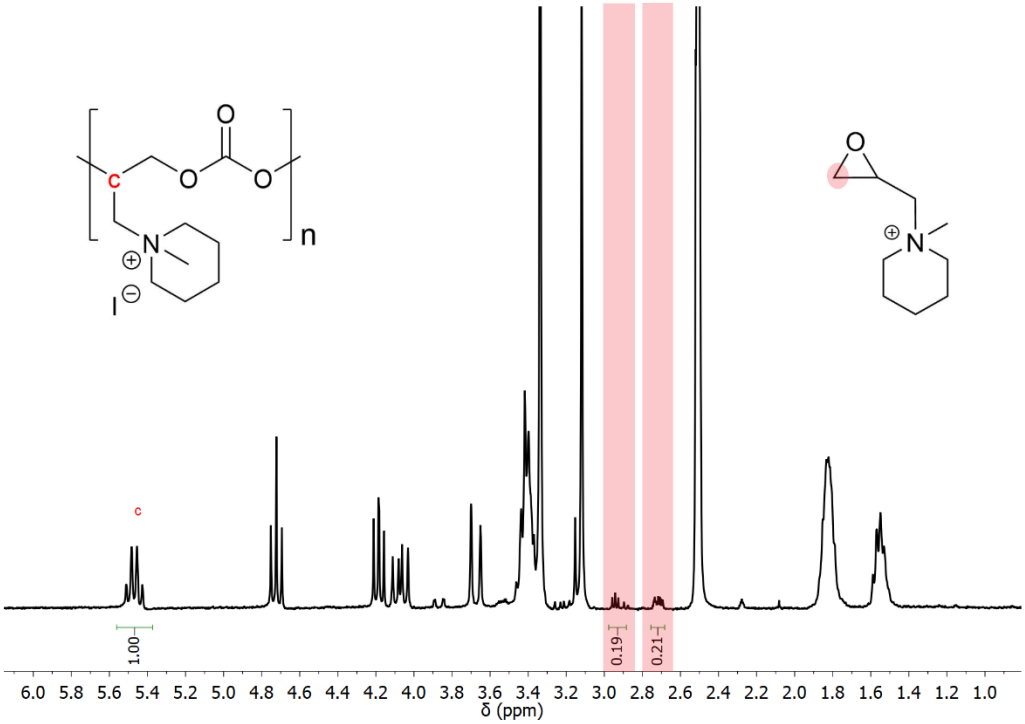

Figure S 6: ^{1}H NMR spectrum (DMSO-*d6*, 300 MHz) of the crude product P5. Example for calculating the conversion.

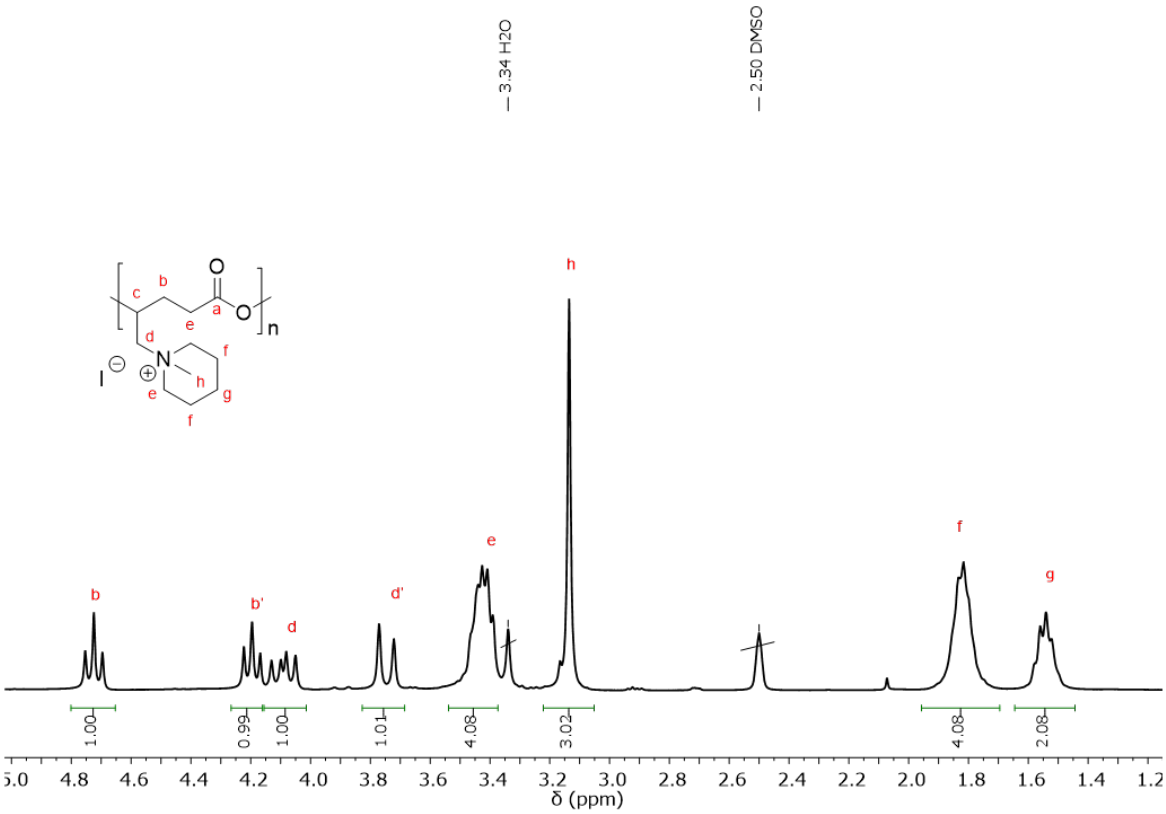

Figure S 7: ^{1}H NMR spectrum (DMSO-*d6*, 300 MHz) of P(PiGA[I]C).

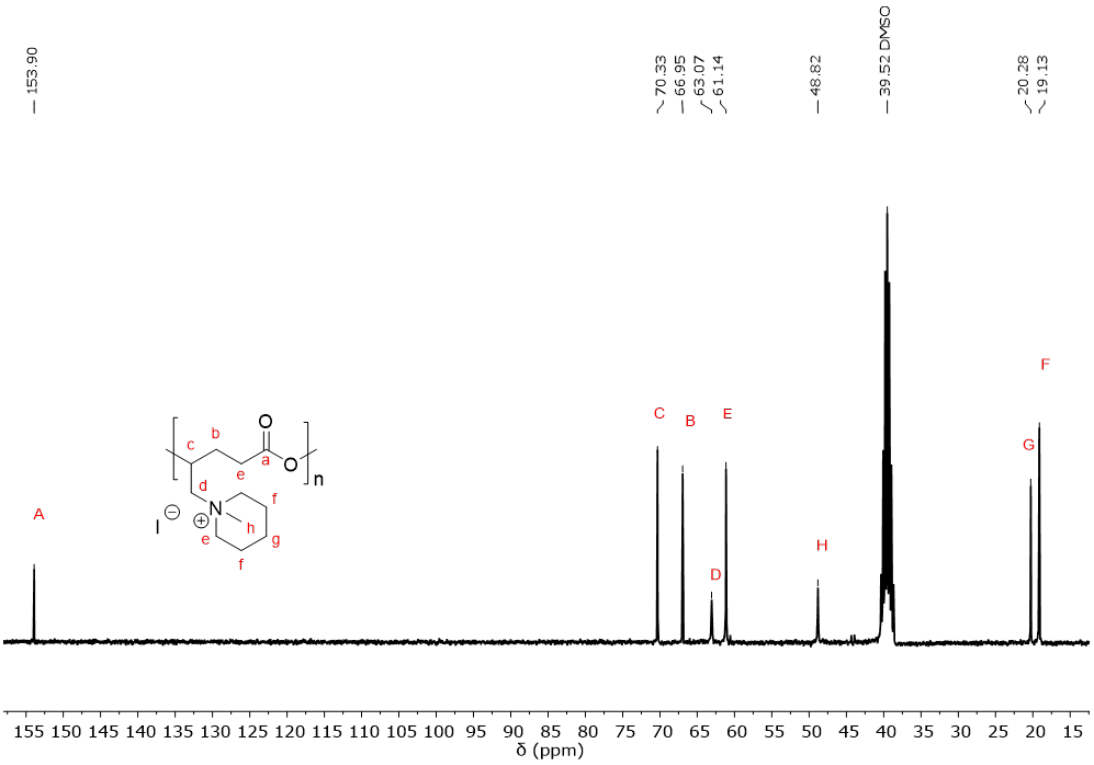

Figure S 8: ^{13}C NMR spectrum (DMSO-*d6*, 75 MHz) of P(PiGA[I]C).

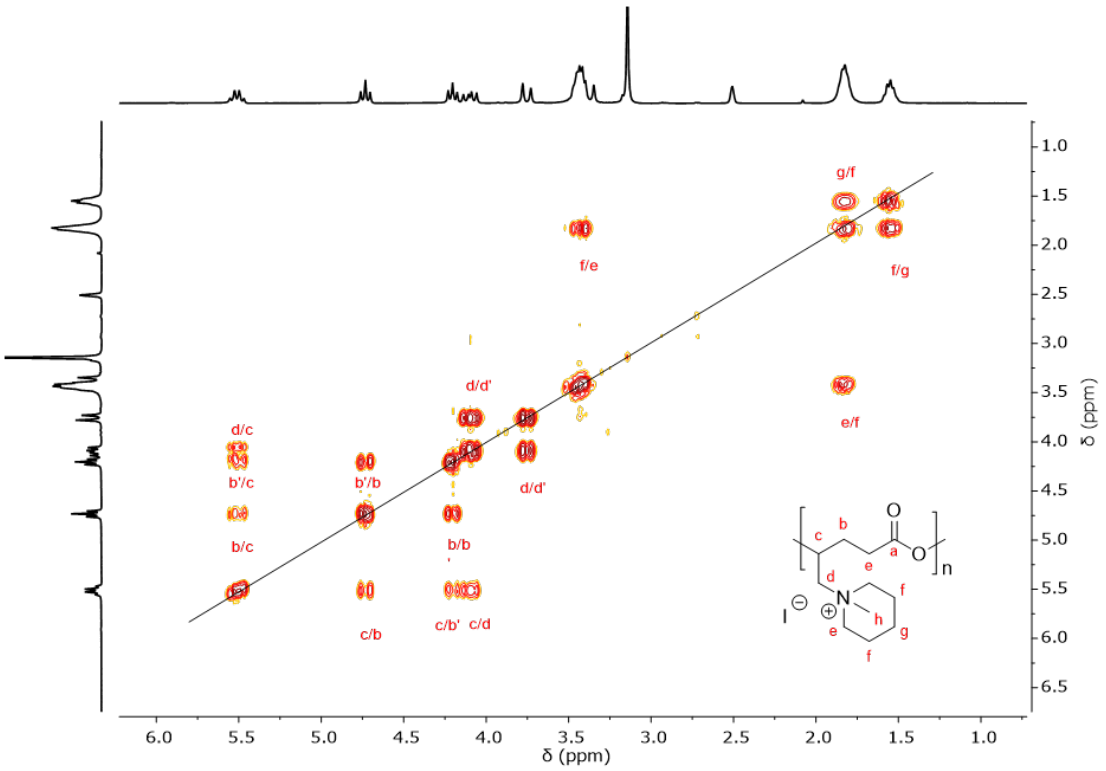

Figure S 9: ^{1}H ^{1}H COSY NMR spectrum (DMSO-d6, 300 MHz) of P(PiGA[I]C).

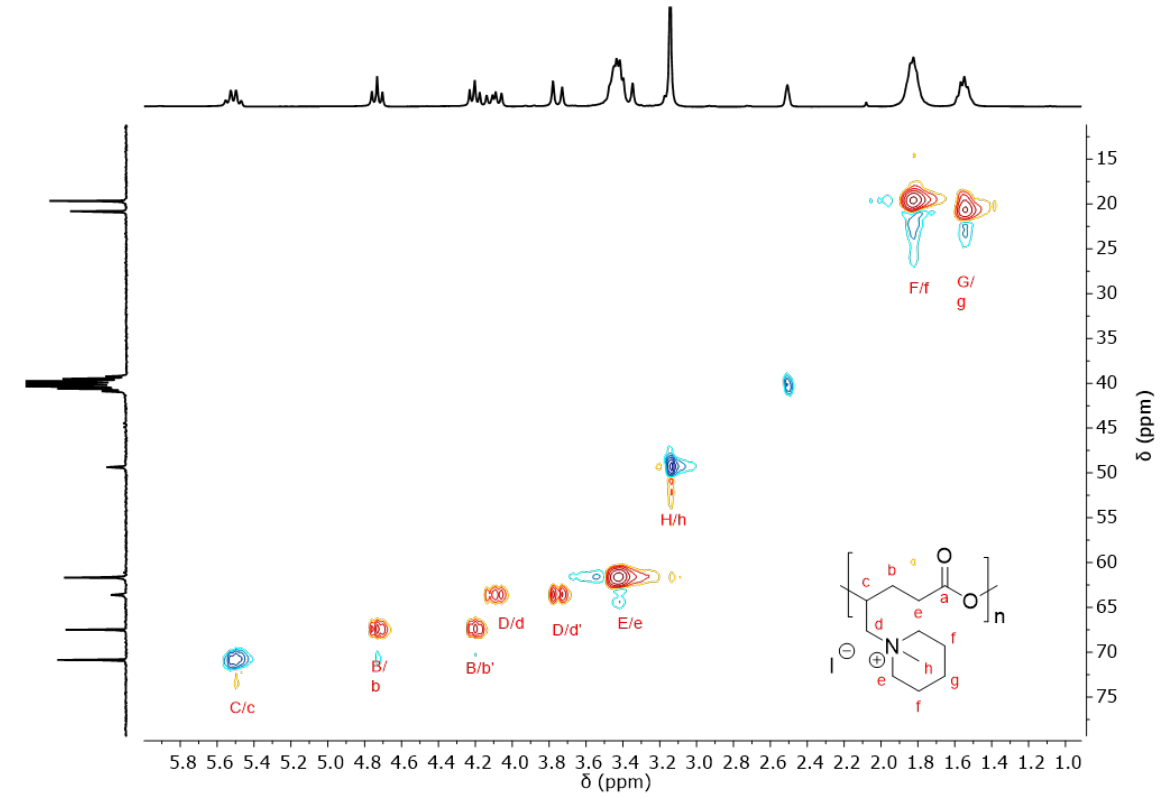

Figure S 10: ^{1}H ^{13}C HSQC NMR spectrum (DMSO-*d6*, 300/75 MHz) of P(PiGA[I]C).

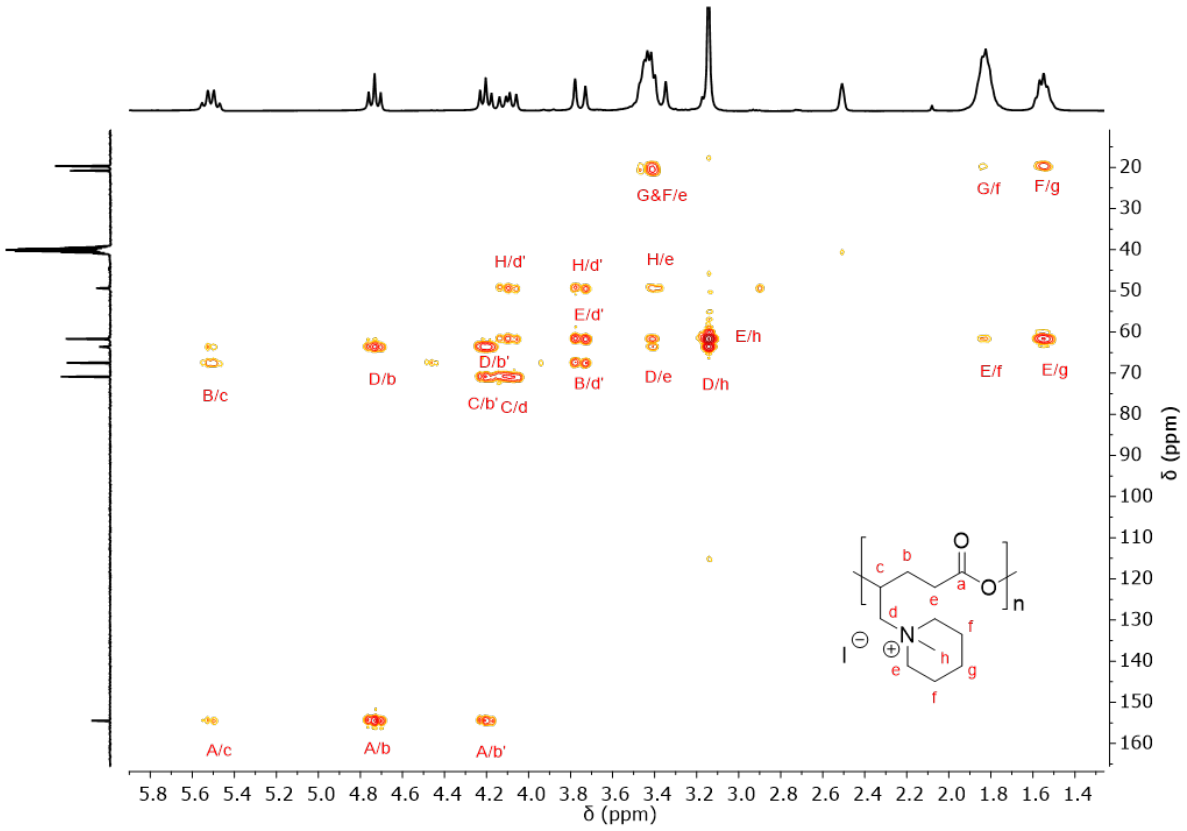

Figure S 11: ^{1}H ^{13}C HMBC NMR spectrum (DMSO-*d6*, 300/75 MHz) of P(PiGA[I]C).

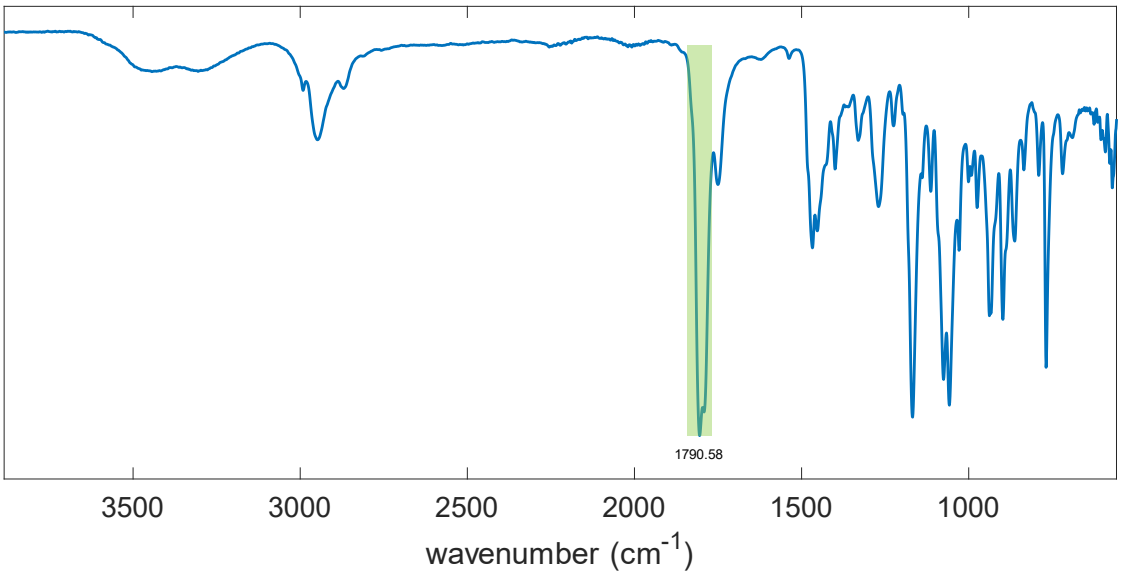

Figure S 12: IR spectrum of P(PiGA[I]C] (P7). The C=O vibration of the polycarbonate is highlighted in green.

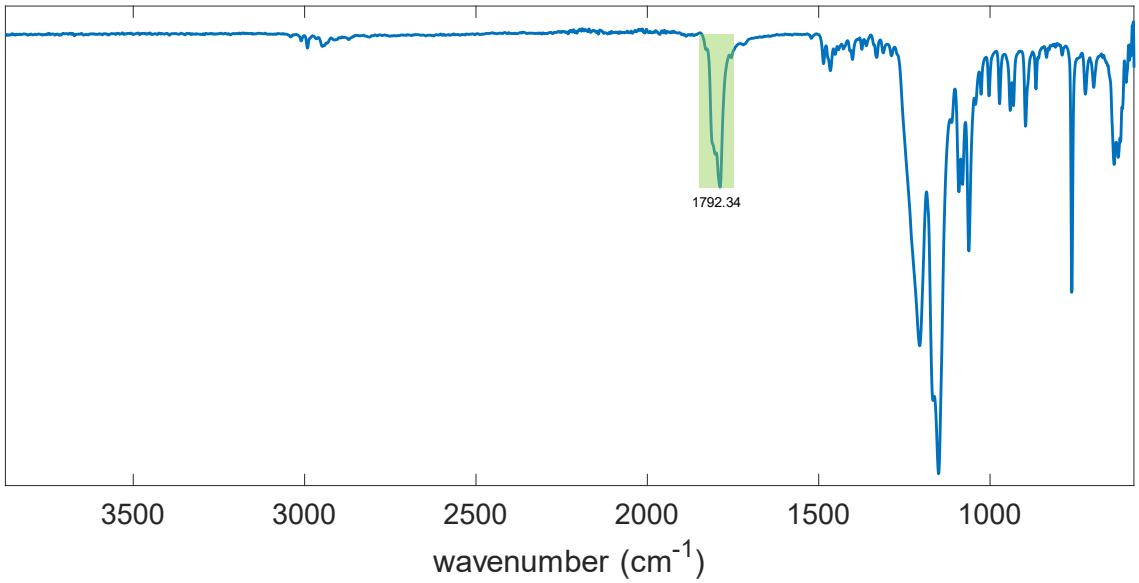

Figure S 13: IR spectrum of P(PiGA[I]C] (P10). The C=O vibration of the polycarbonate is highlighted in green.

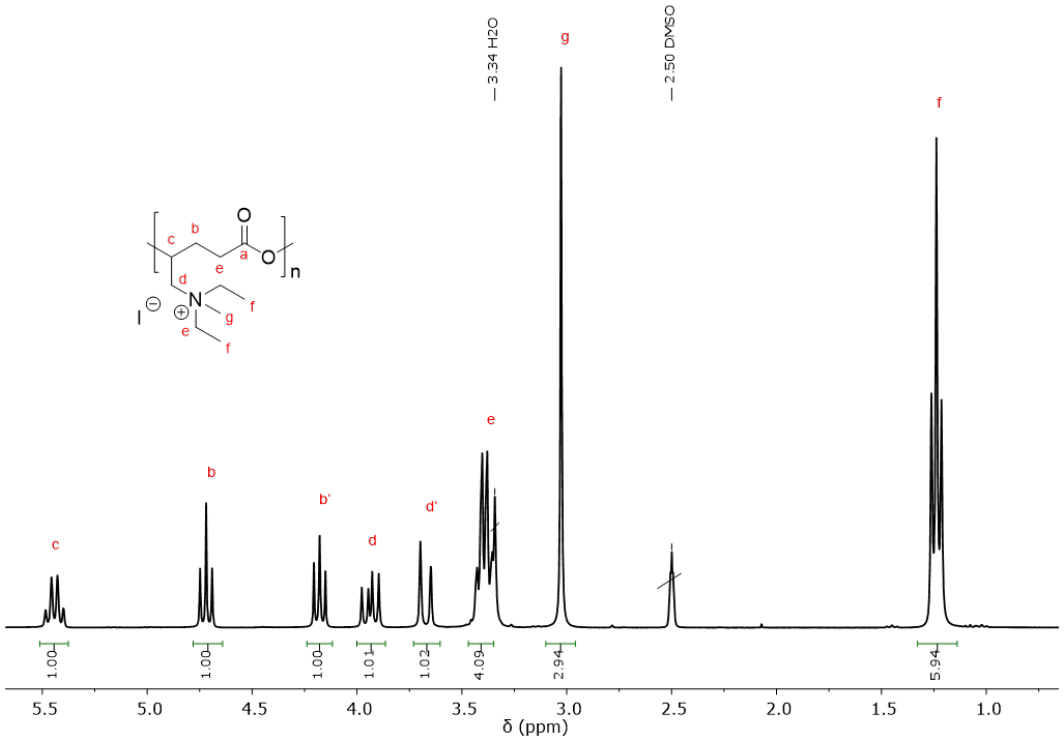

Figure S 14: ^{1}H NMR spectrum (DMSO-*d6*, 300 MHz) of P(DEGA[I]C).

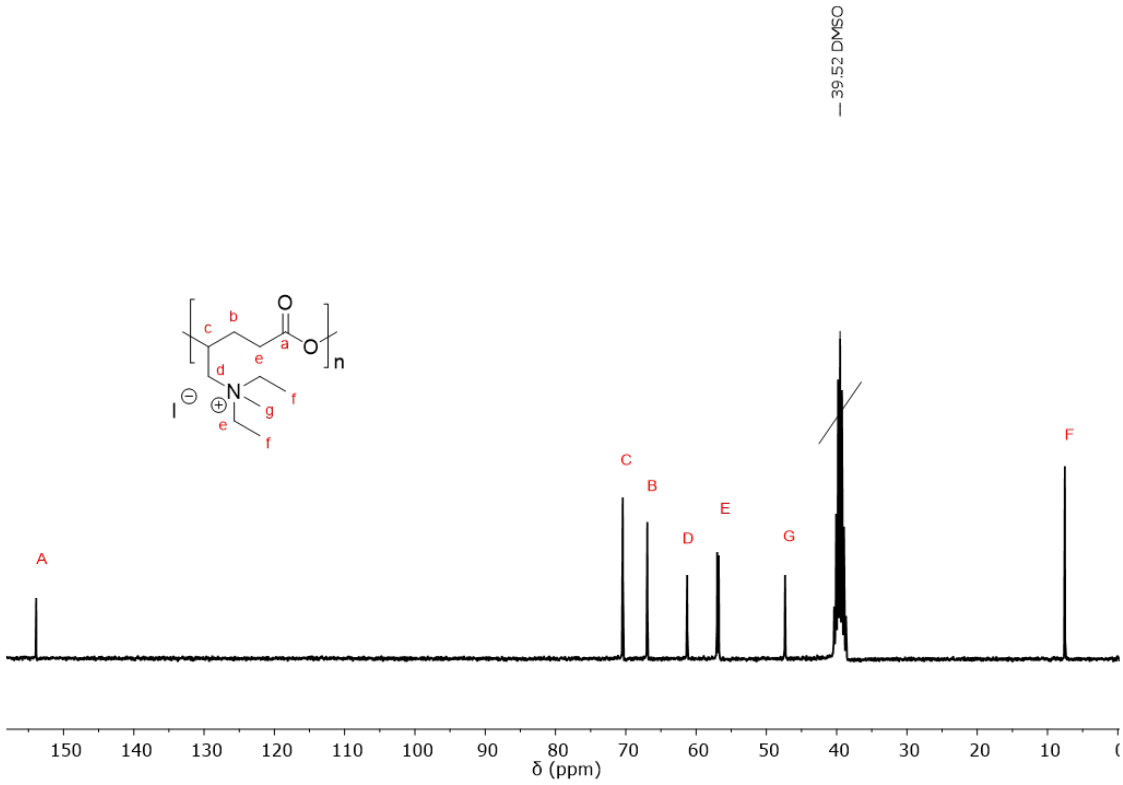

Figure S 15: ^{13}C NMR spectrum (DMSO-*d6*, 75 MHz) of P(DEGA[I]C).

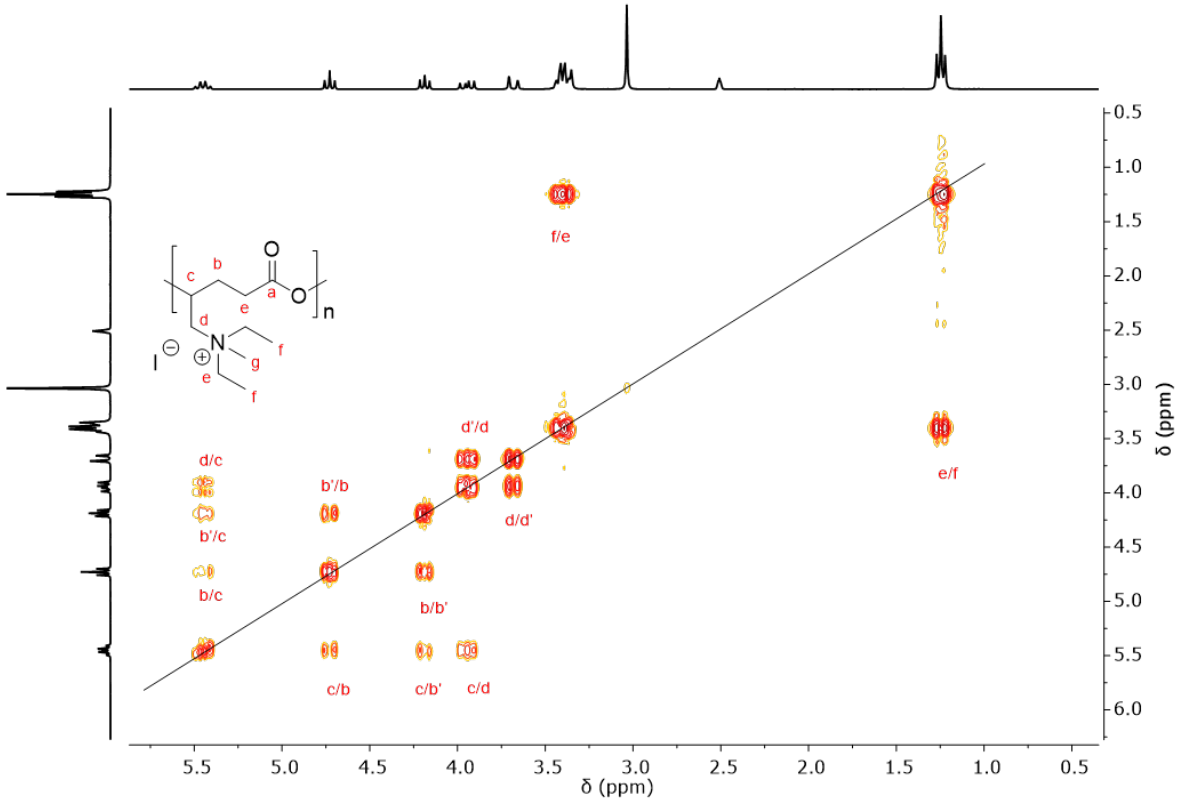

Figure S 16: ^{1}H ^{1}H COSY NMR spectrum (DMSO-*d*6, 300 MHz) of P(DEGA[I]C).

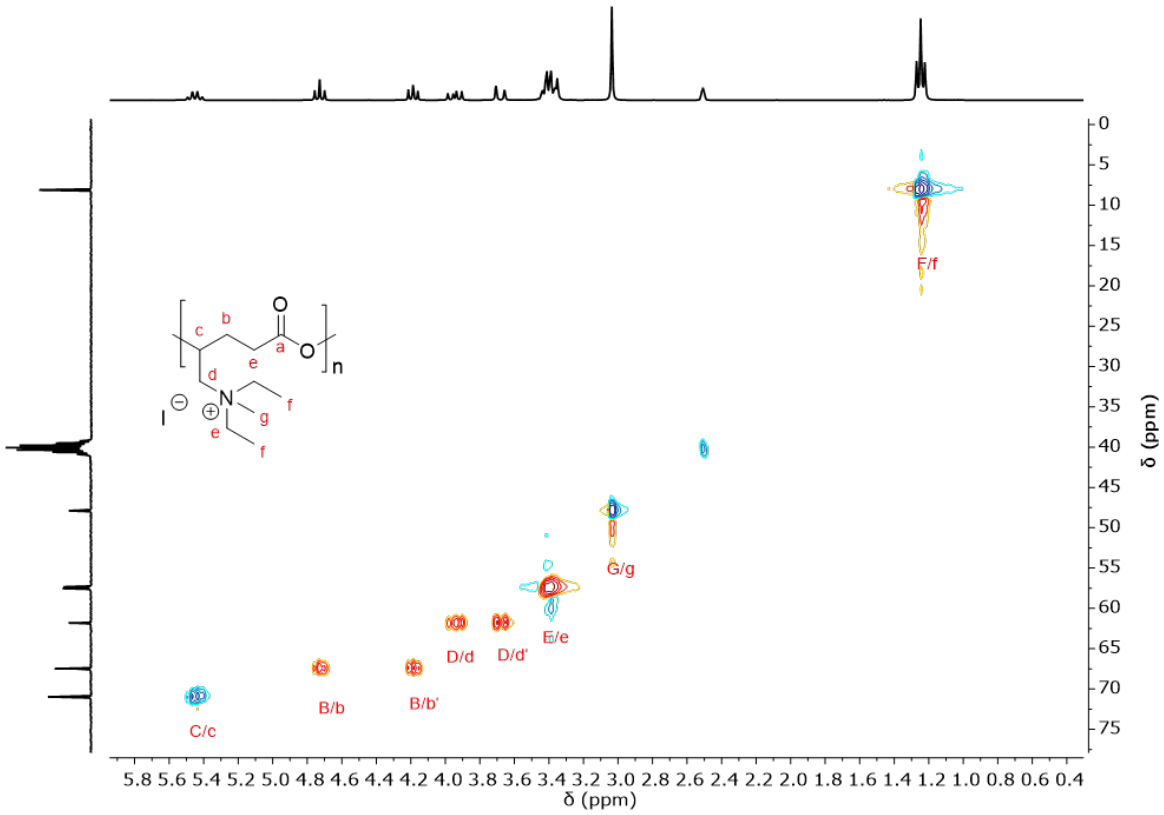

Figure S 17: ^{1}H ^{13}C HSQC NMR spectrum (DMSO-*d6*, 300/75 MHz) of P(DEGA[I]C).

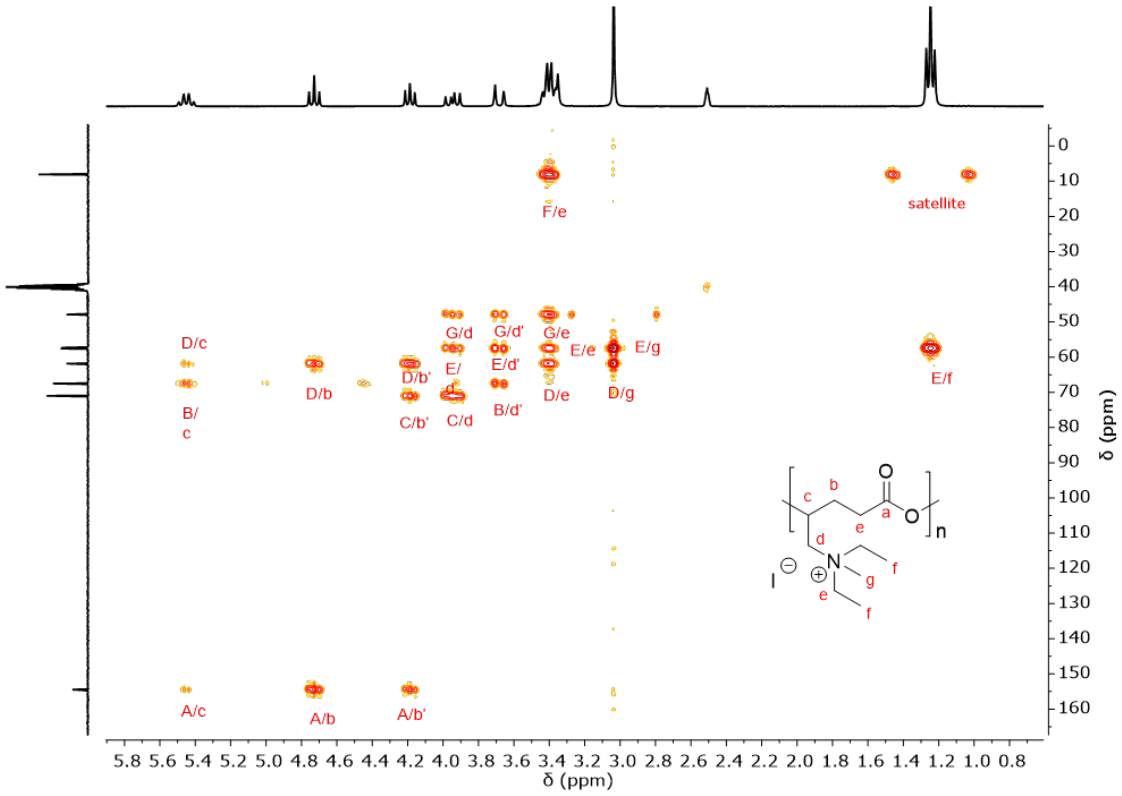

Figure S 18: ^{1}H ^{13}C HMBC NMR spectrum (DMSO-*d*6, 300/75 MHz) of P(DEGA[I]C).

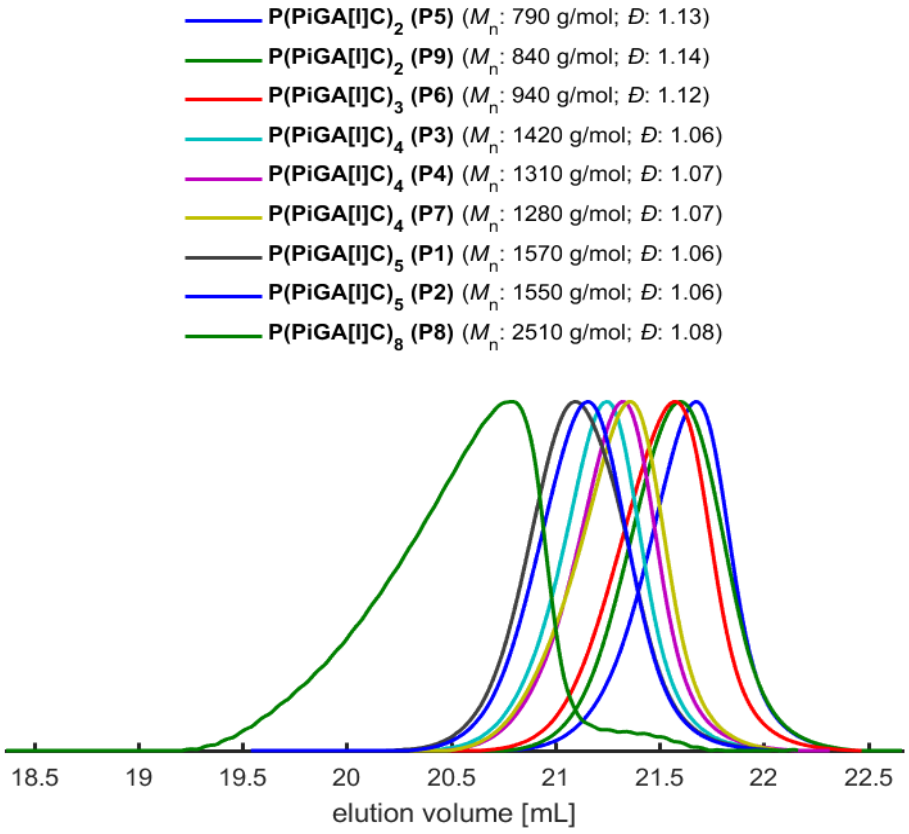

Figure S 19: SEC curves (eluent: HFIP, standard: PMMA) of P(PiGA[I]C) homopolymers.

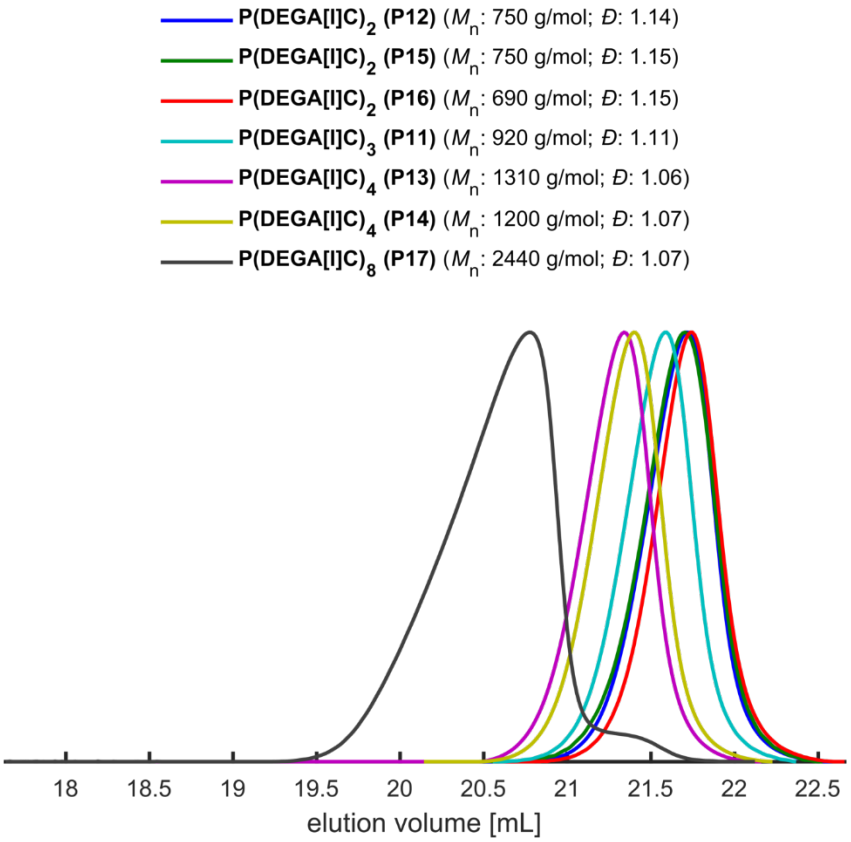

Figure S 20: SEC curves (eluent: HFIP, standard: PMMA) of P(DEGA[I]C) homopolymers.

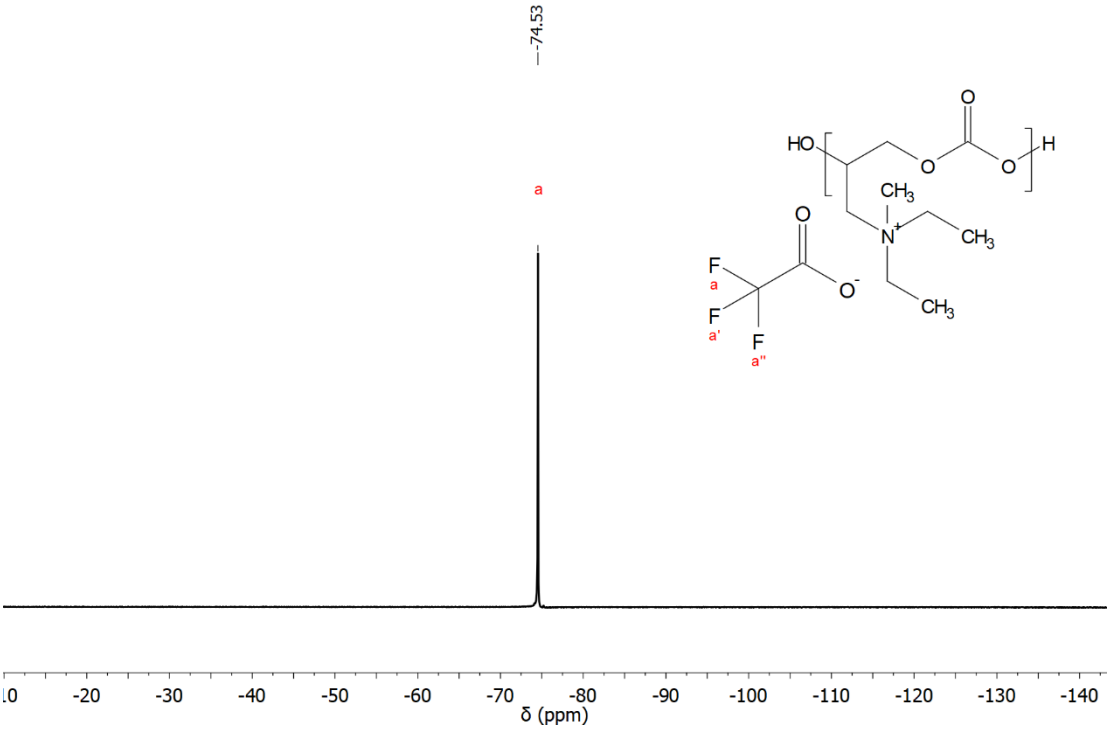

Figure S 21: ^{19}F NMR Spektrum (DMSO-*d6*, 300 MHz) of P(DEGA[TFA]C) (P14).

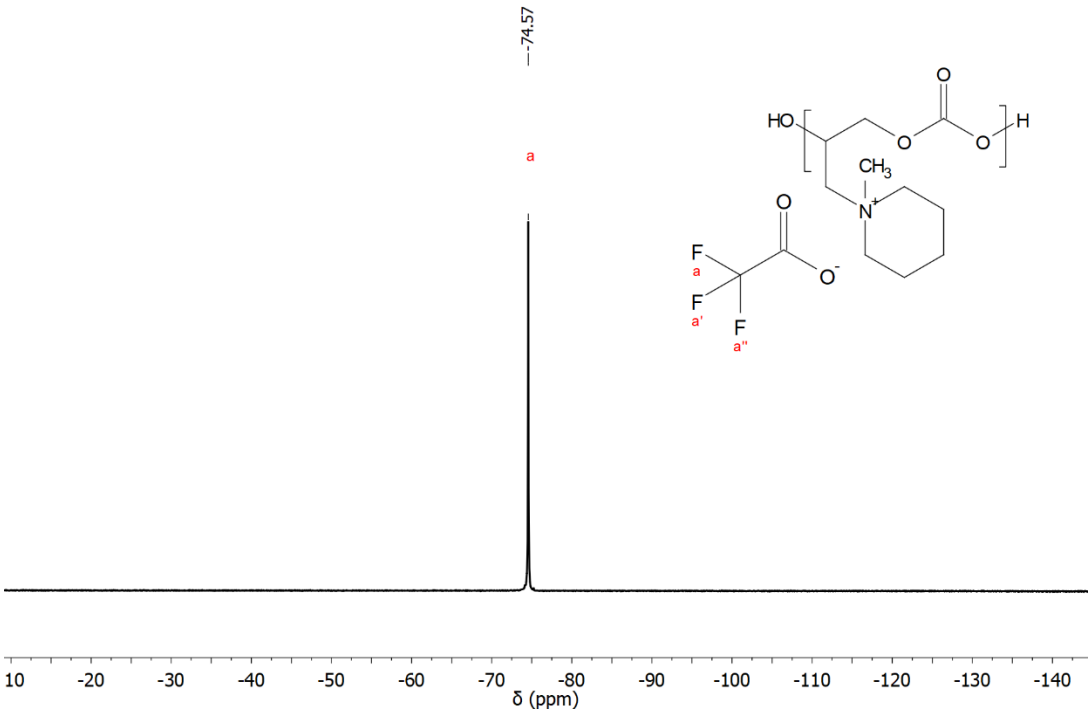

Figure S 22: ^{19}F NMR Spektrum (DMSO-*d6*, 300 MHz) of P(PiGA[TFA]C) (P4).

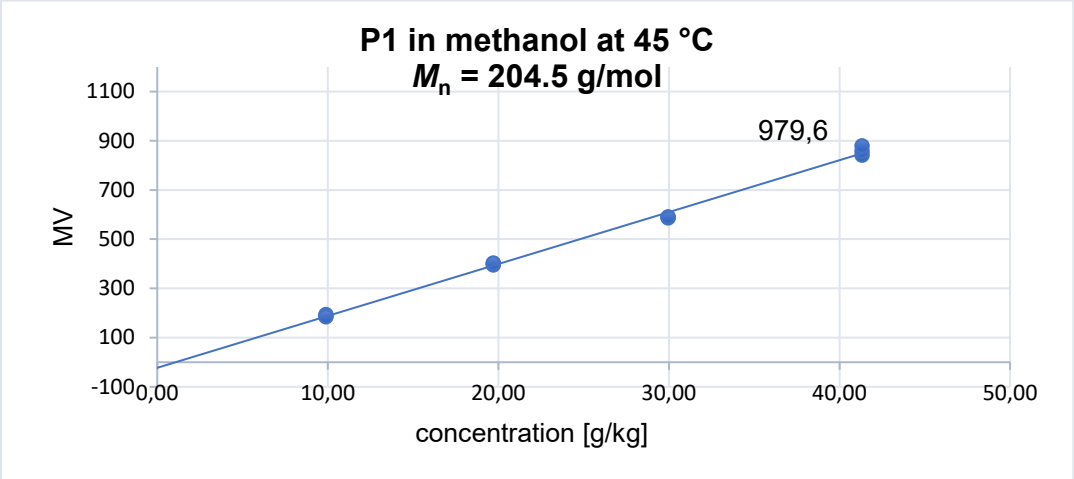

Figure S 23: Calibration graph of VPO measurement of P(PiGA[I]C) (P1). Calculating M_n = 204.5 g/mol. Benzil was used as standard.

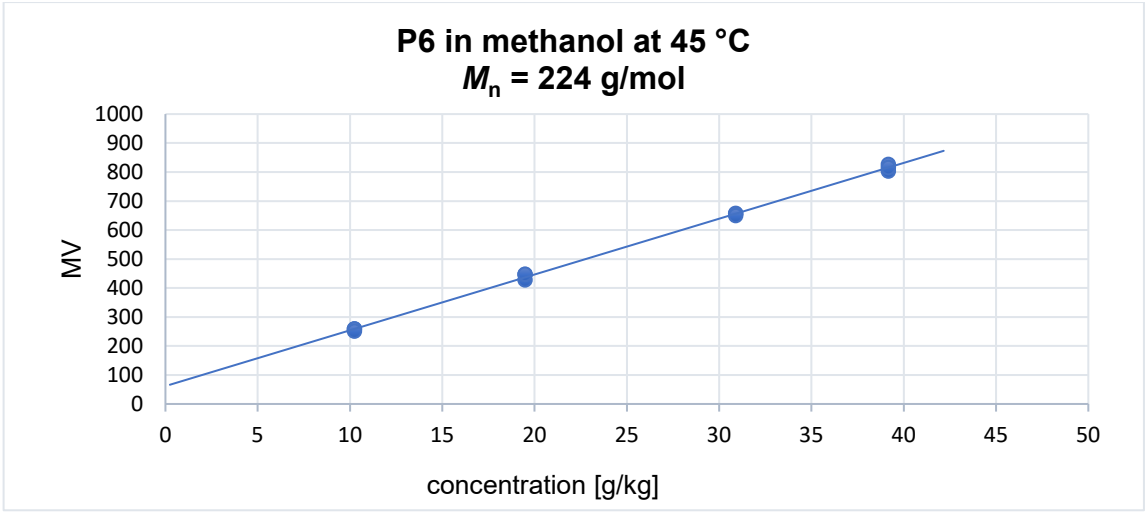

Figure S 24: Calibration graph of VPO measurement of P(PiGA[I]C) (P6). Calculating M_n = 224 g/mol. Benzil was used as standard.

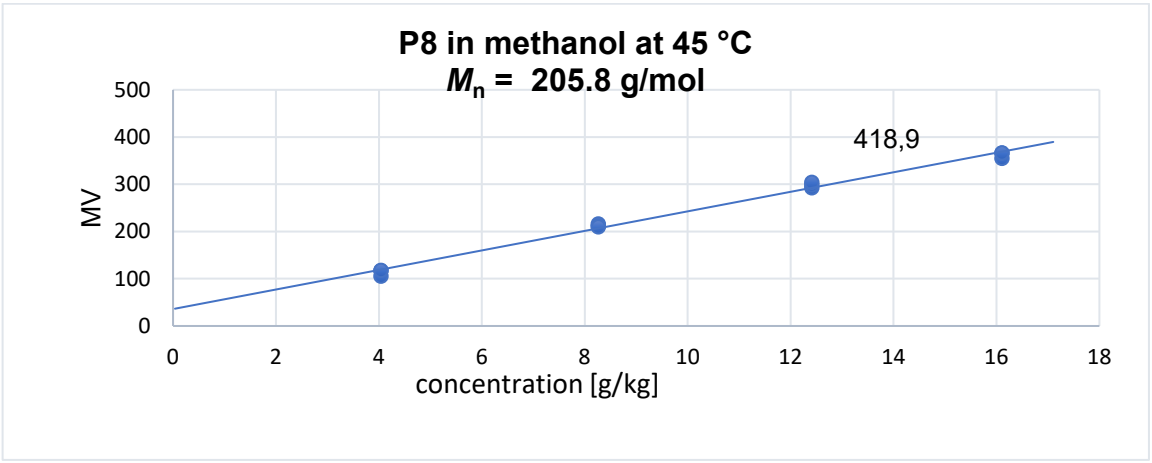

Figure S 25: Calibration graph of VPO measurement of P(PiGA[I]C) (P8). Calculating M_n = 205.8 g/mol. Benzil was used as standard.

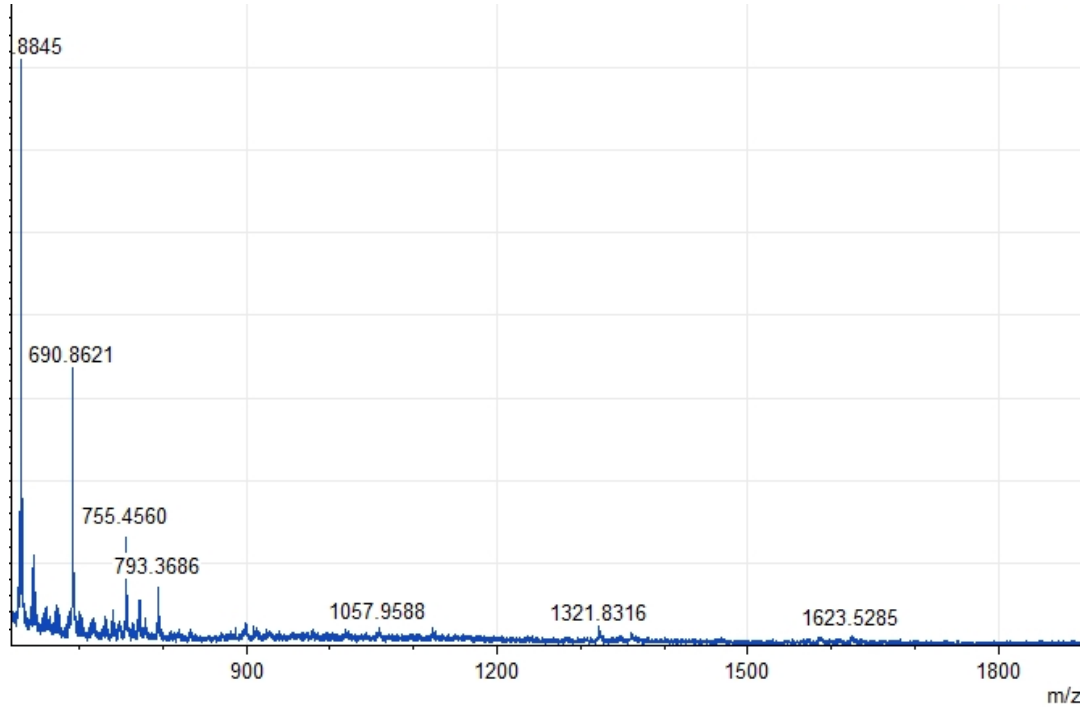

Figure S 26: An example of the mass spectrum of P(DEGA[I]C) (P13) recorded via MALDI ToF MS in dithranol. It was not possible to identify a clear molecular weight distribution corresponding to the molecular weight of the unit $C_{10}H_{18}INO_3$ (316.17 g/mol).

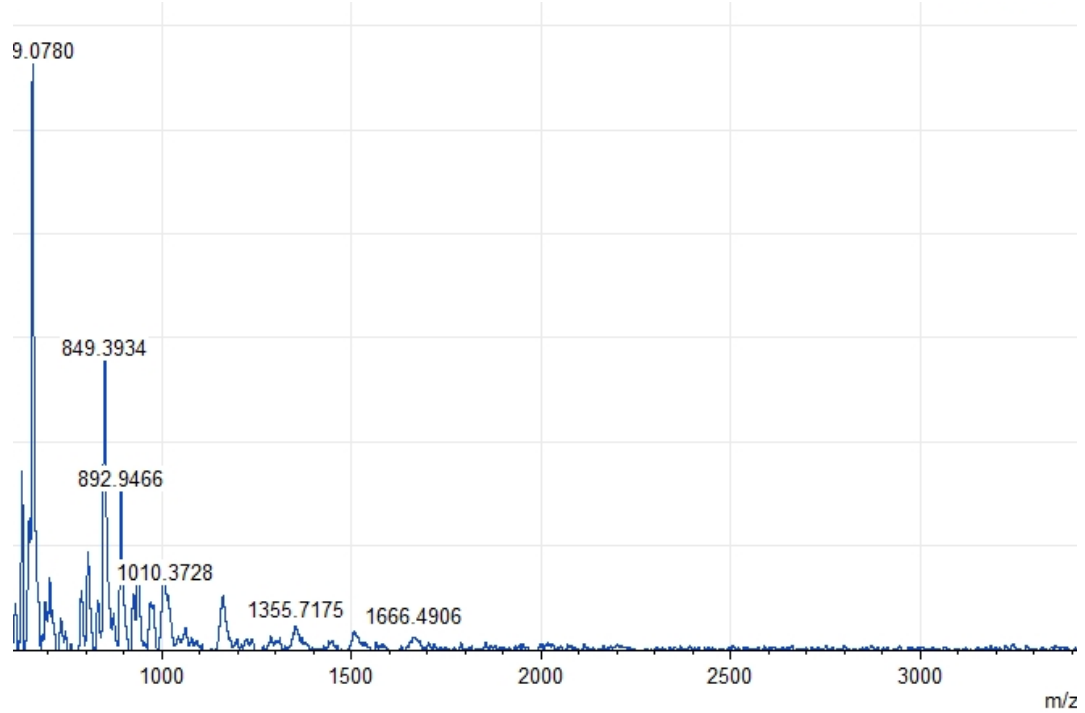

Figure S 27: An example of the mass spectrum of P(DEGA[I]C) (P9) recorded via MALDI ToF MS in CHCA. It was not possible to identify a clear molecular weight distribution corresponding to the molecular weight of the unit $C_{10}H_{18}INO_3$ (316.17 g/mol).

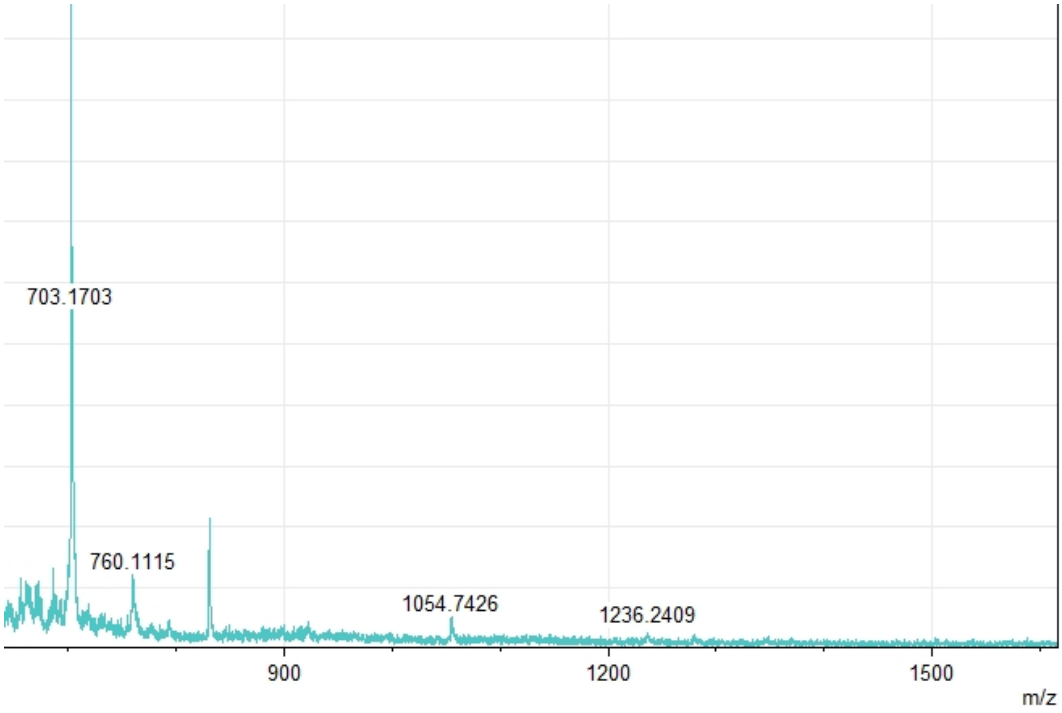

Figure S 28: An example of the mass spectrum of P(DEGA[I]C) (P9) recorded via MALDI ToF MS in dithranol. It was not possible to identify a clear molecular weight distribution corresponding to the molecular weight of the unit $C_{10}H_{18}INO_3$ (316.17 g/mol).

3. Thermal properties

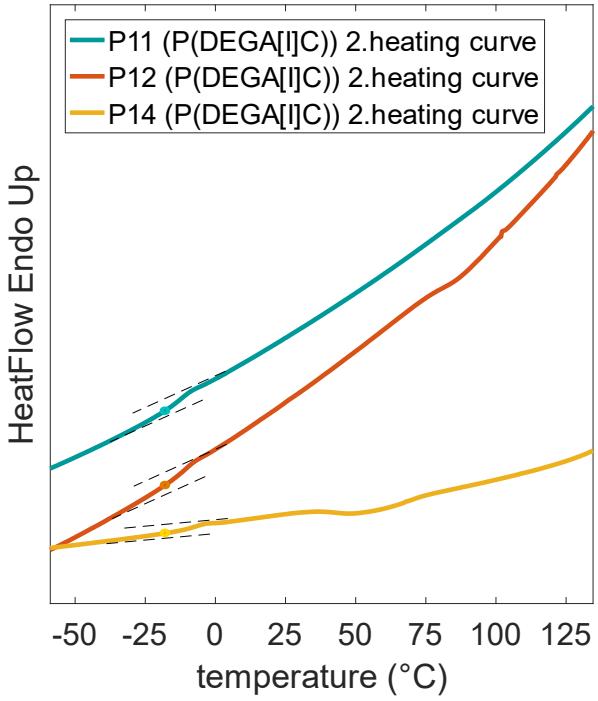

Figure S 29: DSC curves of the P(DEGA[I]C) homopolymers. The second heating curve is illustrated. The dot marks the T_g.

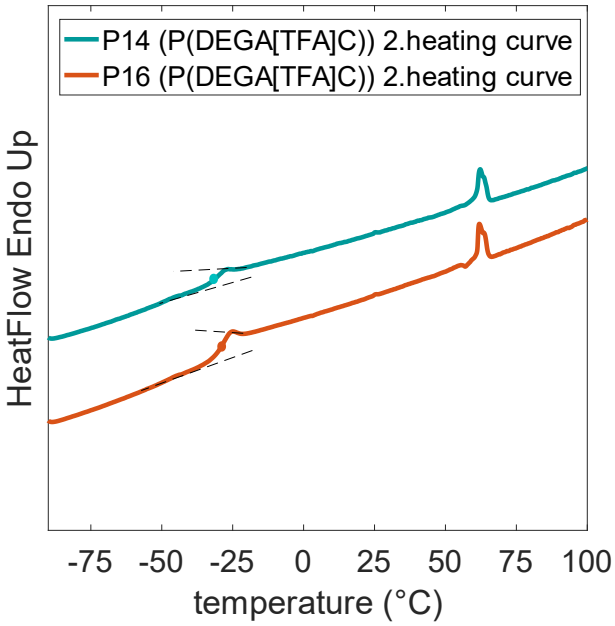

Figure S 30: DSC curves of the P(DEGA[TFA]C) homopolymers. The second heating curve is illustrated. The dot marks the T_g.

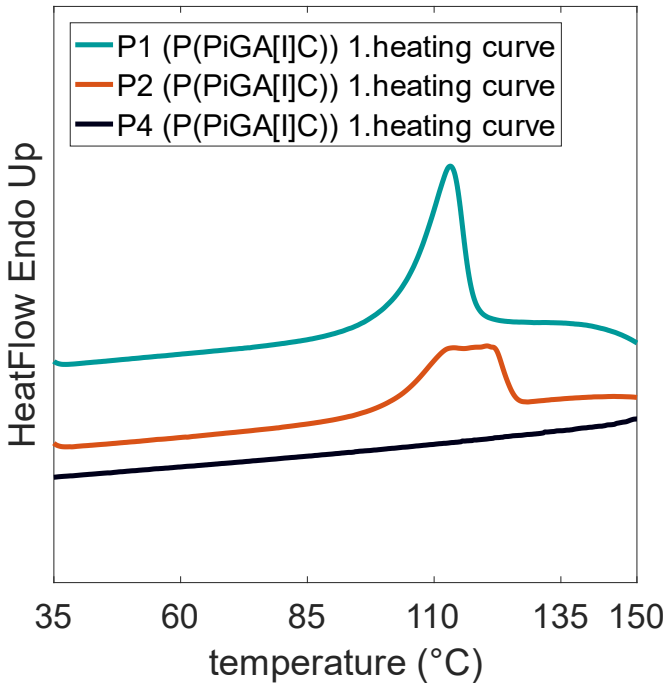

Figure S 31: DSC curves of the P(PiGA[I]C) homopolymers. The first heating curve is illustrated.

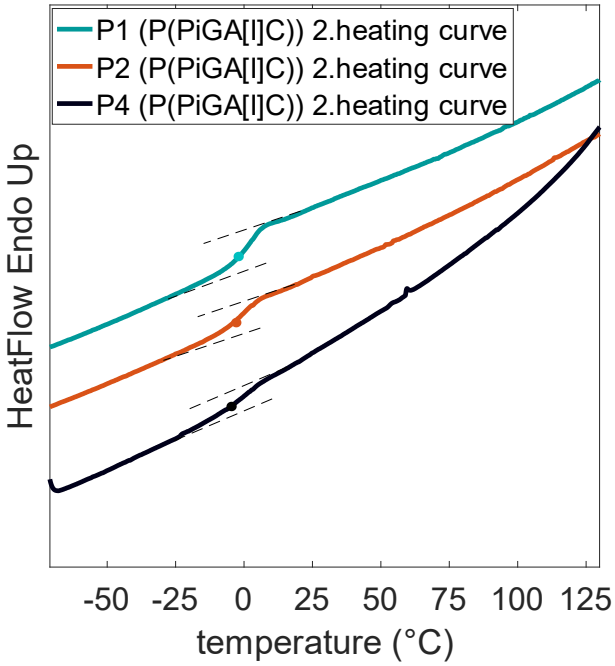

Figure S 32: DSC curves of the P(PiGA[I]C) homopolymers. The second heating curve is illustrated. The dot marks the T_g.

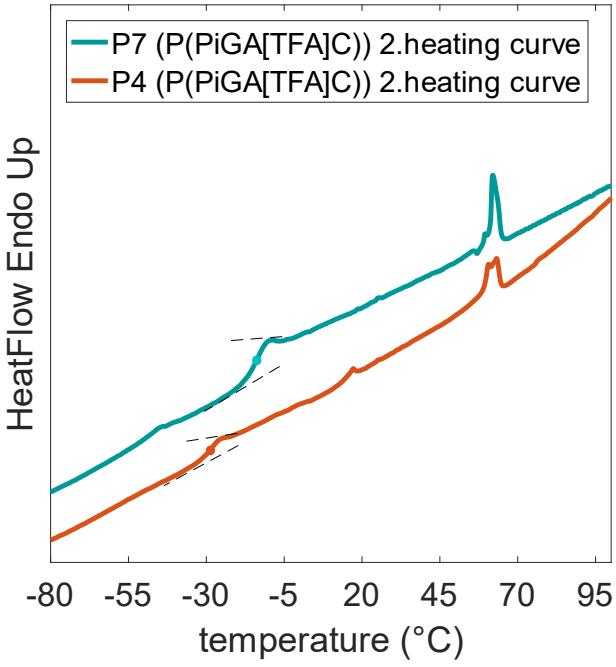

Figure S 33: DSC curves of the P(PiGA[TFA]C) homopolymers. The second heating curve is illustrated. The dot marks the T_g.

4. Acidic degradation

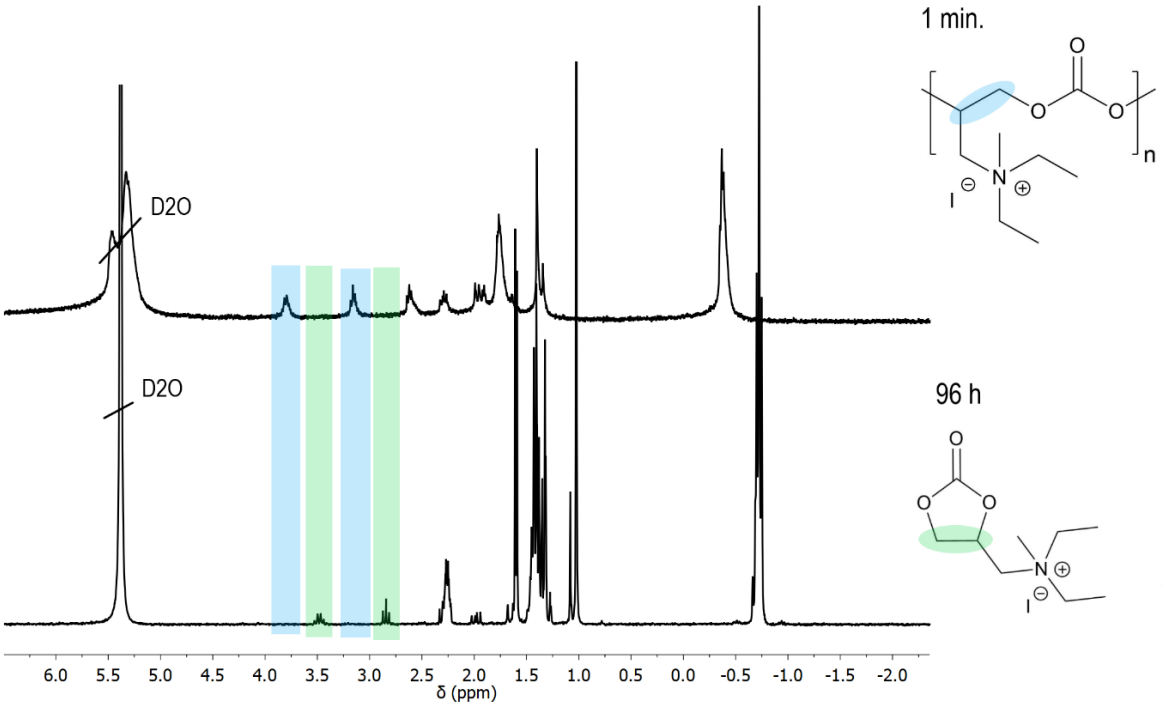

Figure S 34: Comparison of the ^{1}H NMR spectra (DCl/D_2O, 300 MHz) of P13 after the addition of DCl, recorded after 1 min. (top) and 96 h (bottom).

CHAPTER 6

Siloxane Functionalized Polyether-Polycarbonates with Amphiphilic Properties: A New Class of Surfactants

CHAPTER 6

Siloxane Functionalized Polyether-Polycarbonates with Amphiphilic Properties: A New Class of Surfactants

Tatjana Daenzer[a], Christina Gardiner[a], Lena Kunze[a], Shih-Yu Tseng[b], Tassilo Gleede[c], Thomas Sottmann[b]*, Holger Frey[a]*

[a]Institute of Organic Chemistry, Johannes Gutenberg University of Mainz, Duesbergweg 10-14, 55128 Mainz, Germany.

[b]Institute of Physical Chemistry, University of Stuttgart, Pfaffenwaldring 55, 70569 Stuttgart, Germany.

[c]Max Planck Institute for Polymer Research, Ackermannweg 10, 55128 Mainz, Germany.

To be submitted.

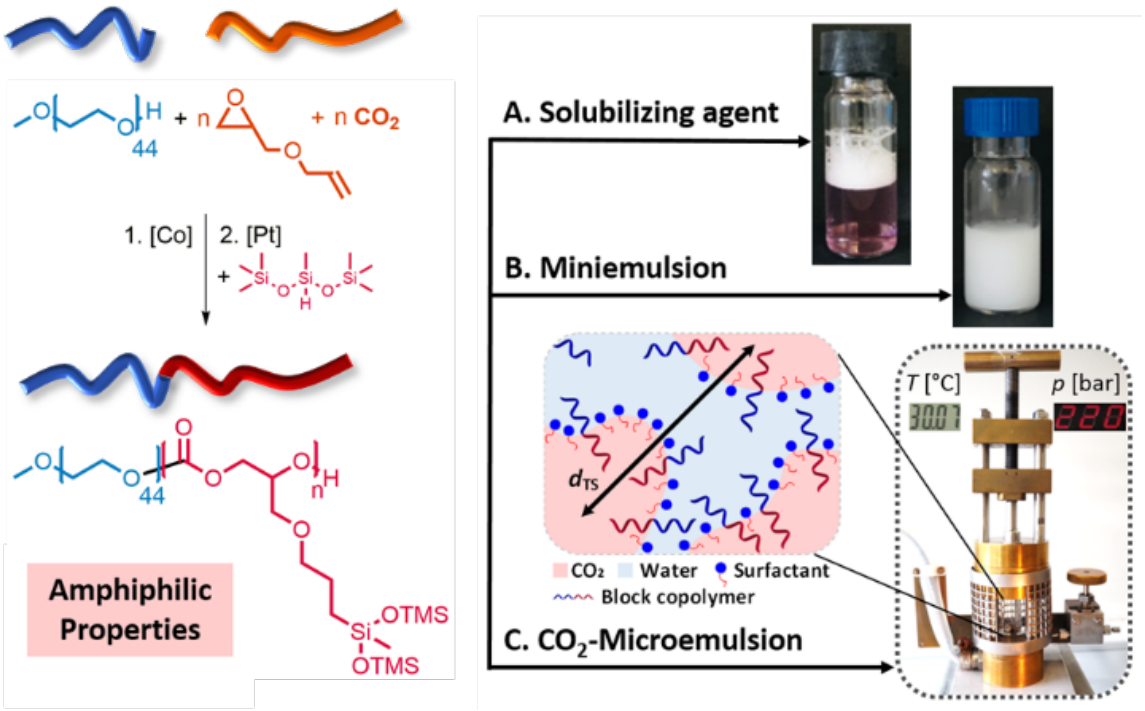

ABSTRACT

In this work, we present a convenient approach to siloxane functionalized polycarbonates (P(AGE-HMTS)C) and the respective amphiphilic nonionic diblock copolymers (mPEG-*b*-PAGEC and mPEG-*b*-P(AGE-HMTS)C). The polymers were synthesized *via* catalytic ring opening copolymerization of allyl glycidyl ether (AGE) with CO_2 by using an established catalytic system consisting of (R,R)(salcy)DNP and [PPN]DNP, followed by hydrosilylation with HMTS. Amphiphilic diblock copolymers with varying polycarbonate block lengths were synthesized and analysed by standard NMR spectroscopy, SEC, MALDI-TOF and FTIR. Thermal properties have been investigated by DSC and TGA measurements. The molecular weight of the amphiphilic copolymers ranges between 3 200–19 000 g mol^{-1}, the homopolymer P(AGE-HMTS)C_{76} has a molecular weight of about 21 000 g mol^{-1}. The micellization behaviour is characterized by surface tension measurements, DLS and TEM measurements. Miniemulsion polymerization of styrene in water is performed in the presence of a selected block copolymer to demonstrate emulsifying properties. The addition of small amounts of this new type of diblock polymers boost the efficiency of the surfactant tetraethylene glycol monodecyl ether ($C_{10}E_4$) to form microemulsions containing equal amounts of water and *n*-decane. Interestingly, at a high pressure of 220 bar (22 MPa) these polymers were also capable of increasing the efficiency of a technical grade PEG-HMTS surfactant to enhance miscibility of H_2O and supercritical CO_2.

INTRODUCTION

Carbon dioxide (CO_2) is a non-flammable, non-toxic, renewable and sustainable C_1 resource. Additionally, as a side product of blast furnace, it is a cheap and readily available established building block for polyether carbonates. However, in general the use of carbon dioxide is limited because of its thermodynamic stability and low reactivity.[1,2] Since the development of the immortal carbon dioxide/epoxide polymerization by Inoue et al. in 1969, carbon dioxide has been used as a monomer in polymerizations. In recent years, polymer architectures based on CO_2 have attracted increasing attention and are studied by a number of groups.[1,3–10] Some groups were also interested in poly(allyl glycidyl ether carbonates) and their copolymers, since this permits to conveniently postmodify the resulting polymer. Listos et al. used a $ZnEt_2$/pyrogallol catalyst system, and Müller et al. employed a multi-component polymerization to synthesize homo-PAGEC.[11,12] Additionally, Kuo and co-workers copolymerized AGE and CO_2 with a Zn-catalyst system and modified the allyl-arms with 3-(trimethoxysilyl)propyl methacrylate *via* a free radical reaction with subsequent sol-gel process to obtain polyether carbonate silica nanocomposites.[13] Meng et al. statistically copolymerized PO, AGE and CO_2 to introduce carboxyl groups by a thiol-ene click reaction to acquire polymers which may find application in lithium batteries.[14] Nanostructured systems comprising ABA triblock copolymers with PAGEC as block A have been synthesized by Darensbourg et al. and functionalized *via* thiol-ene click reaction with a variety of thiols.[15]

To the best of our knowledge, no reports have been published to date regarding side chain functionalization of poly(allyl glycidyl ether carbonates) (PAGEC) and poly(ethylene glycol)-poly(carbonate) block copolymers ($mPEG_{44}$-*b*-$PAGEC_n$) with siloxanes *via* hydrosilylation.

Aiming at the solubilization of CO_2 in polar media, such polymers should possess a "CO_2-philic" and a polar part. In addition, the "CO_2-philic" part should be hydrophobic, while the polar part should be CO_2-phobic. Because of the weak van der Waals interactions of CO_2, it is crucial to identify a suitable CO_2-philic part.[16] In the field of polymeric CO_2-surfactants fluorinated segments achieve a high compatibility with CO_2.[17,18] However, fluorinated oligomers are expensive and environmentally problematic, since they do not degrade but accumulate. Johnston et al. and Eastoe et al. observed that highly branched and oxygenated hydrocarbon chains can interact with CO_2.[19–21] Other promising results were obtained with trisiloxane surfactants, which appear to be effective emulsifying agents, forming both water-in-CO_2 and CO_2-in-water emulsions.[22] Thus, due to the high CO_2-affinity of siloxanes and carbonates, amphiphilic structures that combine both

moieties in their hydrophobic segment are promising candidates for the solubilization of supercritical carbon dioxide in polar media.[22–26]

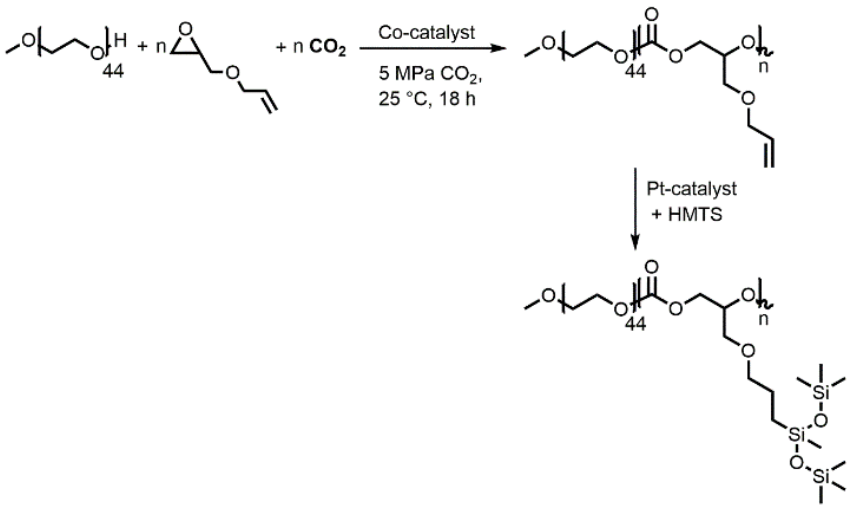

Scheme 1: Synthesis of mPEG$_{44}$-*b*-P(AGE-(bis-trimethylsiloxy) methyl silane)C)$_n$ from mPEG, allyl glycidyl ether, CO_2 and heptamethyltrisiloxane

Besides the promising emulsifying properties of amphiphilic side chain-functionalized polycarbonates, polycarbonates in general can benefit from the outstanding properties of the siloxane group:

On the one hand, siloxane moieties incorporated in various copolymers has been shown to enhance the thermal stability of these polymers.[27–29] On the other hand, trisiloxane surfactants are well known for their lowering effect on the surface energy of aqueous solutions, rendering them favoured additives for wetting applications.[30–32] A combination of a carbonyl backbone with siloxane side chain functionality can combine the advantages of both structures. To the best of our knowledge, polycarbonates based on CO_2 have not yet been covalently combined with siloxanes. Thus, the trisiloxane side chain functionality may not only improve the thermal stability of polycarbonates, but can also contribute to their surface activity.

In this work, we present novel siloxane-functionalized amphiphilic polycarbonates. The structure comprising only (AGE-HMTS) units and CO_2 was obtained by co-polymerization of allyl glycidyl ether (AGE) and CO_2. Block copolymers were obtained by polymerization of the same monomers, using monomethoxy poly(ethylene glycol) with a molecular weight of $\bar{M}_n$ = 2 000 g mol^{-1} (mPEG$_{44}$) as a chain transfer agent. In the final step, the addition of the silane HMTS to the allyl groups proceeded *via* hydrosilylation, using Karstedt's catalyst. This strategy affords the P(AGE-HMTS)C homopolymer and mPEG$_{44}$-*b*-P(AGE-HMTS)C$_n$ diblock copolymers (Scheme 1).

All polymers were characterized by NMR spectroscopy, size exclusion chromatography (SEC) and Fourier-transform infrared spectroscopy (FTIR), matrix-assisted-laser-desorption-ionization-time-of-flight (MALDI-TOF), differential scanning calorimetry (DSC), and thermogravimetric analysis (TGA). Amphiphilic block copolymers that were soluble in water were screened for their micellization behaviour by determination of their critical micelle concentration (CMC) via tensiometry, their micelle size by dynamic light scattering with a Malvern Zetasizer and transmission electron microscopy (TEM), and their spreading behaviour on a glass surface by contact angle measurements. To demonstrate application as a surfactant, a selected block copolymer was used as an emulsifier to stabilize a miniemulsion polymerization of styrene in aqueous medium. Both DLS and Transmission Electron Microscopy (TEM) showed that the novel block copolymers can be successfully used as surfactants in the miniemulsion polymerization.

Furthermore, we studied the ability of the new amphiphilic block copolymer $mPEG_{44}$-*b*-P(AGE-HMTS)C_8 to increase the efficiency of *n*-alkyl poly(ethylene glycol) and trisiloxane surfactants to stabilize *n*-alkane/scCO_2 containing microemulsions.

RESULTS AND DISCUSSION

PAGEC and mPEG44-*b*-P(AGE-HMTS)C_n - Synthesis and Characterization

Siloxane functionalized polycarbonate surfactants based on allyl glycidyl ether (AGE), CO_2, monomethoxy poly(ethylene glycol) (mPEG) and 1,1,1,3,3,5,5,5-heptamethyltrisiloxane (HMTS) are introduced in this work.

The polycarbonate homopolymer $PAGEC_{76}$ was synthesized by copolymerization of carbon dioxide and allyl glycidyl ether (AGE) using the established (*R,R*)-(salcy)-CoDNP catalyst system and bis(triphenyl-phosphine)iminium-2,4-dinitrophenol ([PPN]DNP]) (Scheme 1). The (*R,R*)-(salcy) catalyst leads to perfectly alternating incorporation of epoxide monomers and carbon dioxide and results in a moderate dispersity of the polycarbonate.[36] To suppress the formation of cyclic carbonates, which are the thermodynamically favored products of the reaction, the experiments were conducted at room temperature, and the reaction time was adjusted to 18 h.[10] To generate the amphiphilic mPEG-*b*-PAGEC diblock copolymers $mPEG_{44}$ was used as a chain transfer agent (CTA). An equilibrium forms between the CTA containing block copolymer (mPEG) and the homopolymer (PAGEC) as active and dormant species. This usually leads to a controlled reaction and low dispersity diblock copolymers ($mPEG_{44}$-*b*-$PAGEC_n$).[6,10] The byproduct PAGEC homopolymer and the deactivated catalysts were separated from the diblock copolymer by

quenching with HCl ($5_{vol\%}$ in MeOH) and subsequent flash column chromatography using neutral aluminum oxide and THF as an eluent. Considering the formation of PAGEC, no quantitative yield can be achieved in the block copolymerization reactions.

The trisiloxane HMTS was added to the pending double bond *via* hydrosilylation with the Karstedt's catalyst as the best-established catalyst for hydrosilylation.[37,38] The reaction time was adjusted to not exceed 60°C to prevent the isomerization of the allyl ether at elevated temperatures. Purification by refluxing with basic ion exchange resin to remove remaining catalyst and dialysis against dichloromethane resulted in the pure products.

Using this method, a siloxane bearing homopolymer and three silicone-functionalized amphiphilic block copolymers were obtained. The results are listed in Table 1.

Table 1: Overview of the synthesized P(AGE-HMTS)C_{76} and mPEG_{44}-*b*-P(AGE-HMTS)C_n.

No.	sample	M_n[a] g/mol	M_n[b] g/mol	$Đ$[b]	T_g[c] °C	T_m[c] °C	ΔH_m[c] J/g	T_d[d] °C
	mPEG_{44}	2 000	2 400	1.03		52	174	365
1.1	P$AGEC_{76}$	n.a.	12 000	1.21	–30			271
1.2	P(AGE-HMTS)C_{76}	n.a.	21 000	1.32	–44			294
2.1	mPEG_{44}-*b*-P$AGEC_3$	2 400	2 100	1.03		48	121	351
2.2	mPEG_{44}-*b*-P(AGE-HMTS)C_3	3 200	2 500	1.06	–52	37	44.0	346
3.1	mPEG_{44}-*b*-P$AGEC_8$	3 200	4 200	1.03	–30	42	87.0	235
3.2	mPEG_{44}-*b*-P(AGE-HMTS)C_8	5 000	6 200	1.09	–42	38	58.5	243
4.1	mPEG_{44}-*b*-P$AGEC_{45}$	9 100	8 500	1.08	–40	25	0.60	199
4.2	mPEG_{44}-*b*-P(AGE-HMTS)C_{45}	19 000	14 000	1.11	–72	27	4.50	265

[a]Determined by ^{1}H NMR spectroscopy in $CDCl_3$, 400 MHz. [b]Obtained by SEC (RI trace) in THF using PS standards for calibration. [c]Determined by DSC measurements at heating rates of 10 K min^{-1}. [d]$T_{d,onset}$ was determined by thermogravimetric analysis (TGA) at heating rates of 10 K min^{-1}.

All polymers were characterized by ^{1}H NMR spectroscopy, SEC and FTIR spectroscopy to determine the composition and to confirm purity. All signals can be assigned using 2D NMR

spectroscopy (Figure S 1-23). Impurities occur only in traces and consist of the used solvents methanol and diethyl ether or moisture. The successful formation of $PAGEC_{76}$ and the block copolymers is most evidently shown by the appearance of the carbonyl carbon signal at 154.35 ppm (Figure S 2, signal a). Distinctive signals of the polycarbonate backbone in the ^{1}H NMR at 5.05–5.02 ppm and 4.47–4.23 ppm (Figure S 1, signals a and b) and in the ^{13}C NMR at 66.25 ppm, and 74.51 ppm (Figure S 2, signals b and c) further support a successful polymerization. The characteristic signals of the double bond appear at 5.92–5.79 ppm and 5.30–5.17 ppm in the ^{1}H NMR (Figure S 1, signals e and f) and at 134.22 ppm and 117.72 ppm in the ^{13}C NMR (Figure S 2, signals f and g). In the block copolymers the methoxy group of the $mPEG_{44}$ block appears as a singlet at 3.35 ppm and 59.04 ppm respectively (Figure S 12 and S 13, signal a). It was used as a reference for the determination of the number of carbonate units of the block copolymers. The polyether backbone appears at 3.72–3.39 ppm and 70.57 ppm respectively (Figure S 12 and S 13, signal b).

The molecular weight of $PAGEC_{76}$ was determined by SEC in THF (polystyrene standard), since no end group analysis can be performed by ^{1}H NMR spectroscopy (Figure S24). The molecular weight value obtained is 12 000 g mol^{-1}, suggesting a degree of polymerization of $n \approx 76$. The distribution is monomodal, but shows tailing towards lower molar masses. The molecular weight distributions of the block copolymers determined by SEC (Figure S 25–27) are narrow ($Đ<1.1$), but show tailing towards lower molecular weights as well.

Due to the high hydrophobicity of PAGEC a PS standard was used for calibration. In the case of the block copolymers the use of a PEG standard leads to a much higher overestimation of the molecular weight compared to the $\bar{M}_n$ determined by end group analysis. Only the molar mass of the block copolymer with 8 carbonate units is slightly overestimated. Please note that SEC characterization of $mPEG_{44}$ leads to a higher value of $\bar{M}_n$ when using PS as SEC standard. By using a PEG standard, the value is of course much closer to the molecular weight obtained from NMR measurement. PEG is much more hydrophilic than PS and thus owns a much smaller hydrophilic radius, leading to later elution times and higher molar masses.

Carbonate bands at ca 1 750 cm^{-1} and polyether bands at ca 1 100 cm^{-1} in the FT-IR spectra further confirm the successful copolymerization of CO_2 and AGE (Figure S 28 and S 29). No cyclic by-products were observed, which is confirmed by the absence of a band at ca 1 800 cm^{-1}. In the case of the homopolymer, weak bands at ca 2 800 cm^{-1} only refer to the ether bonds of AGE, concluding the formation of only one polymeric species and no undesired formation of polyether defects.

The successful addition of the silane to the double bond *via* hydrosilylation in the post-polymerization step is supported by the disappearance of double bond signals in the ^{1}H NMR spectrum and the appearance of new signals at 1.60–1.50 ppm, 0.47–0.36 ppm, 0.17–0.03 ppm and 0.02–(–0.04) ppm. (Figure S 6, signals e, f, h, and g) and 23.29 ppm, 13.56 ppm, 2.00 ppm and 0.22 ppm respectively (Figure S 7, signals f, g, i, and h). The hydrosilylation was carried out at temperatures around 60 °C to ensure full conversion. It has been reported that allyl ethers tend to isomerize at temperatures exceeding 40 °C.[39] Corresponding signals to the isomerization product are found at 6.22–6.16 and 5.95–5.87 ppm (Figure S 6, zoom-in) and 145.97 ppm and 99.74 ppm respectively. The ^{1}H NMR and ^{13}C NMR spectra also show signals in the range of 0.75–1.00 ppm and 9–12 ppm that correlate to a hydrosilylated isomerization product in the 2D NMR experiments. However, the degree of isomerization did not exceed 2% of the double bonds, as determined by NMR integration and will thus not be considered in the further discussion.

The same findings regarding the hydrosilylation step apply for the block copolymers. The FTIR spectra display bands at 1 250 cm^{-1}, 1 039 cm^{-1}, and 838 cm^{-1} corresponding to the newly formed Si-C and then Si-O bonds of the HMTS unit.

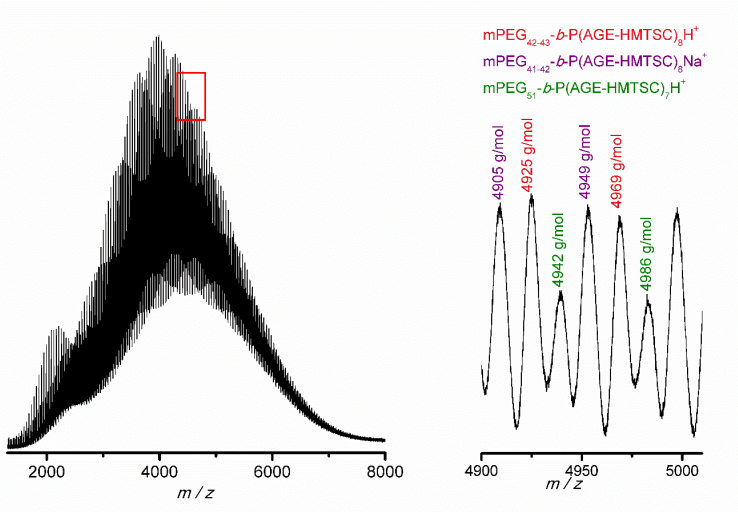

Figure 1. MALDI-TOF spectrum of sample mPEG$_{44}$-*b*-P(AGE-HMTS)C$_8$: complete spectrum (left side) and assigned molar masses (right side) in Dithranol. The repeating units were calculated to 44 g mol^{-1} for C_2H_4O (EO) and 380 g mol^{-1} for $C_{14}H_{32}O_6Si_3$ (AGE-HMTS)C.

Using several established matrix compounds for MALDI-TOF spectrometry of the hydrosilylated PAGEC homopolymer, no mass spectrum could be obtained (Figure S 30). Possibly, the high amount of non-polar siloxane side chains lowers the ionizability of the polymer. However, MALDI-TOF spectrometry of the siloxane-containing block copolymers confirmed full functionalization

with HMTS (Figure 1, the MALDI-TOF spectrum of the unfunctionalized block copolymer is shown in Figure S31). The unfunctionalized polycarbonate shows repeating units of 44 g mol^{-1} (ethylene glycol unit of the PEG block) and 158 g mol^{-1} (allyl glycidyl ether carbonate unit) with a molar mass maximum of 3 232.6 g mol^{-1} (mPEG$_{44}$-*b*-PAGEC$_9$Na$^+$). After hydrosilylation the MALDI-TOF spectrum is shifted to higher molecular masses due to the additional mass of 222.5 g mol^{-1} for each monomer unit with a molar mass maximum of 4 497.0 g mol^{-1} (mPEG$_{40}$-*b*-P(AGE-HMTS)C$_7$K$^+$). Every block exhibits a dispersity according to different potassium and sodium salts, resulting in a broad distribution of different ionized species. It is not possible to distinguish between the product of the hydrosilylation of the double bond or of the isomer since both units have the same molecular weight.

To further explore the effect of the siloxane functionalization on the polycarbonates, their thermal properties were investigated by differential scanning calorimetry (DSC) and thermogravimetric analysis (TGA). Samples **2.1–3.2** are obtained as PEG-like colourless solids, whereas samples **4.1** and **4.2** are slightly yellow viscous liquids at ambient temperature. As shown in Table 1, the melting points of the poly(AGE carbonates) and the HMTS-functionalized polycarbonates decrease with increasing carbonate block length from 52°C for pure mPEG$_{44}$ to 25 °C for mPEG$_{44}$-*b*-PAGEC$_{45}$ because of the growing PAGEC-like nature of the unfunctionalized copolymers and the growing siloxane-like nature of the functionalized copolymers. The amorphous homopolymer PAGEC$_{76}$ does not show any melting points and exhibits a glass transition temperature (T_g) of –30 °C (Figure S32). Experiments of Tan et al. show similar results for the PAGEC block (–18 °C, molecular weight not given).[40] Functionalization with the siloxane moieties lowers the glass transition of P(AGE-HMTS)C$_{76}$ considerably to –44 °C. The same trend applies for the functionalized block copolymers.

Contrary to previous findings for poly(butylene carbonate) block copolymers, the glass transition temperature of poly(AGE carbonate) block copolymers decreases with increasing carbonate chain length after hydrosilylation.[41] This is attributed to the enhanced side chain flexibility due to HMTS in comparison to the allyl ether. This effect called “internal plasticization” has previously been shown for poly(*N*-vinyl caprolactones) grafted with PDMS and for different poly(*n*-alkyl methacrylates).[42–44]

Siloxanes are well known for their high thermal stability.[45] PAGEC-SiO_2 nanocomposites have already shown an increasing stability with increasing Si content.[40] To investigate the influence of the covalently joined siloxane side chain on the thermal stability of the functionalized polycarbonates TGA measurements have been performed of both the non-functionalized and

functionalized polycarbonates (Figures S 33–S 36). Similar to the results of Tan et al., $PAGEC_{76}$ degrades at $T_{d,onset}$ = 271 °C (at 10% degradation).[40] After functionalization with HMTS P(AGE-HMTS)C_{76} exhibits a higher degradation temperature of 294 °C. The same applies to the block copolymers: the degradation temperature of the functionalized polycarbonate block copolymers is generally higher than the degradation temperature of the unfunctionalized polycarbonate block copolymers. $T_{d,onset}$ increases with increasing chain length and siloxane content of the carbonate block after functionalization. The degradation steps of $mPEG_{44}$-*b*-$PAGEC_3$ and $mPEG_{44}$-*b*-P(AGE-HMTS)C_3 do not differ significantly, since the aliphatic block is rather short and the polymers are still PEG-like while $mPEG_{44}$-*b*-P(AGE-HMTS)C_{45} has a significantly larger $T_{d,onset}$ than $mPEG_{44}$-*b*-$PAGEC_{45}$ ($\Delta T_{d,onset}$ = 61 °C) and is more siloxane-like. These findings support the thesis that the thermal stability of polycarbonates benefits from side chain functionalization with HMTS.

Surfactant behaviour of block copolymers in aqueous media

The amphiphilic block copolymers and their micellization behaviour in water were examined. Due to the apolar side chains both $PAGEC_{76}$ and P(AGE-HMTS)C_{76} are highly hydrophobic and insoluble in water. Adding a hydrophilic PEG block significantly increases the aqueous solubility of the block copolymers, depending on the length of the polycarbonate block.

The block copolymers with 45 carbonate units have HLB values of 4 (unfunctionalized polycarbonate) and 2 (HMTS-functionalized polycarbonate) and are both not soluble in water. Apparently, also the unfunctionalized polymer $mPEG_{44}$-*b*-$PAGEC_3$ is not amphiphilic enough to show any surface-active behaviour. However, after functionalization, an aqueous solution of $mPEG_{44}$-*b*-P(AGE-HMTS)C_3 shows heavy foaming while shaking and dissolves the otherwise insoluble dye nile red (right image in Figure 2). This is a first indication of the formation of micelles with a hydrophobic core in which the hydrophobic dye is dissolved. By increasing the length of the hydrophobic chain to eight units, the non-functionalized polycarbonate block copolymer $mPEG_{44}$-*b*-$PAGEC_8$ already shows surface active behaviour. The same observation is made for the functionalized copolymer $mPEG_{44}$-*b*-P(AGE-HMTS)C_8, although the complete dissolution in water takes significantly longer than for the not HMTS-functionalized copolymer. The critical micelle concentrations (CMC) obtained from tensiometry in Milipore water (Figure 2) range between 4–7 mg L^{-1} (Table 2), agreeing with literature values for amphiphilic polycarbonates.[9,10,41,47,48].

Table 2: Micellization properties of the water-soluble block copolymers.

No.	*CMC*[a]	*σ*[a]	*Γ*[a]	*A*[a]	*Θ*[b]	HLB[c]
	mg/L	mN/m	µmol/m²	Å²	°	
2.1	n.a.	n.a.	n.a.	n.a.	n.a.	16
2.2	6	34	4.34	3.8	n.d.	12
3.1	7	45	2.47	6.7	18.6 ± 0.8	10
3.2	4	58	2.30	7.2	14.9 ± 1.4	8

[a]Determined by ring tensiometry using an RG10 Du Noüy ring. [b]Determined by contact angle measurement [c]Calculated by using the method of Griffin for nonionic surfactants.[46]

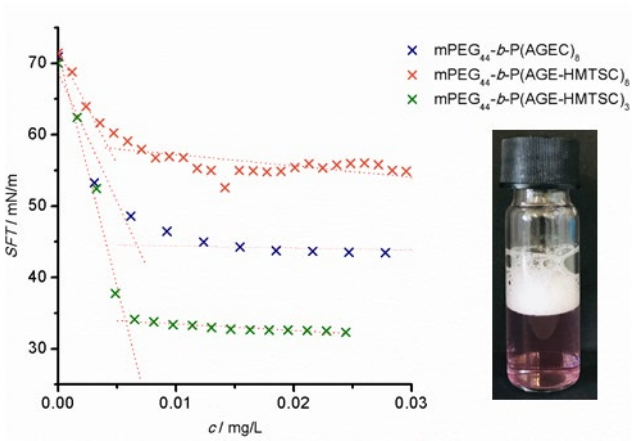

Figure 2: CMC *determination* by tensiometry of all water soluble block copolymers (mPEG$_{44}$-*b*-P(AGE-HMTS)C$_3$, mPEG$_{44}$-*b*-PAGEC$_8$ and mPEG$_{44}$-*b*-P(AGE-HMTS)C$_8$).

Amphiphilic block copolymers very often do not show a distinct CMC, even with a narrow dispersity.[49] However, Figure 2 exhibits a clear trend in the minimal surface tension (SFT) *σ*: with decreasing HLB value, i.e. with increasing carbonate chain length and hydrophobicity, the minimal SFT of the water-air interface increases from 34 mN m^{-1} for 2.1 to 55 mN m^{-1} for mPEG$_{44}$-*b*-P(AGE-HMTS)C$_8$. Polyether-siloxane surfactants have been extensively investigated regarding their influence on the surface tension of aqueous solutions. The minimum surface tensions of solutions of classic trisiloxane surfactants in water are reported to be between 20–21 mN m^{-1} due to the saturation of the water/air interface with CH_3 groups.[22,30,50] None of the newly synthesized surfactants reaches these values. This is tentatively attributed to the carbonate units in the hydrophobic block. Other than in surfactants comprising merely PDMS or trisiloxane, functional

groups with high surface energy in the backbone like CH_2, C=O, and C-O raise the surface energy. In addition to that, model calculations show that polymeric AB diblock surfactants with a shorter apolar chain length are more efficient in reducing the interfacial tension of a water/oil interface than surfactants with a longer chain length, independent of their chemical nature.[51] This is supported by the surface excess concentration Γ in mol m^{-2} and the area per molecule A in nm^2 determined by

$$\Gamma = -\frac{1}{RT}\left(\frac{\delta\sigma}{\delta ln(c)}\right) \quad (4)$$

and

$$\mathrm{A} = \frac{10^{18}}{N\Gamma} \quad (5)$$

with R = 8.314 J mol^{-1} K^{-1}, T = temperature in K, σ surface tension in mN m^{-1}, and c = concentration in mol L^{-1}. The calculated data in Table 2 shows decreasing values of Γ for increasing (AGE-HMTS)C chain lengths due to a higher steric demand of the hydrophobic chain, which translates to an increasing area per molecule. Polyether-trisiloxane surfactants are particularly known as efficient super spreaders and wetting agents due to their low surface tension in water. The wetting behaviour of such surfactants has already been reported in various publications.[30,50,52,53] To investigate the influence on the wetting characteristics of carbonate surfactants, contact angle measurements of droplets of aqueous surfactant solutions on glass were performed. Images of the droplets are shown in the Supporting Information (Figure S 37). Pure water on glass showed a contact angle of Θ = 32.4±0.6° and $mPEG_{44}$ showed a lower contact angle of Θ = 25.0±0.6°. Dissolving the unfunctionalized carbonate in water significantly lowers the contact angle to Θ = 18.6±0.8°. The addition of the siloxane functionality lowers the value even further to Θ = 14.9±1.4°. This demonstrates that adding siloxane moieties to the hydrophobic block of the surfactant enhances the wettability of a low-energy surface with an aqueous solution of an amphiphilic polycarbonate and demonstrates applicability as wetting agents for less demanding wetting problems.

The presence of micelles was proven exemplary for the amphiphilic block copolymer $mPEG_{44}$-*b*-$P(AGE\text{-}HTMS)_3$ by DLS and TEM. The TEM image shows spherically shaped micelles with an average diameter of 97±17 nm (Figure 3) in agreement with preliminary DLS measurements, in which a

slightly smaller hydrodynamic diameter of d_{hyd} = 84 mn (PDI = 0.889, Figure S 38) was found. Note that these values are in the typical order of magnitude found for polymeric surfactants micelles.[54–56]

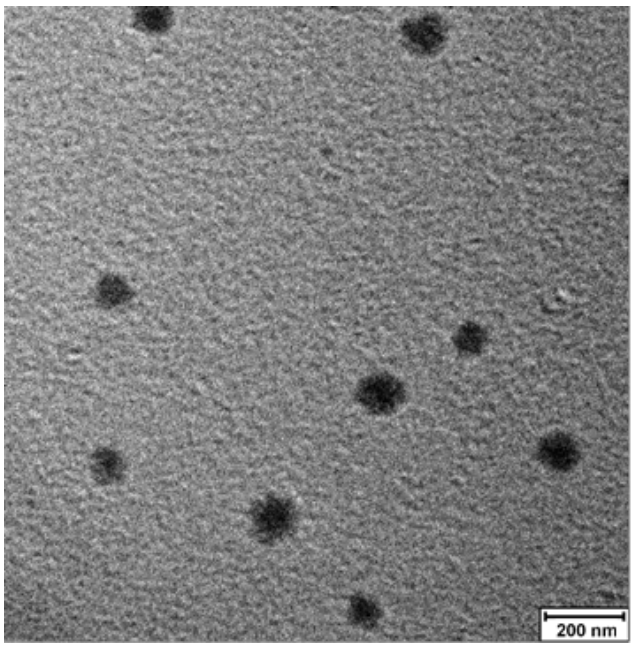

Figure 3: TEM image of mPEG$_{44}$-*b*-P(AGE-HMTS)C$_3$ in water (no staining needed).

Nonionic surfactants with an HLB value of 8–10 are known to be efficient O/W emulsifiers.[57] Various amphiphilic block copolymers, including polycarbonates, have already shown applicability as emulsifiers in the emulsion polymerization of apolar monomers in water.[9,58] The emulsifying properties of mPEG$_{44}$-*b*-P(AGE-HMTS)C$_8$ (HLB value = 8) were investigated in a free radical miniemulsion polymerization of styrene in water. The block copolymer was used at a concentration of 30 mg/mL in water. After addition of a mixture of styrene, hexadecane and the initiator 2,2'-azobis(2-methylbutyronitrile) a stable miniemulsion was obtained by sonication. TEM images (Figure S 39) show that the block copolymer can be used to prepare spherical PS-nanoparticles. The hydrodynamic radius of the nanoparticles was determined by DLS measurement (Figure S 40) and was found to be 92 nm. The PDI of 0.083 indicates a narrow size distribution of the nanoparticles. Besides possible application in miniemulsion polymerization, the outstanding emulsification properties of siloxane functionalized amphiphilic polycarbonate block copolymers regarding scCO$_2$ in water are discussed in the following section.

Efficiency-Boosting Effect of mPEG44-*b*-P(AGE-HMTS)Cn block copolymers in microemulsions

Almost 20 years ago, Jakobs et al. found that small amounts of amphiphilic poly(ethylene propylene)-*co*-poly(ethylene glycol) polymers are able to considerably increase the efficiency of medium-chain surfactants in forming microemulsions.[59] Recently we showed that amphiphilic polyether-*b*-polycarbonate polymers of the type $mPEG_{44}$-*b*-PBC_n strongly increase the efficiency of nonionic *n*-alkyl polyglycol ether surfactants (C_iE_i) to formulate microemulsions containing polymerizable oils, e.g. hexyl methacrylate.[41] In this work, the new type of amphiphilic block copolymers ($mPEG_{44}$-*b*-P(AGE-HMTS)C_n) possessing siloxane functionalized polycarbonate units as nonpolar and CO_2-philic block has been added to two different type of microemulsions. On the one hand, the influence of $mPEG_{44}$-*b*-P(AGE-HMTS)C_8 on the state of the art microemulsion H_2O/NaCl - *n*-decane - $C_{10}E_4$ (tetraethylene glycol monodecyl ether) is studied at ambient pressure. On the other hand, we investigated whether this new type amphiphilic block copolymer is also able to increase the efficiency of the trisiloxane surfactant Q2-5211 to solubilize H_2O and supercritical CO_2.

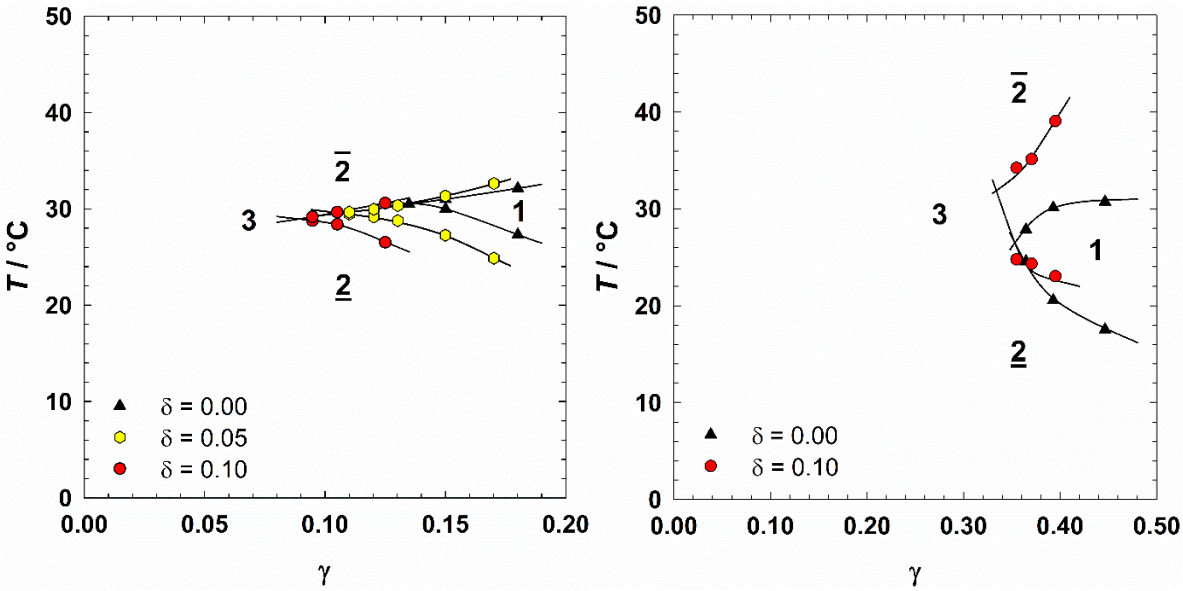

Figure 4: Influence of the $mPEG_{44}$-*b*-P(AGE-HMTS)C_8 polymer on the phase behaviour of two different microemulsion systems. *T*(*γ*)-sections through the phase prism are recorded at equal volumes of water and oil. Left: H_2O/NaCl (0.1 wt%) - n-decane - $C_{10}E_4$/$mPEG_{44}$-*b*-P(AGE-HMTS)C_8. Right: H_2O - $scCO_2$ - Q2-5211/$mPEG_{44}$-*b*-P(AGE-HMTS)C_8 at p = 220 bar.

In Figure 4 (left), the influence of the $mPEG_{44}$-*b*-P(AGE-HMTS)C_8 block copolymer on the phase behaviour of H_2O/NaCl (0.1 wt%) - *n*-decane - $C_{10}E_4$ (tetraethylene glycol monodecyl ether) is

shown. $T(\gamma)$-sections were recorded at equal volumes of water and oil for the system without block copolymer (δ = 0.00) and replacing 5 and 10 wt% of the $C_{10}E_4$ by $mPEG_{44}$-*b*-P(AGE-HMTS)C_8, i.e. δ = 0.05 and 0.10. Note, that the small amount of NaCl (0.1 wt.% in the H_2O/NaCl mixture (brine)) is added to suppress possible electrostatic interactions induced by impurities of the polymer. In general, a phase sequence typical for microemulsions stabilized by nonionic surfactants is found.[34] At low temperatures, an oil-in-water microemulsion co-exists with an oil excess phase (denoted as $\underline{2}$); while at high temperatures, a water-in-oil microemulsion co-exists with a water-excess phase (denoted as $\overline{2}$). At temperatures in between, a three-phases region (denoted as 3) exist at $\gamma < \tilde{\gamma}$ where a microemulsion co-exists with a water-excess phase and an oil-excess phase. When the value of γ is larger than $\tilde{\gamma}$, which is the minimum amount of total surfactant/polymer mixture needed to form a microemulsion at the phase inversion temperature PIT ($\tilde{T}$), the one-phase region can be found.

The influence of the new $mPEG_{44}$-*b*-P(AGE-HMTS)C_8 block copolymer on the phase boundaries is striking. By replacing merely 5 wt% of $C_{10}E_4$ with the new block copolymer (δ = 0.05), $\tilde{\gamma}$ decreases from $\tilde{\gamma}$ = 0.135 to 0.106. A further replacement of the surfactant by the block copolymer (δ = 0.10) causes a further decrease of $\tilde{\gamma}$ to $\tilde{\gamma}$ = 0.089. Furthermore, the phase boundaries and accordingly the phase inversion temperature $\tilde{T}$ decreases slightly from $\tilde{T}$ = 30.5 °C to 29.6 °C and 28.9 °C. This slightly decrease in $\tilde{T}$ might come from the fact that the hydrophobic block of the diblock polymer is larger than the hydrophilic block.[60,61] Due to the mean curvature changes of the surfactant membrane induced by the anchored block polymer, the change in the temperature $\tilde{T}$ can be described as

$$\Delta T \propto \frac{\sigma k T (R_W - R_O)}{\kappa^* c} \tag{6}$$

with the number density of the block copolymer molecules in the membrane σ, end-to-end distances of hydrophilic block R_W or hydrophobic block R_O of the polymer, bending rigidity of the membrane κ and the temperature coefficient of the mean curvature *c* for the system.[62]

Having proven that these new amphiphilic block copolymers show a strong efficiency boosting in state of the art microemulsion systems, the CO_2-philic (AGE-HMTS)C_8 block suggest to use these polymers for the formulations of CO_2-microemulsions which gained a lot of interest lately.[35,63–66] Since it is easy to produce, non-flammable and non-toxic supercritical CO_2 ($scCO_2$) is not only used as replacement for organic solvents, but also interesting blowing agent for producing micro- and

nanocellular foams starting from a CO_2-microemulsion.[35] However, to find efficient non-fluorinated surfactants, that stabilize CO_2-microemulsions efficiently, is a challenging task (as discussed in the introduction).[17,19,21] With this motivation, we also studied the influence of the new $mPEG_{44}$-*b*-P(AGE-HMTS)C_8 on the phase behaviour of the H_2O - $scCO_2$ - Q2-5211 microemulsion system. Here, Q2-5211 is a technical-grade polyethylene heptamethyltrisiloxane surfactant with 10.3 EO units which has a reasonable affinity with CO_2 due to the stubby structure and the CO_2-philic heptamethyltrisiloxane group.[22]

Figure 4 (right) shows the $T(\gamma)$-section of the system H_2O - $scCO_2$ - Q2-5211 recorded at equal volumes of water and $scCO_2$ at constant pressure p = 220 bar. The phase behaviour of this CO_2-microemulsion resembles that of microemulsions stabilized by nonionic surfactants, i.e. the one of the H_2O/NaCl - *n*-decane - $C_{10}E_4$ system shown in Figure 4 (left). However, as can be seen, the efficiency of the Q2-5211 surfactant to solubilize H_2O and $scCO_2$ ($\tilde{\gamma}$ = 0.353) is much smaller than the efficiency of $C_{10}E_4$ solubilizing brine and *n*-decane. Replacing 10 wt% ($\delta = 0.10$) of the Q2-5211 surfactant by the $mPEG_{44}$-*b*-P(AGE-HMTS)C_8 polymer, the one-phase region is largely widened (stabilized). However, the efficiency is only slightly enhanced by the polymer, i.e. $\tilde{\gamma}$ decreases slightly to $\tilde{\gamma}$ = 0.334. The small effect of the polymer with respect to efficiency might also be related to the shift of the phase inversion temperature $\tilde{T}$ from 26.5 °C to 31.9 °C. The polymer seems to induce an increasing curvature of the amphiphilic film around CO_2, which is a strong indication that the size of the P(AGE-HMTS)C_8 block is much smaller in CO_2 than in *n*-decane due to the not perfect interaction between CO_2 and P(AGE-HMTS)C.[60] Pursuing this line of thought, the size of the PEO block has to be decreased to improve the efficiency boosting effect of this new type of amphiphilic block copolymers in CO_2-microemulsions.

CONCLUSION

A series of novel amphiphilic siloxane functionalized block copolymers ($mPEG_n$-*b*-P(AGE-HMTS)C_m) based on $mPEG_{44}$ and CO_2 with varying block lengths of 3, 8, and 45 and one homopolymer (P(AGE-HMTS)C) were successfully synthesized.

The polycarbonates were synthesized by catalytic ring opening copolymerization of CO_2 with AGE in an autoclave at CO_2 pressures of 5.5 MPa at room temperature. The siloxane functionality was introduced *via* subsequent hydrosilylation of the AGE double bond. The resulting polymers exhibit molar masses in the range between 3 200 and 21 000 g mol^{-1} with narrow molecular weight distributions of Đ<1.2. The homopolymer shows a mass of 21 000 g mol^{-1} with a distribution of $Đ$ = 1.31. MALDI-TOF spectra prove the existence of repeating units with a mass of 158 g mol^{-1}

(AGEC) before hydrosilylation and 380 g mol^{-1} (AGE-HMTS)C after the hydrosilylation, thus proving the successful side chain functionalization of the polycarbonate.

DSC measurements showed decreasing glass transition temperatures from –30 °C to –40 °C for the unfunctionalized copolymers to –44 °C to –70 °C for the HMTS functionalized copolymers. Additionally, the decreasing melting points (52 °C to 27 °C) with increasing carbonate chain length and increasing HMTS content underline the increasing siloxane-like properties of the surfactant structures. TGA measurements revealed that functionalization of carbonates with siloxanes also leads to higher degradation temperatures.

CMC determination provided values between 4–7 mg L^{-1}, agreeing with literature values for amphiphilic polycarbonates. Preliminary DLS as well as TEM images prove the formation of micelles. The observation that the contact angle of an aqueous solution can be decreased by adding the functionalized polycarbonate surfactant suggest a possible application as wetting agents. Furthermore, mPEG$_{44}$-*b*-P(AGE-HMTS)C$_8$ was successfully applied in a miniemulsion polymerization of styrene in water. Narrowly distributed PS-nanoparticles with an average radius of 92 nm and a PDI of 0.083 were obtained.

The phase behaviour studies show that the addition of mPEG$_{44}$-*b*-P(AGE-HMTS)C$_n$ diblock copolymers leads to an enhanced efficiency of medium chain surfactants in forming both state of the art *n*-alkane- and scCO$_2$-microemulsions. In this regard, the effect of the mPEG$_{44}$-*b*-P(AGE-HMTS)C$_8$ polymer on the H$_2$O/NaCl - *n*-decane - C$_{10}$E$_4$ microemulsion system is much stronger than on the H$_2$O - scCO$_2$ - Q2-5211 system. The shift of the phase inversion temperature towards higher temperatures in the latter system indicates that the size of the (AGE-HMTS)C$_8$ block is much smaller in CO$_2$ than in *n*-decane due to the non-perfect interaction between CO$_2$ and (AGE-HMTS)C. However, the small decrease in $\tilde{\gamma}$ value and the enlarged one-phase region still implies the potential of mPEG$_{44}$-*b*-P(AGE-HMTS)C$_n$ as promising additives in CO$_2$-microemulsions.

The surfactant-like properties of the siloxane functionalized polycarbonates open several application possibilities, e. g. as stabilizers in the free-radical polymerization of hydrophobic monomers in water or as co-stabilizers in emulsions and microemulsions.

EXPERIMENTAL SECTION

Materials

Allyl glycidyl ether (AGE) (99% *TCI*), was distilled over CaH_2 under reduced pressure prior to use. Argon and CO_2 (>99.99% *Westfalen AG* and *TMG*) were used as received. Monomethoxy poly(ethylene glycol) ($mPEG_{44}$) (Fluka) was dried with benzene under reduced pressure prior to use. All other reagents were purchased from *Sigma Aldrich*, *Acros Organics, Fischer Chemicals* and *AnalR NORMPUR* and were used as received. The catalyst system (*R,R*)-(salcy)-CoDNP and [PPN]DNP was synthesized as previously described.[33]

H_2O was double-distilled. *n*-Decane (purity of 99%) was purchased from *Sigma-Adrich* and used as received. Tetraethylene glycol monodecyl ether ($C_{10}E_4$) was purchased from *Bachem* with an analytical grade of at least >98% and used as received. A technical-grade poly(ethylene glycol) heptamethyltrisiloxane surfactant (Q2-5211) with 10.3 EO degree was purchased from *Dow Corning* with technically grade purity and used as received.

Characterization

Nuclear Magnetic Resonance (NMR) spectroscopy: ^1H and ^{13}C NMR spectra as well as the 2D-NMR techniques were recorded on a *Bruker Avance II HD 400* (400 MHz) spectrometer at 21 °C. The chemical shifts δ are given in part per million (ppm). All spectra are referenced to the residual solvent signal. Analysis of the spectra was performed with the software *MestReNova 9.0.1 (MestreLab Research)*.

Matrix-assisted laser desorption and ionization time-of-flight mass spectrometry (MALDI-TOF): MALDI-TOF measurements were performed on a Bruker rapifleX R^+ MALDI-TOF-MS on a DCTB (trans-2-[3-(4-tert-Butylphenyl)-2-methyl-2-propenylidene]malononitrile) matrix in the presence of KTFA (potassium trifluoroacetate).

Size exclusion chromatography (SEC): All SEC measurements were performed in THF at 50 °C using a flow rate of 0.1 mL min^{-1}. Toluene was added as an internal standard and polystyrene standards provided by PSS were used for calibration. A refractive index (RI) and a UV (275 nm) detector served as integrated instruments.

Differential Scanning Calorimetry (DSC)*:* DSC curves were recorded on a METTLER DSC 823 in the temperature range from –140 to +50 °C with a heating rate of 10 K min^{-1} under nitrogen.

Thermogravimetric Analysis (TGA)*:* The TGA data was obtained using a Perkin Elmer Pyris Thermogravimetric Analyzer in the temperature range from 30 to 600 °C with heating rates of 10 K min^{-1} in air.

IR Spectroscopy*:* FT-IR spectra were recorded on a *Thermo Scientific iS10 FT-IR* spectrometer, equipped with a diamond ATR unit.

Determination of the CMC using ring tensiometry*:* Screening of the surface tension of a polymer solution in water with increasing concentration of the polymer was performed at 24.6 °C with a DataPhysics DCAT 11 EC tensiometer equipped with a TV 70 temperature control unit, a liquid dispenser unit (LDU) 1/1 and a Du Noüy ring RG 11. The ring was heated with a Bunsen burner before each measurement. All solutions were stirred for 120 s at a stirring rate of 50%. Measurements were started after a waiting time of 30 s and repeated twice.

Light Scattering*:* DLS measurements of the micelles were performed in disposable PS cuvettes on a Malvern Zetasizer Nano ZS with a Peltier-controlled thermostat, at a wavelength of 633 nm, an angle of 173° and a constant temperature of 25 °C. DLS of the styrene nanoparticles was performed on an ALV spectrometer consisting of a goniometer and an ALV-5004 multiple-tau full-digital correlator (320 channels) which allows measurements over an angular range from 20°–150°. A He-Ne Laser operating at a laser wavelength of 632.8 nm was used as light source. For temperature-controlled measurements the light scattering instrument is equipped with a thermostat from Julabo. Diluted samples were filtered through PTFE membrane filters with a pore size of 0.45 µm (LCR syringe filters). Measurements were performed at 20 °C at different angles ranging from 30°–150°.

Transmission Electron Microscopy (TEM): The image was recorded on a FEI Tecnai 12 microscope equipped with a LaB6-cathode (120 kV acceleration voltage, nominal magnification: 68 000; nominal underfocus: 0.5–1.5 mm). For sample preparation, carbon grids for TEM applications were negatively glow discharged at 25 mA for 30 s in an Emitech K100X glow discharge system. A droplet of the sample with a concentration of 50 mg L^{-1} was carefully placed on the grid. After an incubation time of 30 s the grid was dried by side-blotting with a filter paper. To obtain an **image** of the PS particle produced by miniemulsion polymerization 2 µl of a diluted aqueous dispersion was placed onto a 300 mesh carbon-coated copper grid (for TEM) and allowed to dry under ambient conditions. Electron micrographs were taken on an Ultrascan 1000 (Gatan) charge-coupled device (CCD) camera. The TEM was operated at 200 kV. The Digital Micrograph software (Gatan) was used to collect the images.

Contact angle measurements*:* A 5 mL drop of a surfactant solution with a concentration of 1 mg mL^{-1} was placed on a microscopy glass cover slip- The surface was rinsed with MilliQ-water water and dried with a Kimtech Kimwipe prior to the measurement. The images were taken 20 s after application of the droplet with a Dataphysics Contact Angle System OCA. Contact angels were determined with the Software SCA20 as the apparent angle between the liquid and the glass surface. The measurements were repeated five times and the average value of Θ was calculated.

Phase behaviour measurements*:* To characterize the phase behaviour of microemulsion systems of the type polar component (A) – nonpolar component (B) – nonionic surfactant (C), it has been proven useful to record a phase diagram as a function of temperature *T* and surfactant mass fraction γ[34]

$$\gamma = \frac{m_C}{\sum m_i} \tag{1}$$

at equal volumes of water and oil. This $T(\gamma)$-section allows the determination of both the phase inversion temperature PIT ($\tilde{T}$) and the minimum mass fraction $\tilde{\gamma}$ of the surfactant to form a microemulsion. The mass fraction of the block copolymer (D) in the surfactant/polymer mixture was defined as

$$\delta = \frac{m_D}{m_C + m_D} \tag{2}$$

Note that γ in this work resembles the mass fraction of total surfactant and block copolymer in the overall mixture, i.e.

$$\gamma = \frac{m_C + m_D}{\sum m_i} \tag{3}$$

For the phase diagram studies on *n*-alkane microemulsions performed at ambient pressure, all samples were weighed in directly into the test tubes with an accuracy of Δm = ±0.0002 g. The test tubes were thermo-stated in a water bath. After homogenizing the sample by stirring, the number and the type of phases were observed visually as a function of temperature. The phase transition temperatures were determined with an accuracy of ΔT = ±0.02 K at given compositions.

In order to prepare the $scCO_2$-microemulsions, the liquid and solid components were weighed into the home-made high-pressure cell with an accuracy of Δm = ±0.0002 g.[35] The liquid CO_2 was

afterwards filled into the high-pressure cell at a pressure of p = 72 bar (7.2 MPa) and room temperature using a home-built filling apparatus consisting of a membrane accumulator. The amount of CO_2 filled-in was controlled by weighing the high-pressure cell before and after filling the CO_2 (with an accuracy of Δm = ±0.01 g). A sapphire cylinder (50 mm in height, $\emptyset_{outside}$ = 32 mm, $\emptyset_{inside}$ = 10 mm), which is the main component of the high-pressure cell allows to observe the entire sample volume visually. Using a piston, the sample volume and thus the pressure can be adjusted. To record $T(\gamma)$-sections at a constant elevated pressure of p = 220 bar, the high-pressure cell was placed in a thermo-stated water bath with an accuracy of ΔT = ±0.02 K.

Synthesis

Synthesis of $PAGEC_{76}$.

The procedure described in the following describes the synthesis of sample 1.1 (Table 1). Allyl glycidyl ether (AGE) (1.5 mL, 12.6 mmol, 1 eq), (*R,R*)-(salcy)-CoDNP (5.9 mg, 0.75 mmol, 0.06 eq) and [PPN]DNP (5.4 mg, 0.75 mmol, 0.06 eq) was filled in the autoclave, equipped with a stir bar, in an inert argon-atmosphere. The reaction mixture was stirred at carbon dioxide pressure of 5.5 MPa at RT for 3 d. The crude product was dissolved in dichloromethane (DCM) and the catalyst was deactivated with 1.0 mL of a solution of 5%$_{vol}$ HCl in methanol and precipitated in ice-cold methanol. The yellow viscous fluid was then dried under reduced pressure for 24 h (yield 41%).

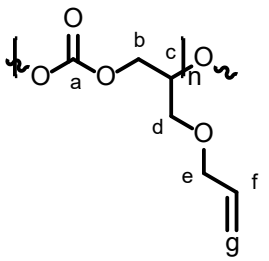

^{1}H NMR (400 MHz, $CDCl_3$) δ/ppm: 5.92–5.79 (m, -*CH*=CH_2); 5.30–5.17 (m, -CH=*CH*$_2$); 5.00 (s, -*CH* carbonyl backbone); 4.47–4.23 (m, -*CH*$_2$- carbonyl backbone); 4.06–3.93 (m, -CH*CH*$_2$O-); 3.63–3.54 (m, -*CH*$_2$CH=CH_2). ^{13}C NMR (400 MHz, $CDCl_3$) δ/ppm: 154.35 (*C*=O); 134.22 (-*CH*=CH_2); 117.72 (-CH=*CH*$_2$); 74.51 (-*CH*- carbonyl backbone); 72.50 (-*CH*$_2$CH=CH_2); 67.74 (-CH*CH*$_2$O-); 66.25 (-*CH*$_2$- carbonyl backbone). FT-IR $\tilde{\nu}$/cm^{-1}: 2 937, 2 864 (H–C(–O)), 1 744 (C=O).

Synthesis of $mPEG_{44}$-*b*-$PAGEC_n$ (exemplified by sample $mPEG_{44}$-*b*-$PAGEC_8$).

mPEG was dried by azeotropic distillation with benzene under reduced pressure. A 200 mL Roth autoclave was dried at 40 °C under reduced pressure.

$mPEG_{44}$ (1.0 g, 0.5 mmol,1 eq), allyl glycidyl ether (AGE) (3.0 mL, 25 mmol, 50 eq), (*R,R*)-(salcy)-CoDNP (11.8 mg, 0.015 mmol, 0.03 eq) and [PPN]DNP (10.8 mg, 0.015 mmol, 0.03 eq) was filled in the autoclave, equipped with a stir bar in an inert argon-atmosphere. The reaction mixture was stirred at carbon dioxide pressure of 5.5 MPa at RT for 70 h. The crude product was dissolved in DCM and the catalyst was deactivated with 0.5 mL of a solution of $5\%_{vol}$ HCl in methanol. A neutral aluminium oxide column and 400 mL THF as eluent was used for the further purification to eliminate the catalyst. The THF was evaporated under reduced pressure and the product, again dissolved in DCM, precipitated from ice-cold diethyl ether. The colourless solid was then dried under reduced pressure for 24 h. This preparation shows the synthesis of sample 4.1**,** $mPEG_{44}$-*b*-$PAGEC_{45}$, (yield 61%). The other $mPEG_{44}$-*b*-$PAGEC_n$ (samples 2.1 and 3.1) diblock copolymers were prepared in a similar procedure using different amounts of CTA and allyl glycidyl ether.

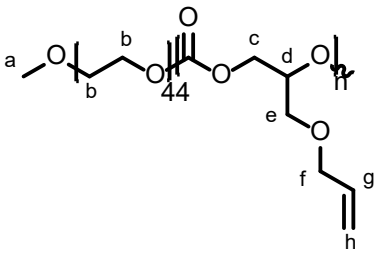

^{1}H NMR (400 MHz, $CDCl_3$) δ/ppm: 5.94–5.76 (m, -*CH*=CH_2); 5.30–5.13 (m, -CH=*CH_2*); 5.00 (s, -*CH* carbonyl backbone); 4.49–4.12 (m, -*CH_2*- carbonyl backbone); 4.06–3.92 (m, -*CH_2*CH=CH_2); 3.72–3.39 (m, *polyether backbone and* -OCH_2CH*CH_2*); 3.35 (s, -O*CH_3*).

^{13}C NMR (400 MHz, $CDCl_3$) δ/ppm: 154.21 (*C*=O); 134.08 (-*CH*=CH_2); 117.58 (-CH=*CH_2*); 74.36 (-*CH*-carbonyl backbone); 72.37 (*CH_2*CH=CH_2); 70.56 (-*CH_2*- polyether backbone); 67.66 (-OCH_2CH*CH_2*); 66.11 (-*CH_2*- carbonyl backbone); 59.04 (-O*CH_3*).

FT-IR $\tilde{\nu}$/cm^{-1}: 2 866 (H–C(–O)), 1 750 (C=O), 1 229 (C–O), 1 095 (C–O–C).

General Procedure for the hydrosilylation of $PAGEC_n$ and $mPEG_{44}$-*b*-$PAGEC_n$ (exemplified by sample $mPEG_{44}$-*b*-P(AGE-HMTS)C_8)

108 mg $mPEG_{44}$-*b*-$PAGEC_{45}$ (0.01 mmol) were dissolved in 1,4-dioxane in a Schlenk tube and degassed twice *via* freeze-pump-thaw cycles. One drop of Karstedt's catalyst was added under Argon atmosphere and the solution was stirred for 30 min at 60 °C. 0.17 mL HMTS (0.63 mmol) were added with a syringe followed by a slow darkening of the solution. After reacting overnight and subsequent cooling to room temperature, the solution was refluxed for approximately one hour with Amberlite® IRA743 free base (basic ion exchange resin) until the colour lightened. The

solution was filtered through a 0.45 µm PTFE syringe filter and the solvent and excess HMTS were evaporated under reduced pressure. The polymers with a high (AGE-HMTS)C content were precipitated from cold methanol after dialysis against dichloromethane three times over night (benzylated tubes, MWCO = 2000 g mol^{-1}) and obtained as very viscous liquids after freeze drying. The diblock copolymers with three and eight (AGE-HMTS)C units were dialysed in dichloromethane and precipitated from cold diethyl ether as colourless, wax-like solids. All polymers were obtained in quantitative yields.

mPEG$_{44}$-*b*-P(AGE-HMTS)C$_{45}$

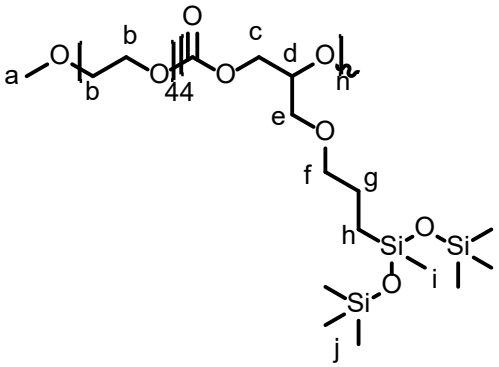

^{1}H NMR (400 MHz, $CDCl_3$) δ/ppm: 5.00 (s, -*CH* carbonyl backbone); 4.52–4.05 (m, -*CH$_2$*- carbonyl backbone); 3.87–3.51 (m, polyether backbone and -OCH$_2$CH*CH$_2$*); 3.48–3.21 (m, -O*CH$_2$*CH$_2$ and -O-*CH$_3$*); 1.65–1.48 (m, -*CH$_2$*CH$_2$Si-); 0.49–0.35 (m, -CH$_2$*CH$_2$*Si-); 0.18–0.03 (m, -Si(*CH$_3$*)$_3$); 0.00–(-0.06) (m, -Si*CH$_3$*).

^{13}C NMR (400 MHz, $CDCl_3$) δ/ppm: 154.26 (*C*=O); 74.38 (-*CH*- carbonyl backbone); 71.94 (-*CH$_2$*CH=CH$_2$); 70.57 (-*CH$_2$*- polyether backbone); 68.81 (-OCH$_2$CH*CH$_2$*); 66.23 (*CH$_2$*- carbonyl backbone); 59.04 (-O*CH$_3$*); 23.15 (-*CH$_2$*CH$_2$Si-); 13.43 (-CH$_2$*CH$_2$*Si-); 1.87 (-Si(*CH$_3$*)$_3$); –0.36 (-Si*CH$_3$*).

FT-IR $\tilde{\nu}$/cm^{-1}: 2 956, 2 881 (H–C(–O)), 1752 (C=O), 1 250 (Si–CH$_3$), 1 224 (C–O), 1 103 (C–O–C), 1 039 (Si–O–Si), 838 (Si(CH$_3$)$_3$).

P(AGE-HMTS)C_{76}:

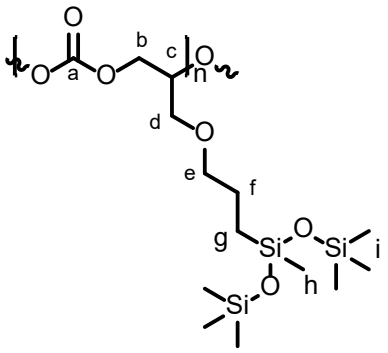

^{1}H NMR (400 MHz, $CDCl_3$) δ/ppm: 5.01 (s, -*CH* carbonyl backbone); 4.54–4.15 (m, -CH_2- carbonyl backbone); 3.60–3.50 (m -OCH_2CH); 3.48–3.33 (m, -OCH_2CH_2); 1.60–1.50 (m, -CH_2CH_2Si-); 0.47–0.36 (-CH_2CH_2Si-); 0.17–0.03 (-Si(CH_3)$_3$); 0.02–(-0.04) (-SiCH_3).

^{13}C NMR (400 MHz, $CDCl_3$) δ/ppm: 154.36 (*C*=O); 74.54 (-*CH*- carbonyl backbone); 73.46 (-OCH_2CH_2-); 68.45 (-OCH_2CHCH_2); 23.29 (-CH_2Si-); 13.56 (-CH_2CH_2Si-); 2.00 (-Si(CH_3)$_3$); 0.22 (-SiCH_3).

FT-IR $\tilde{\nu}$/cm^{-1}: 2 956, 2 881 (H–C(–O)), 1 754 (C=O), 1 258 (Si–CH_3), 1 032 (Si–O–Si), 832 (Si(CH_3)$_3$).

Procedure for the miniemulsion polymerization of styrene stabilized by mPEG44-b-PAGEC8

24 mg mPEG44-b-PAGEC8 (0.005 mmol) were dissolved in 800 mg water (44.4 mmol,). A solution of 200 mg freshly distilled styrene (1.92 mmol), 8.3 mg hexadecane (0.037 mmol) and 3.3 mg 2,2'-azobis(2-methylbutyronitrile) (V59, 0.017 mmol) was prepared and rapidly added to the vigorous stirring aqueous solution containing mPEG44-b-PAGEC8. The emulsion was stirred at 0 °C for one minute at 20 000 rpm using an ultra turrax. The emulsion was ultrasonicated (450 W, two min, 70% amplitude) to produce a stable miniemulsion. The sealed miniemulsion was placed in an oil bath at 70 °C equipped with a stir bar and the polymerization was allowed to proceed overnight. The final nanoparticle dispersion was analyzed with DLS (Particle size = 92 nm) and TEM.

AUTHOR CONTRIBUTIONS

The manuscript was written through contributions of all authors. T.D., C.G., L.K., and S.-Y.T. contributed equally to this work. All authors have given approval to the final version of the manuscript.

Notes: The authors declare no competing financial interest.

ACKNOWLEDGEMENT

We thank Monika Schmelzer for the support during SEC measurements; Elena Berger-Nicoletti for the for MALDI-TOF measurements; Nico Alleva for his first trials on this topic during his bachelor thesis; Petra Raeder (Max Planck Institute for Polymer Research Mainz) for DSC measurements and Maximilian Krappel for helping with the phase diagram studies.

T.D., S.-Y.T., and L.K. thank the German Federal Ministry for Economic Affairs (BMWi) for financial support.

REFERENCES

(1) Sakakura, T.; Choi, J.-C.; Yasuda, H. Transformation of Carbon Dioxide. *Chem. Rev.* **2007**, *107* (6), 2365–2387. https://doi.org/10.1021/cr068357u.

(2) Aresta, M.; Dibenedetto, A. Utilisation of CO_2 as a Chemical Feedstock: Opportunities and Challenges. *J. Chem. Soc. Dalt. Trans.* **2007**, No. 28, 2975–2992. https://doi.org/10.1039/b700658f.

(3) Shi, L.; Lu, X. B.; Zhang, R.; Peng, X. J.; Zhang, C. Q.; Li, J. F.; Peng, X. M. Asymmetric Alternating Copolymerization and Terpolymerization of Epoxides with Carbon Dioxide at Mild Conditions. *Macromolecules* **2006**, 39 (17), 5679–5685. https://doi.org/10.1021/ma060290p.

(4) Inoue, S.; Koinuma, H.; Tsuruta, T. Copolymerization of Carbon Dioxide and Epoxide. Die *Makromol. Chemie* **1969**, 130, 210–220. https://doi.org/10.1002/pol.1969.110070408.

(5) Cheng, M.; Moore, D. R.; Reczek, J. J.; Chamberlain, B. M.; Lobkovsky, E. B.; Coates, G. W. Single-Site β-Diiminate Zinc Catalysts for the Alternating Copolymerization of CO_2 and Epoxides: Catalyst Synthesis and Unprecedented Polymerization Activity. *J. Am. Chem. Soc.* **2001**, 123 (36), 8738–8749. https://doi.org/10.1021/ja003850n.

(6) Cyriac, A.; Lee, S. H.; Varghese, J. K.; Park, E. S.; Park, J. H.; Lee, B. Y. Immortal CO_2/Propylene Oxide Copolymerization: Precise Control of Molecular Weight and Architecture of Various Block Copolymers. *Macromolecules* **2010**, 43 (18), 7398–7401. https://doi.org/10.1021/ma101259k.

(7) Darensbourg, D. J. Making Plastics from Carbon Dioxide: Salen Metal Complexes as Catalysts for the Production of Polycarbonates from Epoxides and CO_2. *Chem. Rev.* **2007**, 107 (6), 2388–2410. https://doi.org/10.1021/cr068363q.

(8) Hauenstein, O.; Reiter, M.; Agarwal, S.; Rieger, B.; Greiner, A. Bio-Based Polycarbonate from Limonene Oxide and CO_2 with High Molecular Weight, Excellent Thermal Resistance, Hardness and Transparency. *Green Chem.* **2016**, 18 (3), 760–770. https://doi.org/10.1039/c5gc01694k.

(9) Scharfenberg, M.; Wald, S.; Wurm, F. R.; Frey, H. Acid-Labile Surfactants Based on Poly(Ethylene Glycol), Carbon Dioxide and Propylene Oxide: Miniemulsion Polymerization and Degradation Studies. *Polymers* (Basel). **2017**, 9 (9), 422. https://doi.org/10.3390/polym9090422.

(10) Scharfenberg, M.; Hilf, J.; Frey, H. Functional Polycarbonates from Carbon Dioxide and Tailored Epoxide Monomers: Degradable Materials and Their Application Potential. *Adv. Funct. Mater.,* **2018**, 28 (10), 1–16. https://doi.org/10.1002/adfm.201704302.

(11) Subhani, M. A.; Köhler, B.; Gürtler, C.; Leitner, W.; Müller, T. E. Transparent Films from CO 2 -Based Polyunsaturated Poly(Ether Carbonate)s: A Novel Synthesis Strategy and Fast Curing. *Angew. Chemie - Int. Ed.* **2016**, 55 (18), 5591–5596. https://doi.org/10.1002/anie.201509249.

(12) Łukaszczyk, J.; Jaszcz, K.; Kuran, W.; Listos, T. Synthesis of Functional Polycarbonates by Copolymerization of Carbon Dioxide with Allyl Glycidyl Ether. *Macromol. Rapid Commun.* **2000**, 21 (11), 754–757. https://doi.org/10.1002/app.21121.

(13) Tan, C.-S.; Kuo, T.-W. Synthesis of Polycarbonate-Silica Nanocomposites from Copolymerization of CO_2 with Allyl Glyciclyl Ether, Cyclohexene Oxide, and Sol-Gel. *J. Appl. Polym. Sci.* **2005**, 98 (2), 750–757. https://doi.org/10.1002/app.22126.

(14) Deng, K.; Wang, S.; Ren, S.; Han, D.; Xiao, M.; Meng, Y. A Novel Single-Ion-Conducting Polymer Electrolyte Derived from CO_2-Based Multifunctional Polycarbonate. *ACS Appl. Mater. Interfaces* **2016,** 8 (49), 33642–33648. https://doi.org/10.1021/acsami.6b11384.

(15) Wang, Y.; Fan, J.; Darensbourg, D. J. Construction of Versatile and Functional Nanostructures Derived from CO_2-Based Polycarbonates. *Angew. Chemie - Int. Ed.* **2015**, 54 (35), 10206–10210. https://doi.org/10.1002/anie.201505076.

(16) O'Neill, M. L.; Cao, Q.; Fang, M.; Johnston, K. P.; Wilkinson, S. P.; Smith, C. D.; Kerschner, J. L.; Jureller, S. H. Solubility of Homopolymers and Copolymers in Carbon Dioxide. *Ind. Eng. Chem. Res.* **1998**, 37 (8), 3067–3079. https://doi.org/10.1021/ie980010x.

(17) Fulton, J. L.; Pfund, D. M.; McClain, J. B.; Romack, T. J.; Maury, E. E.; Combes, J. R.; Samulski, E. T.; Desimone, J. M.; Capel, M. Aggregation of Amphiphilic Molecules in Supercritical Carbon Dioxide: A Small Angle X-Ray Scattering Study. *Langmuir* **1995**, 11 (11), 4241–4249. https://doi.org/10.1021/la00011a014.

(18) DeSimone, J. M.; Guan, Z.; Elsbernd, C. S. Synthesis of Fluoropolymers in Supercritical Carbon Dioxide. *Science (80-.).* **1992**, 257 (5072), 945–947. https://doi.org/10.1126/science.257.5072.945.

(19) Ryoo, W.; Webber, S. E.; Johnston, K. P. Water-in-Carbon Dioxide Microemulsions with Methylated Branched Hydrocarbon Surfactants. *Ind. Eng. Chem. Res.* **2003**, 42 (25), 6348–6358. https://doi.org/10.1021/ie0300427.

(20) Eastoe, J.; Gold, S.; Rogers, S.; Wyatt, P.; Steytler, D. C.; Gurgel, A.; Heenan, R. K.; Fan, X.; Beckman, E. J.; Enick, R. M. Designed CO_2-Philes Stabilize Water-in-Carbon Dioxide Microemulsions. *Angew. Chemie - Int. Ed.* **2006**, 45 (22), 3675–3677. https://doi.org/10.1002/anie.200600397.

(21) Eastoe, J.; Paul, A.; Nave, S.; Steytler, D. C.; Robinson, B. H.; Rumsey, E.; Thorpe, M.; Heenan, R. K. Micellization of Hydrocarbon Surfactants in Supercritical Carbon Dioxide [7]. *J. Am. Chem. Soc.* **2001**, 123 (5), 988–989. https://doi.org/10.1021/ja005795o.

(22) Da Rocha, S. R. P.; Dickson, J.; Cho, D.; Rossky, P. J.; Johnston, K. P. Stubby Surfactants for Stabilization of Water and CO_2 Emulsions: Trisiloxanes. *Langmuir* **2003**, 19, 3114–3120. https://doi.org/10.1021/la026608y.

(23) Sarbu, T.; Styranec, T. J.; Beckman, E. J. Design and Synthesis of Low Cost, Sustainable CO_2-Philes. *Ind. Eng. Chem. Res.* **2000**, 39 (12), 4678–4683. https://doi.org/10.1021/ie0003077.

(24) Sarbu, T.; Styranec, T.; Beckman, E. J. Non-Fluorous Polymers with Very High Solubility in Supercritical CO_2 down to Low Pressures. *Nature* **2000**, 405 (6783), 165–168. https://doi.org/10.1038/35012040.

(25) Wick, C. D.; Siepmann, J. I.; Theodorou, D. N. Microscopic Origins for the Favorable Solvation of Carbonate Ether Copolymers in CO_2. *J. Am. Chem. Soc.* **2005**, 127 (35), 12338–12342. https://doi.org/10.1021/ja0510008.

(26) Parzuchowski, P. G.; Gregorowicz, J.; Fraš, Z.; Wawrzyńska, E. P.; Brudzyńska, E.; Rokicki, G. Hyperbranched Poly(Ether-Siloxane) Amphiphiles of Surprisingly High Solubility in Supercritical Carbon Dioxide. *J. Supercrit. Fluids* **2014**, 95, 222–227. https://doi.org/10.1016/j.supflu.2014.08.030.

(27) Lin, S.-T.; Huang, S. K. Thermal Degradation Study of Siloxane-DGEBA Epoxy Copolymers. Eur. *Polym. J.* **1997**, 33 (3), 365–373.

(28) Chuang, F. S.; Tsen, W. C.; Shu, Y. C. The Effect of Different Siloxane Chain-Extenders on the Thermal Degradation and Stability of Segmented Polyurethanes. *Polym. Degrad. Stab.* **2004**, 84, 69–77. https://doi.org/10.1016/j.polymdegradstab.2003.10.002.

(29) Kumar, S. A.; Narayanan, T. S. N. S. Thermal Properties of Siliconized Epoxy Interpenetrating Coatings. *Prog. Org. Coatings* **2002**, 45, 323–330.

(30) Ananthapadmanabhan, K. P.; Goddard, E. D.; Chandar, P. A Study of the Solution, Interfacial and Wetting Properties of Silicone Surfactants. *Colloids and Surfaces* **1990**, 44 (C), 281–297. https://doi.org/10.1016/0166-6622(90)80202-F.

(31) Ivanova, N.; Starov, V.; Rubio, R.; Ritacco, H.; Hilal, N.; Johnson, D. Critical Wetting Concentrations of Trisiloxane Surfactants. *Colloids Surfaces A Physicochem. Eng. Asp.* **2010**, 354 (1–3), 143–148. https://doi.org/10.1016/j.colsurfa.2009.07.030.

(32) Svitova, T.; Hill, R. M.; Smirnova, Y.; Stuermer, A.; Yakubov, G. Wetting and Interfacial Transitions in Dilute Solutions of Trisiloxane Surfactants. *Langmuir* **1998**, 14, 5023–5031. https://doi.org/10.1021/la980072s.

(33) Lu, X.-B.; Shi, L.; Wang, Y.-M.; Zhang, R.; Zhang, Y.-J.; Peng, X.-J.; Zhang, Z.-C.; Li, B. Design of Highly Active Binary Catalyst Systems for CO_2/Epoxide Copolymerization: Polymer Selectivity, Enantioselectivity, and Stereochemistry Control. *J. Am. Chem. Soc.* **2006**, 128 (5), 1664–1674. https://doi.org/10.1021/ja056383o.

(34) Kahlweit, B. M.; Strey, R. Phase Behavior of Ternary Systems of the Type H_2O-Oil-Nonionic Amphiphile (Microemulsions). *Angew. Chem. Int. Ed.* **1985**, 24 (2), 654–668. https://doi.org/10.1002/anie.198506541.

(35) Schwan, M.; Kramer, L. G. A.; Sottmann, T.; Strey, R. Phase Behaviour of Propane- and $ScCO_2$-Microemulsions and Their Prominent Role for the Recently Proposed Foaming Procedure POSME (Principle of Supercritical Microemulsion Expansion). *Phys. Chem. Chem. Phys.* **2010**, *12*, 6247–6252. https://doi.org/10.1039/b909764c.

(36) Cohen, C. T.; Thomas, C. M.; Peretti, K. L.; Lobkovsky, E. B.; Coates, G. W. Copolymerization of Cyclohexene Oxide and Carbon Dioxide Using (Salen)Co(Iii) Complexes: Synthesis and Characterization of Syndiotactic Poly(Cyclohexene Carbonate). *J. Chem. Soc. Dalt. Trans.* **2006**, No. 1, 237–249. https://doi.org/10.1039/b513107c.

(37) Karstedt, B. D. Platinum Complexes of Unsaturated Siloxanes and Platinum Containing Organopolysiloxanes. US 3775452, 1973. https://doi.org/10.1111/j.1559-3584.1927.tb04229.x.

(38) Troegel, D.; Stohrer, J. Recent Advances and Actual Challenges in Late Transition Metal Catalyzed Hydrosilylation of Olefins from an Industrial Point of View. *Coord. Chem. Rev.* **2011**, 255 (13–14), 1440–1459. https://doi.org/10.1016/j.ccr.2010.12.025.

(39) Lee, B. F.; Kade, M. J.; Chute, J. A.; Gupta, N.; Campos, L. M.; Fredrickson, G. H.; Kramer, E. J.; Lynd, N. A.; Hawker, C. J. Poly(Allyl Glycidyl Ether)A Versatile and Functional Polyether Platform. J. Polym. Sci. Part A *Polym. Chem.* **2011**, 49, 4498–4504. https://doi.org/10.1002/pola.24891.

(40) Tan, C.-S.; Juan, C.-C.; Kuo, T.-W. Polyethercarbonate-Silica Nanocomposites Synthesized by Copolymerization of Allyl Glycidyl Ether with CO_2 Followed by Sol-Gel Process. *Polymer (Guildf)*. **2004**, 45 (6), 1805–1814. https://doi.org/10.1016/j.polymer.2004.01.013.

(41) Kunze, L.; Tseng, S. Y.; Schweins, R.; Sottmann, T.; Frey, H. Nonionic Aliphatic Polycarbonate Diblock Copolymers Based on CO_2 , 1,2-Butylene Oxide, and mPEG: Synthesis, Micellization, and Solubilization. *Langmuir* **2019**, 35 (15), 5221–5231. https://doi.org/10.1021/acs.langmuir.8b04265.

(42) Immergut, E. H.; Mark, H. F. Principles of Plasticization. Adv. Chem. 1965, 48, 1–26. https://doi.org/10.1021/ba-1965-0048.ch001.

(43) Schönenberg, L.; Ritter, H. Polydimethylsiloxane Macromonomer Bearing N-Vinylcaprolactam as End Group: Thermosensitive Graft Copolymers via Free Radical Polymerization. *Polym. Int.* **2015**, *64*, 1309–1315. https://doi.org/10.1002/pi.4952.

(44) Rogers, S.; Mandelkern, L. Glass Formation in Polymers. I. The Glass Transitions of the Poly(n-Alkyl Methacrylates). *J. Phys. Chem.* **1957**, 61 (7), 985–991.

(45) Jovanovic, J. D.; Govedarica, M. N.; Dvornic, P. R.; Popovic, I. G. The Thermogravimetric Analysis of Some Polysiloxanes. *Polym. Degrad. Stab.* **1998**, 61 (1), 87–93. https://doi.org/10.1016/S0141-3910(97)00135-3.

(46) William C. Griffin. Calculation of HLB Values of Non-Ionic Surfactants. *J. Cosmet. Sci.* **1954,** 5 (4), 249–256.

(47) Hilf, J.; Schulze, P.; Frey, H. CO_2 -Based Non-Ionic Surfactants: Solvent-Free Synthesis of Poly(Ethylene Glycol)-Block-Poly(Propylene Carbonate) Block Copolymers. *Macromol. Chem. Phys.* **2013**, 214 (24), 2848–2855.

(48) Chen, L.-J.; Lin, S.-Y.; Huang, C.-C.; Chen, E.-M. Temperature Dependence of Critical Micelle Concentration of Polyoxyethylenated Non-Ionic Surfactants. *Colloids Surfaces A Physicochem. Eng. Asp.* **1998**, 135, 175–181.

(49) Sikora, A.; Tuzar, Z. Association of Two-Block Copolymer Polystyrene-Block-Poly(2-Vinylpyridine) in Toluene. *Makromol. Chem.* **1983**, 184, 2049–2059.

(50) Zhu, S.; Miller, W. G.; Scriven, L. E.; Davis, H. T. Superspreading of Water-Silicone Surfactant on Hydrophobic Surfaces. *Colloids Surfaces A Physicochem. Eng. Asp.* **1994**, 90 (1), 63–78.

(51) Popova, H.; Milchev, A.; Egorov, S. A. Modeling the Interfacial Tension Dependence on Composition and Stiffness of Nonionic Surfactants on Liquid–Liquid Interfaces. *Colloids Surfaces A Physicochem. Eng. Asp.* **2017**, 519, 168–178. https://doi.org/10.1016/j.colsurfa.2016.05.056.

(52) Svitova, T.; Hoffmann, H.; Hill, R. M. Trisiloxane Surfactants: Surface/Interfacial Tension Dynamics and Spreading on Hydrophobic Surfaces. *Langmuir* **1996**, 12 (7), 1712–1721. https://doi.org/10.1021/la9505172.

(53) Radulovic, J.; Sefiane, K.; Shanahan, M. E. R. Dynamics of Trisiloxane Wetting: Effects of Diffusion and Surface Hydrophobicity. *J. Phys. Chem. C* **2010**, 114 (32), 13620–13629. https://doi.org/10.1021/jp910729c.

(54) Kabanov, A. V; Batrakova, E. V; Melik-Nubarov, N. S.; Fedoseev, Nikolai, A.; Dorodnich, T. Y.; Alakho, V. Y.; Chekhonin, V. P.; Nazarova, I.; Kabanov, V. A. A New Class of Drug Carriers :

Micelles of Poly(Oxyethylene)-Poly(Oxypropylene) Block Copolymers as Microcontainers for Drug Targeting from Blood in Brain. *J. Control*. **1992**, 22, 141–158.

(55) Lo, C.-L.; Huang, C.-L.; Lin, K.-M.; Hsiue, G.-H. Mixed Micelles Formed from Graft and Diblock Copolymers for Application in Intracellular Drug Delivery. *Biomaterials* **2007**, 28, 1225–1235. https://doi.org/10.1016/j.biomaterials.2006.09.050.

(56) Hrubý, M.; Koňák, Č.; Ulbrich, K. Poly(Allyl Glycidyl Ether)-Block-Poly(Ethylene Oxide): A Novel Promising Polymeric Intermediate for the Preparation of Micellar Drug Delivery Systems. *J. Appl. Polym. Sci.* **2005**, 95 (2), 201–211. https://doi.org/10.1002/app.21121.

(57) Griffin, W. Classification of Surface-Active Agents By "HLB." *J. Soc. Cosmet. Chem*. **1949**, 311–326.

(58) Riess, G.; Labbe, C. Block Copolymers in Emulsion and Dispersion Polymerization. *Macromol. Rapid Commun.* **2004**, 25 (2), 401–435. https://doi.org/10.1002/marc.200300048.

(59) Jakobs, B.; Sottmann, T.; Strey, R.; Allgaier, J.; Willner, L.; Richter, D. Amphiphilic Block Copolymers as Efficiency Boosters for Microemulsions. *Langmuir* **1999**, 15 (20), 6707–6711. https://doi.org/10.1021/la9900876.

(60) Hiergeist, C. .; Lipowsky, R. Elastic Properties Polymer-Decorated Membranes. *J. Phys. II Fr*. **1996**, 6, 1465–1481.

(61) Lipowsky, R. Flexible Membranes with Anchored Polymers. *Colloids Surfaces A Physicochem. Eng. Asp.* **1997**, 128 (1–3), 255–264. https://doi.org/10.1016/S0927-7757(96)03906-4.

(62) Jakobs, B. Amphiphile Blockcopolymere Als "Efficiency Booster" Für Tenside - Entdeckung Und Aufklärung Des Effekts, University of Cologne, 2001.

(63) Müller, A.; Pütz, Y.; Oberhoffer, R.; Becker, N.; Strey, R.; Wiedenmann, A.; Sottmann, T. Kinetics of Pressure Induced Structural Changes in Super- or near-Critical CO_2-Microemulsions. *Phys. Chem. Chem. Phys.* **2014**, 16 (34), 18092–18097. https://doi.org/10.1039/c3cp53790k.

(64) Holmes, J. D.; Steytler, D. C.; Rees, G. D.; Robinson, B. H. Bioconversions in a Water-in-CO_2 Microemulsion. *Langmuir 1998*, 14 (22), 6371–6376. https://doi.org/10.1021/la9806956.

(65) Desimone, J. M. Practical Approaches to Green Solvents. *Science (80-.).* **2002**, 297, 799–803.

(66) Klostermann, M.; Strey, R.; Sottmann, T.; Schweins, R.; Lindner, P.; Holderer, O.; Monkenbusch, M.; Richter, D. Structure and Dynamics of Balanced Supercritical CO_2-Microemulsions. *Soft Matter* **2012**, 8 (3), 797–807. https://doi.org/10.1039/c1sm06533e.

SUPPORTING INFORMATION

Siloxane Functionalized Polyether-Polycarbonates with Amphiphilic Properties: A New Class of Surfactants

Tatjana Daenzer[a], Christina Gardiner[a], Lena Kunze[a], Shih-Yu Tseng[b], Tassilo Gleede[c], Thomas Sottmann[c], Holger Frey[a]***

[a]Institute of Organic Chemistry, Johannes Gutenberg University of Mainz, Duesbergweg 10-14, 55128 Mainz, Germany.

[b]Institute of Physical Chemistry, University of Stuttgart, Pfaffenwaldring 55, 70569 Stuttgart, Germany.

[c]Max Planck Institute for Polymer Research, Ackermannweg 10, 55128 Mainz, Germany.

Table of content

1. Polymer characterization

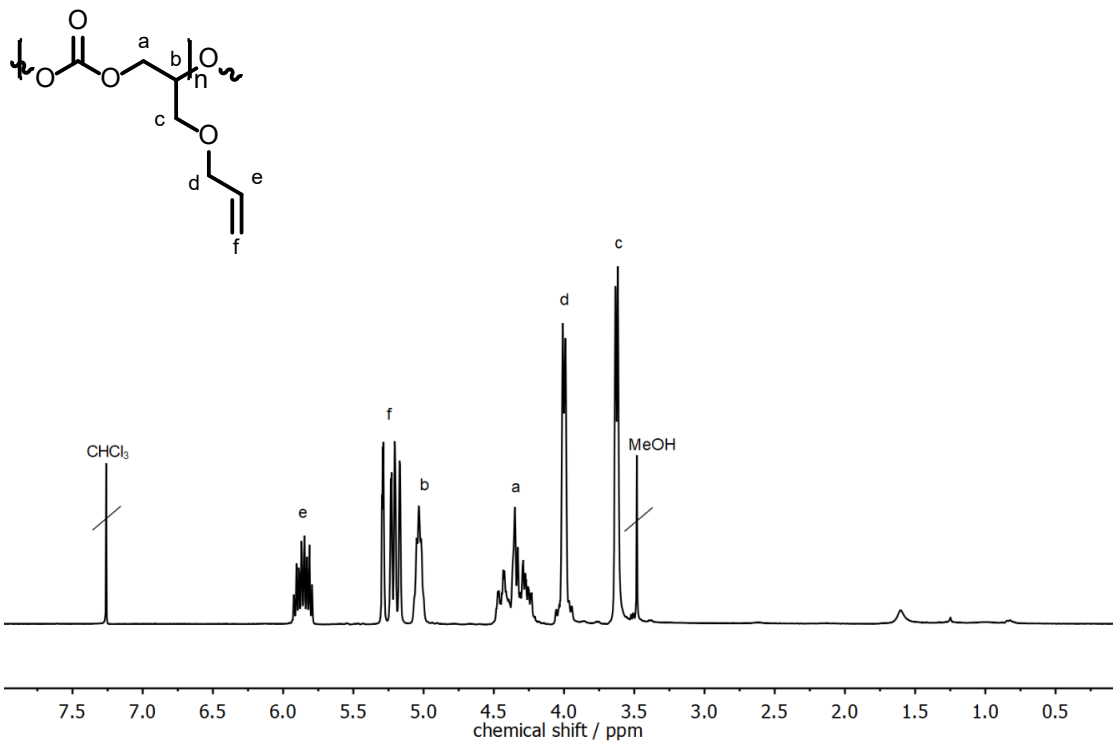

Figure S 1: ^{1}H NMR spectrum of P(AGEC)$_{76}$ in $CDCl_3$, 400 MHz, 21 °C.

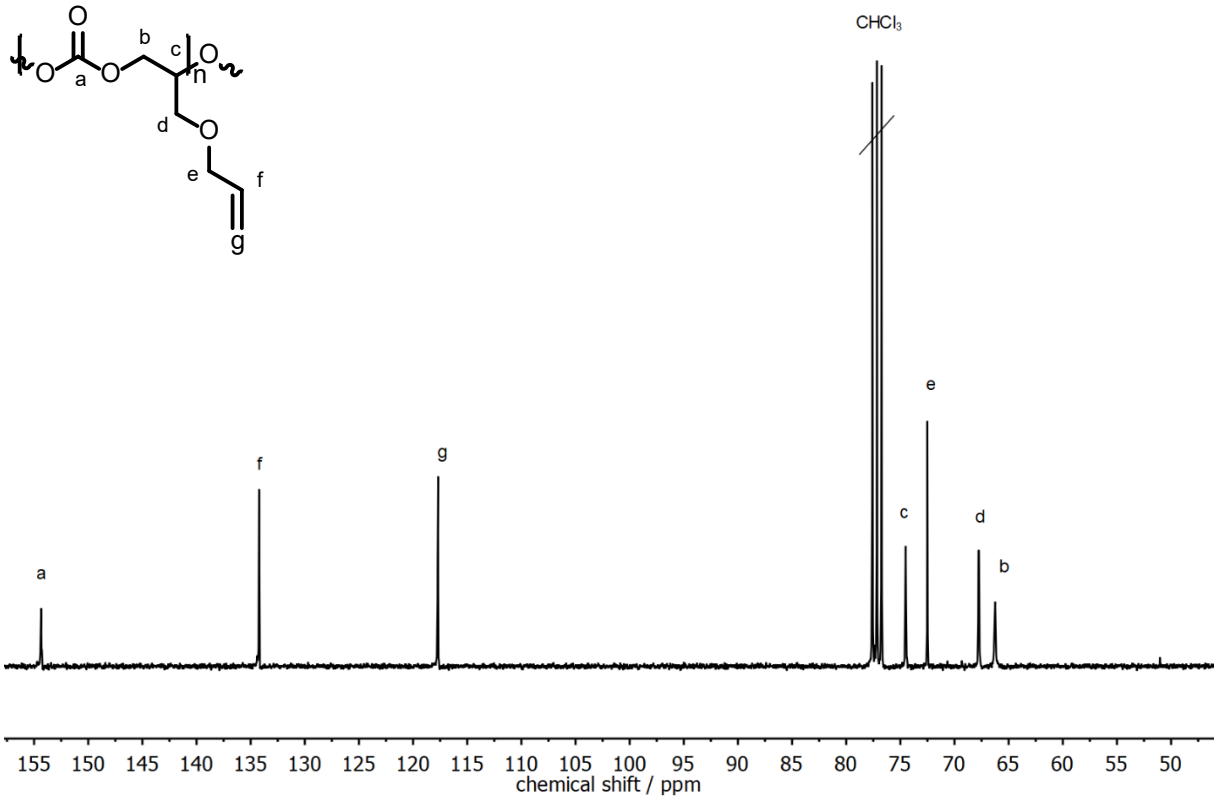

Figure S 2: ^{13}C NMR spectrum of P(AGEC)$_{76}$ in $CDCl_3$, 400 MHz, 21 °C.

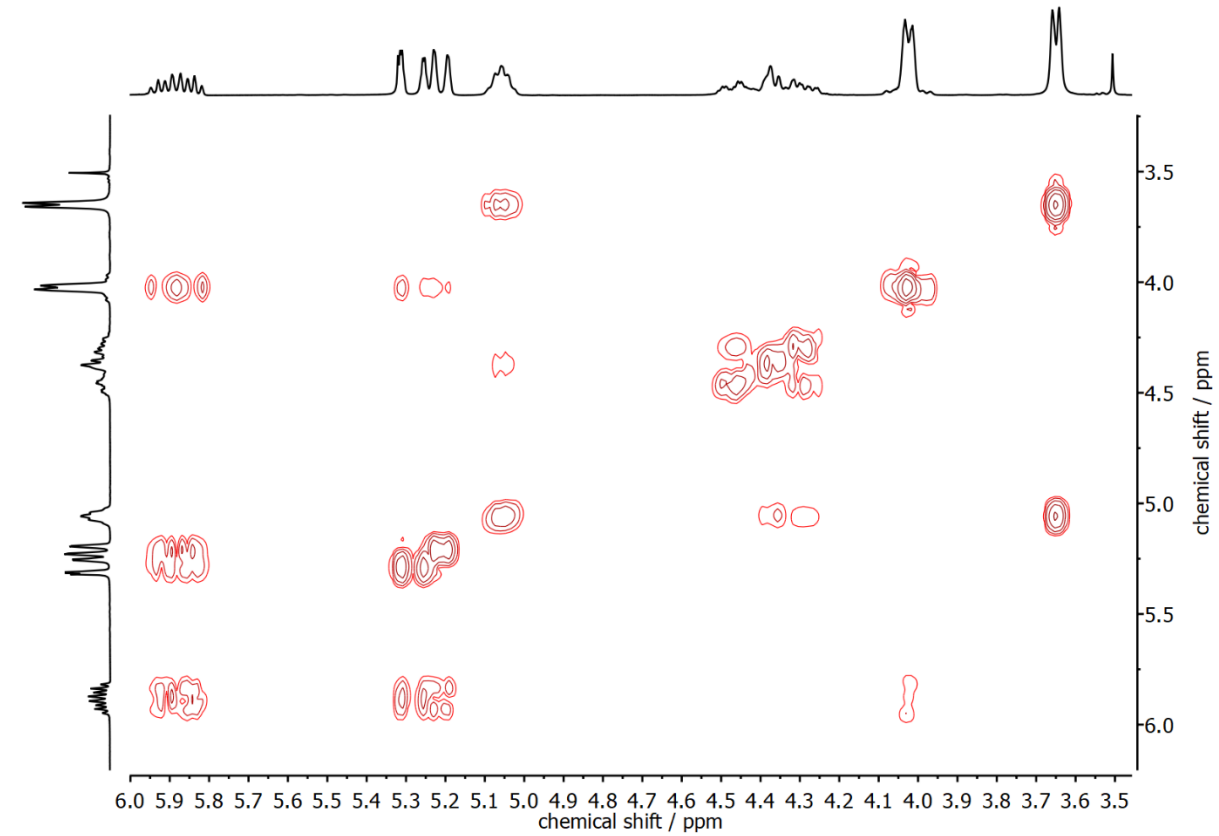

Figure S 3:COSY NMR spectrum of $P(AGEC)_{76}$ in $CDCl_3$, 400 MHz, 21 °C.

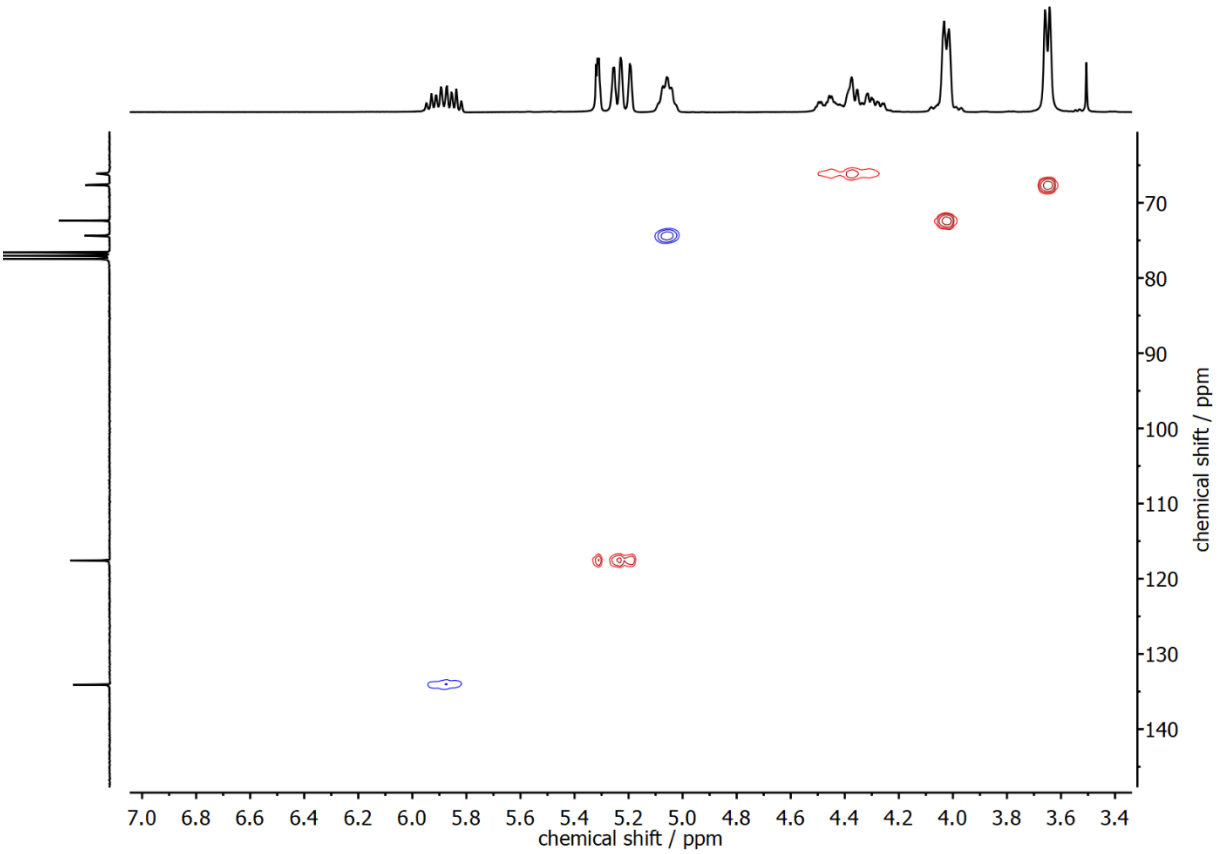

Figure S 4: HSQC NMR spectrum of $P(AGEC)_{76}$ in $CDCl_3$, 400 MHz, 21 °C.

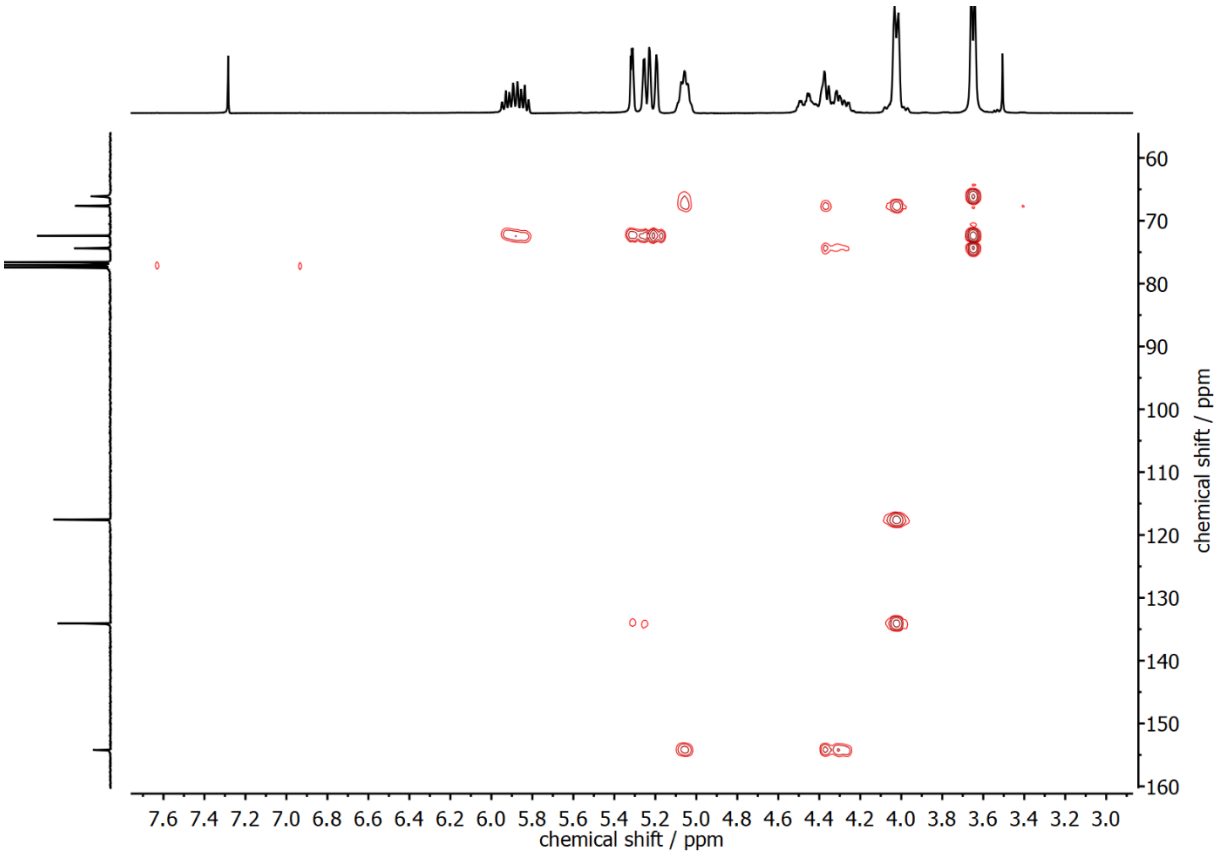

Figure S 5: HMBC NMR spectrum of P(AGEC)$_{76}$ in $CDCl_3$, 400 MHz, 21 °C.

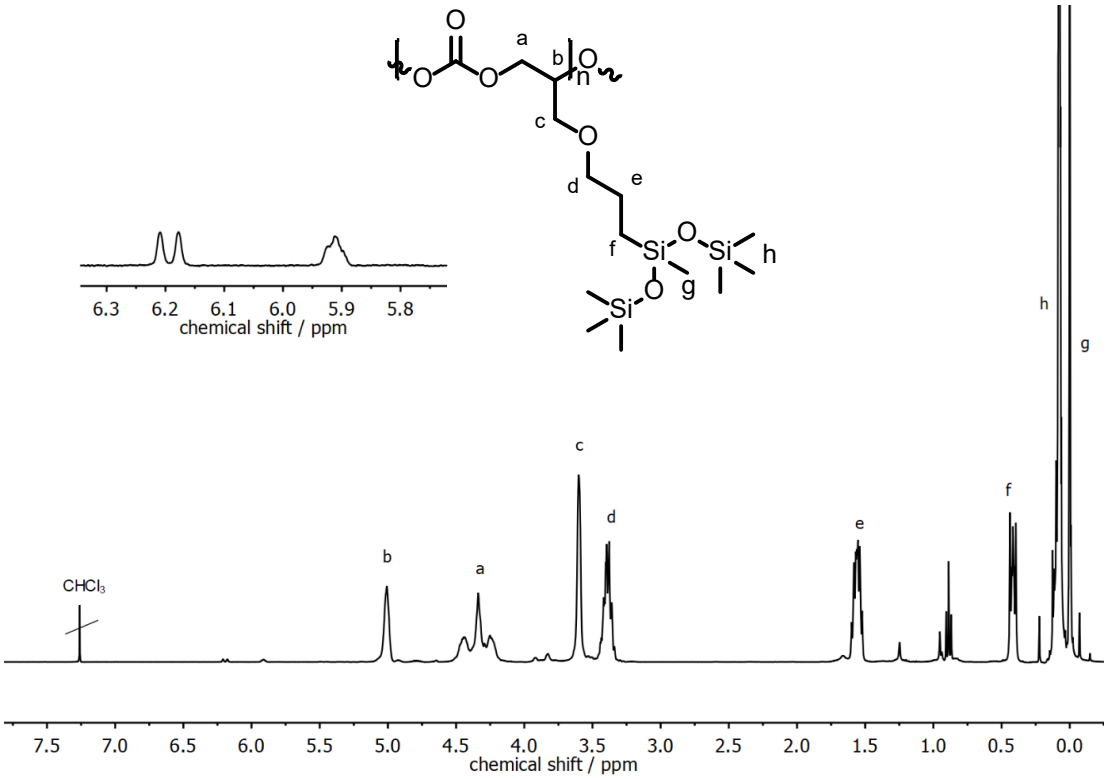

Figure S 6: ^{1}H NMR spectrum of P(AGE-HMTS)C_{76} in $CDCl_3$, 400 MHz, 21 °C.

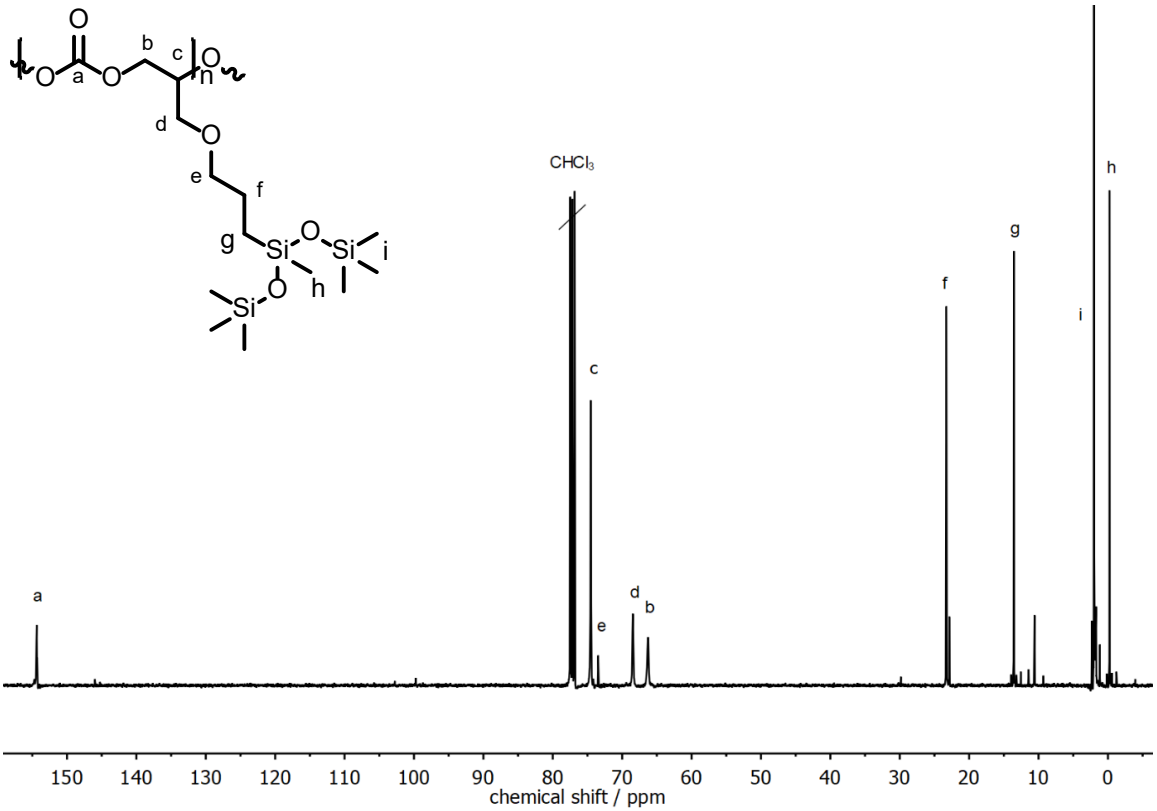

Figure S 7: ^{13}C NMR spectrum of P(AGE-HMTS)C_{76} in $CDCl_3$, 400 MHz, 21 °C.

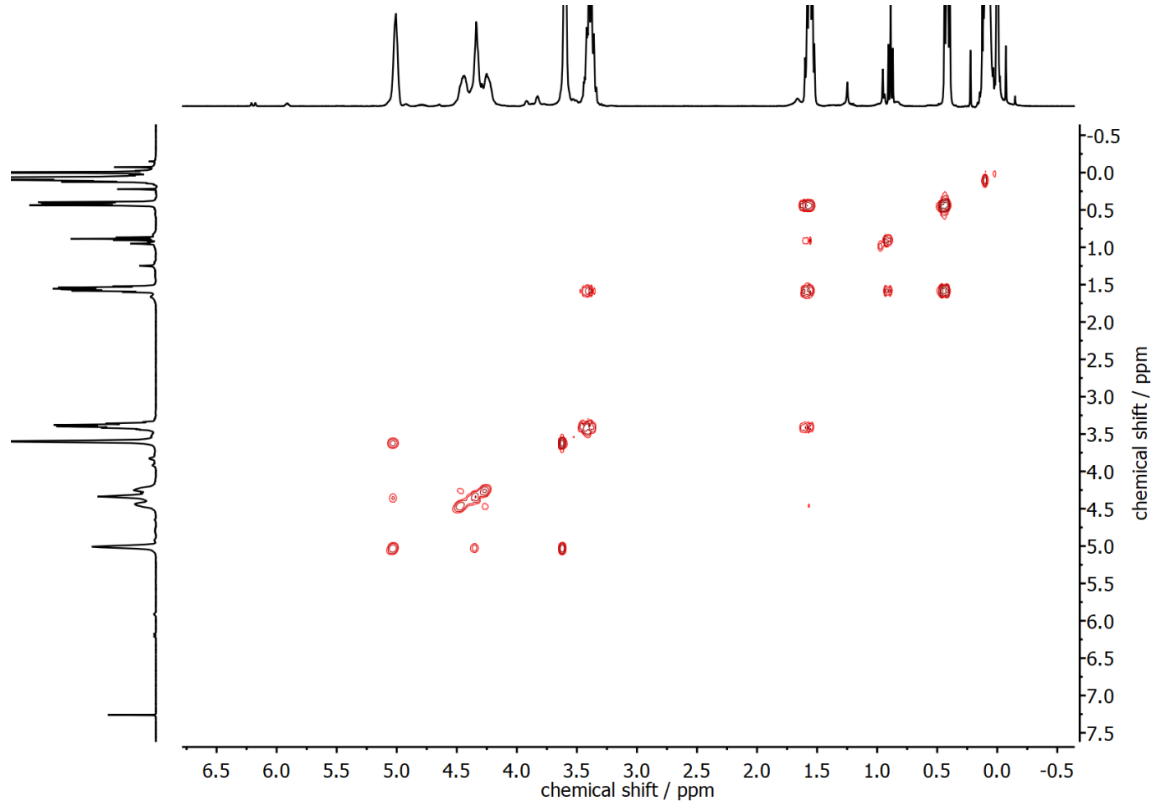

Figure S 8: COSY NMR spectrum of P(AGE-HMTS)C_{76} in $CDCl_3$, 400 MHz, 21 °C.

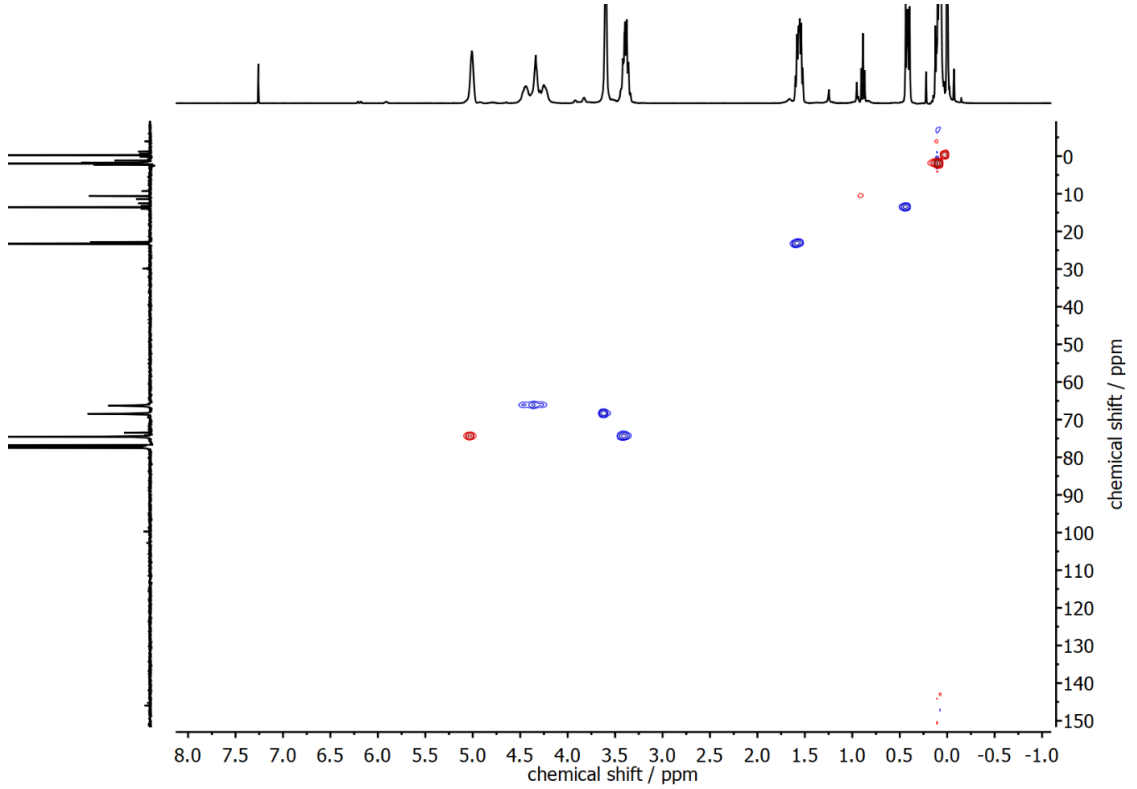

Figure S 9: HSQC NMR spectrum of P(AGE-HMTS)C_{76} in $CDCl_3$, 400 MHz, 21 °C.

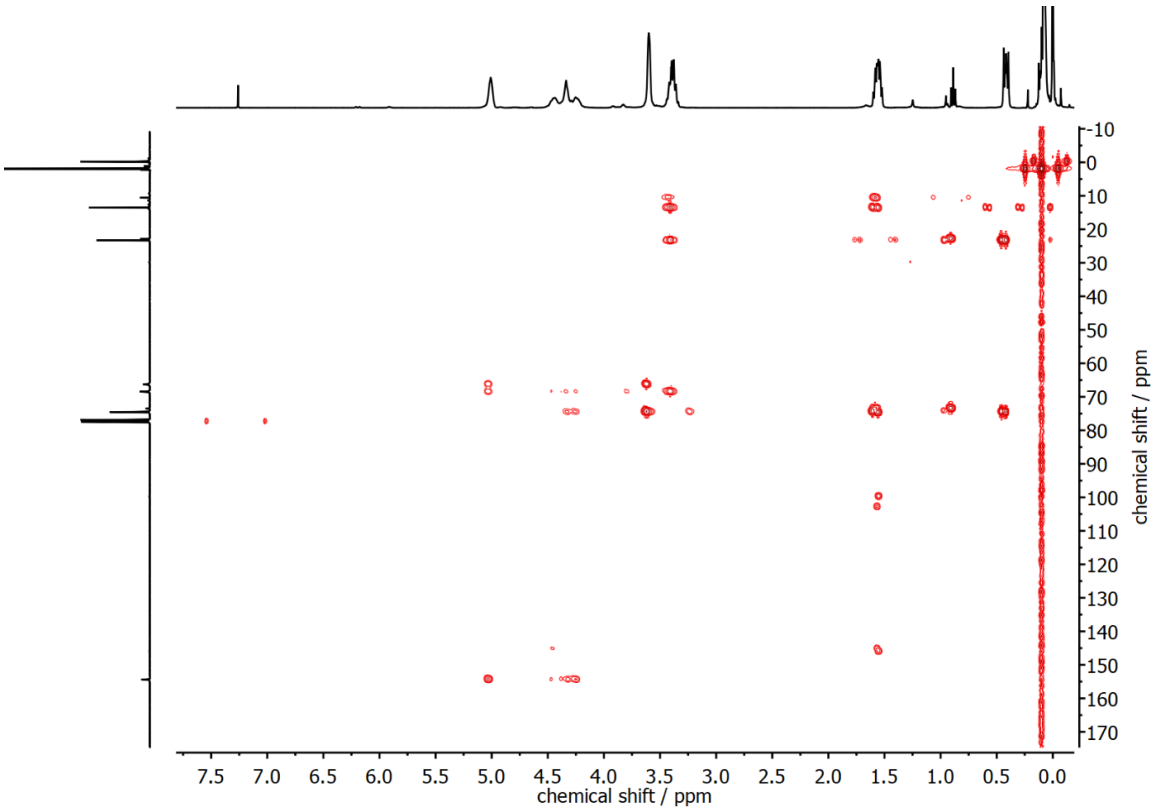

Figure S 10: HMBC NMR spectrum of P(AGE-HMTS)C_{76} in $CDCl_3$, 400 MHz, 21 °C.

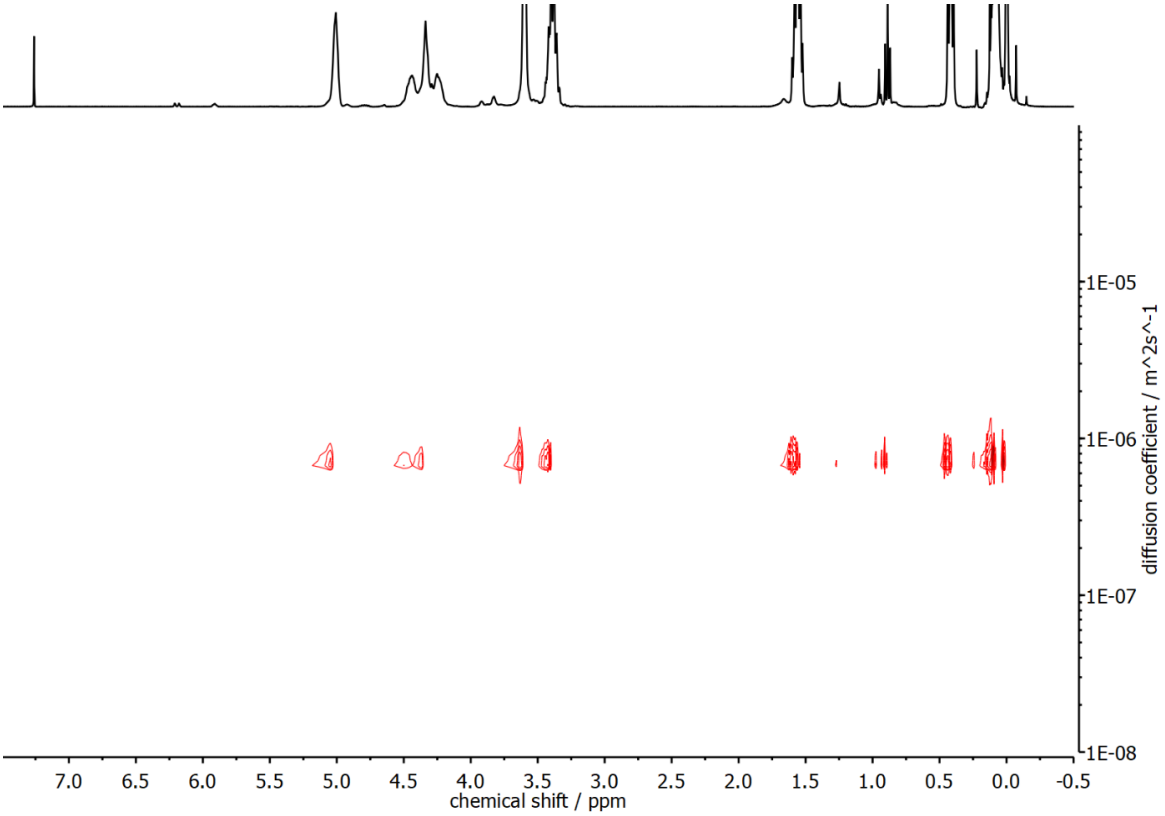

Figure S 11: DOSY NMR spectrum of P(AGE-HMTS)C_{76} in $CDCl_3$, 400 MHz, 21 °C.

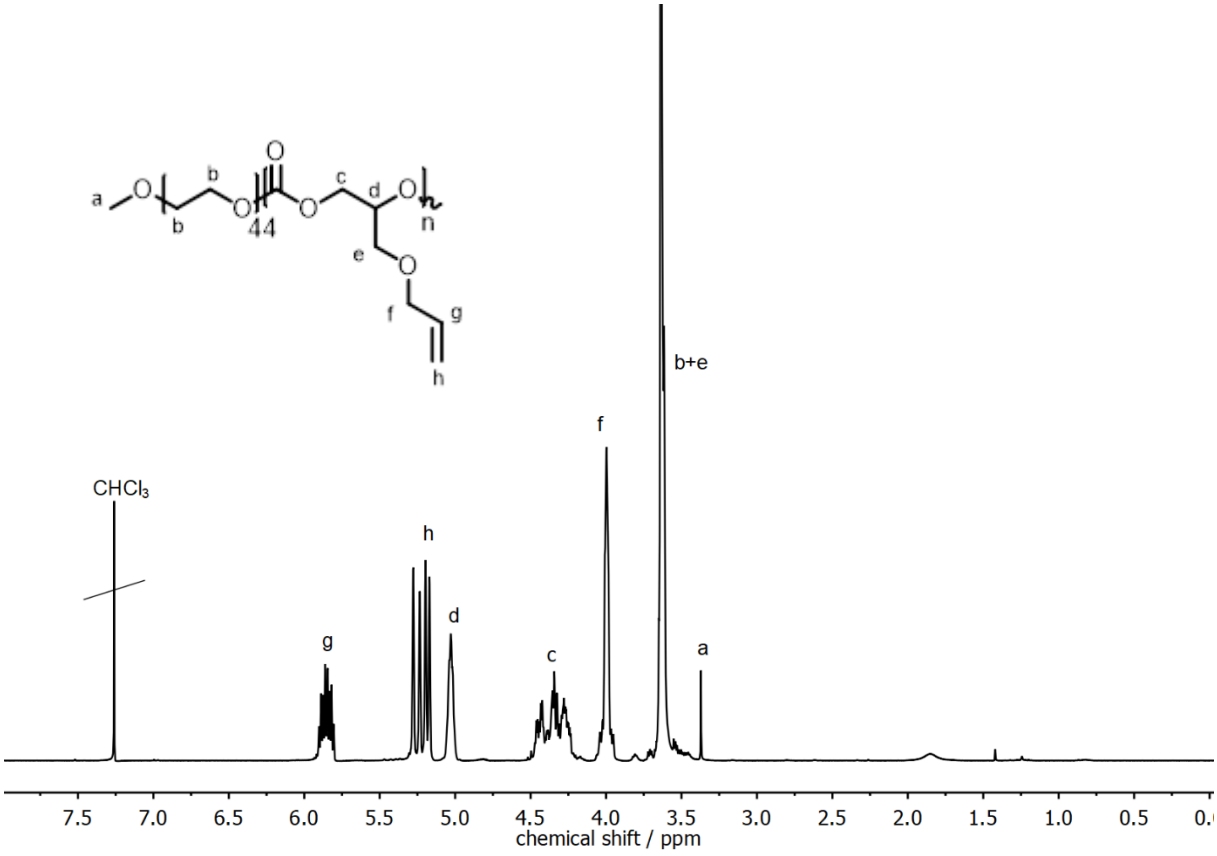

Figure S 12: ^{1}H NMR spectrum of mPEG$_{44}$-*b*-P(AGEC)$_{45}$ in $CDCl_3$, 400 MHz, 21 °C.

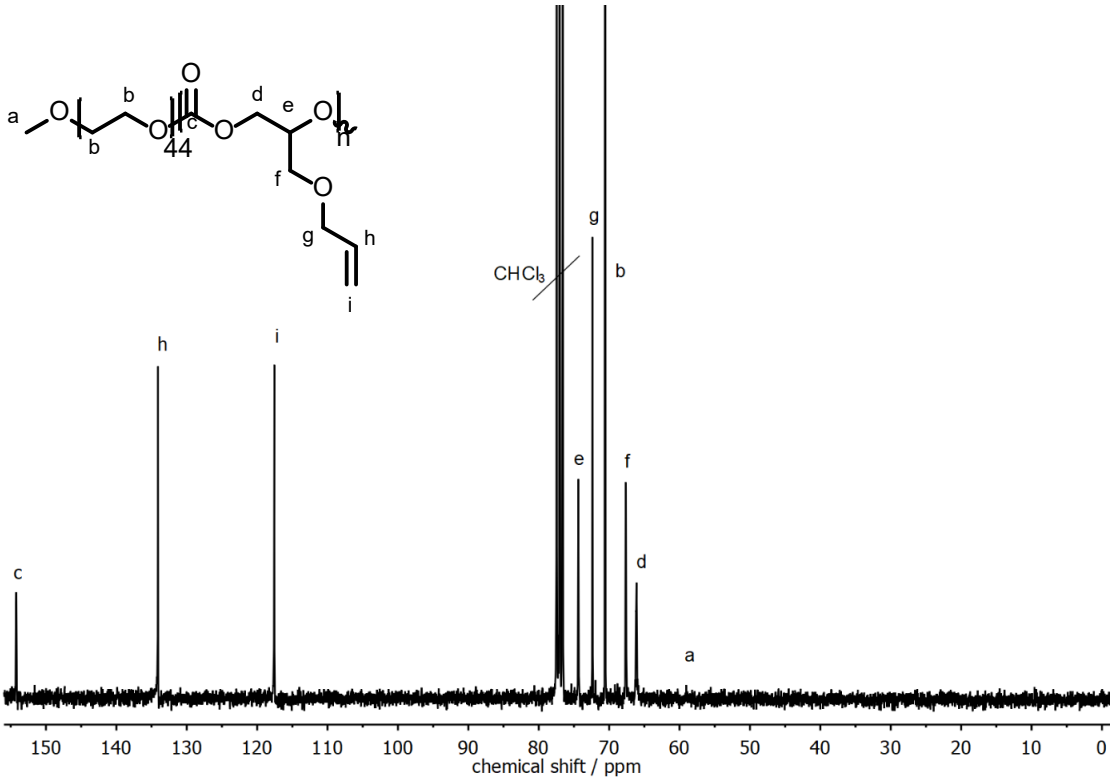

Figure S 13: ^{13}C NMR spectrum of mPEG$_{44}$-*b*-P(AGEC)$_{45}$ in CDCl$_3$, 400 MHz, 21 °C.

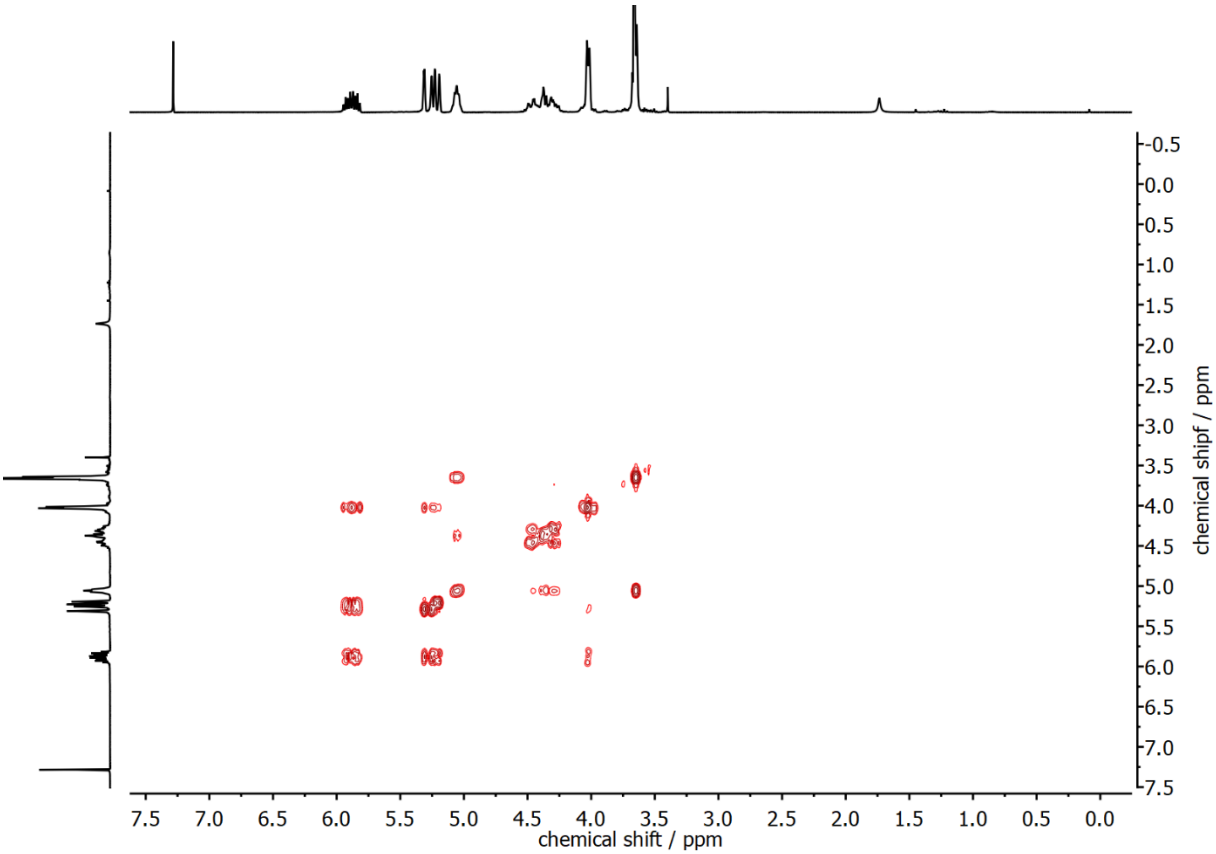

Figure S 14: COSY NMR spectrum of mPEG$_{44}$-*b*-P(AGEC)$_{45}$ in CDCl$_3$, 400 MHz, 21 °C.

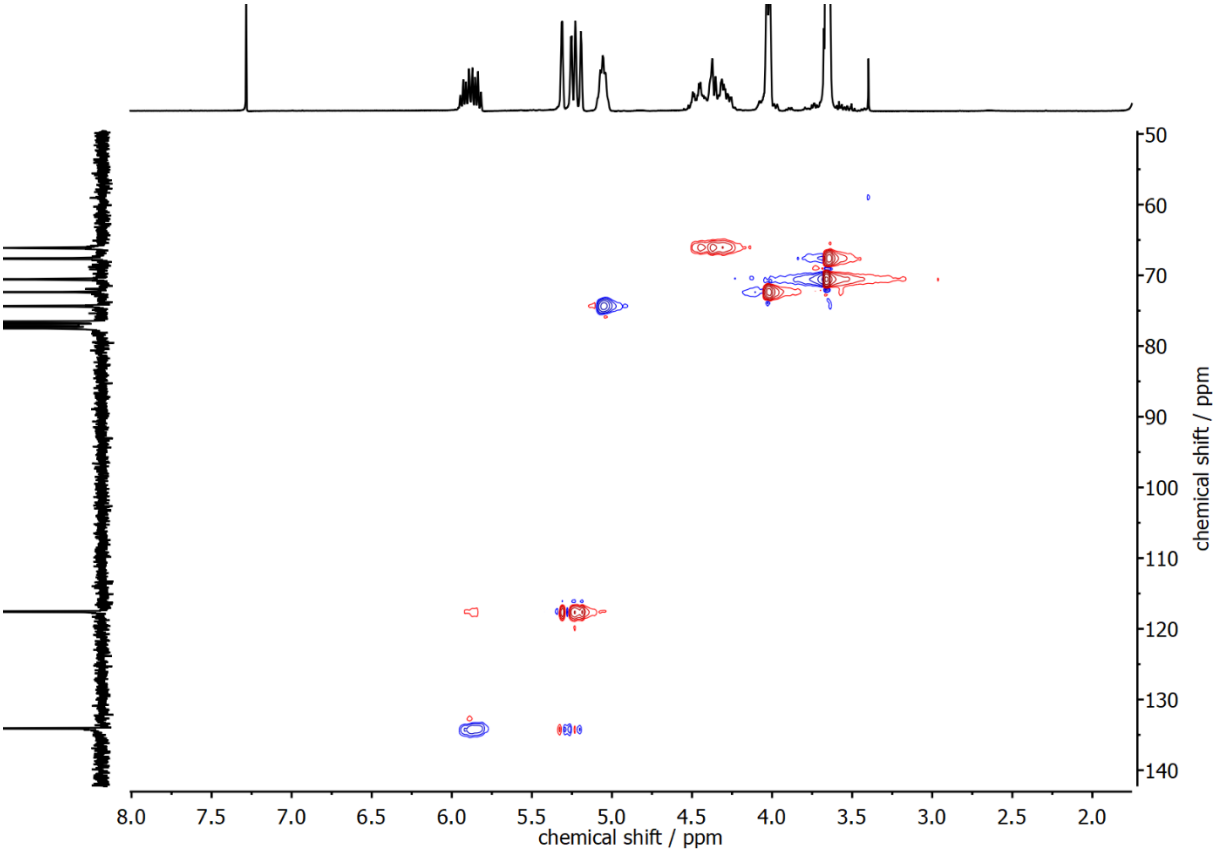

Figure S 15: HSQC NMR spectrum of mPEG$_{44}$-*b*-P(AGEC)$_{45}$ in CDCl$_3$, 400 MHz, 21 °C.

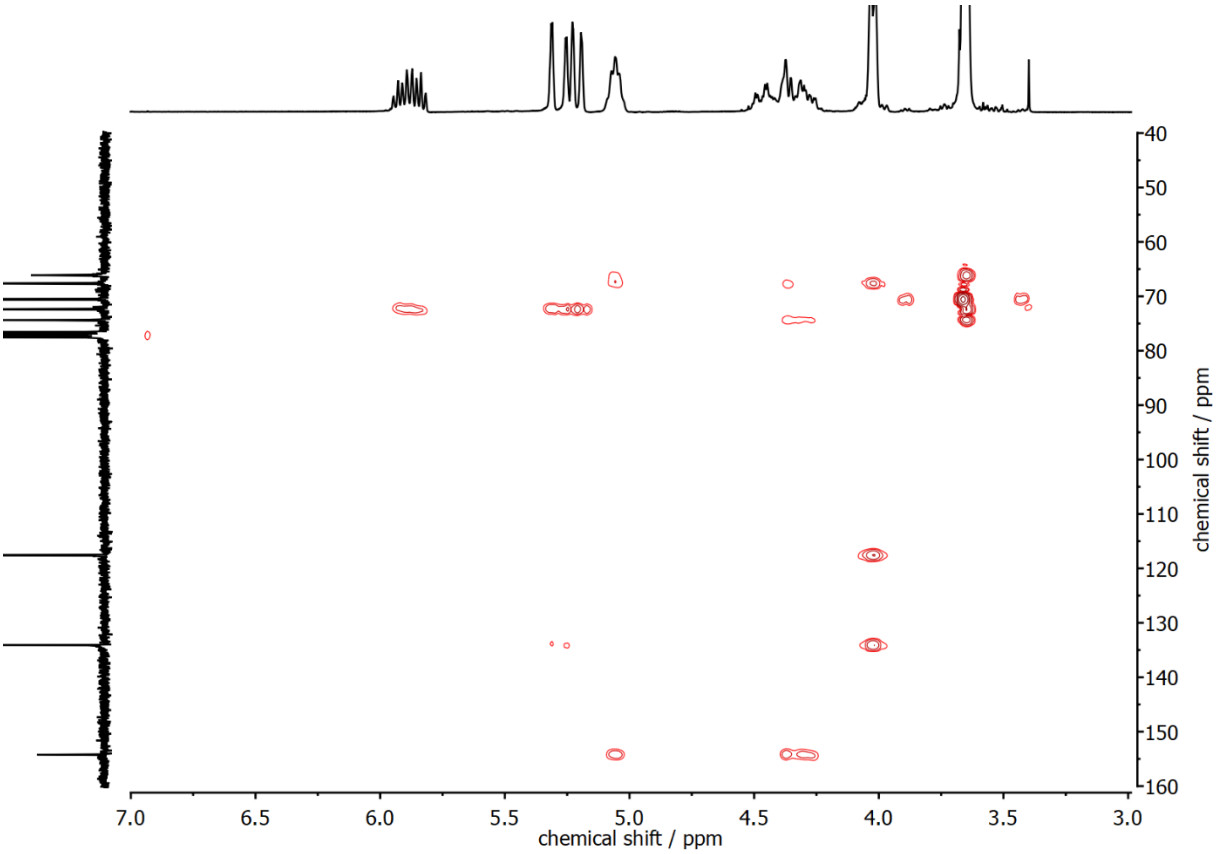

Figure S 16: HMBC NMR spectrum of mPEG$_{44}$-b-P(AGEC)$_{45}$ in CDCl$_3$, 400 MHz, 21 °C.

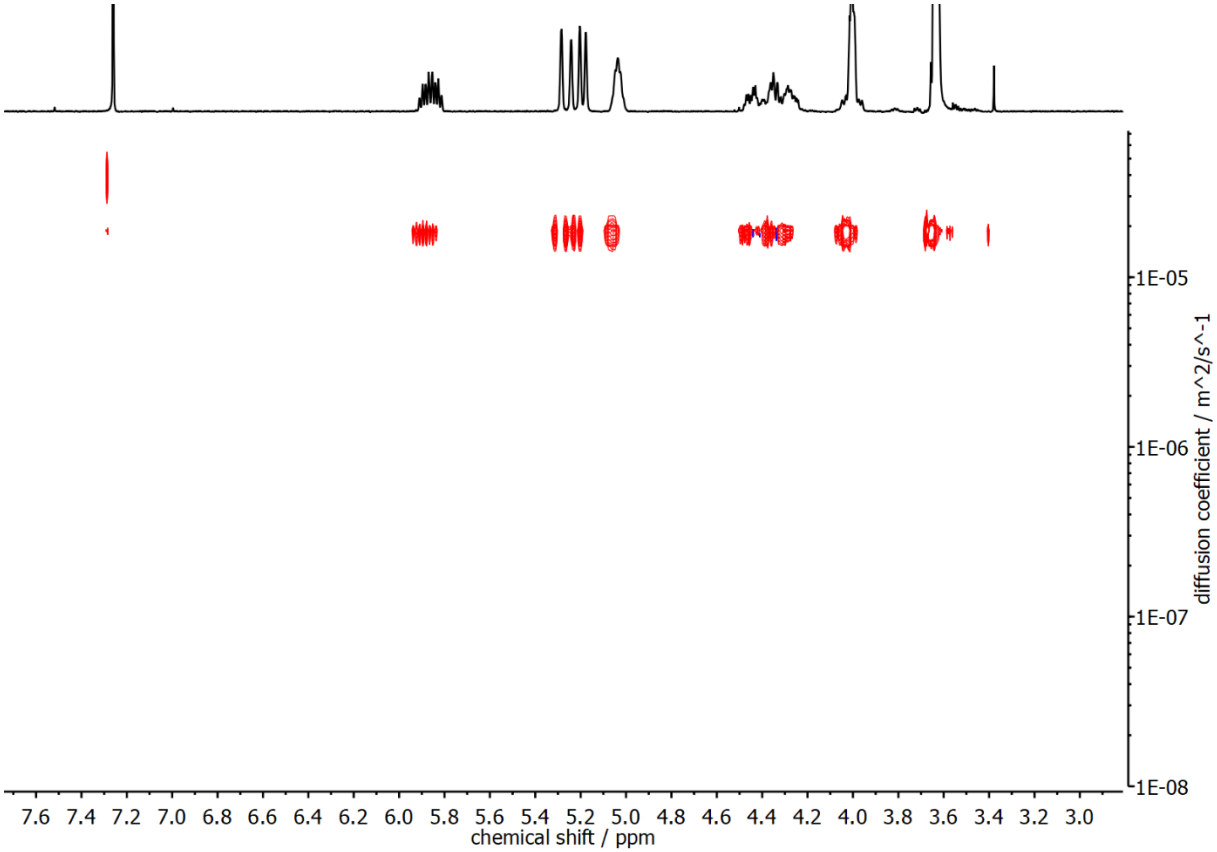

Figure S 17: DOSY NMR spectrum of mPEG$_{44}$-*b*-P(AGEC)$_{45}$ in $CDCl_3$, 400 MHz, 21 °C.

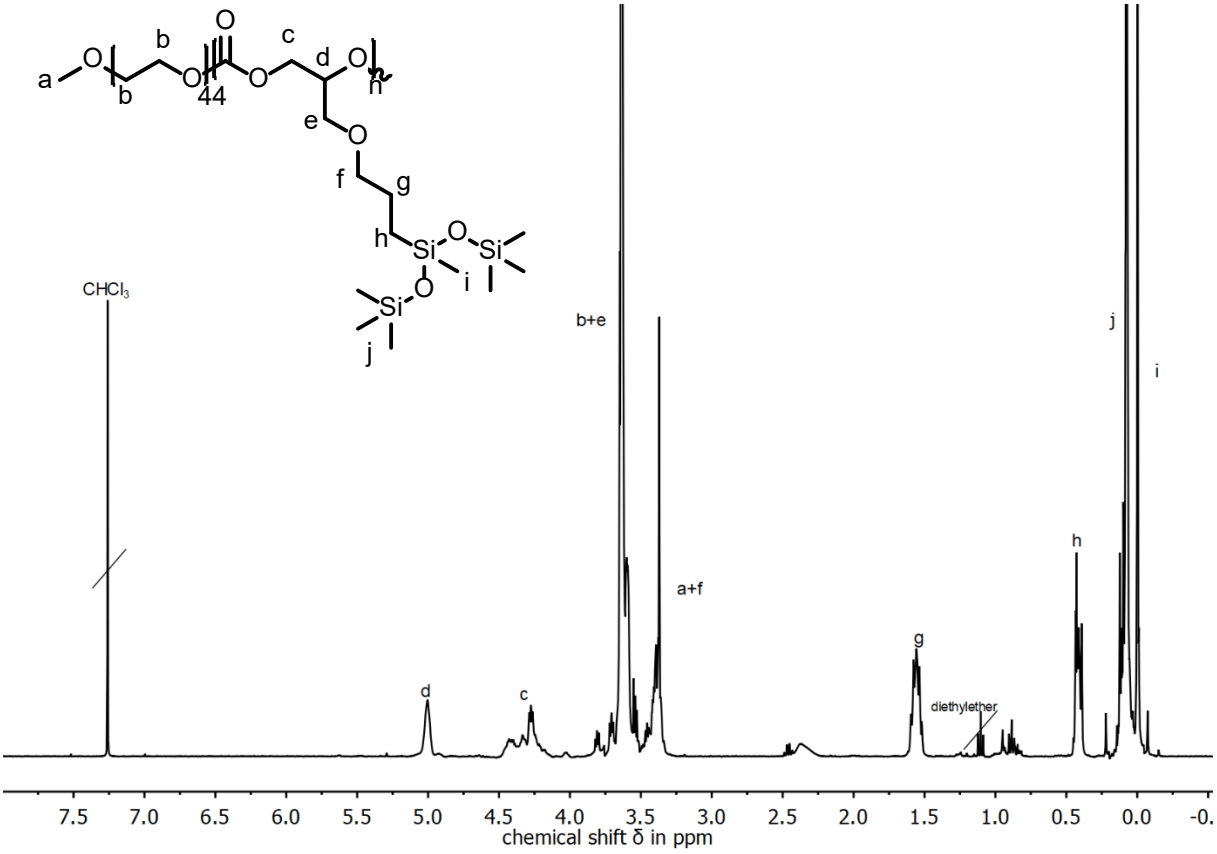

Figure S 18: ^{1}H NMR spectrum of mPEG$_{44}$-*b*-P(AGE-HMTS)C$_{45}$ in $CDCl_3$, 400 MHz, 21 °C.

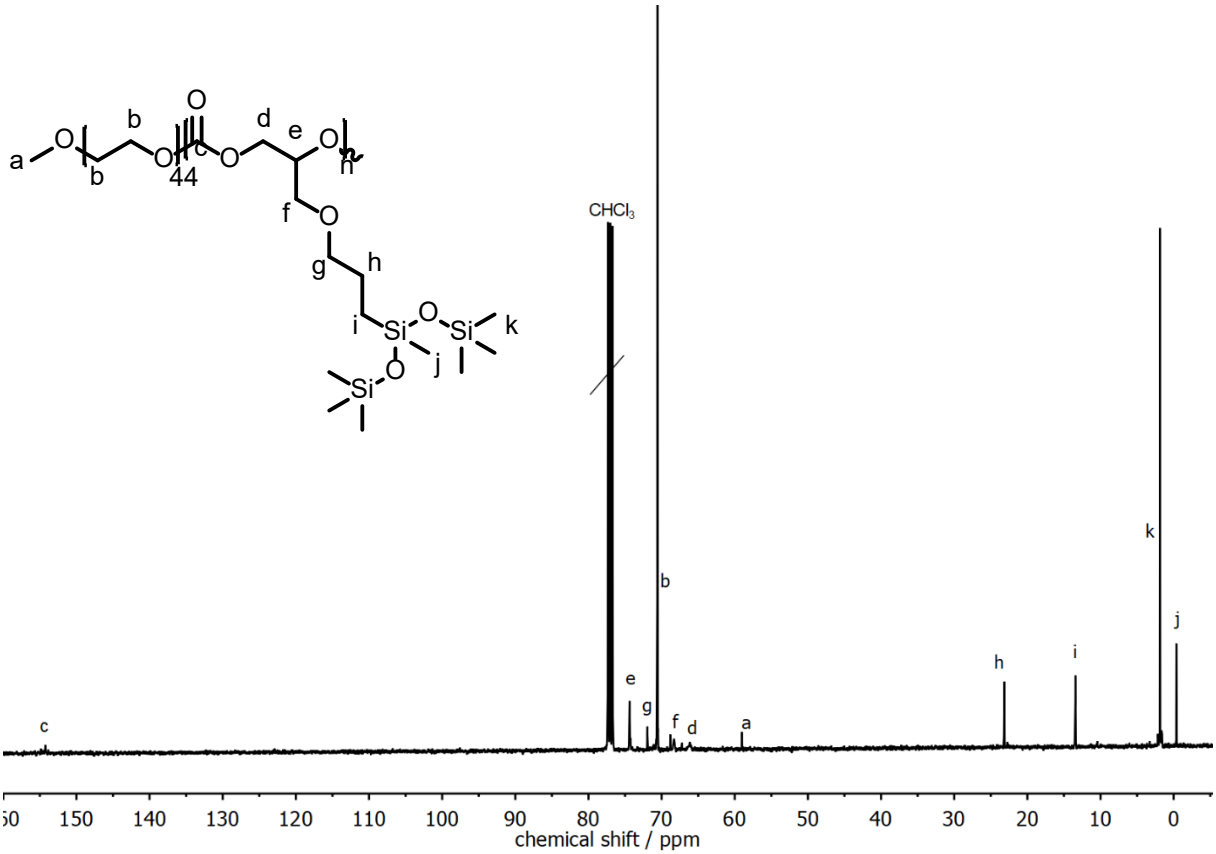

Figure 19: ^{13}C NMR spectrum of mPEG$_{44}$-*b*-P(AGE-HMTS)C$_{45}$ in $CDCl_3$, 400 MHz, 21 °C.

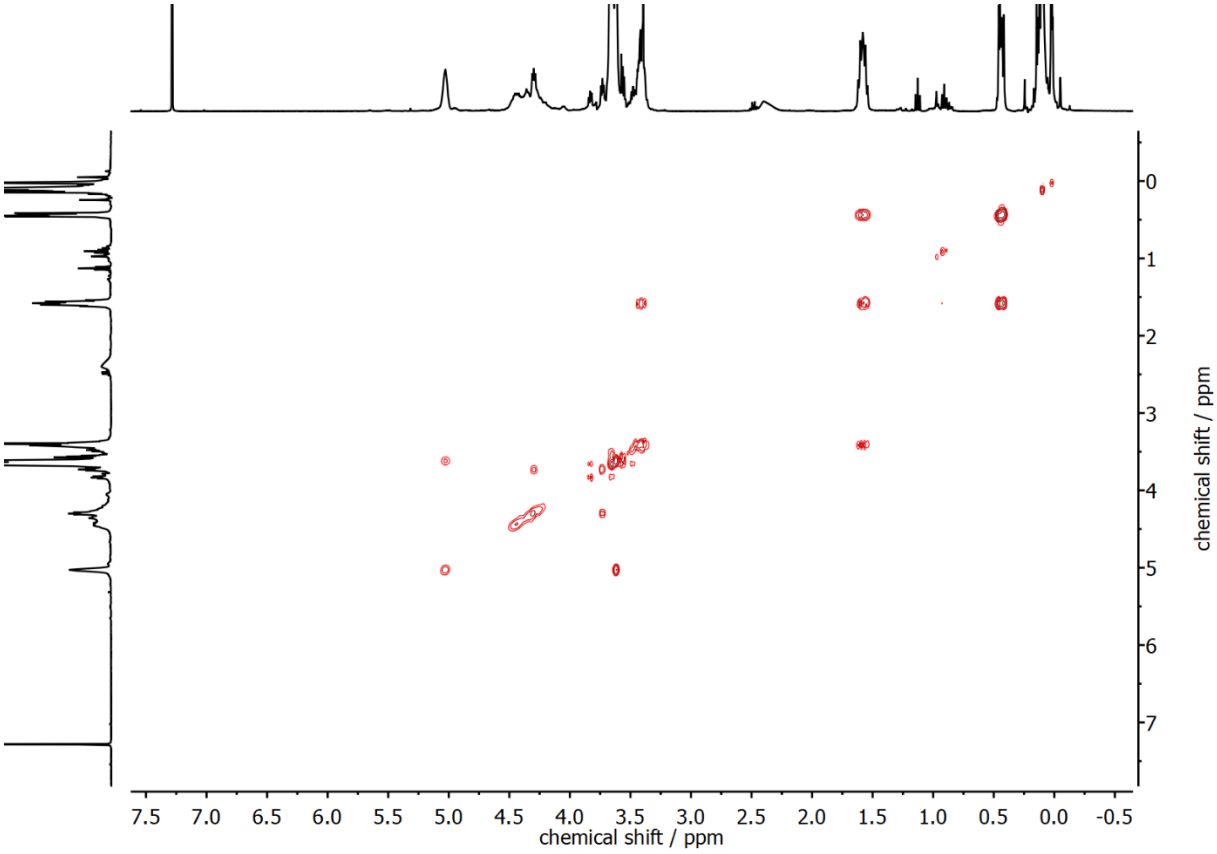

Figure S 20: COSY NMR spectrum of mPEG$_{44}$-*b*-P(AGE-HMTS)C$_{45}$ in CDCl$_3$, 400 MHz, 21 °C.

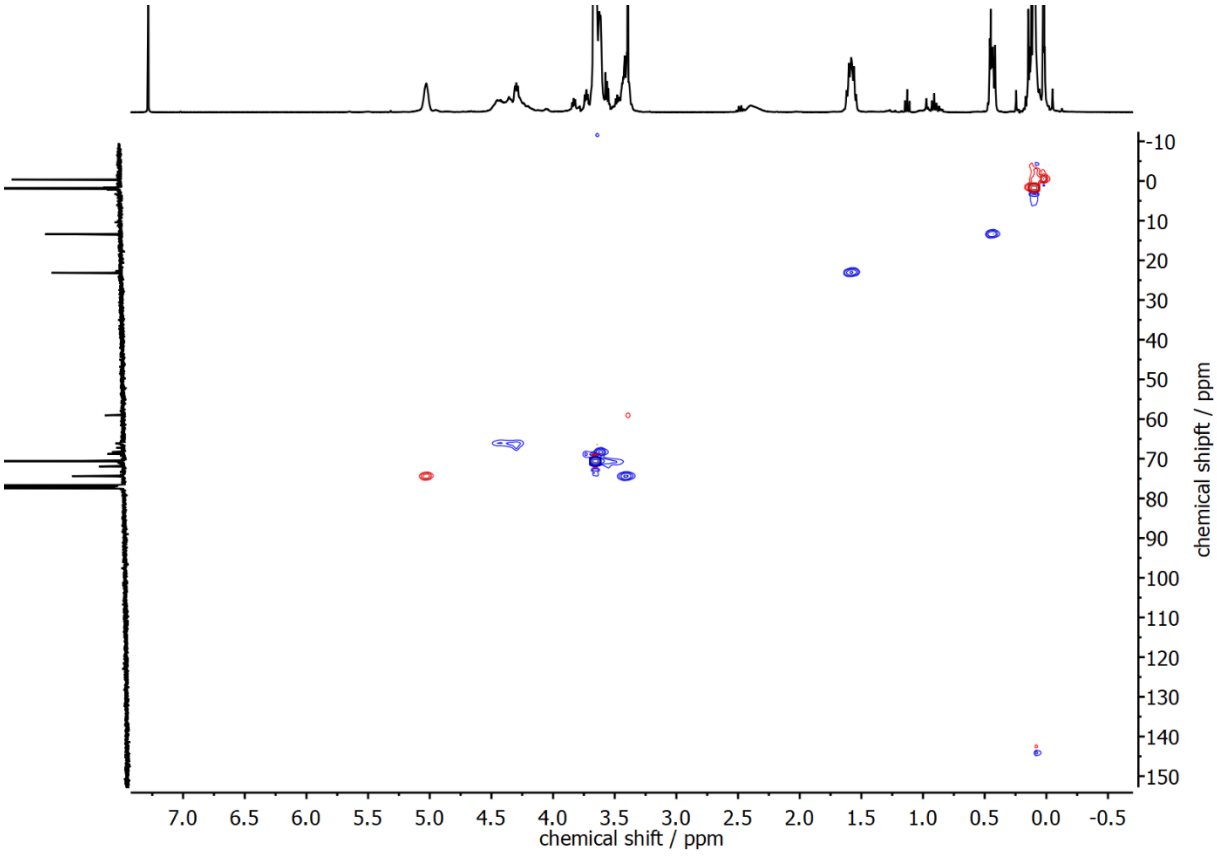

Figure S 21: HSQC NMR spectrum of mPEG$_{44}$-*b*-P(AGE-HMTS)C$_{45}$ in CDCl$_3$, 400 MHz, 21 °C.

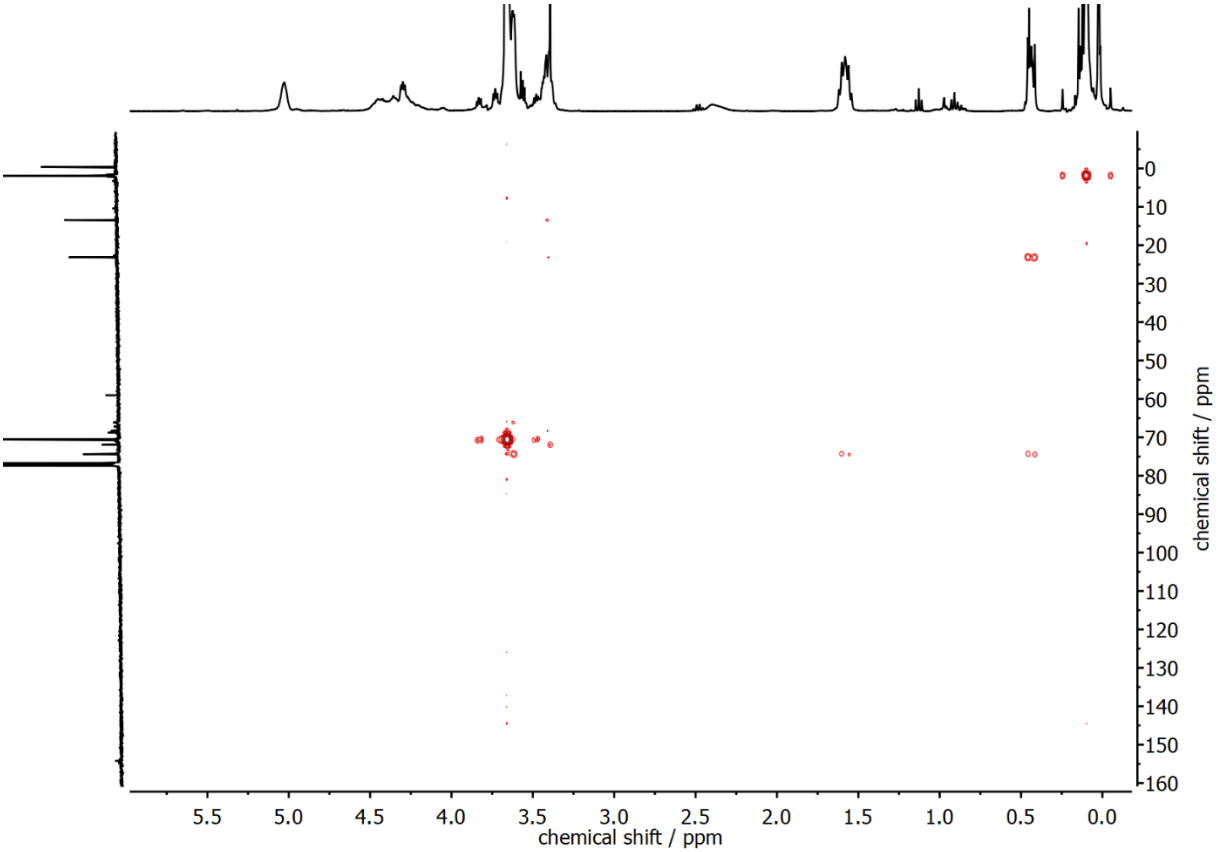

Figure S 22: HMBC NMR spectrum of mPEG$_{44}$-*b*-P(AGE-HMTS)C$_{45}$ in CDCl$_3$, 400 MHz, 21 °C.

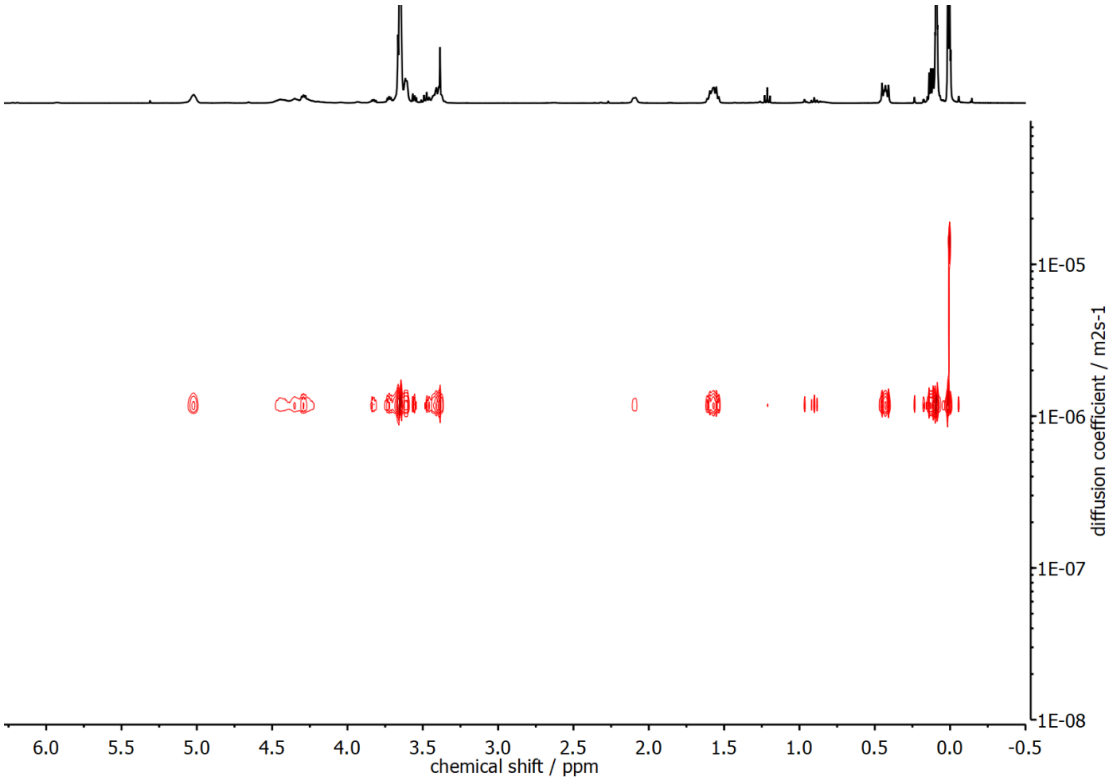

Figure S 23: DOSY NMR spectrum of mPEG$_{44}$-*b*-P(AGE-HMTS)C$_{45}$ in CDCl$_3$, 400 MHz, 21 °C.

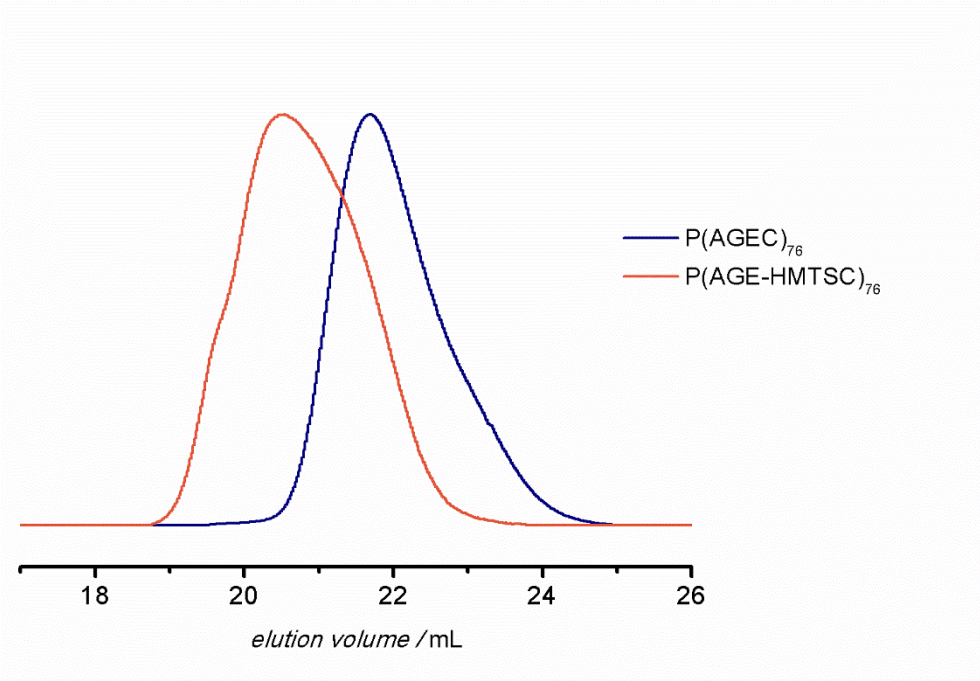

Figure S 24: SEC traces of $P(AGEC)_{76}$ compared with $P(AGE\text{-}HMTS)C_{76}$ in THF, 50 °C, PS standard.

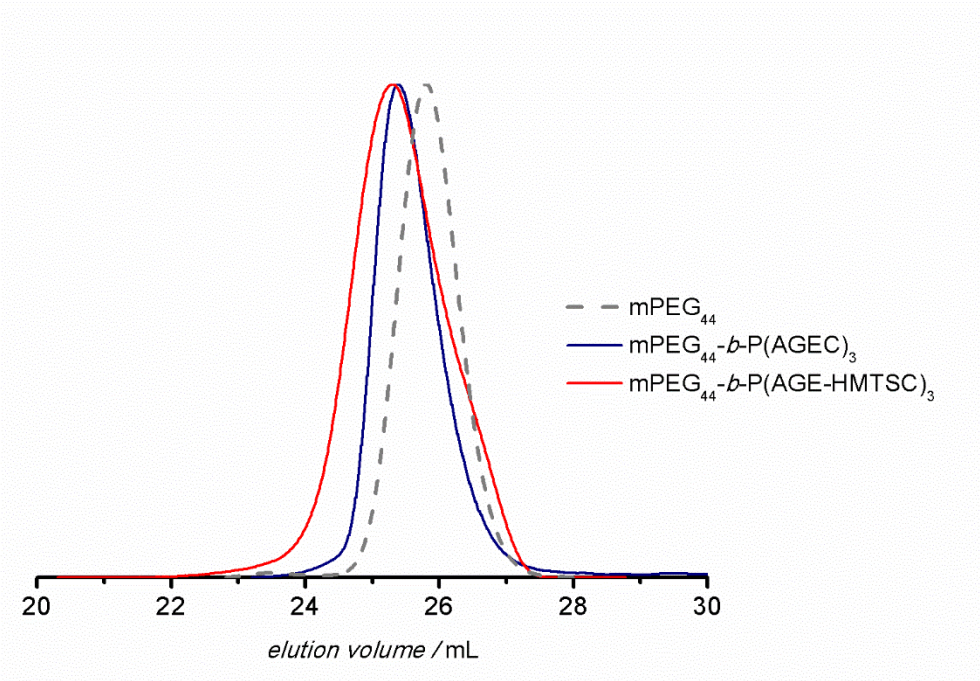

Figure S 25: SEC traces of $mPEG_{44}$-*b*-$P(AGEC)_3$ compared with $mPEG_{44}$-*b*-$P(AGE\text{-}HMTS)C_3$ in THF, 50 °C, PS standard.

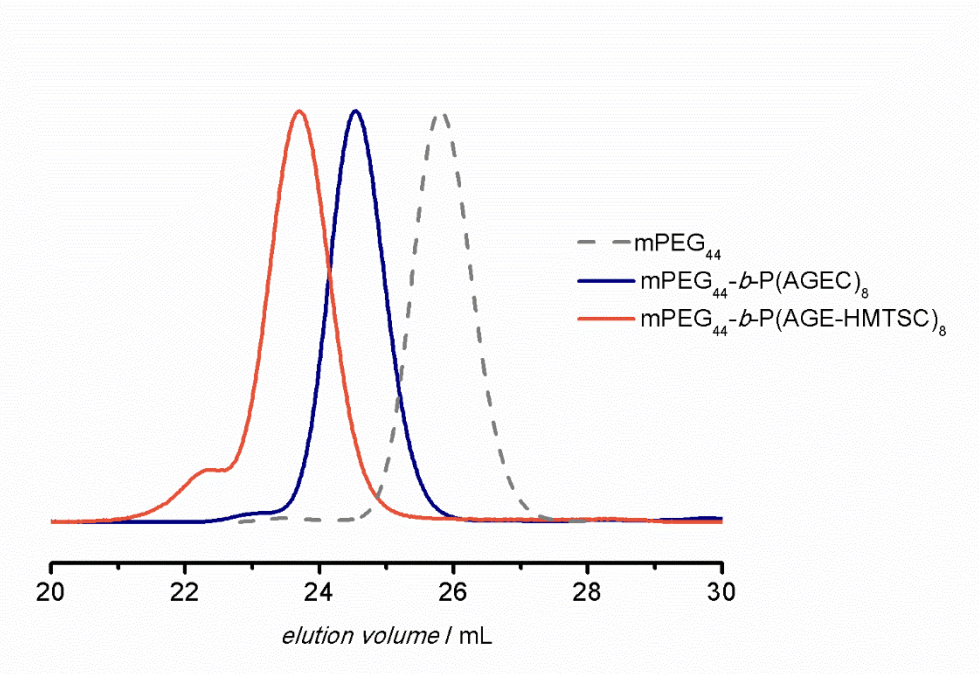

Figure S 26: SEC traces of $mPEG_{44}$-*b*-$P(AGEC)_8$ compared with $mPEG_{44}$-*b*-$P(AGE\text{-}HMTS)C_8$ in THF, 50 °C, PS standard.

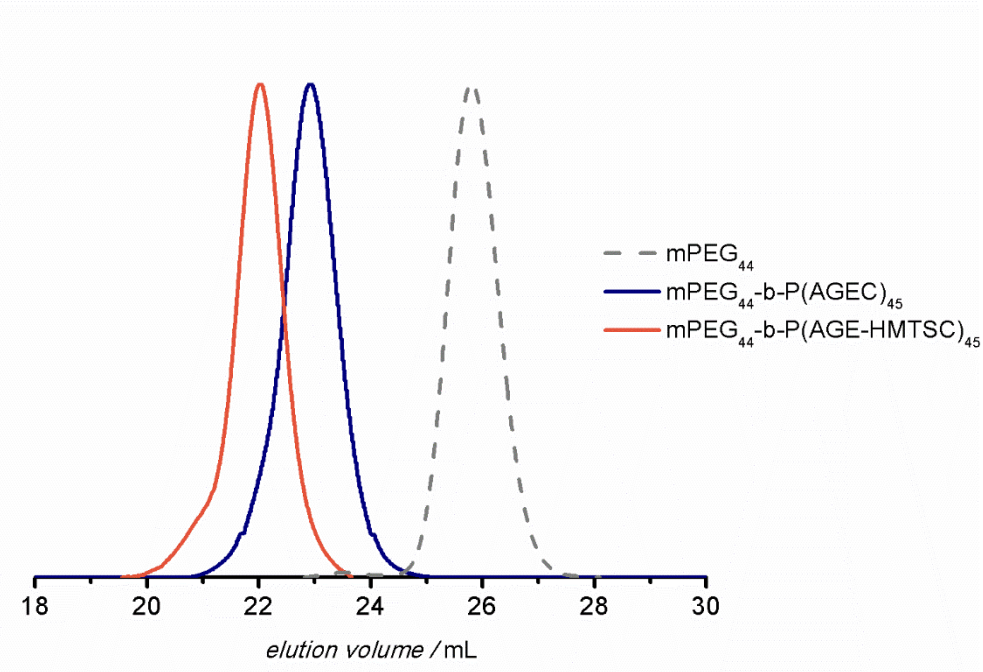

Figure S 27: SEC traces of $mPEG_{44}$-*b*-$P(AGEC)_{45}$ compared with $mPEG_{44}$-*b*-$P(AGE\text{-}HMTS)C_{45}$ in THF, 50 °C, PS standard.

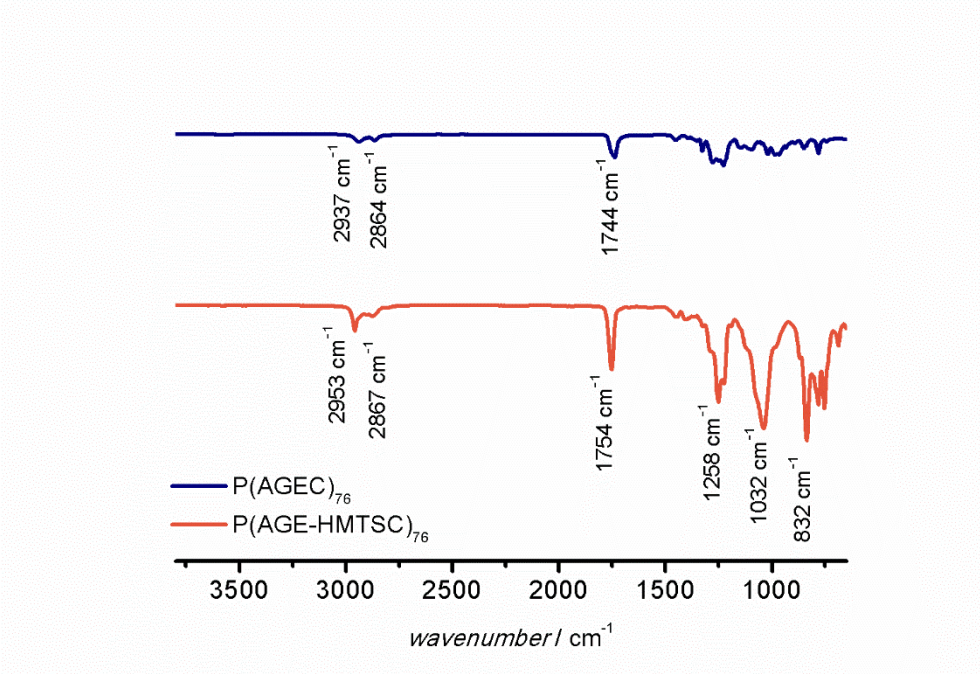

Figure S 28: FT-IR spectra of $P(AGEC)_{76}$ compared with $P(AGE\text{-}HMTS)C_{76}$.

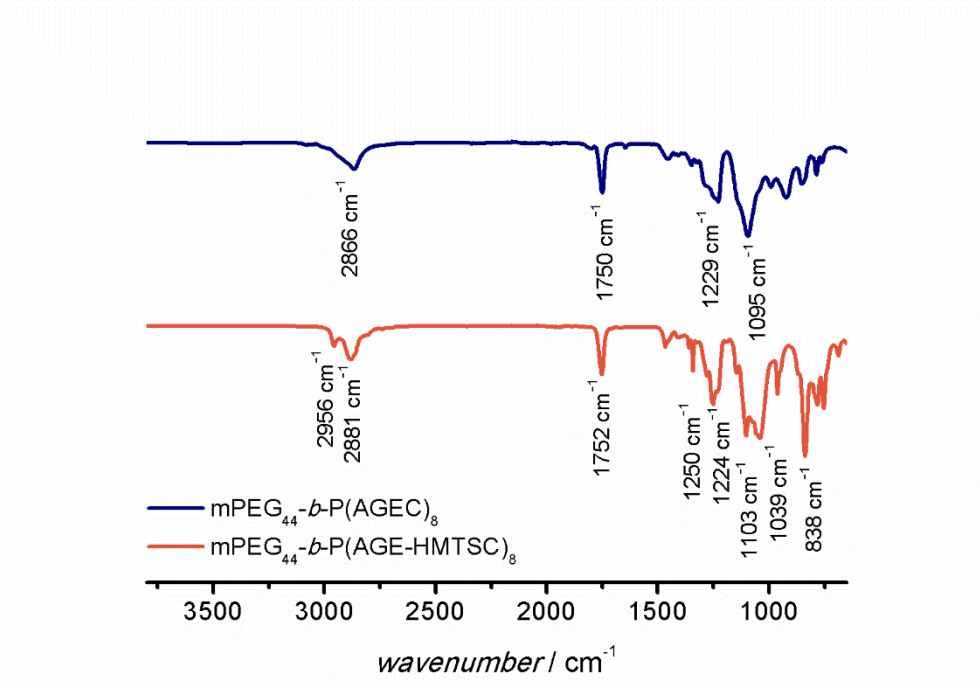

Figure S 29: FT-IR spectra of $mPEG_{44}$-*b*-$P(AGEC)_8$ compared with $mPEG_{44}$-*b*-$P(AGE\text{-}HMTS)C_8$.

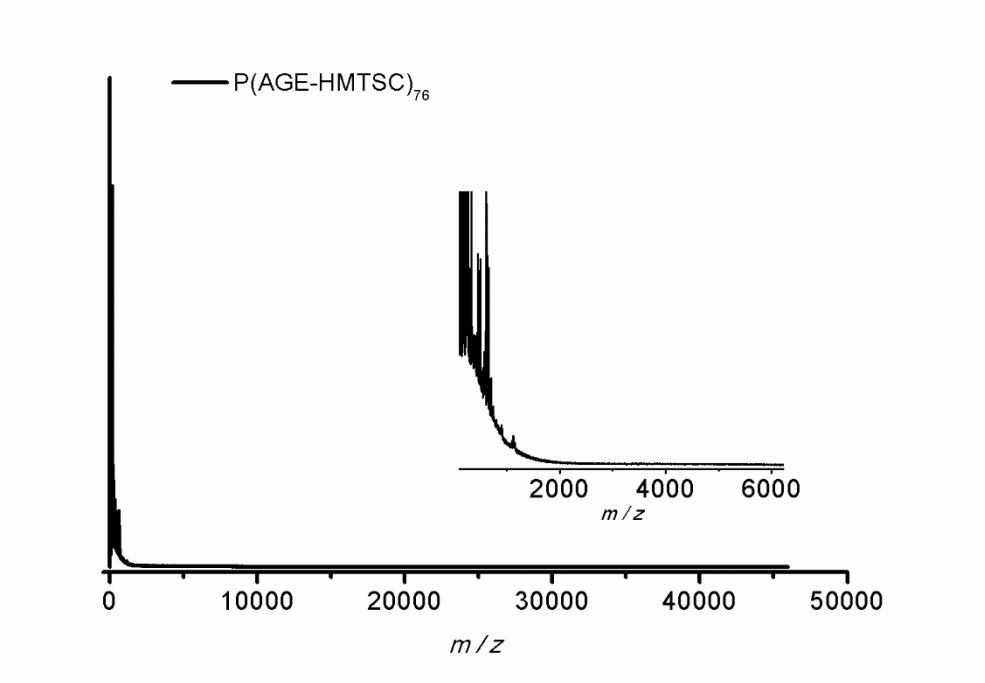

Figure S 30: MALDI-TOF spectra of sample P(AGE-HMTS)C_{76} in Dithranol.

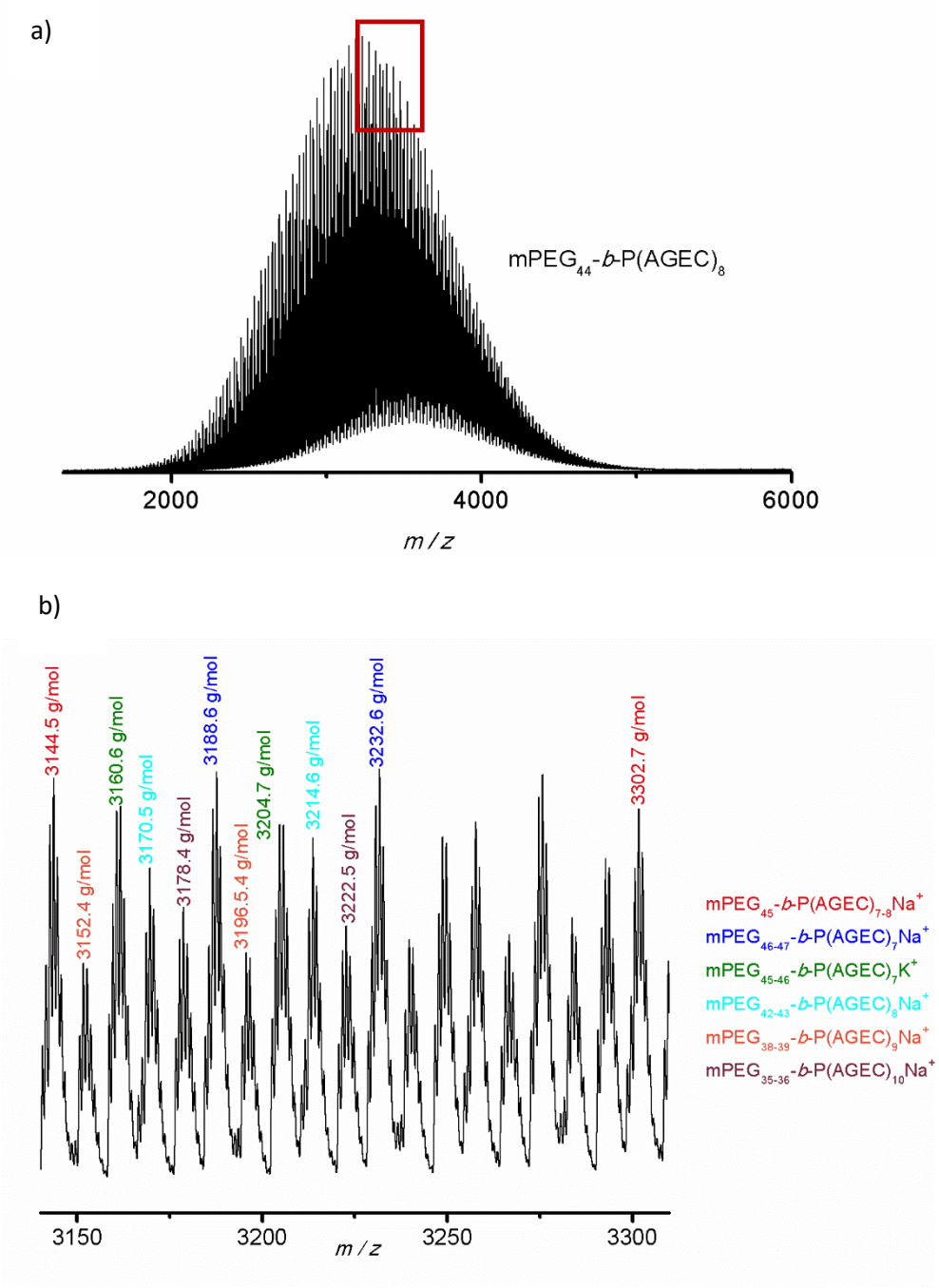

Figure S 31: MALDI-TOF spectra of sample $mPEG_{44}$-*b*-$P(AGEC)_8$: complete spectrum in a), assigned molar masses in b) (repeating units calculated to 44 g mol^{-1} for C_2H_4O and 158 g mol^{-1} for $C_7H_{10}O_4$) in Dithranol.

2. Thermal analysis

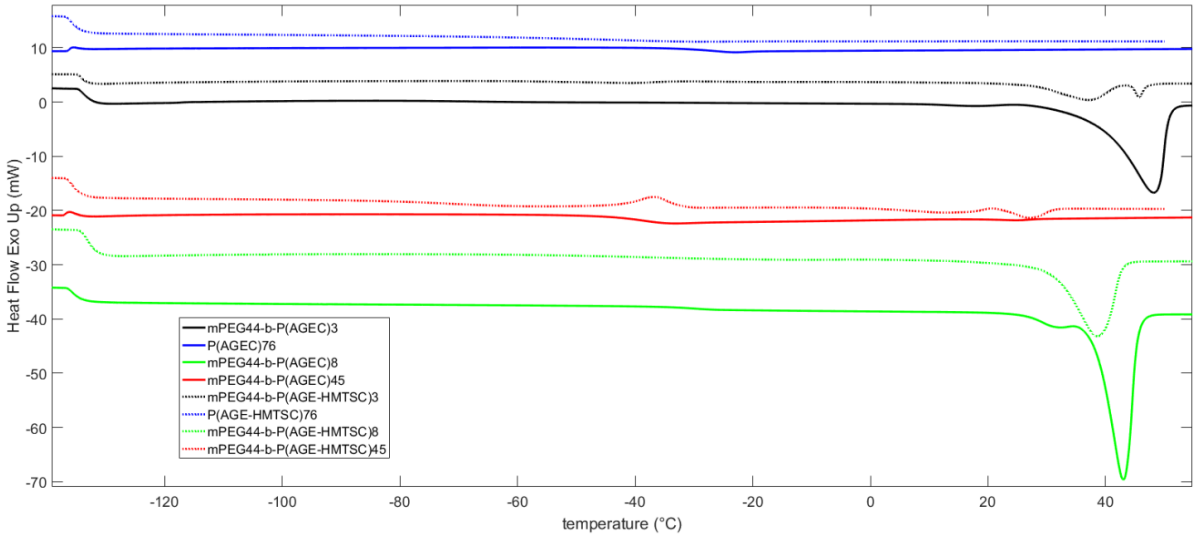

Figure S 32: DSC heating curves of the polycarbonates before and after hydrosilylation.

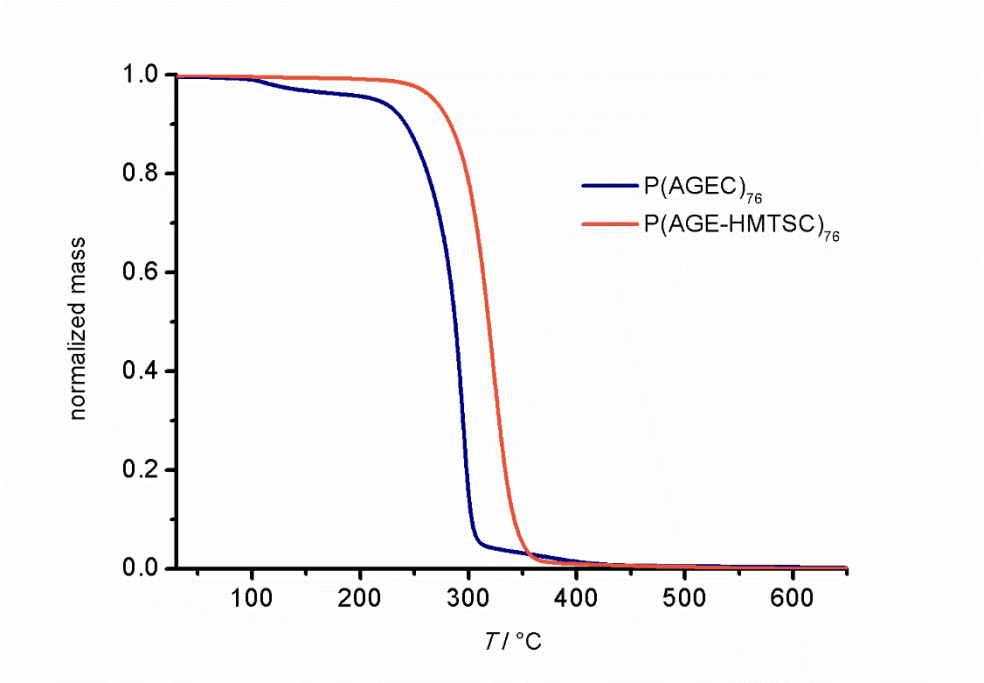

Figure S 33: TGA curve of $P(AGEC)_{76}$ compared with $P(AGE\text{-}HMTS)C_{76}$.

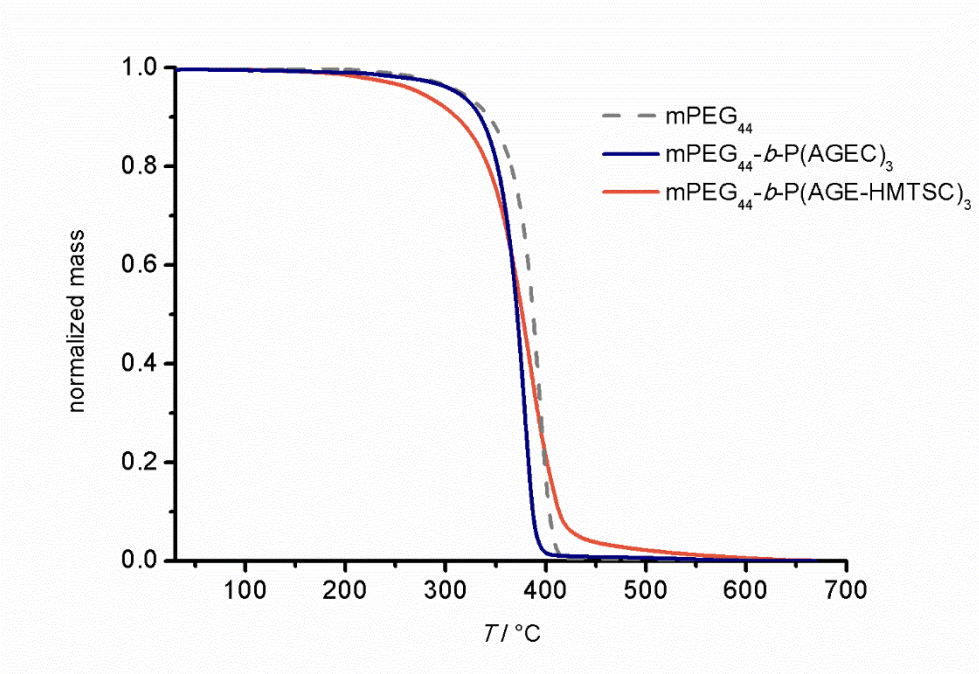

Figure S 34: TGA curve of $mPEG_{44}$-*b*-$P(AGEC)_3$ and $mPEG_{44}$-*b*-$P(AGE\text{-}HMTS)C_3$ compared with $mPEG_{44}$.

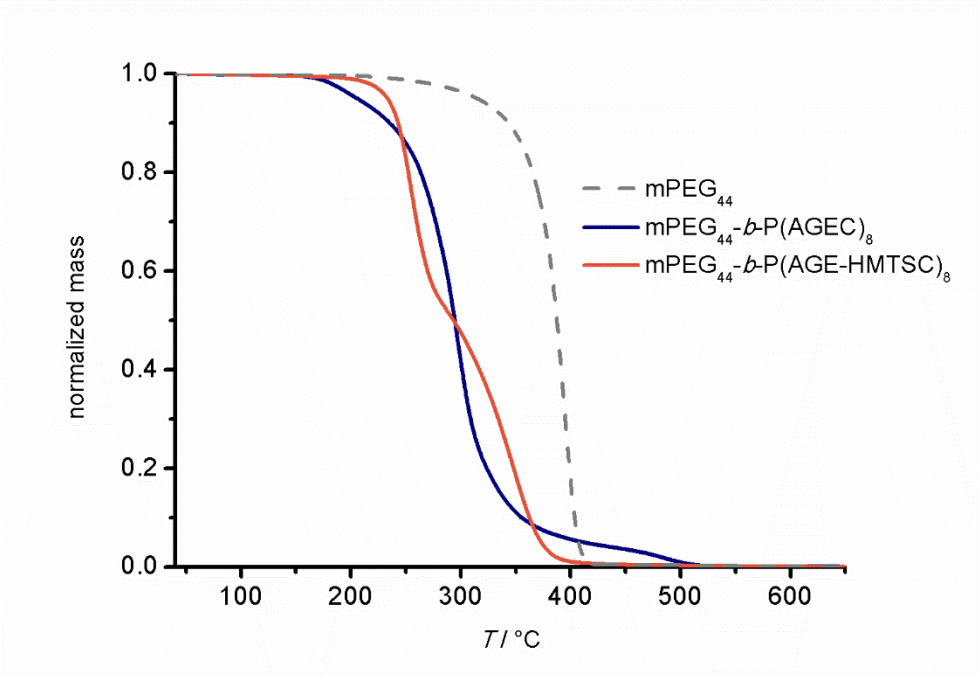

Figure S 35: TGA curve of $mPEG_{44}$-*b*-$P(AGEC)_8$ compared with $mPEG_{44}$-*b*-$P(AGE\text{-}HMTS)C_8$.

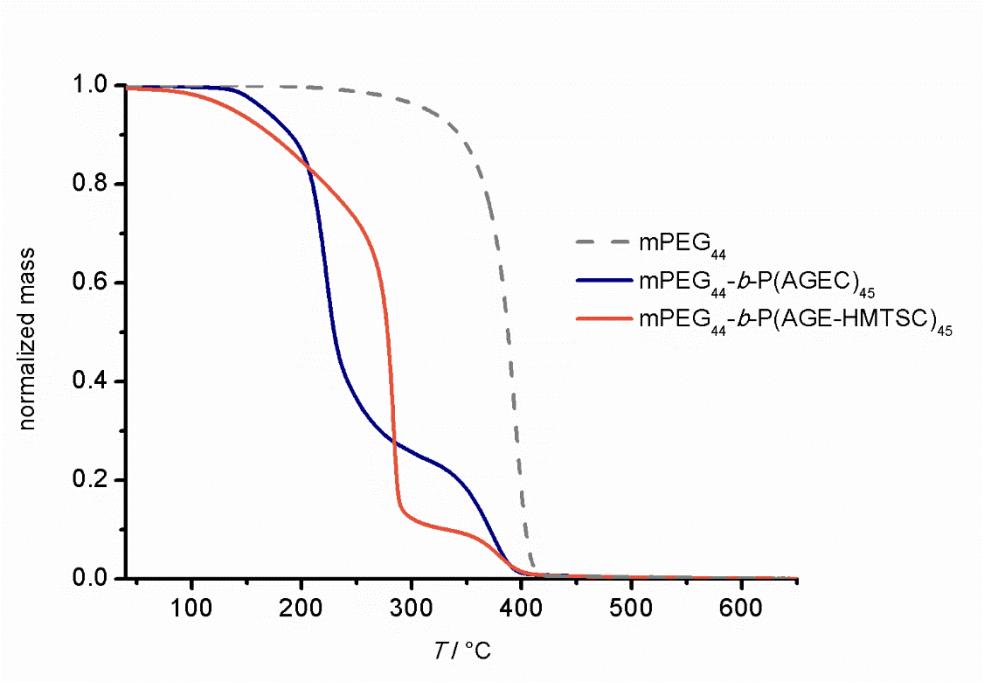

Figure S 36: TGA curve of $mPEG_{44}$-*b*-$P(AGEC)_{45}$ compared with $mPEG_{44}$-*b*-$P(AGE\text{-}HMTS)C_{45}$.

3. Contact Angle Measurements

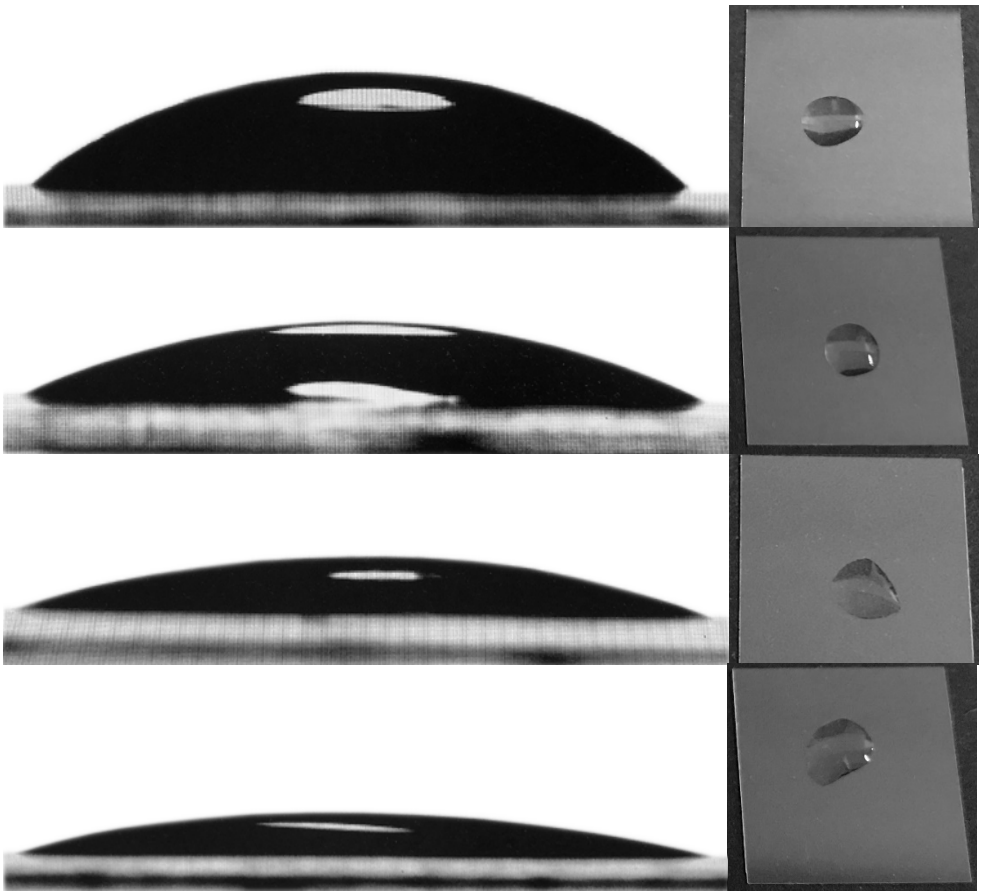

Figure S 37: Images of the droplets used in contact angle measurements (from top to bottom: pure water, $mPEG_{44}$, $mPEG_{44}$-*b*-$PAGEC_8$, and $mPEG_{44}$-*b*-$P(AGE\text{-}HMTS)C_8$).

4. DLS measurements

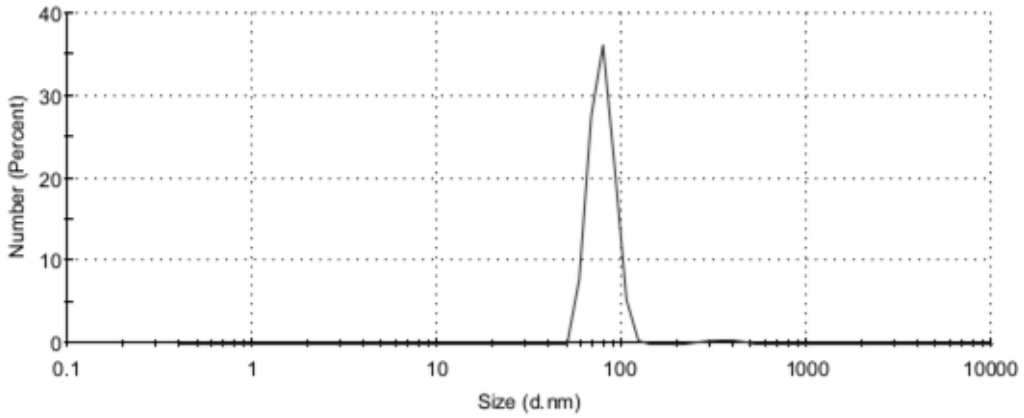

Figure S 38: DLS of mPEG$_{44}$-*b*-P(AGE-HMTS)C$_3$ in water.

5. Miniemulsion Polymerization

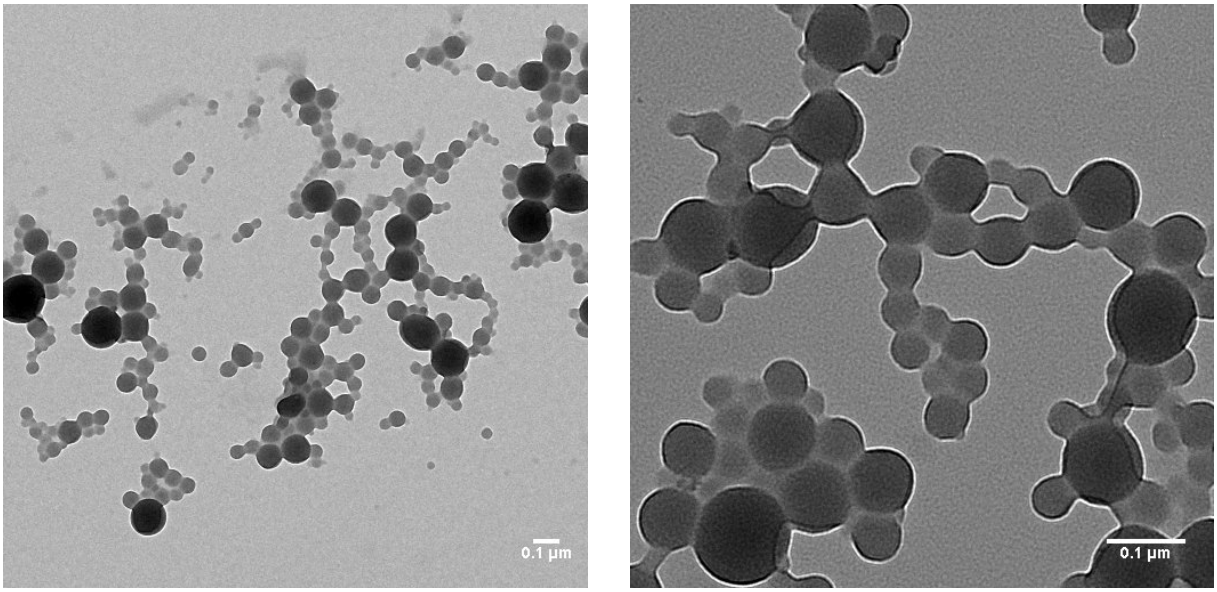

Figure S 39: TEM images at different magnifications of the polystyrene nanoparticles achieved from free-radical miniemulsion polymerization of styrene in water with mPEG$_{44}$-*b*-P(AGE-HMTS)C$_8$ as emulsifier.

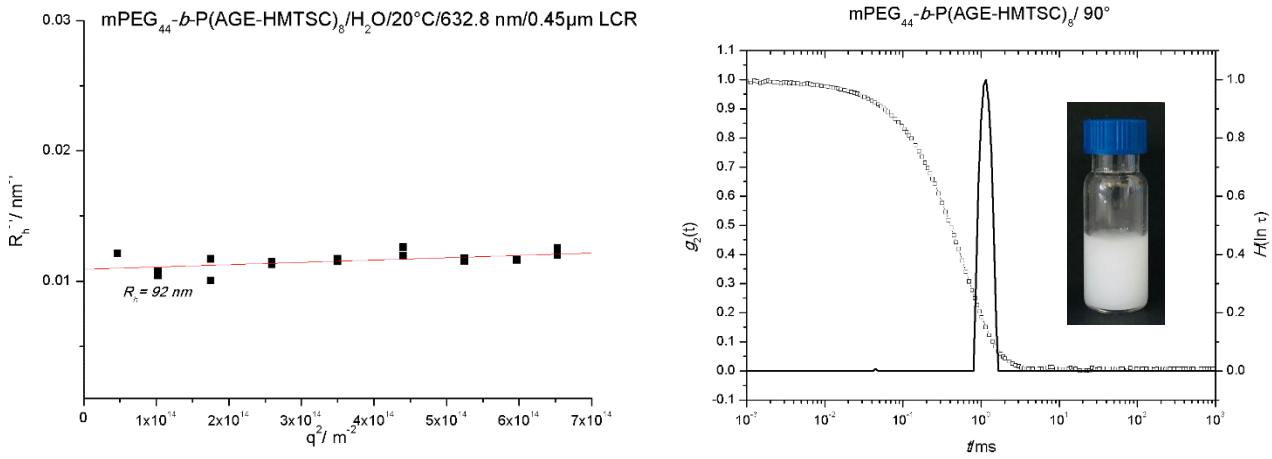

Figure S 40: DLS data of the PS-nanoparticles in water (left) and autocorrelation function (g_2(t)) of PS nanoparticles and the relaxation time distribution (H(ln(t)) with stable miniemulsion (right).

Appendix

CHAPTER A1

Efficiency Boosting of Surfactants with Poly(ethylene oxide)-Poly(alkyl glycidyl ether)s – A New Class of Amphiphilic Polymers

LANGMUIR

pubs.acs.org/Langmuir Article

Efficiency Boosting of Surfactants with Poly(ethylene oxide)-Poly(alkyl glycidyl ether)s: A New Class of Amphiphilic Polymers

Kristina Schneider,[‖] Patrick Verkoyen,[‖] Maximilian Krappel, Christina Gardiner, Ralf Schweins, Holger Frey, and Thomas Sottmann*

Cite This: *Langmuir* 2020, 36, 9849−9866 Read Online

ACCESS | Metrics & More | Article Recommendations | Supporting Information

ABSTRACT: Twenty years ago, it was found that adding small amounts of amphiphilic block copolymers like poly(ethylene propylene)-*co*-poly(ethylene oxide) (PEP-*b*-PEO) to microemulsion systems strongly increases the efficiency of medium-chain surfactants to solubilize water and oil. Although being predestined to serve as a milestone in microemulsion research, the effect has only scarcely found its way into applications. In this work, we propose new types of efficiency boosters, namely, poly(ethylene oxide)-poly(alkyl glycidyl ether carbonate)s (PEO-*b*-PAlkGE) and their "carbonated" poly(ethylene oxide)-poly(carbonate alkyl glycidyl ether) analogs. Their synthesis via anionic ring-opening polymerization (AROP) from commercially available long-chain alkyl glycidyl ethers (AlkGE) and monomethoxypoly(ethylene glycol)s as macroinitiators can be performed at low cost and on a large scale. We demonstrate that these new PEO-*b*-PAlkGE copolymers with dodecyl and hexadecyl side chains in the nonpolar block strongly increase the efficiency of both pure and technical-grade *n*-alkyl polyglycol ether surfactants to form microemulsions containing pure *n*-alkanes or even technical-grade waxes, a result that could be of interest for industrial applications where reduced surfactant needs would have significant economic and ecological implications. For *n*-decane microemulsions, the boosting effect of PEO-*b*-PAlkGE and PEP-*b*-PEO polymers can be scaled on top of each other, when plotting the efficiency semilogarithmically versus the polymeric coverage of the amphiphilic film. Interestingly, a somewhat different scaling behavior was observed for *n*-octacosane microemulsions at elevated temperatures, suggesting that the polymers show less self-avoidance and rather behave as almost ideal chains. A similar trend was found for the increase of the bending rigidity κ upon polymeric coverage of the amphiphilic film, which was obtained from the analysis of small-angle neutron scattering (SANS) measurements.

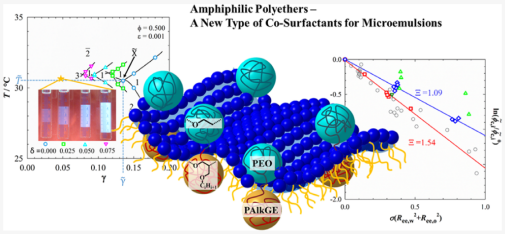

INTRODUCTION

Microemulsions. Microemulsions consist of at least three different components, with two of them being immiscible under standard conditions. The miscibility of these two immiscible components, namely, a hydrophilic/polar component (e.g., water) (A) and a hydrophobic/nonpolar component (e.g., oil) (B), can be facilitated by an amphiphilic component (e.g., surfactant) (C). Such mixtures are referred to as microemulsions[1] if they are thermodynamically stable, macroscopically homogeneous albeit nanostructured mixtures containing an amphiphilic film. Microemulsions are characterized by their multifarious nanostructures[2] as well as their enormous interface, and they excel at reducing the oil/water interfacial tension to low and ultralow values.[3−6] More than half a century of extensive research has shown that these properties can easily be tuned and adjusted by parameters like temperature, pressure, or the addition of components such as cosurfactants and salts.[7] The properties themselves and also their adjustability enable numerous technical applications of microemulsions, for instance, in washing processes,[8,9] enhanced oil recovery,[10,11] or in cosmetic and pharmaceutical applications.[12−14] However, compared to emulsions, which are only kinetically stable, high amounts of surfactant required to formulate microemulsions pose significant economic and ecological drawbacks. The latter may arise from surfactants' potential hazards for humans (e.g., damaged skin from surfactants in cosmetics) and the ecosystem in general (e.g., non-biodegradable surfactants).

Efficiency Boosting Effect. A milestone in microemulsion research was the observation that the addition of small amounts of amphiphilic diblock copolymers can lead to a strong reduction of the amount of surfactant needed to formulate microemulsions.[15,16] By means of ternary nonionic

Received: May 19, 2020
Revised: July 20, 2020
Published: July 21, 2020

https://dx.doi.org/10.1021/acs.langmuir.0c01491
Langmuir 2020, 36, 9849−9866

microemulsions of the type H_2O−*n*-decane−tetraethylene glycol monodecyl ether ($C_{10}E_4$),[16,17] it was shown that amphiphilic diblock copolymers of the type poly(ethylene propylene)-*co*-poly(ethylene oxide) (PEP-*b*-PEO)[18,19] act as a kind of macrosurfactant forced into the amphiphilic film since water and *n*-decane are good solvents for the PEO and PEP block, respectively. In systematic phase behavior and microstructure studies, it was found that in addition to the efficiency boosting, the addition of PEP-*b*-PEO polymers also results in water and oil domains with larger length scales as well as a further decrease of the already ultralow oil/water interfacial tension.[15] Additionally, the formation of liquid crystalline phases, e.g., the lamellar phase (L_α), which are a prominent feature of microemulsion systems stabilized by long-chain surfactants (alkyl chain length longer than C_{10}), can partly be controlled by adjusting the alkyl chain length of the surfactants as well as the concentration and block size of the amphiphilic copolymers.[16,17,20] Endo et al. proved by elaborate neutron scattering experiments employing a high-precision two-dimensional contrast variation technique that the PEP-*b*-PEO polymers are indeed anchored in the amphiphilic film, with the PEP and PEO blocks forming mushroom-like structures in the oil and water domains, respectively.[21] Gompper et al.[22] explained the enormous efficiency boosting effect in terms of the bending elastic energy[23] of fluctuating polymer-decorated surfactant membranes by taking into account the effect of the membrane-anchored copolymers onto the spontaneous curvature and the bending moduli κ and $\bar{\kappa}$.[24,25] Based on these theoretical considerations, it was found that the efficiency boosting effect scales with the number density of block copolymers anchored into the membrane as well as the end-to-end distances of hydrophilic and hydrophobic blocks.[21,26] Over the last two decades, several research groups have investigated the role of the copolymers' molecular structure on their efficiency boosting effect in mostly balanced bicontinuously structured microemulsions,[21,26−31] whereas Foster et al. utilized the boosting effect of PEP-*b*-PEO diblock copolymers to enable the formation of giant water-in-oil microemulsion droplets.[32] Johannson et al. studied the effect of poly(ethylene oxide)-*b*-poly(dodecene oxide), poly(ethylene oxide)-*b*-poly(butylene oxide), and the Ketjenlube comb-polymer on quaternary microemulsion systems of the type D_2O−*n*-octane−*n*-octyl-β-D-glucoside−1-octanol.[27] Frank et al.[33] and Brodeck et al. used different types of sticker polymers (hydrophilic alcohol ethoxylates) and Y-shaped polymers (PEO-*b*-PEP-*b*-PEO) in ternary microemulsion systems of the type D_2O−*n*-decane−$C_{10}E_4$,[34] while Klemmer et al. used poly(ethylene oxide)-*b*-poly(butylene oxide) (PEO-*b*-PBO) to increase the efficiency of pseudo-ternary H_2O/NaCl−*n*-decane−$C_{10}E_4$ microemulsions.[30] Recently, some of us have studied the efficiency boosting effect of a new type of poly(ethylene oxide)-*b*-poly(butylene carbonate) block copolymers (PEO-*b*-PBC) in microemulsion systems containing technically relevant polar oils.[31] Furthermore, the impact of triblock (ABA or ABC) copolymers such as poloxamers (PEO-*b*-PPO-*b*-PEO),[30,35] amphiphilic random copolymers,[36] and charged diblock copolymers consisting of poly(ethylene-*co*-propylene) and sodium poly(styrene sulfonate) (PEP-*b*-PSS)[37] as efficiency boosters has been investigated. While all these amphiphilic copolymers were found to increase the efficiency of surfactants to solubilize water and oil into each other, the boosting strength strongly depends on their amphiphilicity as well as the structure and size of their hydrophilic and hydrophobic blocks. On the contrary, a so-called "anti-boosting" effect was found for non-amphiphilic homopolymers[28] and for some special kinds of poloxamers of the type PEO-*b*-PPO-*b*-PEO, where the PPO unit is significantly larger than the PEO units.[38] Although the boosting effect of amphiphilic diblock copolymers seems to be predestined to eradicate the disadvantage of the need for high surfactant amounts to stabilize microemulsions, it has only scarcely found its way into applications.[39] Some prominent reasons for this are a difficult and expensive large-scale polymer synthesis[17] as well as the weakening of the boosting effect with increasing dispersity of the polymer blocks, especially in the case of remaining homopolymers.

Poly(ethylene oxide)-*b*-Poly(alkyl glycidyl ether)s (PEO-*b*-PAlkGEs): A Promising New Type of Efficiency Boosters. Long-chain alkyl glycidyl ethers (AlkGEs) are highly hydrophobic epoxide monomers that can be polymerized by the conventional anionic ring opening polymerization (AROP) approach adding crown ethers,[40] via catalysts[41,42] or adding phosphazene bases.[43] Using the established AROP approach, the molar masses of the polyethers can be adjusted by the initiator to monomer ratio. Due to the absence of catalysts or other toxic components, a one-step purification protocol yields pure polyethers on a multigram scale. In this work, we report the synthesis of well-defined amphiphilic diblock polyethers with narrow dispersities from $Đ$ = 1.03 to 1.09. Using different macroinitiators and long-chain AlkGE monomers, different block copolymers have been synthesized under systematic variation of the hydrophilic/lipophilic balance (HLB). We emphasize that due to the commercial availability of the macroinitiator (Me-PEO, also called mPEG) and the availability of epoxy monomers in pure and technical grades, the synthesis of these diblock copolymers can be performed at low cost and on a multigram scale via the synthesis route shown in Scheme 1.

Scheme 1. Synthesis of AB Diblock Copolymers Using Me-PEO Macroinitiators and the Long-Chain Alkyl Glycidyl Ethers C_{12}GE, C_{16}GE, and Technical Grade $C_{12/14}$GE

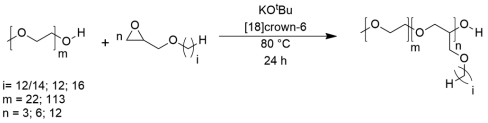

Having this new type of easy-to-synthesize poly(ethylene oxide)-*b*-poly(alkyl glycidyl ether) (PEO-*b*-PAlkGE) polymer with narrow dispersities at hand (cf. Table 1), the objective of this work was to investigate their influence on both model type and technically relevant microemulsions. Thus, in a first step, we studied the effect of Me-P(EO)$_{113}$-*b*-P(C_{12}GE)$_7$ on the phase behavior and microstructure of the model microemulsion system H_2O/NaCl−*n*-decane−$C_{10}E_4$. For technical applications, such as enhanced oil recovery, efficient solubilization of long-chain *n*-alkanes is of interest, which is why we investigated the extent of boosting of PEO-*b*-PAlkGE polymers in H_2O/NaCl−*n*-octacosane−$C_{16}E_6$ microemulsions[44] in the next step. By means of this microemulsion system, the effect of varying both the alkyl chain length and the number of repeating units of the alkyl glycidyl ether block was studied. With respect to their technical application, the

https://dx.doi.org/10.1021/acs.langmuir.0c01491
Langmuir 2020, 36, 9849−9866

influence of technical-grade "carbonated" poly(ethylene oxide)-poly(alkyl glycidyl ether carbonate) copolymers was investigated in the *n*-octacosane microemulsion and in the technical-grade system consisting of H_2O/NaCl−Sasolwax 5805−Genapol O 050/O 080. In all microemulsion systems studied, the size of both the PEO and the PAlkGE block was chosen to be considerably smaller than the diameter of the water and oil domains to suppress the formation of liquid crystalline phases. With the analysis of the recorded phase diagrams and small-angle neutron scattering (SANS) curves, we finally not only quantified the effect of the polymers on the bending rigidity κ but also used the scaling relation suggested by Gompper et al.[22,26,29] in order to compare the boosting of the PEO-*b*-PAlkGE polymers with the extensively investigated PEP-*b*-PEO polymers.

EXPERIMENTAL PART

Reagents. Solvents, reagents, and surfactants were purchased from Acros Organics, Bachem, Clariant, Deutero, Eurisotop, Fluka, Sasol Germany GmbH, Sigma-Aldrich and TCI and used as received, unless otherwise stated.

For the synthesis of the diblock polyethers, the two different alkyl glycidyl ethers C_{12}GE and C_{16}GE were synthesized to ensure high purity of the epoxide monomers. Additionally, the synthesized C_{12}GE was copolymerized with CO_2 to generate hydrophobic polycarbonate blocks. Since the living anionic ring-opening polymerization (AROP) is limited to epoxide monomers with high purity, additional copolymerization reactions of CO_2 with a commercially available alkyl glycidyl ether mixture ($C_{12/14}$GE, technical-grade) were carried out. All epoxide monomers were dissolved in benzene and dried overnight under reduced pressure before polymerization to remove water residues. The dispersities of the purchased macroinitiator Me-P(EO)$_{113}$ (5 kg mol^{-1}, $Đ$ = 1.04) were determined by size-exclusion chromatography (SEC) (eluent: dimethylformamide (= DMF), calibration: PEO, M_n = 238−44,000 g mol^{-1}). The deuterated solvent (chloroform-*d*) used for nuclear magnetic resonance (NMR) measurements was received from Deutero GmbH.

For the phase behavior studies, double-distilled H_2O, *n*-decane ($C_{10}H_{22}$, Sigma-Aldrich, purity of >99%), and *n*-octacosane ($C_{28}H_{58}$, Acros Organics, purity of 99%) were used. Sasolwax 5805 (Sasol Germany GmbH) was used as a technical-grade mixture of linear (*n*) and branched (iso) alkanes ranging from C_{19} to C_{46} with an average carbon number of 30.5 (see gas chromatography (GC) spectrum in ref 44). As pure surfactants, tetraethylene glycol monodecyl ether (= $C_{10}E_4$, $C_{18}H_{38}O_5$, Bachem AG, purity of >99%) and hexaethylene glycol monohexadecyl ether (= $C_{16}E_6$, $C_{28}H_{58}O_7$, Fluka, purity of >98%) were used. Technical-grade nonionic surfactants of the Genapol O series (Clariant (Frankfurt, Germany)), which consist of ethoxylated oleyl alcohols with a broad distribution of their ethoxylation degrees, were utilized. For Genapol O 050 and Genapol O 080, the mean ethoxylation degrees are 5 and 8, respectively. For the SANS measurements, H_2O was replaced by D_2O (Eurisotop, purity of 99% D) to adjust bulk contrast.

Synthesis. The synthesis and purification of the commercial monomers as well as the pure C_{12}GE and C_{16}GE epoxide monomers were carried out as reported before. Additionally, the synthesis of the homopolymers was performed as reported in ref 40. The synthesis of the novel diblock copolymers employed in the current study is described in the following.

Diblock Copolymer Synthesis. In the following, the general reaction procedure for the synthesis of the PEO-*b*-AlkGEs is described by means of Me-P(EO)$_{113}$-*b*-P(C_{12}GE)$_6$. In a 50 mL Schlenk flask, 1 g (0.2 mmol, 1 equiv) of Me-P(EO)$_{113}$ (M_n = 5.000 g mol^{-1}), 17.9 mg (0.16 mmol, 0.8 equiv) of potassium *tert*-butoxide (KO^{t}Bu), and 84.6 mg (0.3 mmol, 1.6 equiv) of 18-crown-6 were dissolved in 5 mL of a benzene/methanol mixture (4.5 mL benzene / 0.5 mL methanol). Subsequently, the mixture was dried overnight under reduced pressure at 60 °C to yield the partly deprotonated initiator. The reaction mixture was heated to 80 °C and 290 mg (1.2 mmol, 6 equiv) of the dried C_{12}GE were added with a syringe under argon (1 atm). The reaction mixture was then stirred for 24 h at 80 °C. After completion of the reaction, 1 mL of methanol and 3 mL of dichloromethane (DCM) were added at room temperature. The product was precipitated in diethyl ether at room room temperature, centrifuged, and the precipitated product was dried under reduced pressure at 40 °C. Subsequently, the polymer was dialyzed in methanol to fully remove salts and crown ether residues. ^{1}H NMR (300 MHz, chloroform-*d*) δ (ppm) = 3.93−3.39 (m, 588 H, backbone), 3.37 (s, 3 H, CH_3−O), 1.60−1.46 (m, 12 H, O CH_2 CH_2), 1.37−1.18 (m, 108 H, O CH_2 CH_2 $(CH_2)_9$ CH_3), 0.86 (t, 18 H, J = 7.0 Hz, CH_3).

The "carbonate" polymers used in this work contain a CO_2 group within the hydrophobic alkyl glycidyl ether block of the polymer. The general reaction procedure is described for Me-P(EO)$_{113}$-P($CO_2C_{12/14}$GE)$_7$. An autoclave equipped with a stirring bar was filled with 1 g (0.2 mmol, 1 equiv) of Me-P(EO)$_{113}$ (M_n = 5000 g mol^{-1}), 1.95 g (8 mmol, 20 equiv) of the dried $C_{12/14}$GE (technical-grade), 15.3 mg (0.024 mmol, 0.6 equiv) of Co(Salen)Cl, and 13.7 mg (0.024 mmol, 0.6 equiv) of [PPN]Cl under an argon atmosphere. The reaction mixture was stirred under a carbon dioxide pressure of 50 bar at room temperature for 20 h. The crude product was dissolved in DCM, and the catalyst was deactivated with 0.5 mL of a solution of 5 vol % HCl in methanol. A neutral aluminum oxide column and 400 mL of tetrahydrofuran (THF) as the eluent were used for further purification of the product to eliminate the catalyst. The solvent was evaporated under reduced pressure, and the product was dissolved again and precipitated in ice-cold diethyl ether. The colorless solid was then dried under reduced pressure for 24 h. ^{1}H NMR (300 MHz, chloroform-*d*) δ (ppm) = 5.04 (s, 7 H, carbonyl backbone), 4.43−4.21 (m, 14 H, carbonyl backbone), 3.96−3.75 (m, 14 H, O CH_2 CH), 3.75−3.60 (m, 538 H, polyether backbone and −O−CH_2−CH_2−), 3.41 (s, 3 H, CH_3−O), 1.65−1.48 (m, 14 H, O CH_2 CH_2), 1.39−1.15 (m, 246 H, O CH_2 CH_2 $(CH_2)_9$ CH_3), 0.92−0.87 (m, 21 H, CH_3). The synthesis protocol for the diblock copolymers with the general structure Me-P(EO)$_{113}$-P(CO_2C_{12}GE)$_n$ that contain pure C_{12}GE in combination with carbon dioxide follows the same procedure as the use of the $C_{12/14}$GE mixture (technical-grade) but with decreased amounts of the catalyst system (0.06 equiv).

While the poly(ethylene oxide)-poly(alkyl glycidyl ether)s (PEO-*b*-PAlkGE) were synthesized with a high yield between 70 and 98%, the yield of the "carbonated" poly(ethylene oxide)-poly(carbonate alkyl glycidyl ether) analogs was moderate (30 to 60%, Table S1).

Phase Behavior Studies. The procedure for the investigation of the phase behavior of nonionic microemulsion systems can be found elsewhere.[44] Here, we will only focus on the most important procedures for the water/NaCl (A)−oil (B)−nonionic surfactant (C)/amphiphilic diblock copolymer (D) systems studied in this work. For sample preparation, all components are weighed in test tubes with an accuracy of Δm = ± 0.001 g, starting with the amphiphilic diblock copolymer (smallest amount) and the surfactant(s) followed by the respective oil, which are known to be good solvents for nonionic surfactants. To avoid the formation of liquid crystals, water/NaCl ("brine", with ε = 0.001) was added in the last step. Before the test tubes were sealed with a polyethylene stopper, a stirring bar was added to the sample. After homogenization at low and high temperatures, the samples' phase behavior was studied as a function of temperature with the help of a temperature-controlled water bath (Thermo-Haake DC30, with a temperature control up to ΔT = 0.02 K). For this, the samples were stirred until the temperature equilibrium was reached. The stirring was then stopped, and the numbers and types of coexisting phases were determined by visual inspection of both transmitted and scattered light using crossed polarizers to recognize anisotropic phases. After the phase transition temperatures were determined with a precision of ΔT = ±0.05 K for a given composition, the sample was diluted with brine and oil to repeat the process for lower values of γ.

In order to characterize the phase behavior of a microemulsion system in general and the efficiency boosting effect of amphiphilic

https://dx.doi.org/10.1021/acs.langmuir.0c01491
Langmuir 2020, 36, 9849−9866

block copolymers in particular, it has been proven useful to perform the so-called $T(\gamma)$ sections through the Gibbs phase prism.[44−46] To be more precise, the phase behavior was studied as a function of temperature and mass fraction

$$\gamma = \frac{m_C + m_D}{m_A + m_B + m_C + m_D} \quad (1)$$

of amphiphiles, which comprises both surfactant(s) (C) and block copolymer (D). The mass fraction α of oil (B) in the brine (A)/oil (B) mixture was adjusted to a value that corresponds to a volume fraction

$$\phi = \frac{V_B}{V_A + V_B} = 0.500 \quad (2)$$

using the respective components' densities. Note that for these symmetric systems, using equal volumes of oil and water results in a zero mean curvature of the amphiphilic film at the phase inversion temperature (PIT or $\tilde{T}$).[2] Traces of sodium chloride (= NaCl) were added to water (mass fraction ε = 0.001) to screen possible electrostatic interactions of ionic impurities.

The amount of polymer (D) within the overall amphiphilic mixture is defined as follows

$$\delta = \frac{m_D}{m_C + m_D} \quad (3)$$

For the analysis of the recorded phase diagrams and scattering curves with respect to the scaling of the efficiency boosting effect,[22,25] the respective volume fractions $\phi_{C,i}$ of the surfactant in the amphiphilic film is needed. $\phi_{C,i}$ can be calculated from the volume fraction

$$\phi_C = \frac{V_C}{V_A + V_B + V_C + V_D} = \frac{V_C}{V_{total}} \quad (4)$$

of surfactant in the overall mixture taking into account the monomeric solubility

$$\phi_{C,monb} = \frac{V_{C,monb}}{V_{C,monb} + V_B} \quad (5)$$

of the nonionic surfactants in the oil according to

$$\phi_{C,i} = \phi_C - \frac{\phi_{C,monb}(1 - \phi_C)\phi}{V_{tot}} \quad (6)$$

Here, $V_{C,monb}$ is the surfactant volume monomerically solubilized in the oil volume V_B. For the studied systems, monomeric solubilities of $\phi_{C10E4,monb}$ = 0.016 in *n*-decane[47] and $\phi_{C16E6,monb}$ = 0.014 in *n*-octacosane were used for the respective phase inversion temperatures (PIT). Both values were determined from measurements of the microemulsion (middle) phase volume as a function of γ at the PIT. Note that the monomeric solubility of $C_{10}E_4$ and $C_{16}E_6$ as well as of technical-grade Genapol O 050 and Genapol O 080 in water (cmc) can be neglected.[47] For the sake of completeness, the volume fraction of copolymer

$$\phi_D = \frac{V_D}{V_A + V_B + V_C + V_D} \quad (7)$$

can be estimated assuming a polymer density of 1 g cm^{-3}.

Instrumentation. ^{1}H NMR (300 MHz) spectra were recorded on a Bruker Avance III HD (300 MHz, 5 mm BBFO-head with *z* gradient and ATM, BACS 60 sample changer) and referenced internally to the proton signal of the deuterated solvent (here: chloroform-*d*).

Size exclusion chromatography (SEC) was performed in DMF with 1 g/L lithium bromide as the eluent and MZ-Analysetechnik HEMA 300/100/40 columns at 50 °C, using an RI detector at a flow rate of 1 mL/min. Calibration was carried out using poly(ethylene glycol) (PEO) standards provided by PSS. Additional SEC measurements were performed in THF using an MZ-Gel SD plus eS/e3/100 column at 30 °C. Calibration was carried out using polystyrene standards provided by PSS.

Differential scanning calorimetry (DSC) measurements were carried out under a nitrogen atmosphere using a PerkinElmer DSC 8500 in the temperature range of −50 to 70 °C, with heating rates of 20 K min^{-1} and 10 K min^{-1} for the first and second heating cycle, respectively. A temperature plateau at 70 °C for 1 min was used after the first heating followed by a cooling run with a rate of 10 K min^{-1}.

Small-angle neutron scattering (SANS) measurements were performed to study the influence of the new PEO-*b*-PAlkGE copolymers on the microstructure of the respective microemulsions and to determine the end-to-end distances of some of the homopolymers in the respective solvents. All scattering curves were recorded by adjusting the so-called bulk contrast. Therefore, H_2O was replaced by D_2O while keeping the sample composition constant with respect to their volume ratios. Note that for D_2O, the phase boundaries are about 2 K lower than for H_2O.[48] For the determination of the end-to-end distances of the PAlkGE homopolymers, deuterated *n*-alkanes were used.

All scattering experiments on microemulsion systems were performed using the D11 spectrometer of the Institut Laue-Langevin (ILL) in Grenoble (France), where a neutron wavelength of λ = 5.5 Å with a wavelength spread of $\Delta\lambda/\lambda$ = 9% (fwhm, specified by the ILL) was adjusted. Three different detector/collimation distances, namely, 39 m/40.5 m, 8 m/20.5 m, and 1.5 m/8 m, were used to obtain a scattering vector

$$q = \frac{4\pi}{\lambda} \cdot \sin\left(\frac{\theta}{2}\right) \quad (8)$$

ranging from 0.0016 Å^{-1} to 0.4695 Å^{-1}. The SANS experiments on homopolymers in their respective solvents were performed at the instrument NG7 30 m SANS at the National Institute of Standards and Technology (NIST) in Gaithersburg, Maryland (USA) and the KWS-1 instrument operated by the Jülich Centre for Neutron Science (JCNS) at the Heinz Maier-Leibnitz Zentrum (MLZ), Garching (Germany). While at the NIST, the following settings were used: wavelength λ = 6 Å and detector/collimation distances of 1.33 m/5.42 m, 4 m/8.52 m, and 13.17 m/14.72 m, resulting in a q range from 0.0126 to 0.4450 Å^{-1}; at the MLZ, λ = 5 Å and det./coll. = 1.5 m/8 m, 8 m/8 m, and 20 m/20 m were adjusted, resulting in a q range from 0.0097 to 0.5835 Å^{-1}. The wavelength distribution was $\Delta\lambda/\lambda$ = 13.8% (fwhm) at the NG7 30 m SANS and 10% at KWS-1.

The measured scattering intensities were normalized to the absolute scale using the incoherent scattering of H_2O (optical path length 1 mm) at the ILL, empty beam measurements at the NIST, and Plexiglas (optical path length 1.5 mm) at MLZ. The software packages LAMP (ILL), IGOR Pro (NIST), and QtiSAS (MLZ) were used to perform the reduction of the raw data. To obtain the differential cross section $d\sigma(q)/d\Omega = I(q)$, the data were radially averaged masking defective detector pixels and taking into account dark current and empty cell scattering as well as the detector dead time.

Prior to the SANS measurements, the phase behavior of the microemulsion samples was checked in a water bath at the desired temperatures. All samples were then filled into Hellma quartz QS glass cells with an optical path length of 1 mm. Afterward, the samples were transferred into our home-built 5 position cell holder, which allows temperature adjustments with an accuracy of ±0.1 K. Note that this cell holder can be shaken manually to ensure the mixing and homogeneity of the microemulsion samples. Before and after each measurement, the homogeneity of the samples was checked visually after several minutes of waiting time. Note that at the NIST, where only homopolymer samples were studied, the onsite cell holder was used.

RESULTS AND DISCUSSION

This section starts with the characterization of the Me-P(EO)$_{113}$-*b*-P(C$_i$GE)$_n$, Me-P(EO)$_{113}$-*b*-P(CO$_2$C$_i$GE)$_n$, and Me-P(EO)$_{113}$-P(CO$_2$C$_{12/14}$GE)$_n$ copolymers. Subsequently,

https://dx.doi.org/10.1021/acs.langmuir.0c01491
Langmuir 2020, 36, 9849−9866

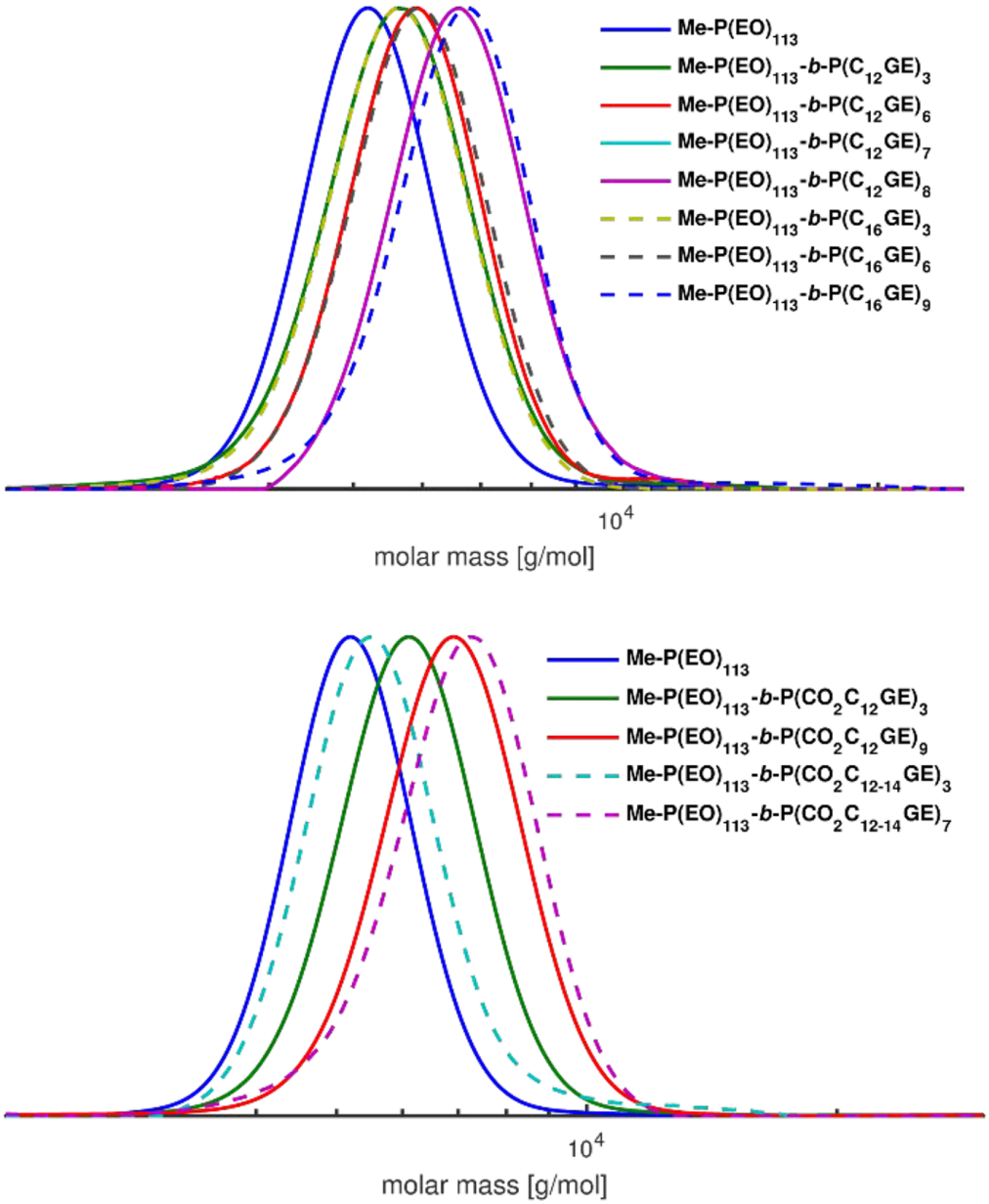

Figure 1. SEC traces of the synthesized diblock copolymers using Me-P(EO)$_{113}$ as a macroinitiator in combination with pure C_{12}GE, pure C_{16}GE, and technical-grade $CO_2C_{12/14}$GE (eluent: DMF, calibration: PEO standards).

the influence of this new type of amphiphilic copolymers on the solubilization efficiency and microstructure of microemulsions containing *n*-decane or *n*-octacosane is demonstrated by varying the copolymer concentration (δ) as well as the alkyl side chain length (i) and the number of repeating units of the alkyl glycidyl ether block (n). To suppress the

https://dx.doi.org/10.1021/acs.langmuir.0c01491
Langmuir 2020, 36, 9849−9866

formation of liquid crystalline phases, the size of the PEO block was set to 113 EO, while the PAlkGE block was chosen to not be larger than $i = 16$ and $n = 9$, ensuring that the end-to-end distances of the two blocks are considerably smaller than the diameter of the water and oil domains in the microemulsion (see Table 2 and Table S4).[20,30] To prove that the efficiency boosting effect can be successfully transferred to technical applications, the technical-grade Me-P(EO)$_{113}$-P(CO$_2$C$_{12/14}$GE)$_7$ polymer was used to boost the efficiency of technical-grade Genapol O surfactants to solubilize Sasolwax 5805 in brine. The last part of this section deals with the quantification of the copolymers' effect on the bending rigidity κ as well as the comparison of the boosting strength of this new copolymer type with the extensively investigated PEP-*b*-PEO polymers by applying the scaling relation of Gompper et al.[22,26]

Synthesis and Characterization. The polymerization of hydrophobic long-chain alkyl glycidyl ethers (here: C$_{12}$GE and C$_{16}$GE) with commercially available monofunctional Me-PEO macroinitiators (M_n = 5000 g mol^{-1}) leads to amphiphilic diblock copolymers with tailorable hydrophobic/hydrophilic ratios on a multigram scale. Due to the underlying mechanism of the anionic ring opening polymerization (AROP), the different polymerizations yield diblock polyethers with monomodal and narrow molar mass distributions ranging from $Đ$ = 1.03 to 1.08 (see Figure 1).

The experimentally determined molar masses ($M_{n,exp}$) (Table 1 and Table S1) are in good agreement with the theoretically calculated molar masses ($M_{n,theo}$). However, it should be noted that for Me-P(EO)$_{113}$-*b*-P(C$_{12}$GE)$_8$ and Me-P(EO)$_{113}$-*b*-P(C$_{16}$GE)$_9$, a higher degree of polymerization of n = 12 was targeted. The lower values could be explained by impurities in the epoxide monomers or the reaction mixture (e.g., water), leading to termination of the polymerization reaction or to the formation of additional living chain ends and the formation of homopolymers with increasing amount of monomer. However, narrow molar mass distributions for all synthesized diblock copolymers were obtained, indicating a controlled polymerization.

Differential scanning calorimetry (DSC) measurements of the synthesized amphiphilic diblock copolymers reveal the presence of two different melting temperatures T_m that can be assigned to the melting points of the PAlkGE and the PEO block, respectively. These results are in good agreement with previous investigations of ABA triblock copolymers and similar systems, indicating a phase segregation of the respective blocks driven by crystallization of both PEO and the long alkyl chains (Figures S2 to S11 and Table S1).[40,49−51]

Efficiency Boosting of Me-P(EO)$_{113}$-*b*-P(C$_{12}$GE)$_7$ in H$_2$O/NaCl−*n*-Decane−C$_{10}$E$_4$. It was 20 years ago that Jakobs et al. discovered the efficiency boosting effect by adding small amounts of amphiphilic block copolymers of the type PEP-*b*-PEO to the symmetric (equal volumes of water and *n*-decane; ϕ = 0.500) model microemulsion system H$_2$O−*n*-decane−C$_{10}$E$_4$.[16] By considering these studies as a kind of benchmark, we systematically studied the influence of the new type of poly(ethylene oxide)-*b*-poly(alkyl glycidyl ether) copolymer on the phase behavior and microstructure of the same microemulsion system. Note that we added traces of NaCl to water (mass fraction ε = 0.001) to screen possible electrostatic interactions of ionic impurities. Besides the facile synthesis, the adjustability of the molecular structure of the PEO-*b*-PAlkGE copolymers is an outstanding property. By deliberately varying m, n, and i, the number of repeating units of the two blocks and also the length of the alkyl side chain within the AlkGE block can be adjusted.

Table 1. Synthesized Amphiphilic Diblock Copolymers, Their Experimentally Determined Molar Masses Obtained from ^{1}H NMR,[a] Molar Mass Distribution $Đ$ Obtained from SEC,[b] and Melting Temperatures (T_m) of the Two Polymer Blocks within the Diblock Copolymer[d]

polymer sample	$M_{n,theo}$ (g mol^{-1})	$M_{n,exp}$ (g mol^{-1})[a]	$Đ$[b]	T_m (°C)[c]
Me-P(EO)$_{113}$-*b*-P(C$_{12}$GE)$_3$	5699	5700	1.05	−4; 55
Me-P(EO)$_{113}$-*b*-P(C$_{12}$GE)$_6$	6426	6400	1.08	1; 53
Me-P(EO)$_{113}$-*b*-P(C$_{12}$GE)$_7$	6668	6670	1.06	
Me-P(EO)$_{113}$-*b*-P(C$_{12}$GE)$_8$*	6911	6910	1.06	3; 53
Me-P(EO)$_{113}$-*b*-P(C$_{16}$GE)$_3$	5866	5870	1.04	56
Me-P(EO)$_{113}$-*b*-P(C$_{16}$GE)$_6$	6760	6760	1.06	35; 53
Me-P(EO)$_{113}$-*b*-P(C$_{16}$GE)$_9$*	7654	7650	1.05	38; 52
Me-P(EO)$_{113}$-*b*-P(CO$_2$C$_{12}$GE)$_3$	5831	5830	1.04	−3; 54
Me-P(EO)$_{113}$-*b*-P(CO$_2$C$_{12}$GE)$_9$	7549	7550	1.05	−2; 54
Me-P(EO)$_{113}$-*b*-P(CO$_2$C$_{12/14}$GE)$_3$	5872	5870	1.06	3; 55
Me-P(EO)$_{113}$-*b*-P(CO$_2$C$_{12/14}$GE)$_7$	7072	7070	1.05	−3; 53

[a]Determined by ^{1}H NMR (300 MHz, CDCl$_3$). [b]Determined by SEC (eluent: DMF, calibration: PEO standards). [c]Measured by DSC; the first listed melting temperature (T_m) can be assigned to the alkyl glycidyl ether block and the second T_m can be assigned to the PEO block. [d]Asterisk (*) indicates that more repeating units were targeted.

As a starting point, similar to Jakobs et al. in their 1999 paper,[16] we demonstrate the boosting effect of the new Me-P(EO)$_{113}$-*b*-P(C$_{12}$GE)$_7$ copolymer by preparing four different samples of the symmetric microemulsion H$_2$O/NaCl−*n*-decane−C$_{10}$E$_4$/Me-P(EO)$_{113}$-*b*-P(C$_{12}$GE)$_7$. When using the same overall volume, equal volumes of oil and water (ϕ = 0.500), and a constant surfactant plus copolymer mass fraction γ = 0.050 (yellow star), all samples form three phases at the phase inversion temperature T = 30.7 °C of the system without the polymer. The photos in Figure 2 impressively show that the volume of the microemulsion (middle) phase strongly increases when the mass fraction δ of Me-P(EO)$_{113}$-*b*-P(C$_{12}$GE)$_7$ in the C$_{10}$E$_4$/Me-P(EO)$_{113}$-*b*-P(C$_{12}$GE)$_7$ mixture is increased from δ = 0 to δ = 0.075. Thus, much more water and oil can be solubilized by the same amount of amphiphile. This emphasizes a strong increase of efficiency, which is also reflected by the changing visual appearance of the microemulsion phase from opalescent to whitish. The increasing length scale of the water and oil domains obviously leads to a stronger light scattering. Furthermore, the water and oil excess phases exhibit almost identical volumes, which strongly indicates that the hydrophilic−lipophilic balance seems to be unaffected by the addition of copolymer.

As a next step, the influence of the Me-P(EO)$_{113}$-*b*-P(C$_{12}$GE)$_7$ copolymer on the phase behavior of the H$_2$O/NaCl−*n*-decane−C$_{10}$E$_4$ system was quantitatively studied as a function of temperature and mass fraction of amphiphile (surfactant and copolymer) at a constant ϕ = 0.500 and ε = 0.001. The recorded phase diagrams are shown on the left side of Figure 2. In general, the phase behavior of all systems resembles the well-known phase behavior of nonionic microemulsion systems.[46] A fishtail-shaped one-phase region

https://dx.doi.org/10.1021/acs.langmuir.0c01491
Langmuir 2020, 36, 9849−9866

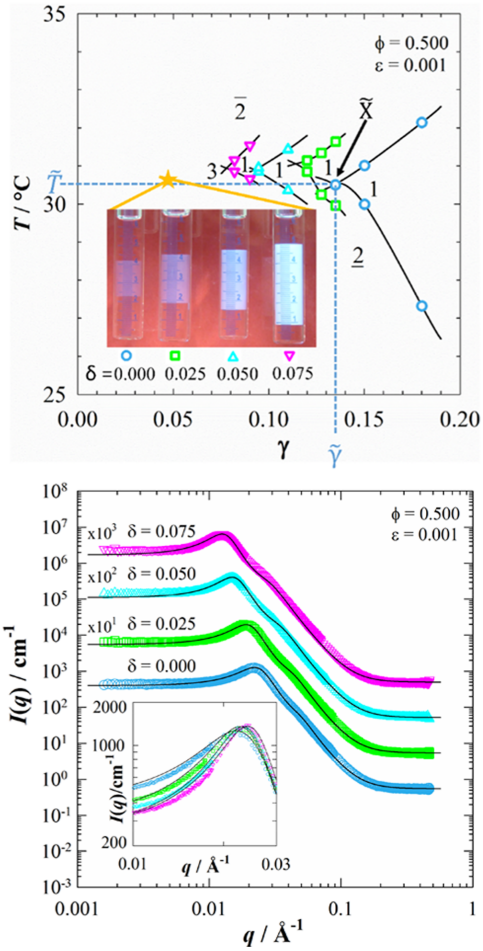

Figure 2. Left: $T(\gamma)$ diagrams of the system H_2O/NaCl–*n*-decane–$C_{10}E_4$/Me-P(EO)$_{113}$-*b*-P(C_{12}GE)$_7$, recorded at δ = 0 (blue circle), 0.025 (green square), 0.050 (light blue triangle up), and 0.075 (fuchsia triangle down) with ϕ = 0.500 and ε = 0.001. 1, $\underline{2}$, $\overline{2}$, and 3 denote the regions where a one-phase microemulsion (1), or coexistences of an o/w microemulsion with an oil excess phase ($\underline{2}$), a w/o microemulsion with water excess phase ($\overline{2}$), and a bicontinuous microemulsion with water and oil excess phases (3) can be observed. The shift of the $\tilde{X}$ points toward lower values of γ upon increasing δ clearly proves the strong efficiency boosting, which is also visible by the growth of the microemulsion phase shown in the photos of samples prepared at T = 30.7 °C and γ = 0.050 (yellow star) with varying δ values. Right: bulk contrast SANS curves of samples recorded along two pathways: Close to the respective $\tilde{X}$ points, the scattering peak shifts to smaller q values and higher intensities with increasing polymer content. Note that the curves are displaced by a factor of 10. Inset: Scattering curves of samples at ϕ_C = 0.144 exhibit an increasing sharpness of the scattering peak with increasing δ. All curves are analyzed using the TS model[53] taking into account double scattering.[54,55]

occurs at intermediate temperatures between two phase boundaries. While at lower temperatures, an oil-in-water microemulsion co-exists with an oil excess phase ($\underline{2}$), a water-in-oil microemulsion co-exists with a oil excess phase ($\overline{2}$) at higher temperatures. With decreasing mass fraction γ of the amphiphile, the phase boundaries converge and eventually coincide in the so-called optimum point $\tilde{X}$, defined by the minimum amount $\tilde{\gamma}$ of the surfactant plus the polymer needed to form a microemulsion at the phase inversion temperature PIT ($\tilde{T}$). At mass fractions below $\tilde{\gamma}$, a three-phase region (3) can be found between the two-phase regions. Note that in this study, we primarily focus on the influence of the new amphiphilic block copolymers on the so-called optimum point $\tilde{X}$. Therefore, mainly the phase boundaries limiting the one phase region at $\gamma \geq \tilde{\gamma}$ were determined.

Starting with the phase diagram of the pseudo-ternary microemulsion system, the $\tilde{X}$ point can be found at $\tilde{\gamma}$ = 0.135 and $\tilde{T}$ = 30.6 °C, which is in an almost quantitative agreement with the literature.[16] Upon replacing only a small fraction of $C_{10}E_4$ with Me-P(EO)$_{113}$-*b*-P(C_{12}GE)$_7$ (δ = 0.025), $\tilde{\gamma}$ decreases to $\tilde{\gamma}$ = 0.114; i.e., the efficiency to formulate a microemulsion increases. At the same time, the PIT increases to $\tilde{T}$ = 31.1 °C because the hydrophilic Me-P(EO)$_{113}$-block is larger than the hydrophobic P(C_{12}GE)$_7$-block.[52] A further increase of δ shifts the minimum amount of $C_{10}E_4$ and Me-P(EO)$_{113}$-*b*-P(C_{12}GE)$_7$ needed to formulate a microemulsion to even lower values. For δ = 0.075, a value of $\tilde{\gamma}$ = 0.077 is found. Thus, both the phase diagrams and the swelling of the volume of the microemulsion phase prove the strong efficiency boosting of the PEO-*b*-PAlkGE copolymers. Whether the boosting effect of the new type of copolymer is comparable to the extensively investigated PEP-*b*-PEO polymers will be discussed at the end of this section by applying the scaling relation of Gompper et al.[22,26] Note that the $\tilde{X}$ points are compiled in Table S2 of the Supporting Information in the form of $\tilde{\gamma}$ and $\tilde{T}$ values.

Subsequently, the influence of the Me-P(EO)$_{113}$-*b*-P(C_{12}GE)$_7$ copolymer on the microstructure of the D_2O/NaCl–*n*-decane–$C_{10}E_4$ systems was studied by two sets of systematic SANS experiments. The scattering curves recorded in bulk contrast are shown on the right side of Figure 2. All curves resemble the typical shape found for bicontinuous microemulsions:[53] Starting from low q values, where the curves show a plateau, a scattering peak is found at middle $q = q_{max}$ after which the intensity decreases proportionally to q^{-4} before the incoherent background is reached. However, due to the strong scattering and the neutron path length of 1 mm, contributions of multiple scattering can be observed especially around $q \approx 2q_{max}$.

In the main part of Figure 2 (right), the scattering curves of the first set of experiments, which were performed to determine the length scale and the ordering of the efficiency-boosted microemulsions, are shown. These samples were prepared near the $\tilde{X}$ point of the respective system, i.e., in the one-phase region at $\phi_{C+D} \approx \tilde{\phi}_{C+D} + 0.02$. Here, the surfactant/copolymer volume fraction ϕ_{C+D} is used instead of the mass fraction γ (taking into account the higher density of D_2O) in order to adjust the same volume composition of phase behavior and SANS samples. Considering the trend of the scattering curves with increasing Me-P(EO)$_{113}$-*b*-P(C_{12}GE)$_7$ content, a strong shift of the scattering peak to lower q and higher I can be observed when δ is increased from δ = 0 to 0.075. This shift is a clear indication of increasing water and oil

https://dx.doi.org/10.1021/acs.langmuir.0c01491
Langmuir 2020, 36, 9849−9866

domain sizes in the bicontinuous microstructure, which is in agreement with the shift of the $\tilde{X}$ point to lower surfactant mass fractions $\tilde{\gamma}$ induced by the efficiency boosting of Me-P(EO)$_{113}$-*b*-P(C$_{12}$GE)$_7$ copolymers. Furthermore, the sharpness of the scattering peak increases slightly, indicating that the copolymer induces a better structural ordering of the bicontinuous microemulsion.

The scattering curves are analyzed using the model by Teubner and Strey[53] taking into account double scattering contributions[54,55] according to

$$I(q) = \frac{I_{0,1}}{\left(1 - \frac{I_{0,1}}{I_{\max,1}}\right)\left(\frac{q^2}{q_{\max}^2} - 1\right)^2 + \frac{I_{0,1}}{I_{\max,1}}} + \frac{I_{0,2}}{\left(1 - \frac{I_{0,2}}{I_{\max,2}}\right)\left(\frac{q^2}{4q_{\max}^2} - 1\right)^2 + \frac{I_{0,2}}{I_{\max,2}}} + I_{\text{incoh}} \quad (9)$$

where $I_{0,1} = I_0 \cdot (1 - f \cdot x)$ and $I_{0,2} = I_0 \cdot f \cdot x$ are the single and double scattering contributions of the scattering intensity at $q = 0$, respectively. f specifies the fraction of double scattering and x is the additional broadening due to higher order multiple scattering contributions and the wavelength spread of the neutrons. Similarly, $I_{\max,1} = I_{\max}(1 - f)$ and $I_{\max,2} = I_{\max} \cdot f$ are the single and double scattering contributions of the scattering at $q = q_{\max}$ and $q = 2q_{\max}$, respectively.

Relating $I_{0,1}$, $I_{\max,1}$, and $q_{\max}$ to the coefficients of the order parameter expansion via $a_2 = 1/I_{0,1}$, $c_2 = (1/I_{0,1} - 1/I_{\max,1})/q_{\max}^4$, and $c_1 = -2c_2 q_{\max}^2$, the periodicity d_{TS}, the correlation length ξ_{TS}, and the amphiphilicity factor f_a can be determined

$$\xi_{TS} = \left[\frac{1}{2}\left(\frac{a_2}{c_2}\right)^{1/2} + \frac{1}{4}\frac{c_1}{c_2}\right]^{-1/2} \quad (10)$$

$$d_{TS} = 2\pi\left[\frac{1}{2}\left(\frac{a_2}{c_2}\right)^{1/2} - \frac{1}{4}\frac{c_1}{c_2}\right]^{-1/2} \quad (11)$$

and

$$f_a = \frac{a_1}{\sqrt{4a_2c_2}} \quad (12)$$

f_a is an important parameter to quantify the amphiphilic strength of an amphiphile and the structural order of a microemulsion system. While positive values are found for uncorrelated interfaces in disordered systems, negative f_a values are observed for systems with correlated interfaces.[56−58] By crossing the Lifshitz line, located at $f_a = 0$, toward negative f_a values, a peak develops in the scattering curve.[56,57] Typically, for microemulsions the f_a value ranges between −0.6 and −0.9. The more negative the amphiphilicity factor, the better the structuring of the microemulsion. Note that a perfectly structured lamellar phase exhibits an amphiphilicity factor of $f_a = -1$.[56−58]

Additionally, the parameter d_{TS} and ξ_{TS} can be used to determine the bending rigidity

$$\frac{\kappa_{SANS}}{k_BT} = \frac{10\sqrt{3}\pi}{64}\frac{\xi_{TS}}{d_{TS}} \quad (13)$$

using the model of random interfaces derived by Safran et al.[59] with k_B being the Boltzmann constant. Note that recent simulations on triangulated surfaces[60] as well as elaborate experimental studies, including phase behavior, SANS, and neutron spin echo (NSE) experiments,[61] indicate that κ_{SANS} determined this way (eq 13) is rather a mixture of the bending rigidity κ and the saddle splay modulus $\bar{\kappa}$. Nevertheless, in this study we used the model of random interfaces to analyze the SANS curves because of the following reasons: First, in order to separate the contributions of κ and $\bar{\kappa}$ to κ_{SANS}, one of two parameters has to be determined using independent methods. NSE, which is a reliable but elaborate method to determine the bare bending rigidity κ_0, was not available. Second, the bare saddle splay modulus $\bar{\kappa}_0$ can in principle be determined from the location of the so-called optimum point $\tilde{X}$, i.e., the instability of the bicontinuously structured micoemulsion.[62−64] However, the exact value of $\bar{\kappa}$ at $\tilde{X}$ is not exactly defined. While usually $\bar{\kappa}_0$ is set to 0 at the $\tilde{X}$ point,[62−64] Holderer et al. had to use $\bar{\kappa}_0 = 0.28k_BT$[61] in order to achieve agreement with both the predicted relative contributions of κ and $\bar{\kappa}$ (0.15 and −0.85, respectively[60]) as well as the values of the bare bending rigidity κ_0 determined by NSE.

The fit of the experimental scattering data by eq 9 is shown as black solid lines in Figure 2, right. It not only describes the peak but the entire scattering curve almost quantitatively. The sample composition, measuring temperature, d_{TS}, ξ_{TS}, f_a, and κ_{SANS} (according to eq 13) are summarized in Table 2. In accordance with the shift of the scattering peak to lower q, the periodicity d_{TS} increases by almost a factor two from 272 to 484 Å when δ is increased from $\delta = 0$ to 0.075. Simultaneously, the amphiphilicity factor f_a becomes slightly more negative and the bending rigidity κ_{SANS} increases somewhat. Both trends indicate a slightly better structural ordering, which is most probably caused by an increasing relative distance of the SANS samples from the $\tilde{X}$ point.

In the second set of SANS experiments, the influence of the Me-P(EO)$_{113}$-*b*-P(C$_{12}$GE)$_7$ copolymer on the microstructure was studied at constant surfactant volume fraction $\phi_C = \tilde{\phi}_{C,0} + 0.02 = 0.144$. Note that $\tilde{\phi}_{C,0}$ defines the surfactant volume fraction at the $\tilde{X}$ point of the polymer-free system ($\delta = 0$). The inset in Figure 2 (right) shows the respective scattering curves with focus on the region around the scattering peak. As can be seen, the peak, which stays almost at the same q_{max}, becomes significantly sharper when δ is increased from $\delta = 0$ to 0.075, indicating a considerably better ordering of the bicontinuous structure. Indeed, the analysis of the scattering data by the extended TS model (eq. 9) provides an almost constant periodicity (as expected for $\phi_C = 0.144$ = constant) but an increasingly negative f_a value, decreasing from $f_a = -0.83$ to $f_a = -0.91$, proving the presence of very well-structured bicontinuous microemulsions.[57,58] Simultaneously, the addition of Me-P(EO)$_{113}$-*b*-P(C$_{12}$GE)$_7$ leads to a considerable increase of the amphiphilic film's bending rigidity κ_{SANS}, which increases from $0.44k_BT$ to $0.61k_BT$.

Efficiency Boosting of Me-P(EO)$_{113}$-*b*-P(C$_{12}$GE)$_7$ in H$_2$O/NaCl−*n*-Octacosane−C$_{16}$E$_6$. For some technical applications, as for instance enhanced oil recovery (EOR) but also cleaning and washing processes, the efficient solubilization of long-chain oils and waxes in microemulsions is of great interest because it is closely related to ultralow values of the oil/water interfacial tension and excellent wetting properties.[2,3,65] Very recently, it was shown that symmetric microemulsions containing pure long-chain oils (e.g., *n*-octacosane) or even technical-grade waxes (e.g., Sasolwax 5805) can be formulated using on the order of 15 wt % pure and technical-grade non-

https://dx.doi.org/10.1021/acs.langmuir.0c01491
Langmuir 2020, 36, 9849−9866

Table 2. Composition and Measuring Temperature of SANS Samples of Different Microemulsions Boosted by the New Me-P(EO)$_{113}$-*b*-P(C$_{12}$GE)$_7$ Copolymer Together with the Obtained Fit Parameters[a]

T_{SANS} (°C)	δ	ϕ_C	ϕ_D	ξ_{TS}/Å	d_{TS}/Å	f_a	κ_{SANS} (k_BT)
D$_2$O/NaCl–*n*-decane (C$_{10}$H$_{22}$)–C$_{10}$E$_4$/Me-P(EO)$_{113}$-*b*-P(C$_{12}$GE)$_7$							
29.0	0	0.144	0	142	272	−0.83	0.44
29.0	0.025	0.125	0.003	178	317	−0.85	0.48
29.0	0.050	0.098	0.005	235	406	−0.86	0.49
29.0	0.075	0.083	0.007	285	484	−0.86	0.50
29.0	0.025	0.143	0.004	174	270	−0.89	0.55
29.0	0.050	0.142	0.007	189	264	−0.91	0.61
29.0	0.075	0.142	0.011	183	255	−0.91	0.61
D$_2$O/NaCl–*n*-octacosane (C$_{28}$H$_{58}$)–C$_{16}$E$_6$/Me-P(EO)$_{113}$-*b*-P(C$_{12}$GE)$_7$							
65.3	0	0.155	0	195	307	−0.88	0.54
65.3	0.050	0.112	0.006	277	438	−0.88	0.54
65.3	0.100	0.078	0.008	405	634	−0.89	0.55
65.3	0.050	0.154	0.008	228	300	−0.92	0.65
D$_2$O/NaCl–Sasolwax 5805–Genapol O 050/080/Me-P(EO)$_{113}$-*b*-P(CO$_2$C$_{12/14}$GE)$_7$							
67.6	0.100	0.114	0.012	241	623	−0.71	0.33

[a]Symmetric microemulsions at constant ϕ = 0.500 and ε = 0.001 were studied at the temperature T_{SANS} (close to the PIT). Their composition is specified by the copolymer mass fraction δ within the overall amphiphilic mixture, the surfactant and copolymer volume fractions ϕ_C and ϕ_D, respectively. The accuracy of the periodicity d_{TS}, the correlation length ξ_{TS}, the amphiphilicity factor f_a,[53−55] and the bending rigidity κ_{SANS}[59] is of the order of ±3 Å, ± 4 Å, ± 0.015, and ± 0.015k_BT, respectively.

ionic *n*-alkyl polyglycol ether type surfactants.[44,66] However, in order to decrease the environmental impact of surfactants and the overall costs, a considerable reduction of the amount of surfactant needed to form microemulsions is highly desirable.

This was our motivation to study whether the new PEO-*b*-PAlkGE copolymers can also be used to increase the efficiency of long-chain surfactants to formulate microemulsions containing long-chain oils or even technical-grade waxes. Thus, the influence of Me-P(EO)$_{113}$-*b*-P(C$_{12}$GE)$_7$ on the phase behavior of the H$_2$O/NaCl–*n*-octacosane–hexaethylene glycol monohexadecyl ether (C$_{16}$E$_6$) system was quantitatively studied by recording a $T(\gamma)$ section at constant ϕ = 0.500 and ε = 0.001. The phase diagrams for different polymer contents are shown on the left side of Figure 3. As can be seen, strong efficiency boosting was also found in this microemulsion system, which exhibits a relatively high phase inversion temperature of $\tilde{T}$ = 66.8 °C. Upon replacing only a small fraction of C$_{16}$E$_6$ by Me-P(EO)$_{113}$-*b*-P(C$_{12}$GE)$_7$ (δ = 0.050), the one-phase region extends to lower mass fractions of the amphiphile, with the $\tilde{X}$ point decreasing from $\tilde{\gamma}$ = 0.144 to $\tilde{\gamma}$ = 0.105. Further increasing δ to δ = 0.100 shifts the $\tilde{X}$ point to an even lower value of $\tilde{\gamma}$ = 0.071. Note that the PIT stays almost constant at $\tilde{T} \approx$ 66.8 °C, whereas it slightly increases in the *n*-decane microemulsions with increasing δ. Furthermore, a two-phase coexistence of a lamellar (L$_\alpha$) and a microemulsion phase can be found at relatively large γ values. This behavior is in agreement with the results obtained for the efficiency boosting in *n*-decane microemulsions with PEP-*b*-PEO copolymers. At low values of δ, a suppression of the liquid crystal formation, e.g., the L$_\alpha$ phase, was observed, while the opposite effect, i.e., a stabilization of liquid crystal phases, was found for $\delta \geq$ 0.10.[16,20] Note that the appearance of liquid crystal phases, such as the lamellar phase, is ambiguous. While they are preferentially used, e.g., in food applications[67] or as templates for the synthesis of mesoporous silica,[68] the formation of these often highly viscous phases is undesirable in applications,[69] where microemulsions should be highly dilutable with water or oil.

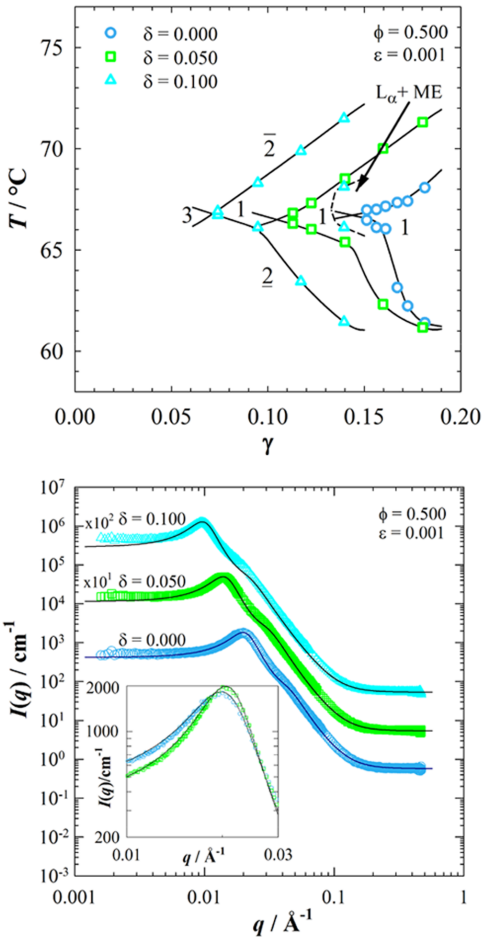

Figure 3. Left: $T(\gamma)$ diagrams of the system H$_2$O/NaCl–*n*-octacosane–C$_{16}$E$_6$/Me-P(EO)$_{113}$-*b*-P(C$_{12}$GE)$_7$, recorded at δ = 0 (blue circle), 0.05 (green square) and 0.10 (light blue triangle) with ϕ = 0.500 and ε = 0.001. The shift of the $\tilde{X}$ points toward lower values of γ upon increasing δ clearly proves the strong efficiency boosting. Right: bulk contrast SANS curves of samples recorded along two pathways: For samples close to the respective $\tilde{X}$ points, the scattering peak shifts to smaller q values and higher intensities with increasing polymer content. Note that the curves are displaced by a factor of 10. Inset: samples at ϕ_C = 0.155 exhibit an increasing sharpness of the scattering peak when increasing δ to δ = 0.050. All curves are analyzed using the TS model,[53] taking into account double scattering.[54,55]

https://dx.doi.org/10.1021/acs.langmuir.0c01491
Langmuir 2020, 36, 9849−9866

The observed efficiency boosting of Me-P(EO)$_{113}$-*b*-P(C$_{12}$GE)$_7$ in the *n*-octacosane microemulsion at high temperatures indicates that the copolymer influences the microstructure of the *n*-decane and the *n*-octacosane microemulsions in a similar way. Indeed, as can be seen in Figure 3 (right), the scattering peak of the samples prepared near the $\tilde{X}$ point ($\phi_{C+D} \approx \tilde{\phi}_{C+D} + 0.02$) also strongly shifts to lower q and higher I when δ is increased from $\delta = 0$ to 0.100. Describing the experimental scattering data by eq 9 (black solid lines) yields an increase of the periodicity d_{TS} by more than a factor two from 307 to 634 Å when δ is increased from $\delta = 0$ to 0.100. Interestingly, the amphiphilicity factor, which stays almost constant at $f_a \approx -0.88$, is more negative than the amphiphilicity factor of the *n*-decane microemulsion. Consequently, the value of the bending rigidity $\kappa_{SANS} = 0.55k_BT$ is larger. Both values indicate a better structural ordering of the C$_{16}$E$_6$-stabilized *n*-octacosane microemulsions, most probably caused by the longer alkyl chain of the surfactant C$_{16}$E$_6$ compared to C$_{10}$E$_4$.

The influence of Me-P(EO)$_{113}$-*b*-P(C$_{12}$GE)$_7$ on the microemulsion microstructure at $\phi_C = \tilde{\phi}_{C,0} + 0.02 = 0.155$ was only studied with one sample ($\delta = 0.050$). The inset in Figure 3 (right) shows the respective scattering curve together with the scattering curve of the polymer-free system with a focus on the region around the scattering peak. As observed for the C$_{10}$E$_4$-stabilized *n*-decane microemulsions, the peak becomes significantly sharper when δ is increased. Accordingly, the analysis of the scattering data provides an increasingly negative f_a value, decreasing from $f_a = -0.88$ to $f_a = -0.92$ and an increase of the amphiphilic film's bending rigidity, which increases from $0.54k_BT$ to $0.65k_BT$. For a more detailed analysis of the copolymers' influence on the bending rigidity, see Figure 8. Note that the composition of the samples, measuring temperatures, and values of d_{TS}, ξ_{TS}, f_a, and κ_{SANS} are summarized in Table 2.

Role of the Molecular Structure of PEO-*b*-PAlkGE Polymers for the Boosting Effect. So far, the efficiency boosting effect has been studied by means of the copolymer Me-P(EO)$_{113}$-*b*-P(C$_{12}$GE)$_7$. However, as mentioned before, the outstanding property of PEO-*b*-PAlkGE copolymers is their easy-to-modify molecular structure. Thus, in this section, the influence of the AlkGE block size and the alkyl side chain on the polymers' efficiency boosting effect is studied by means of the system H$_2$O/NaCl–*n*-octacosane–C$_{16}$E$_6$/Me-P(EO)$_{113}$-*b*-P(C$_i$GE)$_n$, varying the number n of AlkGE repeating units from 3 to 9 and the number i of carbon atoms in the alkyl side chain between 12 and 16. On the left side of Figure 4, the phase diagrams recorded at constant $\phi = 0.500$, $\varepsilon = 0.001$, and a polymer mass fraction $\delta = 0.050$ in the overall amphiphile mixture are shown in comparison to the phase diagram of the polymer-free system (blue circle). As can be seen, all of the used Me-P(EO)$_{113}$-*b*-P(C$_i$GE)$_n$ polymers cause a strong shift of the one-phase region and the $\tilde{X}$ point to lower mass fraction γ of the amphiphile. Since all phase boundaries almost lie on top of each other, the influence of the AlkGE block size and the alkyl side chain on the efficiency boosting is shown in the inset by plotting $\tilde{T}$ versus $\tilde{\gamma}$ (the values are compiled in Table S2 of the Supporting Information).

The effect of the number n of AlkGE repeating units on the $\tilde{X}$ point is discussed by means of Me-P(EO)$_{113}$-*b*-P(C$_{12}$GE)$_n$ polymers with a dodecyl side chain. By increasing n from 3 to 8, a very systematic shift of $\tilde{\gamma}$ to lower amphiphile mass

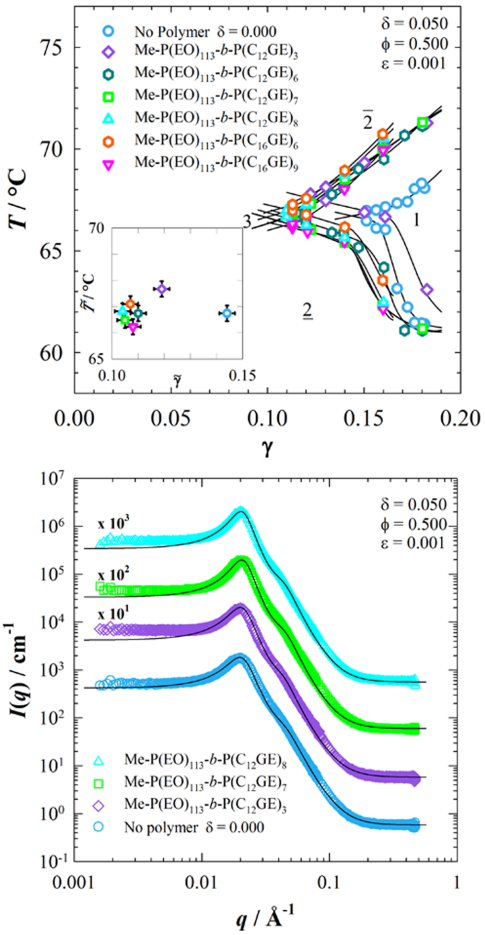

Figure 4. Left: $T(\gamma)$ diagrams of the systems H$_2$O/NaCl – *n*-octacosane – C$_{16}$E$_6$/Me-P(EO)$_{113}$-*b*-P(C$_i$GE)$_n$, recorded at $\phi = 0.500$, $\varepsilon = 0.001$ and $\delta = 0.050$ for the polymers $i = 12$ and $n = 3, 6, 7, 8$ as well as $i = 16$ and $n = 6, 9$ together with the polymer-free system ($\delta = 0$, blue circle). Inset: $\tilde{X}$ points ($\tilde{T}(\tilde{\gamma})$) of the studied systems to visualize the effect of n and i on the efficiency boosting and the PIT. Right: Bulk contrast SANS curves of the polymer-free sample and samples containing different copolymers ($\delta = 0.050$) recorded at $\phi_C = 0.155$. All curves are analyzed using the TS model[53] taking into account double scattering.[54,55]

fractions can be observed. This trend is in agreement with the theoretical prediction of efficiency boosting[21,22,24,26]

$$\ln \tilde{\phi}_{C,i} = \ln \tilde{\phi}^0_{C,i} - \Xi\sigma(R_{ee,w}{}^2 + R_{ee,o}{}^2) \quad (14)$$

which describes the dependence of the volume fraction $\tilde{\phi}_{C,i}$ of surfactant molecules in the amphiphilic film at the $\tilde{X}$ point as a function of the number density $\sigma = N_D/(S/V)$ of block copolymers within the surfactant membrane and the polymer end-to-end distances $R_{ee,w}$ and $R_{ee,o}$ of the hydrophilic and

https://dx.doi.org/10.1021/acs.langmuir.0c01491
Langmuir 2020, 36, 9849−9866

Table 3. Composition and Measuring Temperature of SANS Samples of the D_2O/NaCl−*n*-Octacosane−$C_{16}E_6$ Microemulsions Boosted by Different me-P(EO)$_{113}$-*b*-P(C_{12}GE)$_n$ Copolymers Together with the Obtained Fit Parameters[a]

n	T_{SANS} (°C)	δ	ϕ_C	ϕ_D	ξ_{TS} (Å)	d_{TS} (Å)	f_a	κ_{SANS} (k_BT)
	65.3	0	0.155	0	195	307	−0.88	0.54
3	67.6	0.050	0.154	0.008	203	305	−0.89	0.57
7	65.3	0.050	0.154	0.008	228	300	−0.92	0.65
8	65.3	0.050	0.154	0.008	230	304	−0.92	0.64

[a]Symmetric microemulsions at constant ϕ = 0.500 and ε = 0.001 were studied at the temperature T_{SANS} (close to the PIT). Their composition is specified by the copolymer mass fraction δ within the overall amphiphilic mixture, the surfactant and copolymer volume fractions ϕ_C and ϕ_D, respectively. The accuracy of the periodicity d_{TS}, the correlation length ξ_{TS}, the amphiphilicity factor f_a,[53−55] and the bending rigidity κ_{SANS}[59] is of the order of ±3 Å, ± 4 Å, ± 0.015, and ± 0.015k_BT, respectively.

hydrophobic block, respectively. $\tilde{\phi}^0_{C,i}$ is the surfactant volume fraction at the $\tilde{X}$ point of the polymer-free system, Ξ is a pre-factor, and $N_D = \phi_D/V_D = \phi_D/(M_D N_A/\rho_D)$, M_D and ρ_D are the number density, molar mass, and density of the copolymer (D). $S/V = a_C\phi_{C,i}/v_C = a_C\phi_{C,i}/(M_C N_A/\rho_C)$ is the total specific interface of the amphiphilic film, where M_C and ρ_C are the molar mass and density of the surfactant (C) molecules and a_C is the area of one surfactant molecule calculated according to ref 48. Thus, according to eq 14, an increase of the AlkGE block size should indeed lead to a decrease of the surfactant amount at the $\tilde{X}$ point, which is equivalent to a stronger efficiency boosting.

Considering now the influence of the PEO-*b*-PAlkGE copolymers on the phase inversion temperature $\tilde{T}$, an increase is observed for Me-P(EO)$_{113}$-*b*-P(C_{12}GE)$_3$. Comparing the effect of different copolymers yields an almost systematic decrease of $\tilde{T}$ with an increasing number n of repeating units. These results qualitatively follow the prediction of Lipowsky,[70] according to which the influence of amphiphilic block copolymers anchored to an interfacial film on its mean curvature H can be described by

$$\Delta H = A\frac{\sigma k_B T(R_{ee,w} - R_{ee,o})}{\kappa} \quad (15)$$

where A is a pre-factor. Accordingly, for Me-P(EO)$_{113}$-*b*-P(C_{12}GE)$_3$, a shift of $\tilde{T}$ to higher temperatures is expected as the polymer end-to-end distance $R_{ee,w}$ of the Me-P(EO)$_{113}$ block is larger than the $R_{ee,o}$ of the P(C_{12}GE)$_3$ block (see Supporting Information, Table S4). Furthermore, the observed decrease of $\tilde{T}$ with an increasing number n of repeating units can be explained by eq 15. However, based on the first SANS measurements of the homopolymer P(C_{12}GE)$_{18}$ in *n*-octacosane (see Supporting Information, Table S4), this trend is expected to be less pronounced than what was observed. This may indicate that the conformation of the hydrophobic PAlkGE block (as a part of the amphiphilic block copolymer) in the microemulsions is different from the homopolymer's conformation in the pure solvent *n*-octacosane.

Looking at the influence of the number i of carbon atoms in the side chain of the AlkGE unit, no systematic trend on the location of the $\tilde{X}$ point is found. Within the experimental error, the copolymers with dodecyl (i = 12) and hexadecyl (i = 16) side chains show similar values of $\tilde{\gamma}$ and $\tilde{T}$.

The influence of the number n of AlkGE repeating units on the microstructure of D_2O/NaCl−*n*-octacosane−$C_{16}E_6$/Me-P(EO)$_{113}$-*b*-P(C_iGE)$_n$ microemulsions was studied by bulk contrast SANS experiments performed at $\phi_C = \tilde{\phi}_{C,0}$ + 0.02 = 0.155. Figure 4 (right) shows the respective scattering curves (δ = 0.050) together with the scattering curve of the polymer-free system (δ = 0). As observed for the microemulsions studied so far, at constant ϕ_C, the sharpness of the peak, which stays almost at the same q_{max}, increases upon addition of the PEO-*b*-PAlkGE copolymers. In agreement with the different degree of efficiency boosting found in the phase behavior studies, the value of the amphiphilicity factor becomes only slightly more negative when adding Me-P(EO)$_{113}$-*b*-P(C_iGE)$_3$, i.e., with the factor decreasing only slightly from f_a = −0.88 to f_a = −0.89, while for the copolymers with n = 7 and 8, a value of f_a = −0.92 is found. Accordingly, the value of the amphiphilic film's bending rigidity increases from 0.54k_BT for the polymer-free system to 0.57, 0.65, and 0.64k_BT for the Me-P(EO)$_{113}$-*b*-P(C_iGE)$_n$-doped systems with n = 3, 7, and 8, respectively. Note that the composition of the samples, measuring temperatures, and values of d_{TS}, ξ_{TS}, f_a, and κ_{SANS} are summarized in Table 3.

Efficiency Boosting of "Carbonated" PEO-*b*-PCO$_2$AlkGE Polymers in H_2O/NaCl−*n*-Octacosane−$C_{16}E_6$. In order to bring the PEO-*b*-PAlkGE diblock copolymers to application, technical-grade Me-P(EO)$_{113}$-*b*-P($CO_2C_{12/14}$GE)$_n$ polycarbonate derivatives were synthesized and their influence on the phase behavior of the H_2O/NaCl−*n*-octacosane−$C_{16}E_6$ system was studied at ϕ = 0.500, ε = 0.001, and δ = 0.050. To distinguish between the effects of the additional carbonate group and the technical-grade $C_{12/14}$ side chain in the AlkGE repeating units, "carbonated" Me-P(EO)$_{113}$-*b*-P(CO_2C_{12}GE)$_n$ copolymers with a defined C_{12} side chain were also synthesized.

In Figure 5 (left), the effects of Me-P(EO)$_{113}$-*b*-P(C_{12}GE)$_3$, Me-P(EO)$_{113}$-*b*-P(CO_2C_{12}GE)$_3$, and Me-P(EO)$_{113}$-*b*-P($CO_2C_{12/14}$GE)$_3$ on the phase behavior of the H_2O/NaCl−*n*-octacosane−$C_{16}E_6$ system are compared in the form of the well-known $T(\gamma)$ section. As can be seen, all three copolymers cause a shift of the one-phase region and the $\tilde{X}$ point to lower mass fractions γ of the amphiphile. Interestingly, the copolymer Me-P(EO)$_{113}$-*b*-P(CO_2C_{12}GE)$_3$ enables the strongest efficiency boosting, which might be related to the somewhat larger PAlkGE block. Consequently, the technical-grade nature of the $C_{12/14}$ side chain must be the reason for the weaker efficiency boosting obtained for the technical-grade P(EO)$_{113}$-*b*-P($CO_2C_{12/14}$GE)$_3$ copolymer.

On the right side of Figure 5, the effect of the different PAlkGE blocks on the phase behavior of the H_2O/NaCl−*n*-octacosane−$C_{16}E_6$ system is shown by means of Me-P(EO)$_{113}$-*b*-P(C_{12}GE)$_7$, Me-P(EO)$_{113}$-*b*-P(CO_2C_{12}GE)$_9$, and Me-P(EO)$_{113}$-*b*-P($CO_2C_{12/14}$GE)$_7$. Since these copolymers possess a larger PAlkGE block, a stronger decrease of $\tilde{\gamma}$, i.e., a stronger efficiency boosting than for the n = 3 copolymers, is enabled. Comparing the boosting effects among these larger copolymers, the smallest $\tilde{\gamma}$ value is found for Me-P(EO)$_{113}$-*b*-P(CO_2C_{12}GE)$_9$ since it possesses the largest PAlkGE block (eq

https://dx.doi.org/10.1021/acs.langmuir.0c01491
Langmuir 2020, 36, 9849−9866

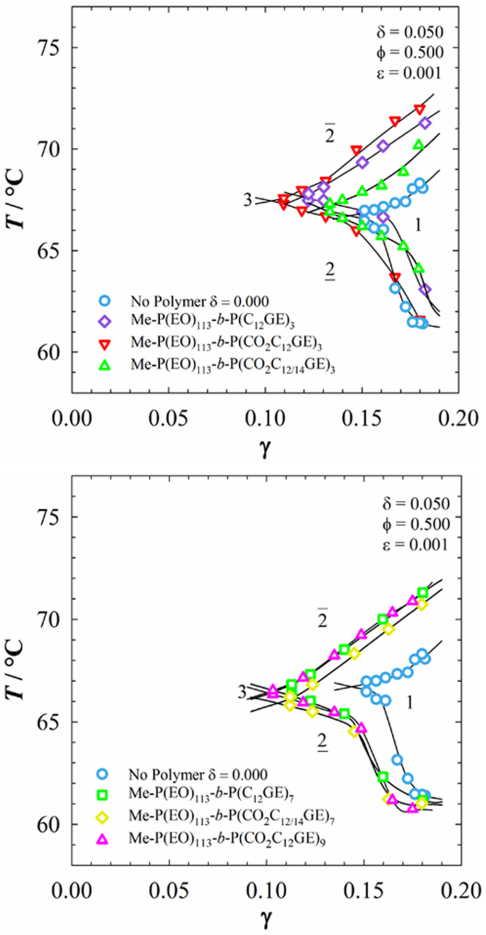

Figure 5. $T(\gamma)$ diagrams of the systems H_2O/NaCl–*n*-octacosane–$C_{16}E_6$/PEO-*b*-PAlkGE recorded at $\phi = 0.500$ and $\varepsilon = 0.001$ for $\delta = 0$ (polymer-free system) and $\delta = 0.050$ with a varying molecular structure of the hydrophobic PAlkGE block, ranging from $P(C_{12}GE)_n$ to the carbonated $P(CO_2C_{12}GE)_n$ to technical-grade $P(CO_2C_{12/14}GE)_n$. Note that all copolymers with $n = 3$ (left) and $n = 7$ and 9 (right), including the technical-grade ones, cause a considerable efficiency boosting effect.

14). A slightly larger $\tilde{\gamma}$ value, i.e., weaker efficiency boosting, is found for Me-$(PEO)_{113}$-*b*-$P(C_{12}GE)_7$. Regarding a technical application, it is promising that the efficiency boosting effect of the technical-grade Me-$P(EO)_{113}$-*b*-$P(CO_2C_{12/14}GE)_7$ copolymer is only slightly weaker than observed with "pure" Me-$P(EO)_{113}$-*b*-$P(C_{12}GE)_7$. For a more detailed comparison of the efficiency boosting effects of the different polymers, the reader is referred to Table S2 in the Supporting Information, where all $\tilde{\gamma}$ and $\tilde{T}$ values are compiled.

Efficiency Boosting of Me-$P(EO)_{113}$-*b*-$P(CO_2C_{12/14}GE)_7$ in H_2O/NaCl–Sasolwax 5805–Genapol O 050/O 080. As already mentioned in the Introduction, the boosting effect of amphiphilic diblock copolymers so far has only scarcely found its way into applications,[39] mainly due to a difficult and expensive large-scale polymer synthesis[17] as well as the weakening of the boosting effect with increasing dispersity of the polymer blocks, especially in the case of the remaining homopolymers. The results obtained in this study, especially those shown in Figure 5 (right), strongly indicate that the technical-grade Me-$P(EO)_m$-*b*-$P(CO_2C_{12/14}GE)_n$ copolymers, which can be synthesized at low cost and on large scale with a yield of the order of 60% (Table S1), are at least capable of strongly increasing the efficiency of the monodisperse nonionic surfactant $C_{16}E_6$ to solubilize water and *n*-octacosane.

In a further step toward an application of the efficiency boosting effect, we studied whether the technical-grade Me-$P(EO)_m$-*b*-$P(CO_2C_{12/14}GE)_n$ copolymers are able to increase the efficiency of technical-grade (polydisperse) *n*-alkyl polyglycol ether surfactants to solubilize technical-grade Sasolwax 5805, which is a technical-grade mixture of linear and branched alkanes ranging from C_{19} to C_{46} with an average carbon number of 30.5.[44] Ethoxylated oleyl alcohols of the Genapol O series, more precisely Genapol O 050 and Genapol O 080 (mean ethoxylation degrees of 5 and 8, respectively), were chosen as technical-grade nonionic surfactants.

Based on a very recent study of Sasolwax 5805-containing microemulsions stabilized by technical-grade surfactants of the Genapol type,[44] we formulated a symmetric ($\phi = 0.500$) microemulsion of the type H_2O/NaCl ($\varepsilon = 0.001$)–Sasolwax 5805–Genapol O 050/O 080, starting with a 1:1 (m/m) mixture of the two Genapol surfactants. The phase behavior of this polymer-free technical grade microemulsion system is shown in Figure 6 in the form of a $T(\gamma)$ section (blue circle). As can be seen, the phase boundaries are strongly distorted because the hydrophobic homologues of the technical-grade surfactants are extracted from the amphiphilic film into the oil-rich domains and the oil excess phase. As a consequence, the amphiphilic film becomes increasingly hydrophilic with decreasing γ, shifting not only the phase boundaries but also the hydrophilic lipophilic balance (HLB) to higher temperatures.[71] Thus, the $\tilde{X}$ point is located at $\tilde{\gamma} = 0.155$ and $\tilde{T} \approx 73.7$ °C. Note that an extended two-phase coexistence of a lamellar (L_α) and a microemulsion phase can be found at low temperatures.

By replacing 10 wt % of the Genapol O 050/O 080 (1:1) mixture with the technical-grade Me-$P(EO)_{113}$-*b*-$P(CO_2C_{12/14}GE)_7$ copolymer ($\delta = 0.100$, green square), the $\tilde{X}$ point is shifted to $\tilde{\gamma} = 0.127$ and $\tilde{T} = 79.6$ °C along the upward-tilted HLB line. Thus, the technical-grade Me-$P(EO)_m$-*b*-$P(CO_2C_{12/14}GE)_n$ copolymers indeed enable efficiency boosting. A further increase in efficiency is obtained by increasing the fraction of the hydrophobic Genapol O 050 in the surfactant mixture to 75 wt %, leaving the copolymer content constant at $\delta = 0.100$ (red triangle). Accordingly, the phase boundaries are shifted to lower temperatures and surfactant mass fractions, yielding an $\tilde{X}$ point located at $\tilde{\gamma} = 0.091$ and $\tilde{T} = 74.6$ °C. Furthermore, the phase boundaries are even more distorted because the fraction of the hydrophobic homologues of the technical-grade surfactants extracted from the amphiphilic film with respect to the overall surfactant mass fraction strongly increases with decreasing γ. The results clearly prove that this new type of technical-grade amphiphilic diblock copolymer allows for the formulation of efficient microemulsions, even when a mixture of long-chain oils has to be

https://dx.doi.org/10.1021/acs.langmuir.0c01491
Langmuir 2020, 36, 9849–9866

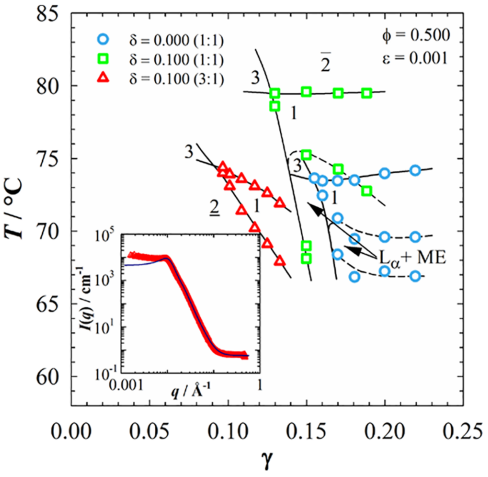

Figure 6. $T(\gamma)$ diagrams of the technical-grade microemulsion system H_2O/NaCl−Sasolwax 5805−Genapol O 050/O 080/Me-P(EO)$_{113}$-*b*-P($CO_2C_{12/14}$GE)$_7$, recorded at ϕ = 0.500, ε = 0.001, δ = 0.100, and different surfactant ratios; shown together with the polymer-free system (δ = 0, blue circle). Two different mixtures of the Genapol surfactants were used, i.e., 1:1 (green square) or 3:1 (red triangle) (O 050/O 080, m/m). Excitingly, the technical-grade Me-P(EO)$_{113}$-*b*-P($CO_2C_{12/14}$GE)$_7$ copolymer also causes an efficiency boosting in this technical-grade microemulsion system. L_α + ME denotes the coexistence of a lamellar phase (L_α) with a microemulsion phase (ME). Inset: bulk contrast SANS curve recorded near the $\tilde{X}$ point of the system D_2O/NaCl−Sasolwax 5805−Genapol O 050/O 080/Me-P(EO)$_{113}$-*b*-P($CO_2C_{12/14}$GE)$_7$ with δ = 0.100 and a 3:1 (m/m) mixture of Genapol O 050/O 080. The curve was analyzed using the TS model,[53] taking into account double scattering.[54,55]

solubilized. From our results, an even stronger efficiency boosting can be predicted upon further increasing the fraction δ of the technical-grade Me-P(EO)$_m$-*b*-P($CO_2C_{12/14}$GE)$_n$ copolymers in the amphiphile mixture. Note that the $\tilde{T}$ and $\tilde{\gamma}$ values are listed in Table S2 in the Supporting Information.

In order to study the microstructure of this efficiency-boosted technical-grade microemulsion, one bulk contrast SANS curve was recorded for the system D_2O/NaCl−*n*-octacosane−Genapol O 050/O 080(3:1)/Me-P(EO)$_{113}$-*b*-P(C_{12}GE)$_7$ with ϕ = 0.500, ε = 0.001, and δ = 0.100 near its $\tilde{X}$ point, i.e., at a surfactant volume fraction of ϕ_C = 0.114 and a temperature of T = 67.6 °C. Note that for D_2O, the phase boundaries are about 2 K lower than for H_2O.[18] The obtained SANS curve is shown in the inset of Figure 6. Qualitatively, the curve resembles the typical shape found for bicontinuous microemulsions. However, two differences with respect to the scattering curves shown so far (Figures 2 to 4) can be observed. On the one hand, the scattering peak is less pronounced, indicating a less ordered structure. On the other hand, an increase of the scattering intensity at low q points to the existence of a structure with a larger length scale. As we can exclude a demixing of the sample during the experiment (by checking before and after the experiment), we presume that the SANS curve was not recorded at the HLB but close to the lower phase boundary, where cylindrical structures are expected.

The fit of the experimental scattering data by eq 9 is shown as a black solid line. As can be seen, it describes almost the entire scattering curve except for the low q regime almost quantitatively. A relatively large value of the periodicity of the structure d_{TS} = 623 Å is found. In agreement with the qualitative discussion of the data, a less negative value of the amphiphilicity factor f_a = −0.71 and a smaller bending rigidity κ_{SANS} = 0.33 are found, indicating a less ordered structure. The sample composition, measuring temperature, d_{TS}, ξ_{TS}, f_a, and κ_{SANS} are summarized in Table 2.

Scaling of the PEO-*b*-PAlkGE Efficiency Boosting: A Synopsis. The results obtained so far clearly show that the new amphiphilic poly(ethylene oxide)-poly(alkyl glycidyl ether) copolymers boost the efficiency of microemulsion systems, containing model type oils like *n*-decane, long-chain oils as *n*-octacosane, or even technical-grade waxes. Similar to the boosting of *n*-decane microemulsions by amphiphilic PEP-*b*-PEO copolymers, which was found 20 years ago,[16,17,72] the strong efficiency increase facilitated by the new type of PEO-*b*-PAlkGE copolymers is expected to be related to the anchoring of the copolymers in the amphiphilic film. Gompper et al. were able to explain the enormous boosting effect in terms of the bending elastic energy[23] of fluctuating polymer-decorated surfactant membranes.[21,22] To obtain a scaling of the efficiency boosting effect, they combined the effect of the membrane-anchored copolymers onto the curvature and the bending moduli κ and $\bar{\kappa}$ predicted by Lipowsky et al.[24,25,52,70] with the model of thermally fluctuating amphiphilic films, for which the bicontinuous microemulsion becomes unstable when the renormalized saddle splay modulus $\bar{\kappa}(\xi)$ approaches zero at the $\tilde{X}$ point.[62−64] This scaling relation (eq 14), whose detailed derivation can be found elsewhere,[21,22] allows predicting the increase of the efficiency (characterized by the volume fraction $\tilde{\phi}_{C,i}$ of surfactant molecules in the amphiphilic film at the $\tilde{X}$ point) as a function of the number density σ of block copolymers in the membrane and the end-to-end distances $R_{ee,w}$ and $R_{ee,o}$ of the hydrophilic and hydrophobic block, respectively.

By using this scaling description, the efficiency boosting effect of the new type of PEO-*b*-PAlkGE diblock copolymers in the different microemulsion systems can not only be analyzed on a quantitative level but also allows for a comparison between the respective degrees of efficiency boosting of PEO-*b*-PAlkGE and PEP-*b*-PEO copolymers. However, in order to perform the analysis according to eq 14, not only $\tilde{\phi}_{C,i}$ and $\tilde{\phi}^0_{C,i}$ must be calculated using eq 6 considering the monomeric solubilities of the surfactants in the respective oil, but also $\sigma = N_D/(S/V)$, $R_{ee,w}$, and $R_{ee,o}$ are required. Although the R_g value and therefore the $R_{ee,w}$ value (calculated via $R_{ee} = 6^{1/2} R_g$) of a larger PEO block (41,500 g mol^{-1}) in D_2O can be found in the literature,[73] we performed additional SANS experiments both at T = 25 °C and T = 60 °C to study the temperature dependence of $R_{ee,w}$ of our PEO block, which possesses a molecular weight of M_w = 5290 g mol^{-1}. Furthermore, a few SANS experiments were performed on PAlkGE homopolymers in *n*-decane and *n*-octacosane at $T \approx$ 25 °C and T = 67 °C to determine $R_{ee,o}$. The scattering data (Figure S24) of PEO were analyzed by using a two-correlation-length model taking into account the scattering contribution of occurring clusters at low q,[73−75] while the data for the PAlkGE homopolymers were described by the Guinier model.[76] Interestingly, within the measuring error, no dependence of the end-to-end distances on temperature and solvent was found (see values of $R_{ee,o}$ and

https://dx.doi.org/10.1021/acs.langmuir.0c01491
Langmuir 2020, 36, 9849−9866

$R_{ee,w}$ in Table S4). The $R_{ee,o}$ values of the PAlkGE blocks containing 3 to 9 AlkGE repeating units were obtained considering the dependence of end-to-end distances $R_{ee,o}$ on the molecular weight, which was similarly found for PEO polymers by Kawaguchi et al.,[77] i.e., $R_{ee,o} = 2.2707 M_w^{0.314}$ (Figure S25).

The determination of $\tilde{\phi}_{C,i}$, $\tilde{\phi}^0_{C,i}$, σ, $R_{ee,w}$, and $R_{ee,o}$ allows for the analysis of the efficiency boosting effect by a scaling representation via plotting $\ln(\tilde{\phi}_{C,i}/\tilde{\phi}^0_{C,i})$ versus the polymeric coverage of the membrane $\sigma(R_{ee,w}^2 + R_{ee,o}^2)$. In a first step, in Figure 7, the efficiency boosting of the new type of PEO-*b*-PAlkGE and the literature-known PEP-*b*-PEO[72] copolymers is compared by means of the model microemulsion H_2O/NaCl–*n*-decane–$C_{10}E_4$. The plot contains data from the Me-P(EO)$_{113}$-*b*-P(C_iGE)$_n$ copolymers with i = 12 and n = 3, 6, 7, and 8. As can be seen, for the model *n*-decane microemulsion, the data of PEO-*b*-PAlkGE (red square)-boosted systems fall onto a single straight line, which confirms the scaling relation (eq 14) and proves that the copolymers indeed modify the saddle-splay modulus of the surfactant membrane. Interestingly, the data of PEO-*b*-PAlkGE (red square) and PEP-*b*-PEO (gray circle)[72] copolymers fall almost on top of each other, yielding almost identical slopes of Ξ(PEO-*b*-PAlkGE) = 1.54 ± 0.08 and Ξ(PEP-*b*-PEO) = 1.51 ± 0.06,[72] respectively. The slopes are roughly twice as large as the theoretical estimate for ideal chains (Ξ(ideal chains) = π/5) due to the fact that self-avoiding chains may have a more pronounced effect on the saddle-splay modulus than ideal chains.[21,78,79]

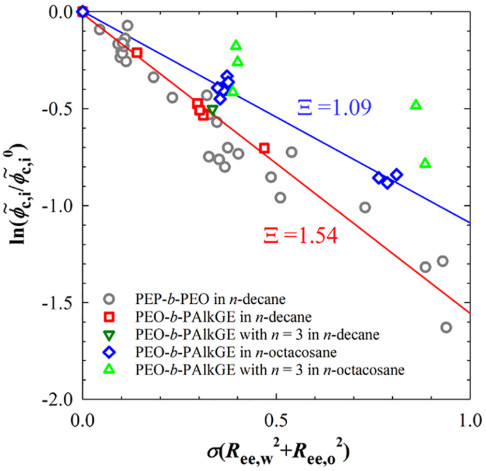

Figure 7. Normalized logarithmic volume fraction of surfactant in the interface at the $\tilde{X}$ point $\ln(\tilde{\phi}_{C,i}/\tilde{\phi}^0_{C,i})$, plotted against the polymer coverage of the membrane $\sigma(R_{ee,w}^2 + R_{ee,o}^2)$, for the systems H_2O/NaCl–*n*-decane–$C_{10}E_4$/PEO-*b*-PAlkGE (red square) and H_2O/NaCl–*n*-octacosane–$C_{16}E_6$/PEO-*b*-PAlkGE (blue diamond). The plot contains data from the Me-P(EO)$_{113}$-*b*-P(C_iGE)$_n$ copolymers with i = 12 and n = 3, 6, 7, and 8 as well as the polymers with i = 16 and n = 6 and 9. Additionally, data for the Me-P(EO)$_{113}$-*b*-P(CO_2C_iGE)$_n$ copolymers with i = 12 and n = 3 and 9 as well as i = 12/14 and n = 3 and 7 are included. Note that the results obtained for the H_2O/NaCl–*n*-octacosane–$C_{16}E_6$ systems with the n = 3 (green triangle) polymers are shown but were not considered in the linear regression (see text). Literature data obtained by Jakobs for the system H_2O–*n*-decane–$C_{10}E_4$/PEO$_m$-*b*-PEP$_n$ with different PEP-*b*-PEO copolymers[72] are shown for comparison (gray circle).

In the next step, the scaling relation is applied to the efficiency boosting of the new PEO-*b*-PAlkGE in the H_2O/NaCl–*n*-octacosane–$C_{16}E_6$ microemulsion (Figure 7; blue diamond and green triangle). The figure contains data from Me-P(EO)$_{113}$-*b*-P(C_iGE)$_n$ copolymers with i = 12, i = 16 and n = 3, 6, 7, 8, and 9 as well as results obtained for Me-P(EO)$_{113}$-*b*-P(CO_2C_iGE)$_n$ with i = 12, 12/14 and n = 3, 7, and 9. As can be seen, the data (with the exception of most of the n = 3 (green triangle) copolymer data) fall onto a single straight line, confirming that the scaling relation (eq 14)) also applies for *n*-octacosane microemulsions formed at high temperatures of around 60 °C. However, the slope of Ξ(PEO-*b*-PAlkGE) = 1.09 ± 0.05 is somewhat smaller than the one found for the *n*-decane microemulsions and may indicate that polymers at higher temperatures come closer to the behavior of ideal chains. Furthermore, while the data points of technical-grade Me-P(EO)$_{113}$-*b*-P($CO_2C_{12/14}$GE)$_7$ follow this scaling relation, most of the n = 3 (green triangle) copolymer data do not fall on the line. A possible reason might be the rather small size of the PAlkGE block, which decreases the tendency of these polymers to tether to the surfactant membrane, when *n*-octacosane is used as the hydrophobic solvent at high temperatures. Note that for the *n*-decane microemulsion, efficiency boosting of the Me-P(EO)$_{113}$-*b*-P(C_{12}GE)$_3$ obeys the general trend.

Influence of the PEO-*b*-PAlkGEs on the Bending Rigidity κ. The analysis of the SANS data was performed with the model of random interfaces derived by Safran et al.[59,80,81] to determine the bending rigidity κ_{SANS}. Due to the reasons given above, we decided to not consider recent indications[60,61] that κ_{SANS} is rather a mixture of the bending rigidity κ and the saddle splay modulus $\bar{\kappa}$.

Taking into consideration the stiffening of the membrane by anchoring of the copolymers in the amphiphilic film[24,25,52,70] as well as its softening through thermal fluctuations,[62−64] κ_{SANS} is given by

$$\kappa_{SANS} = \kappa_0 + \frac{k_B T}{12}\left(1 + \frac{\pi}{2}\right)\sigma(R_{ee,w}^2 + R_{ee,o}^2) - \frac{3k_B T}{4\pi}\ln\frac{d_{TS}a_C}{2v_C} \quad (16)$$

with κ_0 being the pure bending rigidity, $d_{TS}/2$ being the length scale of the respective systems, $v_C = M_C N_A/\rho_C$ being the molecular volume of the surfactant molecule, and a_C being the area of one surfactant molecule calculated according to reference[48] ($C_{10}E_4$: a_C = 54.1 Å^2 and v_C = 579.0 Å^3; $C_{16}E_6$: a_C = 66.5 Å^2 and v_C = 874.4 Å^3).

In Figure 8, the obtained κ_{SANS} values are plotted as a function of the polymeric coverage $\sigma(R_{ee,w}^2 + R_{ee,o}^2)$ of the amphiphilic film for the two systems D_2O/NaCl–*n*-decane–$C_{10}E_4$/Me-P(EO)$_{113}$-*b*-P(C_{12}GE)$_7$ (left) and D_2O/NaCl–*n*-octacosane–$C_{16}E_6$/Me-P(EO)$_{113}$-*b*-P(C_{12}GE)$_7$ (right). Considering at first the values obtained from the analysis of the SANS measurements performed near the respective $\tilde{X}$ points of the systems at $\phi_{C+D} \approx \tilde{\phi}_{C+D}$ + 0.02 (circle), κ_{SANS} turned out to be nearly constant. Being close to the stability limit of bicontinuous microemulsions, separating into three phases at the $\gamma < \tilde{\gamma}$, the effect of membrane stiffening via copolymer

https://dx.doi.org/10.1021/acs.langmuir.0c01491
Langmuir 2020, 36, 9849−9866

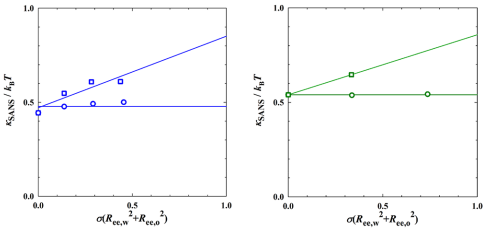

Figure 8. Bending rigidity κ_{SANS} determined by the analysis of the SANS curves according to the model of random interfaces,[59] plotted against the polymer coverage of the membrane $\sigma(R_{ee,w}^2 + R_{ee,o}^2)$ for the systems D_2O/NaCl−*n*-decane−$C_{10}E_4$/Me-P(EO)$_{113}$-*b*-P-(C_{12}GE)$_7$ (left) and D_2O/NaCl−*n*-octacosane−$C_{16}E_6$/Me-P-(EO)$_{113}$-*b*-P(C_{12}GE)$_7$ (right) at constant ϕ = 0.500 and ε = 0.001. Experiments were performed along two pathways varying δ: (circle) close to the respective $\tilde{X}$ points and (square) at constant surfactant volume fraction, i.e., ϕ_C = 0.144 (left) and ϕ_C = 0.155 (right).

anchoring and membrane softening through thermal fluctuations compensate for each other. Note that a similar compensation of membrane stiffening and softening was already observed by Jakobs for the system D_2O−*n*-octane−C_8E_3/PEP_5-*b*-PEO_5.[72]

Analyzing the second set of experiments (square), which were conducted at a constant surfactant volume fraction $\phi_C = \tilde{\phi}_{C,0}$ + 0.02 = const. close to the surfactant volume fraction $\tilde{\phi}_{C,0}$ at the $\tilde{X}$ point of the polymer-free system, a linear increase of κ_{SANS} with increasing polymer decoration of the membrane ($\sigma(R_{ee,w}^2 + R_{ee,o}^2)$) is found. Due to the fact that ϕ_C and therewith the length-scale $d_{TS}/2$ of the structure remains constant, the thermal fluctuations provide a constant contribution to κ_{SANS} (eq 16), which amounts to 0.61k_BT and 0.59k_BT for the *n*-decane and *n*-octacosane systems, respectively. Thus, the increase of κ_{SANS} can only be attributed to the increasing polymer decoration. Assuming a linear behavior, slopes of 0.38 and 0.32 were obtained, which in close agreement with Ξ found for the scaling of the efficiency are larger than the theoretically expected value for ideal chains of $(1 + \pi/2)/12$ = 0.214. Last but not least, the values of the intercept, i.e., 0.47 ± 0.03k_BT and 0.54 ± 0.04k_BT can be used for the determination of the bare bending rigidity κ_0, yielding κ_0($C_{10}E_4$/*n*-decane) = 1.08 ± 0.05k_BT and κ_0($C_{16}E_6$/*n*-octacosane) = 1.13 ± 0.06k_BT at T = 302.2 K and T = 338.5 K, respectively. Thus, the pure $C_{10}E_4$ membrane in the microemulsion containing *n*-decane is slightly less rigid compared to the pure $C_{16}E_6$ membrane in the *n*-octacosane microemulsion.

■ CONCLUSIONS

In this study, poly(ethylene oxide)-poly(alkyl glycidyl ether)s (PEO-*b*-PAlkGE) and their "carbonated" poly(ethylene oxide)-poly(alkyl glycidyl ether carbonate) analogs were synthesized as promising efficiency boosters for microemulsions. These new types of amphiphilic block copolymers excel in terms of their facile synthesis, which can be performed at low cost and on a large scale, as well as their easy-to-modify molecular structure. Systematic phase behavior studies revealed that the Me-P(EO)$_{113}$-*b*-P(C_iGE)$_n$ copolymers not only strongly increase the efficiency of the medium-chain nonionic surfactant $C_{10}E_4$ to solubilize water and *n*-decane at room temperature but also boost the efficiency of the longer-chain surfactant $C_{16}E_6$ to stabilize water/*n*-octacosane microemulsions at elevated temperatures. The influence of the molecular structure on the boosting effect was studied by increasing the number n of C_iGE repeating units from 3 to 9 and by varying the number i of carbon atoms in the alkyl side chain between 12 and 16. The observed very systematic increase in efficiency is in agreement with theoretical predictions.[21,22,24,29]

The "carbonated" Me-P(EO)$_{113}$-*b*-P(CO_2C_{12}GE)$_n$ copolymers and their technical-grade Me-P(EO)$_{113}$-*b*-P-($CO_2C_{12/14}$GE)$_n$ derivatives were also found to enable a strong efficiency boosting. By means of the H_2O/NaCl−*n*-octacosane−$C_{16}E_6$ system, we were able to show that the boosting efficiency of technical-grade Me-P(EO)$_{113}$-*b*-P-($CO_2C_{12/14}$GE)$_7$ is only slightly weaker than that of the "pure" Me-P(EO)$_{113}$-*b*-P(C_{12}GE)$_7$. In a further step toward application, we added the technical-grade Me-P(EO)$_m$-*b*-P($CO_2C_{12/14}$GE)$_7$ copolymer to a technical-grade microemulsion consisting of brine, Sasolwax 5805 (linear and branched alkanes with an average carbon number of 30.5[44]), and a mixture of technical-grade nonionic surfactants (Genapol O 050/ O 080). We emphasize that our data show that the mass fraction of amphiphiles needed to stabilize this technical-grade microemulsion can be strongly reduced from 15.5 to 9.1 wt % when only 10 wt % of an optimized surfactant mixture is replaced by the Me-P(EO)$_{113}$-*b*-P($CO_2C_{12/14}$GE)$_7$ copolymer. This result could be of interest for industrial applications where reduced surfactant needs would have significant economic and ecological implications.

The scaling description of the efficiency boosting[21,22,24,29] was then used to analyze the boosting of the new type of PEO-*b*-PAlkGE diblock copolymers on a quantitative level and to compare the respective degrees of efficiency boosting of PEO-*b*-PAlkGE and PEP-*b*-PEO copolymers. We found that for *n*-decane microemulsions, the boosting of PEO-*b*-PAlkGE and PEP-*b*-PEO polymers can be scaled on top of each other, when the efficiency is plotted semilogarithmically versus the polymeric coverage of the amphiphilic film. Interestingly, a somewhat different scaling behavior was observed for *n*-octacosane microemulsions stable at elevated temperatures, suggesting that the polymers show less self-avoidance and rather behave as almost ideal chains.

The influence of the new PEO-*b*-PAlkGE copolymers on the microstructure of the D_2O/NaCl−*n*-decane−$C_{10}E_4$ systems was studied by systematic SANS experiments performed close to the $\tilde{X}$ point of the boosted microemulsions and at a constant surfactant volume fraction close to the $\tilde{X}$ point of the polymer-free system. Particularly, the SANS curves obtained from the latter experiments indicate that the copolymers induce a considerably better ordering of the bicontinuous microstructure. To study the influence of the PEO-*b*-PAlkGE on the membrane's bending rigidity κ_{SANS}, the SANS data were analyzed using the model of random interfaces derived by Safran et al.[59,80,81] We found that the bending rigidity κ_{SANS} remains almost constant for boosted microemulsion prepared near their $\tilde{X}$ point. Being close to the stability limit of bicontinuous microemulsions, the effects of membrane stiffening via copolymer anchoring and membrane softening through thermal fluctuations compensate for each other. For the boosted microemulsions studied at a constant surfactant volume fraction close to the $\tilde{X}$ point of the polymer-free

https://dx.doi.org/10.1021/acs.langmuir.0c01491
Langmuir 2020, 36, 9849−9866

system, however, an increase of κ_{SANS} upon the polymeric coverage of the amphiphilic film is found.

By determining the bare bending rigidities κ_0, it was found that the pure $C_{10}E_4$ membrane in the *n*-decane microemulsion ($\kappa_0(C_{10}E_4/n\text{-decane}) = 1.08k_BT$ at $T = 302.2$ K) is slightly less rigid compared to the pure $C_{16}E_6$ membrane in the *n*-octacosane microemulsion ($\kappa_0(C_{16}E_6/n\text{-octacosane}) = 1.13k_BT$ at $T = 338.5$ K).

■ ASSOCIATED CONTENT

Supporting Information

The Supporting Information is available free of charge at https://pubs.acs.org/doi/10.1021/acs.langmuir.0c01491.

Synthesis of the amphiphilic diblock polycarbonates, overview of synthesized homopolymers and diblock copolymers, SEC measurements of the synthesized homopolymers, ^{1}H NMR spectra as well as DSC measurements of the synthesized diblock copolymers, tabular overview of the phase behavior and SANS results, and SANS curves of homopolymers and their analysis (PDF)

■ AUTHOR INFORMATION

Corresponding Author

Thomas Sottmann − *Institute of Physical Chemistry, University of Stuttgart, 70569 Stuttgart, Germany;* orcid.org/0000-0003-3679-3703; Phone: +49(0)711-685-64494; Email: thomas.sottmann@ipc.uni-stuttgart.de; Fax: +49(0) 711-685-64443

Authors

Kristina Schneider − *Institute of Physical Chemistry, University of Stuttgart, 70569 Stuttgart, Germany*

Patrick Verkoyen − *Department of Chemistry, Johannes Gutenberg University Mainz, 55128 Mainz, Germany*

Maximilian Krappel − *Institute of Physical Chemistry, University of Stuttgart, 70569 Stuttgart, Germany*

Christina Gardiner − *Department of Chemistry, Johannes Gutenberg University Mainz, 55128 Mainz, Germany*

Ralf Schweins − *Institut Laue-Langevin, 38042 Grenoble CEDEX 9, France;* orcid.org/0000-0001-8078-2089

Holger Frey − *Department of Chemistry, Johannes Gutenberg University Mainz, 55128 Mainz, Germany;* orcid.org/0000-0002-9916-3103

Complete contact information is available at: https://pubs.acs.org/10.1021/acs.langmuir.0c01491

Author Contributions

[‖]K.S. and P.V. have contributed equally.

Author Contributions

The manuscript was written through contributions of all authors. All authors have given approval to the final version of the manuscript.

Notes

The authors declare no competing financial interest.

■ ACKNOWLEDGMENTS

The authors thank the companies Clariant Produkte (Deutschland) GmbH and SASOL Germany GmbH for providing the technical-grade Genapol surfactants as well as for providing the technical-grade wax Sasolwax 5805. Furthermore, we would like to acknowledge the Institut Laue-Langevin (ILL) in Grenoble (France) for the allocation of beam-time under proposal 9-12-573 [doi: 10.5291/ILL-DATA.9-12-573] and David Bowyer for help with setting up the SANS environment. Additionally, we thank the Jülich Centre for Neutron Science (JCNS) at the Heinz Maier-Leibnitz Zentrum (MLZ) in Munich (Germany) and the National Institute of Standards and Technology (NIST) in Gaithersburg (USA) for providing the facilities for preliminary SANS experiments on PEO and PAlkGE homopolymers in D_2O and deuterated *n*-alkanes as well as the valuable support of the local contacts H. Frielinghaus (JCNS) and Y. Liu (NIST). Also, we acknowledge the help of the SANS teams consisting of K. Abitaev, J. Bruckner, S. Dieterich, J. Fischer, F. Gießelmann, S. Tseng and D. Zauser (Institute of Physical Chemistry, University of Stuttgart) during the SANS measurements. The authors also thank Monika Schmelzer for SEC measurements.

■ REFERENCES

(1) Schulman, J. H.; Stoeckenius, W.; Prince, L. M. Mechanism of Formation and Structure of Micro Emulsions by Electron Microscopy. *J. Phys. Chem.* **1959**, *63*, 1677−1680.

(2) Strey, R. Microemulsion microstructure and interfacial curvature. *Colloid Polym. Sci.* **1994**, 272, 1005−1019.

(3) Langevin, D. Low Interfacial Tensions in Microemulsion Systems. In *Structure and Dynamics of Strongly Interacting Colloids and Supramolecular Aggregates in Solution*; Springer Netherlands: Dordrecht, 1992, DOI: 10.1007/978-94-011-2540-6_14.

(4) Aveyard, R.; Binks, B. P.; Clark, S.; Mead, J. Interfacial tension minima in oil−water−surfactant systems. Behaviour of alkane−aqueous NaCl systems containing aerosol OT. *J. Chem. Soc., Faraday Trans. 1* **1986**, *82*, 125−142.

(5) Sottmann, T.; Strey, R. Shape Similarities of Ultra-Low Interfacial Tension Curves in Ternary Microemulsion Systems of the Water-Alkane-C_iE_j Type. *Ber. Bunsenges. Phys. Chem.* **1996**, *100*, 237−241.

(6) Sottmann, T.; Strey, R. Ultralow interfacial tensions in water−*n*-alkane−surfactant systems. *J. Chem. Phys.* **1997**, *106*, 8606−8615.

(7) Sottmann, T.; Strey, R. Microemulsions, In: Fundamentals of Interface and Colloid Science: Soft Colloids, 1. Aufl. In *Fundamentals of Interface and Colloid Science*; Elsevier professional, s.l., 2005.

(8) Scheibel, J. J. The evolution of anionic surfactant technology to meet the requirements of the laundry detergent industry. *J. Surfactants Deterg.* **2004**, *7*, 319−328.

(9) Bajpai, D.; Tyagi, V. K. Laundry Detergents: An Overview. *J. Oleo Sci.* **2007**, *56*, 327−340.

(10) Shah, D. O. *Improved oil recovery by surfactant and polymer flooding*; Elsevier, 2012.

(11) Nazar, M. F.; Shah, S. S.; Khosa, M. A. Microemulsions in Enhanced Oil Recovery: A Review. *Pet. Sci. Technol.* **2011**, *29*, 1353−1365.

(12) Anderberg, E. K.; Nyström, C.; Artursson, P. Epithelial transport of drugs in cell culture. VII: Effects of pharmaceutical surfactant excipients and bile acids on transepithelial permeability in monolayers of human intestinal epithelial (Caco-2) cells. *J. Pharm. Sci.* **1992**, *81*, 879−887.

(13) Merchán Arenas, D. R.; Martínez Bonilla, C. A.; Kouznetsov, V. V. Aqueous SDS micelle-promoted acid-catalyzed domino ABB' imino Diels-Alder reaction: a mild and efficient synthesis of privileged 2-methyl-tetrahydroquinoline scaffolds. *Org. Biomol. Chem.* **2013**, *11*, 3655−3663.

(14) La Sorella, G.; Strukul, G.; Scarso, A. Recent advances in catalysis in micellar media. *Green Chem.* **2015**, *17*, 644−683.

(15) Sottmann, T. Solubilization efficiency boosting by amphiphilic block co-polymers in microemulsions. *Curr. Opin. Colloid Interface Sci.* **2002**, *7*, 57−65.

https://dx.doi.org/10.1021/acs.langmuir.0c01491
Langmuir 2020, 36, 9849−9866

(16) Jakobs, B.; Sottmann, T.; Strey, R.; Allgaier, J.; Richter, D. Amphiphilic Block Copolymers as Efficiency Boosters for Microemulsions. *Langmuir* **1999**, *15*, 6707−6711.
(17) Jakobs, B.; Sottmann, T.; Strey, R. Efficiency boosting with amphiphilic block copolymers: a new approach to microemulsion formulation. *Tenside, Surfactants, Deterg.* **2000**, *37*, 357−364.
(18) Allgaier, J.; Poppe, A.; Willner, L.; Richter, D. Synthesis and Characterization of Poly[1,4-isoprene- b -(ethylene oxide)] and Poly[ethylene- co -propylene- b -(ethylene oxide)] Block Copolymers. *Macromolecules* **1997**, *30*, 1582−1586.
(19) Poppe, A.; Willner, L.; Allgaier, J.; Stellbrink, J.; Richter, D. Structural Investigation of Micelles Formed by an Amphiphilic PEP−PEO Block Copolymer in Water. *Macromolecules* **1997**, *30*, 7462−7471.
(20) Frank, C.; Sottmann, T.; Stubenrauch, C.; Allgaier, J.; Strey, R. Influence of amphiphilic block copolymers on lyotropic liquid crystals in water-oil-surfactant systems. *Langmuir* **2005**, *21*, 9058−9067.
(21) Endo, H.; Allgaier, J.; Gompper, G.; Jakobs, B.; Monkenbusch, M.; Richter, D.; Sottmann, T.; Strey, R. Membrane decoration by amphiphilic block copolymers in bicontinuous microemulsions. *Phys. Rev. Lett.* **2000**, *85*, 102−105.
(22) Gompper, G.; Endo, H.; Mihailescu, M.; Allgaier, J.; Monkenbusch, M.; Richter, D.; Jakobs, B.; Sottmann, T.; Strey, R. Measuring bending rigidity and spatial renormalization in bicontinuous microemulsions. *Europhys. Lett.* **2001**, *56*, 683−689.
(23) Helfrich, W. Elastic properties of lipid bilayers: Theory and Possible Experiments. *Z. Naturforsch., C* **1973**, *28*, 693−703.
(24) Lipowsky, R. Bending of Membranes by Anchored Polymers. *Europhys. Lett.* **1995**, *30*, 197−202.
(25) Lipowsky, R.; Döbereiner, H.-G.; Hiergeist, C.; Indrani, V. Membrane curvature induced by polymers and colloids. *Phys. A* **1998**, *249*, 536−543.
(26) Endo, H.; Mihailescu, M.; Monkenbusch, M.; Allgaier, J.; Gompper, G.; Richter, d.; Jakobs, B.; Sottmann, T.; Strey, R.; Grillo, I. Effect of amphiphilic block copolymers on the structure and phase behavior of oil−water-surfactant mixtures. *J. Chem. Phys.* **2001**, *115*, 580−600.
(27) Nilsson, M.; Söderman, O.; Johansson, I. The effect of polymers on the phase behavior of balanced microemulsions: diblock-copolymer and comb-polymers. *Colloid Polym. Sci.* **2006**, *284*, 1229−1241.
(28) Byelov, D.; Frielinghaus, H.; Holderer, O.; Allgaier, J.; Richter, D. Microemulsion efficiency boosting and the complementary effect. 1. Structural properties. *Langmuir* **2004**, *20*, 10433−10443.
(29) Gompper, G.; Richter, D.; Strey, R. Amphiphilic block copolymers in oil-water-surfactant mixtures: efficiency boosting, structure, phase behaviour and mechanism: Efficiency boosting, structure, phase behaviour and mechanism. *J. Phys.: Condens. Matter* **2001**, *13*, 9055−9074.
(30) Klemmer, H. F. M.; Allgaier, J.; Frielinghaus, H.; Holderer, O.; Ohl, M. Influence of the amphiphilicity profile of copolymers on the formation of liquid crystalline mesophases in microemulsions. *Colloid Polym. Sci.* **2017**, *295*, 911−923.
(31) Kunze, L.; Tseng, S.-Y.; Schweins, R.; Sottmann, T.; Frey, H. Nonionic Aliphatic Polycarbonate Diblock Copolymers Based on CO2, 1,2-Butylene Oxide, and mPEG: Synthesis, Micellization, and Solubilization. *Langmuir* **2019**, *35*, 5221−5231.
(32) Foster, T.; Sottmann, T.; Schweins, R.; Strey, R. Small-angle-neutron-scattering from giant water-in-oil microemulsion droplets II. Polymer-decorated droplets in a quaternary system. *J. Chem. Phys.* **2008**, *128*, No. 064902.
(33) Frank, C.; Frielinghaus, H.; Allgaier, J.; Richter, D. Hydrophilic alcohol ethoxylates as efficiency boosters for microemulsions. *Langmuir* **2008**, *24*, 6036−6043.
(34) Brodeck, M.; Maccarrone, S.; Saha, D.; Willner, L.; Allgaier, J.; Mangiapia, G.; Frielinghaus, H.; Holderer, O.; Faraone, A.; Richter, D. Asymmetric polymers in bicontinuous microemulsions and their accretion to the bending of the membrane. *Colloid Polym. Sci.* **2015**, *293*, 1253−1265.
(35) Hoehn, S.; Schulreich, C.; Hellweg, T. Efficiency Boosting in Technical Grade Sugar Surfactant Based Microemulsions Using Pluronics. *Tenside, Surfactants, Deterg.* **2014**, *51*, 32−39.
(36) Takahashi, Y.; Shirahata, H.; Nishimura, T.; Murai, M.; Wakita, K.; Kondo, Y. Boosting Effect of Amphiphilic Random Copolymers for Bicontinuous Phases. *J. Oleo Sci.* **2018**, *67*, 531−537.
(37) Marchal, F.; Guenoun, P.; Daillant, J.; Holley, D. W.; Mays, J. W. Unprecedented microemulsion boosting effect induced by a charged diblock copolymer: bending modulus and curvature frustration of the surfactant film. *Soft Matter* **2009**, *5*, 4006.
(38) Tchekountieu Mboumi, L. J. Technisch relevante amphiphile Blockcopolymere in Mikroemulsionen: Dissertation. 2010.
(39) Beisser, R.; Allgaier, J.; Hillerich, J. Microemulsion-based cleaning agent comprising an anionic/nonionic surfactant mixture. US 9,150,823 B2, 2015.
(40) Verkoyen, P.; Johann, T.; Blankenburg, J.; Czysch, C.; Frey, H. Polymerization of long chain alkyl glycidyl ethers: a platform for micellar gels with tailor-made melting points. *Polym. Chem.* **2018**, *9*, 5327−5338.
(41) Petrov, P.; Rangelov, S.; Novakov, C.; Brown, W.; Berlinova, L.; Tsvetanov, C. B. Core-corona nanoparticles formed by high molecular weight poly(ethylene oxide)-b-poly(alkylglycidyl ether) diblock copolymers. *Polymer* **2002**, *43*, 6641−6651.
(42) Liu, F.; Frere, Y.; Francois, J. Association properties of poly(ethylene oxide) modified by pendant aliphatic groups. *Polymer* **2001**, *42*, 2969−2983.
(43) Satoh, Y.; Miyachi, K.; Matsuno, H.; Isono, T.; Tajima, K.; Kakuchi, T.; Satoh, T. Synthesis of Well-Defined Amphiphilic Star-Block and Miktoarm Star Copolyethers via t -Bu-P_4 -Catalyzed Ring-Opening Polymerization of Glycidyl Ethers. *Macromolecules* **2016**, *49*, 499−509.
(44) Schneider, K.; Ott, T. M.; Schweins, R.; Frielinghaus, H.; Lade, O.; Sottmann, T. Phase Behavior and Microstructure of Symmetric Nonionic Microemulsions with Long-Chain *n* -Alkanes and Waxes. *Ind. Eng. Chem. Res.* **2019**, *58*, 2583−2595.
(45) Kahlweit, M.; Strey, R.; Busse, G. Microemulsions: a qualitative thermodynamic approach. *J. Phys. Chem.* **1990**, *94*, 3881−3894.
(46) Kahlweit, M.; Strey, R. Phase Behavior of Ternary Systems of the Type H_2O-Oil-Nonionic Amphiphile (Microemulsions). *Angew. Chem., Int. Ed.* **1985**, *24*, 654−668.
(47) Burauer, S.; Sachert, T.; Sottmann, T.; Strey, R. On microemulsion phase behavior and the monomeric solubility of surfactant. *Phys. Chem. Chem. Phys.* **1999**, *1*, 4299−4306.
(48) Sottmann, T.; Strey, R.; Chen, S.-H. A small-angle neutron scattering study of nonionic surfactant molecules at the water−oil interface: Area per molecule, microemulsion domain size, and rigidity. *J. Chem. Phys.* **1997**, *106*, 6483−6491.
(49) Shi, W.; McGrath, A. J.; Li, Y.; Lynd, N. A.; Hawker, C. J.; Fredrickson, G. H.; Kramer, E. J. Cooperative and Sequential Phase Transitions in it -Poly(propylene oxide)- b -poly(ethylene oxide)-*b-it* -poly(propylene oxide) Triblock Copolymers. *Macromolecules* **2015**, *48*, 3069−3079.
(50) McGrath, A. J.; Shi, W.; Rodriguez, C. G.; Kramer, E. J.; Hawker, C. J.; Lynd, N. A. Synthetic Strategy for Preparing Chiral Double-semicrystalline Polyether Block Copolymers. *Polym. Chem.* **2015**, *6*, 1465−1473.
(51) Shin, D.; Shin, K.; Aamer, K. A.; Tew, G. N.; Russell, T. P.; Lee, J. H.; Jho, J. Y. A Morphological Study of a Semicrystalline Poly(l -lactic acid- b -ethylene oxide- b - l -lactic acid) Triblock Copolymer. *Macromolecules* **2005**, *38*, 104−109.
(52) Hiergeist, C.; Lipowsky, R. Elastic Properties of Polymer-Decorated Membranes. *J. Phys. II Fr.* **1996**, *6*, 1465−1481.
(53) Teubner, M.; Strey, R. Origin of the scattering peak in microemulsions. *J. Chem. Phys.* **1987**, *87*, 3195−3200.
(54) Schelten, J.; Schmatz, W. Multiple-scattering treatment for small-angle scattering problems. *J. Appl. Crystallogr.* **1980**, *13*, 385−390.

https://dx.doi.org/10.1021/acs.langmuir.0c01491
Langmuir 2020, 36, 9849−9866

(55) Silas, J. A.; Kaler, E. W. Effect of multiple scattering on SANS spectra from bicontinuous microemulsions. *J. Colloid Interface Sci.* **2003**, *257*, 291−298.
(56) Gradzielski, M.; Langevin, D.; Sottmann, T.; Strey, R. Small angle neutron scattering near the wetting transition: Discrimination of microemulsions from weakly structured mixtures. *J. Chem. Phys.* **1996**, *104*, 3782−3787.
(57) Schubert, K.-V.; Strey, R. Small-angle neutron scattering from microemulsions near the disorder line in water/formamide−octane-C_iE_j systems. *J. Chem. Phys.* **1991**, *95*, 8532−8545.
(58) Schubert, K.-V.; Strey, R.; Kline, S. R.; Kaler, E. W. Small angle neutron scattering near Lifshitz lines: Transition from weakly structured mixtures to microemulsions. *J. Chem. Phys.* **1994**, *101*, 5343−5355.
(59) Pieruschka, P.; Safran, S. A.; Marčelja, S. T. Comment on "Fluctuating interfaces in microemulsion and sponge phases". *Phys. Rev. E* **1995**, *52*, 1245−1247.
(60) Peltomäki, M.; Gompper, G.; Kroll, D. M. Scattering intensity of bicontinuous microemulsions and sponge phases. *J. Chem. Phys.* **2012**, *136*, 134708.
(61) Holderer, O.; Frielinghaus, H.; Monkenbusch, M.; Klostermann, M.; Sottmann, T.; Richter, D. Experimental determination of bending rigidity and saddle splay modulus in bicontinuous microemulsions. *Soft Matter* **2013**, *9*, 2308.
(62) Morse, D. C. Topological instabilities and phase behavior of fluid membranes. *Phys. Rev. E* **1994**, *50*, 2423−2426.
(63) Gompper, G.; Kroll, D. M. Membranes with Fluctuating Topology: Monte Carlo Simulations. *Phys. Rev. Lett.* **1998**, *81*, 2284−2287.
(64) Golubović, L. Passages and droplets in lamellar fluid membrane phases. *Phys. Rev. E* **1994**, *50*, 2419−2422.
(65) Lyklema, J. *Fundamentals of Interface and Colloid Science: Soft Colloids*; Fundamentals of Interface and Colloid Science, 1. Aufl.; Fundamentals of Interface and Colloid Science v.v. 5; Elsevier professional, s.l., 2005.
(66) Aubry, J.-M.; Ontiveros, J. F.; Salager, J.-L.; Nardello-Rataj, V. Use of the normalized hydrophilic-lipophilic-deviation (HLDN) equation for determining the equivalent alkane carbon number (EACN) of oils and the preferred alkane carbon number (PACN) of nonionic surfactants by the fish-tail method (FTM). *Adv. Colloid Interface Sci.* **2020**, *276*, 102099.
(67) Sagalowicz, L.; Leser, M. E.; Watzke, H. J.; Michel, M. Monoglyceride self-assembly structures as delivery vehicles. *Trends Food Sci. Technol.* **2006**, *17*, 204−214.
(68) Attard, G. S.; Glyde, J. C.; Göltner, C. G. Liquid-crystalline phases as templates for the synthesis of mesoporous silica. *Nature* **1995**, *378*, 366−368.
(69) Solans, C.; Kunieda, H. *Industrial applications of microemulsions*; In Surfactant science series 66; Dekker: New York, NY, 1997.
(70) Lipowsky, R. Flexible membranes with anchored polymers. *Colloids Surf., A* **1997**, *128*, 255−264.
(71) Sottmann, T.; Lade, M.; Stolz, M.; Schomäcker, R. Phase behavior of non-ionic microemulsions prepared from technical-grade surfactants. *Tenside, Surfactants, Deterg.* **2002**, *39*, 20−28.
(72) Jakobs, B. *Amphiphile Blockcopolymere als Efficiency Booster für Tenside*; 1st ed.; Cuvillier Verlag: Göttingen, 2001.
(73) Hammouda, B.; Ho, D. L. Insight into chain dimensions in PEO/water solutions. *J. Polym. Sci., Part B: Polym. Phys.* **2007**, *45*, 2196−2200.
(74) Hammouda, B.; Ho, D. L.; Kline, S. Insight into Clustering in Poly(ethylene oxide) Solutions. *Macromolecules* **2004**, *37*, 6932−6937.
(75) Hammouda, B.; Ho, D.; Kline, S. SANS from Poly(ethylene oxide)/Water Systems. *Macromolecules* **2002**, *35*, 8578−8585.
(76) Glatter, O.; Kratky, O. *Small angle X-ray scattering*; 2nd printing 36; Academic Press: London, 1982.
(77) Kawaguchi, S.; Imai, G.; Suzuki, J.; Miyahara, A.; Kitano, T.; Ito, K. Aqueous solution properties of oligo- and poly(ethylene oxide) by static light scattering and intrinsic viscosity. *Polymer* **1997**, *38*, 2885−2891.
(78) Auth, T.; Gompper, G. Self-avoiding linear and star polymers anchored to membranes. *Phys. Rev. E* **2003**, *68*, No. 051801.
(79) Auth, T.; Gompper, G. Fluctuation spectrum of membranes with anchored linear and star polymers. *Phys. Rev. E* **2005**, *72*, 031904.
(80) Pieruschka, P.; Safran, S. A. Random Interface Model of Sponge Phases. *Europhys. Lett.* **1995**, *31*, 207−212.
(81) Pieruschka, P.; Safran, S. A. Random Interfaces and the Physics of Microemulsions. *Europhys. Lett.* **1993**, *22*, 625−630.

https://dx.doi.org/10.1021/acs.langmuir.0c01491
Langmuir 2020, 36, 9849−9866

SUPPORTING INFORMATION

Efficiency Boosting of Surfactants with Poly(ethylene oxide)—Poly(alkyl glycidyl ether)s – A New Class of Amphiphilic Polymers

*Kristina Schneider[§,a], Patrick Verkoyen[§,b], Maximilian Krappel[a], Christina Gardiner[b], R. Schweins[c], Holger Frey[b], Thomas Sottmann[a]**

a. Institute of Physical Chemistry, University of Stuttgart, Pfaffenwaldring 55, 70569 Stuttgart, Germany

b. Department of Chemistry, Johannes Gutenberg University Mainz, Duesbergweg 10-14, 55128 Mainz, Germany.

c. Institut Laue-Langevin, DS/LSS, 71 avenue des Martyrs, CS 20156, 38042 Grenoble CEDEX 9, France

*Corresponding author: thomas.sottmann@ipc.uni-stuttgart.de, Tel. +49(0)711-685-64494, Fax. +49(0)711-685-64443

[§]These authors have contributed equally: Kristina Schneider and Patrick Verkoyen.

Table of Contents

1. Route of Synthesis of Amphiphilic Diblock Polycarbonates and Overview of the Synthesized Homopolymers and Diblock Copolymers

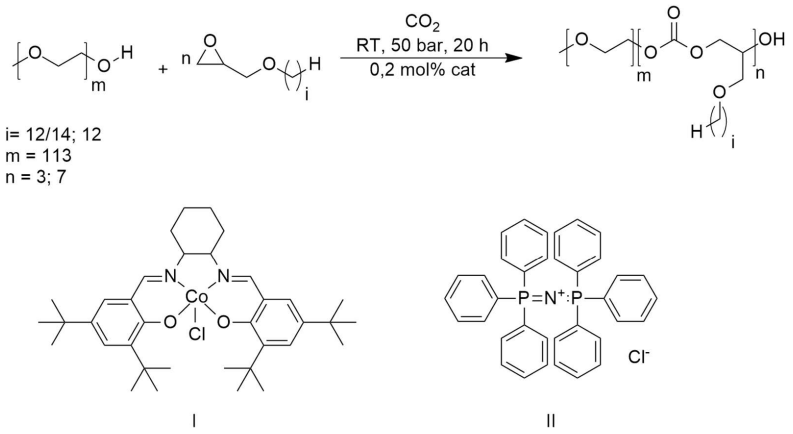

Scheme 1. Synthesis of amphiphilic diblock polycarbonates using Me-PEO as chain transfer agent, long-chain alkyl glycidyl ethers (C_{12}GE and a $C_{12/14}$GE technical-grade mixture) and carbon dioxide as monomers. For polymerization, the catalyst I and the co-catalyst II were used.

Table S1. Synthesized homopolymers and diblock copolymers, calculated molar masses $M_{n,theo}$, experimentally determined molar masses $M_{n,exp}$ and $M_{w,exp}$, as well as molar mass distributions $Đ$ obtained from SEC[b], melting temperatures (T_m) of the two polymer blocks and yields.

Polymer sample	$M_{n,theo}$ / g mol^{-1}	$M_{n,exp}$ / g mol^{-1} [a]	$M_{w,exp}$ / g mol^{-1} [a]	$Đ$ [a]	T_m / °C [b]	ΔH_m / J g^{-1} [b]	Yield / %
BnO-P(C_{12}GE)$_6$	1710	2500	2680	1.06	-	-	80
BnO-P(C_{12}GE)$_{14}$	3649	3600	3960	1.09	-	-	83
BnO-P(C_{12}GE)$_{18}$	4619	4600	4820	1.06	-	-	79
Me-P(EO)$_{113}$-*b*-P(C_{12}GE)$_3$	5699	5400	5810	1.05	-4; 55	2; 136	92
Me-P(EO)$_{113}$-*b*-P(C_{12}GE)$_6$	6426	5800	6520	1.08	1; 53	5; 75	98
Me-P(EO)$_{113}$-*b*-P(C_{12}GE)$_7$	6668	6500	6880	1.06	-	-	80
Me-P(EO)$_{113}$-*b*-P(C_{12}GE)$_8$	6911	6500	6750	1.06	3; 53	14; 131	68
Me-P(EO)$_{113}$-*b*-P(C_{16}GE)$_3$	5866	5400	5660	1.04	56	148	87
Me-P(EO)$_{113}$-*b*-P(C_{16}GE)$_6$	6760	5800	6460	1.06	35; 53	10; 114	82
Me-P(EO)$_{113}$-*b*-P(C_{16}GE)$_9$	7654	6600	6420	1.05	38; 52	20; 103	70
Me-P(EO)$_{113}$-*b*-P(CO_2C_{12}GE)$_3$	5831	5900	6180	1.04	-3; 54	6; 131	40
Me-P(EO)$_{113}$-*b*-P(CO_2C_{12}GE)$_9$	7549	6600	6990	1.05	-2; 54	8; 113	60
Me-P(EO)$_{113}$-*b*-P($CO_2C_{12/14}$GE)$_3$	5872	5500	6160	1.06	3; 55	9; 125	59
Me-P(EO)$_{113}$-*b*-P($CO_2C_{12/14}$GE)$_7$	7072	6800	7150	1.05	-3; 53	6; 107	28

[a] Determined by SEC (eluent: DMF, calibration: PEO standards, and THF, PS standards for the homopolymers); [b] measured by DSC, the first-mentioned melting temperature (T_m) can be assigned to the alkyl glycidyl ether (chain) block and the second T_m can be assigned to the PEO block, respectively. ΔH_m represents the determined melting enthalpy.

2. SEC Measurements of the Synthesized Homopolymers

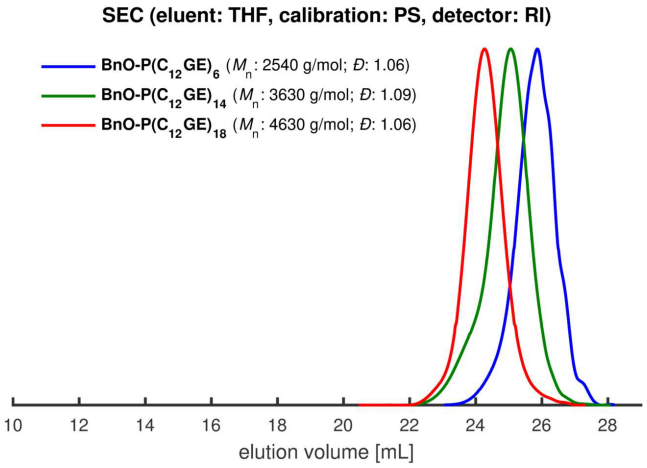

Figure S1. SEC traces of the synthesized homopolymers using C_{12}GE and Benzyloxy ethanol (BnO) as initiator (eluent: THF, calibration: PS standards).

3. DSC Curves of the Synthesized Diblock Copolymers

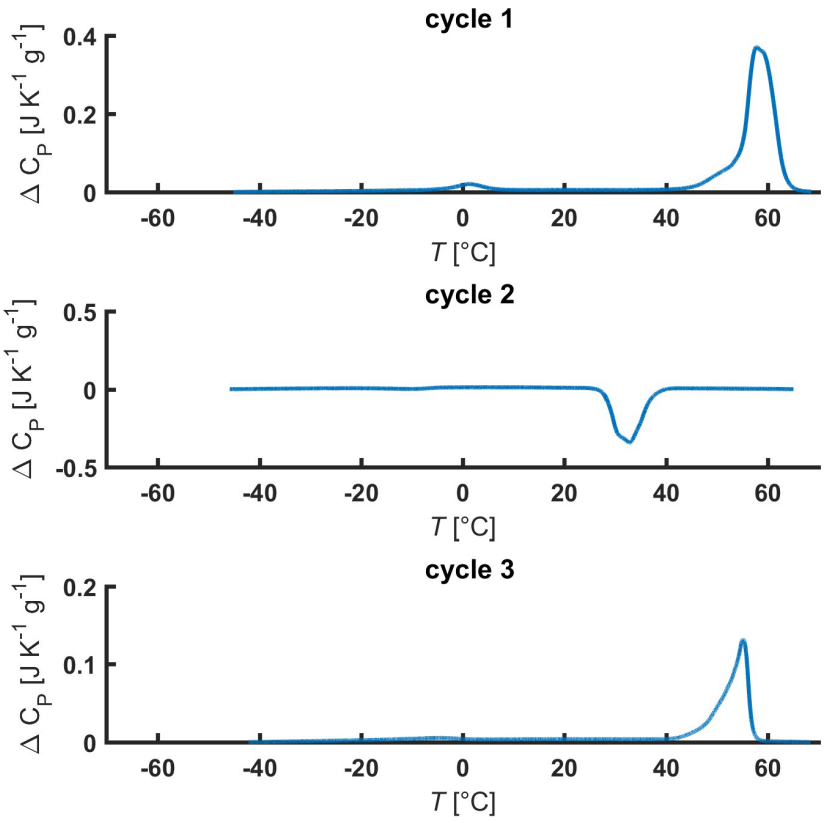

Figure S2. Heating, cooling, and heating cycles of the synthesized diblock copolymer Me-P(EO)$_{113}$-*b*-P(C$_{12}$GE)$_3$; Heating rates: first heating cycle: 20 K min^{-1}, cooling and second heating cycle: 10 K min^{-1}.

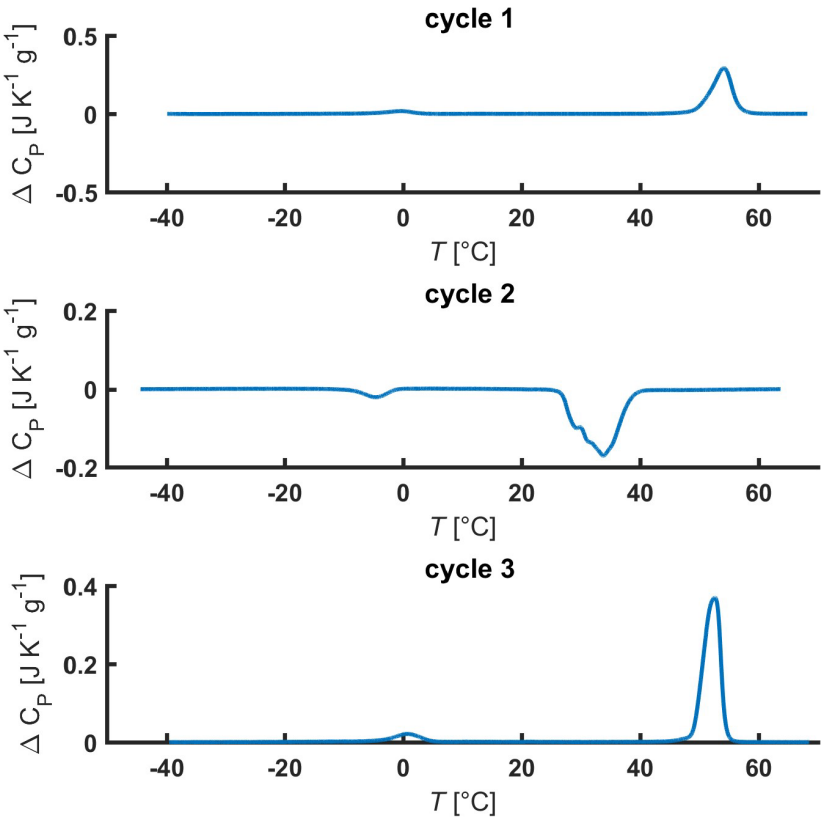

Figure S3. Heating, cooling, and heating cycles of the synthesized diblock copolymer Me-P(EO)$_{113}$-*b*-P(C$_{12}$GE)$_6$; Heating rates: first heating cycle: 20 K min^{-1} , cooling and second heating cycle: 10 K min^{-1}.

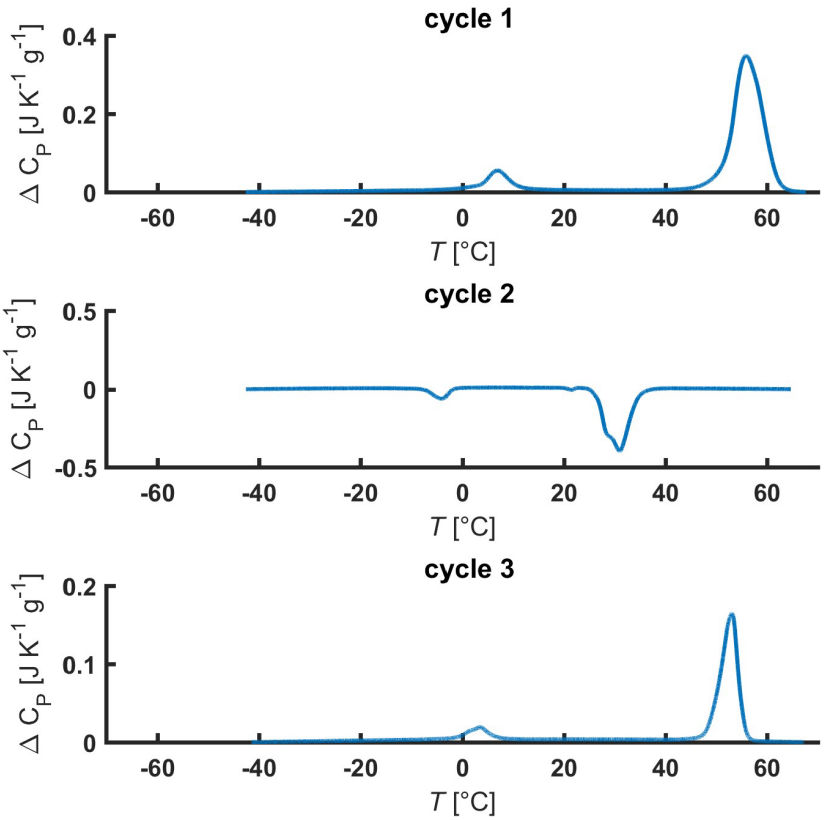

Figure S4. Heating, cooling, and heating cycles of the synthesized diblock copolymer Me-P(EO)$_{113}$-*b*-P(C$_{12}$GE)$_8$; Heating rates: first heating cycle: 20 K min^{-1}, cooling and second heating cycle: 10 K min^{-1}.

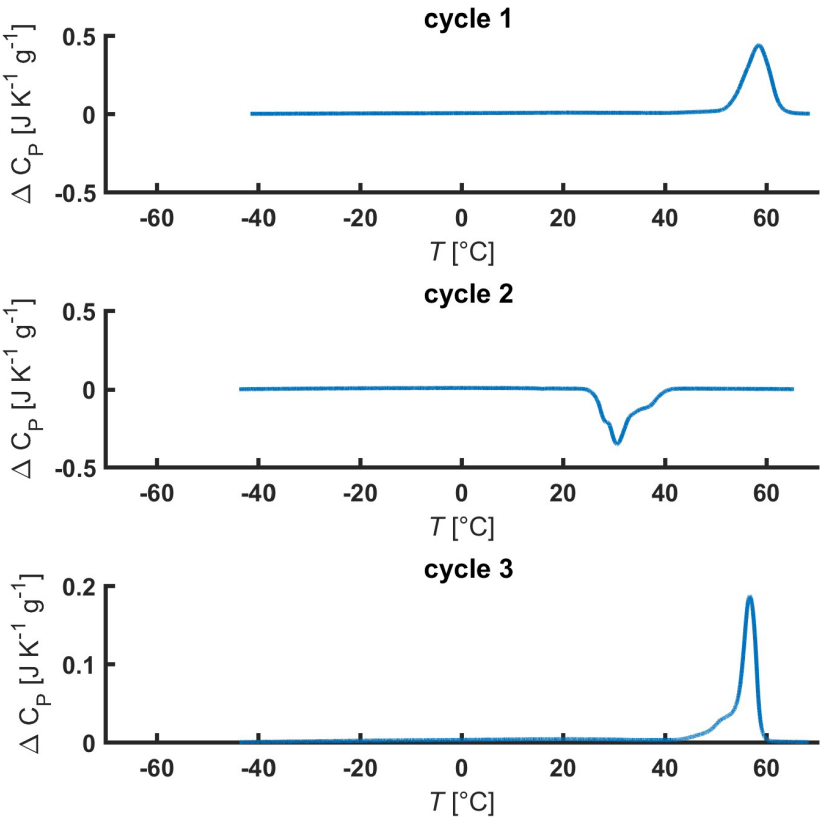

Figure S5. Heating, cooling, and heating cycles of the synthesized diblock copolymer Me-P(EO)$_{113}$-*b*-P(C$_{16}$GE)$_3$; Heating rates: first heating cycle: 20 K min^{-1} , cooling and second heating cycle: 10 K min^{-1}.

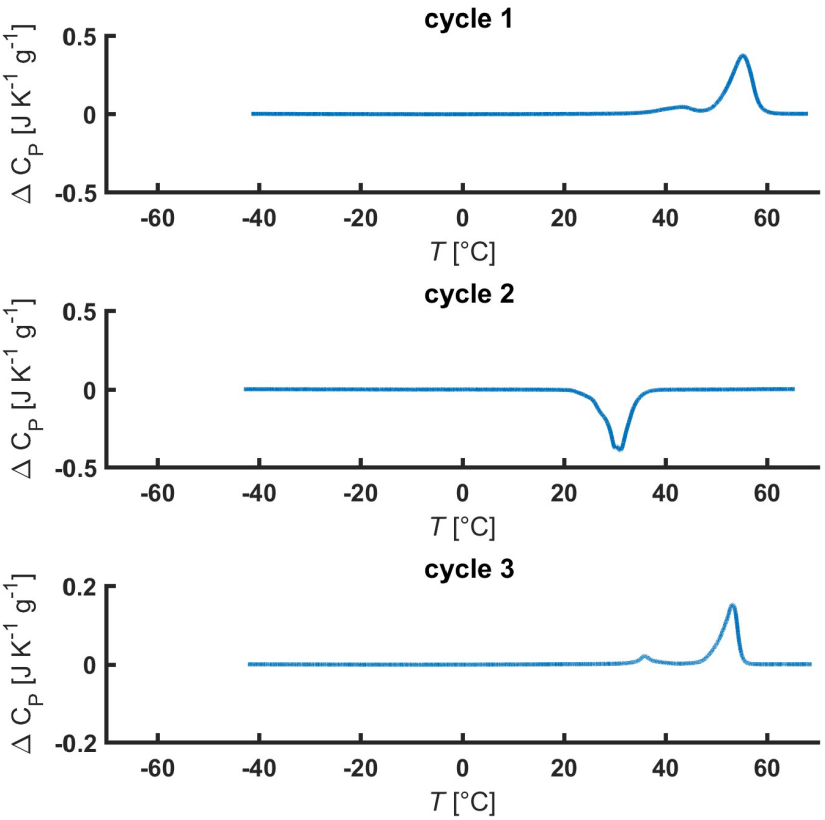

Figure S6. Heating, cooling, and heating cycles of the synthesized diblock copolymer Me-P(EO)$_{113}$-*b*-P(C$_{16}$GE)$_6$; Heating rates: first heating cycle: 20 K min^{-1}, cooling and second heating cycle: 10 K min^{-1}.

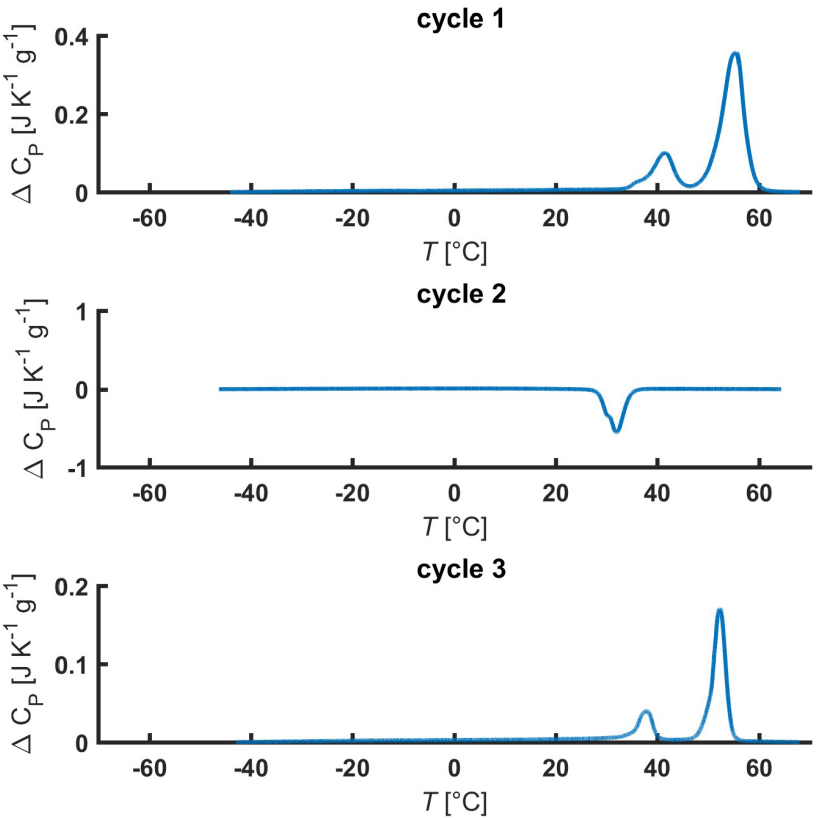

Figure S7. Heating, cooling, and heating cycles of the synthesized diblock copolymer Me-P(EO)$_{113}$-*b*-P(C$_{16}$GE)$_9$; Heating rates: first heating cycle: 20 K min^{-1}, cooling and second heating cycle: 10 K min^{-1}.

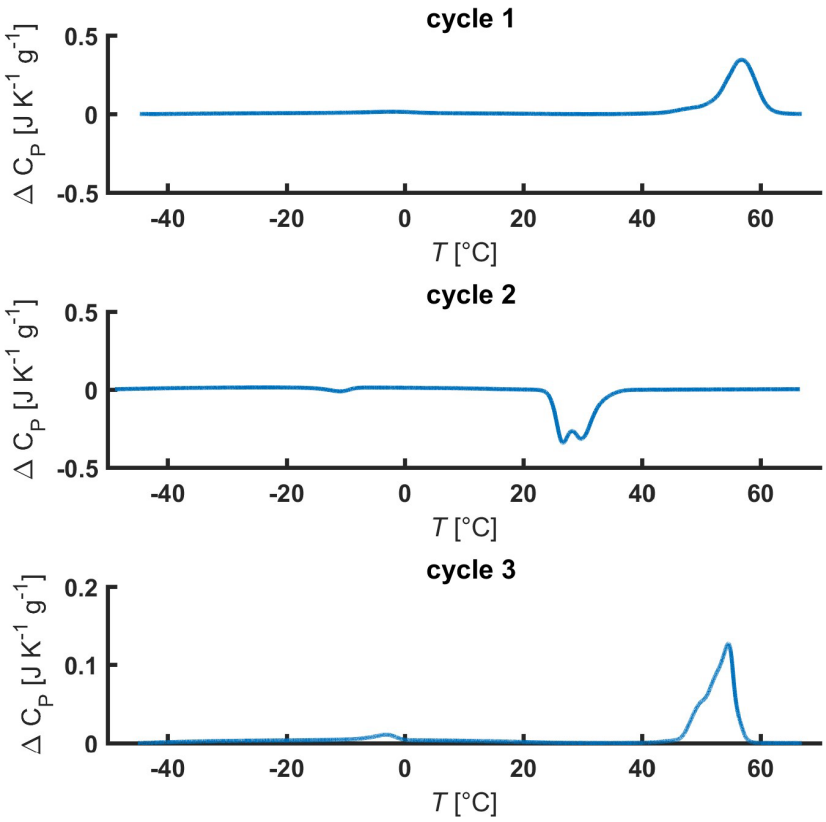

Figure S8. Heating, cooling, and heating cycles of the synthesized diblock copolymer Me-P(EO)$_{113}$-*b*-P(CO$_2$C$_{12}$GE)$_3$; Heating rates: first heating cycle: 20 K min^{-1}, cooling and second heating cycle: 10 K min^{-1}.

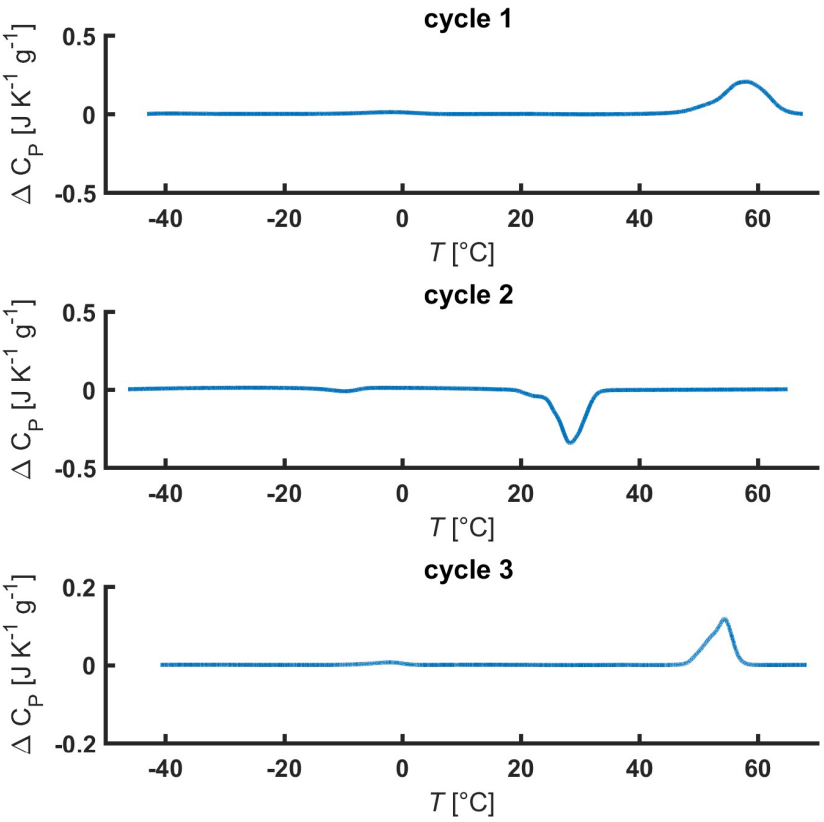

Figure S9. Heating, cooling, and heating cycles of the synthesized diblock copolymer Me-P(EO)$_{113}$-*b*-P(CO$_2$C$_{12}$GE)$_9$; Heating rates: first heating cycle: 20 K min^{-1}, cooling and second heating cycle: 10 K min^{-1}.

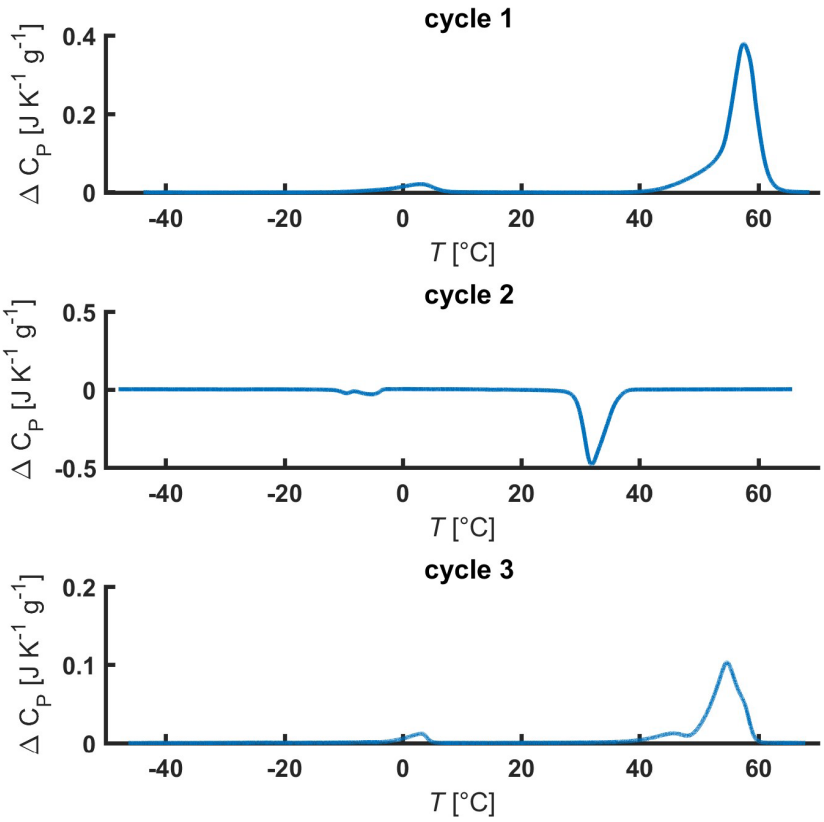

Figure S10. Heating, cooling, and heating cycles of the synthesized diblock copolymer Me-P(EO)$_{113}$-*b*-P($CO_2C_{12/14}$)$_3$; Heating rates: first heating cycle: 20 K min^{-1}, cooling and second heating cycle: 10 K min^{-1}.

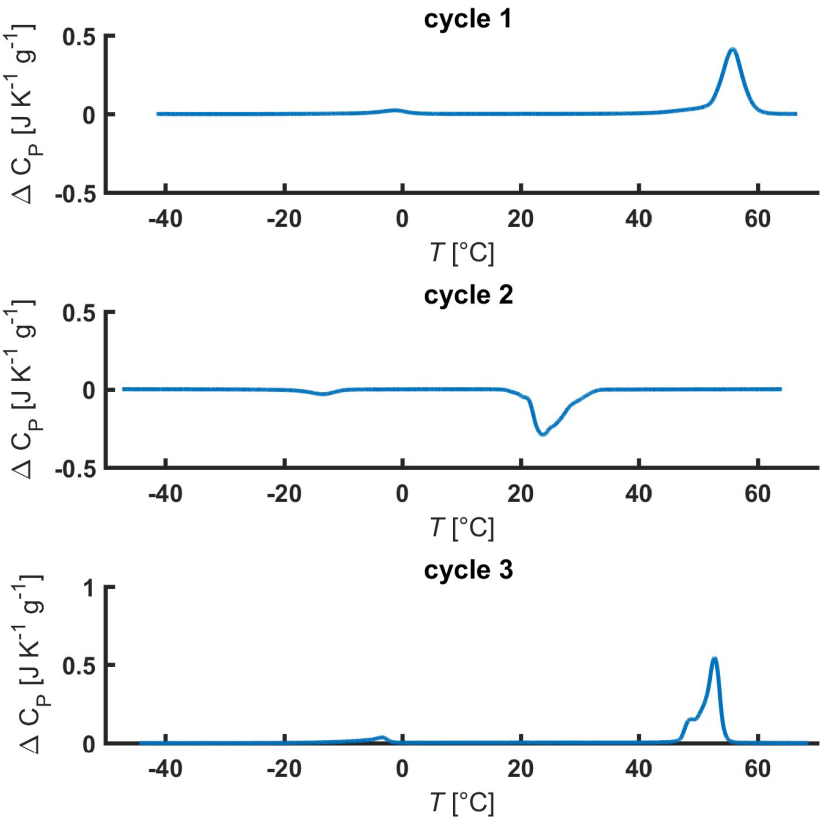

Figure S11. Heating, cooling, and heating cycles of the synthesized diblock copolymer Me-P(EO)$_{113}$-*b*-P(CO$_2$C$_{12/14}$)$_7$; Heating rates: first heating cycle: 20 K min^{-1}, cooling and second heating cycle: 10 K min^{-1}.

4. ^{1}H NMR Spectra of the Diblock Copolymers

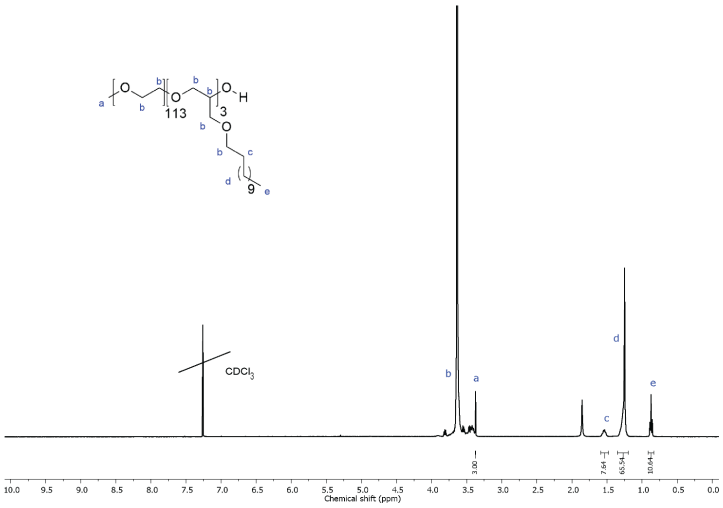

Figure S12. ^{1}H NMR spectrum (300 MHz, chloroform-d) of Me-P(EO)$_{113}$-*b*-P(C$_{12}$GE)$_{3}$.

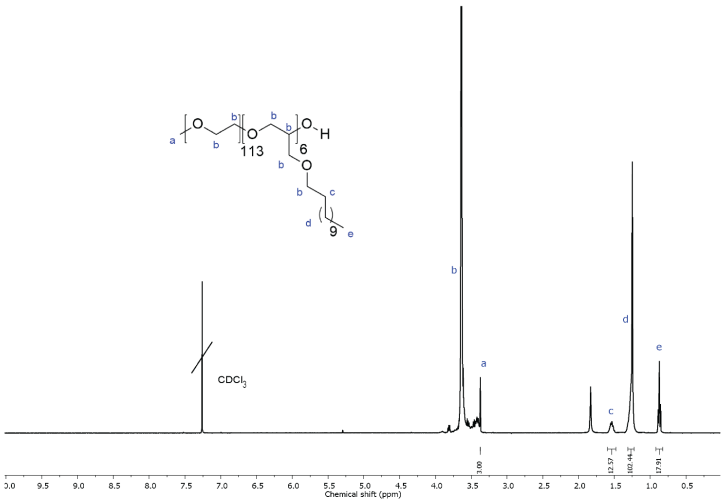

Figure S13. ^{1}H NMR spectrum (300 MHz, chloroform-d) of Me-P(EO)$_{113}$-*b*-P(C$_{12}$GE)$_{6}$.

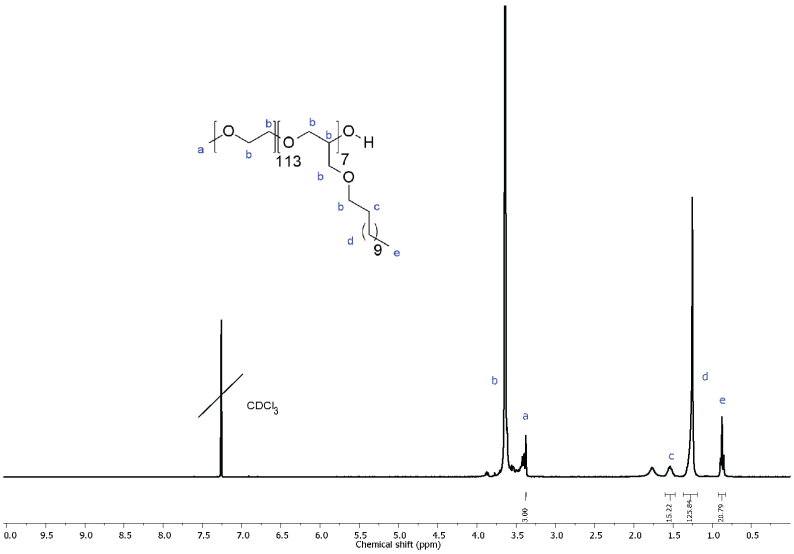

Figure S14. ^{1}H NMR spectrum (300 MHz, chloroform-d) of Me-P(EO)$_{113}$-*b*-P(C$_{12}$GE)$_{7}$.

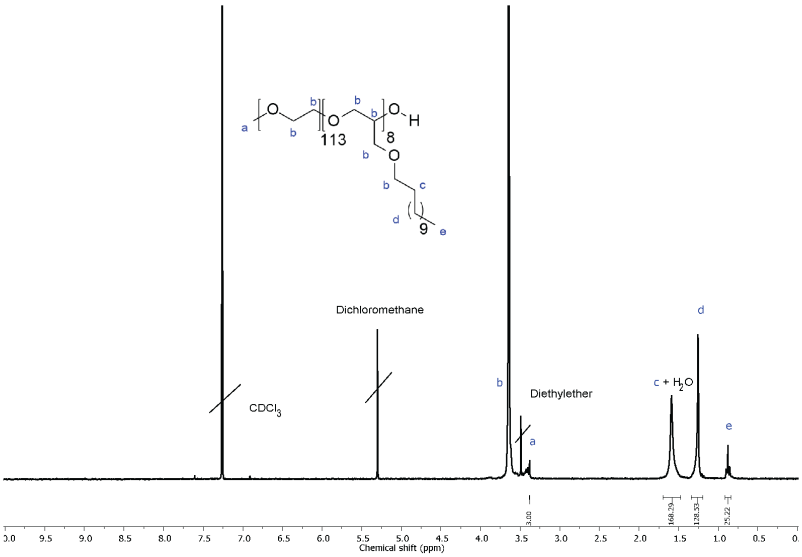

Figure S15. ^{1}H NMR spectrum (300 MHz, chloroform-d) of Me-P(EO)$_{113}$-*b*-P(C$_{12}$GE)$_{8}$.

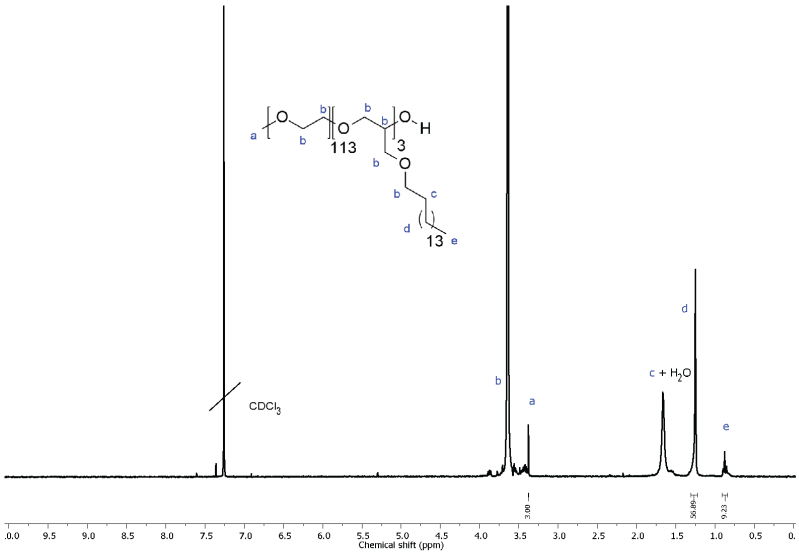

Figure S16. ^{1}H NMR spectrum (300 MHz, chloroform-d) of Me-P(EO)$_{113}$-*b*-P(C$_{16}$GE)$_{3}$.

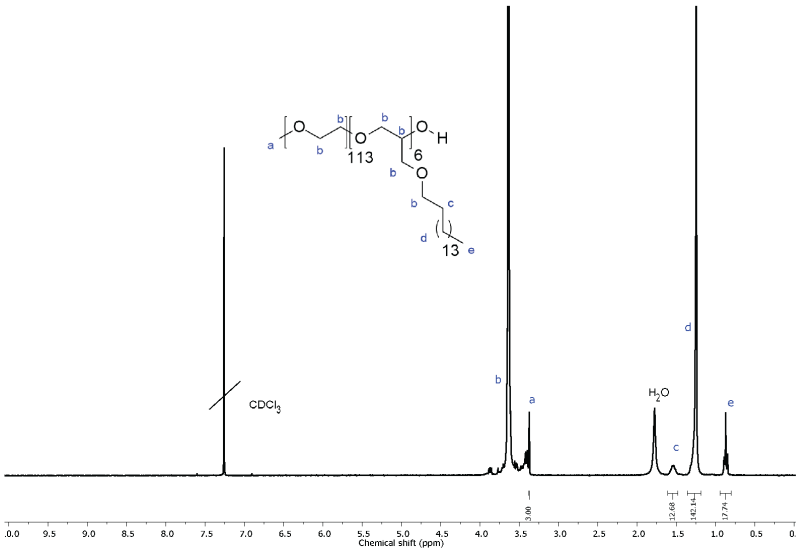

Figure S17. ^{1}H NMR spectrum (300 MHz, chloroform-d) of Me-P(EO)$_{113}$-*b*-P(C$_{16}$GE)$_{6}$.

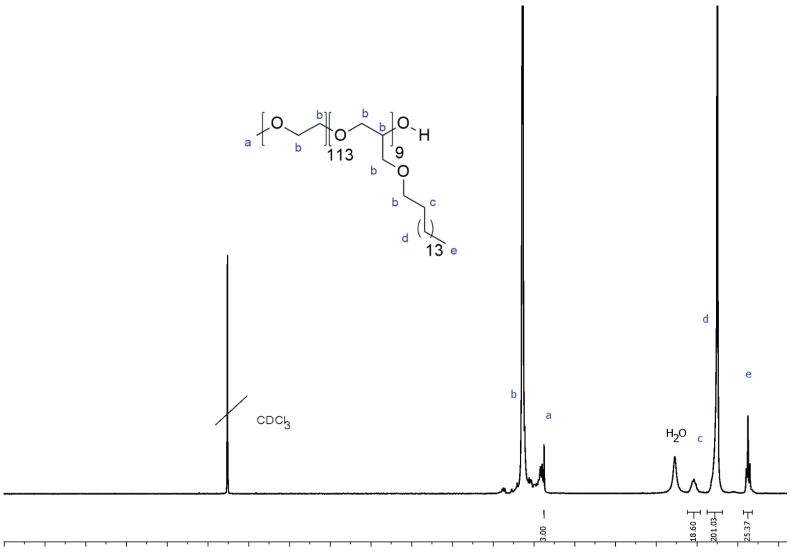

Figure S18. ^{1}H NMR spectrum (300 MHz, chloroform-d) of Me-P(EO)$_{113}$-*b*-P(C$_{16}$GE)$_{9}$.

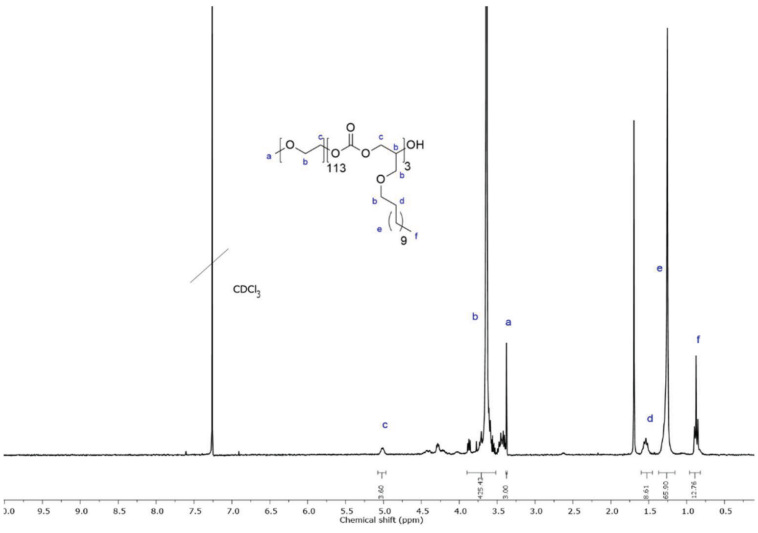

Figure S19. ^{1}H NMR spectrum (300 MHz, chloroform-d) of Me-P(EO)$_{113}$-*b*-P(CO$_2$C$_{12}$GE)$_{3}$.

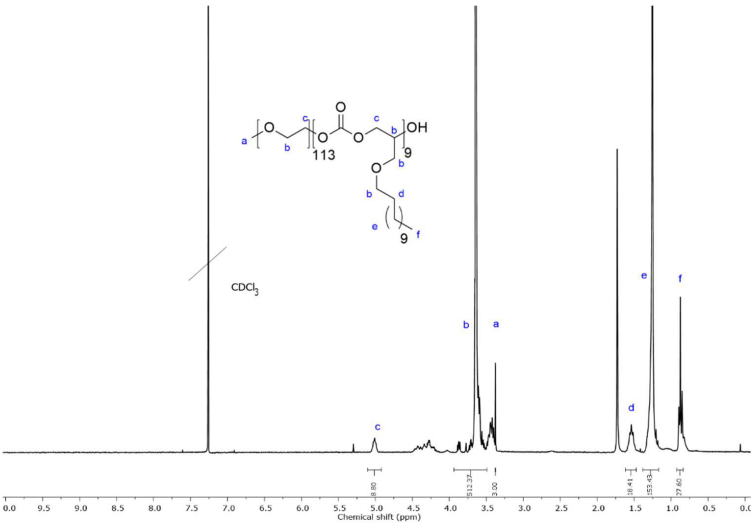

Figure S20. ^{1}H NMR spectrum (300 MHz, chloroform-d) of Me-P(EO)$_{113}$-*b*-P(CO$_2$C$_{12}$GE)$_9$.

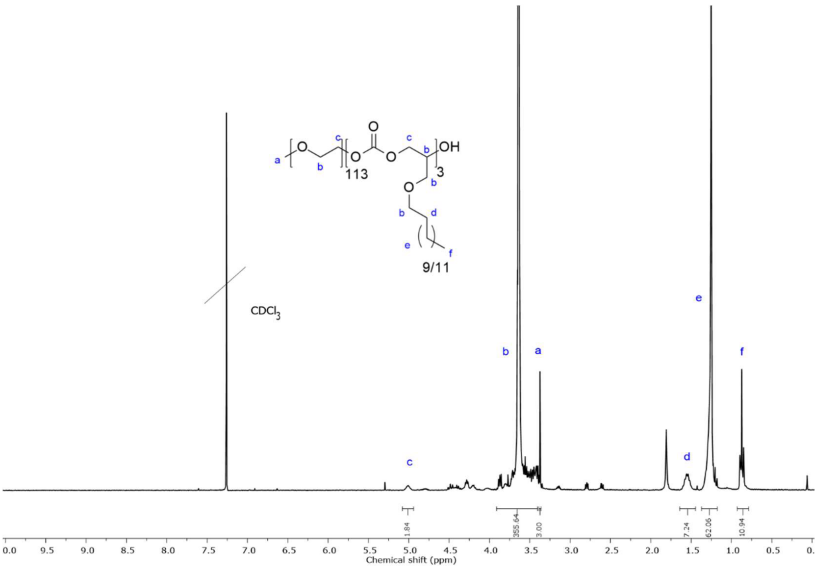

Figure S21. ^{1}H NMR spectrum (300 MHz, chloroform-d) of Me-P(EO)$_{113}$-*b*-P(CO$_2$C$_{12/14}$GE)$_3$.

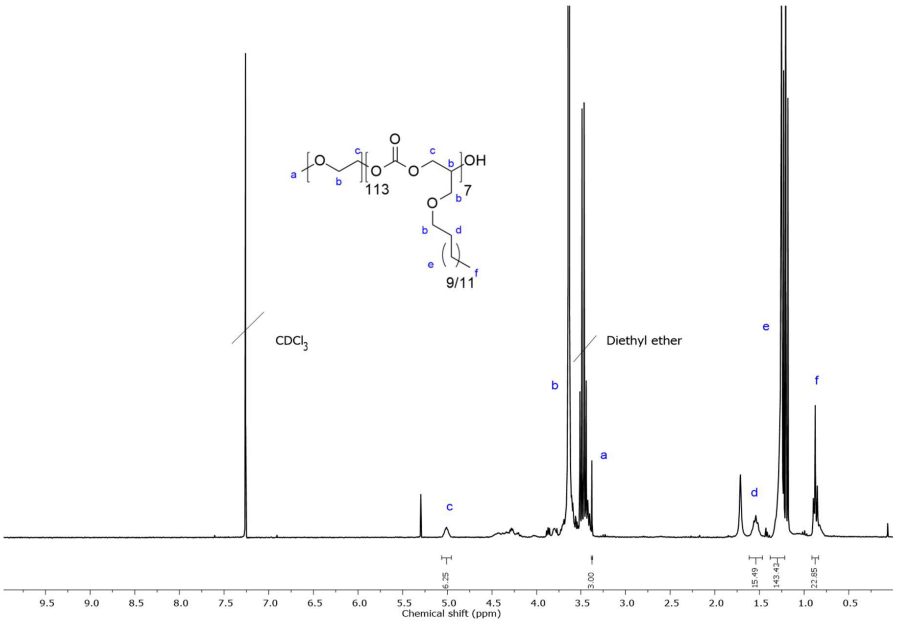

Figure S22. ^{1}H NMR spectrum (300 MHz, chloroform-d) of Me-P(EO)$_{113}$-*b*-P(CO$_2$C$_{12/14}$GE)$_7$.

5. Tabular Overview of the Phase Behavior Studies

Table S2. Sample composition, $\tilde{X}$ point parameters ($\tilde{\gamma}$ and $\tilde{T}$) and surfactant mass fraction $\tilde{\phi}_{C,i}$ within the interface at the $\tilde{X}$ point of the pseudo-ternary systems at constant ϕ = 0.500 and ε = 0.001[a], together with the molecular masses $M_{w,PEO}$ and $M_{w,PAlkGE}$ of the PEO and the ,PAlkGE blocks as well as the end-to-end distances $R_{ee,w}$ and $R_{ee,o}$ calculated from an equation derived by Kawaguchi et al. (see ref.[1]).

Polymer	δ	$\tilde{\gamma}$	$\tilde{T}$/°C	$\tilde{\phi}_{C,i}$	$M_{w,PEO}$/ g mol^{-1}	$R_{ee,w}$/Å	$M_{w,PAlkGE}$ g mol^{-1}	$R_{ee,o}$/Å
H_2O/NaCl – *n*-decane ($C_{10}H_{22}$) – $C_{10}E_4$/pure PEO-*b*-PAlkGE								
No polymer	0.000	0.135	30.6	0.124	-	-	-	-
Me-P(EO)$_{113}$-*b*-P(C_{12}GE)$_3$	0.050	0.090	31.5	0.071	5195	71.8	616	17.1
Me-P(EO)$_{113}$-*b*-P(C_{12}GE)$_6$	0.050	0.088	31.2	0.068	5195	71.8	1331	21.7
Me-P(EO)$_{113}$-*b*-P(C_{12}GE)$_7$	0.025	0.114	31.1	0.094	5195	71.8	1691	23.4
Me-P(EO)$_{113}$-*b*-P(C_{12}GE)$_7$	0.050	0.0923	30.9	0.073	5195	71.8	1691	23.4
Me-P(EO)$_{113}$-*b*-P(C_{12}GE)$_7$	0.075	0.0774	31.0	0.058	5195	71.8	1691	23.4
Me-P(EO)$_{113}$-*b*-P(C_{12}GE)$_8$	0.050	0.0896	31.0	0.070	5195	71.8	1556	22.8
H_2O/NaCl – *n*-octacosane ($C_{28}H_{58}$) – $C_{16}E_6$/pure or technical-grade PEO-*b*-PAlkGE								
No polymer	0.000	0.144	66.8	0.130	-	-	-	-
Me-P(EO)$_{113}$-*b*-P(C_{12}GE)$_3$	0.050	0.119	67.7	0.101	5195	71.8	616	17.1
Me-P(EO)$_{113}$-*b*-P(CO_2C_{12}GE)$_3$	0.050	0.103	67.5	0.086	5195	71.8	982	19.8
Me-P(EO)$_{113}$-*b*-P($CO_2C_{12/14}$GE)$_3$	0.050	0.128	67.1	0.109	5195	71.8	592	16.9
Me-P(EO)$_{113}$-*b*-P(C_{12}GE)$_6$	0.050	0.105	66.5	0.087	5195	71.8	1331	21.7

Me-P(EO)$_{113}$-*b*-P(C$_{12}$GE)$_7$	0.050	0.105	66.5	0.088	5195	71.8	1691	23.4
Me-P(EO)$_{113}$-*b*-P(C$_{12}$GE)$_7$	0.100	0.071	66.8	0.054	5195	71.8	1691	23.4
Me-P(EO)$_{113}$-*b*-P(CO$_2$C$_{12/14}$GE)$_7$	0.050	0.105	66.5	0.088	5195	71.8	1960	24.5
Me-P(EO)$_{113}$-*b*-P(CO$_2$C$_{12}$GE)$_9$	0.050	0.100	66.4	0.083	5195	71.8	1794	23.9
Me-P(EO)$_{113}$-*b*-P(C$_{12}$GE)$_8$	0.050	0.104	66.8	0.087	5195	71.8	1556	22.8
Me-P(EO)$_{113}$-*b*-P(C$_{16}$GE)$_6$	0.050	0.111	66.7	0.093	5195	71.8	1271	21.4
Me-P(EO)$_{113}$-*b*-P(C$_{16}$GE)$_9$	0.050	0.108	66.2	0.091	5195	71.8	1229	21.2
H$_2$O/NaCl – Sasolwax 5805 – Genapol O 050/080/ Me-P(EO)$_{113}$-*b*-P(CO$_2$C$_{12/14}$GE)$_7$								
Mass ratio surfactant mixture	δ	$\tilde{\gamma}$	$\tilde{T}$/°C	$M_{w,PEO}$/ gmol^{-1}	$R_{ee,w}$/Å	$M_{W,PALKGE}$/ gmol^{-1}	$R_{ee,o}$/Å	
1:1	0.000	0.155	73.7	-	-	-	-	
1:1	0.100	0.127	79.6	5195	71.8	1960	24.5	
3:1	0.100	0.091	74.6	5195	71.8	1960	24.5	

[a] Note that for the technical-grade systems, the weight ratio of the two technical-grade surfactants are also given.

6. Complete SANS Curves Recorded at $\phi_C = \tilde{\phi}_{C,0} + 0.02$

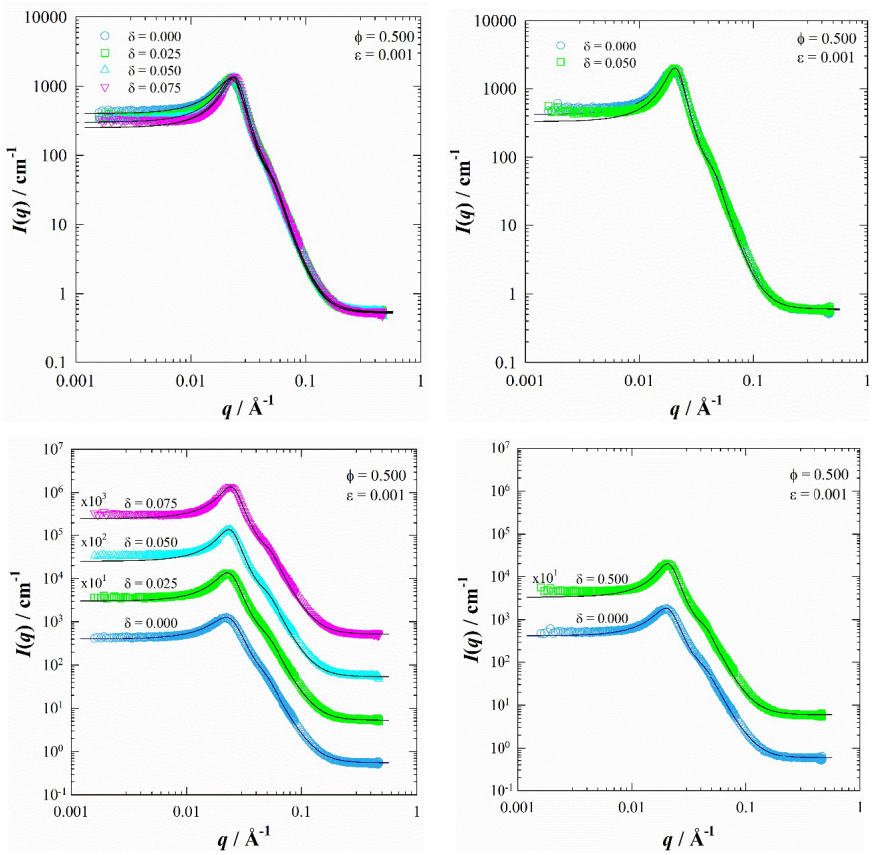

Figure S23. Left: Top :Bulk contrast SANS curves obtained for D_2O/NaCl – *n*-decane – $C_{10}E_4$/Me-P(EO)$_{113}$-*b*-P(C_{12}GE)$_7$ samples recorded close to the $\tilde{X}$ point of the polymer-free system at $\phi_C = \tilde{\phi}_{C,0} + 0.02 = 0.144$. Bottom: Curves from the top figure displaced by a factor of 10. **Right:** Bulk contrast SANS curves obtained for D_2O/NaCl – *n*-octacosane – $C_{16}E_6$/Me-P(EO)$_{113}$-*b*-P(C_{12}GE)$_7$ samples recorded close to the $\tilde{X}$ point of the polymer-free system at $\phi_C = \tilde{\phi}_{C,0} + 0.02 = 0.155$. Bottom: Curves from the top figure displaced by a factor of 10. Note that all shown curves were analyzed using the TS model[2] taking into account double scattering[3,4].

7. Tabular Overview of the Parameters Used to Fit the SANS Curves

Table S3: Composition of the bulk-contrast SANS samples, the corresponding fit parameters of the Teubner-Strey (*TS*) model[2] taking into account double scattering[3,4] as well as the bending rigidity determined from the model of random interfaces[5], alongside the transmission values of the respective SANS measurements.[a]

δ	ϕ_C	ϕ_D	q_{max}/Å^{-1}	I_{max}/cm^{-1}	I_0/cm^{-1}	I_{incoh}/cm^{-1}	f	x	transmission
D_2O/NaCl – *n*-decane ($C_{10}H_{22}$) – $C_{10}E_4$/Me-P(EO)$_{113}$-*b*-P(C_{12}GE)$_7$									
0.000	0.144	0.000	0.022	1280	400	0.550	0.020	1.00	0.66
0.025	0.125	0.003	0.019	1980	550	0.540	0.025	1.30	0.67
0.050	0.098	0.005	0.015	4150	1100	0.520	0.030	1.60	0.67
0.075	0.083	0.007	0.013	6560	1700	0.500	0.030	1.60	0.68
0.025	0.143	0.004	0.023	1370	300	0.530	0.020	1.60	0.66
0.050	0.142	0.007	0.023	1370	250	0.540	0.020	1.60	0.66
0.075	0.142	0.011	0.024	1380	250	0.520	0.020	1.60	0.66
D_2O/NaCl – *n*-octacosane ($C_{28}H_{58}$) – $C_{16}E_6$/Me-P(EO)$_{113}$-*b*-P(C_{12}GE)$_7$									
0.000	0.155	0.000	0.020	1855	420	0.580	0.022	1.60	0.65
0.050	0.112	0.006	0.014	5050	1150	0.540	0.030	1.60	0.66
0.100	0.078	0.008	0.010	13000	2900	0.540	0.025	2.00	0.68
0.050	0.154	0.008	0.021	2020	330	0.600	0.020	1.60	0.65
D_2O/NaCl – Sasolwax 5805 – Genapol O 050/080/Me-P(EO)$_{113}$-*b*-P($CO_2C_{12/14}$GE)									
0.100	0.114	0.012	0.009	9100	4500	0.580	0.022	1.00	0.65

n	δ	ϕ_C	ϕ_D	q_{max}/ Å^{-1}	I_{max}/cm^{-1}	I_0/cm^{-1}	$I_{incoh.}$/cm^{-1}	f	x	Trans-mission
D_2O/NaCl – n-octacosane ($C_{28}H_{58}$) – $C_{16}E_6$/Me-P(EO)$_{113}$-*b*-P(C_{12}GE)$_n$										
-	0.000	0.155	0.000	0.020	1855	420	0.580	0.022	1.60	0.65
3	0.050	0.154	0.008	0.020	2050	420	0.580	0.020	1.20	0.65
7	0.050	0.154	0.008	0.014	5050	1150	0.540	0.030	1.60	0.65
8	0.050	0.154	0.008	0.020	2060	340	0.560	0.020	1.60	0.65

[a]Symmetric microemulsions were studied at constant ϕ = 0.500 and ε = 0.001 for different PEO-*b*-PAlkGEs and polymer mass fractions δ within the overall amphiphilic mixture, with the surfactant and copolymer volume fractions ϕ_C and ϕ_D, respectively. Further listed are the fitting parameters of the extended *TS* model: the scattering vector q_{max} and the intensity I_{max} that define the peak (position) of the SANS curve of the bicontinuously structured microemulsion, the intensity I_0 at q = 0, the incoherent background scattering intensity I_{incoh}, and the fraction of double scattering f and the additional broadening x. For the sake of completeness, the transmission values of the respective SANS measurements are listed, too.

8. Determination of the End-to-End Distances (Ree) of the Homopolymers

SANS experiments were performed for three homopolymers to determine their end-to-end distances R_{ee} in the respective solvent. The SANS measurements were performed for the hydrophilic homopolymer PEO in D_2O, for the hydrophobic BnO-P($C_{12}GE)_{14}$ in deuterated *n*-decane and for the larger BnO-P($C_{12}GE)_{18}$ in deuterated *n*-decane as well as in deuterated *n*-octacosane. Note that the determination of the R_{ee} of the homopolymers was performed near the phase inversion temperature of the polymer-doped microemulsion systems of the type H_2O/NaCl – oil – C_iE_j (see $T(\gamma)$ sections within the manuscript). These measurements were performed Since the SANS investigations were performed at different SANS facilities and under different conditions, Table S4 summarizes the necessary information concerning the measurement conditions etc. whereas the obtained SANS curves are shown in Figure S24. The determined dependencies of the R_{ee} values on the molecular weight M_w of the respective polymer blocks are shown in Figure S25.

Table S4: SANS facilities and measurement conditions used for the investigation of the homopolymers PEO (M_w = 5290 g mol^{-1}), BnO-P($C_{12}GE)_{14}$ and BnO-P($C_{12}GE)_{18}$ within the specified solvents for the determination of their radius of gyration R_g and their end-to-end distances $R_{ee,w}$ or $R_{ee,o}$, respectively.[a, b, c]

Sample	SANS facility	T_{SANS}/ °C	M_w/ g mol^{-1}	R_g/Å	$R_{ee,w}$/Å	$R_{ee,o}$/Å
PEO (5290 gmol^{-1}, 0.25wt% in D_2O)	MLZ	24.9	5290	26.6[b]	65.1	-
PEO (5290 gmol^{-1}, 0.25wt% in D_2O)	MLZ	60.3	5290	26.6[b]	65.1	-
BnO-P($C_{12}GE)_{14}$ (0.5wt% in deut. *n*-decane)	NIST	22.1	3960	12.5[c]	-	30.6
BnO-P($C_{12}GE)_{18}$ (0.5wt% in deut. *n*-decane)	NIST	28.9	4825	13.3[c]	-	32.6
BnO-P($C_{12}GE)_{18}$ (1.0wt% in deut. *n*-octacosane)	NIST	67.0	4825	13.3[c]	-	32.6

[a] The homopolymer samples PEO (5290 g mol^{-1}), BnO-P($C_{12}GE)_{14}$ and BnO-P($C_{12}GE)_{18}$ were studied at different weight fractions (wt%) in the respective deuterated solvents. [b] The SANS data obtained for PEO was evaluated by using a two-correlation length model, taking into account a scattering contribution at low

q obtained from formed clusters.[6–8 c] The SANS data obtained for the PAlkGE homopolymers was evaluated by using the *Guinier* model for spherical structures.[9] Note that both mentioned models initially only provide information about the gyration radius R_g. The end-to-end distances $R_{ee,o}$ and $R_{ee,w}$ can be calculated afterwards from R_g by using the relation $R_{ee} = 6^{1/2} R_g$.[10] It is interesting to note that the determined R_g and therefore R_{ee} values for all homopolymers under investigation seem to be temperature-independent and solvent-independent. Further experiments are necessary to verify the observed independence of R_{ee} on temperature and solvent.

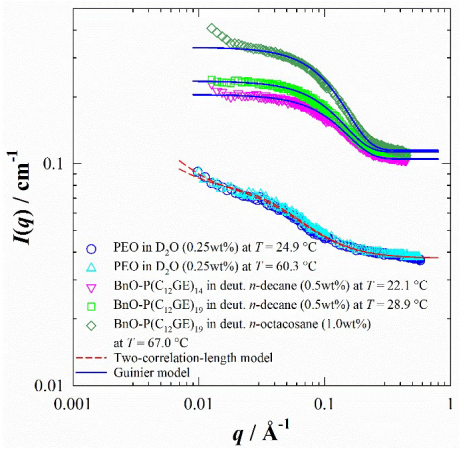

Figure S24. SANS curves obtained for the three homopolymers PEO (M_w = 5290 g mol^{-1}), BnO-P(C_{12}GE)$_{14}$ and BnO-P(C_{12}GE)$_{18}$ in the respective solvents. Scattering curves of PEO, in D_2O (0.25wt%), were fitted by using a two-correlation-length model displayed as a dashed red line, which takes into account the scattering contribution of occurring clusters at low q.[6–8] The hydrophobic homopolymers BnO-P(C_{12}GE)$_{14}$ and BnO-P(C_{12}GE)$_{18}$ were studied in deuterated *n*-decane (0.5wt%) and fitted using the Guinier model (blue solid lines).[9] The more hydrophobic BnO-P(C_{12}GE)$_{18}$ homopolymer was additionally investigated in deuterated *n*-octacosane (1.0wt%) and again fitted using the Guinier model.[9] Note that the shown scattering curves correspond to the data without the subtraction of the scattering contribution of the pure solvents and the incoherent scattering background $I_{incoh.}$, respectively.

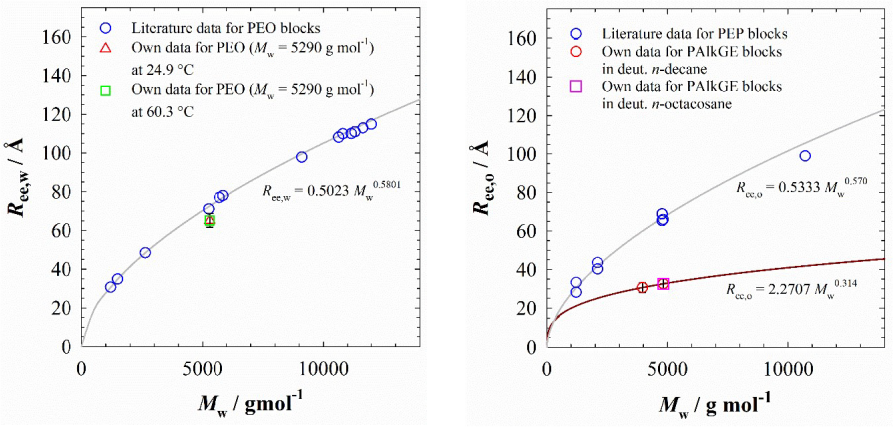

Figure S25. Trends of the end-to-end distance $R_{ee,w}$ (left) and $R_{ee,o}$ (right) as a function of molecular weight M_w for different types of homopolymers/polymer blocks. On the left, the $R_{ee,w}(M_w)$ dependency found for the hydrophilic PEO block within H_2O or D_2O is shown. Note that the theoretical values (taken from[10–13]) are all calculated from an equation derived by Kawaguchi et al. (see ref.[1]), which is based on light scattering experiments performed for varying molecular weights M_w of PEO in water to obtain the radius of gyration R_g of the PEO homopolymer. The red upward triangle represents the result we obtained from SANS investigations of PEO (M_w = 5290 g mol^{-1}) in D_2O at T = 24.9 °C, whereas the green square corresponds to the measurement performed at T = 60.3 °C. As can be seen, the temperature has a negligible effect upon the $R_{ee,w}$ of the PEO homopolymer and our value determined with SANS almost quantitatively agrees with the literature data calculated with the equation derived by Kawaguchi et al.. On the right, the $R_{ee,o}(M_w)$ dependency of the hydrophobic PAlkGE polymer blocks is shown. To the best of our knowledge, there are no comparable data on alkyl glycidyl ether polymers so far. We therefore show the values we obtained via SANS for the two homopolymers BnO-P(C_{12}GE)$_{14}$ and BnO-P(C_{12}GE)$_{18}$ (cf. Table S4), alongside literature data on PEP blocks in cyclohexane or benzene[10–12]. The red circles are displaying the results obtained for these two polymers in deuterated *n*-decane (BnO-P(C_{12}GE)$_{14}$ at T = 22.1 °C and BnO-P(C_{12}GE)$_{18}$ at T = 28.9 °C) whereas the pink square illustrates the result obtained for BnO-P(C_{12}GE)$_{18}$ in deuterated *n*-octacosane at T = 67.0°C. On the basis of this result it can be concluded, that using either *n*-decane or *n*-octacosane has no influence upon $R_{ee,o}$.

References

(1) Kawaguchi, S.; Imai, G.; Suzuki, J.; Miyahara, A.; Kitano, T.; Ito, K. Aqueous solution properties of oligo- and poly(ethylene oxide) by static light scattering and intrinsic viscosity. *Polymer* **1997**, *38*, 2885–2891.

(2) Teubner, M.; Strey, R. Origin of the scattering peak in microemulsions. *J. Chem. Phys.* **1987**, *87*, 3195–3200.

(3) Schelten, J.; Schmatz, W. Multiple-scattering treatment for small-angle scattering problems. *J. Appl. Crystallogr.* **1980**, *13*, 385–390.

(4) Silas, J. A.; Kaler, E. W. Effect of multiple scattering on SANS spectra from bicontinuous microemulsions. *J. Colloid Interface Sci.* **2003**, *257*, 291–298.

(5) Pieruschka, P.; Safran, S. A.; Marčelja, S. T. Comment on ''Fluctuating interfaces in microemulsion and sponge phases''. *Phys. Rev. E* **1995**, *52*, 1245–1247.

(6) Hammouda, B.; Ho, D.; Kline, S. SANS from Poly(ethylene oxide)/Water Systems. *Macromolecules* **2002**, *35*, 8578–8585.

(7) Hammouda, B.; Ho, D. L.; Kline, S. Insight into Clustering in Poly(ethylene oxide) Solutions. *Macromolecules* **2004**, *37*, 6932–6937.

(8) Hammouda, B.; Ho, D. L. Insight into chain dimensions in PEO/water solutions. *J. Polym. Sci. Part B: Polym. Phys.* **2007**, *45*, 2196–2200.

(9) Glatter, O.; Kratky, O. *Small angle X-ray scattering*, 2nd printing 36; Academic Press: London, 1982.

(10) Endo, H.; Mihailescu, M.; Monkenbusch, M.; Allgaier, J.; Gompper, G.; d. Richter; Jakobs, B.; Sottmann, T.; Strey, R.; Grillo, I. Effect of amphiphilic block copolymers on the structure and phase behavior of oil–water-surfactant mixtures. *J. Chem. Phys.* **2001**, *115*, 580–600.

(11) Byelov, D.; Frielinghaus, H.; Holderer, O.; Allgaier, J.; d. Richter. Microemulsion efficiency boosting and the complementary effect. 1. Structural properties. *Langmuir* **2004**, *20*, 10433–10443.

(12) Jakobs, B. *Amphiphile Blockcopolymere als Efficiency Booster für Tenside*, 1st ed.; Cuvillier Verlag: Göttingen, 2001.

(13) Tchekountieu Mboumi, L. J. *Technisch relevante amphiphile Blockcopolymere in Mikroemulsionen: Dissertation*, 2010.

CURRICULUM VITAE

LIST OF PUBLICATIONS

Contribution as first author or equally

2021

(1) Gardiner, C.; Johann, T.; Hanewald, A.; Frey, H. Addressing a key challenge of CO_2-based polycarbonates: low glass transition capitalizing on citronellol glycidyl ether. *to be submitted*.

(2) Gardiner, C.; Frey, H. Tailoring the glass transition temperatures of the established aliphatic polycarbonates PPC and PCHC using biobased citronellol glycidyl ether: kinetic studies and post-modification. *to be submitted*.

(3) Gardiner, C.; Schüttner, S.; Petrov, F.; Floudas, G.; Frey, H. Biobased and biodegradable thermoplastic elastomers based on citronellol glycidyl ether, CO_2 and polylactide. *to be submitted*.

(4) Gardiner, C.; Koynov, K.; Frey, H. Tough hydrogels based on poly(ethylene oxide), carbon dioxide and cyclohexene oxide: Improvement of the toughness via polyurethane multiblock synthesis. *to be submitted in polymer chemistry*.

(5) Daenzer, T.; Gardiner C.; Kunze, L.; Tseng, S., H.; Gleede T.; Sottmann S.; Frey H.; Siloxane Functionalized Polyether-Polycarbonates with Amphiphilic Properties: A New Class of Surfactants. *to be submitted*.

2018

(6) Güney, A.; Gardiner, C.; McCormack, A.; Malda, J.; Grijpma, D. W. Thermoplastic PCL-*b*-PEG-*b*-PCL and HDI Polyurethanes for Extrusion-Based 3D-Printing of Tough Hydrogels. *Bioengineering*, **2018**, DOI: 10.3390/bioengineering5040099.

Contribution as coauthor

2020

Efficiency Boosting of Surfactants with Poly(ethylene oxide)-Poly(alkyl glycidyl ether)s – A New Class of Amphiphilic Polymers. *Langmuir,* **2020***,* DOI: 10.1021/acs.langmuir.0c01491.